ISSN 2542-1565

Vol. 17 2024 No. 04

GEOGRAPHY ENVIRONMENT SUSTAINABILITY

Special issue «CATCHMENT EROSION AND POLLUTION PROBLEMS»

«The journal GEOGRAPHY, ENVIRONMENT, SUSTAINABILITY was founded in 2008 by Russian Geographical Society, the Lomonosov Moscow State University Geography Department, and the Russian Academy of Sciences Institute of Geography. Since that time the journal publishes **4 issues per year**, containing original research papers and reviews. The journal issues are open source and distributed through subscriptions, library exchanges of leading universities, and via the website through the world»

FOUNDERS OF THE JOURNAL: Russian Geographical Society, Faculty of Geography, Lomonosov Moscow State University and Institute of Geography of the Russian Academy of Sciences

The journal is published with financial support of the Russian Geographical Society.

The journal is registered in Federal service on supervision of observance of the legislation in sphere of mass communications and protection of a cultural heritage. The certificate of registration: ПИ № ФС77-67752, 2016, December 21.

PUBLISHER
Russian Geographical Society
Moscow, 109012 Russia
Novaya ploshchad, 10, korp. 2
Phone 8-800-700-18-45
E-mail: press@rgo.ru
www.rgo.ru/en

EDITORIAL OFFICE
Lomonosov Moscow State University
Moscow 119991 Russia
Leninskie Gory, 1,
Faculty of Geography, 1806a
Phone 7-495-9391552
Fax 7-495-9391552
E-mail: ges-journal@geogr.msu.ru
www.ges.rgo.ru

DESIGN
Layout designer: Tereshkin Anton
Moscow, 115088,
26 Simonovsky Val str., bldg. One
Phone: +7 (903) 108-04-44
E-mail: smile.tai@gmail.com

DOI prefix: 10.24057

Format A4 (210x297mm)

"GEOGRAPHY, ENVIRONMENT, SUSTAINABILITY" is the only original English-language journal in the field of geography and environmental sciences published in Russia. It is supposed to be an outlet from the Russian-speaking countries to Europe and an inlet from Europe to the Russian-speaking countries regarding environmental and Earth sciences, geography and sustainability. The main sections of the journal are the theory of geography and ecology, the theory of sustainable development, use of natural resources, natural resources assessment, global and regional changes of environment and climate, social-economical geography, ecological regional planning, sustainable regional development, applied aspects of geography and ecology, geoinformatics and ecological cartography, ecological problems of oil and gas sector, nature conservations, health and environment, and education for sustainable development.

OPEN ACCESS POLICY. "GEOGRAPHY, ENVIRONMENT, SUSTAINABILITY" is an open access journal. All articles are made freely available to readers immediately upon publication. Our open access policy is in accordance with the Budapest Open Access Initiative (BOAI) definition - it means that articles have free availability on the public internet, permitting any users to read, download, copy, distribute, print, search, or link to the full texts of these articles, crawl them for indexing, pass them as data to software, or use them for any other lawful purpose, without financial, legal, or technical barriers other than those inseparable from gaining access to the internet itself.

Date of publication: December 31st, 2024.

© Russian Geographical Society, 2024

EDITORIAL BOARD

EDITORS-IN-CHIEF:

Kasimov Nikolay S.
Lomonosov Moscow State University,
Faculty of Geography, Russia

Kotlyakov Vladimir M.
Russian Academy of Sciences
Institute of Geography, Russia

DEPUTY EDITORS-IN-CHIEF:

Solomina Olga N. - Russian Academy of Sciences, Institute of Geography, Russia
Tikunov Vladimir S. - Lomonosov Moscow State University, Faculty of Geography, Russia

Vandermotten Christian - Université Libre de Bruxelles Belgium
Chalov Sergei R. - (Secretary-General) Lomonosov Moscow State University, Faculty of Geography, Russia

Alexeeva Nina N. - Lomonosov Moscow State University, Faculty of Geography, Russia
Baklanov Alexander - World Meteorological Organization, Switzerland
Chubarova Natalya E. - Lomonosov Moscow State University, Faculty of Geography, Russia
De Maeyer Philippe - Ghent University, Department of Geography, Belgium
Dobrolubov Sergey A. - Lomonosov Moscow State University, Faculty of Geography, Russia
Ferjan J. Ormeling - University of Amsterdam, Amsterdam, Netherlands
Sven Fuchs - University of Natural Resources and Life Sciences
Haigh Martin - Oxford Brookes University, Department of Social Sciences, UK
Golosov Valentin N. - Lomonosov Moscow State University, Faculty of Geography, Russia
Golubeva Elena I. - Lomonosov Moscow State University, Faculty of Geography, Russia.
Gulev Sergey K. - Russian Academy of Sciences, Institute of Oceanology, Russia
Guo Huadong - Chinese Academy of Sciences, Institute of Remote Sensing and Digital Earth, China
Jarsjö Jerker - Stockholm University, Department of Physical Geography and Quaternary Geography, Sweden
Jeffrey A. Nittrouer - Rice University, Houston, USA
Ivanov Vladimir V. - Arctic and Antarctic Research Institute, Russia
Karthe Daniel - German-Mongolian Institute for Resources and Technology, Germany
Kolosov Vladimir A. - Russian Academy of Sciences, Institute of Geography, Russia
Kosheleva Natalia E. - Lomonosov Moscow State University, Faculty of Geography, Russia
Konečný Milan - Masaryk University, Faculty of Science, Czech Republic
Kroonenberg Salomon - Delft University of Technology, Department of Applied Earth Sciences, The Netherlands
Kulmala Markku - University of Helsinki, Division of Atmospheric Sciences, Finland
Olchev Alexander V. - Lomonosov Moscow State University, Faculty of Geography, Russia
Malkhazova Svetlana M. - Lomonosov Moscow State University, Faculty of Geography, Russia
Maslakov Alexey A. - Lomonosov Moscow State University, Faculty of Geography, Russia
Minkina Tatiana M. - Southern Federal University, Russian Federation
Moreido Vsevolod M. - Russian Academy of Sciences, Water Problems Institute, Russia
Meadows Michael E. - University of Cape Town, Department of Environmental and Geographical Sciences South Africa
O'Loughlin John - University of Colorado at Boulder, Institute of Behavioral Sciences, USA
Paula Santana - University of Coimbra, Portugal
Pedroli Bas - Wageningen University, The Netherlands
Pilyasov Alexander N. - Institute of Regional Consulting, Moscow, Russia
Radovanovic Milan - Serbian Academy of Sciences and Arts, Geographical Institute "Jovan Cvijić", Serbia
Samsonov Timofey E. - Lomonosov Moscow State University, Faculty of Geography, Russia
Sebentsov Alexander B. - Russian Academy of Sciences, Institute of Geography, Russia
Sokratov Sergei A. - Lomonosov Moscow State University, Faculty of Geography, Russia
Tishkov Arkady A. - Russian Academy of Sciences, Institute of Geography, Russia
Wuyi Wang - Chinese Academy of Sciences, Institute of Geographical Sciences and Natural Resources Research, China

EDITORIAL OFFICE

ASSOCIATE EDITOR

Maslakov Alexey A.
Lomonosov Moscow State University,
Faculty of Geography, Russia

ASSISTANT EDITOR

Mozolevskaya Irina V.
Lomonosov Moscow State University,
Faculty of Geography, Russia

ASSISTANT EDITOR

Komova Nina N.
Lomonosov Moscow State University,
Faculty of Geography, Russia

PROOF-READER

Denisova Irina S.
Lomonosov Moscow State University,
Faculty of Geography, Russia

CONTENTS

SPECIAL ISSUE
«CATCHMENT EROSION AND POLLUTION PROBLEMS»

Part 1. Catchment erosion and management

Part 2. Channel processes and river hydrogeochemistry

Disclaimer:

The information and opinions presented in the Journal reflect the views of the authors and not of the Journal or its Editorial Board or the Publisher. The GES Journal has used its best endeavors to ensure that the information is correct and current at the time of publication.

Check for updates

CC BY

EDITORIAL PAPER

ADVANCES IN CATCHMENT AND RIVER EROSION AND POLLUTANTS' TRANSPORT STUDIES: FROM MONITORING TO MODELLING TO MANAGEMENT

Sergey R. Chalov[1*], Vsevolod Moreido[2], Marko Urošev[3], Valentin Golosov[1], Miodrag Zlatić[4], Nikolay Kasimov[1]

[1] Faculty of Geography, Lomonosov Moscow State University, Leninskie Gory 1, Moscow 119991, Russia
[2] Water Problems Institute, Russian Academy of Sciences, Gubkina 3, Moscow, 119333, Russia
[3] Geographical Institute "Jovan Cvijić", Serbian Academy of Sciences and Arts, Djure Jakšića 9, Belgrade, 11000, Serbia
[4] Faculty of Forestry, University of Belgrade, Kneza Višeslava 1, Belgrade, 11030, Serbia
***Corresponding author:** hydroserg@mail.ru

Received: November 29th 2024 / Accepted: December 3rd 2024 / Published: October 31st 2024
https://doi.org/10.24057/2071-9388-2024-0608

ABSTRACT. Catchment erosion, channel erosion and sediment transport are connected processes within fluvial system forming a sediment cascade. Studies related to connectivity between a specific source and its multiple sinks within catchment, and rivers, and their multiple impacts have expanded in scope and sophistication during the last two decades, and were recently broadly presented at numerous international conferences and workshops. The International conference on transboundary catchment erosion and pollution problems was held in Belgrade, Serbia, in July 2023. The outcome of this conference as comprehensive literature review on the topic initiated this review which is aimed at classification the functional scheme of soil erosion, channel processes and sediment transport, and their impacts which include natural hazards, river pollution and hydrogeochemistry, catchment management, and hazards prevention, and technologies. We summarize established and emerging papers related to both regional studies on catchment erosion and management, as well as channel processes modelling and hydrogeochemical impact in streams and rivers. Finally, we discuss future directions and challenges to bridge scientific and management gaps by promoting a holistic understanding of river systems and catchment conditions.

KEYWORDS: sediment transport, river pollution, catchment science

CITATION: Chalov S. R., Moreido V., Urošev M., Golosov V, Zlatić M., Kasimov N. (2024). Advances In Catchment And River Erosion And Pollutants' Transport Studies: From Monitoring To Modelling To Management. Geography, Environment, Sustainability, 4(17), 6-9
https://doi.org/10.24057/2071-9388-2024-0608

ACKNOWLEDGEMENT: This review on soil erosion studies is supported by the Ministry of Science and Higher Education of Russian Federation, grant number 075-15-2024-614.
Study of river pollution was supported by the Russian Science Foundation (Project no. 22-17-00102).

Conflict of interests: The authors reported no potential conflict of interest.

INTRODUCTION

In a river, sediments and particulate pollutants go through erosion, transport, and deposition by flowing water. Connectivity between a specific source and its multiple sinks in which the output of one process is the input of another is a dominant feature of catchment-river interaction. Various terms have been proposed to this phenomena such as sediment cascade (Burt and Allison 2010) or integrated erosion-deposition processes (Alekseevskiy et al. 2008). A plethora of studies in this area are motivated by various impacts associated with erosion and particulate transport phenomena. The International conference on transboundary catchment erosion and pollution problems was held in Belgrade, Serbia, in July 2023. It was organized by the University of Belgrade, Center of Russian Geographical Society in Serbia, Lomonosov Moscow State University, Geographical Institute "Jovan Cvijić" SASA, University of Banja Luka, and under auspices of World Association of Soil and Water Conservation (WASWAC), and International Association of Hydrological Sciences (IAHS). It encompassed around 50 presentations addressing numerous aspects of hydrological studies in catchments ranging from bed erosion to transboundary river systems' management.

Here, based on the outcomes of this conference, we reveal two major categories of studies according to spatial scale of research (Table 1): catchment erosion and channel processes. For each of the categories we reviewed potential impacts related to the focus of the particular research: natural hazards, hydrogeochemistry and water pollution, catchment management and hazard mitigation, technologies underlined by technologies in erosion, sediment and pollutants transport monitoring and modelling. We assume that catchment and river management is generally complex, such that continual

research is needed, ranging from improved sediment and pollutants mobilization models to large-scale river experiments (Rheinheimer and Yarnell 2017). The aim of this paper is to provide classification of the erosion and channel processes studies based on the contribution of the International conference on transboundary catchment erosion and pollution problems with a focus on the different aspects of its contributions.

CATCHMENT EROSION

Quantifying catchment erosion under different conservation practices is crucial for watershed management framework. The reviewed collection of papers includes two chapters in soil erosion problems: Management and hazard mitigation and Technological advances.

Management and hazard mitigation issues are observed by (Kovačević-Majkić et al. 2024) for extreme flood events due to torrential rainfall in three catchments of Morava tributaries in Serbia. The catchments are zoned according to the potential exposure to flood impact without river runoff observation data, only based on satellite images, digital elevation model analysis and slope geomorphology.

Catchment erosion due to delivery of sediment into the rivers system is the main global threat to sustainability of reservoirs (Vörösmarty et al. 2003) which requires catchment management plans. In the paper (Minchev et al. 2024) results of soil erosion calculations using the Gavrilovich method (or EPM) for two contrasting river basins in North Macedonia are presented. One of the river basin, the Globocica River, belongs to the territories with high projective slopes covered with vegetation, while there are several hot spot with high rates of water erosion in the other river basin (Spilje). The obtained calculation data were compared with the results of field evaluation of the total sedimentation in reservoirs located in the lower reaches of each of the basins. In general, the calculation results coincide very well (error of the order of 10%) for the Globocica river basin. However, in the case of the Spilje catchment, where the average annual sedimentation volumes in reservoir are an order of magnitude higher, the calculations based on the EPM model underestimate the volumes of sediment inflow by 30%.

Technological advances in catchment science and soil erosion include development of novel approaches to attempt more methods and perform comparative studies to attain accurate results for assessing soil erosion vulnerability (Pandey et al. 2021). In (Gartsman et al 2024) a new method for parameter calibration of distributed hydrological models in river catchments with a complex structure and a large number of gauges is considered. While the search for a local minimum of the optimization function is a complex multicriterial problem, using the principal component analysis, the most representative gauge or gauges are selected for optimization, and the rest are considered as information noise and removed. A fundamentally new concept for river catchment description, the catchment "compactness", is introduced as a measure of the consistency of water content fluctuations within the river network.

A comparison of the results of calculations of water erosion rates in the basin of the transboundary river Strumica, obtained on the basis of the RUSLE and the regional EPM model is presented in the article by (Trendafilov et al. 2024). The authors come to the conclusion that the accuracy of calculations undertaken with application of the RUSLE is higher than EPM model. Therefore, they recommend using RUSLE approach to assess erosion in this region.

RIVER EROSION AND POLLUTANTS' TRANSPORT

Rivers have been manipulated by humans for millennia, with built structures resulting in significant impacts to water flow, sediment transport, and channel stability (Nittrouer et al. 2012). The driving factors of the ongoing changes in channel processes include climate-related water flow changes and engineering projects which carry the potential for unintended consequences, including endangering human lives and infrastructure, and disrupting the commercial and ecological viability of river channels, floodplains, and deltas.

Erosion processes especially in mountain areas are typically associated with **natural hazards**. Example of these studies is given by (Pavlukevich et al. 2024) with the monitoring and assessment of Bashkara Glacier Lakes system after their outburst on September 1st, 2017. The Bashkara Glacier Lakes are located in the most glaciated and populated part of the Central Caucasus of Russia, in the Mt. Elbrus region. This area has been chosen as a polygon for international research in terms of sediment transport (e.g. (Rets et al. 2019; Tsyplenkov et al. 2020)). Studies highlight necessity to take measures to reduce the level of Bashkara Lake to prevent it from re-outburst.

In (Milanović Pešić et al. 2024) the flow patterns of rivers in Serbia and northern Montenegro are considered, and differences and trends in the current climate conditions are discussed. With no significant trends in precipitation an increase in air temperature has led to flow reduction in both winter and summer months. However, only climatic factors were analyzed as drivers for flow alteration, and not land use change in the catchment.

Technological advances in riverine sediment transport relate both to in *situ* automated measurements of water quality constituents, including both solutes and particulates (Bieroza et al. 2023), as well as novel modelling approaches (Gautier et al. 2021). Some recent examples include extended 1- and 2-dimensional models

Table 1. Classification of the erosion and channel processes impacts presented at the International conference on transboundary catchment erosion and pollution problems (Serbia, Belgrade, 2023)

Impacts	Catchment erosion	Channel processes
Natural hazards	-	Pavlyukevich et al. 2024 Milanović Pešić et al. 2024
Hydrogeochemestry and pollution	-	Lychagin et al. 2024 Korjenić, 2024
Management and hazard mitigation	Kovačević-Majkić et al. 2024 Minchev et al. 2024	Matić, 2024
Technological advances	Trendafilov et al. 2024 Gartsman et al. 2024	Krylenko et al. 2024 Nyiri and Török 2024

of large rivers which enable to provide long-scale temporal estimate the impact of interventions. In (Nyiri and Török, 2024), the upper Hungarian reach of Danube River is analyzed to quantify the impact of structural measures on sediment transport, such as: wing dam fields, water dams, artificial cutoffs. In (Krylenko et al. 2024) a novel approach in hydrodynamic 2D modelling and channel evolution forecasting of the most comprehensive channel patterns types strongly impacted by climate change is discussed on a case study of flow distribution and climate related projections of bed level changes of the Lena river anabranching channel.

These models' outputs are typically used to develop **management plans** for management schemes. In (Matić 2024) the integrated water management plan for the transboundary Tisza River (shared by Ukraine, Slovakia, Hungary, Romania and Serbia) is discussed. Methods for flood risk reduction through ecosystem services are considered, such as flood risk management by incorporating natural retention basins (floodplains, marshes).

Finally, in-channel processes are related to water and constituents' fluxes from the continents to the Ocean and highlights the topic of **hydrogeochemistry and pollutants transport** in riverine studies. In Polar regions snow and ice melting are associated with dramatic changes in the hydrological regime and significantly enhance erosional processes. Such changes are the most important driver of the hydrological cycle of Polar rivers and dominate the fluxes of dissolved and particulate substances from land to the Arctic Ocean. In (Lychagin et al. 2024) the results of long-term observations of metals and metalloids migration in dissolved and suspended forms in the Pur River system located in the oil and gas province in Western Siberia are discussed. The dynamics of element concentration in three groups – dissolved, transitional and suspended – by hydrological seasons are analyzed. This paper significantly enhances existing databanks on Artic Polar geochemistry mostly presented by dissolved modes of pollutants transport (e.g. (Szumińska et al. 2023; Savenko and Savenko 2024)) and underlie studies to estimate background, baseline, and anthropogenic levels of dissolved and suspended metal(loid)s.

Another aspect of pollution problem in relation to channel behavior is migration of radioactive waste disposal (Bonavigo et al. 2009). Due to deposition in channel and floodplain sediment and secondary resuspension, studies of radionuclides fate in rivers is strictly related to sediment transport approaches (Chalov et al. 2017). In the paper by (Korjenić 2024) the potential impacts of the planned construction of radioactive waste disposal in the Croatian reach of the Una River basin is discussed. The smaller part of catchment is located in Croatia, while most of the catchment area is located in Bosnia and Herzegovina. The author has carried out a detailed analysis of the landscape features of the river catchment area and its hydrological regime and has convincingly shown that the placement of this waste disposal can lead to significant pollution of the river valley flowing in Bosnia and Herzegovina.

Studies related to connectivity between catchment erosion, channel erosion and sediment transport and their multiple impacts have expanded in scope and sophistication during the last few decades (Collins et al. 2024). Due to climate and land use change international attention should be focused on improvement of understanding of their impacts on river systems and improving their quantification through monitoring and modeling in order to better manage these issues. Advances in soil erosion and channel processes studies are essential for tackling transboundary catchment erosion and pollution problems (Chapman et al. 2016). Although the papers presented in this special issue of Geography, Environment, Sustainability seems to be very diverse in both processes and territory they analyze, we hope that they will provide excellent starting point for future joint research in this field.

CONCLUSION

This review and thorough analyses of the literature emphasized future need in comprehensive research of sediments and pollutants transport based on catchment-river approach which consider particles which are eroded and transported by flowing water or other transporting media. Existing examples demonstrate increased sediment-related hazards possibility over different regions which require. The latter consider both modelling and monitoring techniques development, in particular related to series of physical and chemical approaches for the characterization of river sediment and contaminants in river flow. This should underlie complementary options for sediment management which include catchment-scale conceptual models and budgets for sediment, basin land management (e.g., reforestation, better agriculture practices, etc.), sediment management through dams, and sediment augmentation below dams. There is a growing need to work internationally in developing a commonly accepted databanks and international protocol for measuring erosion, sediment transport and sedimentation in river systems.

REFERENCES

Alekseevskiy N.I., Berkovich K.M., Chalov R.S. (2008). Erosion, sediment transportation and accumulation in rivers. International Journal of Sediment Research, 23(2), 93-105. https://doi.org/10.1016/S1001-6279(08)60009-8

Bieroza M., Acharya S., Benisch J., et al. (2023). Advances in catchment science, hydrochemistry, and aquatic ecology enabled by high-frequency water quality measurements. Environmental Science & Technology, 57(12), 4701-4719. https://doi.org/10.1021/acs.est.2c07798

Bonavigo L., Zucchetti M., Mankolli H. (2009.) Water radioactive pollution and related environmental aspects. Journal of International Environmental Application & Science 4(3), 357-363

Burt T.P., Allison R.J. (2010). Sediment cascades in the environment: an integrated approach. In T.P. Burt and R.J. Allison eds., Sediment Cascades: An Integrated Approach. John Wiley & Sons, Ltd., Online ISBN:9780470682876, 1–15. https://doi.org/10.1002/9780470682876.ch1

Chalov S., Golosov V., Tsyplenkov A., Theuring P., Zakerinejad R., Märker M., Samokhin M. (2017). A toolbox for sediment budget research in small catchments. Geography, Environment, Sustainability 10(4), 43–68. https://doi.org/10.24057/2071-9388-2017-10-4-43-68

Chapman D.V., Bradley C., Gettel G.M., Hatvani I.G., Hein T., Kovács J., Liska I., Oliver D.M., Tanos P., Trásy B., Várbíró G., (2016) Developments in water quality monitoring and management in large river catchments using the Danube River as an example. Environment Science & Policy, 64, 141–154. https://doi.org/10.1016/j.envsci.2016.06.015

Collins A.L., Walling D.E., Golosov V., Porto, P., Gellis, A.C., da Silva, Y.J., Chalov, S. (2024). The International Commission on Continental Erosion (ICCE): a brief overview of its scientific focus and example outputs. Proceedings of IAHS 385, 489–497. https://doi.org/10.5194/piahs-385-489-2024

Gartsman et al. (2024). A method of multi-site calibration of distributed hydrological models for large river basins. Geography, Environment, Sustainability 17(4). https://doi.org/10.24057/2071-9388-2024-3564

Gautier E, Dépret T, Cavero J, Costard F., Virmoux C., Fedorov A., Konstantinov P., Jammet M., Brunstein D. (2021). Fifty-year dynamics of the Lena River islands (Russia): Spatio-temporal pattern of large periglacial anabranching river and influence of climate change. Science of the Total Environment 783, 147020. https://doi.org/10.1016/j.scitotenv.2021.147020

Korjenić A. (2024). Physical-geographical characteristics of the Una River basin – contribution to the analysis of the state and possibilities of radioactive waste disposal in the border zone. Geography, Environment, Sustainability 17(4). https://doi.org/10.24057/2071-9388-2024-3306

Kovačević-Majkić J., Štrbac D., Ćalić J., Milošević M.V., Milivojević M., Polovina S. (2024). Fluvial processes and landforms as indicators in torrential flood hazard assessment. Geography, Environment, Sustainability 17(4). https://doi.org/10.24057/2071-9388-2024-3378

Krylenko I., Pavlyukevich (Kornilova) E., Zavadskii A., Golovlyov P., Fingert E., Borisova N., Belikov V (2024). Modelling of potential impact of climate change on water regime and channel processes in the Lena River near city Yakutsk: possibilities and limitations. Geography, Environment, Sustainability 17(4). https://doi.org/10.24057/2071-9388-2024-3723

Lychagin M., Porsheva S., Sokolov D., Erina O., Krastyn E., Efimov V., Dubrovskaya T., Kasimov N. (2024). Levels, D,S-patterns and source identification of metals and metalloids in river waters of the gas-producing region in the north of Western Siberia (Pur River basin). Geography, Environment, Sustainability 17(4). https://doi.org/10.24057/2071-9388-2024-3741

Matić B.B. (2024). Integrated transboundary river basin management reinforcement by natural water retention measures. Geography, Environment, Sustainability 17(4). https://doi.org/10.24057/2071-9388-2024-3354

Milanović Pešić A., Jakovljević D., Ćulafić G., Milivojević M. (2024). Water regime variability of selected rivers on the Balkan Peninsula: a comparative study of Central Serbia and northern region of Montenegro. Geography, Environment, Sustainability 17(4). https://doi.org/10.24057/2071-9388-2024-3404

Minchev I, Trendafilov B, Blinkov I, Trendafilov A, Ivanovski D (2024). Measuring and modeling erosion in two successive reservoir catchments on the Drim River in North Macedonia. Geography, Environment, Sustainability 17(4). https://doi.org/10.24057/2071-9388-2024-0581

Nyiri E., Török G.T. (2024). Impact assessment of river regulations using 1D morphodynamic modeling on the upper Hungarian Danube. Geography, Environment, Sustainability 17(4). https://doi.org/10.24057/2071-9388-2024-3390

Nittrouer J.A., Shaw J., Lamb M.P., Mohrig D. (2012). Spatial and temporal trends for water-flow velocity and bed-material sediment transport in the lower Mississippi River. Geological Society of America Bulletin 124(3-4), 400–414. https://doi.org/10.1130/B30497.1

Pandey S., Kumar P., Zlatic M., Nautiyal R., Panwar V.P. (2021). Recent advances in assessment of soil erosion vulnerability in a watershed. International Soil and Water Conservation Research 9(3), 305-318, https://doi.org/10.1016/j.iswcr.2021.03.001

Pavlyukevich E.D., Krylenko I.N., Krylenko I.V. (2024). Modern evolution and hydrological regime of the Bashkara glacier lakes system (central Caucasus, Russia) after the outburst on September 1, 2017. Geography, Environment, Sustainability 17(4). https://doi.org/10.24057/2071-9388-2024-3717

Rets E.P., Popovnin VV., Toropov P.A., et al (2019). Djankuat Glacier Station in the North Caucasus, Russia: A Database of complex glaciological, hydrological, meteorological observations and stable isotopes sampling results during 2007-2017. Earth System Science Data 11(3), 1463–1481. https://doi.org/10.5194/essd-11-1463-2019

Rheinheimer D.E., Yarnell S.M. (2017). Tools for sediment management in rivers. In A.C. Horne, J.A. Webb, M.J. Stewardson, B. Richter, M. Acreman eds., Water for the Environment: from Policy and Science to Implementation and Management, Academic Press, ISBN 9780128039076, 237-263, https://doi.org/10.1016/B978-0-12-803907-6.00012-7

Savenko A.V., Savenko V.S. (2024). Trace element composition of the dissolved matter runoff of the Russian Arctic Rivers. Water 2024, 16(4), 565; https://doi.org/10.3390/w16040565

Szumińska D., Kozioł K., Chalov S.R., Efimov V.A., Frankowski M., Lehmann-Konera S., Polkowska Ż. (2023). Reemission of inorganic pollution from permafrost? A freshwater hydrochemistry study in the lower Kolyma basin (North-East Siberia). Land Degradation & Development 34(17), 5591-5605. https://doi.org/10.1002/ldr.4866

Trendafilov B, Minchev I, Trendafilov A, Blinkov I (2024). Comparison of EPM with RUSLE for soil erosion modeling in the Strumica River basin. Geography, Environment, Sustainability 17(4). https://doi.org/10.24057/2071-9388-2024-0580

Tsyplenkov A., Vanmaercke M., Golosov V., Chalov S. (2020). Suspended sediment budget and intra-event sediment dynamics of a small glaciated mountainous catchment in the Northern Caucasus. Journal of Soils and Sediments 20, 3266–3281. https://doi.org/10.1007/s11368-020-02633-z

Vörösmarty C.J., Meybeck M., Fekete B., Sharma K., Green P., Syvitski J.P.M. (2003). Anthropogenic sediment retention: major global impact from registered river impoundments. Global and Planetary Change 39(1-2), 169–190. https://doi.org/10.1016/S0921-8181(03)00023-7

Check for updates

CC BY

RESEARCH PAPER

ASSESSMENT OF NATURAL RESOURCE POTENTIAL AND ANTHROPOGENIC LOAD IN THE MACROREGION OF NORTHERN EURASIA BASED ON A BASIN APPROACH

Oleg P. Yermolaev[1], Nurgul S. Sihanova[2*], Yerlan A. Shynbergenov[2*], Roman O. Yantsitov[1]

[1] Kazan (Volga Region) Federal University, Institute of Ecology and Environmental Management, Kremlevskaya, 18, Kazan, 420000, Russia

[2] Korkyt Ata Kyzylorda University, Engineering and Technology Institute, Ayteke bi, 29A, Kyzylorda, 120014, Kazakhstan

***Corresponding author:** sihanova.nurgul@mail.ru, shynbergenov.erlan@mail.ru

Received: April 17th 2024 / Accepted: July 25th 2024 / Published: October 1st 2024

https://doi.org/10.24057/2071-9388-2024-3359

ABSTRACT. The environmental component of Sustainable Development for large regions of the Earth can be assessed through the evaluation of the natural resource potential of the territory. The methodological challenge of such assessments is always determined by the type of operational-territorial unit within which the geodatabase is formed. This article details the possibilities of using the basin approach as such units. This approach is one of the most important in humid climate regions where a river network has been developed. Using the example of the Ob' river basin in Northern Eurasia, the article illustrates the application of the basin approach to assess the environmental determinants of Sustainable Development. The studies were conducted in three stages: formation of an GIS database of basin geosystems of the Ob' river basin; creation of a geospatial database on the natural resource potential in the small river basins; selection of criteria and assessment of anthropogenic load on the basin geosystems of the Ob'. A total of 30,738 small river basins were delineated automatically based on GMTED DEM, with a mean area of 66 km^2. GIS integrated geoinformation represents the natural and anthropogenic characteristics of river basins. The assessment of the environmental state of the territory should considerthe types and strengths of anthropogenic loads. For this purpose, the integral indicators used, which directly or indirectly reflect anthropogenic impact: population density, road network density, and the percentage of arable land in the total area. The final indicator of anthropogenic load was calculated as a linear combination of specific variables and ranked into six categories. Thematic and complex maps were created, allowing us to identify the natural background in which the geosystems of small river basins are formed and function, as well as the types and strength of anthropogenic loads on the territory.

KEYWORDS: the Ob' river basin, Western Siberia, small river basins, anthropogenic load, GIS geosystems, geodatabase, geoecology

CITATION: Yermolaev O. P., Sihanova N. S., Shynbergenov Y. A., Yantsitov R. O. (2024). Assessment Of Natural Resource Potential And Anthropogenic Load In The Macroregion Of Northern Eurasia Based On A Basin Approach. Sustainability, 4(17), 10-25

https://doi.org/10.24057/2071-9388-2024-3359

ACKNOWLEDGEMENTS: This research has been funded by the Committee of Science of the Ministry of Science and Higher Education of the Republic of Kazakhstan (Grant No. BR21882415).

Conflict of interests: The authors reported no potential conflict of interest.

INTRODUCTION

The scale of human economic activity has led the biosphere in many regions of the planet to the brink of pre-crisis ecological states. The resistance and compensatory reactions of the abiotic environment are often insufficient to counteract degradation and mitigate negative external impacts on the Earth's biosphere (Ivanov et al. 2020). Currently, in many regions of the planet, especially where economic growth is driven by the involvement of significant natural resource flows with deep processing, the ecological capacity of the environment is exceeded[1]. The cumulative impact of anthropogenic activities poses a significant threat to the regenerative capabilities of regional biosphere sections.Anthropogenic interactions and processes can trigger mechanisms within natural-technical geosystems, potentially leading to cumulative effects that amplify anthropogenic changes in the natural environment. Therefore, prioritizing environmentally safe sustainable development is paramount in the global community's Sustainable Development concept. Within this paradigm, the ecological aspect plays a crucial role in shaping strategies for global economic development. However, effective implementation requires tailored programs adapted to specific regions. The selection of appropriate territorial units for data aggregation and spatial analysis of

[1] Florczyka A.J., Corbanea Ch., Ehrlich D. (2019). GHSL - GlobalHumanSettlementLayer [online]. Available at: https://ghsl.jrc.ec.europa.eu/index.php [Accessed 31 Aug. 2024].

ecological aspects is fundamental. In our view, river basins can serve as the best unit in humid climate conditions of extensive land areas, as they are natural, geosystem units (Yermolaev et al. 2017a, b, 2023a). The river basin, being a unified natural-territorial complex with natural boundaries in the form of orographic watersheds, within which the accumulation, transformation, and movement of solid and liquid substances occur, is a spatial unit that allows for the most objective characterization of the territory (Yermolaev, 2002; Korytnyj, 2001; Lisetskii et al., 2014; Osipov & Dmitriev, 2017). The advancement of Geographic Information Systems (GIS), enhanced availability of remote sensing data, and improved computational capabilities have elevated geographic and ecological studies to new heights.The establishment of a detailed vector database covering river basins and their inter-basin areas across a large region of Russia, coupled with comprehensive geospatial data encompassing natural resource potential, landscape diversity, and land use patterns, enables thorough spatial analysis (Gordeev et al. 1996; Ivanov et al. 2022). This infrastructure not only facilitates ecological studies but also supports environmental management, hydrological assessments, and spatial planning (Yermolaev et al., 2023b).

The aim of this study is to assess the natural resource potential and anthropogenic impact in Russia's macroregion, located in the Asian part of the country - the Ob' river basin. This assessment is based on a basin approach. The study area is characterized by a lack of data on the natural resource potential and economic loads in small rivers geosystems, as well as by fact that the Ob' river, running in a north-south direction, crosses a wide range of landscape zones, including tundra and forest-tundra in the north, steppes and semi-deserts in the south, lowland wetlands, mountainous areas, and high-altitude Alpine meadows and snowfields, all experiencing diverse anthropogenic pressures.

Brief Characterization of the Territory

The Ob' river basin is located in the northern part of the Eurasian continent and is considered the main waterway of Western Siberia. The river Ob' originates in the city of Biysk, in the Altai, at the confluence of the Katun and Biya rivers. The river flows from south to north through vast lowland areas of the West Siberian Plain, resulting in a slow flow. Approximately 85% of the Ob' basin is situated on this plain, often featuring forests and swamps. The river flows through the territories of the Altai Krai, Novosibirsk, Tomsk regions, the Khanty-Mansi Autonomous Okrug (Yugra), and the Yamalo-Nenets Autonomous Okrug. The river flows into the Arctic Ocean, specifically into the Kara Sea. There, the river forms a large estuary with numerous branches and islands, creating the Gulf of Ob'. The Ob' river is listed among the largest rivers in the world, ranking 7th in length in Eurasia and 16th globally. The total area of the Ob' basin is 2,026,457.05 km^2. It is 3680 km long. The Ob' river, along with the Irtysh river, ranks 1st among the rivers of Russia in terms of length and basin area, and 3rd in the Russian Federation (after the Lena and Yenisei rivers) in terms of annual streamflow.

RESEARCH METHODOLOGY

Creation of a Cartographic Model of Small River Basins

The development of a problem-oriented GIS combined with mathematical-statistical methods allows the assessment of the environmental status of small basins and the determination of the causes and intensity of their changes over a wide territory. The foundation of such a geoinformation system is the creation of a GIS layer (GIS database) of river basins. In this case, the river basin serves as the basic operational-territorial unit that allows the formation of a geospatial database (Yermolaev, 2017a, c).

The availability of a GIS database for delineating basin geosystems facilitates a wide range of tasks. These include assessing the natural conditions under which various processes and phenomena develop, the formation of water and sediment runoff in rivers, various types of thematic and complex zoning (e.g., climatic, geomorphological, agro-climatic, anthropogenic, landscape), and evaluating anthropogenic impacts on geosystems. Automated delineation of basin boundaries was conducted using global Digital Elevation Models (DEMs) available in open access. The Ob' river basin's topography can be represented by several well-known and publicly available global models, including:: GTOPO30 with a spatial resolution of 1000 m (30 arc seconds); GEBCO2023 with a spatial resolution of 500 m (15 arc seconds); GMTED2010 with a spatial resolution of 250 m, 500 m, 1000 m (7.5 arc seconds, 15 arc seconds, and 30 arc seconds respectively; spatial coverage 84°N - 56°S (Danielson & Gesch, 2011); SRTM with a spatial resolution of 30 m and 90 m (1 arc second and 3 arc seconds respectively, spatial coverage 60°N - 56°S (Rodriguez et al., 2005), etc. All these models utilize the World Geodetic System 1984 (WGS84) coordinate system and are provided by the United States Geological Survey (USGS). For the creation of the river basin boundary layer, the GMTED2010 model (Global Multi-resolution Terrain Elevation Data 2010) (Danielson & Gesch, 2011, Yermolaev, 2017c) with a spatial resolution of 250 m (7.5 arc seconds) was selected, along with the hydrographic network model from 1:1,000,000 scale maps. The Albers Equal Area projection is chosen coordinate system. These parameters correspond to the accepted level of spatial resolution used in the study, adhering to the cartographic principle of scale consistency. The methodology for identifying basins is detailed in our previous work (Yermolaev et al., 2003a).A total of 30,738 small river basins were delineated within the Ob' river basin. In the next stage, a geodatabase and GIS were created for the natural resource potential and anthropogenic load indicators in the basins. Open data sources were used, with characteristics detailed in the thematic sections below. The set of indicators was determined based on data availability and their relevance for characterizing natural potential, assessing environmental favourability for humans, and understanding the conditions for geo- and ecosystem formation.

RESULTS AND DISCUSSION

Geospatial Database of Small River Basins

A geospatial database of small river basins was developed based on several indicators, including morphometric indicators of relief (Table 1) and hydroclimatic factors. The types of land cover and anthropogenic impacts were also taken into account. All these indicators were added as attributes to small river basins (Fig. 1.)

Basin Area

The area of a basin is an important characteristic that reflects the complexity of the hydrographic network, the intensity of fluvial processes, and the volume of water flow (Fig. 3a). The average basin area is 65.9 km^2. Only ten basins have the smallest area (0.25 km^2). The largest basin, located in the southeastern part of the Ob', has an area of 10,449.7 km^2. According to the calculations, about 62% of the basins have areas up to 50 km^2 (16%) and are evenly distributed across the entire small basin.

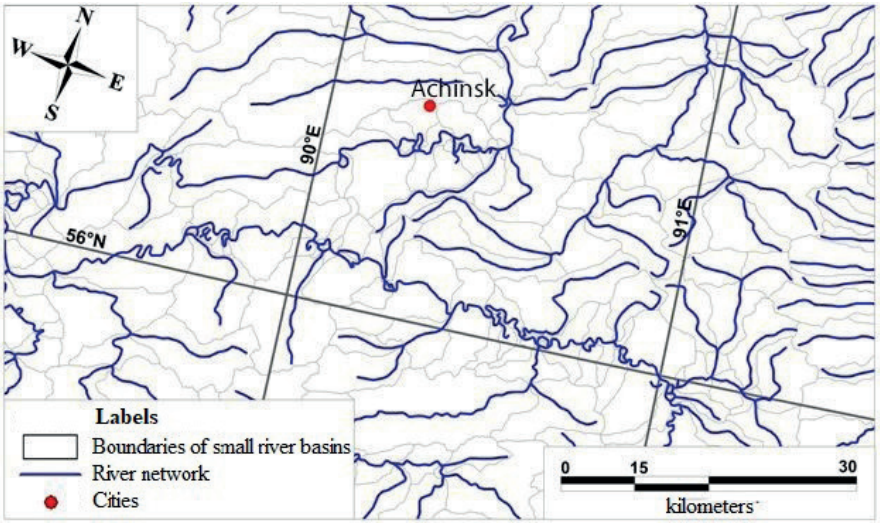

Fig. 1. Fragment of a GIS database of small river basins of the Ob' River

Table 1. Terrain characteristics determined for each basin

Data		Field name
Small basin ID	Dimensionless	Id
Area	km^2	Area
Height	Mean, m	Hmean
	Maximum, m	Hmax
	Minimum, m	Hmin
	2% - percentile, m	CMRobi_Q2
	98% - percentile, m	CMRobi_Q98
	Verticaldissection, m	Rel_Elev
Surface slope steepness	Mean steepness, deg.	Slope
Slope length	Mean, m	_Fl_Path_lenmean

Slightly more than 19% of the basins have areas of 50-100 km^2 (20.8%). Larger basins (100-500 km^2) are densely grouped throughout the Ob' basin (5,377 basins), covering 47.9% of the study area. Basins with a maximum area (>1000 km^2) are mainly located in the southern and southeastern parts of the Ob' (in the steppe regions) and number 73, covering 9.1% of the basin area.

Morphometric Analysis

Morphometric analysis is widely used in dynamic geomorphology for assessing hazardous exogenous processes and ecology. In this study, we calculated the following morphometric characteristics of the relief: average height and slope steepness (Fig. 3c, d), aspect, flow line length, and depth of relief dissection. The average values of these indicators were calculated in the Quantum GIS (v.3.10) application using the "Zonal statistics" tool. In SAGA GIS, the 2nd and 98th percentiles of heights were calculated. Thematic maps based on the morphometric characteristics of the relief were created using the MapInfo Pro V. 15.0 GIS application. The Statgraphics package was used for statistical analysis and distribution of the indicators. Below are examples of evaluating some relief parameters.

Average Height

When distributing the basins according to their average height (Table 2), a standard classification of terrain by absolute height was used. A more detailed gradation was applied to the thematic map in order to ensure readability (Fig. 3b). Lowlands account for 81.2% of basin geosystems with an average height of less than 200 m). This category occupies 78.4% of the area of the Ob' basin. Highlands comprise 11.5% of all basins and cover 14.1% of the Ob' basin area. They are mainly located in the south (the Altai and Kuznetsk-Salair mountain regions) and north parts (along the Ural Mountains). Low, medium, and high mountains account for 3%, 2.6%, and 1.6%, respectively, of basins located in northern Altai, covering 7.4% of the total small basin area. The basin with the maximum height (3,151 m) is located in this region.

Various schemes can be used to classify the distribution of average slope steepness within basins. For this study, we classified the small rivers of the Ob' basin according to slope steepness based on Braude's classification (Braude, 1965). The thematic map (Fig. 2) was created with expert input to ensure appropriate gradation.

For the studied area, basins with a slope steepness of up to 10° are predominant, comprising 95.5% of the small river basins and covering 95.3% of the Ob' basin area. The steepest slopes (10° and above) account for 4.5% of the Ob' basins. These are found in the basins of small rivers located in the upper reaches of the Ob', at the sources of the Tom' River, and along the Biya, the Katun', and the Charysh rivers. Basins with very steep slopes (20-30°) occur sporadically in the upper reaches of the Biya and Katun' rivers (210 basins). Extremely steep slopes are found in only four basins, located in the extreme southern part of the Ob' basin, in the Altai Mountains (Table 3).

Table 2. Classification of small basin by height

Meanheight, m	Landform	Number of small basin, pcs.	Share to percentage	Area, km²	Share to percentage
0-200	Lowlands	24,972	81.2	1,582,519.02	78.4
200-500	Hills	3,548	11.5	285,566.9	14.1
500-1000	Lowmountains	924	3	63,542.68	3.15
1000-2000	Middle mountains	809	2.6	56,734.04	2.8
>2 000	High mountains	485	1.6	29,643.48	1.47
Total		30,738	100	2,026,457.05	100

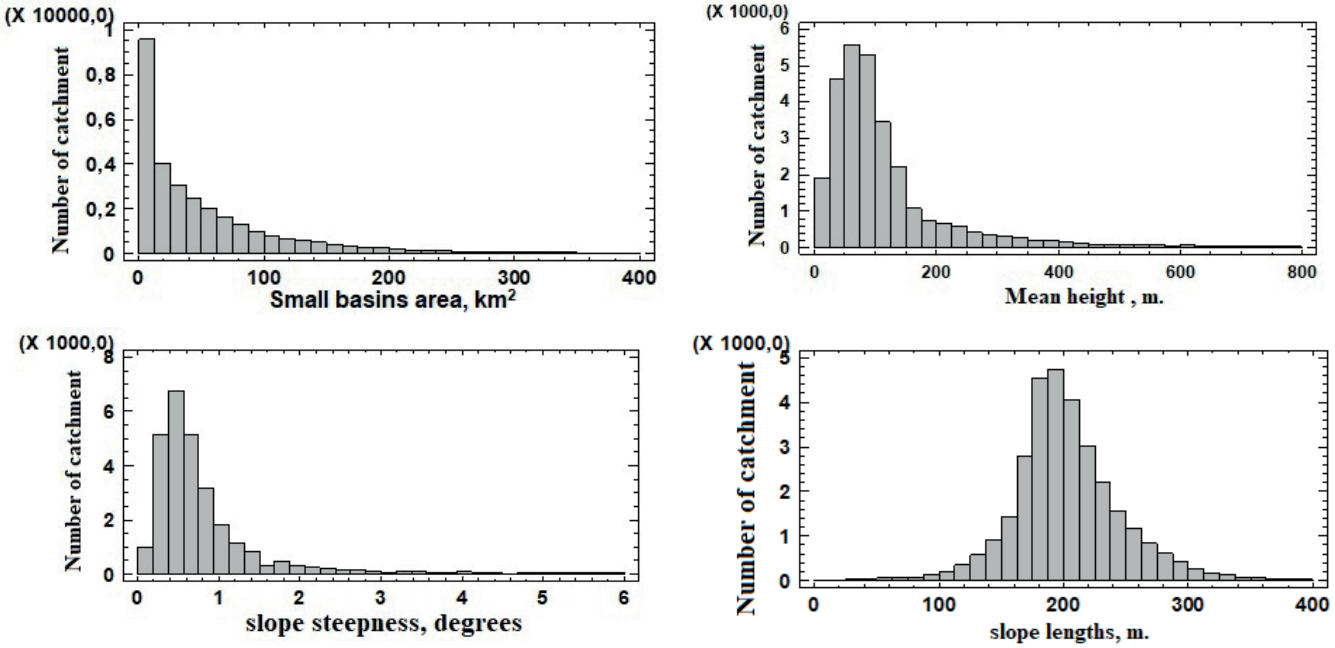

Fig. 2. Distribution of small basin by morphometric characteristics

Table 3. Basic statistics of morphometric characteristics of basin

Indicator	Min.	Max.	Mean	Median	Mode	Std. dev.
Area, km²	0.25	10 449.7	65.9	31.7	0.31	182.2
Height, m	1	3 150.6	198.7	89.7	6	384.3
Slope steepness, degrees	0.0	33.2	1.7	0.6	0.4	3.4
Slope length, m	0	1 096.6	203.8	198.6	0	47.7

Flow Line Length

Flow line length refers to the distance over which any material can move downslope under the influence of gravity. This indicator was classified in the MapInfo Pro application using the "equalcount" function.

For the basin geosystems, the average flow line length is 204 m. The most common basins have flow line lengths in the ranges of 0-180 m, 180-200 m, and 220-500 m (27.2%, 24.6%, and 28.8% of all basins, respectively). These categories collectively cover 80.6% of the territory. Basins with flow line lengths of 0-180 and 180–200 m are densely distributed in the middle course of the Ob', as well as along both banks of the Irtysh and Tobol rivers. The upper, middle, and lower courses of the Ob' scatter small river basins with flow line lengths of 200–220 m in groups. Basins with the longest flow line lengths (220-500 and >500 m) are located along the Ural Mountains to the west, in the Kuznetsk-Salair mountain region to the south and southeast, and partially in the northern part of the basin (along the 60°N parallel).

Climate

Climatic characteristics of river basins were obtained from the All-Russian Research Institute of Hydrometeorological Information – World Data Center (RIHMI-WDC), which is publicly accessible[2]. Data from 73 weather stations is used for the period 1966-2021. In this section, the following climate parameters are considered

[2] Vserossijskijnauchno-issledovatel'skijinstitutgirometeorologicheskojinformacii - MirovojCentrDannyh (All-Russian Research Institute of Gyrometeorological Information - World Data Center) (VNIIGMI-MCD). (2023). Federal'nyjcentr po gidrometeorologiiimonitoringuokruzhajushhejsredy. Temperaturavozduhaikolichestvoosadkov (ezhednevnyedannye) [online]. Available at: http://meteo.ru/data/162-temperature-precipitation#opisanie-massivadannyh. (in Russian) [Accessed 31 Aug. 2024].

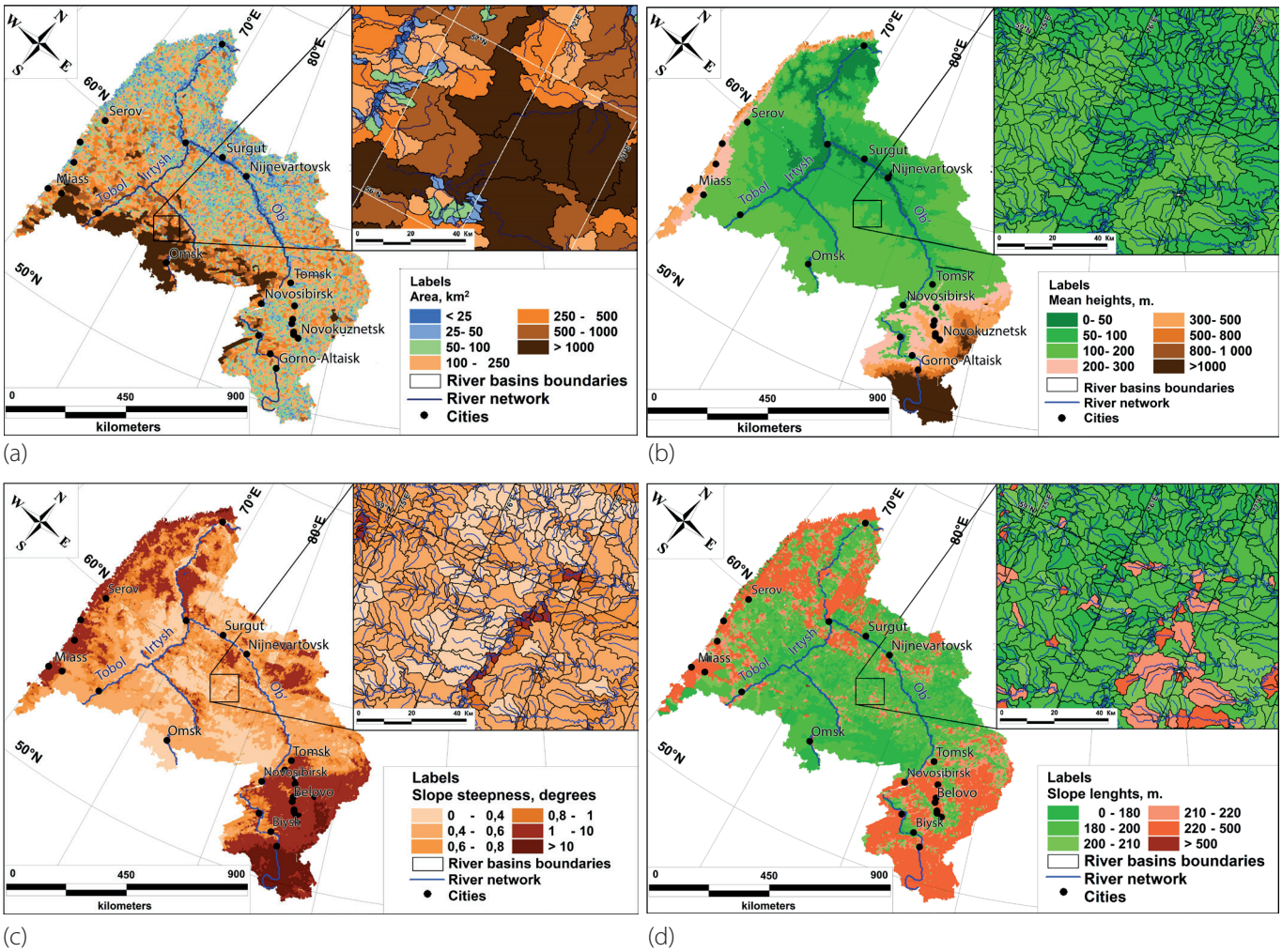

Fig. 3. Maps of morphometric characteristics of small river basins

and analyzed: average air temperature, average January temperature, average July temperature, climate "severity" (expressed as the recurrence of severe frosts below -30° in %), sum of active temperatures, average annual precipitation, average precipitation during the cold period, and average precipitation during the warm period.

Corresponding thematic maps for these parameters were created in MapInfo Pro (Fig. 4), their distribution (Table 4), and statistical analysis was performed (Fig. 5).

The National Atlas of Russia[3] was used as a reference for creating thematic maps, especially for scales and gradations. In the absence of reference maps, values were ranked by expert judgment. Examples of evaluating several climate parameters are provided below.

Mean Annual Air Temperature

The average annual air temperature ranges from -7.7°C in the Ob' River delta (Yamal-Nenets Autonomous Okrug) to 4.1°C in the southern (Altai Krai) and southwestern (Chelyabinsk region) parts of the Ob' basin. This indicator varies in a latitudinal direction. For the lower course of the Ob', the temperature range is from -7.7°C to -2°C (from the Ob' delta to almost the 62nd parallel). Basins with the minimum average annual air temperature values (25 basins) are located in the Ob' River delta near Salekhard. For the middle (from 56-60°N) and upper (from 51-56°N) courses of the Ob', temperatures range from -2-0°C and 0-4.1°C, respectively. The upper course includes basins with the maximum average annual air temperature values (5 basins). The southern and southeastern extremities of the basin (near the mountain structures of the Altai and Sayan mountains) have a temperature range of -2-0°C. The average value of the studied indicator for the entire Ob' river basin is -0.1°C (see Fig. 4).

Mean temperature in January

This indicator moves in a latitudinal direction. Basins with minimum temperatures (from -27.9°C to -22°C) are located in the lower course of the Ob' (the northern and northeastern extremities of the basin) and the southernmost extremity of the Ob' basin. There are minimal values of the analyzed indicator in only four basins (in the upper course of the Ob', near mountain structures). Here, basins with maximum January average temperatures (in the form of areas) are also located, totaling 4. Most small river basins have an average temperature in the range of -22 to -14°C (81.7% of basins), covering 85.9% of the Ob' watershed area. For the entire Ob' river basin, the average value of the studied indicator is -19.4°C.

Mean temperature in July

For this indicator, a pattern similar to the average January temperature is observed. The values range from 7.1 to 20.2°C, with 87.2% of the basins falling within the 16-20.2°C range (covering 90.3% of the Ob' basin area). These basins are located from 64°N latitude up to the mountain structures in the southern part of the basin. Due to the right-skewed distribution of the histogram, the average July temperature for the Ob' river basin is 17.2°C, which is relatively high for this region.

[3] National Atlas of Russia, tom 2, (2007). [online]. Available at: https://nacional'nyjatlas.rf/cd2/territory.html (in Russian) [Accessed 31 Aug. 2024].

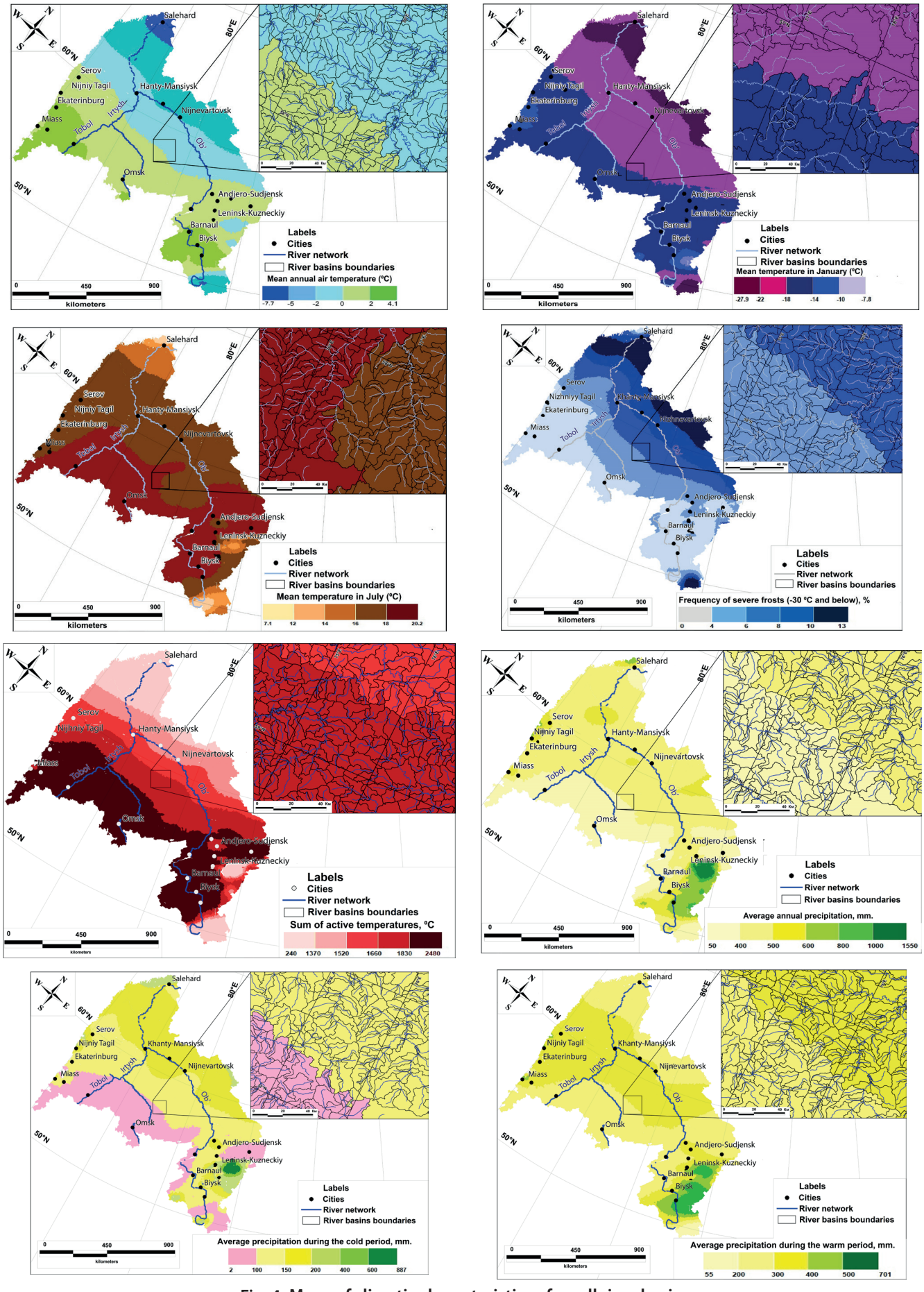

Fig. 4. Maps of climatic characteristics of small river basins

Climate Severity

The intensification of winter frosts, the increased duration of the cold period, and similar factors all contribute to climate severity. It largely determines the suitability of the environment for human habitation. In this study, this indicator is expressed as the number of days (%) with temperatures ≤ -30°C during the cold period (with an average monthly temperature < 0°C). The analyzed indicator varies from 0-14%. In this case, a different pattern is observed compared to the previously mentioned indicators: in the Ob' delta near the Gulf of Ob', the climate is "milder" (0-4%). Then, the climate severity increases up to 64°N latitude, after which it becomes milder again in a latitudinal direction up to the Altai Mountains, where, due to the altitudinal zonation, the climate becomes more severe. Here are the basins with the most severe climate (31 basins). Basins with no days of temperatures ≤ -30°C are located in the steppe regions of the southern part of the Ob' basin (207 basins). The average climate severity for the Ob' basin is 6.2%. 52.7% of the basins have a climate severity indicator in the range of 0-6% (covering 69.1% of the Ob' river basin area).

Precipitation

For the Ob' river basin, the mean annual precipitation is 463 mm. In most basin ecosystems (69% of basins), the average annual precipitation ranges from 400 to 500 mm. The minimum mean annual precipitation (59 mm) is recorded only in one basin, located at the beginning of the Altai Mountains. The highest value (1545 mm) is also recorded in only one basin, located in the southern part of the Ob' basin, in the interfluve of the Tom' and Biya rivers. This is where a cluster of basins with the maximum mean annual precipitation (800-1545 mm) is located. Additionally, the extreme northern end of the Ob' basin hosts a small cluster of basins with relatively high mean annual precipitation (600–800 mm). 69% of small river basins have mean annual precipitation in the range of 400-500 mm and cover 57.9% of the studied area.

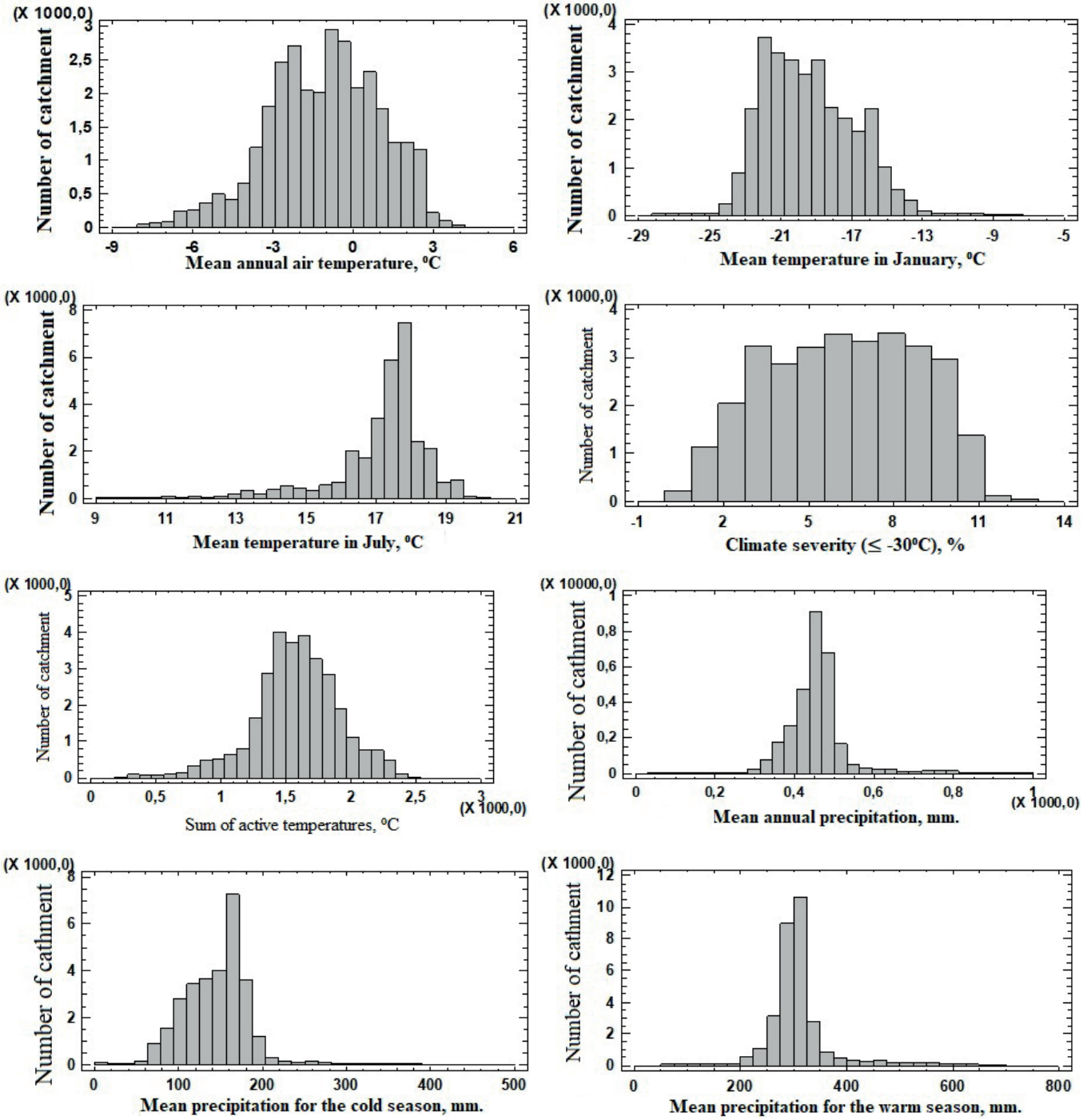

Fig. 5. Distribution of basins by climatic characteristics

Land use is expressed through the predominant types of land cover

The main source of data for creating a geospatial database on land cover types is the raster layer TerraNorte RLC, built based on satellite observations from the MODIS spectroradiometer on the Terra satellite (Bartalev et al., 2012) (Table 5). According to Table 5, the predominant land cover type in the Ob' river basin is deciduous forests (16.5% of the total area of the Ob' basin). This is followed by swamps (15%), meadows (14.2%), and light coniferous evergreen forests (14.1%). The less common are eternal snow and ice (0.04%), deciduous shrubs (0.1%), shrub tundra (0.3%), shrub tundra (0.4%), urbanized areas (0.2%), and deciduous coniferous trees (0.4%).

Table 4. Basic statistics of climatic characteristics

Indicators	Min.	Max.	Mean	Median	Mode	Std. dev.
Mean annual air temperature, °C	-7.7	4.1	-0.1	-1.0	-1.0	2.1
Mean temperature in January, °C	-27.9	-7.8	-19.4	-19.7	-21.3	2.6
Mean temperature in July, °C	7.1	20.2	17.2	17.5	17.8	20.2
Climateseverity, %	0	13	6.2	6.0	8.0	2.8
Sum of active temperatures, °C	249.7	2476.0	1583.9	1590.4	1445.3	330.2
Meanannualprecipitation, mm	59	1545	463	456	472	114
Mean precipitation for the cold season, mm	2	886	153	151	169	71
Mean precipitation for the warm season, mm	55	701	310	303	313	63

Table 5. Land cover types in the Ob' river basin

Code	Typesoflandcover	Area, km^2	Share to percentage
1	Dark coniferousevergreens	120,163.8	5.9
2	Light coniferousevergreens	284,842.1	14.1
3	Deciduous	334,311.3	16.5
4	Coniferousdeciduous (larch) forests	56,275.6	2.8
6	Swamps	304,957.7	15
8	Meadows	288,682.5	14.2
9	Deciduousshrubs	1,771.9	0.1
10	Mixed forests with a predominance of conifers	117,621.4	5.8
11	Mixedforests	89,133.6	4.4
12	Mixed forests with a predominance of deciduous trees	108,427.9	5.4
13	Open soils and rock outcrops	16,943.6	0.8
14	Steppes	24,729.5	1.2
15	Coastalvegetation	65,755.9	3.2
16	Shrubtundra	6,810.2	0.3
17	grassytundra	20,935.4	1
18	Shrubtundra	8,426.8	0.4
20	Riversandreservoirs	29,038.9	1.4
23	Deciduousconiferoustrees (larch)	8,994.3	0.4
24	Freshburning	15,757.7	0.8
31	Urbanizedareas	4,384.8	0.2
32	Eternalsnowandice	845	0 (0.04)
33	Arableland	117,647.2	5.8
Total		2,026,4571	100

For simplifying the construction of a thematic map of land cover types in the Ob' river basin, they were grouped as follows: coniferous forests (dark coniferous evergreens, light coniferous evergreens, coniferous deciduous (larch) forests); deciduous forests; shrubs (deciduous shrubs); aquatic and marsh complexes (swamps, rivers and reservoirs); other vegetation (meadows, coastal vegetation, deciduous coniferous trees, fresh burnings); mixed forests (mixed forests with a predominance of conifers, mixed forests, mixed forests with a predominance of deciduous trees); lands without vegetation cover (open soils and rock outcrops (projected coverage of all plant species less than 20%); steppes; tundra (shrub tundra, grassy tundra, shrub tundra); settlements (urbanized areas); eternal snow and ice; arable land (Fig. 6).

In the upper reaches of the Ob' River, coniferous and mixed forests are fragmented, mainly along the right bank of the basin, closer to the mountainous areas. In the middle and lower reaches of the river, a uniform distribution is observed, but with a prevalence of coniferous forests (see Fig. 6). The area of urbanized areas is 4,384.8 km^2 (0.2%).

Assessment Of Anthropogenic Load On Basin Systems

Human activities have always impacted the surrounding natural environment, but until the 20th century, this influence was not so noticeable due to the Earth's biosphere's ability to regenerate. In the second half of the 20th century, the Earth's population growth and intensified economic activities have led to substantial anthropogenic pressure on the Earth's biosphere, resulting in significant and often detrimental alterations to natural environments. Anthropogenic load is defined as a measure (quantitative and qualitative) of the impact of human economic activity on the surrounding natural environment, leading to its direct or indirect alteration. The impact affects both individual natural components and elements (such as landscapes, biota, river basins, etc.) and natural complexes as a whole. At the same time, their significant transformation occurs (Didenko et al., 2018). The most important elements of the natural environment, including atmospheric air, soil environment, vegetation cover, surface, and groundwater, biotic complexes, are objects of anthropogenic impact exerted by human activity (Miller, 1993). In this study, anthropogenic load was considered based on the definition proposed by Rejmers (Rejmers, 1990). The environmental aspects of sustainable regional development were evaluated through a quantitative assessment of anthropogenic load on basin systems using GIS technologies (Ivanov, 2019; Ivanov et al., 2020; Yermolaev et al., 2023b). For this purpose, a selected range of integral indicators was used, reflecting anthropogenic load directly or indirectly: 1. population density in the basin; 2. road network density (taking into account road type); 3. agricultural development of basins (without ploughing). These indicators comprehensively reflect the degree of economic development in a given area, as they provide a constant impact that is not significantly subject to spatial or temporal fluctuations. Another criterion for selecting these indicators was their availability and potential for data updates over time. The methodology used to calculate the integral indicator of anthropogenic load requires the transformation of selected indicators into a single numerical scale. In scientific literature, logarithmic transformations of the form *log(x+1)* are widely used for a comprehensive assessment of anthropogenic load. This transformation is used for each individual indicator that affects any natural environmental object. Logarithmic transformation is applied to avoid excessive dominance of extreme values on the resulting cumulative map of anthropogenic impact and to adjust frequency distributions, which are usually distorted (Andersen et al., 2013). To ensure the comparability of different indicators, it is necessary to

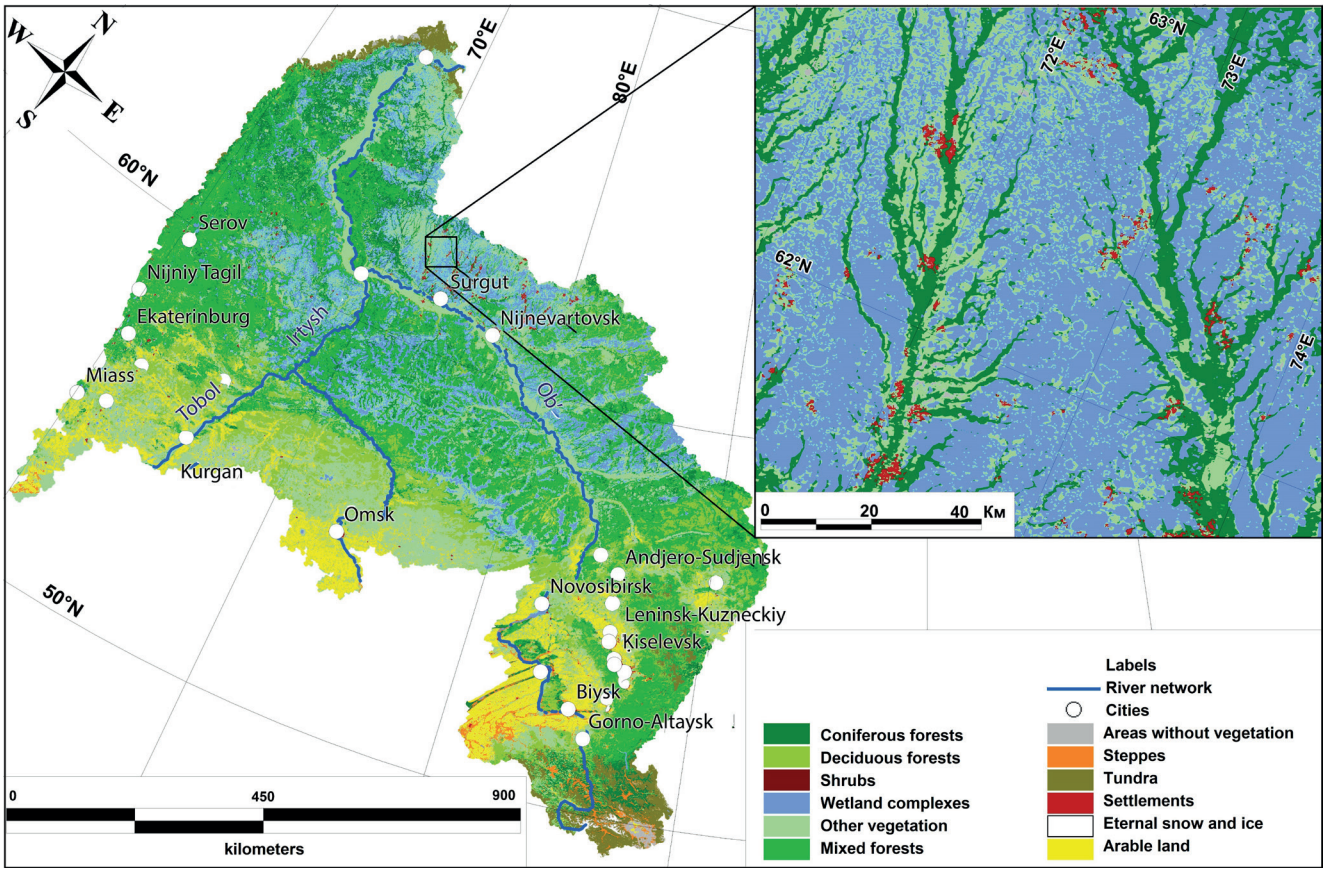

Fig. 6. Land Cover/Land Use map of the Ob' river basin

standardize data on a scale of 0 – 1 according to Eq. (1) (Allan et al., 2013):

$$\left(x_i - x_{min}\right) / \left(x_{max} - x_{min}\right) \quad (1)$$

Population density. Population density is an important measure that indirectly shows how much and what kind of land development (industrial and agricultural) is happening. It also shows how much human activity is affecting natural geosystems.

The primary source of information used is the freely available data from the Global Human Settlement Layer (GHSL) project[1]. This project provides global spatial information about the population over time in the form of built-up area maps, population density maps, and settlement maps. The information is generated using scientifically grounded analytics and advanced technologies for intelligent spatial data analysis. The processing structure of GHSL utilizes heterogeneous data, including global archives of small-scale satellite imagery, census data, and geographic information provided by volunteers. The data are processed fully automatically, resulting in analytical and objective reports on population presence and infrastructure creation.

The project offers a range of products for different time periods, resolutions, and coordinate systems. In our study, the raster grid with population data GHS-POP for the year 2015 was used, with a resolution of 250 m (9 arc-seconds) and the WGS-84 coordinate system. This spatial raster product consists of a set of raster "tiles" depicting the distribution and population density expressed in the number of people per cell (Fig. 7). GHS-POP provides raster grids with population figures for key years: 1975, 1990, 2000, and 2015, provided by the Center for International Earth Science Information Network (CIESIN) Gridded Population of the World (GPW v4.10).

For the Ob' river basin, several raster tiles were downloaded, merged into a single raster, and clipped according to the common boundary of the Ob' river basin and the boundaries of small river basins in the GIS application QGIS. Using the field calculator in QGIS, the total population for each basin was determined. The resulting values were then divided by the area of each basin.

For basins with non-zero density, basic statistics were calculated (Table 6) and a frequency distribution histogram was plotted (Fig. 8).

To account for population density in calculating anthropogenic pressure, this indicator was normalized to a dimensionless form with a range of values from 0 to 1. Therefore, basins with a population density greater than or equal to 1000 people/km^2 were assigned a value of 1 (the maximum possible value). For the remaining basins, the indicator was normalized using the following Eq. (2):

$$\left(\log\left(P_{dens} + 1\right) - 0\right) / \left(\log\left(1000 + 1\right) - 0\right) \quad (2)$$

where P_{dens} is the population density, people/km^2.

As a result, we obtained the normalized indicator (see Fig. 8, Table 7):

We created a corresponding thematic GIS database based on the transformed population density indicator (Fig. 9), where the following pattern is observed: basins with the highest population density are located along the industrial centers of the Urals region (western part of the basin); in the southwest, in the Kurgan, Omsk, and partially in the Tyumen regions. Basins with relatively high population density are concentrated around the oil production centers in the Khanty-Mansi Autonomous Okrug (northeast of the basin). In the south of the basin, the highest population density is observed in the Novosibirsk and Kemerovo regions, in the Altai Republic, and in Altai Krai. Overall, most basins have zero or

Fig. 7. Population raster grid from the GHS-POP project of GHSL

Table 6. Basic statistics of population density in basins (people/km^2)

Quantity(basin)	Min.	Max.	Mean	Mode	St.Dev.	Percentile, %								
						1	5	10	25	50	75	90	95	99
5507	1	4467	46.96	1	204.78	1	1	1	1	4	14	69	199	967

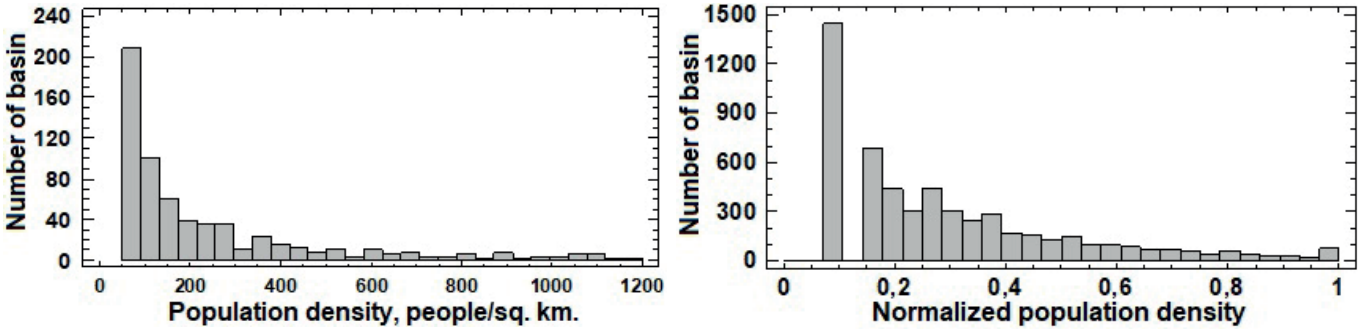

Fig. 8. Distribution of basins by population density indicator

Table 7. Basic statistics of the population density indicator in basins with population density >0 (people/km²)

Quantity (basin)	Min.	Max.	Mean	Mode	St. Dev.	Percentile, %								
						1	5	10	25	50	75	90	95	99
5507	0.1	1	0.3	0.1	0.21	0.1	0.1	0.1	0.1	0.4	14	0.61	0.77	0.99

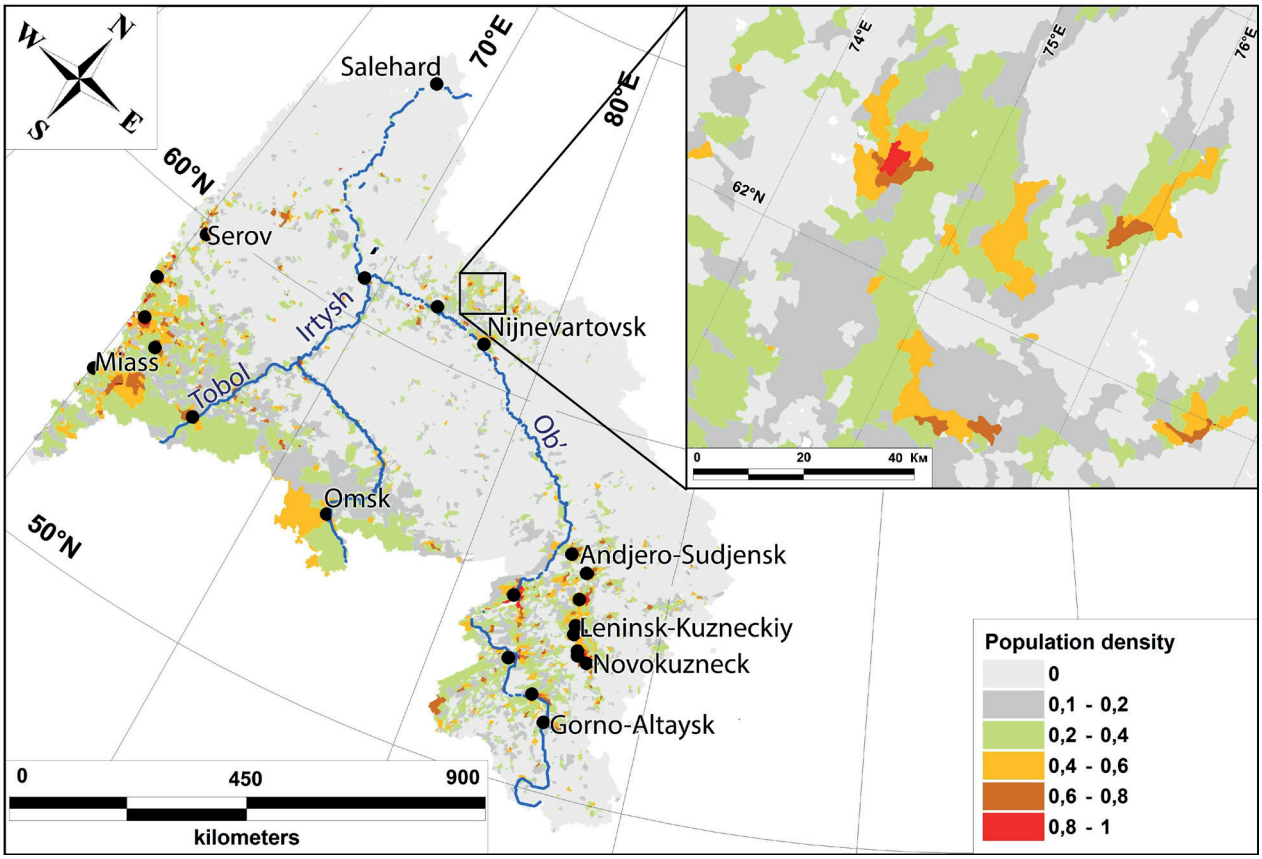

Fig. 9. Normalized indicator of population density in basin geosystems of the Ob' river basin

very low population density due to harsh climatic conditions, vast marshlands (middle reaches of the Ob'), and mountainous terrain (extreme southern part of the basin).

The density of the road network

A well-developed road network is an essential component of any modern state. The road network is a basic component of infrastructure. Roads serve as fundamental infrastructure components, reflecting territorial and industrial development while contributing to anthropogenic pressure. The type and development of the road network largely determine anthropogenic loads of both linear and areal types. Thus, roads passing through various parts of the basin slopes can have anthropogenic effects due to the transformation of surface runoff. It can both interrupt and concentrate. As a result, significant restructuring occurs in erosion, transport, and pollutant accumulation processes. Railways require large land clearances, and in forested areas, they require clear-cutting.

To calculate the road network density in the basins, data from[4] (Haklay& Weber, 2008), as of 2023 was used. During the work, roads and railways were processed. Roads were classified based on their type, with expert-assigned scores ranging from 1 to 5, indicating increasing levels of importance and impact. The scoring system for roads was derived from discussions and consensus within the Russian OSM community[5]). In addition,

[4] OpenStreetMaps. (2023). [online]. Available at: https://www.openstreetmap.org [Accessed 31 Aug. 2024]
[5] OpenStreetMapWiki -RU:Key: highway. (2018). [online]. Available at: https://wiki.openstreetmap.org/wiki/RU:Highway_classification (in Russian) [Accessed 31 Aug. 2024].

load scores were assigned for railways based on the "railway" attribute field. The railway tag is used to denote all types of railways or other transport using rails[6].

Before performing the calculations, the OSM road and railway layers were merged into one layer. All calculations were carried out in the ArcGIS software package (v. 10.4.1). First, in each layer, polylines with the same load score were merged using the "Merge by Attribute" geoprocessing tool. In the next step, the roads were intersected with the boundaries of the small river basins using the "Identify" tool,.Total lengths of roads and railways with the same load score within each basin were calculated using the "Calculate Geometry" tool. As a result, fields with total lengths of two layers of OSM roads with load scores from 1 to 5 were added to the geospatial database of basin geosystems in the Ob watershed.

The density of roads for each category in the basin is calculated as the ratio of length to basin area (km/km^2) (Table 8). The overall indicator (Rpress) for assessing the impact of road density was calculated using the following Eq. (3):

$$R_{press} = R_1 + 2 * R_2 + 3 * R_3 + 4 * R_4 + 5 * R_5 \quad (3)$$

where R_1 represents road density with a score of 1 for anthropogenic impact, R_2 represents road density with a score of 2, and so forth.

They adjusted the indicator based on statistical analysis. As a result, it was found that 95% of basins exhibit a road density value below 4. Consequently, a maximum score of 1 was assigned to basins exceeding this threshold. For the remaining basins, the indicator was normalized using Eq. (4):

$$\left(R_{press} - 0\right) / (4 - 0) \quad (4)$$

where R_{press} –the overall road density indicator.

Because of this normalization, the indicator ranged from 0 to 1. Here is the corresponding thematic GIS database (Fig. 10) and Table 9 with the normalized values.

The thematic map constructed using the final road density indicator, shown in Fig. 11, reflects its spatial distribution. The findings are as expected and rational: basins with the highest road density indicators are predominantly located in urbanized areas, mirroring the patterns observed in population density.Additionally, basins with relatively high road density indicators are those intersecting highways and railway lines connecting major cities, regional administrative centers, industrial areas, and major oil production centers. About 56% (17,381) of basins lack road networks due to challenging terrain conditions (e.g., extensive marshlands, etc.). These basins are scattered along the middle course of the Ob' River and in the northern and southern parts of its basin.

Agricultural Land Use

The extent of agricultural land use serves as the foundation upon which any country's agricultural sector grows and develops. It also serves as a crucial indicator of anthropogenic pressure. In this study, the plowed of basins serves as the key characteristic of agricultural land use, reflecting the primary activity of the agro-industrial complex. Often, primary cultivation leads to the complete destruction of native vegetation, which is replaced by agrocenoses or pasturelands. Soils under cultivation, where various crops are grown, undergo disruptions in horizon structure, leading to soil degradation, accelerated anthropogenic erosion, and the movement of organic and mineral pollutants in dissolved form with surface runoff into small rivers and soil-groundwater.

At the initial stage, arable lands were identified separatelyseparately from the TerraNorte RLC raster layer in ArcGIS using the "reclassification by table" tool. The resulting raster layer was vectorized, and the freely available data in each basin was calculated as the ratio of the area of cultivated lands to the total area of the basin. For basins containing arable lands, a frequency histogram was constructed (Fig. 12), and basic statistical indicators were calculated (Table 10), forming the resulting layer of plowed land map (Fig. 13).

Table 8. Basic Statistics of Road Density Indicator in Basins (km/km^2)

Quantity (basin)	Min.	Max.	Mean	Mode	St. Dev.	Percentile, %								
						1	5	10	25	50	75	90	95	99
13357	0.000003	82.7	1.14	0.57	2.96	0.006	0.03	0.07	0.19	0.47	1.06	2.25	3.86	13.02

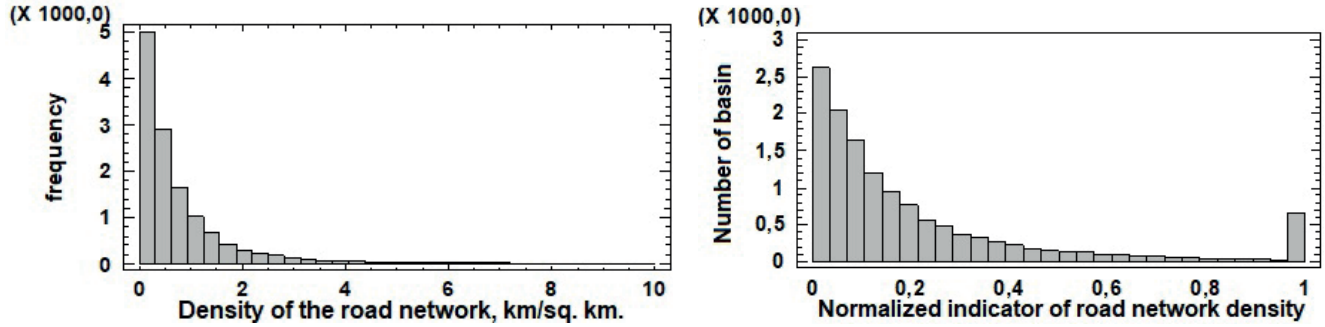

Fig. 10. The distribution of basins according to road density

Table 9. The basic statistics of the normalized road density in the basins (km/sq.km)

Quantity (basin)	Min.	Max.	Mean	Mode	St.Dev.	Percentile, %								
						1	5	10	25	50	75	90	95	99
30738	0	1	0.09	0	0.20	0	0	0	0	0	0.09	0.28	0.50	1

[6] OpenStreetMapWiki - RU:Key:railway. (2016). [online]. Available at: https://wiki.openstreetmap.org/wiki/RU:Key:railway (in Russian) [Accessed 31 Aug. 2024].

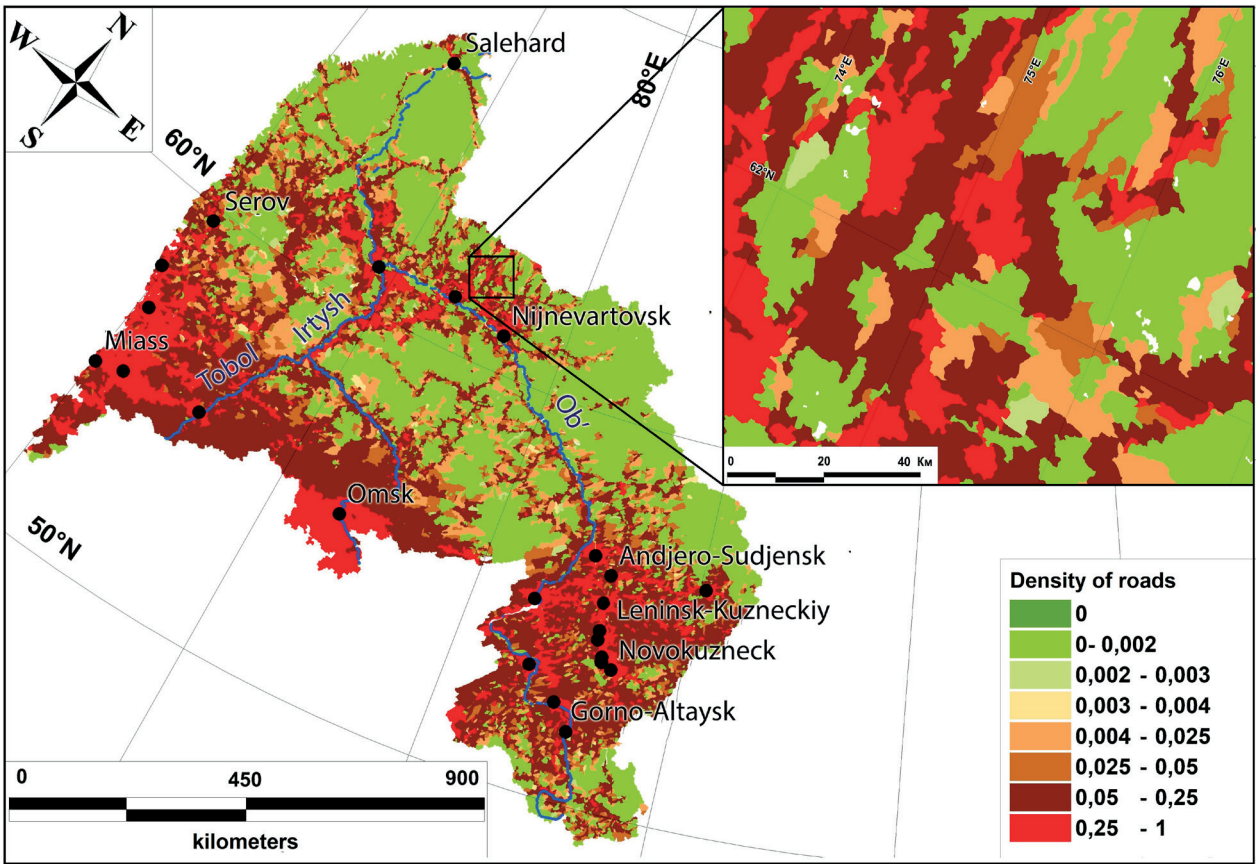

Fig. 11. Final road density indicator in the basins of small rivers within the Ob' river basin

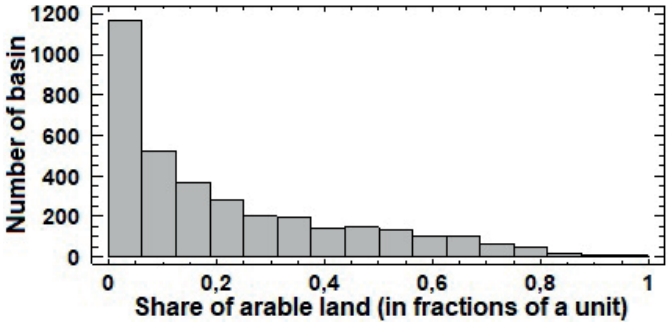

Fig. 12. Distribution of Basins by Agricultural Land Use

Table 10. Basic Statistics and Percentiles of Agricultural Land Use in Basins(%)

Quantity (basin)	Min.	Max.	Mean	Mode	St. Dev.	Percentile, %								
						1	5	10	25	50	75	90	95	99
3493	0	100	21	8	2.47	0.0002	0.003	0.008	0.04	0.13	0.34	0.56	0.67	0.82

Anthropogenic Load

The final indicator of anthropogenic load is calculated as the average of three integral indicators: population density, road network density, and agricultural land use, i.e., a simple linear assessment is used.

The final indicator of anthropogenic load is ranked as follows: very low, low, moderate, high, and very high anthropogenic load (Table 11).

For spatial visualization of the final anthropogenic load indicator, a corresponding thematic map (Fig. 14) has been created, and key statistics have been determined (Fig. 15, Table 12).

Basin ecosystems that do not contain arable land, road networks, or population are classified as basins with zero anthropogenic load (54.3% of basins). These basins, by area, cover 35% of the territory. Basins with a very weak anthropogenic load (35.7%) have a very low population density, averaging 0.73 people/km^2, low road density (measured in hundredths and thousandths of km/km^2), and consequently a very low percentage of arable land, averaging 1.8%. Basins in this category cover almost half of the entire Ob' River basin, accounting for 49.5% of it. Basins of small rivers experiencing weak anthropogenic load (6.6%) have an average population density of 10.7 people/km^2, arable land percentage of 19.4%, predominantly containing field roads (4.68 km/km^2), and cover 6.6% of the territory. Basins with a moderate anthropogenic load form the outer "ring" of urbanized areas, where the average population density reaches 63.4 people/km^2, arable land percentage is 19.4%, and road density begins to increase (0.05 - 0.24 km/km^2). Basin ecosystems with strong and very strong anthropogenic loads (summing up to just over 1% of the total number

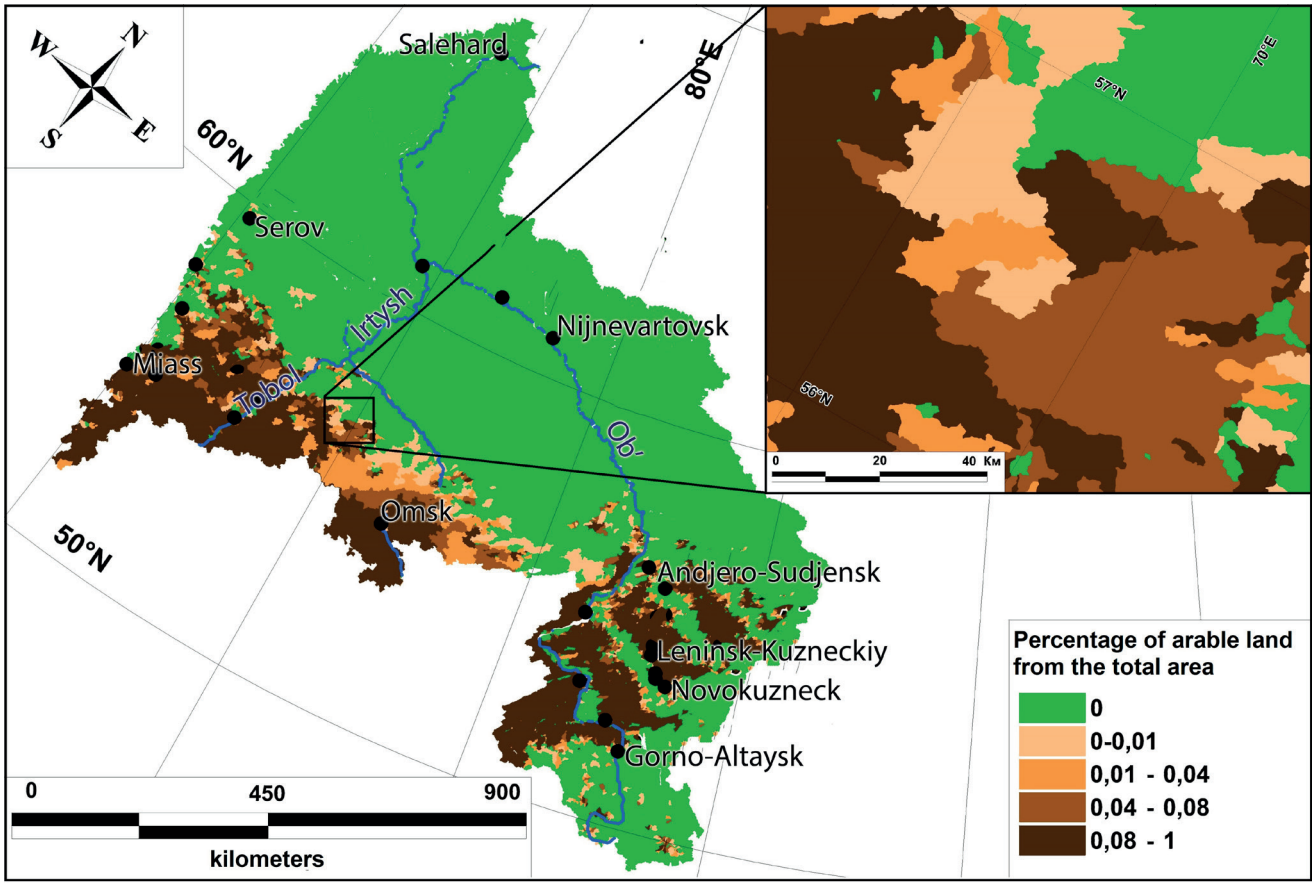

Fig. 13. Map of Agricultural Land Use in Basins of Small Rivers within of the Ob' river basin

Table 11. CategoriesofAnthropogenicLoad

Anthropogenicload			Absent	Veryweak	Weak	Mean	Strong	Verystrong
Interval			0	0–0.2	0.2–0.4	0.4–0.6	0.6–0.8	>0.8
Ploughness, %	Min.		0	0	0	0	0	58.3
	Mean		0	1.76	19.4	16.3	12.5	74.5
	Max.		0	66.7	100	100	100	100
Roading, km/km^2	R_1	Mean	0	0,11	4.68	0.45	1.14	0.62
	R_2	Mean	0	0,08	0.30	0.97	3.33	3.72
	R_3	Mean	0	0,04	0.15	0.24	0.57	0.06
	R_4	Mean	0	0,003	0.017	0.0	0.16	0.24
	R_5	Mean	0	0,006	0.06	0.19	0.67	0.019
Populationdensity, people/km^2	Min.		0	0	0	0	11	322
	Mean		0	0.73	10.7	63.4	589.8	525.7
	Max.		0	0.43	415	505	4467	750

of basins) constitute the inner "core" of urbanized areas, characterized by high population densities averaging 589.8 and 525 people/km^2 respectively, noticeable increase in road density including highways and railways. The average arable land percentage in these areas is 12.5% and 74.5% respectively. Together, they cover approximately 1% of the entire Ob' River watershed.

Overall, the situation is as follows: basins with zero, weak, and very weak anthropogenic loads are evenly distributed throughout the entire Ob' river basin territory (totaling 95.1% of the total area). Basins with moderate, strong, and very strong loads are located in the western, northwestern, southwestern (agricultural and industrially developed regions of the Urals), southern (Kuzbass), central, and eastern parts of the Ob' river basin (areas of intensive coal, gas, and oil extraction).

The obtained results effectively reflect the differences in anthropogenic pressure in the spatial aspect. The indicators used to assess anthropogenic pressure on geosystems reflect how much human activity affects the territory , as well as the significant influence of each category of anthropogenic load. The data obtained can be used to address a range of spatial development tasks in this macro-region of Russia and to develop compensatory measures within river basins.

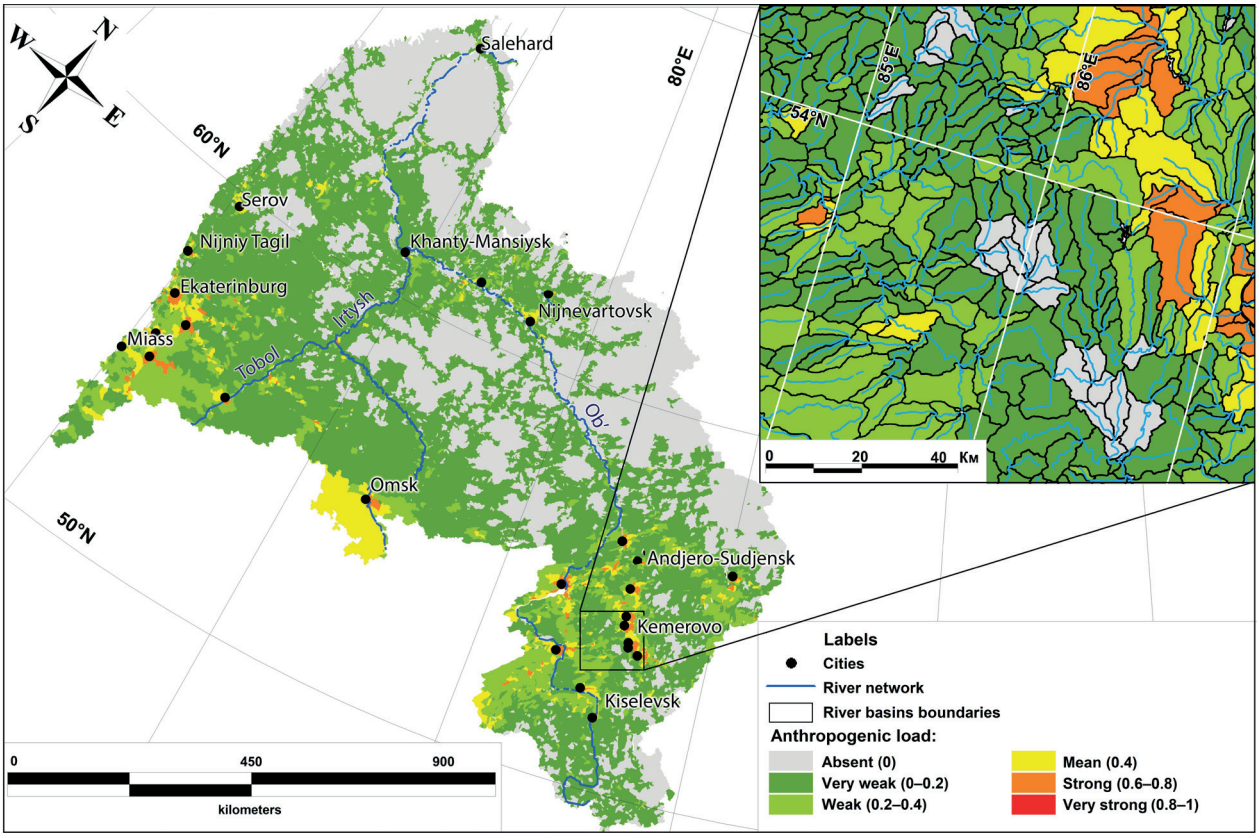

Fig. 14. Map of anthropogenic load on the geosystems of the Ob' river basin

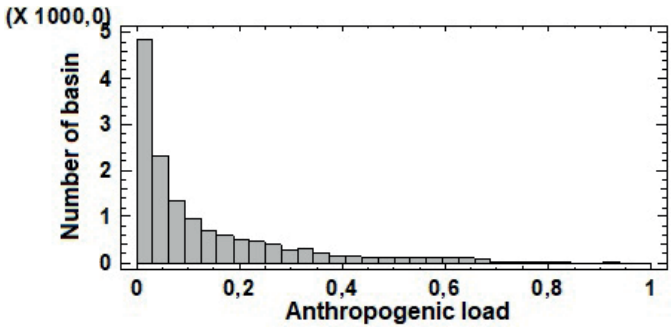

Fig. 15. Distribution of Basins by Anthropogenic load

Table 12. Basic statistics and percentiles of anthropogenic load on basins

Quantity	Min.	Max.	Mean	Mode	St.Dev.	Percentile, %								
						1	5	10	25	50	75	90	95	99
30738	0	0.91	0.06	0	0.12	0	0	0	0	0	0.05	0.2	0.32	0.6

CONCLUSIONS

For the macro-region of Russia within the Ob'river basin, a GIS database of small river basins has been created for the first time, allowing the implementation of a geosystem (basin) approach to territorial assessment. Additionally, a geospatial database has been developed for the first time, detailing the natural-resource potential and indicators of economic development in this territory with the formation of a specialized GIS. The total number of parameters in the database amounts to 12, including morphometric and climatic characteristics, land use types, and anthropogenic load.

The geospatial database enabled an assessment of the territory based on key morphometric relief characteristics, hydro-climatic parameters, types of land cover, and human economic activity. Thematic GIS databases were created for all parameters, the main statistical indicators were determined, and a spatial analysis of the most general patterns of their development in the Ob' river basin was conducted.

Through the system of integrals (population density, road density, and arable land), an assessment of anthropogenic pressure on the geosystems of the small rivers of the Ob' was carried out. According to this assessment, basins with no anthropogenic load predominate (54.3%), due to the low population density in the northern territories, while 35.7% are subject to very weak pressure and 6.6% to weak pressure. Only 3.4% of the territory, located around urbanized areas, is subject to moderate, strong, and very strong anthropogenic pressure.

The results obtained can be used in the implementation of Government Programs for the spatial development of the Western Siberia and Arctic regions within of Russia.

REFERENCES

Allan J.D., McIntyre P.B., Smith S.D., Halpern B.S., Boyer G.L., Buchsbaum A., Steinman A.D. (2013). Joint analysis of stressors and ecosystem services to enhance restoration effectiveness. Proceedings of the National Academy of Sciences, 110 (1), 372-377. DOI:10.1073/pnas.1213841110

Andersen J.H., Stock A., Mannerla M., Heinänen S., Vinther M. (2013). Human uses, pressures and impacts in the eastern North Sea. Technical Report from DCE – Danish Centre for Environment and Energy, 18, 136. http://www.dmu.dk/Pub/TR18.pdf

Bartalev S.A., Egorov V.A., EfremovV.Ju., Loupian E.A., Stycenko F.V., Flitman E.V. (2012). Assessment of the area of fires based on integration of satellite data of various spatial resolutions MODIS and Landsat-TM/ETM+. Sovremennye problemy distancionnogo zondirovanija Zemli iz kosmosa, 9(2), 9-27 (in Russian).

Bartalev S.A., Egorov V.A., Loupian E.A., Khvostikov S.A. (2014). A new locally-adaptive classification method LAGMA for large-scale land cover mapping using remote-sensing data. Remote Sensing Letters, 5(1), 55-64. DOI:10.1080/2150704X.2013.870675

Braude D.I. (1965). Soil erosion, drought and their control in the CBER. M., Nauka, 140 (in Russian).

Danielson J.J. Gesch D.B. (2011). Global multi-resolution terrain elevation data 2010 (GMTED2010) U.S. Geological Survey Open-File Report, 26. DOI:10.3133/ofr20111073

Didenko P.A., Vodop'janova D.S., Skripchinskaja E.A. (2018). Assessment of the stability of landscapes of the Stavropol Territory to anthropogenic load. Nauka. Innovacii. Tehnologii, 2, 127-138 (in Russian).

Ermolaev O.P. Vedeneeva E.A., Mal'cev K.A., Mozzherin V.V., Muharamova S.S., Harchenko S.V., Shynbergenov E.A. (2017c). Mapping basin geosystems of Russia. Treshnikovskie chtenija-2017, Sovremennaja geograficheskaja kartina mira I tehnologii geograficheskogo obrazovanija, Mat. nauch.-prakt. konf., 266-268 (in Russian).

Ermolaev O.P., Mal'cev K.A., Muharamova S.S., Harchenko S.V., Vedeneeva E.A. (2017a). Cartographic model of river basins of European Russia. Geografija I prirodnye resursy, 2, 27-36 (in Russian).

Ermolaev O.P., Mal'cev K.A., Muharamova S.S., Ivanov M.A., Shynbergenov E.A. (2017b). Creation of the GIS «River Basins of Russia». Mat. VI Mezhd. nauch.-prakt. konf. «Aktual'nye voprosy geodezii I geoinformacionnyh sistem», 50-53 (in Russian).

Gordeev V.V., Martin J.M., Sidorov I.S., Sidorova M.V. (1996). A reassessment of the Eurasian river input of water. Sediment, major elements, and nutrients to the Arctic ocean. Amer. J. of Science, 296, 664-691.

Haklay M., Weber P. (2008). Openstreetmap, User-generated street maps. IEEE Pervasive computing, 7(4), 12-18. DOI:10.1109/MPRV.2008.80.

Ivanov M.A. (2019). Geography and geoecology of basin geosystems of the Volga Federal District, dis. …kand. geogr. nauk. Kazan', 197 (in Russian).

Ivanov M.A., Muharamova S.S., Ermolaev O.P. (2020). Assessment of anthropogenic load on the territory of the Volga Federal District using the basin approach. Cifrovaja geografija, materialy Vseros. nauch.-prakt. konferencii s mezhdunar. uchastiem. [online]. Available at, https,//dspace.ncfu.ru/bitstream/20.500.12258/4067/1/127138%20%5BSKFU%5Dnit-2-2018.pdf (in Russian).

Ivanov V., Milyaev I., Konstantinov A., Loiko S. (2022). Land-use changes on Ob River floodplain (Western Siberia, Russia) in context of natural and social changes over past 200 years. Land, 11(12), 2258. DOI:10.3390/land11122258

Korytnyj L.M. (2001). Basin concept in environmental management, monografija. Irkutsk, Izd-vo IG SO RAN, 163. (in Russian)

Criteria and parameters of permissible anthropogenic loads on agricultural landscape components (2005). Kursk, VNIIZiZPJe RASHN, 58 (in Russian).

Lisetskii F.N., Buryak J.A., Zemlyakova A.V., Pichura V.I. (2014). Basin organizations of nature use, Belgorod region. Biogeosystem Technique, 2(2), 163-173. DOI:10.13187/bgt.2014.2.163.

Miller T. (1993). Living in the environment. - M., Progress (in Russian).

O'Callaghan J., Mark D.M. (1984). The extraction of drainage networks from digital elevation data. Comput. Vis., Graph., Image Process., 28(3), 323-344.

Osipov G.K., Dmitriev V.V. (2017). Basin-landscape approach to territorial planning. Informacija I kosmos, 3, 112–117. (in Russian with English summary)

Pogorelov A.V., Dumit Zh.A. (2009). Relief of the river basin Kuban, morphological analysis. M., GEOS, 218 (in Russian).

Rejmers N.F. (1990). Environmental Sciences. Slovar'-spravochnik. M., Mysl', 637 (in Russian).

Rodriguez E., Morris C.S., Belz J., Chapin E., Martin J., Daffer W., Hensley S. (2005). An assessment of the SRTM topographic products. Technical Report JPL D-31639. Pasadena, Jet Propulsion Laboratory, 143.

Serbenjuk S.N. (1990). Cartography and geoinformatics - their interaction. Moskva, Izd-vo MGU, 157 (in Russian).

Shynbergenov Y.A., Sihanova N.S. (2017). Identification of Large Rivers of Siberia (Ob, Yenisei, Lena) by using GIS technology based on remote sensing of Earth from Cosmos. Astra Salvensis, 5(10-1), 541-545.

Vogt J.V., Colombo R., Bertolo F. (2003). Deriving drainage networks and watershed boundaries. A new methodology combining digital elevation data and environmental characteristics. Geomorphology, 53, 281-298. DOI:10.1016/S0169-555X(02)00319-7

Yermolaev O.P. Erosion in the basin's geosystems. Kazan, Publishing House of KSU, 2002, 264 p.

Yermolaev O.P., Mukharamova S.S., Maltsev K.A., Ivanov M.A., Gafurov A.M., Saveliev A.A., Shynbergenov Y.A., Yantsitov R.O. (2023a). Geography and Geoecology of Russia in the Mosaic of River Basins. Geography and Natural Resources, 44(3), 208-214 (in Russian with English summary), DOI:10.1134/S1875372823030046.

Yermolaev O.P., Shynbergenov Y.A., Mukharamova S.S. (2023b). Geoinformation system "River Basins of Russia". InterCarto. InterGIS. GI support of sustainable development of territories, Proceedings of the Int. conf. Moscow, MSU, Faculty of Geography, 29(1), 546–559 (in Russian with English summary), DOI:10.35595/2414-9179-2023-1-29-546-559 (in Russian)

Check for updates

CC BY

RESEARCH PAPER

FLUVIAL PROCESSES AND LANDFORMS AS INDICATORS IN TORRENTIAL FLOOD HAZARD ASSESSMENT

Jelena Kovačević-Majkić[1*], Dragoljub Štrbac[1], Jelena Ćalić[1], Marko V. Milošević[1], Milovan Milivojević[1], Siniša Polovina[2]

[1] Geographical Institute "Jovan Cvijić" Serbian Academy of Sciences and Arts, Đure Jakšića 9/III, Belgrade, 11000, Serbia
[2] University of Belgrade – Faculty of Forestry, Kneza Višeslava 1, Belgrade, 11000, Serbia
***Corresponding author:** j.kovacevic@gi.sanu.ac.rs
Received: May 1st 2024 / Accepted: November 22nd 2024 / Published: December 31st 2024
https://doi.org/10.24057/2071-9388-2024-3378

ABSTRACT. Torrential flood hazard assessment is always a challenge, especially if the aim is to do it on the level of the whole watershed. When there are no required data available, there are traces in nature, morphological indicators, that show the extent of previous floods, in period longer then instrumental period. Therefore, in this paper we deal with fluvial and slope both erosional and accumulation processes and landforms, which doubtlessly indicate torrential flood prone areas. We have selected eight indicators and grouped them into three segments: erosional process, morphometric characteristics of watershed, and accumulation processes and landforms. Selected indicators serve for fluvial processes determination and therefore could be used for proper water and flood risk management. The research was done in three middle-sized watersheds in Serbia which belong to the Velika Morava River basin, showing that integrative approach is necessary for rational watershed management, meaning for selection of measures for torrential flood hazard mitigation.

KEYWORDS: flood hazard, flood zone, fluvial landforms, alluvial plain, fan, Serbia

CITATION: Kovačević-Majkić J., Štrbac D., Ćalić J., Milošević M. V., Milivojević M., Polovina S. (2024). Fluvial Processes And Landforms As Indicators In Torrential Flood Hazard Assessment. Geography, Environment, Sustainability, 4(17), 26-34
https://doi.org/10.24057/2071-9388-2024-3378

ACKNOWLEDGEMENT: We thank the reviewer who helped us to improve the manuscript. The research was funded by the Ministry of science, technological development and innovations of the Republic of Serbia (contract number 451-03-66/2024-03/200172).

Conflict of interests: The authors reported no potential conflict of interest.

INTRODUCTION

Life by the rivers, either lowland or mountainous, has always attracted people, offering a bare necessity – available water. The growth of population density and the resulting human impact (e.g. concreting the riverbanks, thus preventing natural processes; introduction of large amounts of wastewater into streams, etc.) disturbed the human–nature relation, thus in countless cases the nature made a sharp counter-strike. In these circumstances, floods become a threat that endangers the population living on the riversides and get the character of a natural disaster. Water pollution also leads to consequences (acute hydric diseases, but also other diseases with long-term consequences that can be characterized as chronic). Large number of studies dealing with natural disasters begin with devastating statistics which show that their intensity and frequency are increasing, with consequences increasing both in terms of damage and the number of victims (EM-DAT 2024). The reason for this, on one hand, lies in natural processes that have their own dynamics and trends of intensity and frequency. Although the scientists argue about the causes that lead to changes in the timing of hydrometeorological processes and phenomena, the direction in which they take place and the significance of these changes, most of them agree that changes at the global level are evident, especially in the atmosphere and hydrosphere (Arnell 2002; Shiklomanov and Rodda 2003; National Research Council 2011; Hartmann et al. 2013; Gosling and Arnell 2013). On the other hand, the studies of disasters have changed from the perspective mainly focused on a physical or natural event towards the integration to the social system (Alcántara-Ayala 2002).

In order to assess flood hazard, determination of flood zones is the first and complex task to be done. Directive of the European Parliament and of the Council establishing a framework for Community action in the field of water policy – WFD (Directive 2000), as well as the directive on the European Parliament and of the Council on the assessment and management of flood risks – Flood Directive (Directive 2007) recommend the determination of the extent of a flood zone for different scenarios (for high, common and low probability of occurrence), which are important for the preparation of hazard and risk maps, and subsequently for risk management, including spatial planning. Therefore, the basic task in this paper is to determine the indicators for defining the food zone in torrential watersheds and subsequently to assess flood hazard. Existing maps of floodplains at the global level are characterized by lower data resolution, while higher data resolution maps were made for smaller spatial units, created for river regulation in certain sections (hydro-engineering approach and

method), while in mountainous areas there are no data on flood zones. In this sense, the aim of this paper is to use geographical method and an aspect that connects hydrological and geomorphological processes.

In accordance with the characteristics of torrential floods as two-phase fluid (maximum flow and high sediment concentration) as described by Coussot and Meunier (1996), the terms "debris flows", "torrent flows", "mudflows", "debris floods", "torrent floods", "flash floods", "lave torrentielle" are used in the literature and it is very difficult to precisely distinguish these phenomena. Therefore, in this paper we will deal primarily with torrential floods, as a natural process of increased intensity, which is the outflow of water with a high concentration of sediments in the riverbed. Torrential floods are associated with small streams that drain basins up to 100 km^2 (Wang et al. 1996). They refer to occasional, periodic and permanent watercourses whose watersheds are affected by erosion processes. They appear suddenly after intense rains and sudden melting of snow, have a high speed of the flood wave and last relatively short. Torrential floods often occur with other natural disasters, most often hurricanes, typhoons and their combinations with earthquakes and volcanic eruptions, and in these cases they occur as secondary disasters (Jakob and Hungr 2005), i.e. they are a consequence of multihazard (Zhou et al. 2015; Varazanashvili et al. 2012). They can also occur together with other slope processes, most often with landslides, and Jakob and Hungr (2005) state that torrential floods occur as triggers of large landslides. Kovačević-Majkić et al (2013) selected indicators for torrential risk assessment and for hazard component they selected discharge regime and erosion as segments of hazard, which is in accordance with the fact that there are two key factors that determine torrential floods:

1) The key factor and at the same time the trigger for the occurrence of torrential floods is the intense short-term precipitation (usually less than 24 hours), whereby in that time the total amount can reach several tens of millimeters per hour, e.g. 42 mm/h (Radović and Todorović 1989), 80 mm/h (Shimizu et al. 2002), 35-40 mm/ 30 min (Brajković and Gavrilović 1989), up to several hundred mm (320 mm/24h; Kompare and Rismal 1989). High soil moisture, caused by previous precipitation or melting snow, is also important for the occurrence of sudden floods, due to which the soil cannot receive new amounts of water (Jakob and Hungr 2005; Ristić and Malošević 2011).

2) Another key factor for the occurrence of torrential floods is the high prevalence of erosion in the basin and high sediment transport during torrential floods, which reaches more than ten times higher values than the average sediment transport (Costa 1988; Shimizu et al. 2002).

In addition to the two mentioned basic factors, there are also the conditions for the occurrence of torrents: a) physical-geographical: climatic (which in addition to precipitation includes air temperature), geological (type of rock), pedological (type of substrate), morphometric related to the basin (slope and shape of the basin), morphometric related to the riverbed (slope of the riverbed), vegetation (type, structure, age of vegetation) and b) anthropogeographic (land use). Their influence was assessed by Jakob and Hungr (2005), as well as by Ristić and Malošević (2011). Land use changes as urgent issue are pointed out by Gradel et al (2019). The authors appeal that forests are crucial for hydrological balance and land degradation prevention. Nolos et al. (2022) also write about the importance of good forest management. Generally, the trend in research of erosional processes is to put them in the context of environment and ecology, as well as sustainability. Researches expanded in the sphere of modelling and estimation of erosion processes. By the analyses of Zhuang et al. (2015) before 2001 the soil erosion research was mainly distributed across the USA and Europe, and afterwards the research was spread in Asia (dominantly in China and India) and Australia.

Considering the spatial distribution of mentioned erosional and accumulation processes, there are usually three characteristic zones in the torrential watersheds: 1) the "collection zone" that covers the upper parts of the watershed, where the process of soil erosion takes place to a greater or lesser extent, depending on the physio-geographical and anthropogeographical conditions in the watershed, 2) the "transit zone" or "torrent throat", represented by riverbeds in which the transport of torrent material primarily takes place or, as explained by Mazzorana et al. (2013), one-dimensional (1D) flow processes are active, the valleys are often gorge-like, with pronounced vertical erosion, and 3) "flood zone" which represents the part of the basin where the sedimentation material settles and most often has the shape of a fan, the space where two-dimensional (2D) flow occurs (Mazzorana et al. 2013). This zone is important as morphological indicator or "trace" of flooding (Milošević et al. 2015) which testifies about previous cases of torrential floods. Therefore, fluvial erosional and accumulation processes and the resulting landforms, as well as morphometric characteristics of watersheds presented by selected indicators, are appropriate for torrential flood hazards assessment.

Even though torrential floods are characteristic of the relatively small and middle-sized watersheds, they manifest and have impact on large-scale river basins as well, which is also stressed by Borga et al (2014). Therefore, it is difficult and almost impossible to determine the exact boundary where one or another type of flood occurs. Thus, the question is whether it is necessary to draw the exact line between river floods in the lower parts of large river basins and torrential floods that occur at higher elevations. Furthermore, the integral approach and work are the only correct and purposeful options. The results obtained are useful for numerous users, responsible and interested stakeholders, such as decision makers, spatial planners, researchers, insurance companies etc.

MATERIALS AND METHODS

The study area

Floods are among the most common disasters in Serbia causing the greatest damage (Official Gazette 2011; Dragićević et al. 2011; Gavrilović et al. 2012). In addition, torrential floods are the most common disaster, since 86.4% of the territory of Serbia (hilly and mountainous areas mainly south of the Sava and Danube River) is exposed to erosion processes (Ristić et al. 2012). The torrential floods inventory in Serbia was made by Petrović et al. (2014), and contains register of 848 torrential floods in which 133 people lost their lives in the period 1915-2013. The largest number of torrential floods occurred in the Južna Morava River basin, most commonly in May and June. In this paper we have selected three watersheds (the Skrapež River watershed, Belica River watershed and Lužnica River watershed) that belong to the Velika Morava River basin (Fig. 1).

The Skrapež River watershed (647 km^2) belongs to the upper part of the Zapadna Morava River basin. It is located in a mountainous region where the average elevation of the basin is 600.76 m. About 65% of the watershed lies between 400 and 700 m asl, less than 2% above 1000 m asl. (the

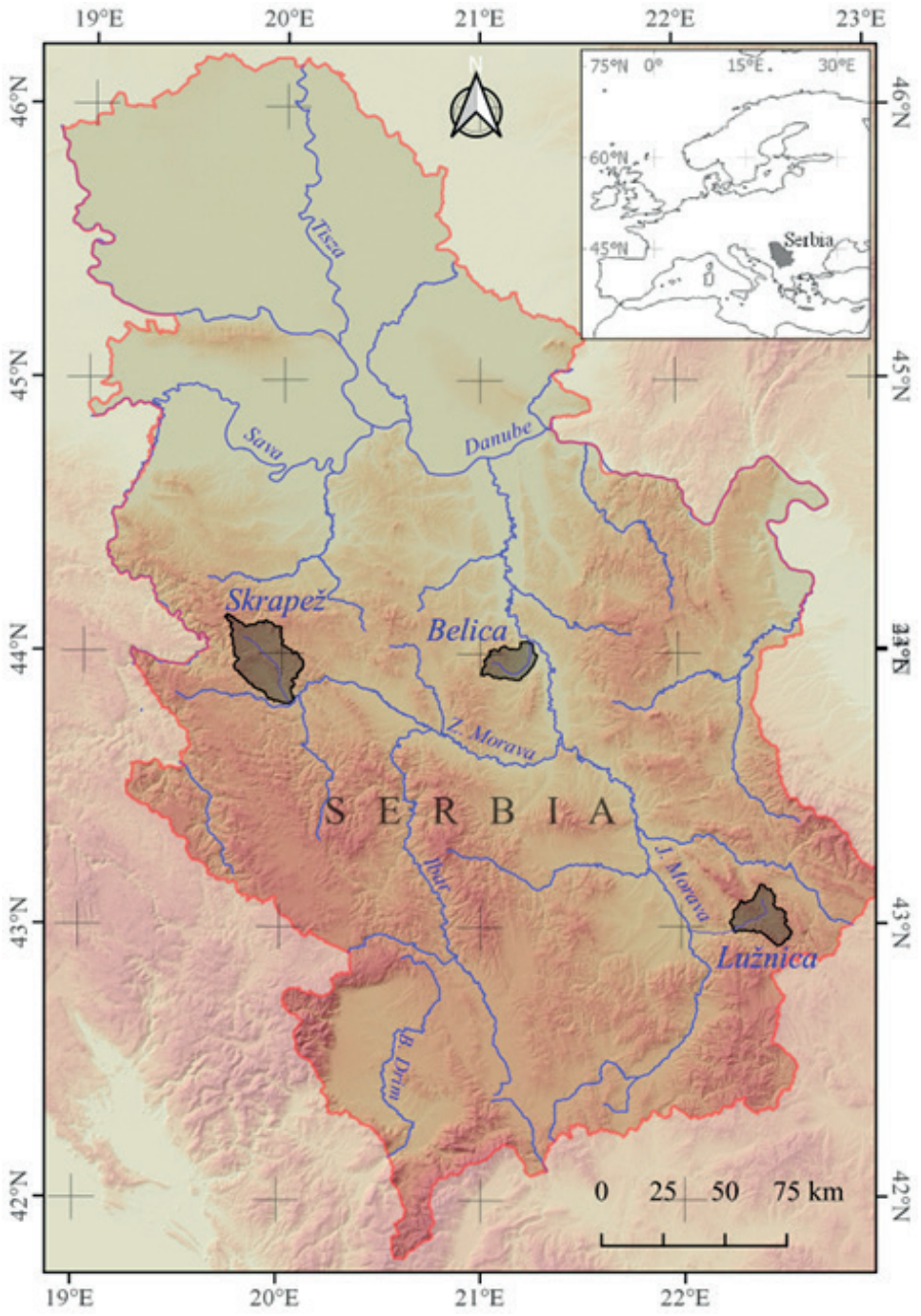

Fig. 1. Location of the Skrapež, Belica and Lužnica watersheds in Serbia

slopes of Povlen Mt. and Maljen Mt.), and about 10% below 400 m asl. (alluvial plains of the Skrapež River watershed and its largest tributary Lužnica River) (Kovačević-Majkić, 2009). Since most of the basin is built of metamorphites prone to decomposition and Miocene clastic rocks and sediments, this has resulted in increased erosion.

The Belica River watershed (233 km^2) is located in central Serbia and is one of the watersheds on the left side of the Velika Morava basin. The average elevation of the basin is 229.5 m. The basin of the Belica River consists of three morphological units: plains (with slopes up to 3°), hilly areas (with slopes up to 10°) and mountainous parts (with slopes up to 40°). The plains are the most represented, followed by hilly landscapes, and areas above 500 m asl. - the slopes of Crni vrh (708 m asl). Lithologically, the basin consists of clastic sediments of considerable thickness (sands, siltstones, sandy clays, clayey sands, clays) and regoliths composed of compact rocks, most often metamorphites (gneisses, mica-schists, dolomite marbles and amphibole shales) (Vujisić et al. 1981). Considering the mentioned lithological composition, which is subject to decay, and the slopes, areas with intensive erosion are poorly represented, and processes with medium and weak erosion dominate, while the lower part of the watershed is characterised by accumulation process.

The Lužnica River watershed (325 km^2) is located in southeastern Serbia. It belongs to the watershed of the Vlasina River, which is a right tributary of the Južna Morava River. Among the morphological units, the most represented are hilly (51%) and mountainous areas (46%) with the highest peak of 1385 m asl, while the plains cover the smallest area of the basin (3%). The lithological composition of the watershed consists of (1) limestones and dolomites of Suva Planina Mt, whose slopes represent the right valley side; (2) flysch, conglomerates and sandstones that form the left valley side, while (3) the Lužnica Miocene basin, located in the middle part of the basin, consists of conglomerates, gravel, sand and clay (Vujisić et al. 1980). Considering the spatial distribution of lithological units, the left valley side is more characterized by erosion than the right side.

Defining indicators for the flood hazard assessment

Floods about which there are no written sources happened in watersheds where there are potentials or conditions that lead to the occurrence of torrential floods. In accordance with character of torrential floods, we have selected the indicators that describe them. The challenge of proper indicators selection (thematically adequate, spatially and temporally available, and approved by scientific community) was elaborated by Kovačević-Majkić et al. (2013) and Kovačević-Majkić (2018). After meeting all of the mentioned criteria, we have grouped the indicators to: (1) segment on erosional fluvial processes, (2) watersheds morphometry segment; as well as traces in nature that testify that torrential floods occurred (morphological indicators), evidenced by (3) segment of landforms of fluvial and slope accumulation (floodplains, alluvial plains, fans). Selected indicators are presented in Table 1.

Data on erosional fluvial processes testify on erosion intensity and are described through four indicators: Areas affected by erosion processes of I, II and III category (H1a and H1b), Erosional coefficient Z (H1c) and Watercourses' density (H1d). Required data were collected from topographical maps 1:25000, Shuttle Radar Topography Mission (SRTM), pedological maps 1:50000, pedlogical map of Serbia (Mrvić et al, 2013), and Corine Land Cover (2018). Erosion was calculated by the method of Gavrilović (1972) in which the first class means the most intensive erosion. The method is widely used in the region and in countries of former Yugoslavia.

For selected morphometric characteristics of watersheds data, sources were the topographical maps 1:25000, SRTM, and Google Earth Service (2019). *Module of watershed divide line development* explains the role of the shape of the watershed in the formation of a torrential flood wave, meaning more rounded watershed means smaller *Module of watershed divide line development*, and subsequently higher probability of rapid water concentration. Whereas we need the indicator that is directly proportional to flood hazard, we have used the variation of the mentioned module, *Reciprocal module of watershed divide line development*, as indicator, whereby more rounded watershed means higher *Reciprocal module of watershed divide line development*.

Data on the landforms of fluvial and slope accumulation originate from the process of flooding and thus represent data on past floods, i.e. the area they covered. These landforms are alluvial plains and fans (Fig. 2), and based on their identification and spreading, the extent of the flood zone is determined. To determine the flood zone as a source of data on traces of torrential floods from the past, it is possible to use geomorphological maps 1:100,000 archived by the Geological Survey of Serbia. Selected torrent watersheds are presented on the maps by Menković and Košćal (1981), Menković and Košćal (1982), Menković, Košćal and Mijatović (1988). An example of a map is presented in Fig. 2. For a flood zone determined in that way, we use the term "geomorphological flood zone" (Geomorphological flood zone as indicators H3a and H3b in Table 1).

In purpose of obtaining the results, the following software packages were used: *Microstation, Global Mapper, QGIS,* and *Microsoft Excel*.

Table 1. Torrential flood hazard indicators

Indicators		Segment
Area affected by erosion of I, II and III category (km^2)	H1a	Erosional fluvial processes
Area affected by erosion of I, II and III category (%)	H1b	
Erosion coefficient Z	H1c	
Watercourses density (km/km^2)	H1d	
Main course slope (‰)	H2a	Watersheds morphometry
Reciprocal module of watershed divide line development	H2b	
Geomorphological flood zone (km^2)	H3a	Accumulation fluvial and slope landforms
Geomorphological flood zone (%)	H3b	

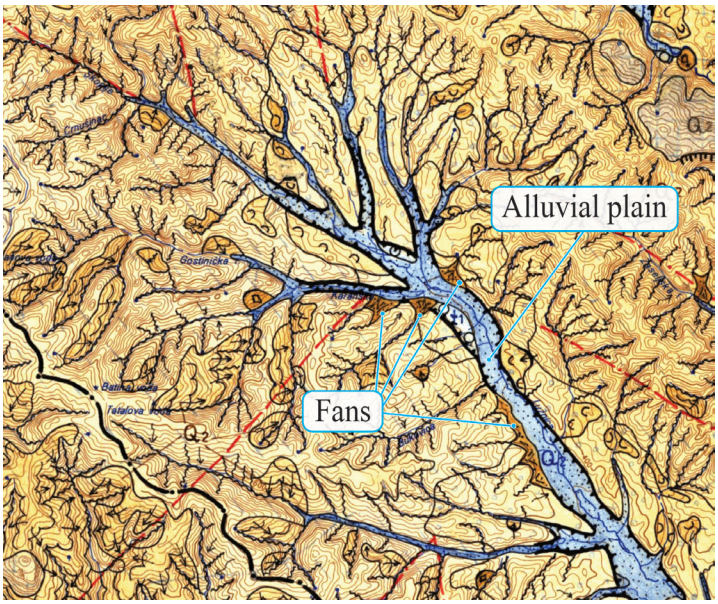

Fig. 2. Segment of the geomorphological map with marked flood-derived landforms, sheet Užice (Menković and Košćal, 1982)

RESULTS

The results used are obtained for three watersheds in Serbia. They were selected following several criteria.

First criterion was presence of erosion of I, II and III categories. According to the results of the calculation of erosion and sediment production by the method of S. Gavrilović (1972), which refers to the period 2012-2016, in all three watersheds there was a decrease in erosion processes, the most significant in the Lužnica watershed, which moved from the category of strong (II) erosion to the category of very weak (V) erosion (Kovačević-Majkić 2018). The erosion processes are presented in Fig. 3. In the selected basins, the characteristics of erosion and river regime are such that they represent the conditions for the formation and occurrence of torrential floods. Moreover, with a large amount of sediment they endanger the accumulations in the higher order basins to which they belong, and according to Gavrilović et al. (2009) they belong to the I and III category of areas affected by extreme torrential floods. Second criterion was detected floods. According to the torrential floods inventory in Serbia made by Petrović et al. (2014) in all three watersheds the torrential floods have happened and been registered. Larger floods in the Skrapež River basin occurred in 1910, 1926, 1938, 1965, 1975, 2001, 2006 and 2014; in the Belica River basin in 1929, 1964, 1965, 1976, 1999, 2002, 2010 and 2014; and in the Lužnica River basin in 1976, 1988, 2003 and 2007. (Gavrilović, 1981; Petrović et al, 2014; UN, EU & World Bank, 2014). Third criterion was morphometric characteristics of watershed which are described above in the Study area. All selected watersheds are positive to these criteria. Additionally, onomastic indicators (hydronyms) in selected watersheds and described cases of torrential floods (literature sources, case studies containing data on victims and other consequences of torrential floods, torrent inventory, newspaper articles) were criteria for torrential watershed selection and at the same time verification that selected indicators are the proper ones.

Based on geomorphological maps of 1:100,000 scale, 50 floodplains were identified in the Skrapež River watershed, 10 in the Belica River watershed, and 8 in the Lužnica River watershed. Milić (1984) dealt with a more detailed analysis of fans in the Lužnica River watershed and identified 60 fans. They differ in type and age, but also in size. Those less than 100 m in range were also identified. Regardless of the characteristics, they undoubtedly testify that torrential floods occurred. The Skrapež River watershed has the largest geomorphological flood zone, while the percentage share of the geomorphological flood zone is the largest in the Belica River watershed (Fig. 4).

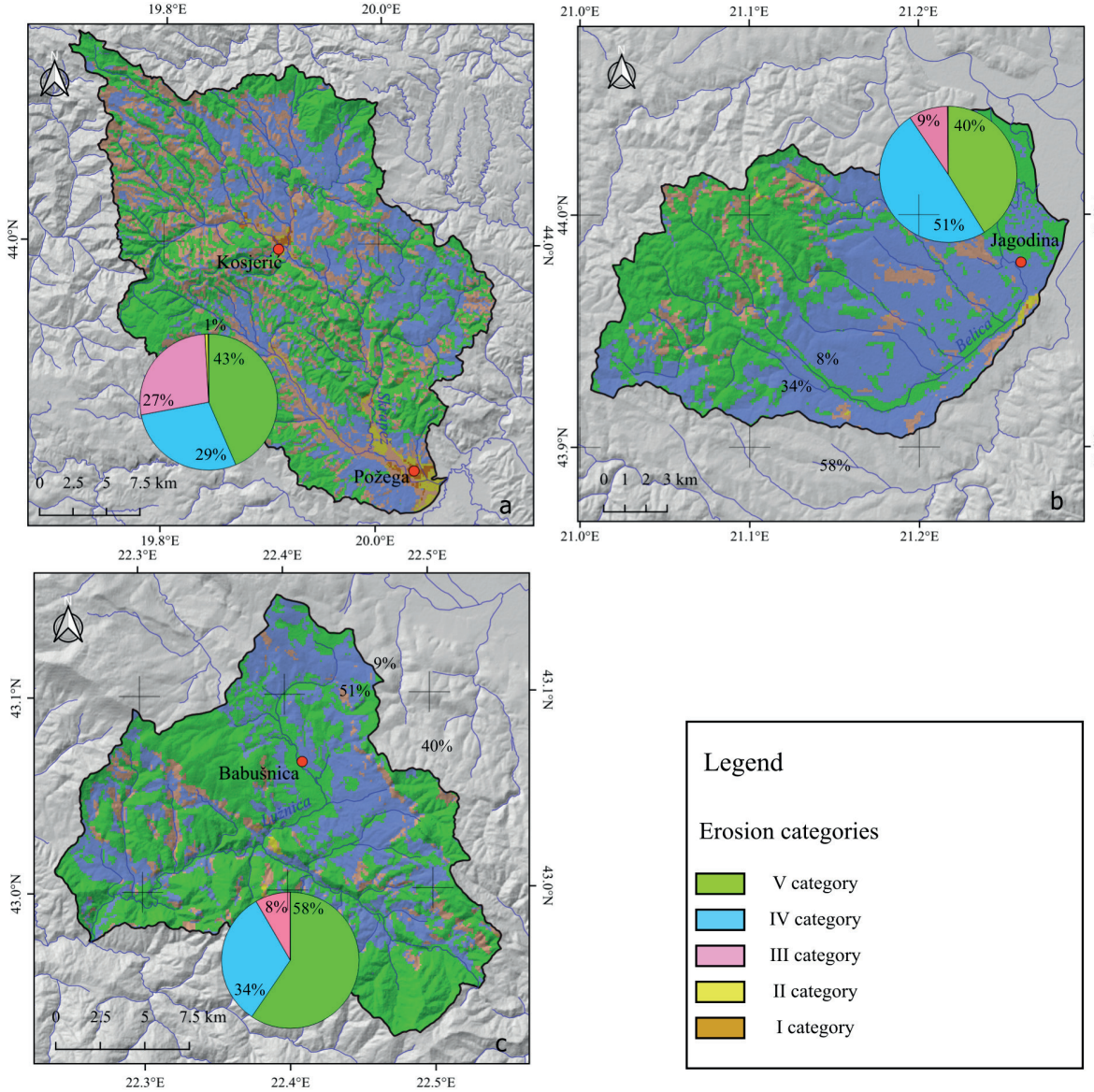

Fig. 3. Spatial distribution of erosional processes in Skrapež River watershed (a), Belica River watershed (b) and Lužnica River watershed (c)

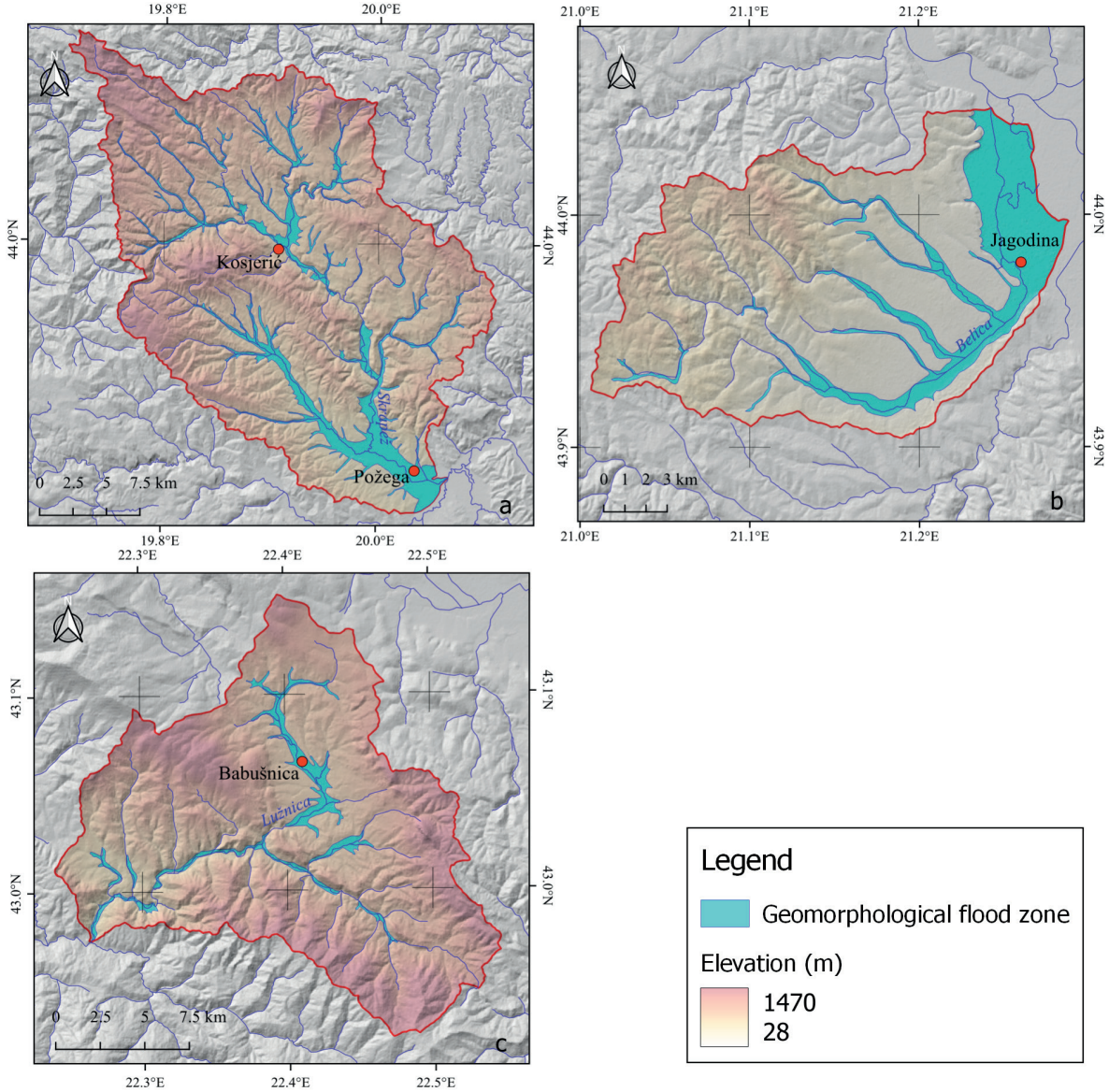

Fig. 4. Geomorphological flood zone in watersheds of the Skrapež River (a), Belica River (b) and Lužnica River (c)

The values of all selected indicators are shown in Table 2. Six of eight indicators are the highest in the Skrapež River watershed. Areas under erosion of I, II and III categories are the largest in the Skrapež River watershed, while they are almost equally represented in the Belica and Lužnica watersheds in absolute measure units and in relation to the size of watershed. The erosion coefficient is slightly higher in the Skrapež River watershed than in the other two basins. The Skrapež River has the most developed river network, as well as the largest watercourse slope, and the Belica River has the smallest. The development of the watershed divide line is unique, but the greatest for the Belica River watershed.

DISCUSSION

The motivation for starting the research process on torrential flood assessment was based on difficulty in determining the flood zone at the level of the entire watershed. Despite the fact that flood hazard could be assessed using hydrological data and geomorphological data, hydrological data have the relatively short series related to instrumental data collection. They are usually analysed using probability in order to obtain data on discharge and water levels for certain return periods. Also, there is a problem that generally there are no hydrological stations on small watercourses. Many hydrological and hydraulic models are developed in order to obtain the extent and depths of floods. Assessing flood hazard also includes other characteristics such as water velocity and for torrential floods erosion processes and deposits (except water, second important phase) are necessary to obtain and have in flood hazard assessment. Therefore the geomorphological data – landforms resulting from the processes of fluvial accumulation (alluvial plains and fans) – are distributed over the whole watershed and testify about floods that happened long time before the instrumental period. The solution to the problem of torrential flood hazard assessment was in detection of traces that point to large and as many floods in history as possible. Such data and their sources may be geomorphological maps that present the flooding-derived landforms, originating within the process of fluvial and slope accumulation. Arnaud-Fassetta et al (2009) point out that fluvial geomorphology can make a significant contribution to understanding the spatio-temporal distribution of flood hazard and flood risk management. Since the only correct water management is at the level of the entire watershed, then for determination of the flood zone, in addition to the landforms of the fluvial accumulation of the main river (alluvial plains), the landforms of fluvial accumulation of tributaries, must be observed. If tributaries have torrential character, then fans are the landforms we must determine as well.

Table 2. Flood hazard indicators in the Skrapež, Belica and Lužnica Rivers watersheds

Indicators	Skrapež River	Belica River	Lužnica River
Area affected by erosion of I, II and III category (km^2)	181.06	21.87	27.02
Area affected by erosion of I, II and III category (%)	27.95	9.37	8.32
Erosion coefficient Z	0.269	0.215	0.176
Watercourses' density (km/km^2)	2.04	1.52	1.63
Main course slope (‰)	15.01	8.99	12.40
Reciprocal module of watershed divide line development	0.63	0.74	0.68
Geomorphological flood zone (km^2)	65.20	45.53	15.16
Geomorphological flood zone (%)	10.06	19.50	4.67

The choice of methods for determining the flood zone also depends on the level of detail, i.e. the size of the area for which the flood zone is determined. The nature of torrential floods, i.e. the area they cover and the consequences they have, implies that it is best to work on risk assessment studies at the regional and local level (UNDP 2004). This is supported by the statement of Stojkov et al. (1998) that the causes of natural hazards such as landslides and torrents are developing at the regional level, and that they should be considered in this way. However, their participation in the total risk of disasters is also significant at the macro (national) level because it is accumulated at the local level and increases the risk at both the national and global level (UNDP, 2004).

Limitations of geomorphological method are the problem of intrazonality and the fact that this method determines the horizontal extent of the flood zone, while the vertical extent or depth of flooding is not detected. Geomorphological flood zone is not registered in areas where fluvial erosion processes dominate, and fluvial accumulation processes are absent. These are narrowed river valleys (canyons, gorges, epigenetic valleys) on whose steep valley sides there are elements exposed to floods (most often they are infrastructural objects - roads, railways). Such areas, depending on the water level, can be directly endangered by floods (with consequences such as casualties and material damage), or indirectly endangered by floods when they become isolated and have difficulty functioning because the flood affected the surrounding areas (Kovačević-Majkić 2018; Kovačević-Majkić et al. 2020). In that sense, it is necessary to upgrade this method, i.e. to solve the problem when there is only a vertical extent of the flood.

Presence of selected indicators could serve for fluvial and slope processes determination. In Table 3 we determined the fluvial and slope processes considering the presence of erosional, accumulation and morphometric indicators. If there are both erosional and accumulation processes, torrential floods are possible and certain, even if do not have data on flood events (registered floods). In watersheds without erosional processes and river network and flood zone are detected, floods are possible, but their character is not torrential (Table 3).

Therefore, type of present fluvial processes is an eliminatory factor for flood type determination. This fluvial process determination is important for water and flood management, meaning for the selection of measures that should be used for flood hazard mitigation.

CONCLUSIONS

Almost everyday cases of torrential floods with significant consequences around the world indicate that permanent water and flood management is necessary. This implies constant data collection and research of all risk components, including hazard, more precisely determining the extent of flood prone areas. The assumption in this research is that fluvial and slope processes and landforms in the watershed are relevant indicators for torrential flood hazard assessment. Eight selected indicators were grouped

Table 3. Possible fluvial and slope processes

Fluvial erosion	Fluvial accumulation	Watershed morphometry	Fluvial and slope process
+	+	+	Torrential flood
+	+	-	There is no such process[1]
-	+	+	Flood
-	+	-	There is no such process[2]
+	-	+	Proluvial and/or colluvial slope processes[3]
+	-	-	There is no such process[4]
-	-	+	Potential flood

1 – It is not possible that there are erosion and accumulation indicators and that there are no selected morphometric indicators of watershed
2 – This means that the erosion process is finished and that we have plain without slope
3 – These processes are present in upper parts of the watershed, i.e. in collection and/or transport zone of the watershed
4 – It is not possible that there are erosion indicators and that there are no selected morphometric indicators of watershed

into three segments: erosional process, morphometric characteristics of watershed, and accumulation processes and landforms. In three middle-sized watersheds in Serbia (Skrapež River, Belica River and Lužnica River watersheds), which belong to the Velika Morava River basin, selected indicators were detected, proving that rivers and their tributaries have torrential character. They indicate that torrential floods happened, and that there is probability that floods will happen again. Flood prone areas determined in this way are wider than those determined by hydrological-hydraulic methods, but it is on the side of safety and in accordance with holistic approach to watershed management. Presence of selected indicators also can help in flood and slope processes determination, and subsequently can be used for selection of measures for torrential flood hazard mitigation.

REFERENCES

Alcántara-Ayala I. (2002). Geomorphology, natural hazards, vulnerability and prevention of natural disasters in developing countries. Geomorphology, 47, 107-124, DOI: 10.1016/S0169-555X(02)00083-1

Arnell N. (2002). Hydrology and Global Environmental Change. London and New York: Pearson Education Limited. p 364.

Arnaud-Fassetta G. and Astrade L, et al. (2009). Fluvial geomorphology and flood-risk management. Géomorphologie, 15(2), 109-128, DOI: 10.4000/geomorphologie.7554

Brajković M. and Gavrilović Z. (1989). Natural and anthropogenous factors important for flash floods apearance. Collection of papers from conference „Flash floods – causes and consequences". JUSOP 89, Kopaonik, Serbia: 46-53. (in Serbian)

Borga M., Stoffel M., Marchi L., Marra F, and Jakob M. (2014). Hydrogeomorphic response to extreme rainfall in headwater systems: Flash floods and debris flows. Journal of Hydrology, 518, 194-205, DOI: 10.1016/j.jhydrol.2014.05.022

Costa J.E. (1988). Rheologic, geomorphic, and sedimentologic differentiation of water floods, hyperconcentrated flows and debris flows. In: V.R. Baker, R.C. Kochel, and P.C. Patton, eds., Flood Geomorphology, 7. John Wiley & Sons, Chichester, England: 113–122.

Coussot P. and Meunier M. (1996). Recognition, classification and mechanical description of debris flows. Earth-Science Reviews, 40, 209-227, DOI: 10.1016/0012-8252(95)00065-8

Directive 2000/60/EC of the European Parliament and of the Council establishing a framework for Community action in the field of water policy. (EU Water Framework Directive). (2000). Official Journal of the European Union L 327, 22.12.2000, pp. 0001 - 0073

Directive 2007/60/EC on the European Parliament and of the Council on the assessment and management of flood risks (EU Flood directive). (2007). Official Journal of the European Union L288, 6.11.2007, pp. 27-34

Dragicevic S., Filipovic D., Kostadinov S., Ristic R., Novkovic I., Zivkovic N., Andjelkovic G., Abolmasov B., Secerov V., and Djurdjic S. (2011). Natural Hazard Assessment for Land-use Planning in Serbia. Int. J. Environ. Res., 5(2), 371-380, DOI:10.22059/IJER.2011.322

Gavrilović Lj., Milanović Pešić A., and Urošev M. (2012). A Hidrological Analysis of the Greatest Floods in the Serbia in the 1960-2010 Period. Carpathian Journal of Earth and Environmental Sciences, 7(4):107-116.

National Research Council (2011). Global Change and Extreme Hydrology: Testing Conventional Wisdom Washington, DC: National Research Council, The National Academies Press.

Gavrilović Lj. (1981). Poplave u Srbiji u 20. veku - uzroci i posledice (Floods in Serbia in XX century – causes and consequences). Posebno izdanje SGD, no 52. Belgrade

Gavrilović S. (1972). Inženjering o bujičnim tokovima i eroziji (Engineering of torrents and erosion). Izgradnja – special issue, Belgrade.

Gavrilović Z., Stefanović M., Milovanović I., Milojević M., and Jurišić S. (2009). Achieved results of the fight against torrential floods and soil erosion. In: D. Isailović and S. Petković, eds. Water resources management in Serbia '09. Institute for Water resources Management „Jaroslav Černi". Belgrade: 233-244. (in Serbian)

Gradel A., Sukhbaatar G., Karthe D., and Kang H. (2019). Forest Management In Mongolia – A Review Of Challenges And Lessons Learned With Special Reference To Degradation And Deforestation. Geography, Environment, Sustainability, 12, (3), 133-166, DOI-10.24057/2071-9388-2019-102

Gosling S. and Arnell N. (2013). A global assessment of the impact of climate change on water scarcity. Climatic Change, 134, 371–385. DOI: 10.1007/s10584-013-0853-x

Hartmann D.L, Klein Tank A.M.G, Rusticucci M, Alexander L.V., Brönnimann S., Charabi Y., Dentener F.J., Dlugokencky E.J., Easterling D.R., Kaplan A., Soden B.J., Thorne P.W., Wild M., and Zhai P.M. (2013). Observations: Atmosphere and Surface. In: T.F. Stocker, D. Qin, G.-K. Plattner, M.Tignor, S.K. Allen, J. Boschung, A. Nauels, Y. Xia, V. Bex, and P.M. Midgley, eds. Climate Change 2013: The Physical Science Basis. Contribution of Working Group I to the Fifth Assessment Report of the Intergovernmental Panel on Climate Change. Cambridge University Press, Cambridge, United Kingdom and New York, NY, USA.

EM-DAT (2024). Number of global reported natural disaster and economic damages. http://www.emdat.be [Accessed 30 Apr. 2024].

Jakob M. and Hungr O. (2005). Debris-flow hazards and related phenomena. Berlin: Springer-Praxis. p 731.

Kompare B. and Rismal M. (1989). Analysis of the causes of floods in Nova Gorica and protection measures taken. Collection of papers from conference „Flash floods – causes and consequences". JUSOP 89, Kopaonik, Serbia: 244-254. (in Serbian)

Kovačević-Majkić, J. (2009). Hidrogeografska studija reke Skrapež (Hydrogeographical study of the Skrapež River). Belgrade: Geographical institute „Jovan Cvijić" SASA and The Serbian Geographical Society. p 133. (in Serbian with English summary)

Kovačević-Majkić J., Urošev M., Štrbac D., and Milanović Pešić A. (2013). Torrential Floods Prevention Possibilities – Case Study of the Skrapež River watershed (Western Serbia). In: B. Raskovic, and S.Mrdja, eds. Natural Disasters: Prevention, Risk Factors and Management. Nova Science Publishers, Inc. New York: 175-202

Kovačević-Majkić J. (2018). Torrential flood risk assessment. PhD thesis, Belgrade University, Faculty of Geography, Belgrade. p 220. (in Serbian with English summary)

Kovačević-Majkić J., Miljanović D., and Doljak D. (2020). Spatial aspects of flood exposure in Serbia. In A. Milanović Pešić and D. Jakovljević, Eds. Water Resources Management: Methods, Applications and Challenges. Nova Science Publishers, Inc. New York: 69–122.

Mazzorana B., Comiti F., and Fuchs, S. (2013). A structured approach to enhance flood hazard assessment in mountain streams. Natural Hazards, 67(3), 991-1009, DOI: 10.1007/s11069-011-9811-y

Menković M. and Košćal M. (1981), Interpretation for the Geomorphological map of Serbia 1:100,000. Sheets: Zvornik, Vladimirci, Ljubovija, Valjevo, and Gornji Milanovac. Belgrade: Fond of expert documents of the Geological Institute of Serbia (in Serbian)

Menković Lj. and Košćal M. (1982). Interpretation for the Geomorphological map of Serbia 1:100,000. Sheets: Višegrad, Titovo Užice, Čačak, Kraljevo, and Paraćin. Belgrade: Fond of expert documents of the Geological Institute of Serbia (in Serbian)

Menković Lj., Košćal M., and Mijatović M. (1988). Interpretation for the Geomorphological map of Serbia 1:100,000. Sheets: Bela Palanka, Pirot, Breznik, and Vlasotince. Belgrade: Fond of expert documents of the Geological Institute of Serbia (in Serbian)

Milić Č. (1984). Fossil and recent fans in the valley system of the Vlasina River. Journal of The Geographical Institute Cvijić, 36, 49-76 (in Serbian)

Milošević M.V., Ćalić J., Kovačević–Majkić, J., and Petrović, A. (2015). Geomorphological indicators of natural disasters – case study of Tekija mudflow in 2014 (eastern Serbia). In D. Filipović, V. Šećerov, and Z. Radosavljević, eds. Planned and normative protection of space and environment. VIII scientific-professional conference with international participation. Belgrade: Serbian Spatial Planners Association and University of Belgrade - Faculty of Geography: 563–570 (in Serbian with English summary)

Mrvić V., Antonović G., Čakmak D., Perović V., Maksimović S., Saljnikov E., and Nikoloski M. (2013). Pedological and pedogeochemical map of Serbia. Proceedings of The First International Congress on Soil Science and XIII National Congress in Soil Science "Soil-Water-Plant". Beograd: 93-104

Nolos R.C., Zamroni A., and Evina K.P. (2022). Drivers Of Deforestation And Forest Degradation In Palawan, Philippines: An Analysis Using Social-Ecological Systems (SES) And Institutional Analysis And Development (IAD) Approaches. Geography, environment, sustainability, 15(4), 44-56. https://doi.org/10.24057/2071-9388-2022-081

Official Gazette of RS 86/11 (2011) National strategy for protection and rescue in emergency situations. Belgrade (in Serbian)

Petrović A., Kostadinov S., and Dragićević S. (2014). The Inventory and Characterization of Torrential Flood Phenomenon in Serbia. Pol. J. Environ. Stud., 23(3), 823-830

Radović R. and Todorović N. (1989). Announcement of flood wave on small watercourses by MRL-5 meteorological radar. Analysis of the causes of floods in Nova Gorica and protection measures taken. Collection of papers from conference „Flash floods – causes and consequences". JUSOP. 89, Kopaonik, Serbia. pp 191-198. (in Serbian)

Ristić R. and Malošević D. (2011). Hydrology of torrential watercourses. Belgrade: Faculty of Forestry (in Serbian)

Ristić R., Kostadinov S., Abolmasov B., Dragićević S., Trivan G., Radić B., Trifunović M., and Radosavljević Z. (2012). Torrential floods and town and country planning in Serbia. Nat. Hazards Earth Syst. Sci., 12, 23-35, DOI: 10.5194/nhess-12-23-2012

Shiklomanov I.A. and Rodda J.C., eds. (2003). World Water Resources at the Beginning of the 21st Century. Cambridge: Cambridge University Press. p 435.

Shimizu Y, Tokashiki N, and Okada F. (2002). The September 2000 Torrential Rain Disaster in the Tokai Region: Investigation of a mountain disaster caused by heavy rain in three prefectures; Aichi, Gifu and Nagano. Journal of Natural Disaster Science, 24(2), 51-59

Stojkov K., Šušić N., and Šijaković J. (1998). Geological hazards and risks. Announcements from the XIII Congress of Geologists of Yugoslavia, book V - Hydrogeology and engineering geology. Herceg Novi, Montenegro: 461-467. (in Serbian)

UN, EU, and World bank group (2014). Poplave u Srbiji 2014 (Floods in Serbia 2014). Belgrade, p.176

UNDP Bureau for Crisis Prevention and Recovery (2004). Reducing Disaster Risk: A Challenge for Development. A Global Report. Pelling M, Maskrey A, et al., eds. USA: John S. Swift Co. p 146.

Varazanashvili O., Tsereteli N., Amiranashvili A., Tsereteli E., Elizbarashvili E., Dolidze J., Qaldani L., Saluqvadze M., Adamia S., Arevadze N., and Gventcadze A. (2012). Vulnerability, hazards and multiple risk assessment for Georgia. Natural Hazards, 64:2021-2056. DOI: 10.1007/s11069-012-0374-3

Vujisić T, Kalenić M, Navala M., and Lončarević Č. (1981). Interpretation for the Basic Geological map, sheet Lapovo. Belgrade: Federal Geological Survey (in Serbian)

Vujisić T, Navala M, Kalenić M, Krstić B, Maslarević Lj, Marković B, and Buković J. (1980). Interpretation for the Basic Geological map, sheet Bela Palanka. Belgrade: Federal Geological Survey (in Serbian)

Wang L., Zhang Z., and Klaghofer E. (1996). Torrent classification and hazard zone mapping with GIS in the PR China. Internationales Symposion, Interpraevent 1996. Tagungspublikation 3, Garmisch-Partenkirchen, Deutschland: 5-18.

Zhou Y., Liu Y., Wu W., and Li N. (2015). Integrated risk assessment of multi-hazards in China. Natural Hazards, 78, 257-280, DOI: 10.1007/s11069-015-1713-y

Zhuang Y., Du C., Zhang L., Du Y., and Li, S. (2015). Research trends and hotspots in soil erosion from 1932 to 2013: a literature review. Scientometrics 105, 743–758. https://doi.org/10.1007/s11192-015-1706-3

Check for updates

CC BY

RESEARCH PAPER

WATER REGIME VARIABILITY OF SELECTED RIVERS ON THE BALKAN PENINSULA: A COMPARATIVE STUDY OF CENTRAL SERBIA AND NORTHERN REGION OF MONTENEGRO

Ana Milanović Pešić[1*], Dejana Jakovljević[1], Golub Ćulafić[2], Milovan Milivojević[1]

[1] Geographical Institute "Jovan Cvijić" Serbian Academy of Sciences and Arts, Djure Jakšića 9, 11000, Belgrade, Serbia

[2] Institute of Hydrometeorology and Seismology, IV Proleterske 19, 81000 Podgorica, Montenegro

***Corresponding author:** a.milanovic@gi.sanu.ac.rs

Received: May 18th 2024 / Accepted: November 22nd 2024 / Published: December 31st 2024

https://doi.org/10.24057/2071-9388-2024-3404

ABSTRACT. River discharge and its variations are often the subject of research from different aspects. This study aims to examine the discharge variability of selected rivers in central Serbia and the northern part of Montenegro, which belong to the Danube River basin (Black Sea Drainage basin). In general, all these rivers have uneven water regimes, a large share of evaporation in the water balance during the year, and very low values in discharges in the summer. In this regard, an analysis of mean annual and monthly discharge changes in ten hydrological stations from nine rivers in the 1961–2020 period was made. By using the t-test, a comparison of two 30-year periods (1961–1990 and 1991–2020) was made to examine if there were significant changes in the discharges. The obtained results indicate that in all rivers, annual discharge decreased in the second period compared to the earlier one, and a statistically significant decrease is recorded in 3 rivers, Lepenica, Lugomir and Lim. Changes in monthly discharges between the two 30-year periods are statistically very significant in the summer period in the selected rivers of Montenegro. In contrast they are not statistically significant in selected rivers of Serbia, with several exceptions in spring and autumn. The obtained results indicate mainly a statistically significant discharge decreasing in the second period, which is primarily correlated with a significant increase in air temperature. As discharge changes influence water resource management, the results obtained in this study are important for decision-makers.

KEYWORDS: discharge variability, air temperature, precipitation, t-test, Serbia, Montenegro

CITATION: Milanović Pešić, A., Jakovljević D., Ćulafić G., Milivojević M. (2024). Water Regime Variability of Selected Rivers on The Balkan Peninsula: A Comparative Study of Central Serbia and Northern Region of Montenegro. Geography, Environment, Sustainability, 4(17), 35-43

https://doi.org/10.24057/2071-9388-2024-3404

ACKNOWLEDGEMENT: This study was supported by the Ministry of Science, Technological Development and Innovation of the Republic of Serbia (Contract No. 451-03-66/2024-03/200172).

Conflict of interests: The authors reported no potential conflict of interest.

INTRODUCTION

Water resources are the subject of various hydrological studies worldwide, mainly due to potential water scarcity. Water quantity is usually analysed throughout discharge changes and variability. Long-term changes in discharges are often estimated by comparing two periods (Georgiadi et al. 2023). Changes in discharges (both increase and decrease) cause many consequences. Temporal and spatial variations in discharges impact on river morphology (Miao et al. 2010). Discharge decrease affects water supply, reduces crop production, and causes problems in river transportation and hydroelectric production (Souza and Reis 2022; Balistrocchi et al. 2021), while its prolonged duration leads to hydrological drought (Leščešen et al. 2020; Urošev et al. 2016). On the other hand, discharge increase often contributes to river bank erosion (Kärkkäinen and Lotsari 2022; Moody 2022; Gao et al. 2021; Brown et al. 2020; Botero-Acosta et al. 2017; DiBiase and Whipple 2011; Larsen et al. 2006) and an augmented risk of flooding, especially in the regions where climate change induced increase in precipitation quantity is expected. According to Langović et al. (2021), variations of discharge values (extremely high or low discharges) are the most important natural factor of riverbank erosion intensity and soil loss. Increased discharges often lead to floods, which further cause infrastructure damage, transportation disruption, and loss of human lives and property (Souza and Reis 2022; Petrović 2015).

Mean annual and seasonal discharge trends were analysed on 94 hydrological stations in Serbia from 1961 to 2010. Results of this study show negative annual, spring, winter and summer trends and positive trends on most stations in autumn and at a small number of stations in winter (Kovačević-Majkić and Urošev 2014). Đorđević et al. (2020) forecasted decreasing average annual discharges in

the river basins of Velika, Zapadna and Južna Morava, Ibar, Timok and Drina with especially negative distribution of seasonal discharges in the vegetative period, from July to October for the following three periods: 2011–2040, 2041–2070, and 2071–2100, comparing with the reference period 1971–2000. Haddeland et al. (2013) projected increased maximum values of discharges in the Kolubara River basin and no increase in the peak annual discharges in the Toplica River basin for the periods 2001–2030 and 2071–2100, compared with the reference period 1961–1990. Also, this study forecasted an increase in drought events in both the Kolubara and Toplica river basins at the end of the 21st century (Haddeland et al. 2013). Dragićević et al. (2013) determined the maximum discharge probability for the Kolubara River and its tributaries in order to assess future flood impacts on bank erosion. Kolubara River has the highest coefficient of discharge variation among the Serbian rivers, which causes a significant impact on river bank erosion (Dragićević et al. 2017). Radulović et al. (2014) analysed the river regime of the Temštica River basin in south-east Serbia for the period 1980–2012. Results of this study showed that maximum discharges occurred in April, while the minimum discharges were recorded in September (Radulović et al. 2014). Milanović Pešić (2019) analysed the water regime and discharge trends of rivers in the Šumadija Region for the period 1961–2019 and concluded that these rivers have low amounts of water, especially in summer, with the lowest discharges in August and September and the highest discharges in March and April.

Despite the richness of water, due to the influence of geological features (karst terrains cover over 60% of the territory), rivers in Montenegro have a significantly uneven distribution of water regimes during the year. In rainy seasons, discharges could reach a thousand times higher values compared with the dry seasons (Sekulić and Radulović 2019). Rajović and Bulatović (2014) also stated spatial and temporal discharge variability in north-eastern Montenegro. According to this study, the maximum discharge of Lim River, which occurs in May, is about six times higher than the minimum discharge in September (Rajović and Bulatović 2014).

This study aims to address discharge changes in annual and monthly discharges of rivers in the Šumadija Region in Serbia and the Lim River basin in Montenegro for the periods 1961–1990 and 1991–2020. Also, the paper aims to analyse the impact of various factors (climate changes, land cover and use, anthropogenic impacts), as well as to explain how discharge changes impact on erosion and human activities.

MATERIALS AND METHODS

The study area

The study area includes seven rivers in the central part of Serbia and two rivers in the northern part of Montenegro (Fig. 1). All rivers belong to the Black Sea Drainage Basin and are characterized by a natural regime with no or minor hydropower and hydromorphological alteration, which makes them suitable for comparative analysis of changes in discharge trends. In Serbia, the following rivers were selected: Kubršnica (48 km, 743.2 km^2), Lepenica (55.4 km, 638.9 km^2), Belica (36.8 km, 222.7 km^2), Lugomir (19.5 km, 447.7 km^2), Čemernica (41 km, 625 km^2), Peštan (32.1 km, 171 km^2) and Ljig (31.3 km, 559.4 km^2). These rivers are located in the Šumadija Region, one of the central areas of Serbia. The high abundance of Neogene sediments causes landslides and erosion in this area. Šumadija Region is a lowland area because 91.6% of this territory is below 500 m a.s.l. (Milanović Pešić 2015). This area is characterized by a moderate continental climate with a continental pluviometric regime, which indicates that the maximum precipitation is registered in May and June. In the period 1961–2010, the mean annual temperature was 11–11.6 ºC at most meteorological stations in this area (Milanović Pešić and Milovanović 2016), and the mean annual precipitation ranged between 700 and 800 mm (Milovanović et al. 2017a). According to Milovanović et al. (2017b), who modified Köppen's classification for Serbia, Cfaq climate is present in the largest part of the Šumadija Region, and Dfbq on lowland terrains. The selected rivers have a pluvio-nival regime, with frequent occurrence of extreme water discharges.

In Montenegro, the Lim River (123 km, 2807 km^2) and its tributary Ljubovidja (35.8 km, 351 km^2) were selected (Hrvačević, 2004). Hydrologically, the Lim River is the most significant river in Montenegro. Its total length is 219 km, of which 123 km are in the territory of Montenegro (Ćulafić, 2020). The rest of this river basin is located in Serbia, and a small part of it is in Bosnia and Herzegovina. In this study, only the data of Lim River was analysed in Montenegro because four hydropower plants were built in the Lim River basin in Serbia, which affects the river regime. In Montenegro, the Lim River basin is located in the northeastern part of the country (600–1500 m a.s.l.) (Fig. 1), framed by high mountains (Komovi, Prokletije and Bjelasica). These mountains are dissected by streams and rivers that are Lims tributaries. Considerable parts of the area are underlain by clastic and flysch, clayey-sandy-marly sediments. Therefore, landslides and degradation processes often occur in this territory (Radojičić 2008). The Lim River basin has a moderate continental climate, which belongs to the following types by Köppen's classification: Cfsb, Cfb, Cfws"bx' and Dfbx., with cold winters (-1.2ºC) and mild summers (17.7–19.1ºC) (Burić et al. 2012). Mean annual air temperature values rangesfrom 8.4 to 9.4ºC, while precipitation ranges from 900 to 1004 mm. Maximum precipitation occurs in November and minimum in August. The Lim River and its tributaries have the nival-pluvio regime (Dukić and Gavrilović 2008), with the highest water discharge in May, April and June, and the lowest in August and September.

Data

The discharge dataset for the selected rivers was analysed based on mean annual and monthly values in the 1961–2020 period from seven hydrological stations in Serbia and three hydrological stations in Montenegro. They are: Bogovađa (Ljig River), Zeoke (Peštan River), Preljina (Čemernica River), Smederevska Palanka (Kubršnica River), Batočina (Lepenica River), Jagodina (Belica River) and Majur (Lugomir River) in Serbia; and Plav (Lim River), Bijelo Polje (Lim River) and Ravna Rijeka (Ljubovića River) in Montenegro. The criteria for selecting the hydrological stations implied that they are located on rivers with almost natural regimes and had continuity in long-term measurements of the discharge. Data were collected from hydrological yearbooks of the Republic Hydrometeorological Service of Serbia (RHSS) and the Institute of Hydrometeorology and Seismology (IHMS) of Montenegro. At the stations where small recording gaps were observed during 60-year measurements (for a particular month or year), the data were obtained from neighbouring stations the best correlation on a monthly basis.

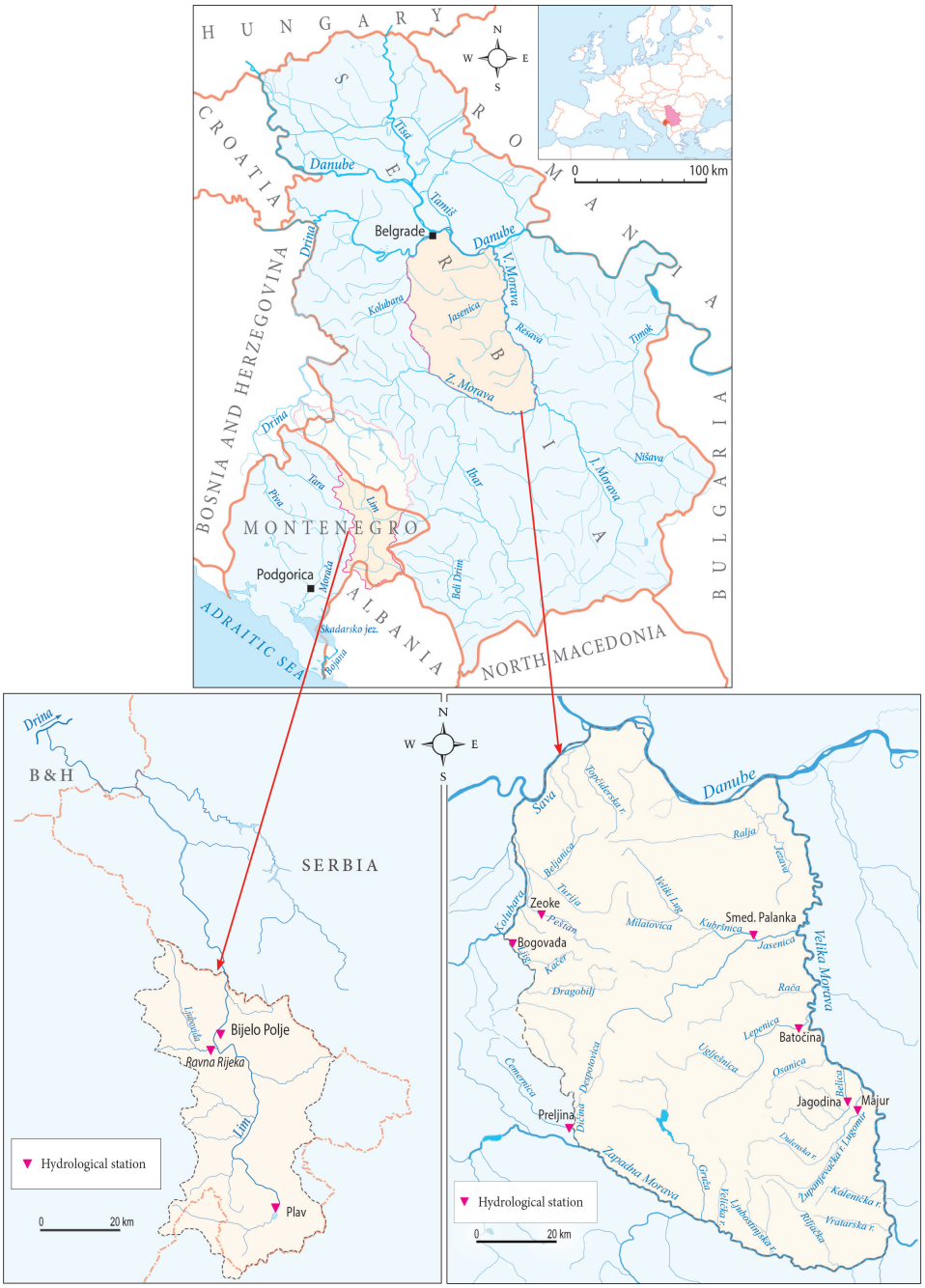

Fig. 1. Study area

Methodology

Previous analysis of the discharge datasets by using the non-parametric Mann–Kendall test and Sen's slope showed water regime variation in some rivers in the Šumadija Region in Central Serbia (Milanović Pešić 2019). In addition, it was observed that a significant change in annual and seasonal discharge occurred around 1990. Hence, the discharge datasets can be divided into two 30-year periods (1961–1990 and 1991–2020) for further analysis. These two data subsets can be used to assess whether there were statistically significant changes in annual and monthly discharge, as well as the level of difference in the two time periods. By using a t-test, discharge values were compared in these two periods to estimate differences in distributions. Calculations were performed for statistical significance specified at the 99% (p value≤0.01) and 95% (0.01<p value≤0.05) levels applying Paired-Samples t-tests within the SPSS Statistics 20.

As the t-test enables to examine whether the means of two subsamples are statistically different (Zheng et al. 2007), it is commonly accepted and often used in hydrological studies. Among others, it was applied for trend analysis in annual maximum, mean and 1-day and 7-day low discharge of rivers in 24 hydrological regions of Turkey (Cigizoglu et al. 2004), for identifying the trends and change points in discharge, precipitation and potential evapotranspiration in Taoer River in China (Li et al. 2010), to examine trend and abrupt changes in discharge regime of the Yellow River (Zheng et al. 2007) and East River in China (Zhang et al. 2012), to determine the statistical significance of the daily discharge variability and trends of Mackenzie River in Canada (Yang et al. 2015) and for analysing runoff variability due to land use changes in Puhe River Basin in China (Zhang and Yu 2020).

RESULTS

Annual discharge variability

In this study, rivers of various mean discharges are selected for analysis. For all selected rivers in Serbia, results

showed a decrease in mean annual discharge in the latter period compared to the earlier one (Fig. 2). This decrease in the Lepenica and Lugomir rivers is statistically very significant (Table 1). These findings are in line with some other studies. Kovačević-Majkić and Radovanović (2006) stated that discharge decrease of the Ljig River in the period 1993–2003 compared with the period 1961–1989. Milanović Pešić (2019) found a decreasing trend in the annual discharge of the Lepenica River for 55-year periods.

The results in Montenero showed a decrease in annual discharge in the latter period compared to the earlier one (Fig. 3). This decrease in the Lim River is statistically significant (Table 3). These results are similar to those of Spalević et al. (2016) findings, who concluded that the discharge peak of the Seoski Potok in Lim River basin decreased from 1975 to 2015, due to changes in vegetation cover. Forest increase in the period from 1975 to 2020 also caused discharge decrease in Miocki Potok basin in the upper Lim River basin (Spalević et al. 2020).

Monthly discharge variability

The inter-annual distribution of discharges shows that the maximum discharge in the rivers in Serbia is recorded mainly in March and the minimum discharge mainly in September. In general, river discharge decreases from March to September and increases from October to March. It is interesting to note that, in the first period, in two rivers (Ljig and Peštan) the maximum discharges were recorded in February, while in the second period, they were recorded in March, and the lowest discharge recording moved from the autumn months (September and October) to August. The possible reason for the maximum discharge move could be the result of increased amount of monthly precipitation and heavy rainfall in March and the minimum discharge move by extremely high air temperatures and the absence or little precipitation. At the meteorological station Kragujevac, located in Šumadija Region, amount of precipitation in March increased from 44.4 mm in the first period to 46.6 mm in the second period. At the same station, temperature in February increased from 2.2 °C in the first period to 3°C in the second period (Jovanović et al. 2023). Sudden snow melt, followed by heavy rainfall in early spring, mainly in March, also contributed the highest discharges in this month (Petrović et al. 2024). The shift of the lowest discharge from autumn to August is caused by increased temperatures in July and August and decreased precipitation from May to July in the second period. At

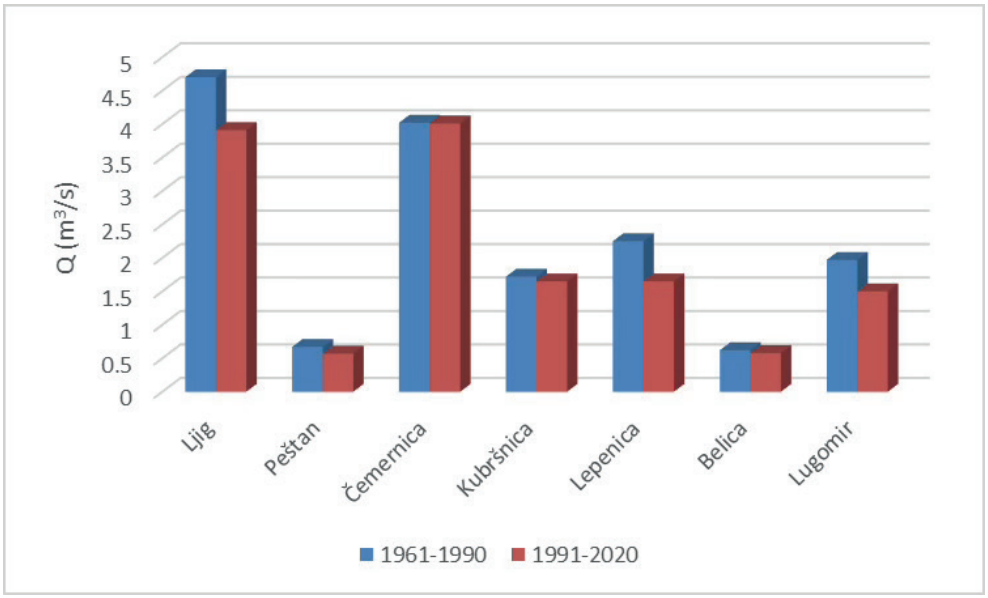

Fig. 2. Mean annual discharges (m³/s) at the selected rivers in Serbia in 1991–2020 relative to 1961–1990

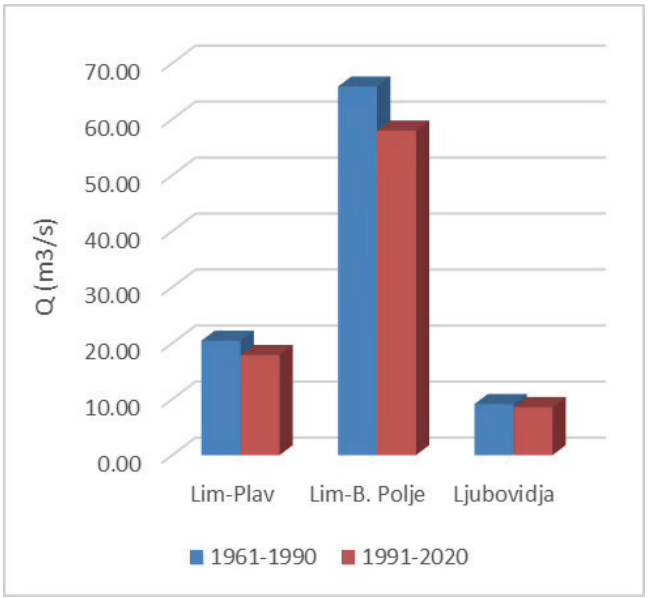

Fig. 3. Mean annual discharges (m³/s) at the selected rivers in Montenegro in 1991–2020 relative to 1961–1990

the meteorological station Kragujevac, temperatures increased from 20.6 °C in the first period to 22.6 °C in the second period in July and from 20.2 °C to 22.3 °C in the second period in August. Comparing these two periods, the amount of precipation decreased in the second period from: 73.8 mm to 70.3 mm in May, 84.7 mm to 77.2 mm in June, and 68 mm to 65.8 mm in July (Jovanović et al. 2023).

In the 1991–2020 period, all rivers experienced a discharge decrease from January to June and a slightly increased from July to December compared to the 1961–1990 period (Table 1).

According to the results obtained in Table 1, the changes in monthly discharges between two thirty-year periods are generally not statistically significant, but there are some exceptions. A significant decrease ($p \leq 0.01$) in discharge was observed on the Lepenica River in February and May and on the Lugomir River in June and September. In addition, a significant decrease ($p \leq 0.05$) was registered at Lepenica River in January and March. Contrary to that, a significant increase ($p \leq 0.05$) in discharge was observed on the Kubršnica River in September and October and Peštan River in October, which can be related to significant precipitation. For example, at rain gauge Mihajlovac, near Kubršnica River, daily amount of precipitation recorded 15 September, 2014 were 180.3 mm, which was the absolutely maximum for the whole period of measurement of 57 years (Petrović. 2021).

Table 1. Mean monthly and annual discharges (m^3/s) at the selected rivers in 1991–2020 relative to 1961–1990

Station	Period	I	II	III	IV	V	VI	VII	VIII	IX	X	XI	XII	Year
Bogovađa	Ljig River													
	1961–1990	5.33	9.86	9.61	6.85	6.88	5.81	2.56	1.09	0.93	0.97	2.20	4.32	4.7
	1991–2020	4.30	6.82	9.03	5.53	4.60	3.90	2.58	1.22	1.28	1.55	2.24	3.83	3.91
	Difference	1.03	3.04	0.58	1.32	2.28	1.91	-0.02	-0.13	-0.35	-0.58	-0.04	0.49	0.8
Zeoke	Peštan River													
	1961–1990	0.82	1.50	1.35	0.74	0.97	0.95	0.32	0.36	0.15	0.13	0.27	0.55	0.68
	1991–2020	0.68	0.91	1.04	0.79	0.76	0.48	0.41	0.20	0.24	0.25	0.40	0.66	0.57
	Difference	0.14	0.59	1.31	-0.05	0.21	0.47	-0.09	0.16	-0.09	-0.12	-0.13	-0.11	0.11
Preljina	Čemernica River													
	1961–1990	4.39	7.25	7.71	5.16	6.58	4.68	2.29	1.48	1.30	1.49	2.32	3.63	4.02
	1991–2020	3.78	6.23	8.80	5.87	5.03	3.73	2.89	1.65	1.71	2.00	2.58	3.67	3.99
	Difference	0.61	1.02	-1.09	-0.71	1.55	0.95	-0.6	-0.17	-1.41	-0.51	-0.26	-0.04	0.02
Smed. Palanka	Kubršnica River													
	1961–1990	1.76	4.33	3.71	2.28	2.22	2.35	0.77	0.37	0.32	0.40	0.67	1.16	1.7
	1991–2020	2.05	3.21	3.57	2.01	1.77	1.52	1.47	0.62	0.49	0.63	0.79	1.65	1.65
	Difference	0.29	1.12	1.14	0.27	0.45	0.83	-0.7	-0.25	-0.17	-0.23	-0.12	-0.49	0.05
Batočina	Lepenica River													
	1961–1990	1.98	3.71	4.45	2.88	2.95	2.72	1.43	1.43	1.08	1.12	1.39	1.82	2.25
	1991–2020	1.45	2.17	2.49	2.26	1.65	1.93	1.80	1.22	1.11	1.08	1.15	1.45	1.65
	Difference	0.53	1.54	1.96	0.62	1.30	0.79	-0.37	0.21	-0.03	0.04	0.24	0.37	0.60
Jagodina	Belica River													
	1961–1990	0.67	1.17	1.35	0.88	0.95	0.67	0.30	0.19	0.18	0.23	0.33	0.50	0.62
	1991–2020	0.59	0.87	1.07	1.02	0.83	0.66	0.42	0.26	0.17	0.25	0.31	0.51	0.58
	Difference	0.08	0.30	0.28	-0.14	0.12	0.01	-0.12	-0.07	0.01	-0.02	0.02	-0.01	0.04
Majur	Lugomir River													
	1961–1990	2.01	3.62	4.53	3.01	2.90	2.51	0.93	0.66	0.53	0.54	0.87	1.51	1.97
	1991–2020	1.48	2.58	3.67	2.84	2.22	1.27	0.89	0.42	0.31	0.50	0.59	1.24	1.50
	Difference	0.53	1.04	0.86	0.17	0.68	1.24	0.04	0.24	0.22	0.04	0.28	0.27	0.47

Statistical significance – $p \leq 0.01$ and $p \leq 0.05$

On Lim River in Montenegro, the maximum discharge is observed in May and in its tributary Ljubovića in April. The minimum discharges were recorded mainly in August. Generally, river discharge decreases from December to February, increases from March to April or May, then decreases by August, and increases from September to December. By comparing two thirty-year periods, it was noted that at the upstream hydrological station Plav, the minimum discharge was moved from September to August in the later period. At the downstream hydrological station Bijelo Polje, the maximum discharge moved from May to April. The recording of maximum discharge in April at this station coincides with secondary maximum of precipitation amount, contributed by the earlier snow cover melting in the downstream sector of the Lim River basin due to the increased trend in air temperature. The lowest discharges coincide with the lowest amount of precipitation and highest air temperatures (Ćulafić and Krstajić, 2024).

According to the inter-annual distribution, discharge generally decreased in almost all months, except March (and April in one station) and December in 1991–2020 compared to 1961–1990.

According to the results, the decrease in monthly discharges between two thirty-year periods is statistically very significant from May to August in the Lim River and August on the Ljubovidja River. Also, a significant decrease ($p \leq 0.05$) was registered at Ljubovića River in July. During the other months, changes in monthly discharges are not statistically significant (Table 2).

DISCUSSION

Studies worldwide found discharges correlation with climate variation, such as air temperature, precipitation, snow cover melting, as well as anthropogenic activities. General decrease of discharges is caused by global change, such as precipitation, land use change and increase of water consumption (Billi and Fazzini, 2017). The discharge decrease resulting from this study indicate its correlation with the variability of climatic elements, especially with air temperature. In the Šumadija Region, for instance, a statistically significant increase in air temperature was recorded in the 50 year period. According to Milanović Pešić and Milovanović (2016), the calculated trends of mean annual air temperatures in the Šumadija Region for 1961–2010 indicate a statistically significant increase in almost all meteorological stations and ranges from 0.02 to 0.04 °C/year. The absolute maximum air temperature trends have a statistically significant increase in half of the analyzed stations and range from 0.05 to 0.07 °C/year. At the monthly level, the calculated trends of mean air temperatures in July and August showed that almost all stations have a statistically significant increase (0.04 to 0.07 °C/year), while the trends of the mean air temperatures in January are not statistically significant, although is recorded slight temperature increasing.

Regarding precipitation, the calculated changes in Serbia ranged from -2 mm to +2 mm/year from 1961–2010, and there is no statistically significant trend (Milovanović et al. 2017a). In the Šumadija Region, a decrease in the mean annual precipitation was observed in parts of the Zapadna Morava River basin (from Kraljevo to Prokuplje). At the same time, in the rest of the area, there was an increase in the mean annual precipitation. As regards the spring and summer precipitation, there were no statistically significant changes in the observed period. In the entire territory of Serbia, a slight decrease in precipitation in spring and a slight increase in precipitation in summer were observed. In addition, a slight increase in precipitation is recorded during autumn and winter (Milovanović et al. 2017a). Analyzing the water balance in Serbia, it was calculated that about 75% of the precipitation evaporates. Considering air temperature increasing, evaporation is even more pronounced, which has an unfavourable effect on discharge. This trend is also observed in Region Šumadija, and it was calculated that about 81.4% of precipitation evaporates in the Lepenica River basin (Milanović 2007). Therefore, it can be concluded that the discharge decrease in the selected river of Region Šumadija is mainly influenced by significant air temperature increases. In addition, a decrease in discharge could be caused by human activities, including land cover change, urbanization, and population increase. As it was stated by Vuksanović-Macura et al. (2018), in the 20th century,

Table 2. Mean monthly and annual discharges (m^3/s) at the selected rivers in 1991–2020 relative to 1961–1990

Station	Period	I	II	III	IV	V	VI	VII	VIII	IX	X	XI	XII	Year
Plav	Lim River													
	1961–1990	15.62	14.08	15.64	32.46	46.04	31.18	15.45	8.17	7.91	14.78	22.67	21.33	20.44
	1991–2020	15.07	12.57	16.67	31.43	37.09	20.91	9.78	4.90	6.70	12.81	22.60	24.17	17.89
	Difference	0.55	1.49	-1.03	1.03	**8.95**	**10.27**	**5.67**	3.27	1.21	1.97	0.07	-2.84	2.55
Bijelo Polje	Lim River													
	1961–1990	61.05	61.72	72.34	120.60	136.32	77.99	36.46	20.69	22.77	38.77	64.88	76.27	65.82
	1991–2020	52.62	50.49	77.92	119.45	109.23	53.07	23.54	15.27	20.40	33.89	62.02	77.70	57.97
	Difference	8.43	11.23	-5.58	1.15	**27.09**	**24.92**	**12.92**	**5.42**	2.37	4.88	2.86	-1.43	7.85
Ravna Rijeka	Ljubovića River													
	1961–1990	9.93	11.16	12.71	17.02	13.47	7.75	4.29	2.96	3.26	5.61	9.39	11.87	9.12
	1991–2020	9.03	8.50	13.55	17.16	12.26	6.65	3.38	2.03	2.63	4.78	9.83	13.23	8.59
	Difference	0.90	2.66	-0.84	-0.14	1.21	1.1	0.91	**0.93**	0.63	0.83	-0.44	-1.36	0.53

Statistical significance – **$p \leq 0.01$** and $p \leq 0.05$

the population in the Šumadija Subregion of the capital Belgrade area increased from 68,480 to 930,000, forest and agricultural areas gradually decreased, and artificial land cover increased from 6.0% to 34.6% of the subregion area, which was an increase of 479.7%. Based on the results of Drobnjaković et al. (2021), changes in the population of the Šumadija Region and the type of settlement took place in favour of urban settlements from 1948 to 2011. The most intensive migrations occurred in 1961–1981 when the urban population of several municipalities increased by up to 50%. Demographic changes and intensive urbanization also caused changes in the land cover.

Our results and interpretations are in line with several studies provided for other areas of Serbia. These studies examined the connection of discharges with precipitation, air temperatures and human influence, as well as the consequences of discharge changes on human activities. Krtolica et al. (2024) concluded that decreasing annual discharge trends were observed in many rivers in Serbia, including Velika Morava, Nišava, Južna Morava, Timok and Toplica rivers, as a consequence of climate variables (increased air temperatures and decreased precipitation), land use changes and natural vegetation changes, as well as increased water demand for irrigation. On the other side, Đokić et al. (2022) found that discharge decreased due to vegetation growth during June, with the highest precipitation in the Nišava River basin. Idrizović et al. (2020) have projected changes in discharges, precipitation and temperature for two periods: 2021–2050 and 2071–2100 compared with the reference period 1971–2000 in the Toplica River basin. The authors forecasted no notable changes on an annual scale but an increase in discharge, air temperature and precipitation during the winter months and a decrease in discharges during the warm season. Discharges in Južna Morava River and Zapadna Morava River basins are determined by air temperature and precipitation, terrain slope and geological structure, pedological and vegetation cover and human impact (Langović 2019; Langović et al. 2017). Manojlović et al. (2021) found a significant decrease in discharge for the Južna Morava River basin in the 1961–2007 period but no significant changes in precipitation. Decreased discharge has been caused by human activities and interventions such as water extraction, agricultural irrigation, industrial and urban use, engineering works, and conservation measures in the 1960s and 1970s (Manojlović et al. 2021).

In the selected rivers of the northern part of Montenegro, the statistically significant decrease in discharge from May to August is a direct consequence of climatic elements variability, especially the air temperature increasing trend. Ćulafić et al. (2017) analysed the impact of climate change in the Lim River basin and concluded that there was a tendency for the mean annual discharge to decrease in in 1948–2014, along with an increase in air temperature, especially with high oscillations during the winter months. Analysing the relationship between discharge and precipitation in the Lim River basin for the 1966-2014 period, Ćulafić (2020) found that there is a decrease in discharge during the summer (July and August), especially from 1989, while on the other hand, a constant increase in air temperature is recorded, as well as a slight decrease in the amount of precipitation.

The decreasing trend in the discharge of the selected rivers in 1991–2020 compared to 1961–1990 carries significance in water resources management, especially through the negative effect on water supply, water quality, agriculture, biodiversity, etc. Although the studied rivers in Šumadija Region are not directly used for the water supply of settlements, they have multiple purposes, and preserving their good water quality is important. Continuous monitoring is necessary to analyse the correlation of discharge variability and the impact on water quality. Unfortunately, some of these rivers do not have water quality monitoring, and others are not continuously monitored. By analysing data in the water quality of the Lepenica River in 2001–2005, Milanović and Kovačević (2007) concluded that the Lepenica River is a polluted watercourse. The highest level of water pollution is during the summer and early autumn, when the discharge rate is the lowest, and it is mainly polluted by wastewater from industrial facilities. In recent years, water quality testing of Lim River has been carried out 3 to 4 times per year. Reports indicate that the water quality in the upstream sector near Andrejevica is good. The water quality is moderate in the downstream sector near Bijelo Polje and on its tributary Ljubovića (IHMS, 2024). However, it is necessary to provide continuous water quality measurements in the Lim River basin to research the impact of discharge change on its water quality.

Discharge variability also has an impact on erosion processes in watersheds. Until now, no studies have dealt with the influence of discharge changes on erosion intensity in this study area. Ristić et al. (2013) analysed the impact of land-use changes in the Dičina River basin from 1966 to 2012 and concluded that maximal discharges had been reduced since 2002 due to land-use changes, including erosion and control torrent works. Spalević et al. (2020) analysed land-use changes and their impact on erosion, primarily on fluvial erosion in the Miocki Potok basin, Lims tributary. They found that changes in land use in the last 50 years have reduced soil erosion intensity by 14%.

According to the Erosion Map of Serbia (1983), made in the 1966–1971 period, 86.39% of Serbia was affected by varying erosion intensities, and excessive and very strong erosion covered about 14.3% of the territory. However, during that time, the relationship between erosion categories changed, and according to data from 2009, the area under excessive erosion decreased by 50–70%, and the areas under severe erosion were reduced by about 75% and moved into the medium erosion category (Lazarević 2009). According to Dragićević et al. (2011), areas with strong erosion potential cover about 3.76% of the territory in Serbia. Numerous factors influenced the change in erosion intensity, and it would be significant to examine the correlations between the discharge decrease and erosion intensity changes in specific river basins.

CONCLUSIONS

In this study, discharge changes during sixty years on selected rivers of the Danube basin in central Serbia and northern Montenegro were analysed. The maximum discharge on the rivers in Serbia is recorded mainly in March, and the minimum discharge is mainly in September, while on the analysed rivers in Montenegro, maximum discharges were in May (or April) and minimum in August.

By using a t-test, it is concluded that in all the study rivers, a decrease in mean annual discharge was recorded in the 1991–2020 compared to the 1961–1990 period. This discharge decrease is statistically very significant ($p \leq 0.01$) in rivers Lepenica and Lugomir in Serbia and statistically significant ($p \leq 0.05$) in Lim in Montenegro. The monthly discharges decrease observed in the 1991–2020 period is statistically very significant ($p \leq 0.01$) from May to August on Lim River and in August on its tributary Ljubovića River in Montenegro, in February and May on Lepenica River and in June and September on Lugomir River in Serbia, and statistically significant ($p \leq 0.05$) in July Ljubovića River in

Montenegro and in January and March on Lepenica River in Serbia. In contrast a statistically significant ($p \leq 0.05$) discharge increase is registered in September and October on the Kubršnica River and in October on the Peštan River in Serbia. In other months, no statistically significant changes in monthly discharges were observed between the two 30-year periods.

Discharge decreases in selected rivers correlate with a statistically significant air temperature increase in the entire region, whereas it is barely influenced by precipitation, which has slightly changed. Further research on discharge variation in the study rivers should consider additional factors, such as snow cover and melting, geological structure, land-use changes, etc. Considering that the decreasing trends of discharge negatively affect the water resources management, their use, water quality degradation and other natural processes, further research on the factors affecting the hydrological changes outlined in the study rivers should be undertaken.

REFERENCES

Balistrocchi M., Tomirotti M., Muraca A., and Ranzi R. (2021). Hydroclimatic variability and land Cover transformations in the Central Italian Alps. Water, 13, 963, DOI: 10.3390/w13070963

Billi, P. and Fazzini, M. (2017). Global change and river flow in Italy. Global and Planetary Change, 155, 234-246. DOI: 10.1016/j.gloplacha.2017.07.008

Botero-Acosta A., Chu M.L., Guzman J.A., Starks P.J., and Moriasi, D.N. (2017). Riparian erosion vulnerability model based on environmental features. Journal of Environmental Management, 203, 592-602, DOI: 10.1016/j.jenvman.2017.02.045

Brown D.R., Brinkman T.J., Bolton W.R., Brown C.L., Cold H.S., Hollingsworth T.N., and Verbyla D.L. (2020). Implications of climate variability and changing seasonal hydrology for subarctic riverbank erosion. Climatic Change, 162, 1-20, DOI: 10.1007/s10584-020-02748-9

Burić M., Micev B., and Mitrović L. (2012). Atlas klime Crne Gore [Climatic Atlas of Montenegro]. Podgorica: CANU (in Serbian).

Cigizoglu H.K., Bayazit M., and Önöz B. (2005). Trends in the maximum, mean, and low flows of Turkish rivers. Journal of Hydrometeorology, 6(3), 280-290. DOI: 10.1175/JHM412.1

Ćulafić G., Mitrović L., Ivanov M., and Golijanin J. (2017). Uticaj klimatskih promjena na vodni režim u slivu Lima. Zbornik radova povodom obilježavanja 20 godina rada Prirodno–matematičkog Fakulteta Univerziteta u Banjoj Luci. Banja Luka: Republika Srpska, Bosna i Hercegovina, p. 141-147 (in Serbian).

Ćulafić G. (2020). Impact of climate change on river discharge regimes in the Danube river basin: Example of Lim River (Montenegro). In: A. Milanović Pešić, and D. Jakovljević, eds., Water Resources Management: Methods, Application and Challenges, 35-68. New York: Nova Science Publishers.

Ćulafić G. and Krstajić J. (2024). Hydrology of Surface Water and Climate Characteristics of Montenegro. In: G. Barović, ed., Speleology of Montenegro, 51-65. Cham: Springer International Publishing.DiBiase R.A. and Whipple K.X. (2011). The influence of erosion thresholds and runoff variability on the relationships among topography, climate, and erosion rate. Journal of Geophysical Research: Earth Surface, 116(F4), DOI: 10.1029/2011JF002095

Dragićević S., Pripužić M., Živković N., Novković I., Kostadinov S., Langović M., Milojković B., and Čvorović Z. (2017). Spatial and temporal variability of bank erosion during the period 1930–2016: Case Study—Kolubara River Basin (Serbia). Water, 9(10), 748. DOI: 10.3390/w9100748

Dragićević S., Ristić R., Živković N., Kostadinov S., Tošić R., Novković I., Borisavljević A., and Radić B. (2013). Floods in Serbia in 2010–case study: the Kolubara and Pcinja River basins. In: D. Lóczy, ed., Geomorphological impacts of extreme weather: Case studies from Central and Eastern Europe. Dordrecht: Springer, 155-169, DOI: 10.1007/978-94-007-6301-2_10

Dragicevic S., Filipovic D., Kostadinov S., Ristic R., Zivkovic N., Andjelkovic G., Abolsamov B., and Djurdjic S. (2011). Natural Hazard Assessment for Land-use Planning in Serbia. International Journal of Environmental Research, [online] Volume 5(2), 371-380. Available at: https://www.sid.ir/paper/300933/en [Accessed 20 Feb. 2024]

Drobnjaković M., Petrović G., Karabašević D., Vukotić S., Mirčetić V., and Popović, V. (2021). Socio-economic transformation of Šumadija District (Serbia). Journal of the Geographical Institute "Jovan Cvijić" SASA, 71(2), 163-180, DOI: 10.2298/IJGI2102163D

Dukić D. and Gavrilović Lj. (2008). Hidrologija. [Hydrology]. Belgrade: Zavod za udžbenike i nastavna sredstva (in Serbian).

Đokić M., Stričević L.J., Gocić M., Golubović N., and Miletić M. (2022). Analysis of Discharge Fluctuation Using Modified Streamflow Drought Index (SDI) and Standardized Precipitation Index (SPI) in the Upper Nišava River Basin. Serbian Journal of Geosciences, 8, 15-26. DOI: 10.18485/srbjgeosci.2022.8.1.3

Đorđević B., Dašić T., and Plavšić J. (2020). Impact of climate change on Serbian water management and measures for protection against negative impacts. Vodoprivreda, [online] Volume 305-309, p. 39-68 (in Serbian with English abstract). Available at: https://grafar.grf.bg.ac.rs/handle/123456789/2520 [Accessed 20 Feb. 2024]

Gao P., Li Z., and Yang H. (2021). Variable discharges control composite bank erosion in Zoige meandering rivers. Catena, 204, 105384, DOI: 10.1016/j.catena.2021.105384

Georgiadi A.G., Milyukova I.P., Borodin O.O., and Gusarov A.V. (2023). Water Flow Changes in the Don River (European Russia) during 1891–2019. Geography, Environment, Sustainability, 16(2), 6–17, DOI: 10.24057/2071-9388-2022-083

Haddeland I., Langsholt E., Lawrence D., Wong W.K., Andjelic M., Ivkovic M. and Vujadinovic M. (2013). Effects of climate change in the Kolubara and Toplica catchments, Serbia, Report number 62 [online]. Oslo: Norwegian Water Resources and Energy Directorate. Available at: https://publikasjoner.nve.no › rapport2013_62 [Accessed 20 Feb. 2024]

Hrvačević S. (2004). Resursi površinskih voda Crne Gore, Elektroprivreda Crne Gore AD Nikšić, Nikšić (in Serbian).

Idrizovic D., Pocuca V., Mandic M.V., Djurovic N., Matovic G., and Gregoric, E. (2020). Impact of climate change on water resource availability in a mountainous catchment: a case study of the Toplica River catchment, Serbia. Journal of Hydrology, 587, 124992, DOI: 10.1016/j.jhydrol.2020.124992

Institute of Hydrometeorology and Seismology (IHMS) (2024). Stanje kvaliteta vode u Crnoj Gori 2023 (in Montenegrin).

Jovanović S., Petrović J., Nikolic D., Djordjevic Z., and Sustersic V. (2023). Climate changes – Trends and perspectives in the Republic of Serbia. In: 14th International Quality Conference , Conference Manual (Kragujevac, Serbia, 2023). Kragujevac: Faculty of Engineering, University of Kragujevac, pp. 1753-1760

Kärkkäinen M. and Lotsari E. (2022). Impacts of rising, peak and receding phases of discharge events on erosion potential of a boreal meandering river. Hydrological Processes, 36(10), e14674, DOI: 10.1002/hyp.14674

Kovačević-Majkić J. and Radovanović M. (2006). Hydrological features of Ljig municipality. Journal of the Geographical Institute "Jovan Cvijic" SASA, 55, 37-52 (in Serbian with English abstract).

Kovačević-Majkić J. and Urošev M. (2014). Trends of mean annual and seasonal discharges of rivers in Serbia. Journal of the Geographical Institute "Jovan Cvijić" SASA, 64(2), 143-160, DOI: 10.2298/IJGI1402143K

Krtolica I., Todorov M., Prohaska S., and Stojković, M. (2024). Annual and Low-Flow Trends in Serbia. Journal of Hydrologic Engineering, 29(3), 05024008. DOI: 10.1061/JHYEFF.HEENG-6030

Langović M. (2019). Annual and seasonal variations of river discharges in the South Morava River Basin (Republic of Serbia). In: Proceedings of the International Scientific Symposium "New Trends in Geography" (Ohrid, North Macedonia, 2019). Ohrid: Macedonian Geographical Society, pp. 27-36.

Langović M., Dragićević S., Novković I., Živković N., Tošić R., Milojković B., and Čvorović Z. (2021). Assessment of the soil loss caused by riverbank erosion in Serbia. Bulletin of the Serbian Geographical Society, 101(1), 31-47, DOI: 10.2298/GSGD2101031L

Langović M., Manojlović S. and Čvorović Z. (2017). Trends of mean annual river discharges in the Zapadna Morava river basin. Bulletin of the Serbian Geographical Society, 97(2), 19-45. DOI: 10.2298/GSGD1702019L

Larsen, E.W., Premier A.K., and Greco S.E. (2006). Cumulative effective stream power and bank erosion on the Sacramento river, California, USA. JAWRA Journal of the American Water Resources Association, 42(4), 1077-1097, DOI: 10.1111/j.1752-1688.2006.tb04515.x

Lazarević R. (2009). Erozija u Srbiji. Belgrade (in Serbian).

Leščešen I., Dolinaj D., Pantelić M., Telbisz T., and Varga G. (2020). Hydrological drought assessment of the Tisza River. Journal of the Geographical Institute "Jovan Cvijić" SASA, 70(2), 89-100, DOI: 10.2298/IJGI2002089L

Li L.J., Li B., Liang L.Q., Li J.Y., and Liu Y.M. (2010). Effect of climate change and land use on stream flow in the upper and middle reaches of the Taoer River, northeastern China. Forestry Studies in China, 12, 107-115, DOI: 10.1007/s11632-010-0301-1

Manojlović S., Sibinović M., Srejić T., Hadud A., and Sabri I. (2021). Agriculture land use change and demographic change in response to decline suspended sediment in Južna Morava River basin (Serbia). Sustainability, 13(6), 3130, DOI: 10.3390/su13063130

Miao C., Ni J. and Borthwick A.G.L. (2010). Recent changes of water discharge and sediment load in the Yellow River basin, China. Progress in Physical Geography: Earth and Environment, 34(4), 541-561, DOI: 10.1177/0309133310369434

Milanović A. (2007). Analiza rečnog režima i vodnog bilansa u slivu Lepenice [Analysis of river regime and water balance in the Lepenica River basin]. Journal of the Geographical Institute "Jovan Cvijić" SASA, 56, 35-50, DOI: 10.2298/IJGI0756035M (in Serbian)

Milanović A. and Kovačević-Majkić J. (2007). Evaluation of surface water quality and pollution in Lepenica River basin Bulletin of the Serbian Geographical Society, 87(1), 175-184, DOI: 10.2298/GSGD0701173M (in Serbian with English abstract).

Milanović Pešić A. (2019). Water regime and discharges trends of the rivers in the Šumadija region (Serbia). In: Proceedings of the International Scientific Symposium "New Trends in Geography" (Ohrid, North Macedonia, 2019). Ohrid: Macedonian Geographical Society, pp. 3–13.

Milanović Pešić A. (2015). Geographical Aspects of Natural Disasters in Šumadija. University of Belgrade, Faculty of Geography, PhD Dissertation (in Serbian with English abstract)

Milanović Pešić A. and Milovanović B. (2016). Thermic Regime and Air Temperature Trends in Šumadija Region (Serbia). Journal of the Geographical Institute "Jovan Cvijić" SASA, 66(1), 19-34, DOI: 10.2298/IJGI1601019M

Milovanović B., Radovanović M., Stanojević G., Pecelj M., and Nikolić J. (2017a). Klima Srbije [Climate of Serbia]. In M. Radovanović ed., Geografija Srbije (Posebna izdanja, Knjiga 91) [Geography of Serbia (Special issues, Book 91)]. Belgrade: Geographical Institute "Jovan Cvijić" SASA, 94-156 (in Serbian).

Milovanović B., Ducić V., Radovanović M., and Milivojević, M. (2017b). Climate regionalization of Serbia to Köppen climate classification. Journal of the Geographical Institute "Jovan Cvijić" SASA, 67(2), 103–114, DOI: 10.2298/IJGI1702103M

Moody J.A. (2022). The effects of discharge and bank orientation on the annual riverbank erosion along Powder River in Montana, USA. Geomorphology, 403, 108134. DOI: 10.1016/j.geomorph.2022.108134

Petrović A.M. (2015). Challenges of torrential flood risk management in Serbia. Journal of the Geographical Institute "Jovan Cvijić" SASA, 65(2), 131-143, DOI: 10.2298/IJGI1502131P

Petrović A.M. (2021). Bujične poplave u Srbiji [Torrential floods in Sebia]. Belgrade: Serbia Geographical Society, Special Issues, Book 73.

Petrović A. M., Leščešen I., and Radevski I. (2024). Unveiling Torrential Flood Dynamics: A Comprehensive Study of Spatio-Temporal Patterns in the Šumadija Region, Serbia. Water, 16(7), 991, DOI: 10.3390/w16070991

Radojičić B. (2008). Geografija Crne Gore, prirodna osnova. Podgorica: DANU (in Serbian).

Radulović M., Leščešen I., and Pavić, D. (2014). Analysis of River regime and Water balance of the Temštica River Basin (South-East Serbia) during the 1980-2012 Period. Forum Geografic 13(2), 178-184, DOI: 10.5775/fg. 2067-4635.2014.082.d

Rajović G. and Bulatović J. (2014). Water geographic values Northeastern Montenegro. Larhyss Journal, [online] 17. Available at: http://larhyss.net/journal.html [Accessed 20 Feb. 2024]

Ristić R., Ljujić M., Despotović J., Aleksić V., Radić B., Nikić Z., Milčanović V., Malušević I., and Radonjić J. (2013). Reservoir sedimentation and hydrological effects of land use changes-case study of the experimental Dičina river watershed. Carpathian Journal of Earth and Environmental Sciences, 8(1), 91-98. Available at: https://www.cjees.ro/viewTopic.php?topicId=298 [Accessed 20 Feb. 2024]

Sekulić G. and Radulović M.M. (2019). The Hydrology and Hydrogeology of Montenegro. In: V. Pešić, M. Paunović, and A. Kostianoy, eds., The Rivers of Montenegro. The Handbook of Environmental Chemistry, Volume 93. Cham: Springer, pp: 13-42. DOI: 10.1007/698_2019_413

Souza S.A. and Reis, D.S.Jr. (2022). Trend detection in annual streamflow extremes in Brazil. Water, 14, 1805. DOI: 10.3390/w14111805

Spalevic V., Barovic G., Fikfak A., Kosanovic S., Djurovic M., and Popovic S. (2016). Sediment yield and Land use changes in the Northern Montenegrin Watersheds: Case study of Seocki Potok of the Polimlje Region. Journal of Environmental Protection and Ecology, [online] Volume 17(3), 990-1002. Available at: https://scibulcom.net/en/article/QolOVlG4vl4PtVviS9fY [Accessed 20 Feb. 2024]

Spalevic V., Barovic G., Vujacic D., Curovic M., Behzadfar M., Djurovic N., Dudic B., and Billi P. (2020). The impact of land use changes on soil erosion in the river basin of Miocki Potok, Montenegro. Water, 12(11), 2973, DOI: 10.3390/w12112973

Urošev M., Dolinaj D., and Štrbac D. (2016). At-site hydrological drought analysis: Case study of Velika Morava River at Ljubičevski Most (Serbia). Journal of the Geographical Institute "Jovan Cvijić" SASA, 66(2), 203-220, DOI: 10.2298/IJGI1602203U

Vuksanović-Macura Z., Radulović S., and Macura V. (2018). Land cover changes of the Belgrade area over the past three centuries. Spatium, 42-50, DOI: 10.2298/SPAT1840042V

Yang D., Shi X., and Marsh P. (2015). Variability and extreme of Mackenzie River daily discharge during 1973–2011. Quaternary International, 380, 159-168, DOI: 10.1016/j.quaint.2014.09.023

Zhang J. and Yu X. (2021). Analysis of land use change and its influence on runoff in the Puhe River Basin. Environmental Science and Pollution Research, 28, 40116-40125, DOI: 10.1007/s11356-020-09798-7

Zheng H., Zhang L., Liu C., Shao Q., and Fukushima Y. (2007). Changes in stream flow regime in headwater catchments of the Yellow River basin since the 1950s. Hydrological Processes: An International Journal, 21(7), 886-893. DOI: 10.1002/hyp.6280

Check for updates

CC BY

RESEARCH PAPER

COMPARISON OF EPM WITH RUSLE FOR SOIL EROSION MODELING IN THE STRUMICA RIVER BASIN

Bozhin Trendafilov, Ivan Minchev*, Aleksandar Trendafilov, Ivan Blinkov

[1]Ss. Cyril and Methodius University, Hans Em Faculty of Forest Sciences, Landscape Architecture and Environmental Engineering, 16-ta Makedonska brigada No.1, 1000 Skopje, North Macedonia

***Corresponding author:** ivan.minchev@sf.ukim.mk

Received: September 5th 2024 / Accepted: November 22nd 2024 / Published: December 31st 2024

https://doi.org/10.24057/2071-9388-2024-0580

ABSTRACT. The most recent climate change scenarios indicate an increase in extreme climate events (rainfall) and therefore an increase in soil loss. Strumica River is a tributary of river Struma/Strimon – a transboundary basin in North Macedonia (Strumica), Bulgaria and Greece that flows to the Aegean Sea. Most of the models incorporated in several software packages, use the USLE (Universal Soil Loss Equation). USLE-based models (RUSLE, MUSLE) are designed to model soil loss on gentler slopes and in agricultural areas. Furthermore, the model considers soil removal, but not the mass movement processes. On the other hand, the EPM (Erosion Potential Method by Gavrilovic), considers all soil particles (including rocks and mass movement) as well as all slope topography. The EPM considers the whole basin area. The aim of this research is to assess the differences between the two methods in the case study of the Strumica river basin. The results show differences in the quantities of the produced sediment. On the basin level, according to EPM, the quantity of annual produced sediment is 3.38 m^3 ha $year^{-1}$ while RUSLE depicted an annual soil loss at 1.59 t $ha^{-1}year^{-1}$. When observing just the agricultural land, according to EPM, the annual produced sediment is 4.22 m^3 ha $year^{-1}$ while according to RUSLE, the annual produced sediment is 2.84 t $ha^{-1}year^{-1}$. The EPM yields higher quantities because it takes into account the gully erosion and mass movement processes.

KEYWORDS: EPM, RUSLE, soil loss, soil erosion, produced sediment, Strumica river, Struma/Strimon

CITATION: Trendafilov B., Minchev I., Trendafilov A., Blinkov I. (2024). Comparison of EPM With RUSLE For Soil Erosion Modeling In The Strumica River Basin. Geography, Environment, Sustainability, 4(17), 44-49
https://doi.org/10.24057/2071-9388-2024-0580

Conflict of interests: The authors reported no potential conflict of interest.

INTRODUCTION

A Hazard is something that has the potential to harm you. Risk is the likelihood of a hazard causing harm (EFSA, online). A hazard is a situation or potential condition to harm or threat to life, health or damage to property or environment, social and economic disruption. The mass movement of soil is an indicator of a soil erosion hazard. This includes gully erosion, riverbank erosion, rock falls, debris-falls and landslides that can create damage to the environment and livelihoods (Senanayake *et al*., 2020).

Erosion hazard refers to the threat of channel migration and/or down cutting, due to erosion during times of flooding, or erosion of the ground around a structure in such a manner as to threaten the stability of the structure. It depicts the susceptibility of a site to erosion, based on soils, conditions and steepness of a slope, rock type, vegetation, and other site factors.

Soil erosion is one of the major environmental threats (Amundson *et al*., 2015) that is forecasted to diffusely increase under the impact of climate change (Borrelli *et al*., 2022; Panagos *et al*., 2022, Bezak *et al*., 2024).

Erosion risk assessment is a much more complex task since it considers various adverse effects that occur both on-site and off-site. The main on-site impact of soil erosion is the reduction in soil quality which results from the loss of the nutrient-rich upper layers of the soil, and the reduced water-holding capacity of many eroded soils. In an affluent area of the world, accelerated water erosion's on-site effects upon agricultural soils can be mitigated by increased use of artificial fertilizers; however, this is not an option for much of the earth's population (Favis-Mortlock, 2017).

Off-site effects, caused by erosion, transport the sediment through the watershed drainage pattern, are less visible and less studied. In the process of runoff on eroded slopes, along with soil particles (erosion sediment), all the other substances contained in the eroded soil layer are also removed. These substances can be natural, organic, inorganic, or artificial. Natural substances vary depending on the slope's or eroded region's geologic and pedologic properties. Most often, various fertilizers and pesticides are applied in agricultural production, and they reach the lower hydrographic network along with the eroded sediment. After reaching the streams and reservoirs, erosion sediment has the following ecological (and other) adverse effects: a) mechanical pollution of the stream and reservoir water, b) chemical pollution of water by manures and fertilizers, and c) chemical pollution by pesticides (Kostadinov, 2002).

Various methods for erosion vulnerability assessment are used by various countries in the world. Development of erosion vulnerability assessment methods, soil loss estimation and erosion intensity estimation, have a long–term tradition and a large number of methods and models have been developed in the past 100 years.

Generally, three types of approaches exist to identify areas at risk: qualitative approach, quantitative approach, and model approach. All these methods vary in their characteristics and applicability (Eckelmann et al., 2006). On the territory of the Republic of North Macedonia, the most practiced method is EPM by Gavrilovic. Considering the worldwide use of the USLE/RUSLE methods globally, it has also been applied in the country (Blinkov *et al*., 2020).

The Erosion Potential Method (EPM) is a complex methodology designed for use in the field of Integrated Water Resources Management and was originally developed for Yugoslavia by Slobodan Gavrilovic in 1972. EPM is factor-based, which means that a series of factors, each quantifying one or more processes and their interactions, are combined to yield an overall estimation of soil loss. The EPM method gives a quantitative estimation of erosion intensity as well as the estimation of sediment production and transportation (Gavrilovic *et al*., 2006).

The Universal Soil Loss Equation (USLE) predicts the long-term average annual rate of erosion on a field slope based on rainfall pattern, soil type, topography, crop system and management practices. USLE only predicts the amount of soil loss that results from sheet or rill erosion on a single slope and does not account for additional soil losses that might occur from gully, wind or tillage erosion. This erosion model was created for use in selected cropping and management systems but is also applicable to non-agricultural conditions such as construction sites. The USLE can be used to compare soil losses from a particular field with a specific crop and management system to "tolerable soil loss" rates. Alternative management and crop systems may also be evaluated to determine the adequacy of conservation measures in farm planning. The Revised Universal Soil Loss Equation (RUSLE) is an upgrade of USLE that is independent of land use. It can be used on cropland, disturbed forestland, rangeland, construction sites, mined land, reclaimed land, military training grounds, landfills, waste disposal sites, and other lands where rainfall and its associated overland flow cause soil erosion. RUSLE maintains the same empirically based equation as USLE to compute sheet and rill erosion (FAO, online).

The first erosion map of the Republic of Macedonia was finished in 1993 by the Institute for water economy (orig: Zavod za vodostopanstvo) in a process that lasted eleven years with extensive field validation and traditional mapping techniques. Thirty years later, in 2020, it was updated with contemporary mapping techniques (GIS and Remote sensing, including field mapping using an expert judgment approach as control of the modelling results). The erosion map EPM and RUSLE were developed in a project funded by UNEP (UN Environmental program) for the Ministry of Environment and physical planning of Republic of North Macedonia. The latest erosion map (update of the first erosion map) was used in the analyses of this paper (Blinkov *et al*., 2020). There are several other erosion maps developed for research purposes (Milevski, 2015).

In the scope of this research, an erosion map using the two methods, EPM by Gavrilovic and RUSLE was produced. Conceptually, EPM was intended to be used for the whole country and RUSLE was intended mainly for the agriculture area.

The aim of this paper is to show the difference between two models for soil erosion estimation: EPM and RUSLE. The separate objectives are: (1) to estimate the produced sediment in the basin using EPM, (2) to estimate the soil loss in the basin using RUSLE, and (3) to compare the modeled values on different land uses.

MATERIALS AND METHODS

Study area

Struma/Strymon is a transboundary river with a basin of 18,078 km^2 (290 km and 10,797 km^2 in southwest Bulgaria; 110 km and 7,281 km^2 in northern Greece), its tributaries even extending into four countries (small parts are in Serbia and Republic of North Macedonia) (INWEB, online).

The river Strumica is a tributary of Struma River. Strumica river basin is 1,649 km^2 which is 6.4% of the territory of North Macedonia. A major part of the total watershed (75%) is in North Macedonia, while the remaining is in Bulgaria and Greece. River Strumica takes its source from the Plackovica Mountain at an altitude of 1,540 m asl running south in a deep valley and known as the Stara Reka (Popovska and Geshovska, 2014).

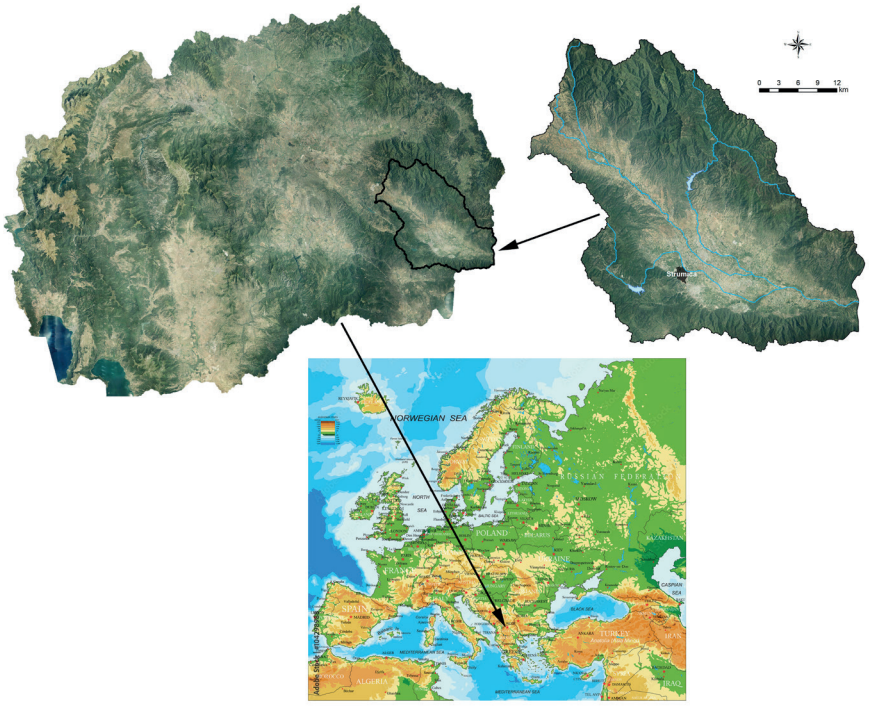

Fig. 1. Location of the basin of Strumica river in North Macedonia

The basin area of the Strumica River is situated in the south-eastern part of North Macedonia (Fig. 1). In this paper, only the part of the basin which is located in North Macedonia is considered. The basin has a total area of 1485 km^2. The land cover is dominated by broad-leaved forests in the higher parts of the basin with 38.9% and transitional woodland 19.7%. On the other hand, agricultural land is present at 35.2% of the total (Fig. 2).

The specific geographical and topographical position of the Strumica region is characterized by two zonal climates: sub-Mediterranean and continental. Sub-Mediterranean with long hot summers, with high average daily temperatures and reduced annual rainfall, decreased winter temperatures and winds from all directions (Lazarevski, 1993).

The climatic characteristics of the basin are strongly influenced by the location, orography, vegetation, and hydrological conditions of the region. The lowest parts of the basins are affected by the sub-Mediterranean climate, hilly and upland areas are affected by moderate continental and mountainous climate and highland areas are affected by typical mountain climate. Within the analysed period (1981-2010), the average annual air temperature for the basin is 11.2°C. The average annual rainfall sum is 626 mm, and in the higher parts of the basin, it can get up to 1014 mm (Aksoy *et al*., 2020).

The basin area of the Strumica River is part mountainous with 2/3 of the area and the flat valley with a dominant agriculture area. The average slope of the catchment is 27%, with maximal value of 230%; most of the mountainous area is with steep slopes in the range of 45-100%.

The dominant soil type in the mountainous part of the basin area is cambisol with 34.4%, on the other hand, in the valley the most dominant are the alluvial soils (12.7%) and colluvial fans (11.8%). Also, in the basin there are regosols (6.8%), complex of cambisol and regosol (6.5%), complex of humic eutric and umbric regosol (6.1%), complex of chromic luvisol on saprolite and regosol (5.6%) and leptosol (4.5%) (Markovski *et al*., 2018).

The geology of the investigated area is very diverse. In the northern and east-northern parts prevail Proterozoic gneisses and shales. In the central part, along the Strumica river, prevail Quaternary alluvial sediments and Neogene clastic sediments. In the central-eastern part and in the south-eastern part magmatic rock are present, while in the south-western part prevail Paleozoic shales with the inclusion of Paleozoic carbonates (Stafilov & Šajn, 2016, Čančalova et. al, 2017). The basin area is dominated by double mica gneiss (15.3%), alluvium (14.9%), biotite granite (10.6%), mica schist and leptynolite (10.3%), deluvium-proluvium 9.1% and marl clay, sandstone and gravel (8.8%).

Modeling produced sediment (soil loss) in the basin of Strumica river with the Erosion Potential Method (EPM)

There are many methodologies which are used for soil erosion estimation. Blinkov and Kostadinov (2010) provide a review of applicability for various usage scenarios of several models for estimation of erosion: EUROSEM, USLE, PESERA, KINEROS, WEP, WEPP and EPM.

The EPM was developed in the Balkan region, south Serbia, which is very similar in climatic conditions to North Macedonia, and therefore it is well adapted to the study area. Also, the model has the ability to predict sediment transport and deposition and it was developed by calibration with the measurement of the deposited sediments in the existing reservoirs. The EPM was validated using bathymetric measurements of several water reservoirs and it show similar results of the model and the measurements (Mincev, 2018).

It was observed that the use of this model increased from 2011 to 2019, and very few studies were conducted in the preceding decade (2000–2010). This method has been widely used in the European continent making it the third (6.7%) most used quantitative method
(Pandey *et al*., 2021).

$$Z = \gamma * Xa * \left(\varphi + \sqrt{I_{sr}}\right) \quad (1)$$

$$W_{year} = T * H_{year} * \pi * \sqrt{Z^3} * F \quad (2)$$

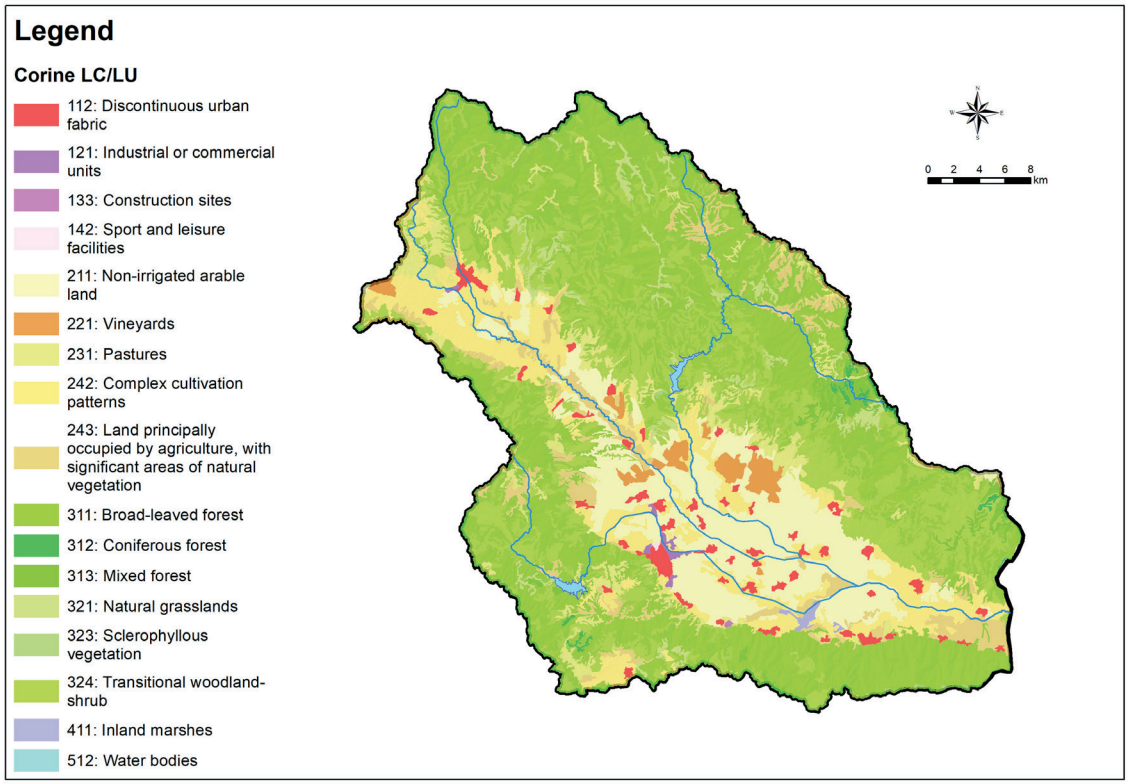

Fig. 2. Land cover/use map of the Strumica River basin

Where:
Z – coefficient of erosion by Gavrilovic (dimensionless)
γ - the reciprocal value of resistance of soils/rocks on erosion processes
Xa – protection of the basin in natural conditions and after erosion control
φ - coefficient of visible processes of erosion
Jsr - mean slope of the basin
W – quantity of produced sediments [m^3 $year^{-1}$]
T – temperature coefficient
H – total annual precipitations [mm]
π – Ludolph number
F – basin area [km^2]

The EPM (by Gavrilovic) was originally designed to be used with hardcopy maps, and the mapping process itself was carried out on a basin level. With the advent of GIS tools and the large variety of geographic data available (Corine LC/LU, soil maps, geology maps, elevation data – DEM, rainfall models, etc.), the mapping process evolved on much smaller mapping units. These datasets can be of good quality, but the production scale should be taken into account, and they could be reclassified according to the given classes in the methodology. The use of a global dataset is recommended due to the easy transferability and comparability of the results (Mincev, 2015).

The input parameters used for the EPM and RUSLE were as follows: National soil map (scale 1:50,000); Land cover: Corine LC/LU 2018 (developed by European Environmental Agency, scale 1:100,000), later improved using visual photo-interpretation of aerial imagery with spatial resolution of 0.3 m (2019) (Fig.2); DEM spatial resolution of 5 m; climatic parameters developed in spatial resolution of 20 m, analysed period (1981-2010) (Aksoy et al. 2020).

Modeling soil loss in the basin of Strumica river with RUSLE

The main factors affecting the rates of soil erosion by water are precipitation, soil type, topography, land use and land management. In a recent inventory, Karydas et al. (2014) identified 82 water-erosion models classified on different spatial/temporal scales with various levels of complexity. The most used erosion model is the Universal Soil Loss Equation (USLE) (Wischmeier and Smith, 1978) and its revised version (RUSLE) (Renard *et al.*, 1997) which estimates long-term average annual soil loss by sheet and rill erosion. It should be noted that soil loss caused by (ephemeral) gully erosion is not predicted by RUSLE (Poesen *et al.*, 2003). Despite its shortcomings, RUSLE is still the most frequently used model at large scales (Renschler and Harbor, 2002; Kinnell, 2010) as it can process data input for large regions and provides a basis for carrying out scenario analysis and taking mitigating measures against erosion (Lu *et al.*, 2003; Panagos *et al.*, 2015e). The equation of USLE (RUSLE) is:

$$E = R * K * C * LS * P \quad (3)$$

Where:
E - annual average soil loss (t ha^{-1} yr^{-1}),
R - rainfall erosivity factor (MJ mm ha^{-1} h^{-1} yr^{-1}),
K - soil erodibility factor (t ha h ha^{-1} MJ^{-1} mm^{-1}),
C - cover-management factor (dimensionless),
LS - slope length and slope steepness factor (dimensionless) and
P - support practices factor (dimensionless).

Each parameter is estimated and defined in detail, in separate papers by Panagos et al., published in 2015 (Panagos et al., 2015a, 2015b, 2015c, 2015d, 2015e). Also, a modification and development of the R factor for North Macedonia was published by Blinkov et al. (2022). More detailed description of the both methods used it can be found in Tavares et al., 2019.

RESULTS AND DISCUSSION

The main difference between RUSLE (and similar to USLE methods) and EPM is different terminology that represents different processes and conditions. Soil loss is in fact loss of consolidated material. Sediment production refers to unconsolidated material. The difference is in bulk density because in situ soil bulk density is higher then bulk density of unconsolidated or partially consolidated erosive material (Blinkov, 2014). Apart from that, the main difference between EPM is that USLE (RUSLE) are limited on sheet and inter-rill erosion. On the other hand, EPM recognizes deep erosion –

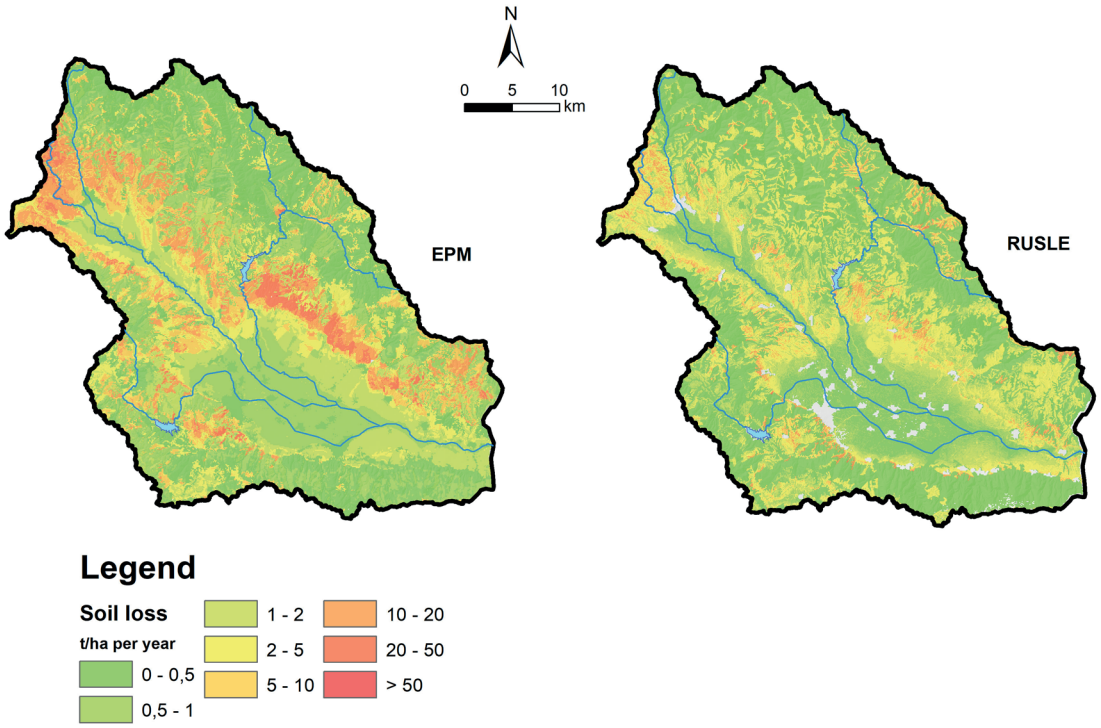

Fig. 3. Comparison of soil loss/produced sediment of EPM vs. RUSLE in the basin of Strumica river

Table 1. Comparison of soil loss/produced sediment of EPM vs. RUSLE on different land cover and slope

Corine Land cover/Land use (Level 3)	EPM-W (t/ha)	RUSLE-E (t/ha)	Slope (%)
Non-irrigated arable land	2.1	1.5	3.3
Complex cultivation patterns	4.2	2.5	7.5
Land principally occupied by agriculture, with significant areas of natural vegetation	3.4	4.2	13.7
Pastures	11.2	6.3	24.6
Vineyards	3.4	3.4	4.4
Broad-leaved forest	1.3	0.2	41.9
Mixed forest	1.4	0.1	37.4
Coniferous forest	1.1	0.1	36.2
Transitional woodland-shrub	6.2	2.1	33.7
Natural grasslands	6.2	3.0	29.2
Sclerophyllous vegetation	3.7	3.8	42.1

gullies, landslides, rockfalls, fluvial, deep erosion etc. (Blinkov and Kostadinov, 2010).

The EPM produces an output expressed in volume units $m^3ha^{-1}year^{-1}$. On the other hand, RUSLE expresses the output in weight measure t $ha^{-1}year^{-1}$. In order to make a comparison of the results of the soil loss or produced sediment the EPM values were converted from m^3 to tons using the bulk density of the soil/erosive material of 1.2 (1 m^3 = 1.2 t).

The map above (Fig. 3) depicts the difference in quantities of soil loss of the two methods. From the visual inspection, it can be seen that the quantities in the valley are similar (mostly green color). On the other hand, larger discrepancies can be observed in the central part of the basin, north of the confluence of the rivers. Focusing on the red/orange color on the EPM map (classes 5-10, 10-20 and 20-50 t ha^{-1}) and the RUSLE map, the same areas have maximum values of 5-10 t ha^{-1}. This can be attributed to the fact that the RUSLE model does not account for the mass movement erosion processes and only quantifies the topsoil removal.

Table 1 depicts how the two models perform on different land cover classes. The values are expressed as average values, which were calculated on a polygon level of the Corine land cover map from 2018. The agriculture areas yield 1.3 times higher values with the EPM than with RUSLE. This was also confirmed before by Bezak *et al.*, 2024, and this was expected. The lower part of the table shows the natural land cover classes. Here the difference is much higher. On average, EPM yielded values that were seven times higher than those of the RUSLE model. This difference can also be accounted for by the slope of the terrain since the RUSLE model was mostly developed for agricultural areas and for slopes up to 15%. Similar comparison can be found in Tavares *et al.*, 2019.

CONCLUSIONS

The results show differences in the quantities of the produced sediment. On the basin level, according to EPM, the quantity of annually produced sediment is 3.38 m^3 km^{-2} $year^{-1}$ and according to RUSLE the annual soil losses is 1.59 t $ha^{-1}year^{-1}$. When observing just the agricultural land according to EPM the annually produced sediment is 4.22 m^3 km^{-2} $year^{-1}$ while according to RUSLE the annual produced sediment is 2.84 t ha^{-1} $year^{-1}$. EPM yields higher quantities because it considers gully erosion and mass movement processes. On the other hand, the RUSLE model is much more adapted for agricultural land and in terms of soil loss estimation, it should yield more accurate results.

REFERENCES

Aksoy, E., Arsov, S., Mincev, I., Fang C. (2020) Agro-ecological atlas of the Republic of North Macedonia. Rome, FAO

Amundson, R., Berhe, A.A., Hopmans, J.W., Olson, C., Sztein, A.E., Sparks, D.L., (2015) Soil and human security in the 21st century. Science (80-.) 348, 1261071. https://doi.org/10.1126/science.1261071

Bezak, N., Borrelli, P., Mikos, M., Auflic, M.J. and Panagos, P., (2024) Towards a multi-model soil erosion modelling: An evaluation of the Erosion Potential Method (EPM) for global soil erosion assessments, CATENA, ISSN 0341-8162, 234, 2024, p. 107596, JRC134173

Blinkov I. and Kostadinov S. (2010). Applicability of various erosion risk assessment methods for engineering purposes, BALWOIS conference 2010, Ohrid, Macedonia

Blinkov I., (2014) An approach for conversion of erosion data produced by EPM method in weight measure, Monograph: Advances in GEOECOLOGY 43 – Challenges: Sustainable Land Management – Climate Change, Edition: Advances in GEOECOLOGY, Editors: Miodrag Zlatic & Stanimir Kostadinov, Publisher: CATENA VERLAG GMBH Armelgasse 11, D-35447 Reiskirchen, Germany

Blinkov I., Trendafilov A., Mukaetov D., Monevska Alcinova S., Stevkova S., Stevkov A., Minchev I. and Trendafilov B. (2020) Erosion, Drought and Desertification Atlas of the Republic of North Macedonia; https://balkansfoundation.org/publications/

Blinkov I., Minchev I. and Trendafilov B. (2022) Calculation of the R-factor (the rainfall erosivity factor) for the needs of modeling soil losses using the RUSLE method, based on annual precipitation (in Serbian); Erozija - Scientific Journal of erosion and torrent control, No.:48, UDK 626 ISSN 0350-9648, https://phaidrabg.bg.ac.rs/view/o:28096

Borrelli, P., Ballabio, C., Yang, J.E., Robinson, D.A., Panagos, P., (2022) GloSEM: High resolution global estimates of present and future soil displacement in croplands by water erosion. Sci. Data 9, 406. https://doi.org/10.1038/s41597-022-01489-x

Čančalova, S., Stafilov, T., Šajn, R., & Alijagić, J. (2017). Spatial distribution of chemical elements in soil from the Strumica region, Republic of Macedonia. Geologica Macedonica, 31(2), 117-130. Retrieved from https://js.ugd.edu.mk/index.php/GEOLMAC/article/view/1954

EFSA, official website, [online] Available at: https://www.efsa.europa.eu/en/campaigns/hazard-vs-risk#:~:text=A%20Hazard%20is%20something%20that,of%20a%20hazard%20causing%20harm [Accessed 3 Apr. 2024].

Eckelmann, W., Baritz, R., Bialousz, S., Bielek, P., Carré, F., Hrušková, B., & Tóth, G. (2006). Common criteria for risk area identification according to soil threats. Office for Official Publications of the European Communities

FAO, [online] Available at: https://www.fao.org/land-water/land/land-governance/land-resources-planning-toolbox/category/details/ru/c/1236444/ ; [Accessed 18 Apr. 2024].

Favis-Mortlock D., (2017) [online] Available at: https://soilerosion.net/on-site_impacts.html#:~:text=The%20main%20on%2Dsite%20impact,capacity%20of%20many%20eroded%20soils [Accessed 15 Feb. 2024].

Gavrilovic S. (1972) Inzenjering o bujicnim tokovima i eroziji (Engineering of torrents erosion) (in Serbian). Izgradnja, Belgrade special edition, pp. 272.

Gavrilovic Z., Stefanovic M., Milojevic M., Cotric J., (2006): "Erosion Potential Method» An Important Support For Integrated Water Resource Management. BALWOIS 2006 conference, Orhid, Republic of Macedonia http://balwois.com/balwois/administration/full_paper/ffp-700.pdf

INWEB, official website, [online] Available at: https://www.inweb.gr/workshops2/sub_basins/11_Strymon.html [Accessed 7 Apr. 2024].

Karydas, C.G., Panagos, P., Gitas, I.Z., (2014) A classification of water erosion models according to their geospatial characteristics. International Journal of Digital Earth 7 (3), 229–250.

Kinnell, P.I.A., (2010) Event soil loss, runoff and the Universal Soil Loss Equation family of models: a review. Journal of Hydrology 385, 384–397.

Kostadinov S., (2002) Erosion and Torrent Control in Mountainous Regions of Serbia; Proceedings,Keynote paper; International Year of Mountainous Conference:" Natural and Socio-Economic Effects of Erosion Control in Mountainous Regions; Edited by: M.Zlatić, S.Kostadinov, N.Dragović; Belgrade/ Vrujci Spa; Dec.10-13,2002; p.p.33-56.

Law Insider official website, [online] Available at: https://www.lawinsider.com/dictionary/erosion-hazard [Accessed 5 Apr. 2024].

Lazarevski A.: Climate in Macedonia, Kultura, Skopje, (1993), (in Macedonian)

Lu, H., Prosser, I.P., Moran, C.J., Gallant, J.C., Priestley, G., Stevenson, J.G., (2003) Predicting sheetwash and rill erosion over the Australian continent. Australian Journal of Soil Research 41 (6), 1037–1062.

Markoski, M., Mitkova, T., Tanaskovik, V., & Spalevic, V. (2018). Soil distribution in Strumica river basin and its importance for agricultural production. Agriculture & Forestry, Vol. 64 Issue 4: 121-128, 2018. DOI: 10.17707/AgricultForest.64.4.14

Milevski I. (2015). An approach of GIS based assessment of soil erosion rate on country level in the case of Macedonia. Proceedings of International scientificconference BALKANIKA 2015, pp. 97-104. http://dx.doi.org/10.18509/GBP.2015.13

Mincev I., (2015) Development of methodology for establishing protection zones in the proximity of water reservoirs from erosion and sediment transport aspect, Doctoral thesis, Ss. Cyril and Methodius University, Faculty of Forestry in Skopje

Mincev I., (2018) Measuring v.s modeling sediment, case study: Kalimanci reservoir, Soil and water resources protection in the changing environment, Ed.: Miodrag Zlatic; Stanimir Kostadinov; Schweizerbart and Borntraeger science publishers; Advances in Geoecology, Volume 45, ISBN 978-3-510-65418-5

Panagos, P., Borrelli, P., Matthews, F., Liakos, L., Bezak, N., Diodato, N., Ballabio, C., (2022) Global rainfall erosivity projections for 2050 and 2070. J. Hydrol. 610, 127865 https://doi.org/10.1016/j.jhydrol.2022.127865.

Panagos, P., Ballabio, C., Borrelli, P., Meusburger, K., Klik, A., et al., (2015a). Rainfall erosivity in Europe. Science of Total Environment 511, 801–814.

Panagos, P., Borrelli, P., Meusburger, C., Alewell, C., Lugato, E., Montanarella, L., (2015b). Estimating the soil erosion cover-management factor at European scale. Land Use Policy 48C, 38–50, http://dx.doi.org/10.1016/ j.landusepol.2015.05.021

Panagos, P., Borrelli, P., Meusburger, K., (2015c). A new European slope length and steepness factor (LS-Factor) for modeling soil erosion by water. Geosciences 5, 117–126.

Panagos, P., Borrelli, P., Meusburger, K., van der Zanden, E.H., Poesen, J., Alewell, C., (2015d). Modelling the effect of support practices (P-factor) on the reduction of soil erosion by water at European Scale. Environmental Science & Policy 51, 23–34.

Panagos, P., Borrelli, P., Poesen, J., Ballabio C., Lugato E., Meusburger K., Montanarella, L., Alewell, C. (2015e) The new assessment of soil loss by water erosion in Europe, Environmental Science & Policy 54, (2015) 438–447

Pandey Sh., Kumar P., Zlatic M., Nautiyal R., Panvar V.P., (2021) Recent advances in assessment of soil erosion vulnerability in a watershed, International Soil and Water Conservation Research, Volume 9, Issue 3, September 2021, Pages 305-318

Poesen, J., Nachtergaele, J., Verstraeten, G., Valentin, C., (2003) Gully erosion and environmental change: importance and research needs. Catena 50 (2–4), 91–133.

Popovska C., Geshovska V. (2014): Water Balance Model for Vulnerability Assessment of Water Resources in Strumica River Basin. Irrigation & Drainage Systems Engineering. Volume 3. Issue 3. pp.1-9.

Renard, K.G., et al., (1997) Predicting Soil Erosion by Water: A Guide to Conservation Planning with the Revised Universal Soil Loss Equation (RUSLE) (Agricultural Handbook 703). US Department of Agriculture, Washington, DC, pp. 404.

Renschler, C.S., Harbor, J., 2002. Soil erosion assessment tools from point to regional scales – the role of geomorphologists in land management research and implementation. Geomorphology 47 (2–4), 189–209.

Senanayake S, Pradhan B, Huete A, Brennan J. (2020) A Review on Assessing and Mapping Soil Erosion Hazard Using Geo-Informatics Technology for Farming System Management. Remote Sensing. 2020; 12(24):4063. https://doi.org/10.3390/rs12244063

Stafilov T., Šajn R.: Geochemical Atlas of the Republic of Macedonia, Faculty of Natural Sciences and Mathematics, Skopje, 2016.

Tavares A., Spalevic V., Avanzi, J., Nogueira D., Silva M, Mincato R. (2019). Modeling of water erosion by the erosion potential method in a pilot subbasin in southern Minas Gerais. SEMINA: CIENCIAS AGRARIAS. 40. 555-572. DOI: 10.5433/1679-0359.2019v40n2p555.

Wischmeier, W., Smith, D., (1978) Predicting Rainfall Erosion Losses: A Guide to Conservation Planning. Agricultural Handbook No. 537 U.S. Department of Agriculture, Washington DC, USA.

Check for updates

CC BY

RESEARCH PAPER

MEASURING AND MODELING EROSION IN TWO SUCCESSIVE RESERVOIR CATCHMENTS ON THE DRIM RIVER IN NORTH MACEDONIA

Ivan Minchev*[1], Bozhin Trendafilov[1], Ivan Blinkov[1], Aleksandar Trendafilov[1], Dragan Ivanovski[2]

[1] Ss. Cyril and Methodius University, Hans Em Faculty of Forest Sciences, Landscape Architecture and Environmental Engineering, 16-ta Makedonska brigada No.1, 1000 Skopje, North Macedonia,

[2] Hidro Konsult Skopje, Hristo Smirnenski 14/1, 1000 Skopje, North Macedonia

***Corresponding author:** ivan.minchev@sf.ukim.mk

Received: September 5th 2024 / Accepted: November 22nd 2024 / Published: December 31st 2024

https://doi.org/10.24057/2071-9388-2024-0581

ABSTRACT. The catchments of the reservoirs Spilje and Globocica are positioned in the western part of North Macedonia. These catchments are situated in the higher part of the Drim/Drin catchment which is a transboundary catchment stretching in several countries. The two catchments were mapped for erosion according to the Erosion potential method by Gavrilovic. In order to assess the Erosion potential method, a bathymetric survey was also carried out. The two erosion maps created for the two reservoir catchments show very different results. The catchment of the reservoir Globocica is one of the most preserved catchments in the country from soil erosion point of view with average erosion coefficient of 0.21, specific annual production of erosive sediment is 394 $m^3\ km^{-2}\ yr^{-1}$, the specific annual transport of erosive sediment is 247 $m^3\ km^{-2}\ yr^{-1}$ and the annual transport of erosive sediment is 74,543 $m^3 yr^{-1}$. On the other hand, the catchment of the reservoir Spilje is one of the most erosive areas in the country, with average erosion coefficient of 0.44, specific annual production of erosive sediment of 776 $m^3\ km^{-2}\ yr^{-1}$, the specific annual transport of erosive sediment of 541 $m^3\ km^{-2}\ yr^{-1}$ and annual transport of erosive sediment is 563,154 $m^3 yr^{-1}$. The sedimentation of both of the reservoirs was measured only once in 2014 and 2015. The accumulated sediment in Spilje is 36.7 $x10^6\ m^3$ or mean annual intensity of sedimentation is 815,555 $m^3 yr^{-1}$. On the other hand, the Globocica reservoir has much lower values for sedimentation, 3.3$x10^6\ m^3$ or mean annual intensity of sedimentation of 67,346 $m^3\ yr^{-1}$.

KEYWORDS: Erosion rates, Erosion modelling, EPM, lake bathymetry, reservoir sedimentation, Drim/Drin

CITATION: Minchev I., Trendafilov B., Blinkov I., Trendafilov A., Ivanovski D. (2024). Measuring And Modeling Erosion In Two Successive Reservoir Catchments On The Drim River In North Macedonia. Geography, Environment, Sustainability, 4(17), 50-57 https://doi.org/10.24057/2071-9388-2024-0581

Conflict of interests: The authors reported no potential conflict of interest.

INTRODUCTION

The soil and the water are the two out of three components of the natural environment. Water is a renewable resource, but the soil genesis on the other hand is long term process. So, in other words the soil practically is not a renewable resource (Blinkov et al, 2003). Soil erosion is deemed as the most important, most dangerous and most spread type of soil degradation and it is the limiting factor of the sustainable use of the land and development of the areas, states and regions.

Soil erosion has been occurring over the geological time. Inappropriate human activities accelerate this process. Soil erosion by water is a widespread problem throughout Europe. It is considered as one of the major threats to European soils, particularly in the Mediterranean areas (CEC, 2002). In order to effectively formulate mitigation strategies and implement conservation measures to counteract soil erosion, it is essential to objectively identify and quantify areas at risk (Gobin et al., 2002).

The South and Southeast regions of Europe are significantly prone to water erosion. In parts of the region, erosion has reached a stage of irreversibility and in some places, erosion has practically ceased because there is no soil left. Scientists from the Balkan countries faced with the erosion problem for years, paid significant attention to solving problems associated with erosion (Blinkov et al., 2019).

Construction of reservoirs is a priority for providing sustainability of the water resources. In the Republic of North Macedonia there are 23 big and over 120 small water reservoirs. On the other hand, erosion and filling the reservoirs with sediment is one of the main problems of reducing the lifespan of the reservoir. The total annual accumulated sediment in all the reservoirs in the Republic of Macedonia is 3,000,000 m^3 (Erosion map of RM, 1993).

Measuring sediment on natural flows is closely related to the examination of the soil erosion intensity in their respective catchments. The erosion intensity can be measured with direct bathymetric measurements of the reservoirs or with measuring the sediment discharge through one or many respective measuring hydrometric profiles on the stream or it can be estimated through modeling produced and transported sediment in the catchment (Gavrilovic, 1972).

Various methods for erosion risk assessment are used by various countries in Europe. Generally, three types of approaches exist to identify areas at risk (Eckelmann et al., 2006): qualitative approach, quantitative approach, and model approach. All these

methods vary in their characteristics and applicability. All of the previously developed models were created for analog data use but in the recent period they are adapted to use with GIS enabled technologies. The most spread erosion type in the East and Southeast Europe as well as in whole continent is water erosion (Blinkov and Kostadinov, 2010).

The difficulty in applying the physically-based erosion models to natural landscapes lies in the fact that sediment yield predictions are still widely based on very simple empirical models developed by multiple regression methods between morpho-climate parameters and limited measurements of sediment yield and/or sediment fluxes (Jansen and Painter, 1974; Ciccacci et al., 1980; Mulder and Syvitski, 1996; Poesen et al., 2003, Lazzari et al, 2015).

Reservoir sedimentation is a serious consequence of soil erosion with large environmental and economic implications. Based on the existing data on reservoir sedimentation trapping rates, Mahmood (1987) estimated the global annual loss of storage capacity of the reservoirs was around 1%. According to the study by Wisser et al. (2013), global annual loss rates compared to original reservoir storage capacity were projected to range between 0.5 and 1%, equivalent to about 30 to 60 billion cubic meters per year.

Over time, sediments build-up in reservoirs and displace usable storage volume, which in turn negatively affects hydropower generation, reduces the reliability of the reservoir, irrigation, water supply, flood management services, and degrades aquatic habitat (Annandale et al., 2016; Icold, 2009; Rakhmatullaev et al., 2011). On the other hand, reservoir sedimentation also provides valuable information on erosion problems and sediment transport within a drainage basin. A reservoir can be considered as a large-scale experiment, as the outlet of a giant erosion plot (de Vente et al, 2000, Mincev, 2015).

The measuring of the deposited sediment in the reservoir is done on the basis of a reservoir bathymetric survey. In order to assess the rate of sedimentation of the catchment there should be constant monitoring of the filling up the reservoirs with sediment. This data is necessary for validation and calibration of the models for determining the sediment production and transport in the catchment.

The first erosion map of the country was finished in 1993 by the Institute for water economy (orig: Zavod za vodostopanstvo) in a process which lasted eleven years with extensive field validation and with traditional mapping techniques. After almost thirty years was updated in 2020 with contemporary mapping techniques (GIS, Remote sensing including field mapping using expert judgment approach as control of results of modelling). The latest erosion map was used in the analyses of this paper (Blinkov et al, 2020).

The aim of this paper is to show the difference between measuring sediment in the reservoirs Globocica and Spilje and estimating the sediment which is deposited in the reservoir by using established modeling schemes. The separate objectives are: (1) to measure the deposed sediment in the reservoir and to estimate the rate of sedimentation of the reservoirs, (2) to estimate the annual transported sediment in the reservoir using the EPM methodology, and (3) to compare the measured and modeled sediment estimations.

MATERIALS AND METHODS

Study area

The catchment areas of the reservoirs Spilje and Globocica are located in the western part of the Republic of North Macedonia. The Black Drim river basin connects with the White Drim in Albania and further flows as Drim (Drin) river up to the Adriatic Sea.

The Drin Basin is positioned in the south-east of the Balkan Peninsula with water bodies and watersheds which spread across Albania, Greece, Serbia, Montenegro and North Macedonia. It comprises the sub-basins of the Black Drin, White Drin, Drin and Buna/Bojana rivers, of the Prespa, Ohrid and Skadar/Shkoder lakes, the underlying aquifers, and the adjacent coastal and marine area (Fig.1). Water also flows through underground karst cavities from Lake Prespa to Lake Ohrid (http://drincorda.iwlearn.org/drin-river-basin/introduction).

The catchment area of Spilje reservoir is 985 km^2 and Globocica reservoir is 328 km^2 respectively, excluding the Ohrid Lake catchment. In this study, the catchment area of the Globocica reservoir is starting from the Ohrid lake. From sediment transport point of view, Ohrid Lake is not considered a sediment source, it is more of a sediment trap, and therefore the calculation of the sediment starts beyond the Ohrid lake. The main water source of the Globocica reservoir is the Drim River. The total storage of the reservoir is projected on 58x10^{6}m^3.

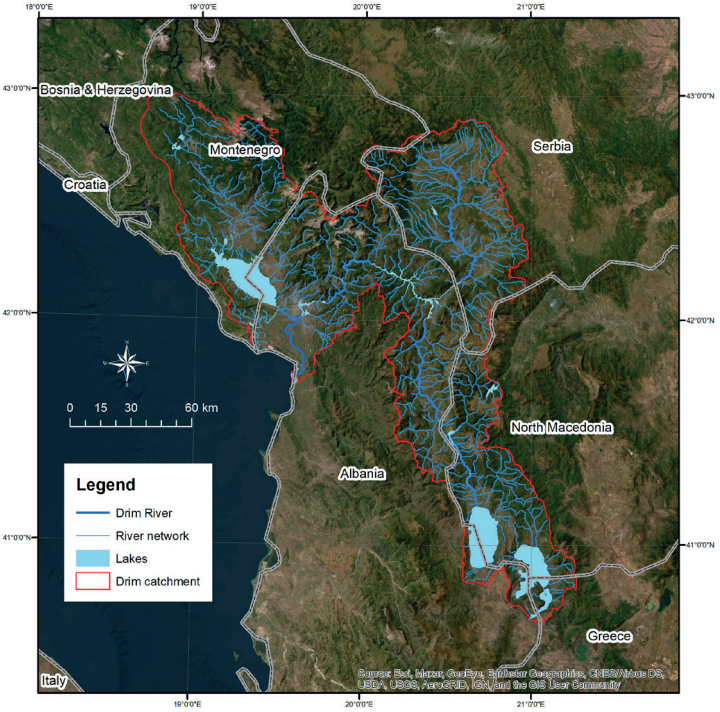

Fig. 1. Drim catchment within the administrative borders

The catchment area of the Spilje reservoir is constituted of two mayor catchment areas: Radika River to the north and to the south extends the catchment area of the river Black (Crn) Drim. Reservoir Spilje (Debar Lake) stretches east and south of the town of Debar. The dam Spilje is located on the Crn Drim River (Black Drin), 3.5 km south of the town Debar, about 300m upstream of the North Macedonian-Albanian border (Fig. 2). The total storage of the reservoir is projected on $543x10^6m^3$.

The climatic characteristics of the catchment of the reservoirs are strongly influenced by the location, orography, vegetation and hydrological conditions of the region. The lowest parts of the basins are affected by the sub-Mediterranean climate, hilly and upland areas are affected by moderate continental and mountainous climate and highland areas are affected by typical mountain climate. The average annual air temperature for the catchment is 7.1°C. The average annual rainfall sum is 860 mm within the analysed period (1981-2010) (Aksoy et al. 2020). The calculated R factor (rainfall-runoff erosivity factor according USLE) for the catchment is in range of 502 and 831 with average value of 633 MJ mm ha^{-1} h^{-1} yr^{-1}.

The catchment area of the reservoir Spilje has heterogeneous geological structure. In the catchment area of the reservoir is dominated by complex phyllites, metasandstones and conglomerates 24%, complex sandstones, clay, argiloshists and limestone 14% and 13% of limestone with chert, clay and massive limestones. As a result, the soil forming factors in the catchment can be found the following soil types: brown forest soils (eutric and distric cambisols) 30%, rankers 28%; calcocambisols 12% and lithosols 10% (Mincev et al, 2017).

The catchment area of the reservoir Globocica has similar geological and soil structure with some differences. Plate dolomite with chert, shale limestone and conglomerate 32%, alluvium 14%, sandstone, shale limestone and conglomerate 12%, marl clay, sands and gravel 11%, phyllite schists 8%, etc. The dominant soils are calcomelanosol 22%, brown forest soils (eutric and distric cambisols) 21%, complex of calcomelanosols, calcocambisols and dolomite 14% and molic fluvisols 11% (ibid).

The land cover in the catchment of Spilje is mostly dominated by broadleaved forest 40% (primarily of oak, beech or beech-fir forests), natural grasslands 36%, transitional woodland-shrub 10% and 6% agriculture area (Corine LC/LU 2018). The upper limit of the forest is dominated by alpine and subalpine meadows, rocky and massive rock formations. In terms of erosion, the existing vegetation basically provides relatively good protection of the land from erosion. The worst situation is in the vicinity of the inhabited areas, where the land use is significantly affected by human. On the other hand, the land cover in the catchment of Globocica is also dominated by broadleaved forest 38%, agriculture 29%, natural grasslands 9% and transitional woodland-shrub 13%. This catchment has more agriculture area but it does not contribute significantly to the erosion and sediment budget because is detached from the vicinity of the reservoir and it is on a flat area. Most of the agriculture area has the lowest erosion category (V).

Slope is a significant factor in increasing erosion and if the two catchments are compared: Spilje has an average slope of 50.2% and Globocica has an average slope of 30.8%. In combination of the slope with the unstable geological substrate on the shores of the Spilje reservoir there can be seen extreme erosive processes which significantly contribute to the reservoir sedimentation (Fig.3).

Bathymetric measurements of the Spilje and Globocica reservoirs

The main task of the echo-sounding measuring of the reservoirs is to determine the volume and the weight of the sediment between two consecutive measurements or from the beginning of the functioning of the reservoir till the moment of the measuring. From these measurements, also some other parameters can be calculated like the annual sediment yield and the reservoir lifespan (Hall, 2010). It is estimated that worldwide, annually, from 0.5% to 1% of the total storage of the reservoirs is lost because of filling up the reservoirs with sediment (White, 2001).

Acoustic echo-sounding relies on accurate measurement of time and voltage. A sound pulse of known frequency and duration is transmitted into the water, and the time required for the pulse to travel to and from a target

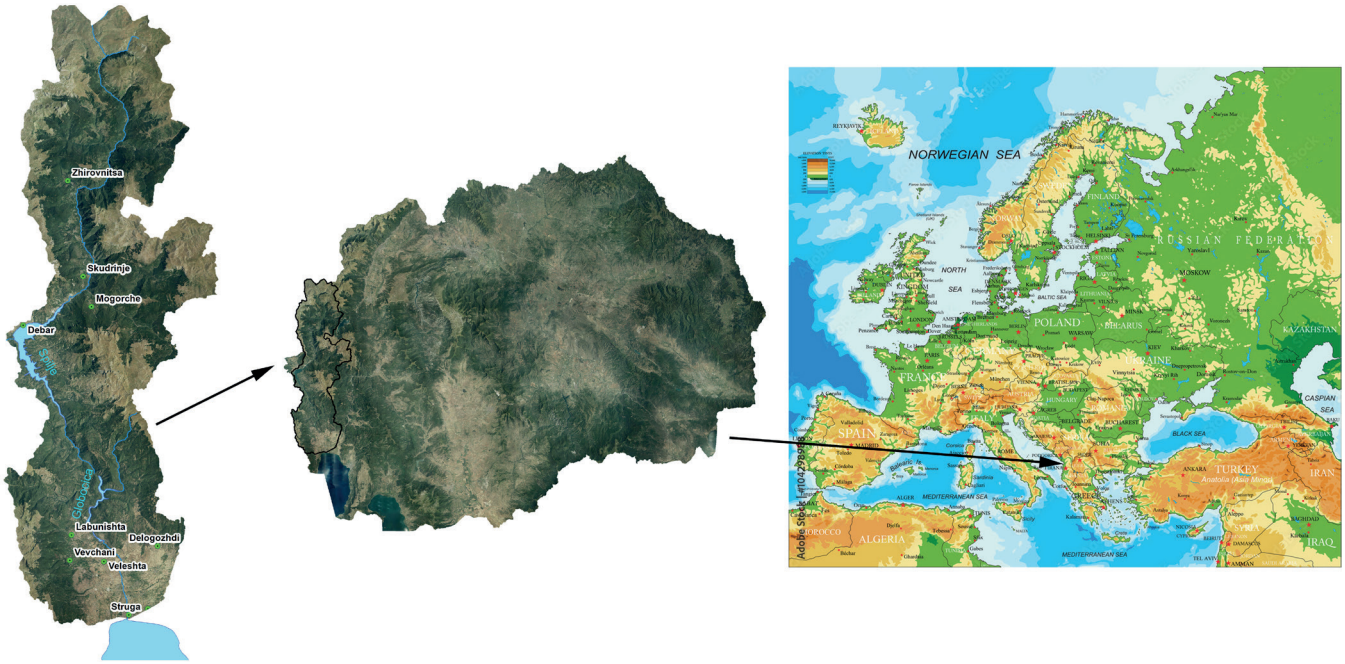

Fig. 2. Location of the catchments of Globocica and Spilje in the Republic of North Macedonia and Europe
Source for map of Europe: https://www.europosters.eu/europe-physical-map-f104298988

(e.g., a submerged object or the bottom of a water body) is measured. To acquire information about the nature of the target, intensity and characteristics of the received signal also are measured. Prior to conducting a bathymetric survey, geospatial data (including geo-referenced aerial photography) of the target lake are acquired, and the lake boundary is digitized as a polygon shape file. Transect lines are predetermined based on project needs and reservoir size (Fig. 4). Immediately before or after the bathymetric survey, elevation of the lake surface is determined (Jakubauskas and deNoyelles, 2008).

The reservoirs Spilje and Globocica were constructed in 1969 and 1965, respectively. The first and only sediment measurement was done in 2014 and 2015. The bathymetric measurement was done using combined transect and contour measurement.

Modeling transported sediment in the reservoirs Globocica and Spilje with the Erosion Potential Method (EPM)

There are several methods which are used for soil erosion estimation. The paper from Blinkov and Kostadinov (2010) give a review of several models for estimation of erosion: EUROSEM, USLE, PESERA, KINEROS, WEP, WEPP and EPM. All of the models provide an estimate of soil erosion, but only few deal with transport and deposition of the sediment: EUROSEM, WEPP and EPM.

The EPM was developed in the Balkan region, south Serbia, which is very similar in climatic conditions with North Macedonia and therefore it is well adapted to the study area. Also, the model has the ability to predict sediment transport and deposition and it was developed

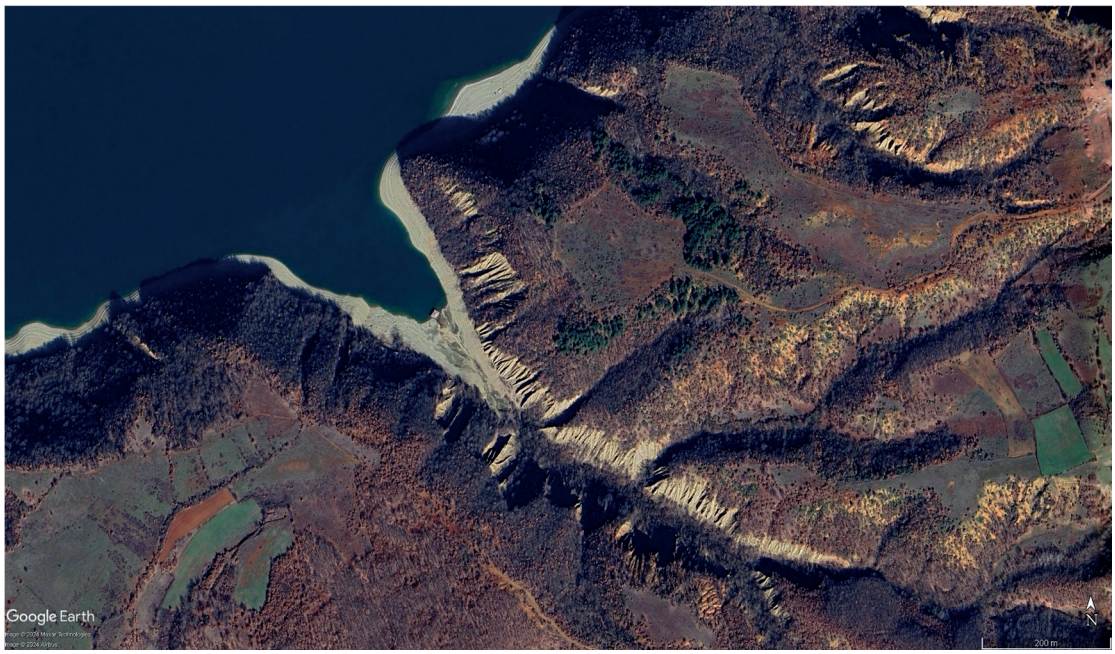

Fig. 3. Gully erosion and extreme erosive processes on the banks of the Spilje reservoir

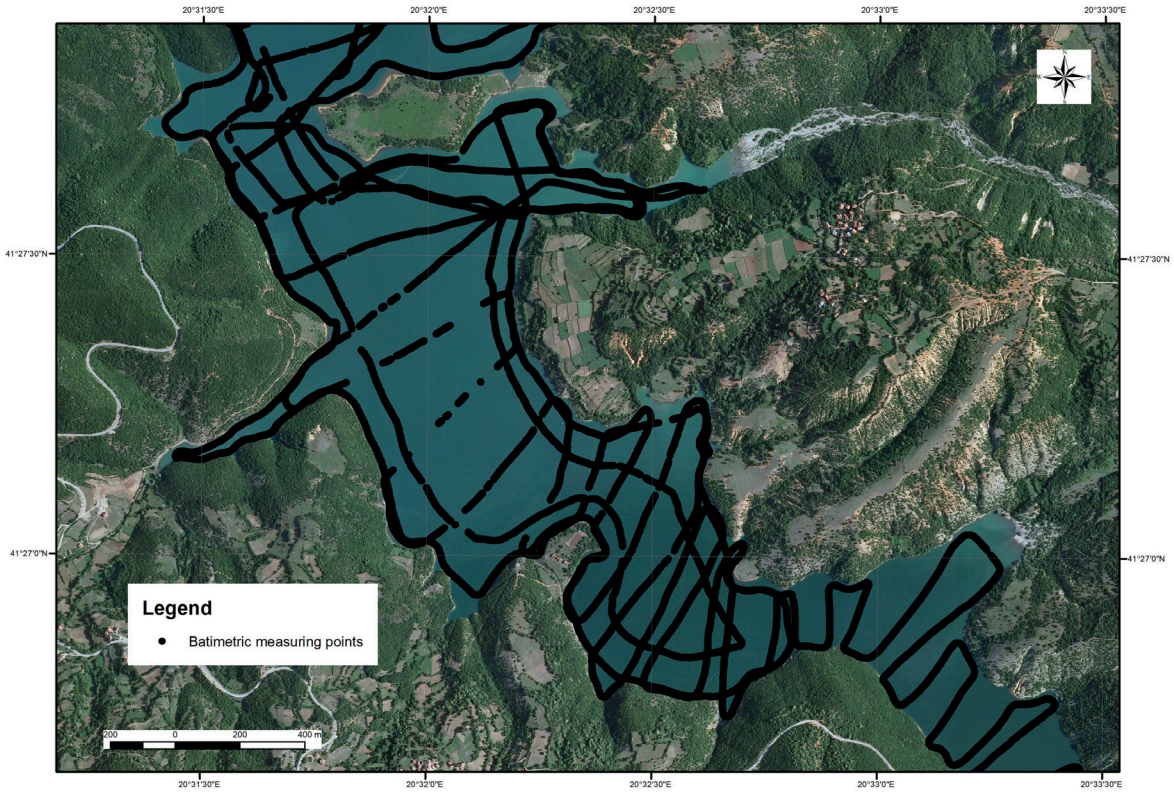

Fig. 4. Bathymetric measurements of the Spilje reservoir

with calibration of deposited sediment in the existing reservoirs. All of the previous studies were developed using EPM and therefore the results would be comparable and the methodology would be transferable (Mincev, 2015b; Blinkov & Kostadinov, 2010).

$$Z = \gamma * Xa * \left(\varphi + \sqrt{I_{sr}}\right) \quad (1)$$

$$G_{year} = T * H_{year} * \pi * \sqrt{Z^3} * F * R_u \quad (2)$$

Where:
Z – coefficient of erosion by Gavrilovic (dimensionless)
γ - reciprocal value of resistance of soils/rocks on erosion processes
Xa – protection of the catchment in natural conditions and after erosion control
φ - coefficient of visible processes of erosion
Jsr - mean slope of the catchment
G – quantity of transported sediments [$m^3\ yr^{-1}$]
T – temperature coefficient
H – total annual precipitations [mm]
π – ludolph number
F – catchment area [km^2]
Ru – retention coefficient

There are several papers clarifying the EPM (see Mincev and Blinkov, 2007) and here only the approach will be shortly explained and the used data in the process and the used modifications will be clarified more elaborately. The EPM (by Gavrilovic) was originally designed to be used with hardcopy maps, and the mapping process itself was mainly done on catchment level. With the advent of the GIS tools and the large variety of geographic data available (Corine LC/LU, soil maps, geology maps, elevation data – DEM, etc.), the mapping process evolved on much smaller mapping units. These datasets can be with good quality but the production scale should be taken into account and they could be reclassified according the given classes in the methodology. It is recommended using global dataset because of the easy transferability and comparability of the results.

The most specific parameter in the EPM is the "Xa" parameter which is connected with the land cover of the catchment and presence of implemented soil erosion measures and works. The determination of the "X" part of this coefficient is done with the use of land cover/use map. The most commonly used land cover map is Corine LC/LU map produced by European Environmental Agency (EEA). This map is good for general purposes but in order to be used for erosion mapping it should be improved. The most obvious example is the class forest. If the class forest is with good cover and in good condition it should take value of 0.05, but in most of the cases the forest polygons are generalized and they do not have the full cover or in some cases there are gaps. To overcome this problem, it was included NDVI (Normalized difference vegetation index). The NDVI was extracted with Google Earth Engine and to each land cover polygon was assigned an average NDVI value. Then the highest values of NDVI were assigned the default Xa value of 0.05 and the lowest value was visually interpreted and assigned a value (Fig. 5). All of the other values in between were rescaled according the NDVI value. The same process was repeated for all of the land cover classes.

The input parameters used for the EPM were as follows: National soil map (scale 1:50,000); Land cover: Corine LC/LU 2018 (developed by European Environmental Agency, scale 1:100,000), later improved using visual photo-interpretation of aerial imagery with spatial resolution of 0.3 m (2019) Fig.5; DEM spatial resolution of 5 m; climatic parameters developed in spatial resolution of 20 m, analysed period (1981-2010) (Aksoy et al. 2020).

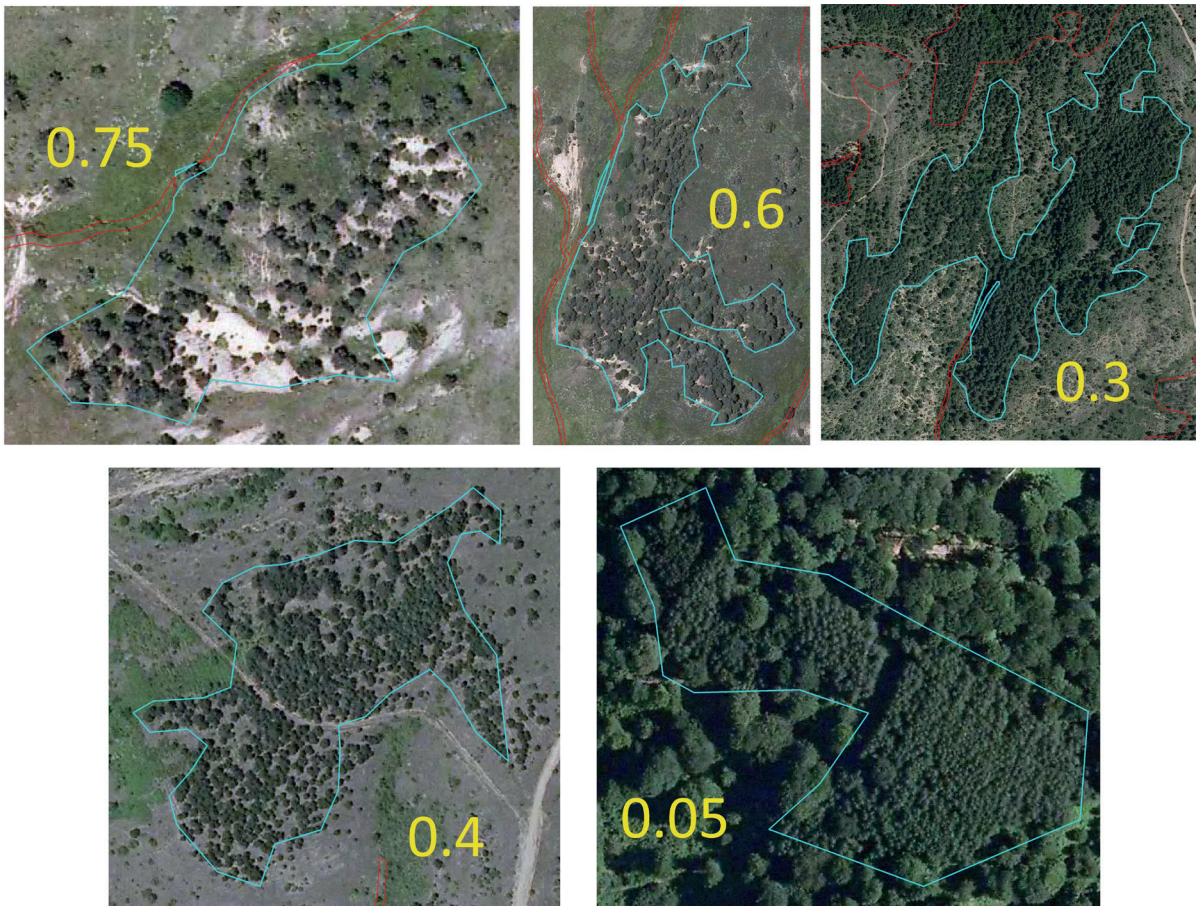

Fig. 5. Xa values for the land cover class forest

RESULTS AND DISCUSSION

The reservoir Spilje was designed with total storage of 543 million m^3. The bathymetric measurements in 2014 showed 36.7 million m^3 deposited sediment in the reservoir or annually 815,555 m^3 yr^{-1} or specific 827.97 $m^3km^{-2}yr^{-1}$. The reservoir Globocica was designed with total storage of 58 million m^3. The bathymetric measurements in 2015 showed 3.3 million m^3 deposited sediment in the reservoir or annually 67,346 m^3yr^{-1} or specific 205.32 $m^3km^{-2}yr^{-1}$.

The EPM model was conducted on both reservoir catchments. The catchment of the reservoir Globocica is one of the most preserved catchments in the country with average erosion coefficient (z) of 0.21, specific annual production of erosive sediment is 394 m^3 $km^{-2}yr^{-1}$, the specific annual transport of erosive sediment is 247 $m^3km^{-2}yr^{-1}$ and the total annual transport of erosive sediment (sediment yield) is 74,543 m^3yr^{-1}. On the other hand, the catchment of the reservoir Spilje is one of the most erosive areas in the country, with average erosion coefficient (z) of 0.44, specific annual production of erosive sediment of 776 $m^3km^{-2}yr^{-1}$, the specific annual transport of erosive sediment of 541 m^3 km^{-2} yr^{-1} and total annual transport of erosive sediment is 563,154 m^3yr^{-1}.

If the measuring and modelling results are compared there can be seen significant difference. Since these two reservoirs do not have continuity of sediment monitoring there can be expected such discrepancies. According the EPM at the moment, the annual transport of erosive sediment is 563,154 m^3yr^{-1} and the bathymetric survey shows reservoir sedimentation of 815,555 m^3 yr^{-1}. The difference is significant. There are two possibilities for this difference: error of the erosion modelling or error in the

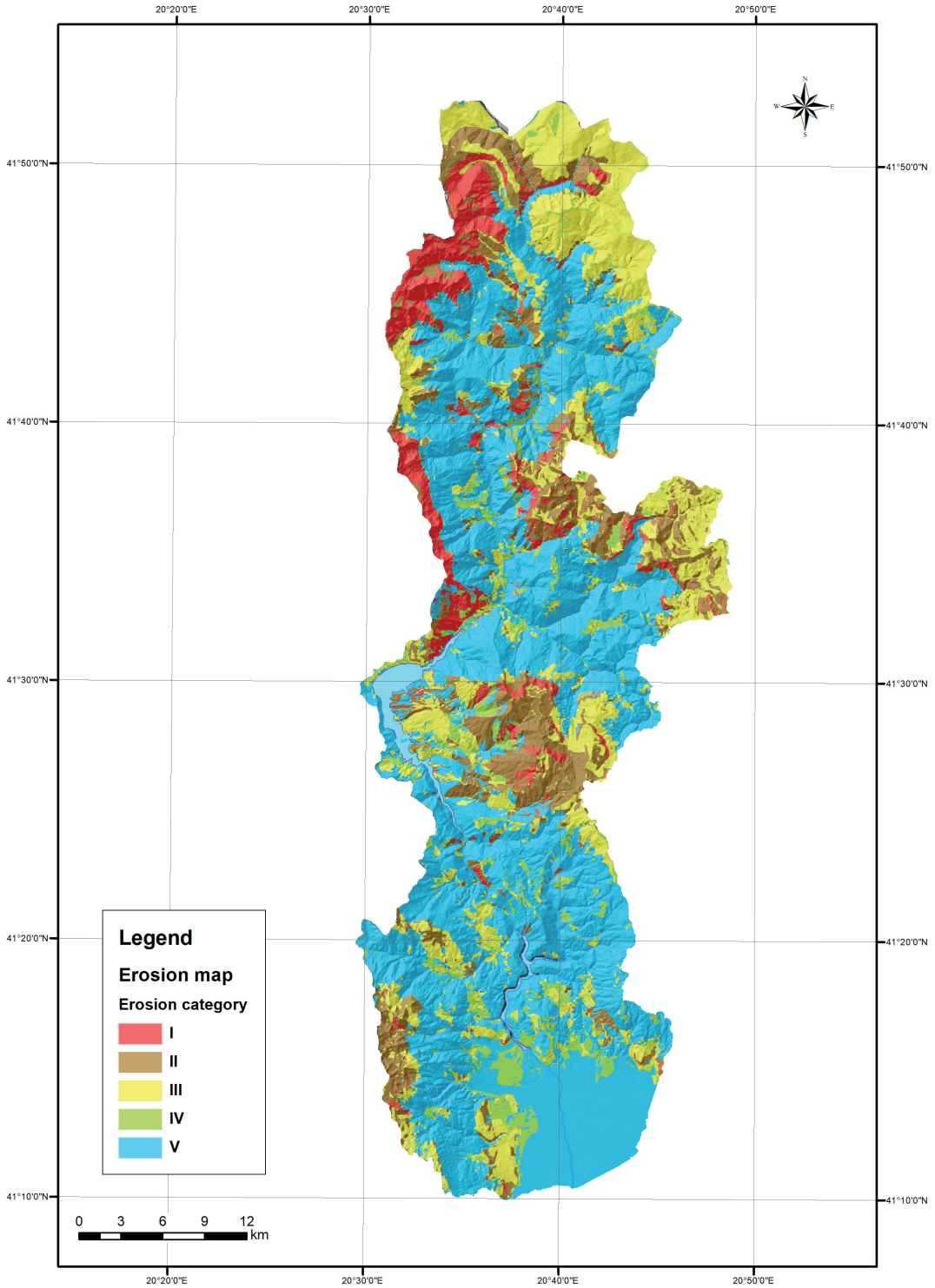

Fig. 6. Soil erosion map of the catchments of the reservoirs Spilje and Globocica

bathymetry. The northern part of the basin is characterized with specific Alpine relief conditions, where numerous so called "point" sources of sediments occur, i.e. rock weathering, landfalls, landslides, even coastal erosion on the lake banks (result of fluctuation level) that in a scale of modelling following the EPM cannot be expressed. It should be mentioned that EPM was developed in the area of old mountains with different relief conditions.

According to Minchev (2018), on a similar study done for the reservoir Kalimanci in the eastern part of the country, the sedimentation rate of the reservoir shows two rates of sedimentation from two periods, 1969-1984 and 1984-2013, in which the latest period has 2.5 times decreased rate of sedimentation. This can be accounted on the decreased pressure on the environment: decreased population, agriculture practices and animal husbandry and significant erosion control measures in the past (Mincev et al. 2019, 2023).

On the other hand, the reservoir Globocica does not have very big differences between the measured and modeled quantities. According to the EPM at the moment, the annual transport of erosive sediment is 74,543 m^3yr^{-1} and the bathymetric survey shows reservoir sedimentation of 67,346 m^3 yr^{-1}. The aforementioned pressures were not present here because this catchment is more natural and there are not so big disturbances and also as previously mentioned, this catchment has much gentler slopes.

CONCLUSIONS AND RECOMMENDATIONS

From the depicted results, it can be concluded that that measuring and modeling sediment does not yield the same results. The modeling results for the Spilje reservoir show that the annual transport of erosive sediment is 563,154 m^3yr-1 and the bathymetric survey measured reservoir sedimentation of 815,555 m^3 yr-1. The difference is significant. Several aforementioned studies show decrease in the severity of the erosive processes in the past decades. This can be accounted on the decrease of the population in the catchment and therefore decrease of the pressure on the environment. So according this theory, the rate of sedimentation of the Spilje reservoir in the past, up till the mid 1980's, was much higher according to Minchev (2018), on a similar study done for the reservoir Kalimanci.

On the other hand, the Globocica reservoir has similar quantities between the measured and modeled quantities. The model shows that the annual transport of erosive sediment is 74,543 m^3yr^{-1} and the bathymetric survey shows reservoir sedimentation of 67,346 m^3 yr^{-1}. This can be accounted on the absence of agricultural practices in the past, and most of the catchment was mostly covered with forest with gentler slopes.

The existing models which estimate sediment transport and deposition give close approximation of the state of the environment. Also, the choice of the model is dependent on the geolocation and site conditions. Another thing to consider is for what kind of purpose the models were developed.

Validation of the model with measured quantities is a prerequisite for a good model. There are a lot of papers which employ model modifications and they end up with just publishing results without any validation. The two catchments examined in this paper are a good example of using the same method of measurement and modeling and yield different results. The Globocica catchment has a good fit of the EPM with the sediment measurements and the Spilje catchment has higher measured values for the sedimentation. This can be accounted on the scarce sediment monitoring data, meaning that having only one measurement data per reservoir is not sufficient enough to assess the current rate of sedimentation. It is recommended that in near future another measurement be executed of the two reservoirs in order to estimate the current sedimentation rate.

Most of the developed theory is not very recent. In order to be implemented with the advances of the new technologies it should be modified.

REFERENCES

Aksoy, E., Arsov, S., Mincev, I., Fang C. (2020) Agro-ecological atlas of the Republic of North Macedonia. Rome, FAO

Annandale, G. W., Morris, G. L., & Karki, P. (2016). Extending the life of reservoirs: Sustainable sediment management for dams and run-of-river hydropower. The World Bank.

Blinkov I., Trendafilov A. and Kaevski I. (2003). The role of the forests on the water and sediment discharge, research project UKIM Forestry faculty Skopje

Blinkov I. and Kostadinov S. (2010). Applicability of various erosion risk assessment methods for engineering purposes, BALWOIS conference 2010, Ohrid, Macedonia

Blinkov I., Trendafilov A., Muaketov D., Monevska Alcinova S., Stevkova S., Stevkov A., Minchev I. and Trendafilov B. (2020) Erosion, Drought and Desertification Atlas of the Republic of North Macedonia; https://balkansfoundation.org/publications/

Blinkov I., Kostadinov S., Mincev I., Petrovic A. (2019) Soil Erosion and Torrent Control in Western Balkan Countries; ch.28 - pgs. 510-536, Title of the book: Degradation of Soil and Water Resources; Editors in Chief: Rui Li, Ted L. Napier, Samir El-Swaify, Mohamed Sabir, Eduardo Rienzi; Science Press, Beijing and Springer

CEC. (2002) Communication on Soil Protection – Towards a Thematic Strategy for Soil Protection,

Ciccacci, S., Fredi, F., Lupia Palmieri, E., Pugliese, F. (1980). Contributo dell'analisi geomorfica quantitativa alla valutazione dell'entita dell'erosione nei bacini fluviali. Boll. Soc. Geol. Ital. 99, 455–516.

de Vente J., Poesen J., and Verstraeten G. (2000). Evaluation of reservoir sedimentation as a methodology for sediment yield assessment in the Mediterranean: challenges and limitations, SCAPE-Soil conservation and protection for Europe;

Eckelmann, W., Baritz, R., Bialousz, S., Bielek, P., Carré, F., Hrušková, B., & Tóth, G. (2006). Common criteria for risk area identification according to soil threats. Office for Official Publications of the European Communities

Erosion map of RM (1993), UKIM, Institute for water economy

Gavrilovic S. (1972) Inzenjering o bujicnim tokovima i eroziji (Engineering of torrents erosion) (in Serbian). Izgradnja, Belgrade special edition, pp. 272.

Gobin A, Govers G, Jones R, Kirkby M, Kosmas C, (2002) Assessment and reporting on soil erosion. Background and workshop report. chRepSoilerosFIN110902.pdf http.//eusoils.jrc.ec. europa.eu/esdb_archive/pesera/pesera_cd/pdf/

ICOLD (2009) Sedimentation and Sustainable Use of Reservoirs and River Systems Draft Icold Bulletin. International Commission on Large Dams (ICOLD), Paris

Jakubauskas M., deNoyelles F. (2008) Methods for assessing sedimentation in reservoirs, pp. 25, Book: Sedimentation in our reservoirs: Causes and Solutions

Jansen, I.M.L., Painter, R.B. (1974). Predicting sediment yield from climate and topography. J. Hydrol. 21, 371–380.

Lazzari M., Gioia D., Piccarreta M., Danese M., Lanorte A., (2015). Sediment yield and erosion rate estimation in the mountain catchments of the Camastra artificial reservoir (Southern Italy): A comparison between different empirical methods, Catena 127 (2015) 323–339

Mahmood, K. (1987) Reservoir Sedimentation: Impact, Extent, Mitigation; World Bank Technical Report No. 71; World Bank: Washington, DC, USA,

Mincev I., & Blinkov I. (2007) GIS model for assessing water and sediment discharge based on the Gavrilovic methodology, International Conference "Erosion and torrent control as a factor in sustainable river basin management" 25-28 September 2007, Belgrade/Serbia

Mincev I., (2015). Measuring deposed sediment in small reservoirs, case study: "Gradče" reservoir, Agriculture & Forestry, Vol. 61, Issue 2: 215-223, 2015, Podgorica

Mincev I., (2015b) Development of methodology for establishing protection zones in the proximity of water reservoirs from erosion and sediment transport aspect, Doctoral thesis, Ss. Cyril and Methodius University, Faculty of Forestry in Skopje

Mincev I., Trendafilov A., Blinkov, I., Ivanoski D., (2017) "Soil erosion rates in two successive reservoir catchments: Spilje and Globocica reservoir", International scientific conference "Sustainable forestry – fact or fiction?", Ss. Cyril and Methodius University, Faculty of Forestry, Skopje, Macedonia 4-6 October 2017. Published in Forest review vol. 47 No. 2, ISSN 1857-9507

Mincev I., Blinkov, I. and Trendafilov A. (2019) Sedimentation rates and lifespan analyses in the "Kalimanci" reservoir, CONTRIBUTIONS, Section of Natural, Mathematical and Biotechnical Sciences, MASA, Vol. 40, No.2, pp. 181–189(2019), ISSN 1857–9027, DOI:10.20903/csnmbs.masa.2019.40.2.142

Minchev I., Blinkov, I., Trendafilov A., Trendafilov B., (2023) Development of Erosion Protection Zones in the Catchment of the Reservoir Kalimanci, North Macedonia, IJERD – International Journal of Environmental and Rural Development (2023)14-1, pp.77-81, ISSN 2433-3700

Mulder, T., Syvitski, J.P.M., (1996). Climatic and morphologic relationships of rivers: implications of sea-level fluctuations on river loads. J. Geol. 104, 509–523.

Poesen, J., Nachtergaele, J., Verstraeten, G., Valentin, C. (2003). Gully erosion and environmental change: importance and research needs. Catena 50, 91–133.

Rakhmatullaev, S., Marache, A., Huneau, F., Le Coustumer, P., Bakiev, M., & Motelica-Heino, M. (2011). Geostatistical approach for the assessment of the water reservoir capacity in arid regions: A case study of the Akdarya reservoir, Uzbekistan. Environmental Earth Sciences, 63(3), 447–460. https://doi.org/10.1007/s12665-010-0711-3

Wisser, D.; Frolking, S.; Hagen, S.; Bierkens, M.F.P. (2013) Beyond peak reservoir storage? A global estimate of declining water storage capacity in large reservoirs. Water Resour. Res. 2013, 49, 5732–5739.

Check for updates

CC BY

RESEARCH PAPER

INTEGRATED TRANSBOUNDARY TISZA RIVER BASIN MANAGEMENT REINFORCEMENT BY NATURAL WATER RETENTION MEASURES

Branislava B. Matić[1*]
[1] Educons University, Vojvode Putnika 87, Sremska Kamenica, 21 208, Serbia
***Corresponding author:** branislava.matic@educons.edu.rs
Received: April 16th 2024 / Accepted: November 22nd 2024 / Published: December 31st 2024
https://doi.org/10.24057/2071-9388-2024-3354

ABSTRACT. Interdependency between river basin water retention capacity and different types of water erosion is well documented and recognized by researchers and practitioners. Erosion adverse effects on sustainable water and land management from local (catchment/ drainage scale) to river basin level are various and generated by natural and anthropogenic drivers. The solutions and measures to address these issues span across Multilateral Environmental Agreements, sectoral policies and legal framework. Consequently, the effective cooperation among different sectors, stakeholders and decision makers is required from local catchment to transboundary river basin level. Natural water retention measures (NWRM) multi-functionality in addressing water-related challenges by integrating different policy objectives at the river basin scale, increased their relevance identification in river basin management plans. Selected NWRM with medium to high benefits with respect to erosion reduction, sediment delivery, flood risk reduction, etc., are summarized. The main steps in flood risk management, "win-win" measures identification by Tisza countries and NWRM included in the Integrated Tisza River Basin Management Plan (2019) are presented. Well-structured data collection approach for different policies integration instead of underlying differences and discrepancies is a good starting point for the productive shared river basins management and governance. If the implementation of the NWRM have potential downstream cumulative effects on low flow water regime the mechanism for evaluation of potential consequences has to be established and defined.

KEYWORDS: enatural water retention measures, flood risk win-win measures, integrated river basin management, transboundary cooperation

CITATION: Matić B. B. (2024). Integrated Transboundary Tisza River Basin Management Reinforcement By Natural Water Retention Measures. Geography, Environment, Sustainability, 4(17), 58-65
https://doi.org/10.24057/2071-9388-2024-3354

ACKNOWLEDGEMENTS: Results and information on Tisza River Basin presented in this paper are funded by DTP Interreg program within the scope of JOINTISZA project (DTP1-152-2.1): Strengthening cooperation between river basin management planning and flood risk prevention to enhance the status of waters of the Tisza River Basin, and joint work by Tisza countries experts within the scope of ICPDR Tisza group, GWP CEE, WWF Hungary, and REC (Regional Environmental Center).

Conflict of interests: The authors reported no potential conflict of interest.

INTRODUCTION

From local hydrologic unit to the large transboundary river basins (Amur, Nile, Danube, Mekong, and so on) complexity of water management and governance is generated by various issues and constrains e.g., extreme events, land use, demand by sectors, natural features, availability, lack of cooperation, etc. Two fundamental forms of water and people relation are benefits of various water use and water adverse effects due to damages and dangers to life and the economy (Jevđević 1946). Increase in multipurpose water use demand by humans and intensive development generates increase in water demand and pollution (Miloradov 1992). Water resources management practice around the world is challenged by serious problems (Simonović 2008). According to Dimkić at al. (2008) abundance, exploitation and sustainable development are three main water management phases. Paradigm change is generated by number of issues that can be addressed by adaptive and integrated water management (Wostl-Pahl et al. 2008) to enable flexibility given the high level of uncertainty with respect floods, droughts, rainfall frequency and intensity, etc. Integrated water resources management (IWRM) concept integrates a large number of processes and their components such as the hydrological cycle, natural characteristics of the basin, environmental sustainability, economic development, institutional and legal framework (Mayfield et al. 2004). The new doctrine - IWRM (Figure 1) is incorporated in policy and legal frameworks at the national, transboundary, and global level to combat increasing pressures on water resources (water scarcity, pollution, climate changes, extreme hydrological events, land use changes, etc.).

Erosion adverse effects on human society and environment accompanied with economic and social consequences are recognized as important for water

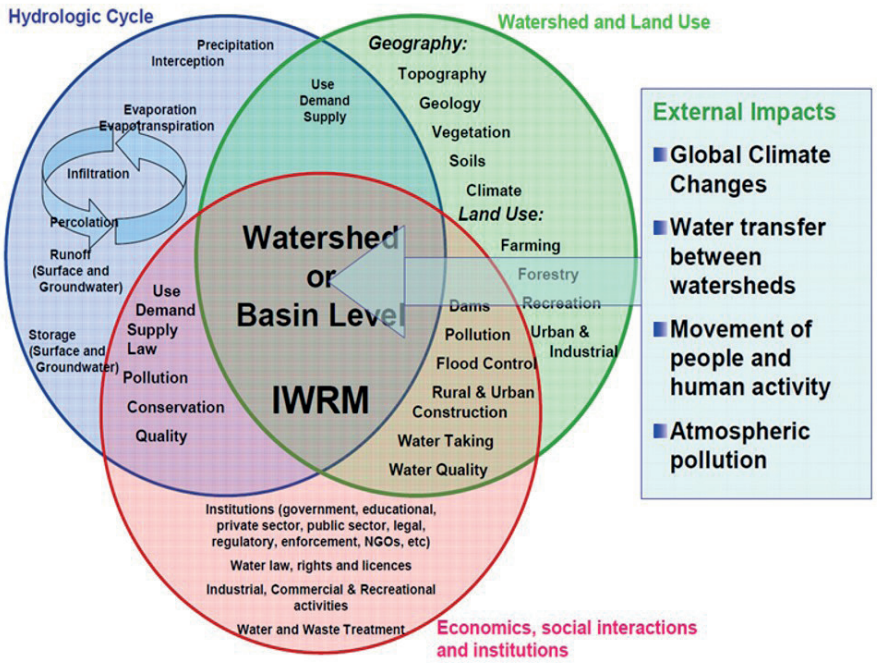

Fig. 1. Conceptual IWRM integration diagram. Source: Mayfield et al. 2004

management with negative impact on water quantity and quality management. Soil erosion by water is estimated to incur a global annual cost of eight billion US dollars to global GDP (Sartori et al. 2019) and falling land productivity due to erosion associated with rice production, is a major driver of the increased water abstraction in Asia. Its consequences span across sectors (water, forestry, environmental protection, spatial planning, disaster risk reduction) and administrative boundaries. Lack of erosion control at the local or country level in the upper part of the river basin generates risks to achieve water management objectives and goals downstream e.g., reservoir sedimentation, landslides, water courses hydromorphology, water quality deterioration that might be decreased if erosion control measures are implemented. Topography, rainfall patterns, land cover and practices are some of the significant factors of relevance for sediment yield and increase in sediment quantity can be a strong signal of various changes that includes watering and erosion, precipitation pattern and frequencies, and human activities (Jaiyeola and Bwapwa 2015). Among the other sources land degradation results in increased erosion intensity, causing elevated sediment loads and enhanced sediment deposition in reservoirs and channels within the river system, environmental and socio-economic losses by decreasing soil fertility, increasing the maintenance costs in hydropower plants and irrigation schemes (Ayele et al. 2021). Land use and land cover (LULC) planning should consider possibilities and constrains to land use practices that reduce erosion to tolerable limits based on soil characteristics, relief, and landowners' socioeconomic aspects (Calegario et al. 2023).

Improved natural water retention capacity by restoring or enhancing natural functioning of ecosystems and the services they provide is achieved by NWRM implementation. The great majority of these measures are qualified as "win-win" solution since their implementation reduce flood risk and support WFD (EU Water Framework Directive) environmental objectives[1]. The integrated and coordinated planning under the WFD and FD (EU Floods Directive) has the potential to identify win-win measures that can deliver on the objectives of both policies[2] and beyond (Green infrastructure, biodiversity, etc). Integrated water management concept is transposed in Republic of Serbia legal framework and implementation advanced for large transnational river basins (Danube, Sava, Tisza) while the action is still pending for sub-basins and their sub catchments (Matić and Simić 2017). The objective of this paper is to underline benefits of the selected NWRM and their identification as the win-win measures that interlink flood risk management and environmental objectives for reinforcement of the integrated Tisza River Basin water management.

ECOSYSTEM SERVICES AND NATURAL WATER RETENTION MEASURES

Ecosystems services (ESS) are benefits provided by ecosystems to society which directly contribute to our well-being and economic wealth (Millennium Ecosystem Assessment 2005). People rely on ecosystems to provide many water related services and hydrologic ecosystem service (HESS) domain includes ESS positive impacts on water regime and water resources, from the supply of water for household use to the mitigation of flood damages (Brauman et.al. 2007). Burkhard et.al. (2009) specified four ESS benefits categories i.e., supporting (nutrient cycling, soil formation), provisioning (supply of drinking water, food, fuel, genetic resources), regulating (regulation of floods, erosion, sediment production, runoff, climate, water purification, etc) and cultural (tourism, recreation, knowledge, and aesthetic experiences).

Their multi-benefits recognition is apparent given the substantial increase in number of publications, implemented or ongoing projects, and their integration in sectoral policies and frameworks in last few decades. Additionally, different definitions and concepts (Eco-DRR,

[1] International Commission for the Protection of the Danube River -ICPDR (2020). Coordinating the WFD and the FD: Focusing on opportunities for improving efficiency, information exchange and for achieving common synergies and benefits, https://www.icpdr.org/sites/default/files/nodes/documents/discussion_paper_coordinating_wfd_and_fd.pdf

[2] EU Commission (2014): Links between the Floods Directive (FD 2007/60/EC and Water Framework Directive (WFD 2000/60/EC), https://op.europa.eu/en/publication-detail/-/publication/5e8ddc30-ed98-47f3-872c-de78851c721f

NWRM, Nature-based Solutions - NbS, Ecosystem-based Adaptation - EbA, etc.) based on ecosystems, their services and benefits are evident (Matić and Karleuša 2022). Estrella and Saalismaa (2013) explain ecosystem-based disaster risk reduction (Eco-DRR) as the "sustainable management, conservation and restoration of ecosystems to reduce disaster risk, with the aim of achieving sustainable and resilient development". Excerpt from study by Sudmeier-Rieux et al. (2019) presented in Table 1 include diverse ecosystems contribution to natural hazards disaster risk mitigation.

For all presented ecosystems and their services contribution to hazards mitigation benefits are primary within regulation and include other aspects (provision, supporting and cultural) regardless spatial distribution. Both floodplains and mountain forests reduce speed and volume of runoff, mitigate droughts, reduce erosion. The reduction rate and mitigation efficiency are more or less site, landscape specific. Governments formally agreed on a definition of nature-based solutions (NbS-NBS), (NbS) as "actions to protect, conserve, restore, sustainably use and manage natural or modified terrestrial, freshwater, coastal and marine ecosystems, which address social, economic and environmental challenges effectively and adaptively, while simultaneously providing human well-being, ecosystem services and resilience and biodiversity benefits"[3].

River basin of any size represents mosaic comprised of various terrestrial and aquatic ecosystems and their services. Study of coherence and inconsistency of European instruments for integrated river basin management (Evers and Nyberg 2013) indicates that the management of water and land resources is poorly connected and achievements of IWRM goals requires consideration of measures that will better connect water management and land use planning. NWRM primary function is enhancing and/or restoring the retention capacity of natural and man-made terrestrial and aquatic ecosystems to deliver a range of services and multiple benefits to people while contributing to the achievement of the objectives of different environmental strategies and policies, e.g., EU Water Framework Directive, EU Flood Directive among the others (Strosser et al. 2015). The NWRM application supports green infrastructure, improves the quantitative status of water bodies, reduces the vulnerability to floods and droughts and restore the natural functioning of ecosystems and the services they provide (Jaritt et al. 2016). Runoff generation primarily depends on the precipitation intensity and distribution and hydrologic unit capacity to retain water (from small catchment to large river basins). Efficient natural capacity to retain precipitation results in more uniform surface water runoff regime with respect to quantity and speed (Jevđević 1956). Subsequently, erosion decrease, infiltration increase, among the other benefits of well-functioning retention capacity to mitigate extreme events. Pećinar (1969) indicated that in watersheds with noticeable terrain slopes, evident torrential flows and intensive erosion processes, the maintenance of existing forest areas and the afforestation of new ones are of great importance and emphasized that lower and denser forests are much more effective for erosion control so the restoration of the forests is necessity.

Research indicated that for forest cover coefficient (ratio of the area covered by forests and basin area) closer to 1 the water regime in the catchment is more uniform and there are less fluctuations in the water level on the basin outlet profiles (Gavrilović 1972). Evidences of the forests ESS benefits for low water regime within Zapadna (Western) Morava River Basin (the largest share of renewable internal - domicile fresh water resources in Serbia) are presented in study by Simić and Matić (2018).

River basin water balance is significantly impacted by terrestrial water storage that is reduced in European part of Russia by approximately 150 mm for 2002-2015 period based on study of Grigoriev et al. (2018) and according to authors it is caused rather by a decline in the storages of surface and ground waters then to changes in soil waters. The function and significance of the river basin retention capacity for water regime and water management are many fold and the understanding of basin retention opportunities gets more and more importance in contemporary water management due to its favourable contributions to sustainable development and integrated water resources management goals achievement (Matić 2019). Evaluation of green infrastructure and agro-environmental measures (filter buffer strips among the others) implementation indicate significant increase in retention of sediments and Total N(nitrogen) and Total P (phosphorus) in Sutla River pilot sub-basins (Ćosić-Flajsig et al. 2023).

Given the benefits of natural water retention capacity there is increasing awareness of various sectors (water, agriculture, forestry, spatial planning, etc), stakeholders and public authorities for measures that mimic natural processes to mitigate anthropogenic and natural adverse effects and provide diverse benefits (NWRM). Based on available knowledge, data and information provided on EU NWRM platform[4], implementation of these measures (53) contributes in IWRM concept implementation at the local scale, support transboundary river basin management and maintain or improve ecosystem services. Excerpt of NWRM with medium to high ESS benefits (Figure 2) are provided for illustrative purposes.

The number of ESS approaches, concepts and definitions is increasing while clear evidence and quantification of multi-functional benefits are missing to great extent. Multi-benefits of the natural water retention

Table 1. Natural hazard mitigation by selected ecosystems

Ecosystem	Hazard mitigation *
Mountain forests Vegetation on hillsides	Floods reduction by peak runoff control Drought mitigation Erosion reduction Increased slope stability
Wetlands Floodplains Lakes and Riverine	Flood control Reduce speed and volume of runoff Realise wet season flows during drought periods

*ESS benefits

[3] The fifth season of the United Nations Environment Assembly. 2022. The UNEA-5 resolution, https://www.unep.org/resources/resolutions-treaties-and-decisions/UN-Environment-Assembly-5-2

[4] Natural Water Retention Measures, http://nwrm.eu

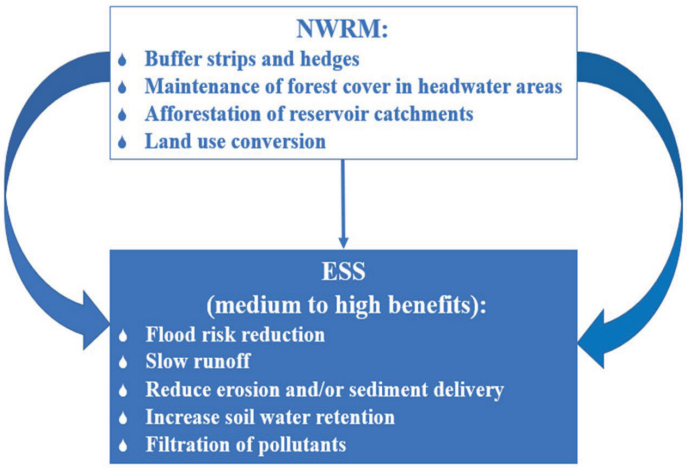

Fig. 2. Schematic display of ESS provided by NWRM based on Catalogue of NWRM[5]

measures for sustainable and integrated river basin management are well documented and quantified by hydrologic analyses. Due to international policy processes and large amounts of funding pledged by both public and private entities, the number of Nature Based Solutions interventions is increasing exponentially and the term NBS is being mainstreamed beyond expectations, for better and for worse, as it is subject to misuse and abuse, and has proponents and opponents (Nehren et al. 2023). The main reason for before mentioned might be advocating NBS as the all-inclusive novel solution superiority against other ESS domain and concepts. Although the benefits provided by NWRM and other ESS concepts and approaches (Eco-DRR, NBS, etc) are numerous, the constraints associated with low-probability events, land ownership, potential space limits in urban areas, etc., should be underlined and mentioned in the planning documents. In addition, their integration with the existing infrastructure has to be elaborated comprehensively (Matić and Karleuša 2023).

STUDY AREA AND METHODOLOGY

Danube River Basin (DRB), the most international river basin in the world, is shared by 19 countries. In 1994, the Danube countries that have territories more than 2,000 km^2 within the DRB signed the Convention on Cooperation for the Protection and Sustainable Use of the River Danube-Danube River Protection Convention[6] (International Commission for the Protection of Danube Rived-ICPDR, 1994). The three main areas for action include the protection of water and associated ecological resources, the sustainable use of water as well as the management of floods and ice hazards within the DRB. All contracting parties (including non-EU members) agreed to coordinate EU WFD[7] and EU FD[8] implementation and participate in the development of a River Basin Management Plan the key tool for implementing the WFD and Flood Risk Management Plan for DRB (Mair and Vasiljević, 2013) as the integral part of integrated river basin management. The largest sub-basin of the DRB is Tisza River Basin (157,186 km^2) shared by five countries (Figure 3).

Transboundary Tisza River Basin (TRB) cooperation

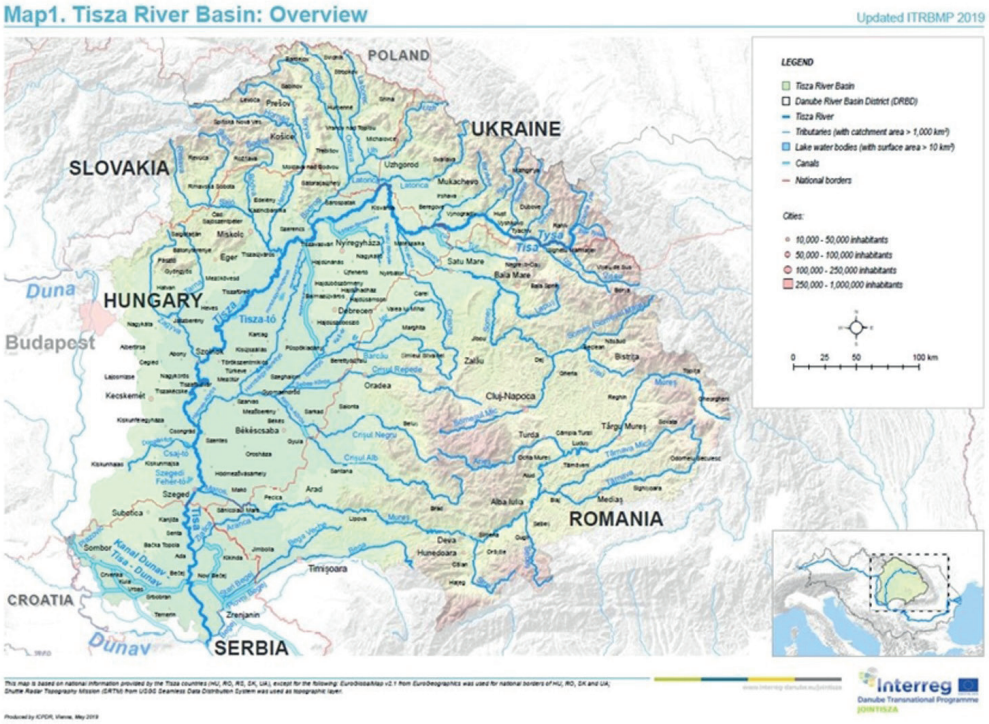

Fig. 3. Tisza River Basin. Source: Updated ITRBMP (Integrated Tisza River Basin Management Plan) 2019[9]

[5] Catalogue of NWRM, https://www.nwrm.eu/measures-catalogue
[6] Danube River Protection Convention: https://www.icpdr.org/about-icpdr/framework/convention
[7] Water Framework Directive (2000/60/EC), https://environment.ec.europa.eu/topics/water/water-framework-directive_en
[8] Floods Directive (2007/60/EC), https://environment.ec.europa.eu/topics/water/floods_en
[9] Updated ITRBMP 2019, https://www.icpdr.org/sites/default/files/nodes/documents/updated_itrbmp_2019.pdf

under the umbrella of the ICPDR started by signature of Memorandum of Understanding[10] and establishing of the ICPDR Tisza Group (ICPDR TG). In 2010 Tisza countries agreed[11] on preparing a sub-basin plan (ITRBMP), which integrates issues on water quality and water quantity, land and water management, floods and droughts[12].

The first ITRBMP (2011) is one of the first river basin management plans that responds to EU Water Framework Directive objectives, considers the ICPDR Flood Action Programme, and reflects the principles of Integrated Water Resources Management (Van Nood et al. 2011). The ITRBMP (2011) introduces water quantity and quality issues interlinkage (Figure 4) identified by ICPDR Tisza Group as a relevant for integrated Tisza River Management and provides comprehensive analysis of pressures from pollution, river engineering works, floods and droughts.

Water quantity and quality issues interlinkage presented above are elaborated in details in Updated ITRBMP 2019 and measures agreed by Tisza countries are presented. ITRBM includes TRB flood risk management plan elements and corresponding measures of basin wide relevance. In addition, flood risk management measures that support WFD environmental objectives, namely win-win measures are identified by Tisza countries based on agreed criteria and included in the updated ITRBMP (2019). The simplified synthesis of the main steps in flood risk management win-win measures identification of these measures are presented in Figure 5.

Incorporated "win-win" measures in ITRBMP Update 2019 are comprehensively elaborated by Tisza countries officially nominated technical experts with respect to field of action and category to emphasize NWRM concept within the TRB following ICPDR procedures and Memorandum of Understanding for TRB (Matić et al 2021).

RESULTS AND DISCUSION

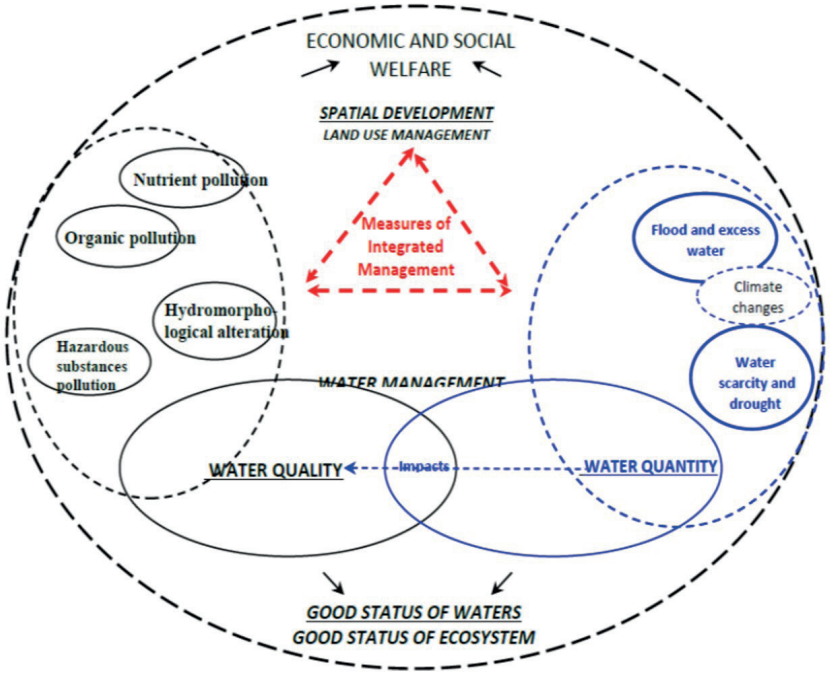

Fig. 4. Inter-linkages between the water quality and water quantity related issue within the TRB identified by ICPDR TG. Source ITRBMP 2011

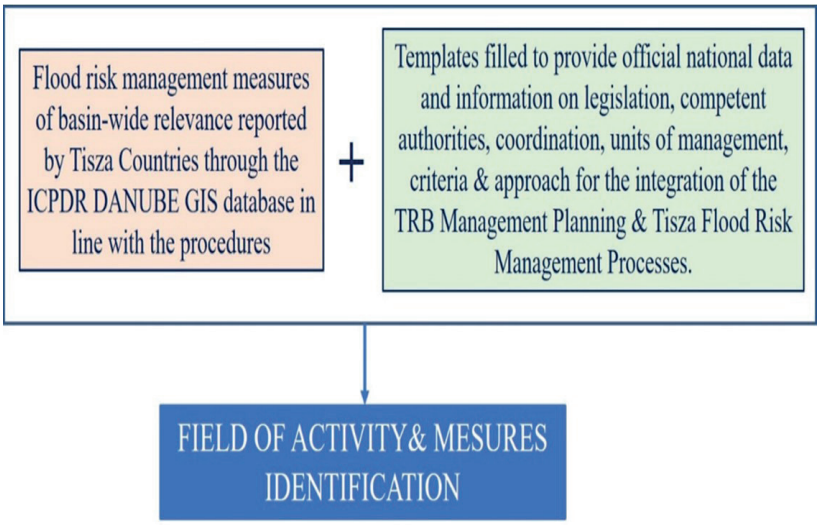

Fig. 5. Methodology for "win-win" flood risk management measures identification

[10] Towards a River Basin Management Plan for the Tisza River supporting sustainable development of the region memorandum of Understanding, https://www.icpdr.org/sites/default/files/FINAL%20-%20Tisza%20-%20MoU%20-%20signature.pdf

[11] Ministerial Statement Towards the Development and Implementation of the RBM Plan for the Tisza Basin (2010), https://www.icpdr.org/sites/default/files/Adopted_Statememt_Tisza_Final.pdf

[12] https://www.icpdr.org/danube-basin/sub-basins/tisza-basin

Table 2. Field of action, category and number of "win-win" TRB flood risk management measures

Field of action	Category	Number
Prevention	Organizational measures (legislative, institutional)	15
Protection	Natural water retention measures (associated to watercourses, wetlands, natural lakes, in line with Directive 2000/60 /EC) and other measures that advocate for increase of retention capacity	36
Public Awareness	Measures to increase community awareness	2
Preparedness	Preparedness measures /Improved preparedness to reduce the floods adverse effects	9
Response and Recovery/ Reconstruction	Post event recovery measures	3

Total number of "win-win" measures of basin wide relevance identified by Tisza countries in line with national policies and legal framework is 65. Summary results for "win-win" flood risk management measures (Table 2) identification clearly indicate natural water retention capacity and NWRM contribution to integrated water resources management at the transboundary river basins level since they connect water and land management. All proposed measures within flood risk management protection field of action (35) are measures that have the potential to increase water retention and provide regulating ESS (e.g., flood risk reduction) benefits with medium to high level. In addition to improved regulating ESS, the majority of measures, e.g., afforestation of the reservoir catchment support provisioning ESS (supply of drinking water, food, fuel, genetic resources) ESS services. NWRM for floodplain restoration and management provides all ESS categories e.g., supporting by nutrient cycling, provisioning, cultural and different regulating benefits (erosion and sediment delivery reduction, flood risk reduction).

The identified NWRMs type of measures are: Measures to restore retention areas (flood plains, wetlands etc.), Natural water retention measures in urban areas, Natural water retention measures by changing or adapting land use practices in forest management (improving forest management in floodplains, maintaining the forests area in catchments of A.P.S.F.R.[13], maintaining and expanding forests in perimeter zones of the reservoirs, expanding the forests in the receiving basins of A.P.S.F.R. - afforestation outside of the forest area), other water retention measures (mainly structural). More details with respect to measures to restore retention areas and other water retention measures are available in Annex 12 of ITRBM (2019) and plan. "Downstream cumulative effects of retentions along the Tisza in Hungary should be evaluated in the frame of bilateral cooperation between Hungary and Serbia"[14] according to disclaimer associated with win-win measures that support maintenance or increase of the natural water retention capacity. This statement is accepted by all Tisza countries to eliminate potential conflict of interest between upstream and downstream country and it is integral part of the Updated ITRBMP (2019) comprised of plan, maps, and annexes and endorsed by high-level Memorandum of Understanding (2019) signature.

All TRB selected NWRMs have moderate to high level of benefits resulting from water retention capacity significance in addressing the great numbers of issues that have to be solved by water management e.g., flood risk reduction, decrease in runoff speed and quantity, reduce erosion and/or sediment delivery, increase soil water retention, pollutants filtration, water demand and supply, etc. The present information and data underline the recognition of multi-benefits provided by NWRM and their role within the integrated water resources management concept and other ecosystem-based approaches and concepts. Finally, they are not "all-inclusive solution" and their efficiency is greatly affected by extreme events frequency.

CONCLUSIONS

Water management objectives achievement requires effective cooperation among sectors and policies given the essence of water as a resource. Natural water retention measures provide framework that support integration of many policies from local to transboundary level required for integrated water resources management due to number of their ecosystem services benefits e.g., flood and drought mitigation, erosion control, pollutants filtration, water purification, improved soil water retention, ground water recharge, among the others. For less frequent, i.e., more sever events their integration with existing grey infrastructure is required. NWRM and other ecosystem-based approaches (NBS, Eco-DRR, etc.) acceptance by practitioners and implementation might be compromised if they continue to be advocated as new approach, solution for all issues and constrains, among the other buzz words and narratives. As presented for Tisza River Basin effective cooperation of the riparian countries technical experts is prerequisite for the integrated water resources management implementation at the level of transboundary river basins. It includes coordinated management of surface and ground water bodies of basin relevance, flood risk management, to support achievement of integrated management of shared river basins. Identification and proposal of the win-win measures to reinforce synergy of the WFD and FD objectives implementation indicated recognition of the NWRM multi-functionality and possibilities for implementation within TRB.

[13] Areas with potentially significant flood risk

[14] Updated ITRBMP 2019, https://www.icpdr.org/sites/default/files/nodes/documents/updated_itrbmp_2019.pdf

REFERENCES

Ayele, G.T.; Kuriqi, A.; Jemberrie, M.A.; Saia, S.M.; Seka, A.M.; Teshale, E.Z.; Daba, M.H.; Ahmad Bhat, S.; Demissie, S.S.; Jeong,J.; et al.(2021). Sediment Yield and Reservoir Sedimentation in Highly Dynamic Watersheds: The Case of Koga Reservoir, Ethiopia. Water,[online] 13(23),p. 3374. Available at: https://doi.org/10.3390/w13233374 [Accessed 14 Apr. 2024].

Brauman, A.K., Daily C.G.,T. Duarte, K.T,.and Mooney A.H. (2007). The Nature and Value of Ecosystem Services: An Overview Highlighting Hydrologic Services. The Annual Review of Environment and Resources, 32, pp.67–98, DOI:10.1146/annurev.energy.32.031306.102758.

Burkhard, B.; Kroll, F.; Müller, F. & W. Windhorst (2009). Landscapes' capacities to provide ecosystem services – a concept for land-cover based assessments. Landscape Online, [online] 15, pp. 1–22. Available at: https://landscape-online.org/index.php/lo/article/view/LO.200915/67 [Accessed 21 Apr. 2024], DOI:10.3097/LO.200915.

Calegario, A.T., da Silva, D.D., Fernandes Filho, E.I. et al. (2023). Characterizing and mapping intensity of land use in large basins through the concept of land use capability. Environmental Earth Sciences, 82,p.151,DOI: https://doi.org/10.1007/s12665-023-10811-8.

Dimkić, M., Brauch, H.J., Kavanaugh, M. (Eds.) (2008) Groundwater Management in Large River Basins. London, UK: IWA Publishing, DOI: doi.org/10.2166/9781780401843.

Jaritt, N., Williams, H., Hanus, A., et al. (2016). A guide to support the selection, design and implementation of natural water retention measures in Europe: capturing the multiple benefits of nature-based solutions. Publications Office. Available at: https://data.europa.eu/doi/10.2779/761211[Accessed 14 Apr. 2024].

Estrella, M. and Saalismaa, N. (2013). Ecosystem-based disaster risk reduction (Eco-DRR): An overview. In The role of ecosystems in disaster risk reduction. Renaud.F.G., Sudmeier-Rieux, K., Estrella, M. (eds.). Tokyo, Japan, UNU Press, ISBN 978-92-808-1221-3, e-ISBN 978-92-808-7190-6.

Evers M., Nyberg L. (2013). Coherence and inconsistency of European instruments for integrated river basin management. International Journal of River Basin Management, [online] Volume11(2),pp.139-152.Available at: https://www.tandfonline.com/doi/full/10.1080/15715124.2013.811416?needAccess=true [Accessed 14 Apr. 2024], DOI: 10.1080/15715124.2013.811416.

G. Ćosić-Flajsig, B. Karleuša, M. Glavan (2023). Green infrastructure and agro-environmental measures for water quality management at the river basin scale, 12th World Congress on Water Resources and Environment (EWRA 2023) "Managing Water-Energy-Land-Food under Climatic, Environmental and Social Instability" Thessaloniki, Greece, 27 June - 1 July 2023: European Water Resources Association (EWRA) ISBN: 978-618-84419-1-0, pp.331-332.

Gavrilović Slobodan (1972). Torrent and erosion Engineering. Beograd, Srbija: Časopis izgradnja, specijalno izdanje, (in Serbian with English summary).

Vadim Yu. Grigoriev, Natalia L. Frolova (2018). Terrestrial water storage change of

European Russia and its impact on water balance. Geography, Environment, Sustainability, [online] Volume11(1), pp. 38-50. Available at: https://ges.rgo.ru/jour/article/view/379/302 [Accessed 14 Apr. 2024], DOI-10.24057/2071-9388-2018-11-1-38-50.

Jaiyeola, A.T.; Bwapwa, J.K. (2015). Dynamics of sedimentation and use of genetic algorithms for estimating sediment yields in a river: A critical review. Natural Resource Modeling, [online] Volume 28 (3), pp.207–218. Available at: https://onlinelibrary.wiley.com/doi/full/10.1111/nrm.12064 [Accessed 14 Apr. 2024], DOI:10.1111/nrm.12064.

Jevđević Vujica (1946). Water management fundamentals - economic and technical study. Novi Sad, Srbija:Štamparija Predsedništva Narodne Skupštine AP Vojvodine, Novi Sad (in Serbian with English summary).

Jevđević V. (1956). Hydrology part I. special ed, book 4, Beograd, Srbija:Hidrotehnički institut "Ing. Jaroslav Černi" (in Serbian with English summary).

Mair, R., Vasiljević, B. (2013). Climate Change Adaptation and Transboundary River Basin Management – Case Study: Strategy on Adaptation to Climate Change for the Danube River Basin, International Conference Climate Change Impacts on Water Resources, 17-18 October 2013, Belgrade, Serbia: Jaroslav Černi Institute for the Development of Water Resources, ISBN 978-86-82565-41-3, pp. 110-116.

Matić, B., Simić, Z. (2017). Prospects for sustainable water resources management within the River Đetinja catchment. European Water, [online] Volume 60, pp.55-60. Available at:https://www.ewra.net/ew/pdf/EW_2017_60_08.pdf, [Accessed 14 Apr. 2024], Publisher: E.W. Publications, ISSN 1105-7580.

Matić B. (2019). Uticaj režima padavina na retencioni kapacitet i upravljanje vodma na slivu, Doktorska disertacija, Fakultet tehničkih nauka, Univerziteta u Novom Sadu, 174 str., 2019. Autorski reprint. (Rainfall impact on river basin retention capacity and water management, Ph.D. Dissertation, FTN University of Novi Sad. National Repository of Dissertations in Serbia, Author reprint).Availbale at: https://nardus.mpn.gov.rs/handle/123456789/11418

Matić, B.; Perović, M.; Vulić, D. (2021). Natural water retention measures contribution to integrated transboundary Tisza River Basin Management - Environmental and Flood risk management objectives synergy. In Proceeding of the International Symposium: Water Resources Management: New Perspectives and Innovative Practices, Novi Sad, Serbia, 23-24 September 2021, pp 113-117.

Matić B.B., and Karleuša, B. (2022). Ecosystem-based disaster risk reduction framework as a tool for improved river basin natural water retention capacity and environmental hazards resilience, Proceedings of EWaS5 International Conference "Moving from Therapy and Restoration to Prognosis and Prevention», Naples, Italy, 12-15 July 2022. Environmental Sciences Proceedings, [online] Volume 21(1), p.40. Available at: https://www.mdpi.com/2673-4931/21/1/40 [Accessed 14 Apr. 2024], DOI:10.3390/environsciproc2022021040.

B.B. Matić and B. Karleuša (2023). Retain for resilience: Natural water retention measures contribution to hydro-meteorological hazards risk reduction at the river basin level, 12th World Congress on Water Resources and Environment (EWRA 2023) "Managing Water-Energy-Land-Food under Climatic, Environmental and Social Instability" Thessaloniki, Greece, 27 June - 1 July 2023: European Water Resources Association (EWRA) ISBN: 978-618-84419-1-0, pp.83-84.

Mayfield, C.I., Grover, V.I. and Daley, R.J. (2004). The United Nations Water Virtual Learning Centre: a flexible distance learning Programme for integrated water resources management. Global Environmental Change – Part A, 13(4): 331-318.

Millennium Ecosystem Assessment (2005). Ecosystems and Human Well-being: Synthesis / Millennium Ecosystem Assessment. Washington, DC, USA: Island Press, ISBN 1-59726-040-1.

Miloradov M. (1992). Planning and Management of Water-Resource Systems in Developing Countries. Journal of Water Resources Planning and Management, 118(6), pp. 603 – 619. https://doi.org/10.1061/(ASCE)0733-9496(1992)118:6(603).

U. Nehren, T. Arce-Mojica, A. Cara Barrett, J. Cueto, N. Doswald, S. Janzen, W. Lange, A. Ortiz Vargas, L. Pirazan-Palomar, F.G. Renaud, S. Sandholz, Z. Sebesvari, K. Sudmeier-Rieux, Y. Walz.(2023). Towards a typology of nature-based solutions for disaster risk reduction. Nature-Based Solutions, [online] Volume 3,p.100057. Available at: https://www.sciencedirect.com/science/article/pii/S2772411523000095?via%3Dihub [Accessed 21 Apr. 2024].DOI:10.1016/j.nbsj.2023.100057, ISSN 2772-4115.

Pećinar, Miladin (1969). Analize pojave erozije tla i antierozionih delovanja, principi borbe protiv erozije tla. Prvi Kongres o vodama Jugoslavije, 28-30 maj, Beograd. Zbornik radova: 189-193.

M. Sartori, G. Philippidis, E. Ferrari, P. Borrelli, E. Lugato, L. Montanarella, P. Panagos (2019). A linkage between the biophysical and the economic: assessing the global market impacts of soil erosion. Land Use Policy [online] Volume 86, pp. 299-312. Available at: https://www.sciencedirect.com/science/article/pii/S0264837718319343[Accessed 14 Apr. 2024]. DOI: https://doi.org/10.1016/j.landusepol.2019.05.014, ISSN 0264-8377.

Simić, Z., Matić, B. (2018). Zapadna Morava river basin zoning based on low flow regime evaluation. Water Utility Journal, [online] Volume 20, pp. 49-56. Available at: http://www.ewra.net/wuj/pdf/WUJ_2018_20_05.pdf [Accessed 14 Apr. 2024].ISSN 1792-748X.

Simonović, S.P. (2008). Managing water resources: Methods and tools for a system approach. In: Proceedings of International Conference Planning and Management of Water Resource Systems (September 25 – 27), Academy of Science and Arts of Vojvodina, pp. 37-47.

P.Strosser, G.Delacámara, A.Hanus, H.Williams and N.Jaritt (2015). A guide to support the selection, design and implementation of Natural Water Retention Measures in Europe -

Capturing the multiple benefits of nature-based solutions. Available at: https://op.europa.eu/en/publication-detail/-/publication/a6de1b15-d277-4753-bc37-3b746b09ef9f [Accessed 14 Apr. 2024]. DOI: https://data.europa.eu/doi/10.2779/761211.

Sudmeier-Rieux, K., Nehren, U., Sandholz, S. and Doswald, N. (2019). Disasters and Ecosystems, Resilience in a Changing Climate - Source Book. Geneva, Switzerland: UNEP and Cologne: TH Köln - University of Applied Sciences. Available at: https://collections.unu.edu/view/UNU:7485[Accessed 21 Apr. 2024]. DOI: 10.5281/zenodo.3493377

Van Nood M., Kovács P., Whalley P., Heilmann D., Milovanović M., Kunikova E., Graziella J., Iarochevitch A. (2011). Integrated Tisza River Basin Management Plan. Water Research and Management. 1 (2), p.1.

Wostl - Pahl, C., Pavel Kabat, P., Jörn Möltgen, J. (Eds.) (2008). Adaptive and Integrated Water Management Coping with Complexity and Uncertainty. Berlin, Heidelberg, Germany: Springer, DOI: https://doi.org/10.1007/978-3-540-75941-6, ISBN 978-3-540-75940-9.

Check for updates

CC BY

RESEARCH PAPER

MODERN EVOLUTION AND HYDROLOGICAL REGIME OF THE BASHKARA GLACIER LAKES SYSTEM (CENTRAL CAUCASUS, RUSSIA) AFTER THE OUTBURST ON SEPTEMBER 1, 2017

Ekaterina D. Pavlyukevich[1,2*], Inna N. Krylenko[1,2], Ivan V. Krylenko[1]

[1] Lomonosov Moscow State University, Faculty of Geography, Moscow, 119991, Russia

[2] Water Problems Institute of the Russian Academy of Sciences, Moscow, 119333, Russia

***Corresponding author:** ekaterina.kornilova.hydro@gmail.com

Received: November 10th 2024 / Accepted: November 22nd 2024 / Published: December 31st 2024

https://doi.org/10.24057/2071-9388-2024-3717

ABSTRACT. In high mountain areas, glacial lake outbursts are often the cause of floods and extreme events. Investigation of these events is especially important in the context of ongoing intensive deglaciation and climate change. This study is focused on the monitoring of the Bashkara Glacier Lakes after their outburst on September 1st, 2017, which are located in the most glaciated and populated part of the Central Caucasus of Russia, in the Mt. Elbrus region. Following the incident, the lakes system has transformed into flow-through. However, the lakes system has undergone significant changes and remains unstable and potentially hazardous. In this research, we used remote sensing data and field observations to assess the condition of the Bashkara Lakes. The water level, area and volume of the lakes are unstable. Between 2018 and 2024, the area of Bashkara Lake increased by 32% and volume by 41%, with the level increasing by 3.2 meters. At the same time, Lapa Lake was rapidly shrinking. The area of Lapa Lake in 2018-2024 decreased by 51%, the volume by 66%, and the level decreased by 4.2 meters. In addition to the continuing rise of the water level, the possibility of future rockfalls cannot be excluded, which can trigger a re-outburst. Ephemeral glacier lakes were also discovered, their merging with the main lake can cause a dramatic increase in the lake volume. On the other hand, other factors, such as the decrease in water temperature of Bashkara lake and its flowage, indicate the stability of the lakes system.

KEYWORDS: mountain hydrology, Central Caucasus, moraine-dammed lake, outburst, GLOF, Bashkara Lake

CITATION: Pavlyukevich E. D., Krylenko I. N., Krylenko I. V. (2024). Modern evolution and hydrological regime of the Bashkara Glacier Lakes system (Central Caucasus, Russia) after the outburst on September 1, 2017. Geography, Environment, Sustainability, 4(17), 66-75

https://doi.org/10.24057/2071-9388-2024-3717

ACKNOWLEDGEMENTS: The authors are grateful to the participants of fieldwork, including the entire team of the MSU debris flow group, especially Vera Kidyaeva, Sergey Chernomorets, and the MSU glacial group, especially Dmitry Petrakov, Kirill Ibrayev, Ivan Durmanov and Ekaterina Rets.

This work was supported by the grant of the The Government of the Russian Federation (Agreement №075-15-2024-614 date 13.06.2024) (satellite image interpretation), was carried out under the Governmental Order to the Water Problems Institute of RAS, subject FMWZ-2022-0001 (water flow measurement) and under the state assignment of Faculty of Geography, Lomonosov Moscow State University part 1.10, CITIS 121051100166-4 (bathymetric survey), 121051400038-1 (level logger installation).

Conflict of interests: The authors reported no potential conflict of interest.

INTRODUCTION

Continuing global warming affects the occurrence of glacier lakes outburst floods (GLOFs) in various mountain regions in the world (Lützow et al., 2023; Shrestha et al., 2023; Veh et al., 2022). A rise in the frequency of GLOFs in areas with extensive glaciers is anticipated by the end of the 21st century (Milner et al., 2017; Zheng et al., 2021). The study and prediction of flash floods is an important task in hydrology and has socio-economic implications, especially in mountainous areas where there is a limited number of measurement stations (Ali Washakh et al., 2024; Chen et al., 2019; Zhou et al., 2024), due to the ongoing intensive economic development of mountainous areas

The issue of studying the process of outburst flood formation, as well as identifying the triggering mechanisms and factors influencing lake outbursts, has received much attention in various studies (Awal et al., 2011; Costa and Schuster, 1987; Adam Emmer and Cochachin, 2013; Liu et al., 2013; Neupane et al., 2019; Westoby et al., 2014). There are external, internal and complex GLOF triggers, such as dam breach initiation caused by mass movement-induced impulse

waves, lake overfilling due to pluvial, nival and glacial runoff (Taylor et al., 2023). Significant factors contributing to a glacial lake outburst flood include a rise in air temperature and heavy rainfalls, which necessitate careful consideration in light of the ongoing climate shifts (Allen et al., 2016; Din et al., 2014). While climate change is a major factor in the deglaciation, it also contributes to the weakening of glacier surfaces, which can lead to catastrophic failures of rock avalanches or other types of landslides (Shugar and Clague, 2011; Vilímek et al., 2014). GLOFs are frequently caused by the collapse of ice and rock, such as rockslides or moraine failures into lakes, resulting in the formation of seiches or displacement waves (Stephan Harrison et al., 2018).

Outburst floods caused by similar processes are observed in various regions of the world (Byers et al., 2019; Adam Emmer and Cochachin, 2013). The article (Shugar et al., 2020) examines the dynamics of glacial lakes and their distribution around the world based on satellite images from 1990 to 2018. It is shown that the number of lakes and their total area increased by 53% and 51%, respectively, during the study period. And the fastest growing lakes (in terms of area) are located in the Scandinavian countries, Iceland and Russia. The first global spatial and temporal assessment of outbursts floods from moraine and glacial lakes based on a regional review (165 moraine dams in the Alps, Pamirs, Tien Shan, Himalayas, USA and South America were selected) is presented in (Harrison et al., 2018). This article provides a historical view of outburst floods and their distribution under current and future global climate change. Currently, there are databases and catalogues of glacial lakes and their outbursts, created on the basis of space image interpretation (Emmer et al., 2016; Zhang et al., 2015).

A critical aspect in the investigation of outburst hazardous lakes is the exploration of the genesis process, evolution, and categorization of stages in their development. Currently, this subject receives limited attention, and scholarly works on the evolution of glacier lakes are few (Aleynikova and Anatskaya, 2019; S. Chernomorets et al., 2007; Dokukin and Khatkutov, 2016; Rasputina et al., 2022). Research shows that the evolution cycle consists of a number of stages, which can be called: 1) the stage of pre-catastrophic preparation, 2) the stage of a debrisflow disaster, 3) the stage of epicatastrophic adaptation, 4) the stage of inter-catastrophic evolution (Chernomorets, 2005). The article (Pryakhina et al., 2021) explores the evolution of the periglacial Lake Nurgan in Northwestern Mongolia, focusing on its stages of formation and development. These stages include the transgressive phase, characterized by the lake's growth, expansion, and increase in volume, the regressive phase, marked by the lake's outburst, and the post-regressive phase, during which the lake persists after the outburst.

Our study objects, the lakes Bashkara and Lapa, are located in the most glaciated and populated part of the Central Caucasus, in the Mt. Elbrus region. On September 1st, 2017, the Bashkara Lake outburst occurred with a total volume of 0.8 million cubic meters of water and 0.35-0.5 million cubic meters of debris (S. Chernomorets et al., 2018). After the outburst on September 1st, 2017, the lake system became permanent flow-through. However, this lake system has begun to evolve and change. The intensive retreat of the Bashkara Glacier took place during the last seven years: two ephemeral small lakes upper the lakes appeared, the size of Bashkara Lake was increasing, and of Lapa Lake was decreasing. Thus, the lakes system is unstable and still potentially hazardous.

Glacier lake may experience repeated outburst floods throughout its evolution (Carrivick and Tweed, 2016; Dussaillant et al., 2010; Adam Emmer, 2017; Kropáček et al., 2015; Petrasov, 1979; Poznanin, 1979) and even mechanisms of outburst formation can differ for the same lake at different events and stages of evolution. In August 1958 and 1959, as well as in October 1960, there were three Bashkara Lake outbursts through the grottoes in the ice wall, causing high-magnitude debris floods downstream the Adylsu River valley (Kovalev, 1964). In 2017, the lake outbursted trough dam erosion and successive glacial channel formation. Despite the formation of a well-developed run-off channel in 2017, it is possible that the lake can outburst again. For example, in summer of 2018 and spring of 2019, large rock falls were observed from Bashkara Peak (4162 m asl.) towards Bashkara Glacier, when rock avalanches had almost reached Bashkara Lake. In future, the possibility of repeated collapses is not excluded, considering the instability of the rocks on the mountain slopes around the lakes (Dokukin et al., 2020), that could trigger the repeated GLOF. Also the drainage channel that was formed follows the ice that is hidden in the moraine, i.e. erosion can be very intense due to thermokarst processes.

This study is focused on the monitoring of Bashkara Glacier lakes after their outburst on 1st September, 2017. The following steps were performed in the research: (1) Determination of the area of the lakes for different years using satellite images; (2) Analysis of changes in the water levels of Lake Bashkara and Lapa; (3) Assessment of the contributions of different water sources to the total outflow from Lapa Lake.

STUDY AREA

The Bashkara Glacier lakes system is located in the upper reaches of the Baksan River and the headwaters of the Adylsu River, its right tributary (Fig. 1). Bashkara Lake appeared in the early 1930s between the right lateral morine and the glacier and was surrounded by ice on three sides for a long time. Lapa Lake appeared at downstream the glacier's tongue in the 1990s. Nowadays, the distance between these two morine-dammed lakes is about 500 meters, the average altitude is from 2480 to 2580, relative excess between the lakes is about 100 meters. Over the past three decades, there has been a noticeable surface lowering at the snout of the Bashkara Glacier adjacent to the lakes. The area and volume of Lapa Lake significantly increased between 1999 and 2017, while Bashkara's size remained quasi-stable (Petrakov et al., 2012).

On the night of 31st August to 1st September 2017, an overflow occurred and a subsequent outburst of Bashkara Lake took place. This was triggered by an extremely heavy rainfall accompanied by strong wetting of the moraine dam. The total precipitation recorded at the Djankuat station near the lake during the night was approximately 100 millimeters (mm) per hour. As a result, significant damage was observed both in the Adylsu River valley, with the total length of 11.5 km, and in the Baksan River valley at a distance of more than 50 km downstream the mouth of the Adylsu River. (S. Chernomorets et al., 2018; Kornilova et al., 2021).

The pre-outburst water level of Bashkara Lake was approximately 2672 meters. According to data from the water level logger, the level in the lake rose by 55 centimeters (cm) in 5 hours during the rainstorm. This led to the erosion of the dam crest during outflow, and the water level in Bashkara Lake dropped by 17 meters relative to its pre-outbreak level. The water volume of Bashkara Lake after the outburst decreased by more than ¾, from more than 1 million m3 to approximately 290 thousand m^3. The GLOF wave first moved from Bashkara Lake across the surface of the glacier's tongue, partially drained Lapa Lake, and then flowed downstream the Adylsu River valley.

At present, lakes Bashkara and Lapa represent a complex system. The Bashkara Glacier supplies water to both the upper and lower lakes. Water from Bashkara Lake flows through a glacier tunnel and feeds Lapa Lake. Lapa Lake is drained by well-developed surface run-off channel to the Adylsu River valley.

MATERIALS AND METHODS

Remote sensing data

We used Sentinel-2, Pleiades and SPOT 6 satellite images to estimate changes in lake area. Typically, the summer months of July through September are considered the ideal time for glacial lake mapping (Zhang et al., 2015). During this time, the amount of snow and ice coverage is minimal, and the area of glacial lakes reaches its maximum. Therefore, we here acquired the best possible images during this period. The collected images were screened for cloud cover and selected for cloud cover <10 % to ensure data reliability. Images were selected for each year from 2017 to 2020 (table 1). We manually mapped the shoreline on all the images using ArcMap 10.4.1.

We examined the area change in Bashkara Glacier during 2017–2024 using Sentinel-2 satellite images. We selected images at the end of the ablation season, when seasonal glacier retreat is maximum (Popovnin et al., 2024).

Hydrological measurements in a lake system

Water level and temperature

Since September 1st, 2017, we continued annual systematic observations of the level of Bashkara Lake using automatic water level recorders, which were initiated in 2007, to monitor the risk of a potential re-outburst (Fig. 2c). In 2018, 2019, 2023 and 2024 we installed water level and temperature loggers Keller to record every 15 minutes data, and also monitored the lake levels relative to a geodetic reference. These measurements are critically important for monitoring the situation and ensuring the safety of the surrounding area. We compared our measurements with the data observed before the outburst from 2007 till 2017 (Petrakov et al., 2012, Chernomorets et al., 2018). The accuracy of the measurements is 0,1% FS.

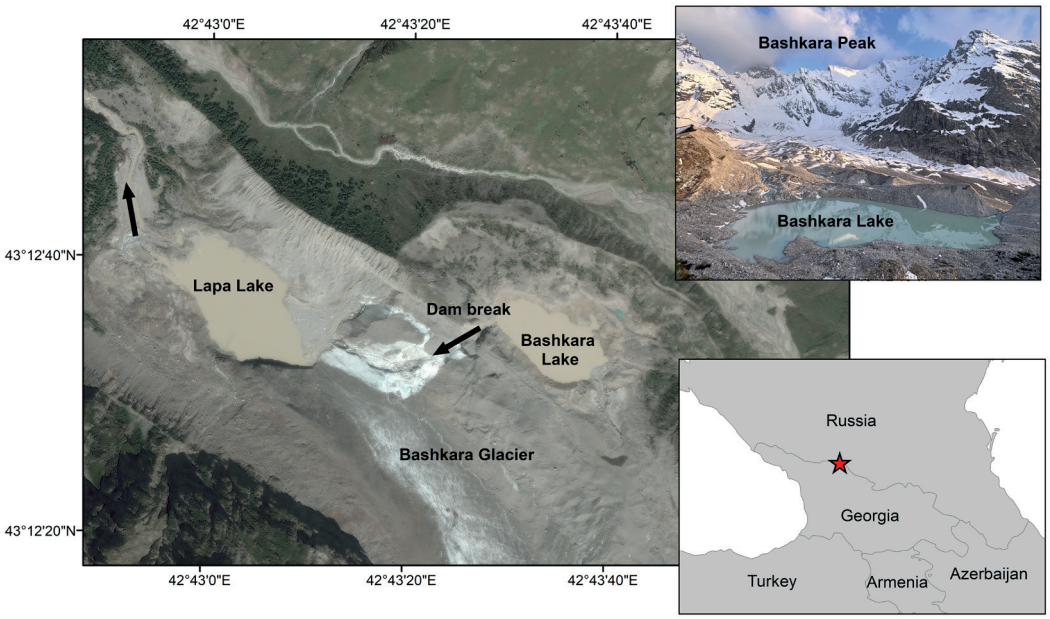

Fig. 1. Study area

Table 1. Multi-source remote sensing datasets

Date	Satellite image	Resolution, m	Objectives
01.08.2017	Pleiades	0.5	Lake area changes
03.09.2017	SPOT 6	1.5	
29.07.2018	Sentinel-2	10	
27.07.2019	Sentinel-2	10	
16.07.2020	Sentinel-2	10	
18.07.2021	Sentinel-2	10	
28.07.2022	Sentinel-2	10	
26.07.2023	Sentinel-2	10	
30.07.2024	Sentinel-2	10	
13.08.2017	Sentinel-2	10	Glacier retreat assessment
30.09.2017	Sentinel-2	10	
28.09.2024	Sentinel-2	10	

Depth measurements

In September 2020, we conducted bathymetric surveying with a boat-mounted Lowrance 525 CF two-frequency echo sounder which produced geo referenced echograms. Sounding points were located along cross-sections at 15-30 m intervals. Surfer 15.3 and ArcMap 10.4.1 software were used to calculate lake volumes and average depths.

Water discharges

From 2018 to 2020, we measured water discharges at various gauging stations in the lakes system to study the hydrological regime of the newly formed flow channels. We installed several discharge gauging stations on streams: Bashkara, Dam Break, Dam Break after the glacier, Lapa (Fig. 2a). Over a period of three years, we collected 20 series of discharge measurements (including four discharges per series). Within each series, we were measuring discharges at each gauge on the same day for two to three hours. Simultaneously, we also measured water levels of both lakes on water level stations (Fig.2a).

The water discharges were measured using the salt dilution method (Fig. 2b). The salt dilution method is an easy-to-use technique for measuring discharge in small turbulent streams that are typically found in mountain areas. To control and compare the results, the water discharges were measured twice at each gauge. The relative error was then calculated. If it was less than 15%, the discharge was considered well-measured.

RESULTS

Glacier retreat assessment

Due to the high thickness of debris-cover on the Bashkara Glacier, it is difficult to estimate the accurate area reduction. However, the retreat of the glacier tongue is clearly visible on the images. According to Sentinel-2 image interpretation data, the area is rapidly decreasing (Fig. 3). The total retreat of the glacier tongue from 2017 to 2024 was about 210 meters.

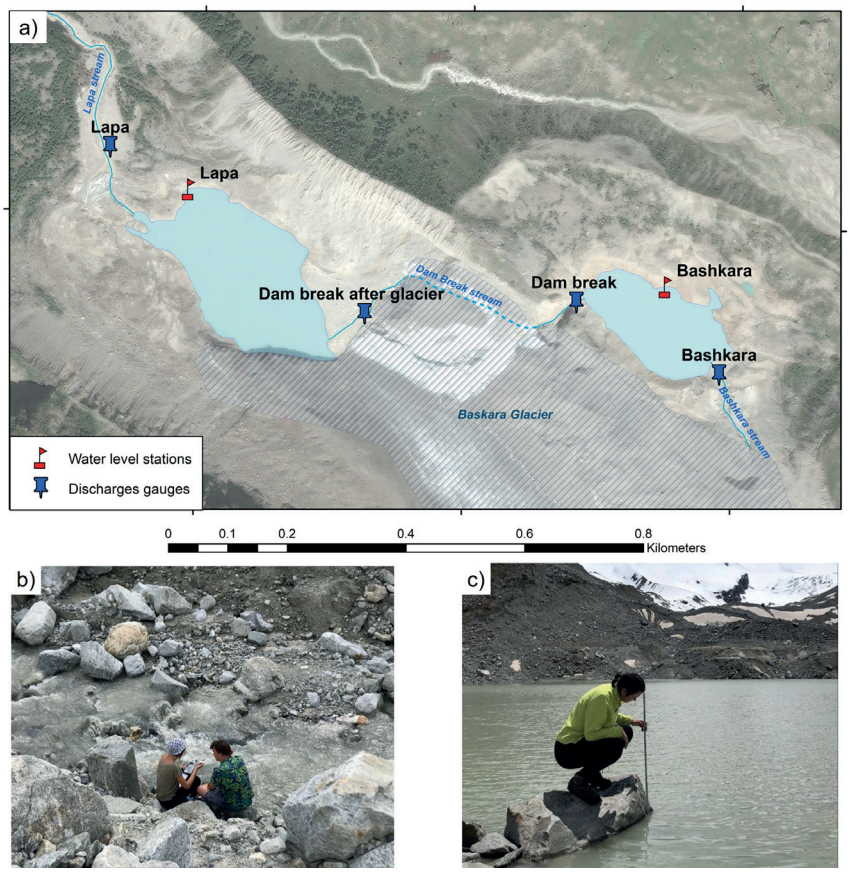

Fig. 2. Location of gauging stations (a), measurement of water discharge by salt dilution method (b) and water level measurement during the logger installation (c)

Fig. 3. State of the Bashkara Glacier in 2017 before and after the outburst and in 2024

Changes in the area, level and volume of lakes

Despite the fact that the lake is flow-through, its level, area, and volume are unstable both seasonally and over several years. The area and volume of Bashkara Lake vary between 26,000–35,000 m^2 and 239,000–339,000 m^3, respectively. We observed that during the period 2018-2020, the area of Bashkara Lake was nearly constant, but it began to expand after 2021 (Fig. 5a). In 2018–2024 the area increased by 32% and the volume increased by 41%. Since the outburst on 1 September 2017, the water level has risen by 3.2 meters, mainly between 2021 and 2024. The maximum measured depth (17,5 m in 2020) was in the center of Bashkara Lake (Fig. 4). Since 2018, the lake bed relief slightly reshaped, as confirmed by the changed volume curve (Fig. 5c). This is probably due to the continued accumulation of sediment on the lake bed. It is also worth noting that the area of ephemeral lakes, formed by uneven deposition of surface moraine on the glacier and in the ice flow stress zones, is increasing.

At the same time, Lapa Lake experienced a rapid decrease (Fig. 5b). Between 2018 and 2024, the level of the lake decreased, which was driven by the glacier tongue retreating, debris sedimintation and siltation (Fig. 4b). sediments from the debris-covered tongue of the Bashkara Glacier form a delta in the southern part of the lake. In 2018–2024 the area decreased by 51%, the volume decreased by 66%, and the water level decreased by 4.2 meters. The maximum depth measured in 2020 was 8.5 meters in the center of the lake. The relief of the lake bed is heterogeneous, with two local depressions, separated in the north-eastern part by a former underwater ridge that has now dried up. It is likely that the lake will split into two in the future. This was already the case in the past, in the late 1990s and 2000s. Initially, two distinct lakes, Lapa and Mizinchik, were formed. Subsequently, these lakes underwent a process of merging.

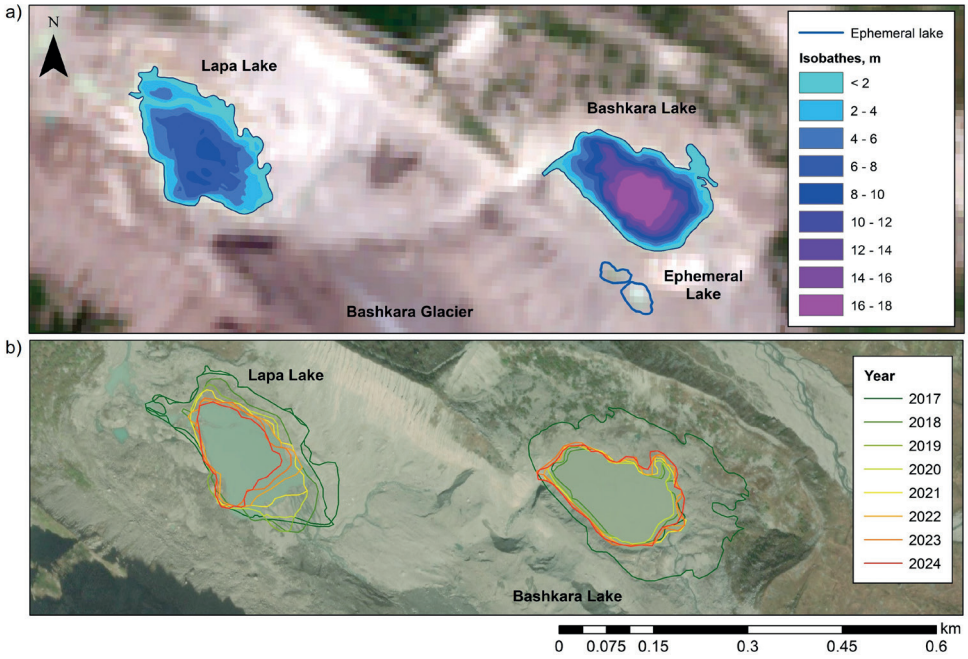

Fig. 4. Bathymetric map of Bashkara and Lapa lakes in 2020 (a); Changing the shape of Bashkara and Lapa lakes (b)

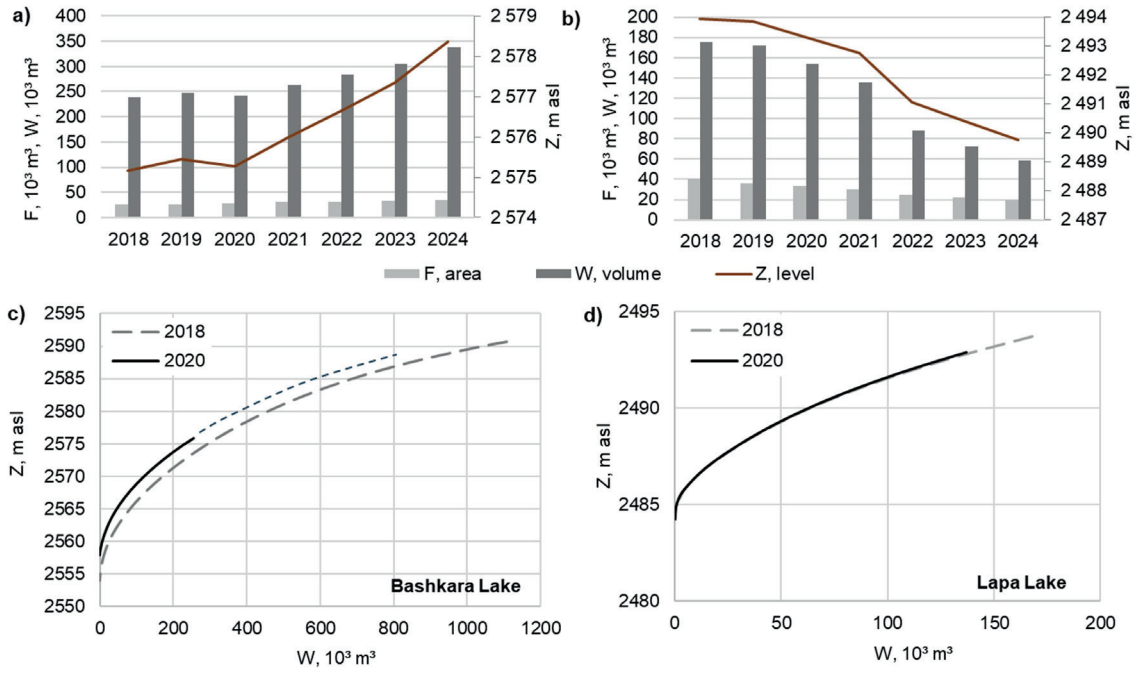

Fig. 5. Area, level and volume change in 2018–2024 of Bashkara Lake (a) and Lapa Lake (b); volume curves of Bashkara Lake (c) and Lapa Lake (d)

Water level fluctuation

Bashkara Lake water level is one of the most important indicators of its re-outburst hazard. After September 1st, 2017 Bashkara Lake is drained by a well-developed run-off channel, so water level fluctuations during the warm season are not high. During summer the lake level varies within a range of 20-50 cm, and remains quasi-stable until late summer. Lake levels sometimes rise sharply in the short term due to intense melting of ice and snow or heavy rainfall. The lake level would decrease to a minimum at the end of the ablation period in late September. October (Fig. 6). However, before the outburst in 2007-2017 the intra-annual water level fluctuations were higher, around 150-300 cm, with the highest level usually observed in June. During the summer of 2008 the level rise was about 400 cm. In 2008, the overflow through the ice-cored moraine dam into the englacial drainage system began due to the lake level increase. However, the surface runoff stopped, the lake didn't burst and the water level stabilised in the following year.

Lake temperature fluctuation

An indirect indication of the state of the lake is its water temperature and its long-term dynamics. In the past, Lake Bashkara was non-flowing and therefore heated up near the shore and on the surface to a depth of 1.5-2 m. The lake is currently flow-through with a short water retention time. At the same time, the main source of water inflow is cold glacial meltwater, resulting in a decrease in the average water temperature of the lake compared to the pre-outburst state. The average water temperature of the lake from June till September was 7.8°C before the lake outburst in 2013-2016; in 2017, as a result of intensive snow and ice melt, the temperature was 3.9°C; after the outburst, the temperature was 1.6°C (Fig. 7b).

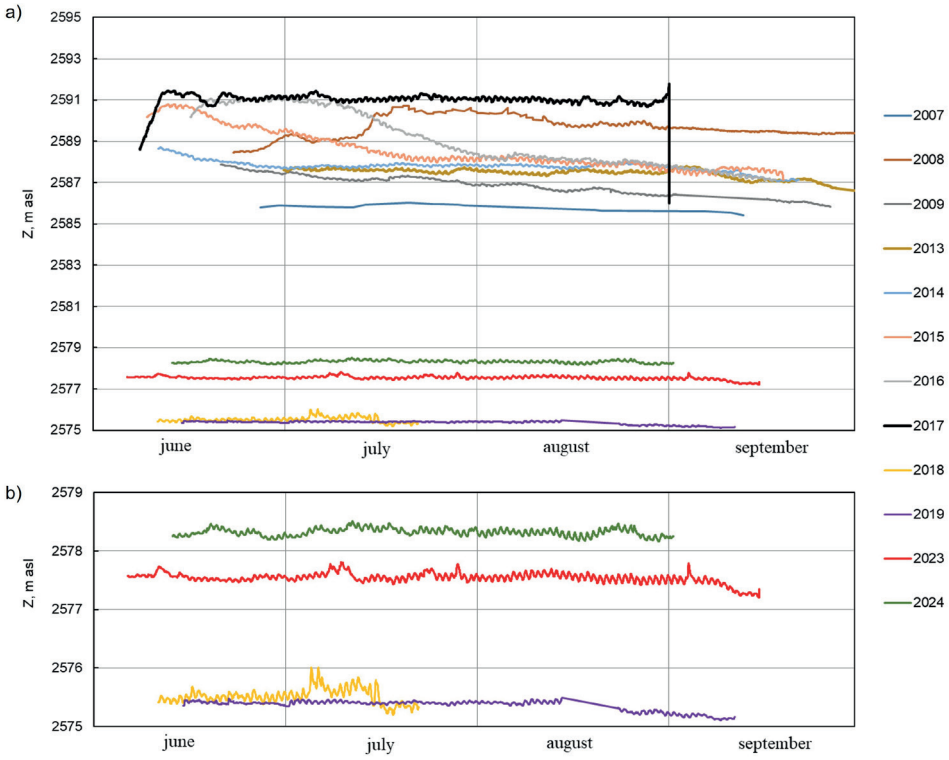

Fig. 6. Lake Bashkara water level fluctuations during warm periods in 2007–2024 (a) (Chernomorets et al., 2018; Petrakov et al., 2012), in 2018–2024 (b)

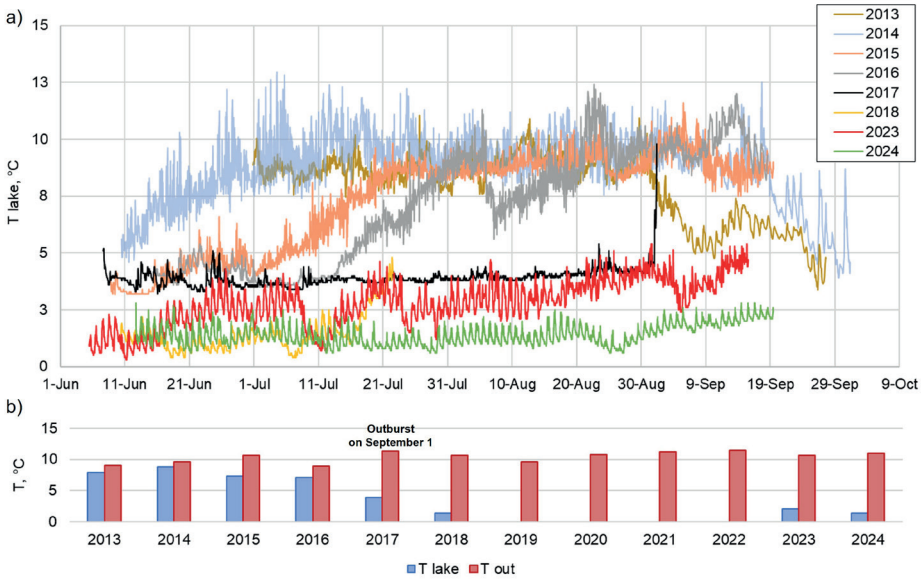

Fig. 7. Lake Bashkara temperature fluctuations during warm periods in 2013–2024 (a), average air (T out) and lake (T lake) temperature from June to September in 2013–2024 (b)

The water temperature fluctuations are in an inverse relationship with the water level: when the water level decreased, the water temperature increased and vice versa (Fig. 7a). This is due to the fact that during periods of low water, the intensity of cold meltwater runoff from the mother glacier decreases and the water mass of the lake warms faster.

Hydrological regime of the Bashkara Glacier Lakes system

For the period 2018-2020, Q(H) curves were plotted for streams flowing from two lakes, Bashkara and Lapa (Fig. 8a,b). Both dependencies were not stable from year to year, indicating the instability of the lake system. Average measured discharges were from 0.1 till 2.4 m^3/s. This is particularly evident for Lapa Lake, because it has changed significantly in size and shape in 7 years due to intensive glacier retreat. After 2021, the discharge of the Dam Break stream visually increased significantly, the water level rose and flooded the shores (or the floodplain), making it impossible for measurements. According to the measurement results, the Dam Break stream is additionally fed by meltwater from the inside the glacier tunnel, as the discharges of the Dam Break stream downstream the glacier were always higher than upstream.

Lake Lapa also receives a large amount of meltwater directly from the Bashkara Glacier tongue. However, as it is impossible to measure the total meltwater inflow, it was assesed by subtracting the contribution of the Dam Break stream from the total outflow from Lapa Lake. The results show that the meltwater from Bashkara Glacier is the largest contributor to the Lapa stream discharge, averaging 65% of the total outflow. The contribution of the Dam Break stream, i.e. water from the upper lake, is small, averaging 24%, and the glacier cave meltwater is 11% (Fig. 8d,e). However, it is likely that this balance has changed in recent years as a result of opposite trends in the level, area and volume of the two lakes.

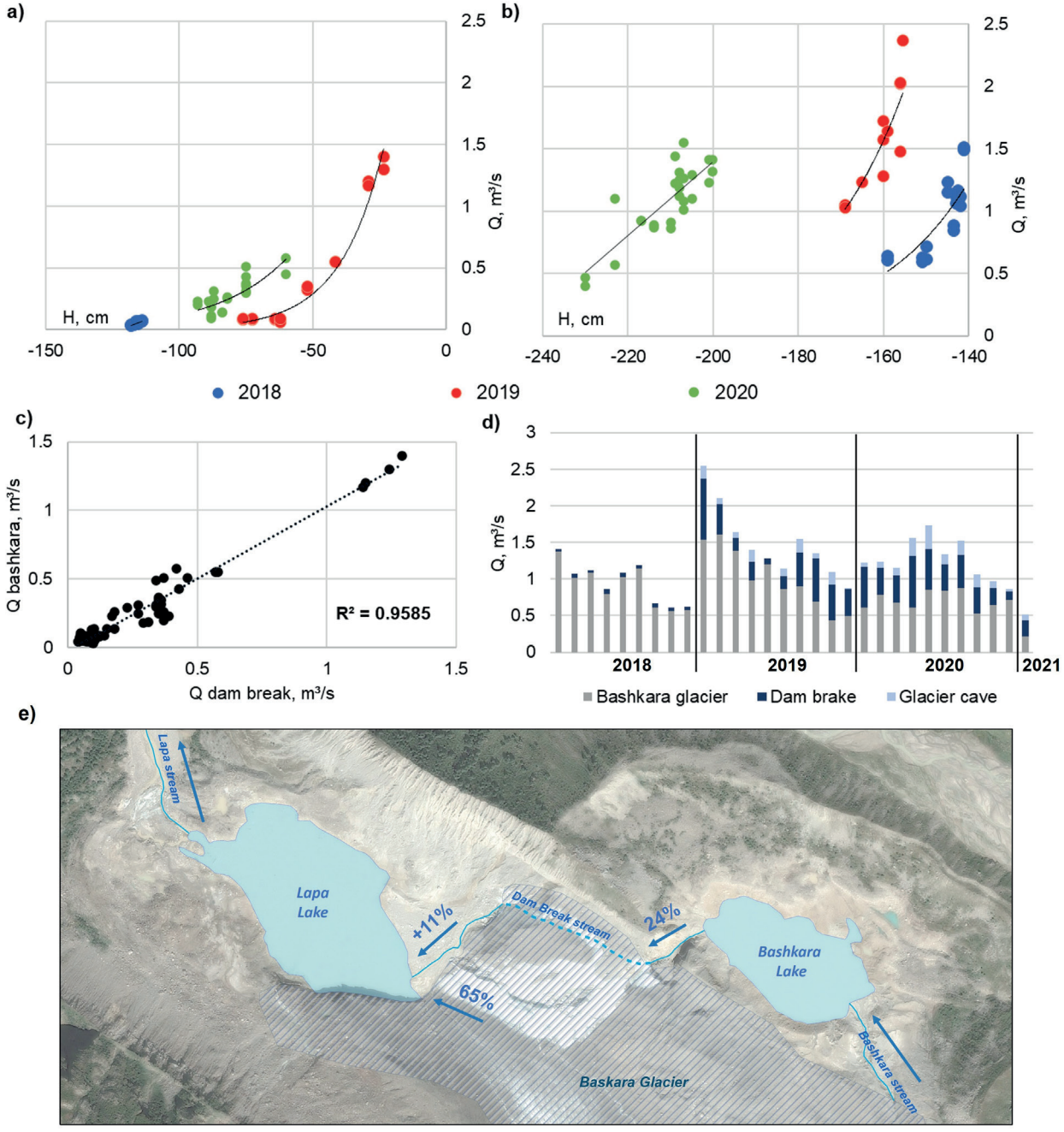

Fig. 8. Q=f(H) curves of Dam Break stream (a) and Lapa stream (b); correlation between discharges of the Bashkara and Dam Break streams (c); contribution of different sources to the total outflow from Lapa Lake (d); spatial distribution of different sources to the total outflow from Lapa Lake (lake outlines of 2018) (e)

DISCUSSIONS

The Bashkara lakes system has gone through several stages of formation and development since its appearance in the 20th century (Fig. 9). The stage of pre-catastrophic preparation, characterised by the growth of the lakes, their area and volume, lasted ~1960 till 2017. Then came the stage of the debrisflow disaster, when Bashkara Lake bursted on September 1st, 2017. From 2018 to 2020, the lake system was quasi-stable; this was the stage of epicatastrophic adaptation. After 2021, however, the volume and area of Bashkara Lake began to increase, marking the transition to the stage of inter-catastrophic evolution. The whole glacial complex is a rather complicated hydraulic system and requires further monitoring of its water balance and dynamics.

A number of factors indicate that the risk of another outburst from Lake Bashkara is on the rise. As before the outburst, there has been a stable trend of intra-annual increases of the water level of Bashkara Lake. In 2018-2019, we did not observe an intra-annual increase of the water level of Bashkara Lake, but in 2023 it was 160 cm higher than 4 years earlier. This trend continued in 2024: the water level was about 60 cm higher than the year before. Extrapolating the *Q=f(H)* curve to the current water level of Bashkara Lake, it can be concluded that the summer discharge of the Dam Break stream could reach 5-6 m^3/s in 2024. The area of ephemeral lakes within the Bashkara Glacier increases. The reduction of the width of the ice-debris dam and its destruction between them and Bashkara Lake could also lead to an outburst. In addition, other factors of moraine complex reformation due to glacier retreat like ice collapses, thermokarst subsidence at the lake bottom, extension and retreat of the delta of the stream flowing into the lake, slope processes on the shores can lead to an unstable condition of the lake. Our observations correlate with glaciologic studies of the potential glacial lake development in the Central Caucasus (Lavrentiev et al., 2020), which predict that Bashkara Lake is expected to continue growing, and the risk of the possible repeated lake outburst is high.

On the other hand, a number of factors indicate a certain stability of the Bashkara lakes system in recent years. According to the results of the water balance study for 2018-2024, the inflow of the Bashkara stream was always close to the outflow of the Dam Break stream, moreover, the flow of the Bashkara stream, the water lake level and the flow of the Dam Break stream correlate with ablation of the Bashkara Glacier (Fig. 8c). This proves that the lake does not have any additional 'hidden' inflow channels and that all the meltwater coming from the catchment leaves the lake via the Dam Break outflow. Consequently, the lake is a self-regulating system as a result of the constant outflow. It also should be noted that the average water temperature of the lake decreases annually in summer (a possible sign of the increased inflow), which reduces the rate of debris-covered dead ice melting.

CONCLUSION

In the seven years since the outburst on September 1st, 2017, there have been significant directional changes in the water level, area and volume of Bashkara Lake, with relatively small seasonal variation. Between 2018 and 2024, the area of Bashkara Lake increasев by 32% and the volume by 41%. At the same time, Lapa Lake has shrunk in size due to silting. Between 2018 and 2024, the area of the lake decreased by 51% and the volume by 66%.

At present, Bashkara Lake is drained by a well-developed surface run-off channel and the water level fluctuations during the summer season are insignificant. The lake level varies within 20-50 cm and remains practically stable until the end of the warm season. At the same time, there has been a directional increase in the water level of Bashkara Lake over the last 5 years. From 2020 to 2024, the lake summer water levels have risen by 3.2 meters.

For the period 2018-2020, *Q(H)* curves were constructed for rivers flowing from the two lakes, Bashkara and Lapa. Both dependencies were not stable from year to year, which also indicates the instability of the lakes system. The results of the water balance studies show that the outflow from Lapa Lake approximately contains of Bashkara Lake runoff (35%) and Bashkara Glacier runoff (65%) (excluding the Bashkara Lake catchment area). Except the inflow from Bashkara Lake, water flows into Lapa Lake in two main ways. About 11% of the total amount of meltwater flows through a sub-glacial channel, which has an outlet at a glacial cave. The rest, about 24%, is dispersed as sub- and inter-glacial meltwater inflow. However, it is likely that this balance has shifted in recent years as a result of opposite trends in the level, area and volume of the two lakes. After 2021, the warm season flow from Bashkara Lake through the surface channel (the 'Dam Break' channel) has visually increased significantly. Extrapolation of the *Q=f(H)* curve to the Bashkara Lake water level in 2024 shows that the discharge through the Dam Break stream could reach 5-6 m^3/s.

It can be concluded that the entire system of the Bashkara moraine-glacial complex, including the glacier, the lakes and the runoff system, has moved from the stage of epicatastrophic adaptation (2017-2020) to the stage of

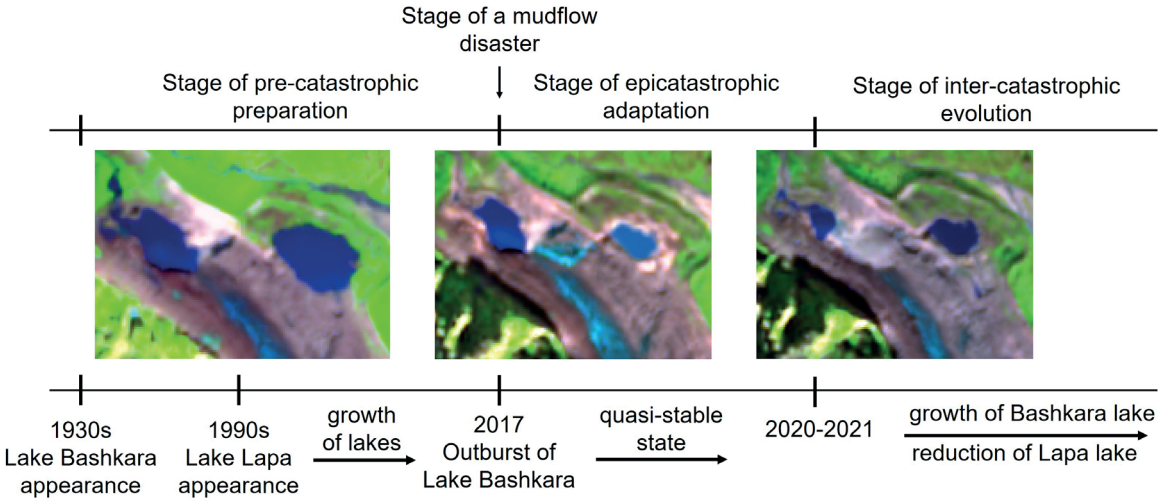

Fig. 9. Stages of formation and development of the Bashkara Lakes system

inter-catastrophic evolution (according to the classification of Chernomorets, 2005).

The results demonstrate the necessity for further monitoring of the glacial complex, i.e. repeated bathymetric surveys, observations of lake sedimentation and siltation, lake temperature surveys and water level measurements. The identified features will allow to identify similar patterns for other glacier lakes in the region. It is also necessary to take measures to reduce the level of Bashkara Lake to prevent it from re-outburst.

REFERENCES

Aleynikova A.M. and Anatskaya E.E. (2019). Dynamics of glaciers and glacial lakes of the ala-arch river basin. Advances in Current Natural Sciences, 42–47. DOI: 10.17513/use.37195

Ali Washakh R.M., Pan X., Almas S., Umar Waque R.M., Li H., Rahman M., Ahmed S.R. and Majid Z. (2024). Deep learning-based GLOF modelling for hazard assessment and risk management. Georisk. DOI: 10.1080/17499518.2024.2379947

Allen S.K., Rastner P., Arora M., Huggel C. and Stoffel M. (2016). Lake outburst and debris flow disaster at Kedarnath, June 2013: hydrometeorological triggering and topographic predisposition. Landslides, 13(6), 1479–1491. DOI: 10.1007/s10346-015-0584-3

Awal R., Nakagawa H., Kawaike K., Baba Y. and Zhang H. (2011). Study on moraine dam failure and resulting flood/debris flow hydrograph due to waves overtopping and erosion. Italian Journal of Engineering Geology and Environment - Book, 3–12. DOI: 10.4408/IJEGE.2011-03.B-001

Byers A.C., Rounce D.R., Shugar D.H., Lala J.M., Byers E.A. and Regmi D. (2019). A rockfall-induced glacial lake outburst flood, Upper Barun Valley, Nepal. Landslides, 16(3), 533–549. DOI: 10.1007/s10346-018-1079-9

Carrivick J.L. and Tweed F.S. (2016). A global assessment of the societal impacts of glacier outburst floods. Global and Planetary Change, 144, 1–16. DOI: 10.1016/j.gloplacha.2016.07.001

Chen Y.M., Liu C.H., Shih H.J., Chang C.H., Chen W.B., Yu Y.C., Su W.R. and Lin L.Y. (2019). An operational forecasting system for flash floods in mountainous areas in Taiwan. Water (Switzerland), 11(10). DOI: 10.3390/w11102100

Chernomorets S., Petrakov D., Aleynikov A.A., Bekkiev M.Y., Viskhadzhieva K., Dokukin M.D., Kalov R., Kidyaeva V., Krylenko V., Krylenko I. V, Krylenko I.N., Rets E., Savernyuk E. and Smirnov A.M. (2018). The outburst of Bashkara glacier lake (Central Caucasus, Russia). On September 1, 2017. XXII. DOI: 10.21782/EC2541-9994-2018-2(61-70)

Chernomorets S., Petrakov D., Krylenko I. V, Krylenko I.N., Tutubalina O., Aleynikov A.A. and Tarbeeva A. (2007). Changes of the Bashkara Glacier-lake system and assessment of debris flow hazard in the Adyl-su River Valley (Caucasus). Earth's Cryosphere, 11, 72–84.

Chernomorets S.S. (2005). Selevye ochagi do i posle-katastrof , Nauchnyj m.

Costa J.E. and Schuster R.L. (1987). The formation and failure of natural dams. In: Open-File Report. DOI: 10.3133/ofr87392

Din K., Tariq S., Mahmood A. and Rasul G. (2014). Temperature and Precipitation: GLOF Triggering Indicators in Gilgit-Baltistan, Pakistan. In: Pakistan Journal of Meteorology , Vol. 10.

Dokukin M.D., Kalov R.K., Chernomorets S.S., Gyaurgiev A.V. and Khadzhiev M.M. (2020). The snow-ice-rock avalanche on Bashkara glacier in the Adyl-Su valley (Central Caucasus) on April 24, 2019. Earth`s Cryosphere, XXIV(1), 55–60. DOI: 10.21782/EC2541-9994-2020-1(55-60)

Dokukin M.D. and Khatkutov A. (2016). Lakes near the glacier Maliy Azau on the Elbrus (Central Caucasus): dynamics and outbursts. Ice and Snow, 56. DOI: 10.15356/2076-6734-2016-4-472-479

Dussaillant A., Benito G., Buytaert W., Carling P., Meier C. and Espinoza F. (2010). Repeated glacial-lake outburst floods in Patagonia: an increasing hazard? Natural Hazards, 54(2), 469–481. DOI: 10.1007/s11069-009-9479-8

Emmer A, Vilímek V., Huggel C., Klimeš J. and Schaub Y. (2016). Limits and challenges to compiling and developing a database of glacial lake outburst floods. Landslides, 13(6), 1579–1584. DOI: 10.1007/s10346-016-0686-6

Emmer Adam. (2017). Geomorphologically effective floods from moraine-dammed lakes in the Cordillera Blanca, Peru. Quaternary Science Reviews, 177, 220–234. DOI: https://doi.org/10.1016/j.quascirev.2017.10.028

Emmer Adam and Cochachin A. (2013). The causes and mechanisms of moraine-dammed lake failures in the cordillera blanca, North American Cordillera, and Himalayas. Acta Universitatis Carolinae, Geographica, 48(2), 5–15. DOI: 10.14712/23361980.2014.23

Harrison S, Kargel J.S., Huggel C., Reynolds J., Shugar D.H., Betts R.A., Emmer A., Glasser N., Haritashya U.K., Klimeš J., Reinhardt L., Schaub Y., Wiltshire A., Regmi D. and Vil\'{\i}mek V. (2018). Climate change and the global pattern of moraine-dammed glacial lakeoutburst floods. The Cryosphere, 12(4), 1195–1209. DOI: 10.5194/tc-12-1195-2018

Harrison Stephan, Kargel J.S., Huggel C., Reynolds J., Shugar D.H., Betts R.A., Emmer A., Glasser N., Haritashya U.K., Klimeš J., Reinhardt L., Schaub Y., Wiltshire A., Regmi D. and Vilímek V. (2018). Climate change and the global pattern of moraine-dammed glacial lake outburst floods. The Cryosphere, 12(4), 1195–1209. DOI: 10.5194/tc-12-1195-2018

Kornilova E.D., Krylenko I.N., Rets E.P., Motovilov Y.G., Bogachenko E.M., Krylenko I. V and Petrakov D.A. (2021). Modeling of Extreme Hydrological Events in the Baksan River Basin, the Central Caucasus, Russia. Hydrology, 8(1). DOI: 10.3390/hydrology8010024

Kovalev P.V. (1964). Traces of ancient glaciation on the Northern slope of the Central Caucasus and glaciological observations (1957-1958). Information Collection about the Work on the International Hydrological Year, 10, 112–131.

Kropáček J., Neckel N., Tyrna B., Holzer N., Hovden A., Gourmelen N., Schneider C., Buchroithner M. and Hochschild V. (2015). Repeated glacial lake outburst flood threatening the oldest Buddhist monastery in north-western Nepal. Natural Hazards and Earth System Sciences, 15(10), 2425–2437. DOI: 10.5194/nhess-15-2425-2015

Liu J., Tang C. and Cheng Z. (2013). The two main mechanisms of Glacier Lake Outburst Flood in Tibet, China. Journal of Mountain Science, 10. DOI: 10.1007/s11629-013-2517-8

Lützow N., Veh G. and Korup O. (2023). A global database of historic glacier lake outburst floods. Earth System Science Data, 15(7), 2983–3000. DOI: 10.5194/essd-15-2983-2023

Milner A.M., Khamis K., Battin T.J., Brittain J.E., Barrand N.E., Füreder L., Cauvy-Fraunié S., Gíslason G.M., Jacobsen D., Hannah D.M., Hodson A.J., Hood E., Lencioni V., Ólafsson J.S., Robinson C.T., Tranter M. and Brown L.E. (2017). Glacier shrinkage driving global changes in downstream systems. In: Proceedings of the National Academy of Sciences of the United States of America , Vol. 114, Issue 37, 9770–9778. National Academy of Sciences. DOI: 10.1073/pnas.1619807114

Neupane R., Chen H. and Cao C. (2019). Review of moraine dam failure mechanism. Geomatics, Natural Hazards and Risk, 10, 1948–1966. DOI: 10.1080/19475705.2019.1652210

Petrakov D.A., Tutubalina O. V., Aleinikov A.A., Chernomorets S.S., Evans S.G., Kidyaeva V.M., Krylenko I.N., Norin S. V., Shakhmina M.S. and Seynova I.B. (2012). Monitoring of Bashkara Glacier lakes (Central Caucasus, Russia) and modelling of their potential outburst. Natural Hazards, 61(3), 1293–1316. DOI: 10.1007/s11069-011-9983-5

Petrasov V.V. (1979). Glacial mudflows in Dagestan. Debrisflows in the mountainous regions of the USSR, 46–57.

Popovnin V., Gubanov A., Lisak V. and Toropov P. (2024). Recent Mass Balance Anomalies on the Djankuat Glacier, Northern Caucasus. Atmosphere, 15, 107. DOI: 10.3390/atmos15010107

Poznanin V.L. (1979). Mechanism of mudflow outbursts of the moraine lake Kakhab-Rosona in Dagestan. Materials of Glaciological Research, 36, 218–223.

Pryakhina G., Boronina A., Rasputina V., Agatova A. and Ganyushkin D. (2021). Formation and evolution of moraine-dammed (periglacial) lake Nurgan, Northwestern Mongolia. Earth's Cryosphere, 25. DOI: 10.15372/KZ20210403

Rasputina V.A., Pryakhina G. V., Ganyushkin D.A., Bantcev D. V. and Paniutin N.A. (2022). The water level regime of periglacial lakes during the growth stage (the lakes of the Tavan-Bogdo-Ola mountain massif, South-Eastern Altai). Led i Sneg, 62(3). DOI: 10.31857/S2076673422030143

Shrestha F., Steiner J.F., Shrestha R., Dhungel Y., Joshi S.P., Inglis S., Ashraf A., Wali S., Walizada K.M. and Zhang T. (2023). A comprehensive and version-controlled database of glacial lake outburstfloods in High Mountain Asia. Earth System Science Data, 15(9), 3941–3961. DOI: 10.5194/essd-15-3941-2023

Shugar D.H., Burr A., Haritashya U.K., Kargel J.S., Watson C.S., Kennedy M.C., Bevington A.R., Betts R.A., Harrison S. and Strattman K. (2020). Rapid worldwide growth of glacial lakes since 1990. Nature Climate Change, 10(10), 939–945. DOI: 10.1038/s41558-020-0855-4

Shugar D.H. and Clague J.J. (2011). The sedimentology and geomorphology of rock avalanche deposits on glaciers. Sedimentology, 58(7), 1762–1783. DOI: 10.1111/j.1365-3091.2011.01238.x

Taylor C., Robinson T.R., Dunning S., Rachel Carr J. and Westoby M. (2023). Glacial lake outburst floods threaten millions globally. Nature Communications, 14(1), 487. DOI: 10.1038/s41467-023-36033-x

Veh G., Lützow N., Kharlamova V., Petrakov D., Hugonnet R. and Korup O. (2022). Trends, Breaks, and Biases in the Frequency of Reported Glacier Lake Outburst Floods. Earth's Future, 10(3), e2021EF002426. DOI: https://doi.org/10.1029/2021EF002426

Vilímek V., Emmer A., Huggel C., Schaub Y. and Würmli S. (2014). Database of glacial lake outburst floods (GLOFs)–IPL project No. 179. Landslides, 11(1), 161–165. DOI: 10.1007/s10346-013-0448-7

Westoby M.J., Glasser N.F., Brasington J., Hambrey M.J., Quincey D.J. and Reynolds J.M. (2014). Modelling outburst floods from moraine-dammed glacial lakes. In: Earth-Science Reviews , Vol. 134, 137–159. Elsevier. DOI: 10.1016/j.earscirev.2014.03.009

Zhang G., Yao T., Xie H., Wang W. and Yang W. (2015). An inventory of glacial lakes in the Third Pole region and their changes in response to global warming. Global and Planetary Change, 131, 148–157.

Zheng G., Allen S.K., Bao A., Ballesteros-Cánovas J.A., Huss M., Zhang G., Li J., Yuan Y., Jiang L., Yu T., Chen W. and Stoffel M. (2021). Increasing risk of glacial lake outburst floods from future Third Pole deglaciation. Nature Climate Change, 11(5), 411–417. DOI: 10.1038/s41558-021-01028-3

Zhou B., Zou Q., Jiang H., Yang T., Zhou W., Chen S. and Yao H. (2024). A novel framework for predicting glacial lake outburst debris flows in the Himalayas amidst climate change. Science of The Total Environment, 946, 174435. DOI: https://doi.org/10.1016/j.scitotenv.2024.174435

Check for updates

CC BY

RESEARCH PAPER

A METHOD OF MULTI-SITE CALIBRATION OF DISTRIBUTED HYDROLOGICAL MODELS BASED ON THE NASH-SUTCLIFFE EFFICIENCY

Boris I. Gartsman[1, 4*], Dimitri P. Solomatine[1, 2, 3], Tatiana S. Gubareva[1]

[1] Water Problem Institute, Russian Academy of Sciences, Gubkina 3, Moscow, 119333, Russia

[2] Water Resources Section, Delft University of Technology, Mekelweg 5, Delft, 2628CD, Netherlands

[3] Department of Hydroinformatics and Socio-Technical Innovation, IHE Delft Institute for Water Education, Westvest 7, Delft, 2611AX, Netherlands

[4] Vernadsky Crimean Federal University, Prospekt Vernadskogo 4, Simferopol, 295007, Russia

***Corresponding author:** Gartsman@inbox.ru

Received: August 24th 2024 / Accepted: November 22nd 2024 / Published: December 31st 2024

https://doi.org/10.24057/2071-9388-2024-3564

ABSTRACT. Contemporary distributed hydrological models are detailed and mathematically rigorous, but their calibration and testing can be still an issue. Often it is based on the quadratic measure of the calculated and observed hydrographs proximity at one outlet gauge station, typically on the Nash-Sutcliffe model efficiency coefficient (NSE). This approach seems insufficient to calibrate a model with hundreds of spatial elements. This paper presents using a multi-dimensional estimator of modeling quality, being a natural generalization of the traditional NSE but which would aggregate data from several hydrological stations using Principal Component Analysis (PCA). The method was tested on the ECOMAG model developed for a sub-basin (24,400 km^2, with 15 gauges) of the Ussuri River in Russia. The results show that the presented version of the multi-dimensional NSE with PCA in calibration of spatially-distributed hydrological models has a number of advantages compared to other methods: the reduced dimensionality without loss of important information, straightforward data analysis and the automated calibration procedure; objective separation of the deterministic signal from the noise, calibration using the "informational kernel" of data, leading to more accurate parameters' estimates. Additionally, the introduced notion of the "compact" dataset allow to interpret physical-geographical homogeneity of the basins in mathematic manner, which can be valuable for hydrological zoning of the basins, hydrological fields analysis, and structuring the models of large basins. There is no doubt that further development and testing of the proposed methodology is advisable in solving spatial hydrological problems based on distributed models, such as managing a cascade of reservoirs, creating hydrological reanalyses, etc.

KEYWORDS: spatially-distributed hydrological models, multi-site calibration, multi-dimensional Nash-Sutcliffe coefficient, prediction for groups of sub-basins

CITATION: Gartsman B. I., Solomatine D. P., Gubareva T. S. (2024). A Method Of Multi-Site Calibration Of Distributed Hydrological Models Based On The Nash-Sutcliffe Efficiency. Geography, Environment, Sustainability, 4(17), 76-87
https://doi.org/10.24057/2071-9388-2024-3564

ACKNOWLEDGEMENTS: This study was partly carried out under the grant from the Russian Science Foundation, No. 23-27-00236.

Conflict of interests: The authors reported no potential conflict of interest.

INTRODUCTION

Hydrological modeling is currently characterized by the prevalence of spatially distributed models. These models are able to adequately reproduce the runoff generation processes within a river basin, and are more reliable for the assessments going beyond the existing observation ranges. The models are also required to solve many problems of spatial water management that are not limited to local tasks like assessing the parameters of bridge dimensions, water intake characteristics or reservoir volume. Contemporary models may be characterized by the detailed representation of watershed characteristics, rigorous mathematical description of processes, and strong hydrometeorological information support, but the issue of adequate diagnostic and verification of these models is still on the agendas of many researchers.

Calibration and verification techniques are primarily based on the use of objective functions in the form of a few quadratic measures of the calculated and observed hydrographs proximity, the most popular of which are the root squared mean error and the Nash-Sutcliffe model efficiency coefficient (NSE) (Nash and Sutcliffe 1970). Sometimes, the NSE is also combined with more measures, as it is done e.g. in the Kling-Gupta-Efficiency (KGE) (Gupta et al. 2009), which combines bias, variability and correlation components to improve the estimation of the performance error. To analyze the temporal variability of model performance and related parameter sensitivity, their interactions, and other aspects of model identifiability,

one may use the DYNamic Identifiability Analysis (DYNIA) method developed by Wagener et al. (2003), and by Reusser et al. (2011).

A more "physically-based" approach is to consider signature measures which are directly related to catchment functions with the aim to consider the relevance of a certain hydrological component individually (e.g. (Yilmaz et al. 2008; Pokhrel et al. 2012; Mohammed et. al. 2021; Huynh et al. 2023)). For example, signature measures based on flow duration curves (FDC) show a model performance for different discharge levels (Yilmaz et al. 2008; Cheng at al. 2012; Pfannerstill et al. 2014). It is worth noting that a calibration problem can be posed as the single-objective optimization problem, typically using algorithms of randomized search in the space of parameters (e.g., (Solomatine et al. 1999)), but also as a multi-objective optimization problem (Pokhrel et al. 2012; Efstratiadis and Koutsoyiannis 2010) with the use of several performance measures. However, we are leaving consideration of the associated possibilities for further studies, concentrating on single-objective calibration.

NSE has a number of advantages, and is still the most widely used performance measure when a model is estimated by a single variable, e.g. by discharge measured at the outlet gauge station. This approach is seen to be justified for simple models, but it seems to be insufficient to calibrate a model with hundreds of spatial design elements and a developed description of a complex set of interrelated processes in each of them.

Hydrological models spatial organization is an important aspect of their calibration and testing. Realization of this fact has led to the interest to the so-called "multi-site calibration" approaches (Wang et al. 2012; Ashu and Lee, 2023; Serur and Adi 2022; Malik et al. 2022; Xu et al. 2022; Ruiz-Pérez et al. 2017), which include comparison of the model outputs to discharge measurements at multiple locations. As presented in the mentioned papers, multi-site calibration allows for developing more reliable models. However, to the best of our knowledge, these approaches can be mostly seen as realizations of "trial and error" strategy, when the model parameters are adjusted in a attempt to iteratively reduce the model error at all the considered locations. For example, Serur and Adi (2022) describe their approach as follows: "the parameter values were changed repeatedly within the allowed ranges until acceptable agreements between observed and simulated streamflow were obtained for each gauged station". Ahu and Lee (2023) describe this procedure as "trial and error were used to acquire the fitted value until the simulated and observed values were consistent". Advantage of this approach is explicit inclusion of an expert in the process, which has certain advantages. However, there are also deficiencies of this method, and we find it important to introduce more rigor to this procedure. This prompts for developing mathematically strict procedures for multi-site calibration, leading to potentially more accurate models. It is done in the presented paper.

It is important to stress the importance of an accurate account of the spatial aspects in calibration. There is a need for comparison of the distributed models outputs not only to the point-wise measurements, but also to the Earth remote sensing data (ERS), where the data is (evenly) distributed over the measurement and calculated grids, and is not necessarily coinciding with the measurement grid. For example, Ruiz-Pérez et al. (2017) calibrate the Eco-hydrological distributed model TETIS-VEG using Normalized Difference Vegetation Index (NVDI) data obtained from the MODIS satellite. They use the method of empirical orthogonal functions (EOF), which is similar to the Principal Component Analysis (PCA) used in this article. Koch et al. (2015) assess the quality of the models by comparing soil temperature maps (LST, land surface temperature) obtained from the model with those obtained from the MODIS satellite, and also using the EOF at one of the stages. Assessment of the model accuracy based on the calculation of soil moisture by comparing the calculated fields with those ones obtained from satellites data and using the EOF apparatus is also considered in the work (Mascaro et al. 2015).

To the best of our knowledge, the problem of spatial calibration of distributed hydrological models based on direct runoff measurements of several stations using the PCA aggregation and analyzing the catchment specifics on the basis of the calculated principal components has not been solved. We see this as a significant gap requiring the novelty in approach.

Hence the main objective of this paper is to develop mathematically strict procedures for multi-site calibration of distributed models.

The approach we propose seems to contributes several innovative aspects in considering the problem of interest. Firstly, the proposed multi-dimensional estimator of modeling quality is a natural generalization of the traditional NSE to the case of modeling runoff simultaneously across a group of hydrological stations within the basin using a single spatially-distributed model. At the same time, all conceptual advantages of the NSE-based assessment are preserved, but the information content used for the model assessment increases substantially.

Secondly, using the PCA method as applied to a group of the daily discharge series improves the adequacy of the model calibration procedure. This becomes possible due to the fairly effective separation of random noise, which is inevitably present in any observational data, and calibrating the model in accordance to an array of the "cleaned" information, which should lead to more accurate parameter estimates.

Thirdly, this approach opens a possibility of obtaining meaningful interpretation of the PCA method results applied to the group of stations data, which is expressed by the proposed concept of a "compact" basin.

Thus, the framework of study presented includes the following stages: assessing the adequacy of NSE under impact of noise; correct calculation of NSE based on the data from multiple gauges; using the PSA as an "integrator" of data from multiple gauges for noise-free calibration; analysis of the case application of the method on a medium-sized basin. The last section pays attention to the formulation of the concept of a "compact" data system and its relationship with the concept of homogeneity of a river basin.

One of the currently popular points of view, consistently presented by K. Beven (2012), insists on the impossibility of determining the "truth" of multiple models (i.e., calibrated on the same data set, but which parameters still differ slightly). It is suggested to consider a wide range of estimates provided by models solely on the basis of rational decision principles under uncertainty. Without delving into further analysis of this approach, we can note that its prevalence is largely related to the dissonance noted above, when calibration tools appear to be limited to deal with the complexity of the models to be compared. Thus, there is a need to develop model calibration and verification tools matching the complexity of the models employed.

METHODOLOGY

Before presenting the essence of the methodology it is important to consider one aspect of application of NSE, which in absolute majority of practical applications is completely overlooked.

Adequacy of NSE for Model Calibration under Assumption of Noise

Let us consider the NSE score in one of the usual formulations, proposed in (Nash and Sutcliffe 1970) and analyzed in detail by Murphy (1998):

$$R^2_{NS} = 1 - \frac{\sum_{i=1}^{n}\left(Qf_i - Qo_i\right)^2}{\sum_{i=1}^{n}\left(Qo_i - Qa\right)^2} \quad (1)$$

where Qf_i and Qo_i are the simulated and observed discharges for the i th day, Qa is the mean observed discharge for the simulated period of time, and n is the number of days in this period. The second term in Eq. (1) is the ratio of the discrepancy quadratic measure between the simulated discharges and the observed ones to the similar measure of the discrepancy between the observed discharges and its "worst" approximation, obtained on the base of available data only (without any model).

According to Eq. (1) for R^2_{NS}, the mean value of the measured discharges for the period is taken as the "worst" approximation. This assessment is the simplest one, but also the "weakest" and not always an adequate one. The issue of applying various approximations as the "worst" is considered in detail in (Murphy 1998). For example, for the rivers with a predominant snowmelt water supply and a stable seasonal distribution of runoff, it would be reasonable to replace the value of Qa in Eq. (1) by $Qnorm_i$, the average annual flow rate for the day i. Such an approach is employed in meteorology, where all estimates are based on anomalies, i.e. the deviations from climatic values at a given moment of the year, which is mathematically equivalent to using "climate" as the "worst" approximation. Yet another, widely used assessment of hydrological forecasts quality (Moreido et al. 2021) $S/\sigma\Delta$ is of similar nature, where S is a root mean squared error of the forecast, and $\sigma\Delta$ is the standard deviation of the observed values during the forecasting period Δ.

In addition, the problem of perfect modeling accuracy estimation deserves special consideration. Many publications indicate that, R^2_{NS} reaches a value of 1, as provided by Eq. (1), when the simulated and observed discharges are completely equal. This result is thought to be an ideal one, and all efforts are focused on its achievement when calibrating the models, although the actual values are typically less than unity. However, each model experiment has a significant random noise, which should not be reproduced by a deterministic model.

Noise is generated by several sources. Firstly, although the model itself is supposed to be strictly deterministic, the results of its operation are strongly influenced by the quality of the input meteorological information. It is appropriate to present the model output Qf_i as the sum of the "true" simulation result Qm_i which could be obtained by feeding accurate and complete meteorological data of the highest spatio-temporal resolution, and a random error ξf resulting from inaccurate and unrepresentative meteorological data. It is impossible to evaluate directly these two components of the simulated signal due to the fundamental lack of "ideal" meteorological data.

Similarly, the measured hydrograph can be represented as the sum of the real discharges Qr_i and the random observation error ξ_o. It is important to bear in mind, that the Qr_i value still contains some internal uncertainty, which, in fact, can also be considered as random. This uncertainty results from the fact that in the real basin there are processes, often random or chaotic, which are beyond the scope of our knowledge, or, at least, beyond the base concepts of the model in use. Model designers often interpret them as "subgrid" processes.

With the above considerations in mind, the formula for R^2_{NS} can be complemented with the independent random variables ξf and ξo with zero mean values, and can be rewritten as follows:

$$R^2_{NS} = 1 - \frac{\sum_{i=1}^{n}\left(\left(Qm_i + \xi_f\right) - \left(Qr_i + \xi_o\right)\right)^2}{\sum_{i=1}^{n}\left(\left(Qr_i + \xi_o\right) - Qa\right)^2} \quad (2)$$

Opening the brackets, we perform the term-wise summation in the numerator and the denominator, assuming n is sufficiently large. Taking into account independence and zero means of ξf and ξo, we can carry out the following derivations:

$$R^2_{NS} = 1 - \frac{\sum_{i=1}^{n}\left(\left(Qm_i + \xi_f\right) - 2\left(Qm_i + \xi_f\right)\left(Qr_i + \xi_o\right) + \left(Qr_i + \xi_o\right)^2\right)}{\sum_{i=1}^{n}\left(\left(Qr_i + \xi_o\right)^2 - 2Qa\left(Qr_i + \xi_o\right) + Qa^2\right)} =$$

$$= 1 - \frac{\sum_{i=1}^{n}\left(Qm_i^2 - 2Qm_i \cdot Qr_i + Qr_{i^2} + \xi_f^2 + \xi_o^2\right)}{\sum_{i=1}^{n}\left(Qr_i^2 + \xi_o^2 - 2Qa \cdot Qr_i + Qa^2\right)} = \quad (3)$$

$$= 1 - \frac{\sum_{i=1}^{n}\left(\left(Qm_i - Qr_i\right)^2 + \xi_f^2 + \xi_o^2\right)}{\sum_{i=1}^{n}\left(\left(Qr_1 - Qa_i\right)^2 + \xi_o^2\right)}$$

With the ideally accurate simulation ($Qm_i = Qr_i$), by dividing the numerator and the denominator by n, we obtain the following estimate of the extreme value of R^2_{NS}:

$$lim_{Qm \to Qr} R^2_{NS} = 1 - \frac{D_{\xi f} + D_{\xi o}}{D_{Qr} + D_{\xi o}} = \frac{D_{Qr} - D_{\xi f}}{D_{Qr} + D_{\xi o}} \quad (4)$$

where Dx is the variable x variance. This expression could also be derived directly based on the general principles of the random variables algebra.

This result is valid only for the assumptions presented earlier. However if, for example, the considered errors are systematic with a non-zero mean value, or variables are not independent, then the final expression will be much more complicated. We assume here that during the calibration process, the systematic part of the analyzed errors is minimized together with the systematic errors inherent in the model itself, which is developed due to the conceptual schematization of real processes.

In real modelling practice one can inevitably expect certain (often significant) random "noise" in the data and simulations. One can see, that in this case the maximum value of NSE for an "ideal" model is below 1. For example, if the variances of errors in input ξf and output ξo are 4% each, then $lim_{Qm \to Qr} R^2_{NS}$ will be 0.923. An attempt of a modeler to exceed (and even achieve) this value cannot be justified, and if this happens, it points at an excessive flexibility of the model. If the number n is not high enough, then the final formula of $lim_{Qm \to Qr} R^2_{NS}$ will also become more complicated, and the estimate will increase slightly,

reflecting the well-known effect of obtaining a fictitiously "better" result of estimates on shorter data samples. We find it important that these considerations must be taken into account for the correct application of the R^2_{NS} measure in rigorous testing of complex models that claim a high degree of proximity to natural processes. Surprisingly, in the majority of papers on (hydrological) modelling the considerations presented above, and their impact on the use of NSE, are not seen as an important part of the calibration and verification process.

Spatial/Dimensional Aspect of Calibration

We will be now considering a more complicated aspect of calibration and testing of the distributed models of extensive basins. Calibration of such models typically uses the data of several gauges damming sub-basins of various sizes and physiographic conditions. The use of all available data for calibration is advisable for the following reasons. Firstly, for the maximum information utilization. Secondly, simulation of a hydrologic event spatial structure is important for solving various tasks, such as operational event planning during floods or reservoir cascade management, when a model should guarantee acceptable accuracy both in the main stream and other stations of the basin. It is also worth mentioning that it would be methodologically attractive to have a unified procedure for such calibration.

In many applications R^2_{NS} estimates are used for distributed models calibration with the data at the outlet gauge station. Along with this, R^2_{NS} is usually evaluated for other gauging stations by experts, so the choice of the most preferred combination of estimates is quite arbitrary. Averaging (simple or weighted) of R^2_{NS} estimates over several gauges can be also employed. It is worth noting that that several stations data in one basin belonging to nested sub-basins are highly correlated and therefore use of simple averaging would be incorrect.

The following question can be posed: is it possible to solve a problem of a multivariate calibration by using the approach similar to the one utilized for the Nash-Sutcliffe model efficiency coefficient proposition? The following consideration answers this question positively. For that, it is possible to use Eq. (1) for multivariate calibration by changing the value of a single gauge discharge to a vector value, that is an ordered set of discharges from multiple gauges:

$$\square^{*}R^2_{NS} = 1 - \frac{\sum_{i=1}^{n}\left(\overline{Qf}_i - \overline{Qo}_i\right)^2}{\sum_{i=1}^{n}\left(\overline{Qo}_i - \overline{Qa}\right)^2} \qquad (5)$$

The asterisk on indicates that this is a multi-dimensional estimate combining all series of the data system considered. The calculation algorithm and the properties of the estimator remain almost unchanged – as a result, one obtains a scalar quantity that reaches 1 in case of perfect modeling without noise, or 0 with the absence of a relationship between the simulated values and the observed ones, and becomes less than zero when their relationship is inverse. In particular, considering Eq. (5) for the simplest case of a two-dimensional vector (i.e., two gauges), in accordance with the rules of vector operations, and after recombination, we obtain:

$$\begin{aligned}
\square^{*}R^2_{NS} &= 1 - \frac{\sum_{i=1}^{n}\left(\left(Qf1_i, Qf2_i\right) - \left(Qo1_i, Qo2_i\right)\right)^2}{\sum_{i=1}^{n}\left(\left(Qo1_i, Qo2_i\right) - \left(Qa1, Qa2\right)\right)^2} = \\
&= 1 - \frac{\sum_{i=1}^{n}\left(Qf1_i - Qo1_i, Qf2_i - Qo2_i\right)^2}{\sum_{i=1}^{n}\left(Qo1_i - Qa1, Qo2_i - Qa2\right)^2} = \\
&= 1 - \frac{\sum_{i=1}^{n}\left(\left(Qf1_i - Qo1_i\right)^2 + \left(Qf2_i - Qo2_i\right)^2\right)}{\sum_{i=1}^{n}\left(\left(Qo1_i - Qa1\right)^2 + \left(Qo2_i - Qa2\right)^2\right)} = \\
&= 1 - \frac{nD_{Qo1}\left(1 - 1 + \frac{\sum_{i=1}^{n}\left(Qf1_i - Qo1_1\right)^2}{nD_{Qo1}}\right) + nD_{Qo2}\left(1 - 1 + \frac{\sum_{i=1}^{n}\left(Qf2_1 - Qo2_1\right)^2}{nD_{Qo2}}\right)}{n\left(D_{Qo1} + D_{Qo2}\right)} = \\
&= 1 - \frac{D_{Qo1}\left(1 - \square^{1}R^2_{NS}\right) + D_{Qo2}\left(1 - \square^{2}R^2_{NS}\right)}{D_{Qo1} + D_{Qo2}} = \frac{D_{Qo1}\square^{1}R^2_{NS} + D_{Qo2}\square^{2}R^2_{NS}}{D_{Qo1} + D_{Qo2}}
\end{aligned} \qquad (6)$$

where $Qf1$, $Qf2$, $Qo1$, $Qo2$, $Qa1$ and $Qa2$ are the modeled, measured and mean discharges in the 1st and 2nd gauges respectively, and и are the regular one-dimensional Nash-Sutcliffe efficiency coefficients for every gauge. The result is that the multi-dimensional is equal to a weighted average of the , and the weights are the corresponding discharge variances. The considered case of two dimensions can be easily extended to deal with higher dimensions (i.e., more than two gauges).

PCA as an "integrator" of data from multiple gauges for noise-free calibration

To analyse and possibly reduce dimension of multi-dimensional sets of highly correlated data the Principal Components Analysis (PCA) method is often used. The principle of the method is the linear transformation of the original coordinate system, in which the initial matrix of correlated data is given, into a new one, which is typically called *U*-space. The first *U*-space axis is oriented along the highest scatter of the initial data, the second one – along the maximum remaining scatter and is orthogonal to the first axis, and further in a sequence. As a result, the initial set of variables is projected to a new set of variables in the *U*-space that is named principal components (PCs). The number of PCs is equal to the initial number of variables, and PCs are non-correlated and orthogonal to each other. Besides, due to the *U*-space conversion method, PCs variance λ is gradually decreasing from the first one to the last one, and thus amounting in the sum the total variance of the initial dataset.

Those properties often make it possible to limit the analysis to only few first PCs representing an expertly defined proportion of the initial dataset variance, of 0.9 or 0.95, for example. Those PCs are considered to be significant, representing the substantial content of the dataset, whereas the rest of the PCs are random noise. Therefore, when applied properly, the PCA makes it possible to decrease the dimensions of the dataset under study and to separate the content-rich data from the noise. Besides, the PCA enables to identify the latent data structures, making it effective in solving classification and zoning tasks.

Apart from using multi-dimensional NSE, using PCA is forms yet another important part of the methodology proposed. PCA serves as an "integrator" of the observed data from multiple (N) gauges and the simulated data for these gauge locations. The information integrated in the major *K* PCs, is considered to represent the deterministic component of the system, and minor (*N* – *K*) components are considered to be representing the noise. The dataset based on the major *K* PCs can be transformed back into multiple *N*-gauges series, and this transformed data is used for the "noise-free" calibration.

A detailed presentation of the PCA and it practical use is provided in a number of publications (e.g., (Pomerantsev 2014; Harris 2001)). The algorithm is implemented in many software packages; we used Minitab Release 14. The PCA transformation is possible both by using the correlation matrix with preliminary standardization of the initial data, and by using the covariance matrix involving initial data processing. The first option scales all variables and equalizes their "weights". Considering that in our investigation the large rivers are more "weighty" compared to small ones, the second option with covariance matrix is adopted.

This section presents the main components of the methodology for calibration of distributed models proposed in this paper, which is based on using a limited number of PCA components, thus concentrating on the main properties of the basin, and reducing noise.

RESULTS: APPLICATION OF THE METHODOLOGY TO A MEDIUM SIZE BASIN

The Ussuri River basin model is considered. It was developed by using the ECOMAG (Ecological Model for Applied Geophysics), developed in the 1990s by Yu.G. Motovilov in the Water Problems Institute of the Russian Academy of Sciences. ECOMAG is a spatially-distributed hydrological model, based on HRU (Hydrological Response Unit) concept. Its complete details are presented in a number of publications (Motovilov et al. 1999; Danilov-Danilyan et al. 2014; Bugaets et al. 2023). The spatial structure of the ECOMAG model splits watershed into sub-basins based on topography, river network structure, soil and vegetation type, land use, and variability of climate characteristics. The main ECOMAG model equations were adopted from the full spatially distributed model by spatial aggregation at subbasin scale, neglecting secondary terms. Daily resolution time series of precipitation, air temperature and air relative humidity are used as inputs. Computation of river basin hydrological response described by the two main phases: calculation of the effective precipitation for each sub-basin, and then routing it through the river network. Runoff from sub-basin is calculated as sum of the three components: Horton overland (surface) flow, soil flow and groundwater outflow. During warm periods precipitation is partially infiltrated and moves along the hillslopes as interflow. Excess water produces surface flow and moves downslope towards the drainage network. The rest of the water that has not been drained to rivers as lateral or surface flow can be evaporated or percolated into deep aquifers. Within cold and mid-season periods the model describes snowpack evolution and soil freezing-thawing cycle. Spatial aggregation made it possible to reduce model calibration to a small number of parameters (Table 1), most of which are correction factors for hydrophysical characteristics.

The basin of Ussuri River near Kirovskiy is 24,400 km^2 (Fig. 1). Its major part is middle altitude taiga with, about 1/3 part is sub-mountain plain-like territory, partially reforested and considerably plowed up. This is a typical Far Eastern river characterized by frequent pluvial floods (Moreido et al. 2021). There were 15 gauges operating in the basin during various time periods, with the highly correlated data.

The data of simultaneous observations of nine gauges for the period beginning 1978 through 1990 (Table 2) were selected for analysis, because the number of synchronously operating gauges is maximal and the quality of network observations is the best during these years. The gauges with watershed areas less than 1,000 km^2 were not included into the data set. Besides, in case of several gauges along one river, they were selected by the watershed area on the condition that the discharges at the neighboring gauges would differ by at least of factor of two. Equal distribution of gauges within the river basin is of course preferred. Discharge data series for the period beginning 1978 through 1990 were simulated with the ECOMAG model. Both observed and simulated datasets were used after every model run for calibration and final estimations of modeling quality by different versions of NSE.

It is important to mention the following. In this paper we are presenting a method able to deal with multi-site calibration and verification of distributed models. However, we are presenting only the results of model calibration on a single data set, but not its testing (on an unseen data set). This is a certain limitation of this study (partly due to the limited resources allocated for this work), but still allows to fully demonstrate the feasibility of the presented approach to calibration well. The comprehensive modelling framework to be developed should include all stages required by modelling theory.

Table 1. ECOMAG calibrated parameters

Parameter	Short Name
Coef. of vertical saturated hydraulic conductivity	GFB
Coef. of horizontal saturated hydraulic conductivity	GFA
Soil evaporation coefficient	EK
Baseflow constant, mm day^{-1}	GROUND
Coef. of snowmelt intensity, mm day^{-1} °C	ALF
Critical air temperature snow/rain, °C	TCR
Snowmelt air temperature, °C	TSN
Air temperature gradient, °C 100 m^{-1}	TGR
Precipitation gradient, mm 100 m^{-1}	PGR
Coef. of vertical saturated hydraulic conductivity	GFB
Coef. of horizontal saturated hydraulic conductivity	GFA

Fig. 1. Hydrological observation network of Ussuri Basin. The runoff gauge stations analysed: 1 – Ussuri–Kirovskiy; 2 – Ussuri–Koksharovka; 3 – Arsenievka–Yakovlevka; 4 –Ussuri–Novomikhalovka; 5 – Pavlovka–Uborka; 6 – Arsenievka–Anuchino; 7 –Ussuri–Verkhniaya Breevka; 8 – Izvilinka–Izvilinka; 9 – Krylovka–Krylovka

Table 2. Model quality estimation by both one- and multi-dimensional NSE on the base of 9 gauges data in Ussuri River basin for 1978 – 1990 years

River – gauge station		Ussuri – Kirovskiy	Ussuri – Koksharovka	Arsenievka – Yakovlevka	Ussuri – Novomikhalovka	Pavlovka – Uborka	Arsenievka –Anuchino	Ussuri – Verkhniaya Breevka	Izvilinka – Izvilinka	Krylovka– Krylovka
Watershed area, km^2		24,400	9,340	5,180	5,170	3,350	2,480	1,800	1,160	1,070
Discharges in initial coordinate system										
Observed discharge series, m^3/sec	Mean	186.0	72.6	36.5	38.5	27.3	20.3	15.6	11.6	8.0
	Standard deviation	268.8	127.4	71.1	62.3	43.4	41.5	27.0	18.3	16.2
	Total variance percentage	70.6%	15.9%	4.9%	3.8%	1.8%	1.7%	0.7%	0.3%	0.3%
Simulated discharge series, m^3/sec	Mean	212.9	90.8	42.5	53.3	31.6	21.8	19.5	14.1	7.6
	Standard deviation	253.1	122.0	57.4	73.9	48.7	34.4	32.3	23.1	13.5
	Total variance percentage	68.9%	16.0%	3.5%	5.9%	2.5%	1.3%	1.1%	0.6%	0.2%
		0.783	0.722	0.625	0.640	0.579	0.650	0.494	0.409	0.229

Multi-dimensional on 9 series is 0.750										
PCs in *U*-space										
		PC1	PC2	PC3	PC4	PC5	PC6	PC7	PC8	PC9
PCs of observanions	Mean	210.4	0.59	−5.72	2.81	1.88	0.77	0.08	−0.17	0.29
	Standard deviation	300.9	93.4	38.6	31.6	16.5	12.0	10.3	8.2	3.4
	Total variance percentage	88.5%	8.5%	1.5%	1.0%	0.3%	0.1%	0.1%	0.1%	0.0%
PCs of simulations	Mean	229.2	9.12	−7.67	2.85	6.34	−2.37	3.03	−1.26	−0.389
	Standard deviation	293.0	73.4	21.5	22.7	14.0	17.8	12.4	9.17	4.08
	Total variance percentage	92.3%	5.8%	0.5%	0.6%	0.2%	0.3%	0.2%	0.1%	0.0%
		0.819	0.358	−0.020	0.170	−0.718	−1.7151	−1.301	−0.9678	−1.054
Multi-dimensional on 9 PCs is 0.767, on the first two PCs – 0.778										

The observed data matrix *Qo (I×J)* presents the sets of daily measured discharges during the calibrating period at 9 gauges, where *I* is the series length (number of days), *J* is the number of variables (gauges). Based on the result of the model simulation performed in an ordinary way (i.e. by calibrating by the outlet gauge data with the expert analysis of other gauges), the simulated daily discharge matrix *Qf (I×J)* is composed. The PCA conversion of *Qo (I×J)* into the *U*-space is carried out, obtaining the eigenvectors *P (J×J)* matrix and the PCs matrix of observations *Uo (I×J)*. Subsequently, the *Qf (I×J)* matrix is converted similarly into the same *U*-space through the *P (J×J)* matrix, that resulted in the PCs matrix of simulations *Uf(I×J)*. The individual values (k=1, 2, …, 9) are evaluated by the series of both observed and simulated discharges at every gauge, and hereafter the multi-dimensional evaluation is done by them. The same procedure is applied for the observed and simulated PCs series from 1 through 9, and the multi-dimensional evaluation is carried out as well. Table 2 presents the summary of the evaluation results.

As presented in Table 2, the variances of PCs decrease very quickly – the sum of the variances of PCo1 and PCo2 amounts for 97% of the total variance, exceeding the threshold estimate at 95%, while the other PCs variances are negligible. So, it is possible to consider the first two PCs as the deterministic part of the system, and the remaining seven ones as the random noise. The individual values of , which show the simulation quality of each PC, confirm this hypothesis - for the first PCo1 the estimate is 0.819 (good), for the second PCo2 it is 0.358 (satisfactory), then the estimate decrease, even reaching large negative values.

Note, that observation variables are also graded in the initial matrix *Qo(I×J)* by variance. Sum of variances of two largest gauges is 86.5% of the total variance, that is so close to the sum of variances of PCo1 and PCo2 of observations. However, the values for all gauge series are still high with the slight downward trend at watershed area reduction. Fig. 2 distinctly shows the difference between the gauge hydrographs and the charts of PCs values at the same positions in the matrixes. The hydrographs' values are essentially positive, and the charts have a specific shape similar to each other, whereas the PCs numbered 3 and higher look like random signals with zero mean.

In other words, the content-rich information from the hydrographs of various gauges is evenly distributed, and is duplicated, which is confirmed by high cross-correlation coefficients. The noises are similarly distributed across all gauges. It is obvious that the PCA transformation brings the initial correlated dataset to the system of uncorrelated PCs collecting independent content-rich data into two first ones, whereas the noise is distributed between the rest. It is known that the random variables' total variance being equal to the sum of variances is true for the independent random variables only. Table 2 really shows that this rule is true for PCs, however the total variance of the initial variables is more than three times higher than the sum of their individual variances. This proportion gives a rough indicator of the data "duplication" in the initial data matrix.

It should be emphasized that it is impossible to strictly separate a signal into a content-rich part and the noise by statistical methods (and, note, the 5% threshold level of noise is set arbitrarily). Therefore, it would be more correct to say that the noise content prevails in the removed seven components, and the content-rich data considerably prevails in the first two components compared to the initial dataset.

The Nash-Sutcliffe multi-dimensional coefficient estimation for a traditionally calibrated model does not depend on the coordinate space – it is calculated according to Eq. (6) and is equal to 0.750. The characteristics of the PCs, including their independent status and the distribution between a content-rich signal and noise, make it possible to perform calibration by only PC1 and PC2 when calculating the multi-dimensional values with this two PCs, that is marked by two asterisks. The is equal to 0.778 by the result of a traditional calibration using standard NSE. By further calibration this value can be risen up to 0.804 for a new PCs matrix of simulations *Uf'(I×J)*. Thereby, the final for all gauges reaches 0.780, so is rising by 4%. Once additional calibration is performed for a content-rich part of data, which can be seen as the "information kernel" of the dataset, it is reasonable to expect that the parameters estimates would be more reliable (however, this should be additionally verified).

Supposedly, the PCs from 3 through 9 mainly contain noise, therefore, it is reasonable to discard them. It is done by zeroing all but the first two matrix columns in *Uf'(I×J)*, and the subsequent reverse *U*-space transformation into the initial one. The resulting *Qf''(I×J)* will have the "noise free" modeled values. The resulting values are equal to 0.789, and remain

practically unchanged. However, it is worth mentioning that this procedure considerably effects the distribution of across individual gauges.

With the traditional calibration, there are typically some stations with the small catchment areas, for which the model performance is very low. The reasons for this phenomenon are not very clear. We observed this effect for the gauge station Krylovrka river near Krylovka, where is only 0.229 (Table 2). To improve that, we have transformed the two-component simulated dataset (based on two PCs) back into nine-gauges series (that is the model was calibrated on the two first PCs thus excluding noise represented by the higher-order components). As a result, we obtained = 0.548 which is much better (albeit not ideal). Thereby, and a watershed area are closely related (Fig. 3). It would be reasonable to conclude that under traditional calibration, uncontrolled distribution of noise concentrates at the gauges at small sub-basins whose contribution to the overall flow is also small. This issue is to a large extent resolved when the noise components are discarded.

Fig. 2b presents the two first PCs obtained as the result of the initial data transformation. Their physical meaning is revealed when zoomed at the X axis (Fig. 4a). The first principal component has typical appearance of a discharge hydrograph and, so to say, presents a "generalized hydrograph" of the basin. The second principal component has zero mean and a specific waveform nearby every peak of the "generalized hydrograph". This component indicates obviously that hydrographs are non-synchronous and systematically deviate from the "generalized" one. In other words, the second principal component reflects the space-time structure of the events within the basin.

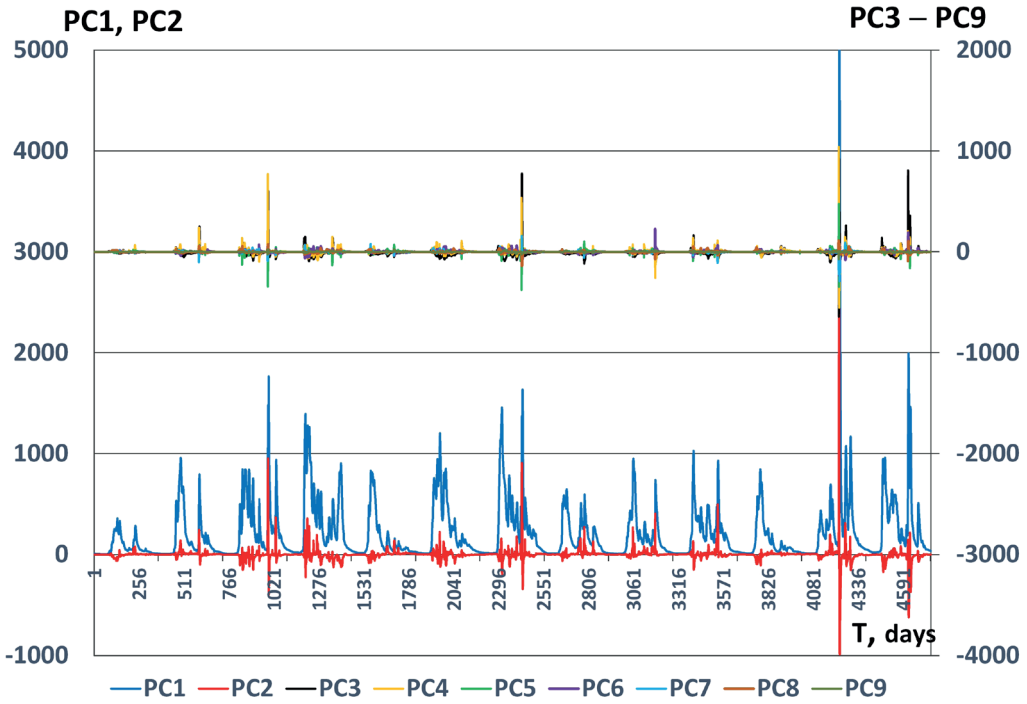

Fig. 2. The series of Ussuri Basin dataset analysed (1978-1990): a) observed daily discharges in initial coordinate system (1 – Ussuri–Kirovskiy; 2 – Ussuri–Koksharovka; 3 – Arsenievka–Yakovlevka; 4 –Ussuri–Novomikhalovka; 5 – Pavlovka–Uborka; 6 – Arsenievka–Anuchino; 7 –Ussuri–Verkhniaya Breevka; 8 – Izvilinka–Izvilinka; 9 – Krylovka–Krylovka); b) PCs in U-space from 1 till 9

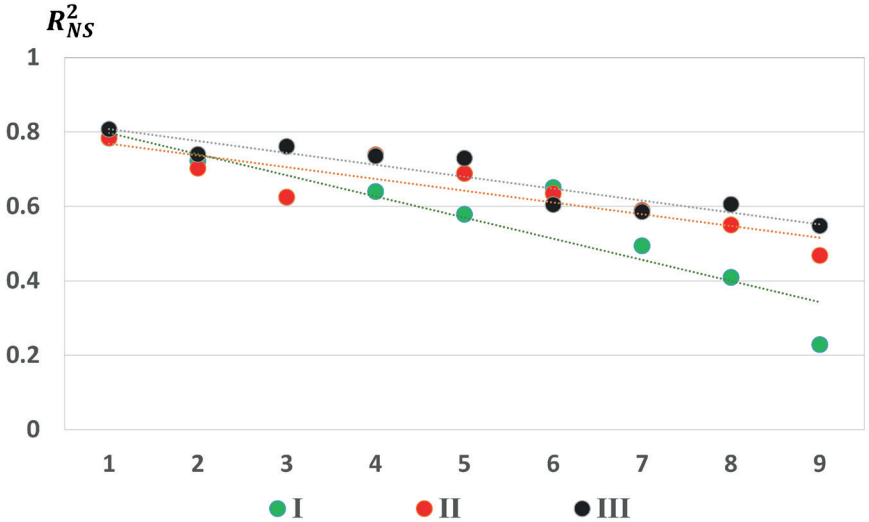

Fig. 3. The one-dimensional Nash-Sutcliffe efficiency coefficients, resulting from different calibration methods, for discharge series: 1 – Ussuri–Kirovskiy; 2 – Ussuri–Koksharovka; 3 – Arsenievka–Yakovlevka; 4 –Ussuri–Novomikhalovka; 5 – Pavlovka–Uborka; 6 – Arsenievka–Anuchino; 7 –Ussuri–Verkhniaya Breevka; 8 – Izvilinka–Izvilinka; 9 – Krylovka–Krylovka. Calibration methods: I – traditional, mainly by discharge measured at outlet gauge station with expert control in others gages; II the same with removing the random noise; III – using the multi-dimensional NSE by all discharge series with removing the random noise

FURTHER EXTENSION: COMPACT DATASETS

It is worth stressing once again some advantages of the multi-dimensional calibration provided in the example above. Firstly, application of a unified measure for a group of gauges reduce the problem of multi-dimensional calibration to the one of one-dimensional problem. Thereby, there is no need in expert evaluation of the relation between model accuracy at various gauges, which facilitates the application of automated procedures. Eq. (6) provides the theoretically justified way of weighting the individual components of NSE by the variances of the corresponding time series, eliminating thus the subjectivity typical of other non-aggregated modeling performance metrices for a group of gauges, designed on the basis of various "practical" considerations.

The example above shows that the PCA procedures allow for considerable reduction of the dimensionality of the datasets for medium-size basins, which are conditionally homogeneous by physiographic conditions and have highly correlated discharge hydrographs at various gauge stations: the useful information is stored in two PCs of varied physical interpretation and the most of the noise can be removed. This opens a possibility to identify the "informational core" of a data set, using which the model calibration would potentially lead to more reliable and stable parameters estimates. It is suggested to name such data sets, as well as their associated basins, the "compact" data sets.

As it may be assumed on the basis of the provided analysis, a "compact" basin is a homogeneous one both by the underlying surface structure and the character of the meteorological forcing, as it is the case for the studied Ussuri River basin. The basin's high homogeneity is expressed by similar response of sub-basins to meteorological forcing, or, in other words, the discharge hydrographs of all sub-basins are similar.

For small basins homogeneity would typically be high. However, we may assume that a certain number of varying sub-basin hydrographs may be averaged without substantial information loss within a basin of few tens of thousands square kilometres (for daily data step), that just is the medium-size. In this case the variance between the hydrographs in different gauges within the basin is determined only by the characteristics of the basin's concentration time and flow in the network. To demonstrate this approach, a simple model demonstrating the properties of a "compact" dataset can be built as follows.

We may use the facts known from hydrological science, such as the linear dependency between discharge and watershed area, and the power dependency between the basin's runoff concentration time and its area, with the exponent close to 0.5 (see, for example, Rodríguez-Iturbe and Rinaldo (1997)). Let us examine the observed hydrograph at the gauge of the Ussuri River near Novomikhaylovka,

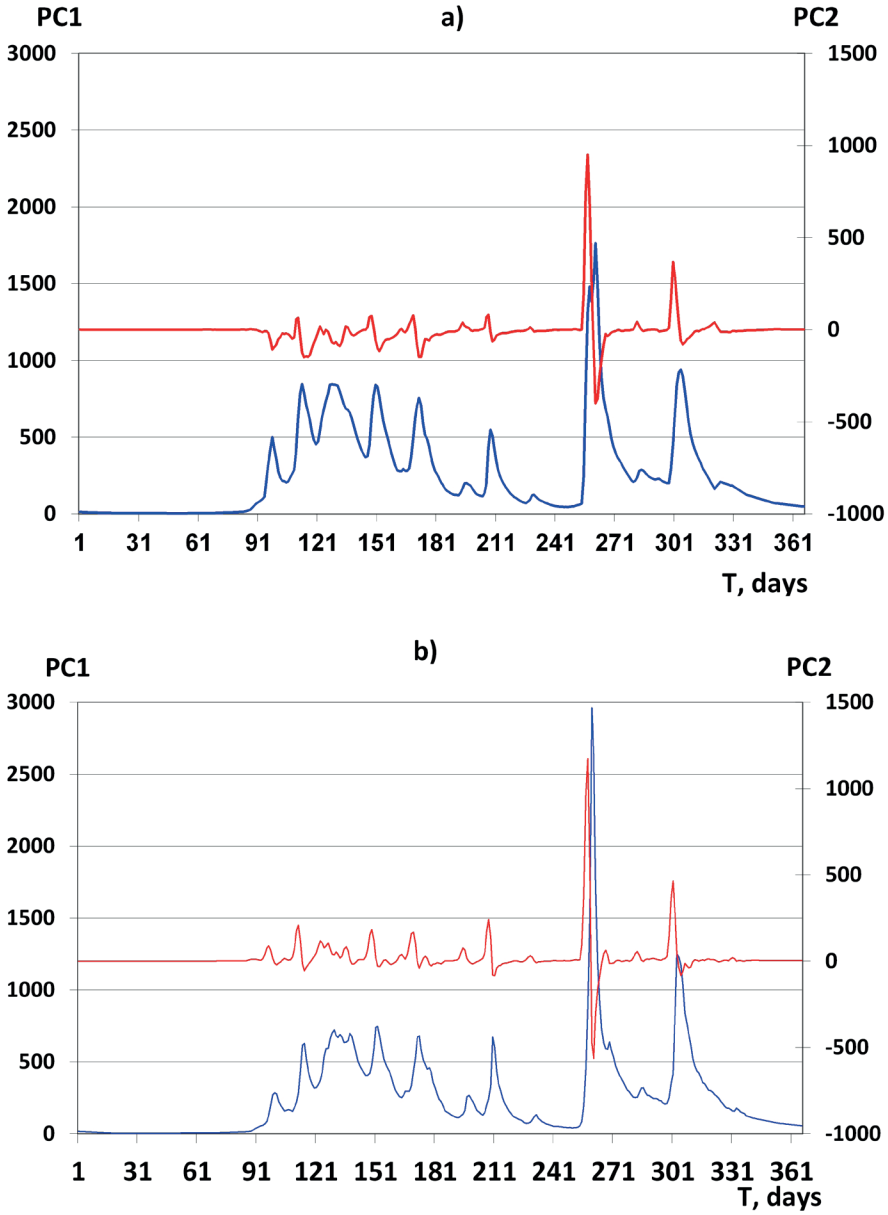

Fig. 4. The example of PC1 (blue line) and PC2 (red line) for the actual observed (a) and the constructed "observed" datasets (b) for 9 gauging stations within Ussuri River Basin (year 1980)

which corresponding sub-basin area is about 5 times higher than that that corresponding to its smallest streams, and 5 times lower than that corresponding to the outlet gauge. We calculate daily runoff specific discharges by the data from the mentioned gauge and transfer them to other gauges according to their watershed areas. As proposed above, the concentration time is proportional to the square root of the area, and we accordingly may shift in time the hydrographs at different gauges relative to one another. Thus, the constructed dataset is obtained from a single observed hydrograph using scaling and shifting transformations only.

For constructing a more realistic dataset, random noise is added to the hydrographs with approximately 20% variance of the main signal. The noise simulates both observational errors and the consequences of other factors, and is modeled by a random number generator with the normal distribution. At each point of time the random noise value is in proportion to discharge and has a considerable inertia described by the coefficient of autocorrelation. The obtained set of hydrographs can be assumed to be the "observed" data. The "simulated" data is the same data, but without the added random noise. This way of constructing the datasets is of course a primitive one, however, it seems sufficient to show the relation between the homogeneity of basin surface and weather conditions, and the statistical "compactness" of observational dataset.

These datasets are processed as described in the previous section regarding the observed and simulated Ussuri River basin data. Table 3 provides the processed results. Tables 2 and 3 mapping confirms that constructed datasets for the period beginning 1978 through 1990 have the properties similar to the actual ones. Thus, "simulated" data have lower variance than the "observed" one. Variance of the constructed series at the gauges is smaller for smaller areas, and the sum of variances for the two largest basins is equal to 88.8% of that for the "observed" data. Individual at gauges vary from 0.872 to 0.316, where the lowest value is related to the smallest basin. estimate is 0.764.

Table 2. Imitation of model quality estimation by both one- and multi-dimensional NSE on the base of constructed data series for 9 gauges in Ussuri River basin for 1978 – 1990 years

River – gauge station		Ussuri – Kirovskiy	Ussuri – Koksharovka	Arsenievka – Yakovlevka	Ussuri – Novomikhalovka	Pavlovka – Uborka	Arsenievka –Anuchino	Ussuri – Verkhniaya Breevka	Izvilinka –Izvilinka	Krylovka– Krylovka
Watershed area, km^2		24,400	9,340	5,180	5,170	3,350	2,480	1,800	1,160	1,070
Discharges in initial coordinate system										
Observed discharge series, m^3/sec	Mean	185	78.4	38.7	41.4	30.9	19.3	12.9	9.2	6.9
	Standard deviation	306	129	72.5	73.6	68.8	34.1	25.6	21.4	10.9
	Total variance percentage	75.4%	13.4%	4.2%	4.4%	3.8%	0.9%	0.5%	0.4%	0.1%
Simulated discharge series, m^3/sec	Mean	192	73.7	40.9	40.8	26.4	19.6	14.2	9.1	8.4
	Standard deviation	312	119	66.2	66.0	42.8	31.7	23.0	14.8	13.7
	Total variance percentage	78.4%	11.5%	3.5%	3.5%	1.5%	0.8%	0.4%	0.2%	0.2%
		0.754	0.818	0.759	0.836	0.777	0.872	0.714	0.769	0.316
Multi-dimensional on 9 series of "observations" and "simulations" is 0.768										
PCs in U-space										
		PC1	PC2	PC3	PC4	PC5	PC6	PC7	PC8	PC9
PCs of observanions	Mean	–212	–15.4	2.3	–3.4	–3.0	–3.9	–1.0	1.9	1.9
	Standard deviation	335	103	55.2	29.3	24.2	18.3	12.7	6.4	6.4
	Total variance percentage	87.7%	8.3%	2.4%	0.7%	0.5%	0.3%	0.1%	0.0%	0.0%
PCs of simulations	Mean	–217	–8.9	–1.4	–7.5	–5.2	–6.0	–2.2	3.2	3.2
	Standard deviation	340	83.1	29.0	11.4	10.9	13.9	6.9	5.7	5.7
	Total variance percentage	93.3%	5.6%	0.7%	0.1%	0.1%	0.2%	0.0%	0.0%	0.0%
		0.818	0.561	0.231	–0.233	–0.254	0.410	–0.052	–0.102	–0.492
Multi-dimensional on 9 PCs is 0.795, on two first PCs – 0.797										

Being projected into the *U*-space, the constructed data is effectively convoluted, and summarized dispersion of the first two PCs is up to 96.0% for the "observed" hydrographs, and it is 98.9% for the "simulated" ones. Individual for PCs are progressively reducing and exceed the 0.5 threshold for the two first PCs only with the estimate equal to 0.796. The PCs following the first two ones look like random stochastic sequences, whereas the charts of the PCc1 and PCc2 are very close to the ones developed by the actual observed and simulated data (Fig. 4).

It can be seen that the Ussuri River basin, being quite homogeneous in structure and dynamics, allows for demonstrating the main properties and usefulness of the proposed notion of a "compact" dataset. For sure, more studies are needed for the further development of this notion.

CONCLUSIONS AND OUTLOOK

The conducted study demonstrates that the presented version of the multi-dimensional NSE with PCA in calibration of spatially-distributed hydrological models, if compared to other calibration methods, has a number of advantages:

– the reduced dimensionality without loss of important information, straightforward data analysis, and the automated calibration procedure;

– objective separation of the deterministic signal from the noise, calibration using the "information kernel" of data, leading to more accurate parameters' estimates.

Additionally, the introduced notion and the procedure of building the "compact" datasets allows for physical interpretation of "compact" or "noncompact" sub-basins, which is valuable for hydrological zoning of the basins, hydrological fields analysis, and structuring the models of large basins. It should be emphasized once again that the proposed methodology seem of most advantageous along the transition to solving those problems of hydrology that can be solved solely on the basis of spatially distributed models.

The methods presented in this paper should be seen as only one of the possible ways of handling the multi-dimensional time series in the context of space-distributed model diagnosis and calibration. The further research may be aimed at:

(a) testing the hypothesis that the parameters estimated by multi-dimensional calibration are more reliable and adequate that those estimated by other calibration procedures;

(b) exploring variability of the simulation accuracy with time, and the spatially aggregated uncertainty;

(c) testing other techniques for data aggregation and dimensionality reduction;

(d) explicit consideration of data series autocorrelation, which is closely related to the issues of their predictability and the overall simulation accuracy.

The presented methodology (and the framework to be created on its basis) should be developed and tested further: verified on more case studies, include explicit testing of the calibrated models on unseen data sets, and perhaps even extended into multi-objective calibration version.

The presented approach opens yet another potential opportunity. Since the multi-dimensional Nash-Sutcliffe index is a single basin characteristic of the simulation accuracy, it is assumed that it can be evaluated according to data from different groups of stations for different time periods in compliance with the principles of sample evaluation, i.e., while respecting the representativeness of these groups of stations in some sense. This opens up the prospect of expanding the information base for calibration of distributed hydrological models, and this may allow using full multi-year archives of standard runoff observations for all gauges in the same basin, despite the existing gaps in the observations and changes in the observation network configuration.

REFERENCES

Ashu A.B. and Lee S.-I. (2023) Multi-Site Calibration of Hydrological Model and Spatio-Temporal Assessment of Water Balance in a Monsoon Watershed. Water, 15, 360. https://doi.org/10.3390/w15020360.

Beven K.J. (2012) Rainfall-Runoff Modelling: The Primer. 2nd ed. Blackwell: Wiley.

Bugaets A., Gartsman B., Gubareva T., Lupakov S., Kalugin A., Shamov V. and Gonchukov L. (2023) Comparing the Runoff Decompositions of Small Experimental Catchments: End-Member Mixing Analysis (EMMA) vs. Hydrological Modelling. Water, 15(4), 752, https://doi.org/10.3390/w15040752.

Cheng L., Yaeger M., Viglione A., Coopersmith E., Ye S. and Sivapalan M. (2012) Exploring the physical controls of regional patterns of flow duration curves - part 1: Insights from statistical analyses. Hydrol. Earth Syst. Sci., 16, 4435–4446, https://doi.org/10.5194/hess-16-4435-2012.

Danilov-Danilyan V.I., Gelfan A.N., Motovilov Y.G. and Kalugin A.S. (2014) Disastrous flood of 2013 in the Amur Basin: genesis, recurrence assessment, simulation results. Water Resources., 41(2), 115-125, https://link.springer.com/article/10.1134/S0097807814020055.

Efstratiadis A. and Koutsoyiannis D. (2010) One decade of multi-objective calibration approaches in hydrological modelling: A review. Hydrol. Sci. J., 55(1), 58–78, https://doi.org/10.1080/02626660903526292.

Gupta H.V., Kling H., Yilmaz K.K. and Martinez G.F. (2009) Decomposition of the mean squared error and NSE performance criteria: Implications for improving hydrological modelling. J. Hydrol., 377, 80–91, https://doi.org/10.1016/j.jhydrol.2009.08.003.

Harris R.J. (2001) A primer of multivariate statistics. 3nd ed. New York: Psychology Press, https://doi.org/10.4324/9781410600455.

Huynh N.N.T, Garambois P.A., Colleoni F. and Javelle P. Signatures-and-sensitivity-based multi-criteria variational calibration for distributed hydrological modeling applied to Mediterranean floods. J. Hydrol., 625, Part A, 129992, https://doi.org/10.1016/j.jhydrol.2023.129992.

Koch J., Jensen K.H. and Stisen S. (2015) Toward a true spatial model evaluation in distributed hydrological modeling: Kappa statistics, Fuzzy theory, and EOF-analysis benchmarked by the human perception and evaluated against a modeling case study. Water Resour. Res., 51, 1225–1246, https://doi.org/10.1002/2014WR016607.

Malik M.A., Dar A.Q., Jain M.K. (2022) Modelling streamflow using the SWAT model and multi-site calibration utilizing SUFI-2 of SWAT-CUP model for high altitude catchments, NW Himalaya's. Model. Earth Syst. Environ., 8, 1203–1213, https://doi.org/10.1007/s40808-021-01145-0.

Mascaro G., Vivoni E.R. and Méndez-Barroso L.A. (2015) Hyperresolution hydrologic modeling in a regional watershed and its interpretation using empirical orthogonal functions. Advances in Water Resources., 83, 190–206, http://dx.doi.org/10.1016/j.advwatres.2015.05.023.

Mohammed S.A., Solomatine D.P., Hrachowitz M. and Hamouda M.A. (2021) Impact of dataset size on the signature-based calibration of a hydrological model. Water., 13, 970, https://doi.org/10.3390/w13070970.

Moreido V., Gartsman B., Solomatine D.P. and Suchilina Z. (2021) How well can machine learning models perform without hydrologists? Application of rational feature selection to improve hydrological forecasting. Water., 13, 1696, https://doi.org/10.3390/w13121696.

Motovilov Yu.G., Gottschalk L., Engeland K. and Belokurov A. (1999) ECOMAG – regional model of hydrological cycle. Application to the NOPEX region. Oslo: Univ. of Oslo, https://studylib.net/doc/11453981/ecomag--regional-model-of-hydrological.

Murphy A. (1988) Skill Scores Based on the Mean Square Error and Their Relationships to the Correlation Coefficient. Monthly Weather Review., 116, 2417–2424, https://doi.org/10.1175/1520-0493(1988)116<2417:SSBOTM>2.0.CO;2.

Nash J.E. and Sutcliffe J.V. (1970) River flow forecasting through conceptual models part I — A discussion of principles. J. Hydrol. 10(3), 282–290, http://dx.doi.org/10.1016/0022-1694(70)90255-6.

Pfannerstill M., Guse B. and Fohrer N. (2014) Smart low flow sig-nature metrics for an improved overall performance evaluation of hydrological models. J. Hydrol., 510, 447–458, https://doi.org/10.1016/j.jhydrol.2013.12.044.

Pokhrel P., Yilmaz K.K. and Gupta H.V. (2012) Multiple-criteria calibration of a distributed watershed model using spatial regularization and response signatures. J. Hydrol., 418-419, 49–60, https://doi.org/10.1016/j.jhydrol.2008.12.004.

Pomerantsev A.L. (2014) Chemometrics in Excel. Hoboken, New Jersey: Wiley, https://doi.org/10.1002/9781118873212.

Reusser D.E., Buytaert W. and Zehe E. (2011) Temporal dynamics of model parameter sensitivity for computationally expensive models with Fourier amplitude sensitivity test. Water Resour. Res., 47, W07551, https://doi.org/10.1029/2010WR009947.

Rodríguez-Iturbe I. and Rinaldo A. (1997) Fractal River Basins: Chance and Self-Organization. Cambrige: Cambrige University Press.

Ruiz-Pérez G., Koch J., Manfreda S., Caylor K. and Francés F. (2017) Calibration of a parsimonious distributed ecohydrological daily model in a data-scarce basin by exclusively using the spatio-temporal variation of NDVI. Hydrol. Earth Syst. Sci., 21, 6235–6251, https://doi.org/10.5194/hess-21-6235-2017.

Serur A.B. and Adi K.A. (2022) Multi-site calibration of hydrological model and the response of water balance components to land use land cover change in a rift valley Lake Basin in Ethiopia. Sci. Afr., 15, e01093, https://doi.org/10.1016/j.sciaf.2022.e01093.

Solomatine D.P., Dibike Y. and Kukuric N. (1999) Automatic calibration of groundwater models using global optimization techniques. Hydrol. Sci. J., 44, 879-894, https://doi.org/10.1080/02626669909492287.

Wagener T., McIntyre N., Lees M.J., Wheater H.S. and Gupta, H.V. (2003) Towards reduced uncertainty in conceptual rainfall-runoff modelling: Dynamic identifiability analysis. Hydrol. Process., 17, 455–476, https://doi.org/10.1002/hyp.1135.

Wang S., Zhang Z., Sun G., Strauss P., Guo J., Tang Y. and Yao A. (2012) Multi-site calibration, validation, and sensitivity analysis of the MIKE SHE Model for a large watershed in northern China. Hydrol. Earth Syst. Sci., 16, 4621–4632, https://doi.org/10.5194/hess-16-4621-2012.

Xu Z., Wu Z., Shao Q., He H., and Guo X. (2022) A two-step calibration framework for hydrological parameter regionalization based on streamflow and remote sensing evapotranspiration, Journal of Hydrology, 613, Part A, 128320, https://doi.org/10.1016/j.jhydrol.2022.128320.

Yilmaz K.K., Gupta H.V. and Wagener T. (2008) A process-based diagnostic approach to model evaluation: Application to the NWS distributed hydrologic model. Water Resour. Res., 44, W09417, https://doi.org/10.1029/2007WR006716.

Check for updates

CC BY

RESEARCH PAPER

IMPACT ASSESSMENT OF RIVER REGULATIONS USING 1D MORPHODYNAMIC MODELING ON THE UPPER HUNGARIAN DANUBE

Emese Nyiri[1*], Gergely T. Török[123]**

[1] Budapest University of Technology and Economics, Faculty of Civil Engineering, Department of Hydraulics and Water Resources Engineering, Műegyetem rakpart, Budapest, 1111, Hungary

[2] HUN-REN-BME Water Management Research Group, Department of Hydraulic and Water Resources Engineering, Budapest University of Technology and Engineering, Műegyetem str. 3,1111 Budapest, Hungary

[3] National Institute of Water and Atmospheric Research, Kyle Street 10, Christchurch 8011, New Zealand

***Corresponding author:** nyiri.emese@edu.bme.hu

****Corresponding author:** torok.gergely@emk.bme.hu

Received: May 5th 2024 / Accepted: November 22nd 2024 / Published: December 31st 2024

https://doi.org/10.24057/2071-9388-2024-3390

ABSTRACT. The geometry of watercourses shows that they undergo continuous deformation towards a dynamic equilibrium state. Once this is reached, further changes in the bed can be observed, but they are not expected to cause significant deviations from the dynamic equilibrium state. The dynamic equilibrium state will likely change due to significant natural or artificial processes. The main question is what new riverbed geometry or flow conditions (peak water levels) can be expected. In our paper, we investigate the impact of past interventions on the dynamic equilibrium state of the Upper Danube in Hungary. We built a 1D morphodynamic model for the section under study. The model was improved by incorporating the mixed grain composition of the bed and bedload material and considering the backwater effect. The model was parameterised with data from the 19th century, i.e. the natural state. The model allowed us to perform a century-scale study. The model gave accurate results of 13 cm and 3 cm for the incorporation of the interventions and also predicted the backfilling in the studied section. Using the 1D approach, we obtained a model that can study a more extended section, such as a more than 100 km reach. The 1D model can provide a temporal estimate of the impact of each intervention, Such as the installation of wing dam fields and water dams and the elaboration of artificial cutoffs.

KEYWORDS: sediment transport, river regulation, 1D model, dynamic equilibrium state

CITATION: Nyiri E., Török G. T. (2024). Impact Assessment Of River Regulations Using 1D Morphodynamic Modeling On The Upper Hungarian Danube. Geography, Environment, Sustainability, 4(17), 88-100
https://doi.org/10.24057/2071-9388-2024-3390

ACKNOWLEDGEMENTS: It has been produced with the technical support of the University Research Scholarship Programme of the Ministry of Culture and Innovation, code number EKÖP-24-2-BME-164, funded by the National Research, Development and Innovation Fund.

The research presented in this publication was supported by the Bolyai János Research Fellowship for the second author and funded by the OTKA Postdoctoral Excellence Grant Programme No PD 135037 from the National Research Development and Innovation Fund. The research was funded by the Sustainable Development and Technologies National Programme of the Hungarian Academy of Sciences (FFT NP FTA).

Conflict of interests: The authors reported no potential conflict of interest.

INTRODUCTION

For all rivers, morphological changes can be observed over time, the effects of which need to be characterized by approximating the dynamic equilibrium state. These changes can be caused by artificial interventions or by natural phenomena. Nowadays, increasing emphasis is being placed on predictions, which can also be necessary for the morphological characteristics of rivers. Natural changes can often only be estimated, but artificial interventions are preceded by planning or consultation, making predicting their impact easier. In the Upper Danube in Hungary, it can also be observed that some interventions have induced changes in riverbed geometry that were not or could not be considered in the design because of the lack of reliable tools (Farkas-Iványi, 2015; Tőry, 1952; Bogárdi, 1955, Holubová, 2004). For example, when deposition and gravel bank formation was caused by excess downstream sediment related to bed erosion from an upstream intervention. In this case, the upstream interventions caused navigational difficulties on the downstream reach, which required further interventions in the river section, which became problematic (Rákóczi, 1993). A suitable model could have predicted the effects of the upstream intervention.

In our study, we focused on a section of the Upper Danube in Hungary and investigated the artificial effects of this section. The section under study starts at Dunaremete and continues to Nagybajcs, as shown in Figure 1.

The Danube has already undergone a lot of regulation, such as the river regulation in the 19th century (1881-1885), where the then braided system (Figure 1.) was transformed into a single thread channel (Figure 1.), which provides better navigation conditions and improved flood protection (Tőry, 1952; VITUKI, 1954).

According to the literature, the length of the section was reduced by 10% (Tőry, 1952). The regulation has reduced by half the widths in the control sections. After regulation, the alluvium was enriched, filling several places. This resulted in the following regulation work (Tőry, 1952; Bogárdi, 1955).

A further intervention was the installation of wing dams/ wing dam rows on the section between 1938 and 1944 (Tőry, 1952) (Figure 2.). This intervention is expected to induce morphodynamic processes that mainly benefit navigability. The braided system regulation upset the sediment balance, which resulted in intensive sediment deposition on the downstream section. The installation of the wing dams was expected to erode these problematic deposits, thus improving the flood risk management and navigability. The wing dams were constructed between 1938 and 1944 (Tőry, 1952). The constructed wing dams narrowed the original channel width by ~30% which means about 120 m in the Nagybajcs (rkm 1801) section.

Several studies have been conducted to investigate the effects of wing dams, which have supported the present work. Evaluation of field measurements and numerical modelling results were also available in the studies processed. The results showed that the consideration of the mixed grain composition plays a significant role in the development of the new equilibrium state (Holubová 2015; Wilcock and Crowe, 2003; Parker et al., 2024). The studies focused on a few km long sections and short time scales. Measurement-based studies (Liedermann et al. 2017; Holubová et al. 2015; Pomázi and

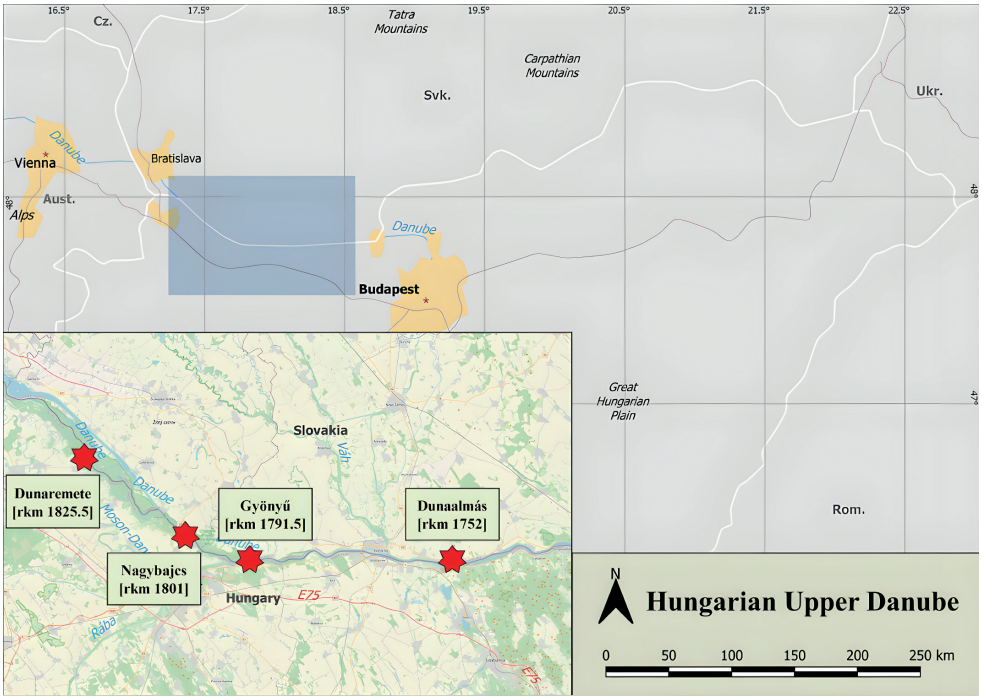

Fig. 1. Description of the section and sections studied on the Upper Danube in Hungary

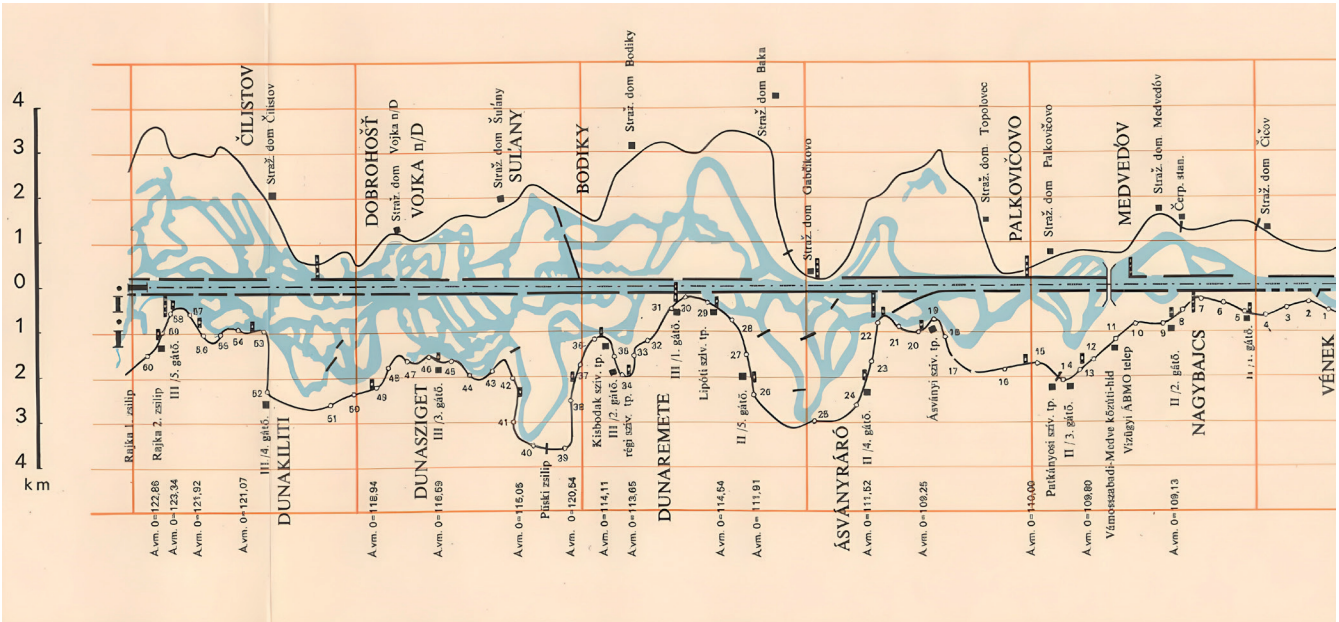

Fig. 2. Braided branch system on the Upper Hungarian Danube (VITUKI, 1954)

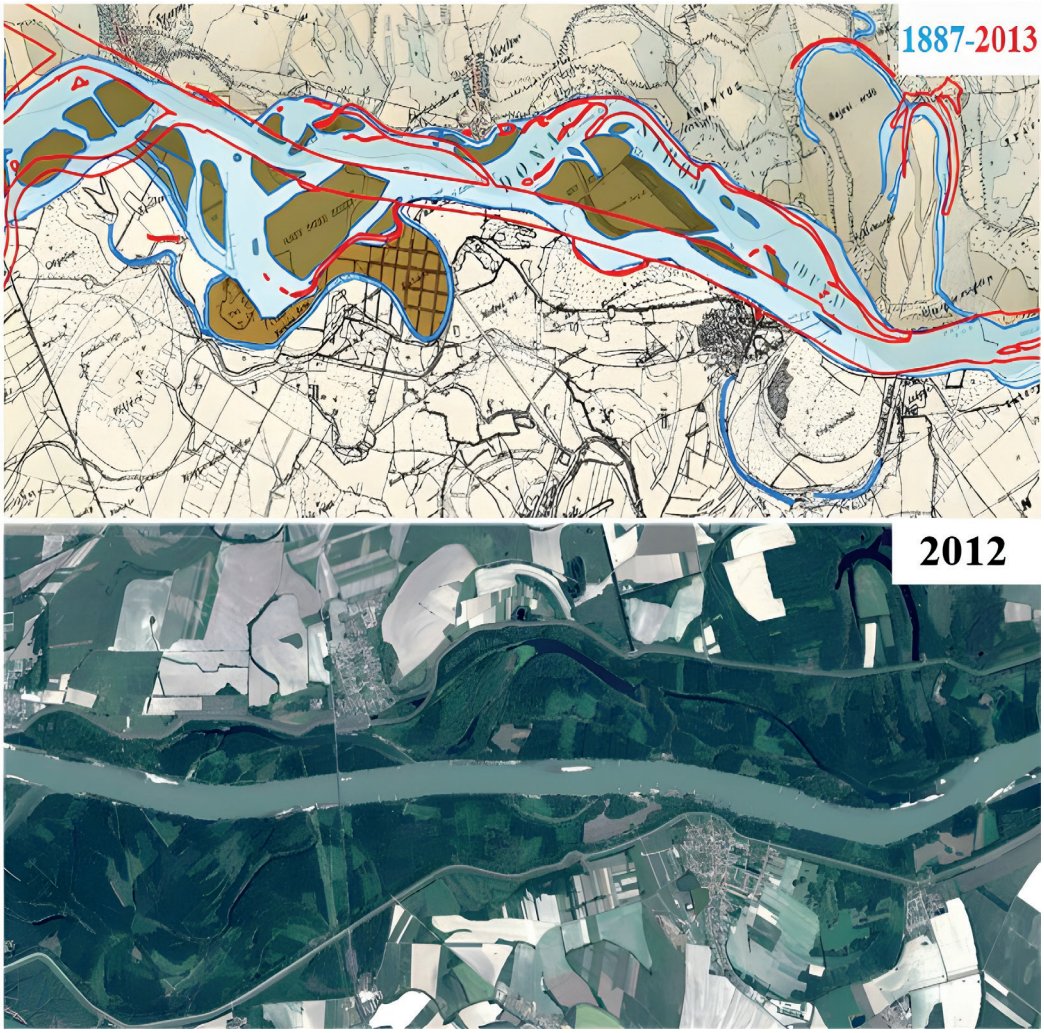

Fig. 3. Danube regulation before/after comparison (DuRe Flood project, 2015)

Baranya 2022) evaluated the present conditions. Numerical modelling-based studies were limited to a few months at most (Fischer- Antze et al., 2008; Baranya & Józsa, 2006). The studies showed no significant riverbed change trend in the examined sections. Based on these, it seems that the 2000s established the new equilibrium state, that is, the effect of previous interventions was no longer detectable.

However, examining the effects of interventions that are more extensive than local, both in space and time is necessary. We believe this is of great importance, as interventions can significantly impact the morphodynamics upstream and downstream.

Based on these, the present study aims to demonstrate that it is possible to predict the morphodynamic effects of reach-scale interventions using a 1D model that is able to take into account the mixed grain composition of sediment transport and is able to consider the interaction between upstream and downstream by applying backwater equation. In this way, we offer a validated tool capable of answering key questions for river regulation. In our particular case, what impact have river management interventions had on the equilibrium state? Can we predict the new dynamic equilibrium state and the time needed to reach it?

MATERIALS AND METHODS

Literature research

The literature search has been emphasized as it provides the model specification and parameterization. From the data collected over several periods, it is possible to identify morphological changes and processes. The impact of two interventions were investigated in this study, so the aim was to collect data before and after the two interventions. One of the two interventions is the braided system regulation in the 19th century and the building of wing dams in the first half of the 20th century. From the period of before the 19th-century regulation, not much substantial data is available. Still, literature research has provided with a very relevant data set: the Danube's longitudinal bed profile (Lanfranconi, 1882) which can be seen in Figure 4. It shows that the section did not follow a constant downward trend. However the upper section was characterized by a steeper slope, which decreased drastically as it reached the lower section. In accordance with previous papers (Holubová et al., 2004; Tőry, 1952), a slope break could be detected in this section under study, as shown in the longitudinal profiles. As additional data, we also found a longitudinal profile from 1910 (M. kir. áll. nyomda, 1910), 1949 (OVH, 1949), and 1970 (VITUKI, 1970).

The longitudinal profiles show that after the regulation in 19th century, the riverbed upstream Gönyű (rkm 1791.5) visibly deepens, while downstream Gönyű a considerable deposition process took place. Comparing the longitudinal profile from 1949 with the pre-regulation section (1882), it can be seen that there is less sedimentation upstream Gönyű (rkm 1791.5) and a gradually filling section downstream. What can also be observed are some significant local changes that an intervention, such as the installation of wing dams, could cause. The amount of sediment has always played an essential role in the ongoing river morphodynamics. The evolution of sediment transport can strongly influence the geometry of the riverbed.

Fig. 4. Row of wing dams at Nagybajcs, rkm 1801 (Google Maps, 2022[1])

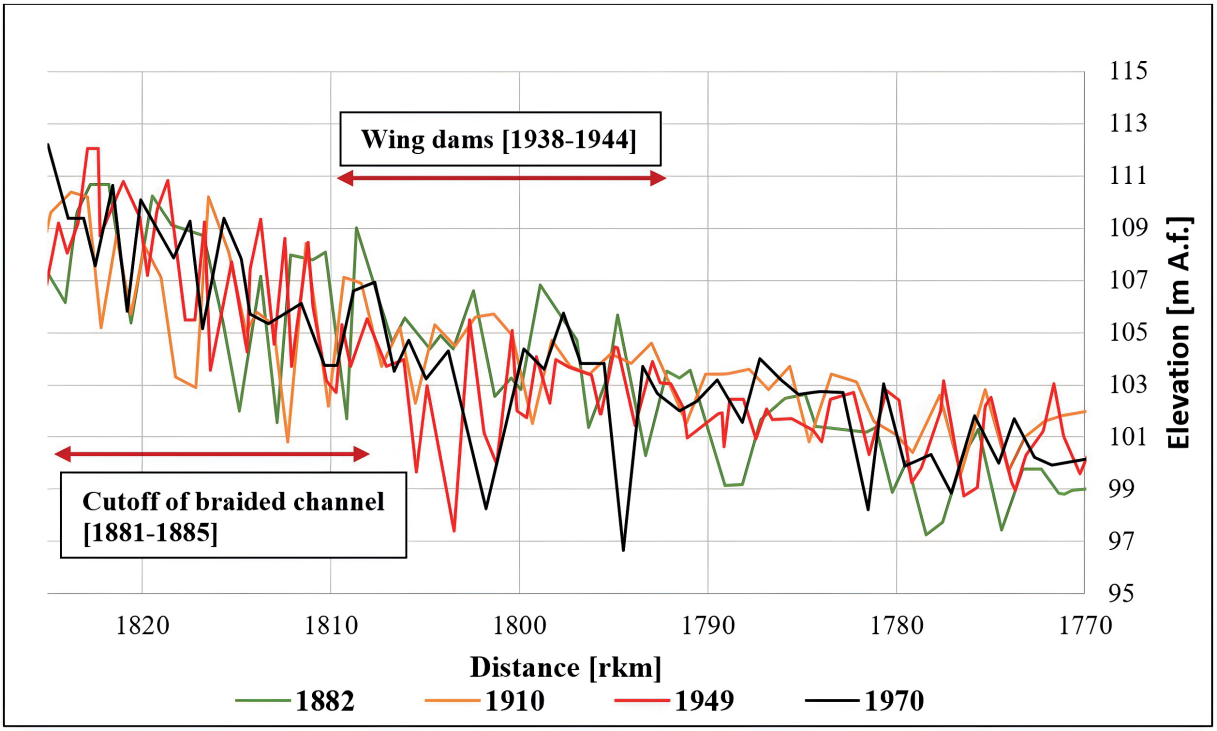

Fig. 5. A comparison chart of past longitudinal profiles

Based on the literature, we had sediment load data for two periods. Between 1952 and 1953, the yield at the Dunaremete (rkm 1825,5) section was 185400 t/year, while at Nagybajcs (rkm 1801), 22000 t/year, and at Dunaalmás (rkm 1752) 38850 t/year (OVF Hydrographic yearbooks 1886-1990[2], Pomázi and Baranya 2020). These data show that erosion is present between Dunaremete (rkm 1825) and Nagybajcs (rkm 1801), and the sediment load of Nagybajcs (rkm 1801) also shows that selective erosion may be the cause of the decline there, as pointed out by several studies (Tőry, 1952; Bogárdi, 1955). The second period is between 1966 and 1992. During this period, the sediment loads were 730607 t/year at Dunaremete (rkm 1825), 483873 t/year at Nagybajcs (rkm 1801) and 65000 t/year at Dunaalmás (rkm 1752) (OVF Hydrographic yearbooks 1886-1990). The later data show that erosion is still present, but not to the same extent as the older data illustrate. For the sediment, not only the sediment load was significant, but also the grain composition.

The section's grain size and sediment values are taken from the measurements made between 1952 and 1953. The average sediment grain size (D_{50}) was 18 mm at Dunaremete (rkm 1825), 7.5 mm at Nagbajcs (rkm 1801), and 0.245 mm at Dunaalmás (rkm 1752) (Bogárdi, 1955).

[1] https://www.google.hu/maps
[2] https://www.vizugy.hu/print.php?webdokumentumid=1524, 2022

The sections' average bed material (D_{sg}) size was 19 mm at Dunaremete (rkm 1825) and 13 mm at Nagybajcs (rkm 1801) (Bogárdi, 1955). The data shows the differences between individual sections. The distance between Dunaremete and Nagybajcs (rkm 1801) is only 25 km and the typical grain size in the Nagybajcs (rkm 1801) section is less than half of the Dunaremete (rkm 1825) value. The decreasing values also confirm the selective deposition within the section.

Another essential data point in our study is the grain composition curves. We aim to develop an inhomogeneous model that considers interactions between several fractions. With this kind of approach, selective erosion can also be investigated. In the section under study, this is a fundamental. The slope break upstream of Gönyű (rkm 1791.5) has a slope rate of 25-40 cm/km on the section and steeper and steeper sections towards Austria (Goda, 1995). Downstream of Gönyű (rkm 1791.5), the predominant slope is 8-10 cm/km or less (Tőry, 1952; Holubová et al. 2004, Rákóczi and Sass, 1995, Rákóczi, 1979).

Four parameters were used to test the model's accuracy. These data were from the contemporary riverbed level at Dunaremete (rkm 1825), the location of the slope break (Holubová, 2004; Tőry 1952), the bed slope upstream and downstream of the reach, and the average sediment diameter in the Dunaremete (rkm 1825) and Nagybajcs (rkm 1801) sections.

1D morphodynamic model setup

The 1D model performs the calculation steps for a whole section, establishing a link between adjacent sections. The approach and simplifications used in the model were based on the online notes of Professor Gary Parker (Parker, 2004[3]). In the model, we approximate the cross-section with a rectangular section and do not consider the floodplain, only the bankfull channel. Because of this approximation, the model takes into account the bankfull discharge. The bankfull discharge along with the intermittency are used to describe the equilibrium bankfull morphodynamic state. Intermittency is the time fraction that shows the morphodynamically active time fraction (Parker, 2004).

The model is based on a system of equations that give the equilibrium stage (Eke et al., 2014; Naito and Parker, 2019).

Continuity equation for a liquid:

$$Q_W = UHB \tag{1}$$

Q the flow discharge [m³/s], U the section average velocity [m/s], B width of the section [m] and H the water depth [m].

Momentum equation:

$$\left(\frac{\tau_b}{\rho}\right) = C_f U^2 = gHS \tag{2}$$

In the equation τ_b is the bed shear stress [N/m²], ρ is the density of water (1000 kg/m³), C_f is the dimensionless bed resistance, g is the acceleration of gravity (9,81 m/s²) and S is the bed slope [-].

The continuity equation for a sediment:

$$Q_b = Bq_b(R+1) \tag{3}$$

Q_b the sediment load [kg/s], q_b the specific sediment load [kg/sm] and R the underwater weight of the sediment.

1D model contexts

The hydrodynamic variables were estimated with the backwater equation:

$$\frac{\partial H}{\partial x} = \frac{S - C_f \dfrac{q_w^2}{gH^3}}{1 - \dfrac{q_w^2}{gH^3}} \tag{4}$$

In the equation, *Sf* is the fall of the energy line.

In the following equation, *Fr* denotes the Froude number, which is a dimensionless number and can be calculated as follows:

$$Fr = \frac{U}{\sqrt{gH}} \tag{5}$$

The dimensionless bed shear stress can be calculated using the following equation:

$$\tau^* = \frac{\tau_b}{\rho g R D} = \frac{HS}{RD} = \frac{C_f U^2}{RgD} \tag{6}$$

Based on the shears stress, the bedload transport formulas are able to estimate the sediment discharges. In the present 1D model, we applied the Wilcock and Crowe formula in order to consider the mixed sediment behavior, such as the selective erosion and bed armouring process. The grain composition is the moving layer and the active and inactive layers of the bed vary in grain composition. So, the transport between these three layers must always be calculated, and then the change in grain composition caused by these must also be modelled for each cell (Wilcock and Crowe, 2003).

The change in the bed elevation of a given cell was calculated from the difference between the sediment loads calculated for the cell of the preceding section and the cell of the following section, using the Exner equation.

$$\left(1 - \lambda_p\right) * \frac{\partial \eta}{\partial t} = \frac{\partial q_b}{\partial x} \tag{7}$$

Steps in the calculation of the Wilcock model:

1. Determination of the dimensionless bed shear stressfor the average grain size as a function of sand content
2. Determination of the reference bed shear stressfor the average grain size as a function of the dimensionless slip stress
3. determination of the reference bed shear stressof the i-th fraction as a function of the reference bed shear stressfor the average grain size and the diameter of the i-th fraction and the diameter of the average grain size
4. Calculation of the dimensionless sediment load of the i-th fraction from the ratio of the reference bottom-slip tension to the bottom-slip tension
5. Calculation of the sediment load per unit width of fraction i-th as a function of the dimensionless yield, fraction ratio and slip velocity
6. calculation of the concentration of the i-th fraction as a function of sediment load, water depth and water velocity

[1] http://hydrolab.illinois.edu/people/parkerg/morphodynamics_e-book.htm

Modell validation

For the model parameterisation, the reach averaged bankfull channel width before interventions were set based on an earlier 0D model-based study in 2020 (Dunaremete: ~600 m) (Nyiri, 2020).

The inlet section of the model was Dunaremete (rkm 1825). The bankfull discharge at Dunaremete is 4100m^3/s (OVF, 1886-1990). Since no data on bed material was available from the 19th century, we assumed that the bed composition didn't change significantly. Therefore, we set the grain size composition curves determined in 1954 as the initial boundary condition (VITUKI, 1954) . The outflow section was the Dunaalmás section (rkm 1752), in order to place the slope break at Gönyű (rkm 1791.5) in the middle of the domain. The grain composition at Dunaalmás (rkm 1752) was determined in a similar way to that at Dunaremete (rkm 1825). The outflow bed level was set at Dunaalmás (rkm 1752), i.e. 97.27 m.A.f (Lanfranconi, 1882). The initial longitudinal profile was calculated assuming a constant bed slope typical downstream of Gönyű (rkm 1791.5), which is ~ 9 cm/km (Tőry, 1952). The measured value of 1953-54 for the inflow sediment load was given, i.e. 185400 t/year (OVF, 1886-1990). After parameterization, the model was run until to get the best match with the real longitudinal profile from 1882, which took 600 years.

As shown in Figure 5, the break is well represented, and the model places it at about rkm 1792.9. Considering that the break is not exactly at Gönyű (rkm 1791.5), this is considered acceptable (Table 1).

The calculated bed elevation at the inlet section is 110.69 m.A.f., while the recorded value is 110.61 m.A.f. (Lanfranconi, 1882), so the model decimetre accurately reproduced the initial level. Regarding the values of the bed slope, the literature defines the slope upstream of Gönyű (rkm 1791.5) as 25-35 cm/km (Tőry, 1952), while the model gave this as 30 cm/km, which slopes within the range of the recorded. Downstream of the slope break, the literature specifies 8-9 cm/km (Tőry, 1952), while the model gave a slope of 8 cm/km (Table 1).

To validate the model, we also considered the calculated average grain sizes of the model, which are shown in Figure 6.

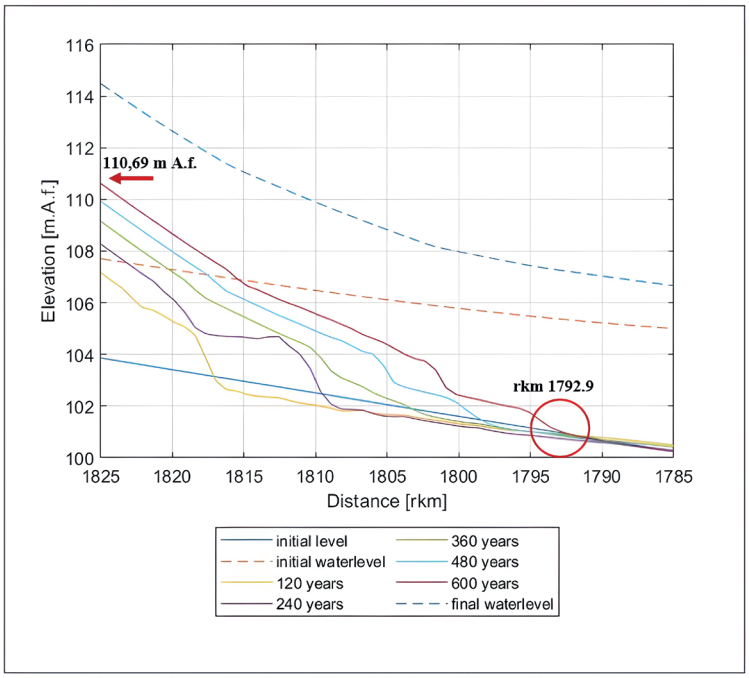

Fig. 6. Calculated longitudinal bed profiles

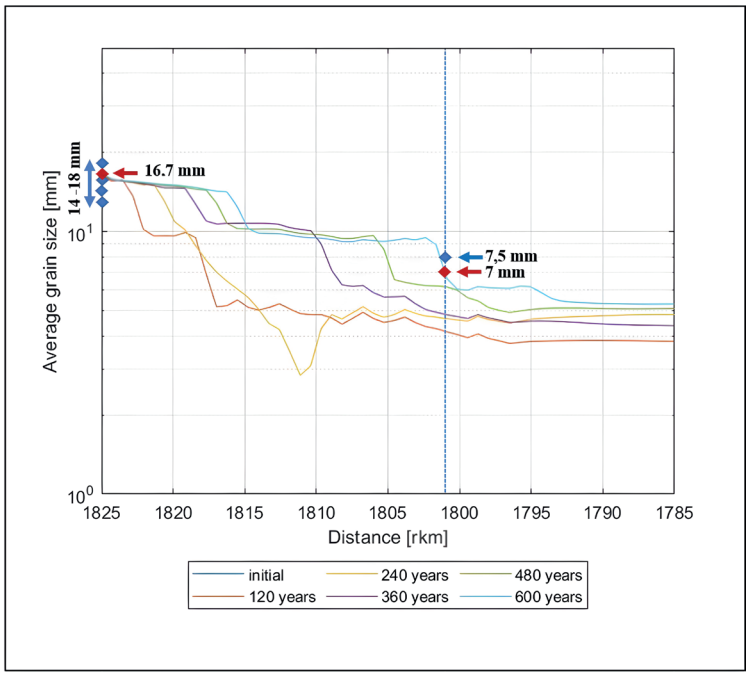

Fig. 7. Change in average grain size

Based on Figure 6, the model calculates 16.7 mm average bed material grain size in the initial section at Dunaremete (rkm 1825), which according to the literature was between 14-18 mm (Bogárdi, 1955; Tőry, 1952), so the model result is considered to be correct. For Nagybajcs (rkm 1801), the model's grain diameter is at 7 mm, which is also very close to the 7.5 mm found in the literature (Bogárdi, 1955).

Implementation of the interventions

Regulation of the braided river system

Prior to the regulation, the Upper Hungarian Danube was braided, and the aim of the regulation was to create a main riverbed that would provide better navigation conditions and improved flood protection. Figure 1 shows the braided character of the studied reach. The artificial cutoffs of the meanders have also shortened the length of the river and thus increased the slope.

The artificial cutoffs were implemented by the fact that the length of the river shortened, so the model accounted for this by reducing Δx cell size by a reduction factor, which was 0.9 (Tőry, 1952).

In addition, the width of the newly created main channel was known from the records. For the 19th century intervention plans, data were available on the extent to which certain sections were narrowed (Tőry, 1952). For the Dunaremete (rkm 1825) section, a planned width of 420 m was used, of which a 325 m channel width was achieved (Tőry, 1952). The model used a width of 325 m on this base.

Installation of the rows of wing dams in the model

The descriptions show that two sets of consecutive row of wing dams were built on the section under study between 1938 and 1944 (Tőry, 1952), one on the section between rkm 1807-1805 and the other on the Nagybajcs-Vének section (rkm 1802-1793). These two rows were included in the model as one continuous wing dam line, because between the two, gravel bars were formed, which narrowed the bed to a similar extent as the wing dams. For this reason, the entire section (rkm 1807-1793) had the same narrowed bed width, that is, it could be considered as a continuous section. The morphodynamic effects of wing dams were implemented in the model with additional equations, which we took from a foreign paper (Török & Parker, 2022). The core of the procedure is that the cross-section are considered to be divided by the wing dams into two parts: one of which will be the narrowed main channel and the other is the wing dam field. However, the hydraulic parameters of the two channels are not identical. The paper recommends using the following two equations to calculate the flow in the two channels. The Bernoulli equation is valid in the following form:

$$\frac{U_m^2}{2g} + z_{ws,m} = \frac{U_{wd}^2}{2g} + z_{ws,wd} \quad (8)$$

Moreover, the continuity equation also hold.

$$Q_{total} = Q_m + Q_{wd} = U_m H_m B_m + U_{wd} H_{wd} B_{wd} \quad (9)$$

By supplementing the original equations with these equations, the system of equations to be solved becomes definite, i.e. the 1D flow pattern in the narrowed main channel can be calculated for each cross-section

MODEL RESULTS

Regulation of the braided river system

Figure 7. shows longitudinal bed profiles from the time of the natural state (solid light blue line) and from the period after the artificial meander cutoffs (but before the wing dam installation). The calculation started from 1880, because that is when the cutoff work started and ended in 1910 for which there was a recorded longitudinal profile dataset. The model results show that the intervention caused about 2.5m bed incision within the affected section (rkm ~1810), while there was a significant, almost 1m rise in the bed level in the downstream of the interventions (downstream of rkm ~1810).

The difference between the calculated and measured bed levels, as well as their average for the section, were also calculated, which can be seen in Figure 8.

As shown in Figure 8, the period 1880-1910 shows a bed level decrease of 1 m on average. The average erosion was also calculated from the model results, resulting in a 1.13 m decrease. The difference between the records and the model results is 13cm, Which indicates the accuracy of the model.

Figure 9 shows the average size of the bed material. It can be seen that initially the average grain size decreased, that is, the bed became finer (orange line). This may be because the bed armor that had formed earlier was broke up as a result of the narrowing (Rákóczi, 2000). Later, however, the bed material became coarser, and eventually returned close to its original dimensions, meaning that the bed armor could develop again (continuous light blue line).

The breakup of the bed armor resulted in the deposition of a large amount of sediment on the downstream. Presumably, this deposition caused the increase of the water levels in the examined section (dashed lines in Figure 7). This flood protection risk caused the plan of wing dam installation in the section where significant sediment deposition took place.

Table 1. Summary table of validation

	Measured data	Calculated data
Dunaremete bed level	110.69 m.A. f	110.61 m.A. f
Location of the slope break	~rkm 1791.5 [Gönyű]	rkm 1792.1
Slope above the break	~25 cm/km – 35 cm/km	30 cm/km
Slope below the break	~ 8 cm/km – 9 cm/km	8 cm/km
Dunaremete average grain size	18 mm – 14 mm	16.7 mm
Nagybajcs average grain size	7.5 mm	7 mm

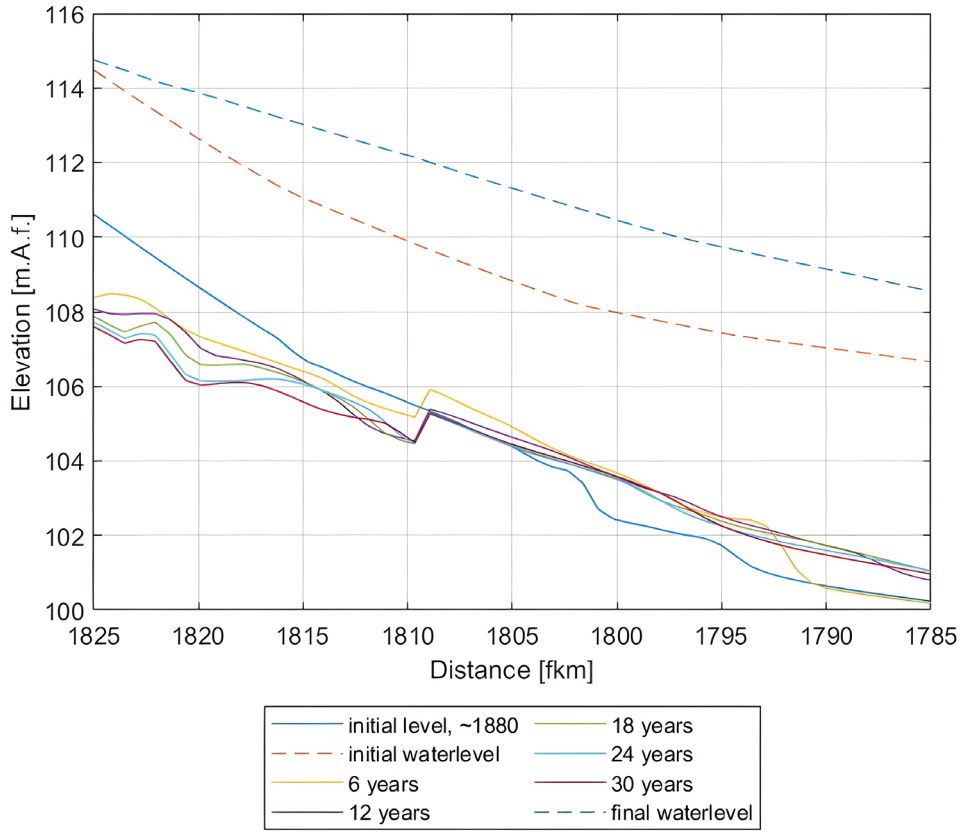

Fig. 8. Calculated longitudinal bed profiles– artificial cutoffs

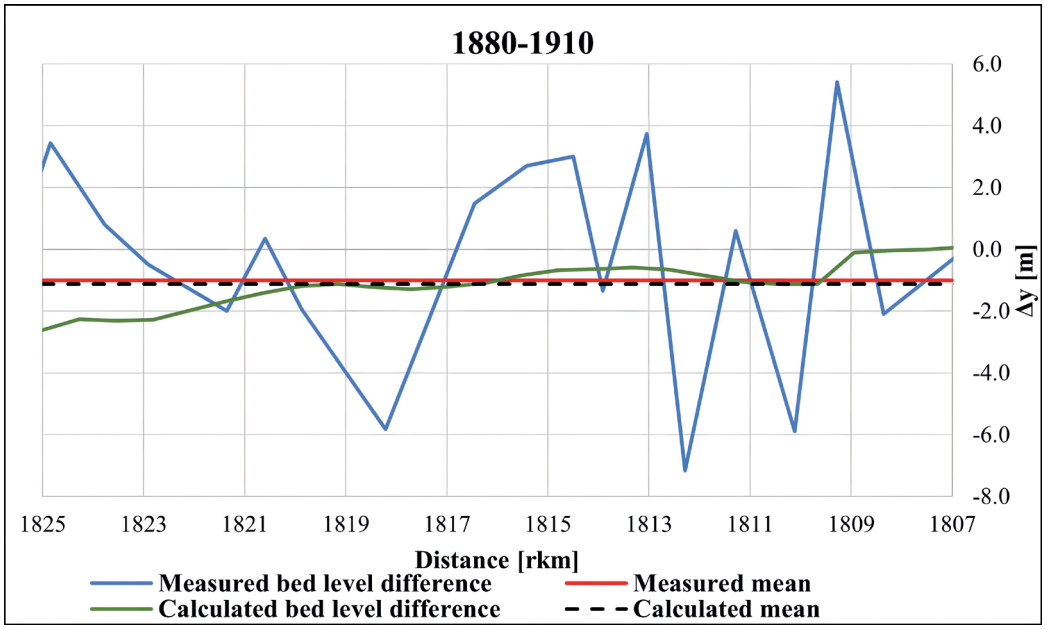

Fig. 9. Comparison of bed level differences – artificial cutoffs

Installation of the wing dam line in the model

The impact assessment of the wing dams was carried out for the following period. The model test was started from 1938, when the wing dams were actually installed on the section and was run until 1949 for which there was recorded longitudinal profile dataset. The result of the model run is shown in Figure 10.

The 1949 status is marked in red. It can be seen that with the construction of the wing dams, the riverbed is beginning to erode, which is one of the expected effects from wing dams. The model shows an average bed incision of about ~90 cm on average for the wing dam section after 10 years. Figure 11 shows the recorded bed changes along the investigated section.

As can be seen in Figure 11, the value of the average bed change is shown by the orange line, which shows an erosion of nearly 1.5 m. The value of the average bed change is shown by the orange line, which shows an erosion of nearly 1.5 m. Based on the topography (Figure 11), it can be seen that there are wing dams on both sides of the river in two places, which caused drastic local depressions (Nyiri et al. 2023). This also significantly affects the average bed erosion value. However, the model cannot take this local effect into account. For this reason, we ignored the two local erosion effects when compiling the results. The lines for the measured values in Figure 12 have already been constructed in this way.

Figure 12 shows that the average erosion rate of the riverbed in this section was 89cm, whereas the model

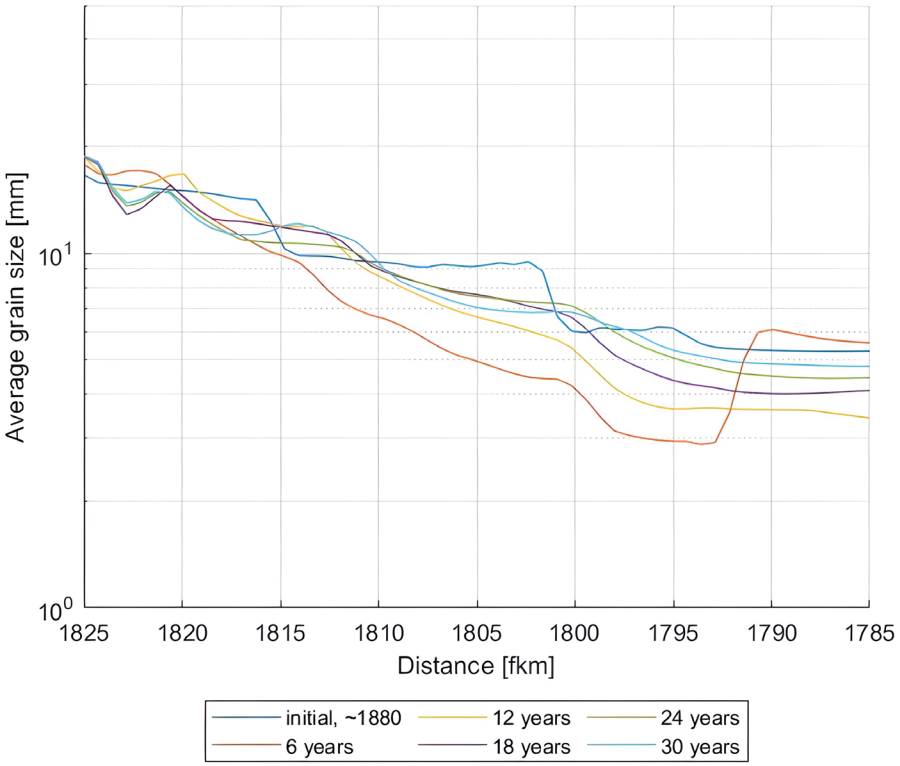

Fig. 10. Change in average grain diameter– artificial cutoffs

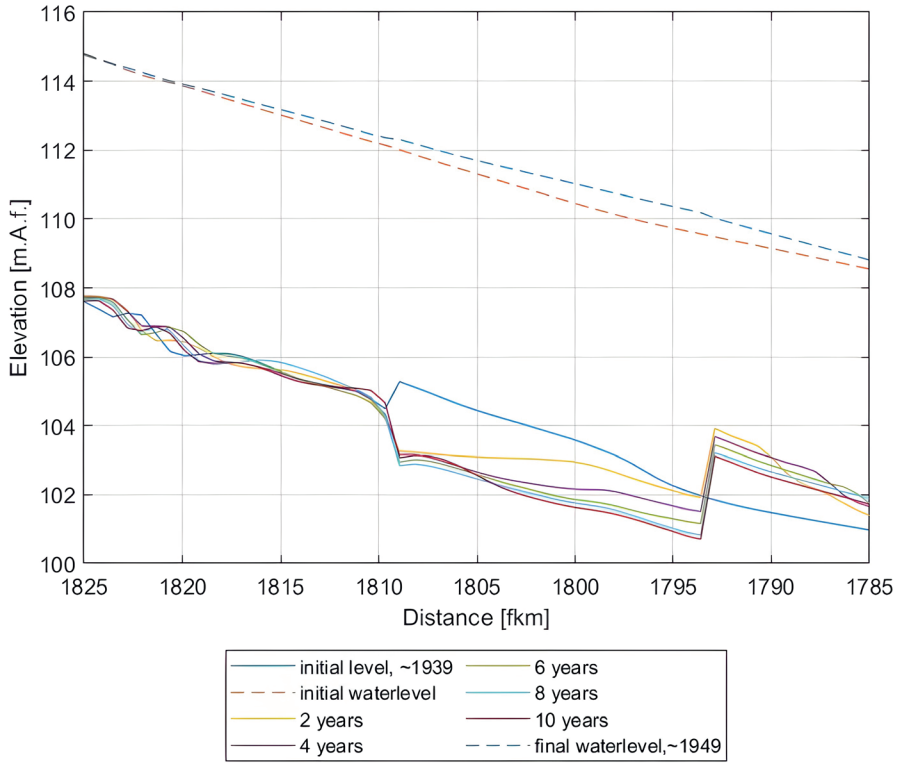

Fig. 11. Calculated longitudinal bed profiles– wing dam installation

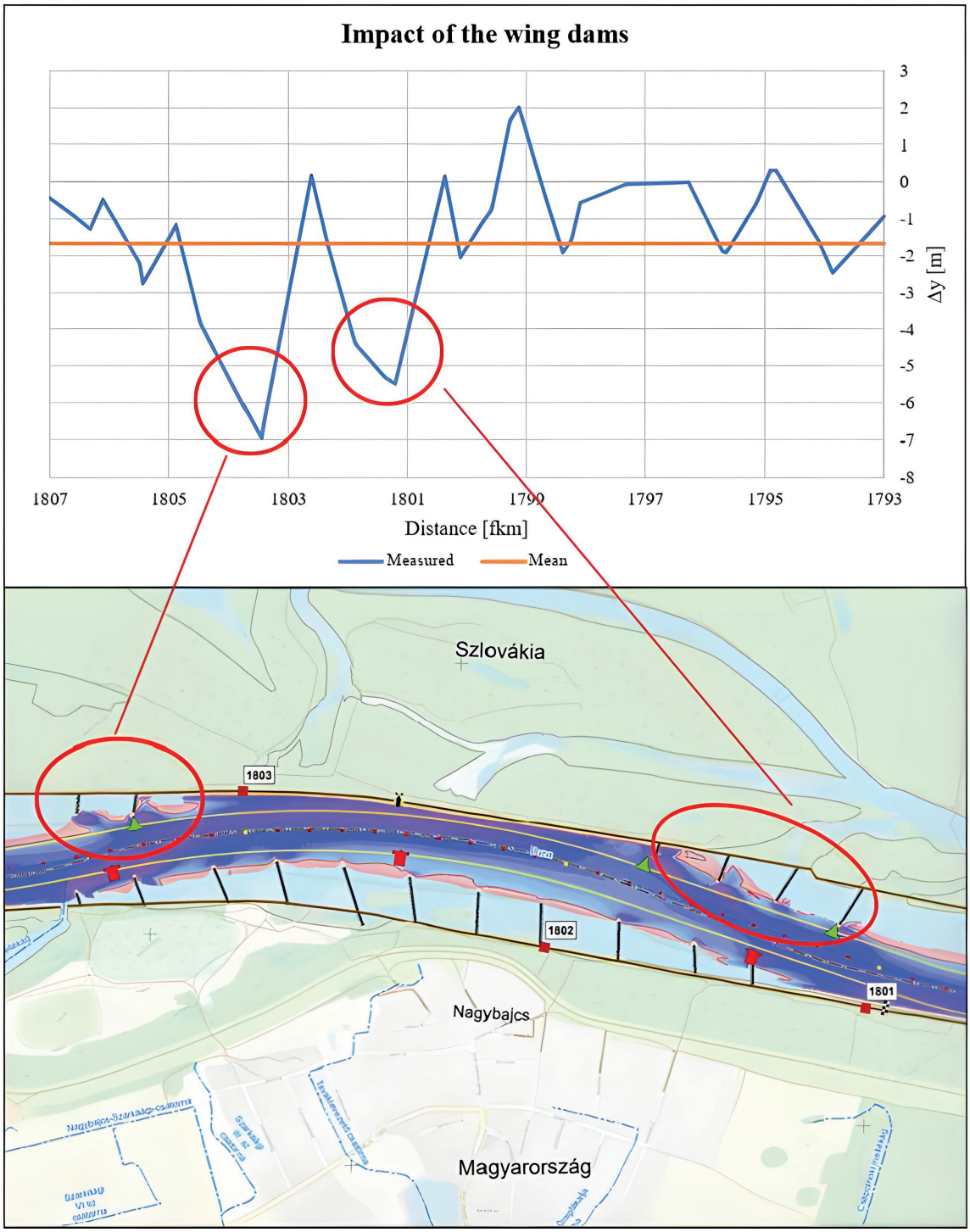

Fig. 12. Changes in bed level at the wing dam between 1938 and 1949 (ÉDUVIZIG, 2022)

resulted in 92cm. This means that there is only a difference of 3cm between the average values of the model and the recorded changes.

Figure 13 shows the change in the bed material. It can be seen that the bed material became significantly coarser in the section affected by the intervention, which indicates the development of the bed armor.

DISCUSSION

River control intervention with wing dams is a fairly common methodology. Finding examples of it all over the world, as a result of which the exploration of the morphodynamic reaction is an important research question. The most widespread methodology for the investigation is based on the statistical analysis of the measured parameters (bed level and water level). On this basis, it was shown, for example, in the case of the Mississippi, Missouri and Rhine rivers (Pinter et al. 2006), that the bed level clearly decreased due to the wing dams. The one we examined showed the same trend. In general, therefore, it is expected that the bed level will decrease. However, from the point of view of the examination of water levels, the expected trend is not so clear. In the case of the Mississippi and Missouri, the trend clearly showed rising water levels, at least in a couple of decades after installation (Pinter and Heine 2004). It has not yet been investigated how long this trend can be expected, or whether it may be followed by a downward trend. In the case of the Rhine River, however, no water level rise was observed. Although in our study we treated the results with reservations regarding the water levels, since they were not validated, we experienced an increasing trend.

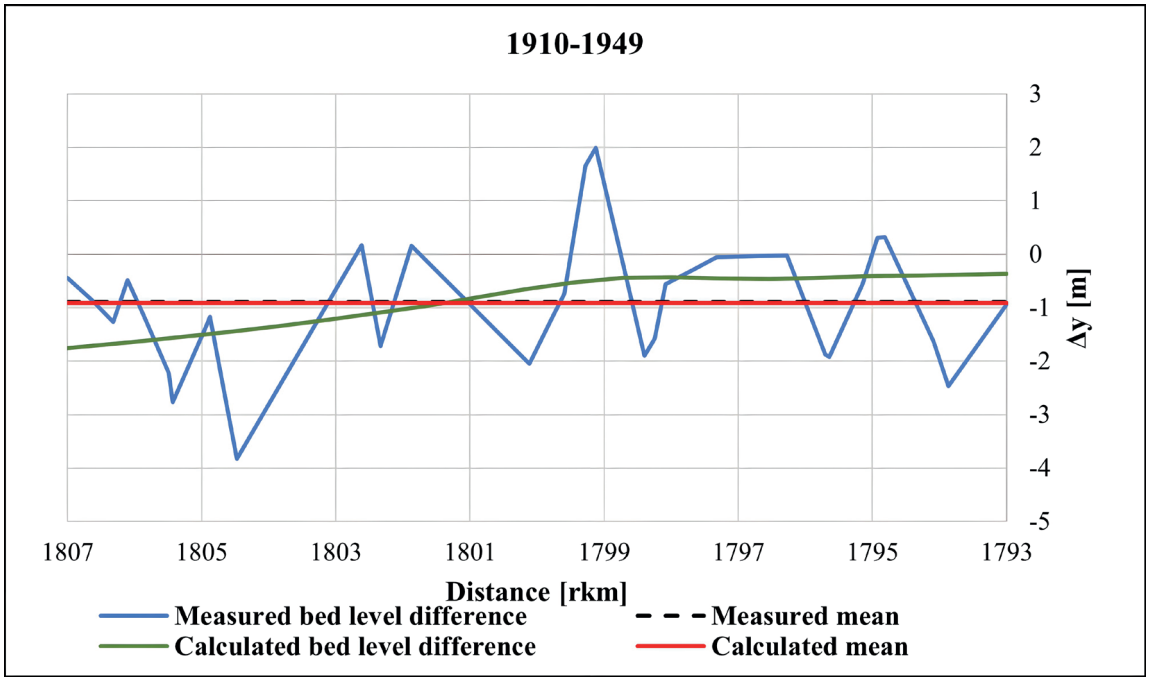

Fig. 13. Comparison of bed level differences – wing dam installation

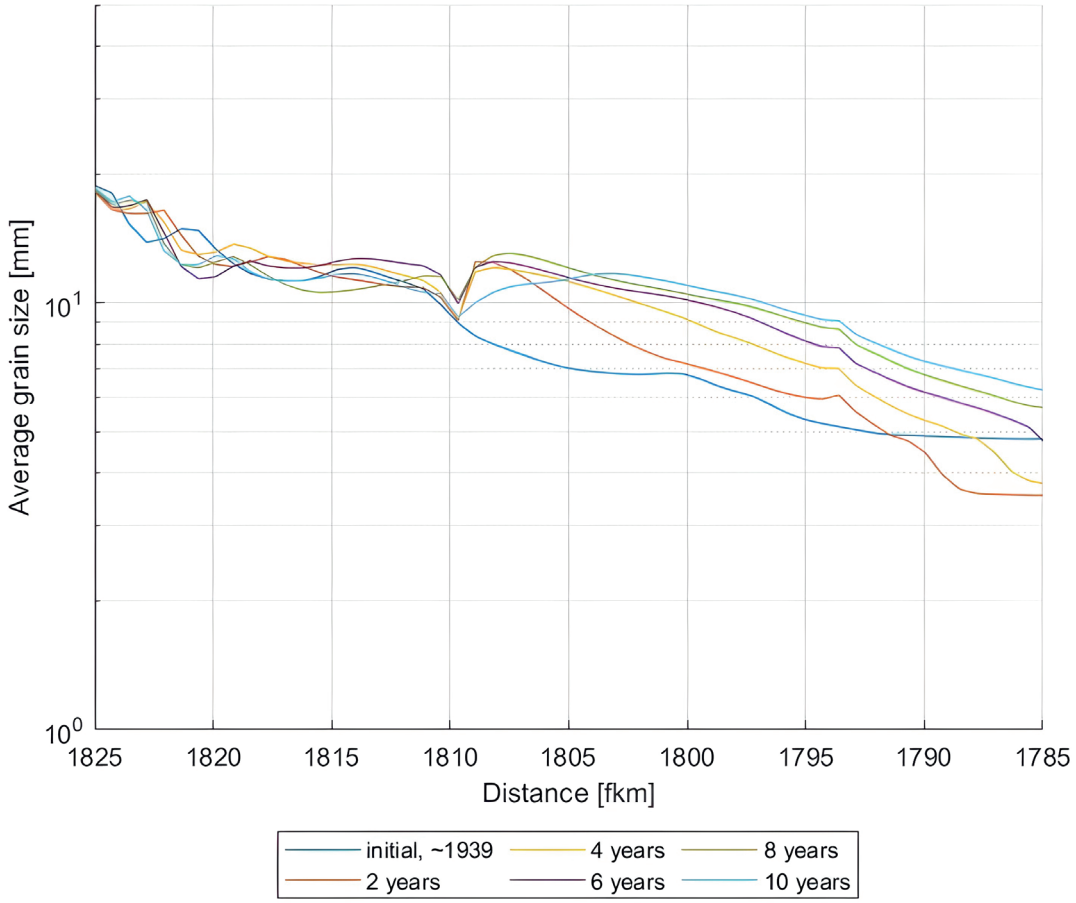

Fig. 14. Evolution of grain sizes

1D morphodynamic model presented in this study provides an opportunity for sensitivity tests and thus an investigation method to reveal the effects that cause water level changes can be revealed. That is, statistical analysis of measured water levels and a 1D morphodynamic model complement each other very well, even in studies of this kind.

CONCLUSIONS

Through the example of the Upper Hungarian Danube, we saw that there is a huge need for tools that can demonstrate the large spatial and temporal morphodynamic effects of artificial river control works, but there is no available means for this. Especially not for cases where the riverbed with a mixed grain composition

can have such a complicated morphodynamic processes (bed armoring, selective erosion and deposition) that simpler sediment transport models cannot even be taken into account. For this reason, our goal was to develop and validate a tool capable of calculating the morphodynamic effects of various artificial river control interventions on a large spatial and temporal scale in the case of rivers with a mixed grain composition.

In our study, we investigated the morphodynamics of a selected section of the Upper Hungarian Danube, focusing on the effect of artificial interventions. The inlet section of the studied reach is Dunaremete (rkm 1825) and the outflow section is Dunaalmás (rkm 1752), with a longitudinal slope break located between these two sections in the vicinity of Gönyű (rkm ~1790). The development to a model which is able to take into account inhomogeneous bed material and bedload was crucial as bed armoring and selective erosion play an important role in forming the bed, including the sudden break in longitudinal profile (Holubová et al., 2015; Liedermann, 2017; Baranya et al., 2008). To gain this experience, we applied the sediment transport model developed by Wilcock and Crowe (2003) for mixed grain composition. A detailed literature search was carried out to be able to validate and calibrate our 1D model. The aim was to assess the impact of interventions with the model. Since the first intervention was river regulation in the late 19th century, it was necessary to have a pre-river regulation state. This state was estimated with the model in such a way that the results showed a good agreement with the location of the break in the longitudinal profile, the value of the upstream and downstream slope and the composition of the bed material. Based on these, on the one hand, the model was validated for the state before the interventions, and on the other hand, this is how we prepared the initial conditions for further model studies.

The first model study was the investigation of the artificial meander cut-offs in the 19th century. The intervention not only changed the bed geometry, but also the sediment transport, not to mention the shortening of the river. The model test showed that the average bed level decrease calculated from the literature was estimated quite well by the model, with only a 13 cm difference between the two average values. The nature of the phenomenon itself was well captured by the model. That is, the intervention caused an important bed level rise in the downstream sections, which eventually resulted in water level rise. Presumably, this triggered the second intervention on the deposited section.

In a second study, a wing dam row from Medve (1807 rkm) to almost Gönyű (1791.5 rkm) was fitted to the existing model. The effects of wing dams were taken into account using a procedure in which the narrowing of the main channel and the distribution of the flow discharge between the main channel and the wing dam field are considered. Based on the comparison of the modelled and measured bed changes, we concluded that the 1D model can reliably predict expected bed changes and changes in the bed material. For example, it can be seen that the bed material on the bottom of the spurs has been significantly refined.

The model tests showed that the presented 1D model is able to reliably assess the impact of the interventions. Keeping in mind the limitations of 1D modelling, we have presented a procedure that can complement the studies based on higher dimensional models. The presented tests exemplify that the 1D model can be a good alternative for the investigation of morphological processes of several decades or even centuries taking place in a river section of up to a few hundreds of kilometers. A higher-dimensional model is still necessary to examine local morphological features, for which the presented 1D model can provide good initial and boundary conditions, even in the case of a bed with a mixed grain composition.

Characterizing the conditions before river regulation, which was typically carried out at least a century ago in the case of large navigable rivers (e.g., Mississippi River), is a big challenge. In the case of such questions, the presented 1D morphological model-based study can play a major role.

The model can also help improve the design of future interventions.

REFERENCES

E. Eke, G. Parker, Y. Shimizu: Numerical modeling of erosional and depositional bank processes in migrating river bends with self–formed width: Morphodynamics of bar push and bank pull, Journal of Geophysical Research: Earth Surface 119 (7), 1455-1483.

E. Lanfranconconi: Magyarország ármentesítése, 1882

. E. Nyiri: Folyók dinamikus egyensúlyi állapotát becslő eljárás kidolgozása és alkalmazása a magyarországi Felső-Dunán, BME-ÉMK TDK, Budapest, 2020.

E. Nyiri, G. T. Török and S. Baranya Impact assessment of river regulations of the past century using 1D morphodynamic modeling on the Upper Hungarian Danube. GEOPHYSICAL RESEARCH ABSTRACTS: EGU GENERAL ASSEMBLY 2023

ÉDUVIZIG: A Duna 2022-2023 évi hajóút-kitűzési terve az 1811-1708 folyamkilométerek közötti szakaszon, 2022

Fischer-Antze, T., N. R. B. Olsen, and D. Gutknecht (2008), Three-dimensional CFD modeling of morphological bed changes in the Danube River, Water Resour. Res., 44, W09422, doi:10.1029/2007WR006402.

F. Pomázi, S. Baranya: Acoustic based assessment of cross-sectional concentration inhomogeneity at a suspended sediment monitoring station in a large river. Acta Geophys 70(5), 2361-2377, 2022

F. Pomázi, S. Baranya Comparative assessment of fluvial suspended sediment concentration analysis methods. Water 12(3):873, 2020

G. Parker: 1D Sediment Transport Morphodynamics with applications To Rivers and Turbidity Currents, e-book, 2004.

G. Parker, C. An, M. P. Lamb, M. H. Garcia, E. H. Dingle and J. G. Venditti: Dimensionless argument: a narrow grain size range near 2 mm plays a special role in river sediment transport and morphodynamics, 2024.

G. T. Török: Vegyes szemösszetételű folyómeder morfodinamikájának numerikus vizsgálata, BME- ÉMK TDK, Budapest, 2011.

G.T. Török, G. Parker: Significance of Time Dependence in The Effect of Wing Dams on Water Levels, 2022

Google Maps, online aerial view, Google, 2022

J. Bogárdi: A hordalékmozgás elmélete. Budapest, Hungary: Akadémiai Kiadó, 1955

K. Farkas-Iványi, A. Trájer: The influence of the river regulations on the aquatic habitats in river Danube, at the bodak branch-system, Hungary and Slovakia, Budapest, 2015

K. Holubová, M. Comaj, M. Lukác, K. Mravcová, Z. Capeková, and M. Antalová: Final report in DuRe Flood project - 'Danube Floodplain Rehabilitation to Improve Flood Protection and Enhance the Ecological Values of the River in the Stretch between Sap and Szob, Bratislava, 2015.

K. Holubová, Z. Capeková, and J. Szolgay: Impact of hydropower schemes at bedload regime and channel morphology of the Danube River, in River Flow 2004: Proceedings of the Second International Conference on Fluvial Hydraulics, 2004, no. 1, pp. 135–142.

K. Naito and G. Parker: Can Bankfull Discharge and Bankfull ChannelCharacteristics of an Alluvial MeanderingRiver be Cospecified From a FlowDuration Curve?, Journal of Geophysical Research: Earth Surface 124 (10), 2381-2401.

K. Tőry: A Duna és szabályozása, Budapest, Hungary: Akadémiai Kiadó, 1952.

L. Goda: A Duna gázlói Pozsony-Mohács között, Vízügyi Közlemények, LXXVII. évf., 1995 évi. 1.füzet, Budapest, 1995

L. Rákóczi: Mederanyag-minták információtartalma és hasznosítása a folyószabályozásban. MIIT országos vándorgyűlése, Keszthely, 1979.

L. Rákócz: A Duna hordalékjárása, Vízügyi Közlemények LXXV. évfolyam/2, 1993

L. Rákóczi and J. Sass: A Felső-Duna és a szigetközi mellékágak mederalakulása a dunacsúnyi duzzasztómű üzembe helyezése után; Vízügyi Közlemények, LXXVII. évf., 1995 évi 1.füzet, Budapest, 1995

L. Rákóczi: A Duna-meder sorsa Szap és Szob között, Vízügyi Közlemények, LXXXII. évf., 2000 évi. 2.füzet, Budapest, 2000

M.kir. Állami nyomda: Duna hossz-szelvénye Dévény-Budapest között 3321/910, 1910

M. Liedermann, P. Gmeiner, A. Kreisler, M. Tritthart, and H. Habersack: Insights into bedload transport processes of a large regulated gravel-bed river, Earth Surf. Process. Landforms 43(2), 2017.

M. Wong and G. Parker: Reanalysis and Correction of Bed-Load Relation of MeyerPeter and Müller Using Their Own Database, Journal of Hydraulic Engineering 132(11), 2006.

N. Pinter, B. S. Ickes, J. h. Wlosinski, R. R. van der Ploeg: Trends in flood stages: Contrasting results from the Mississippi and Rhine River systems, 2006

N. Pinter, R. A. Heine: Hydrodynamic and morphodynamic response to river engineering documented by fixed-discharge analysis,Lower Missouri River, USA, 2004

Országos Vízügyi Főigazgatóság, Vízrajzi Évkönyvek. Budapest, 1886-1190 S. Baranya and J. Józsa: Flow analysis in river danube by field measurement and 3d cfd turbulence modelling, Budapest, 2006

S. Baranya, L. Goda, J. Józsa and L. Rákóczi: Complex hydro- and sediment dynamics survey of two critical reaches on the Hungarian part of river Danube, Budapest, 2008

VITUKI Tanulmánytár XXVI. 5/b (77-78), 1954 51

Wilcock, P. R., and Crowe, J. C., Surface-based transport model for mixed-size sediment, Journal of Hydraulic Engineering, 129(2), 120-128., 2003

Check for updates

CC BY

RESEARCH PAPER

WATER QUALITY MONITORING USING MODELING OF SUSPENDED SEDIMENT ESTIMATION (A CASE STUDY: SEFIDROUD RIVER IN NORTHERN IRAN)

Mohammad Reza Salami[1], Ebrahim Fataei[*1], Fatemeh Nasehi[1], Behnam Khanizadeh[2], Hossein Saadati[1]

[1] Department of Environmental Sciences and Engineering,Ardabil Branch, Islamic Azad University, Ardabil, Iran

[2] Department of Chemistry, Sarab Branch, Islamic Azad University, Sarab, Iran

***Corresponding author:** Ebrahim Fataei, **Email:** eb.fataei@iau.ac.ir; eafataei@gmail.com

Received: October 28th 2024 / Accepted: November 22nd 2024 / Published: October 1st 2024

https://doi.org/10.24057/2071-9388-2024-3511

ABSTRACT. The Sefidroud River, the second largest river in Iran, is located in the north. Since the operation of the Sefidroud (Manjil) dam on the said river, about half of the storage volume of the dam has decreased as a result of the accumulation of sediments. The present research, using 516 suspended sediment data from four regional sediment monitoring stations, was conducted between 2013 and 2020 to check the accuracy of single-linear, bi-linear and middle-class sediment rating curves (SRCs) of four sediment monitoring stations as well as Landsat 8 images to estimate suspended sediment concentration (SSC). After drawing the SRCs based on 46 satellite images and SSC data, 70% of samples were used to prepare the regression models of spectral data versus suspended sediment discharge (Qs) and 30% of samples to evaluate the accuracy of SRC and Landsat 8 data. According to results, the middle-class SRCs had the highest coefficient of determination (R^2, exponential). Four band ratios B4/B3, B4/B2, B6/B5 and B7/B5 had exponential and power correlation with Qs, with the highest value for the band ratio B4/B3 (R^2 = 0.74, exponential). To conclude, the results of the current research showed that the B4/B3 band ratio was more efficient for Qs estimation.

KEYWORDS: Water pollution, suspended sediment discharge, Satellite Spectral Data ,Landsat 8

CITATION: Salami M. R., Fataei E., Nasehi F., Khanizadeh B., Saadati H. (2024). Water Quality monitoring Using Modeling of Suspended Sediment Estimation (A Case Study: Sefidroud River in Northern Iran). Geography, Environment, Sustainability, 4(17), 101-111

https://doi.org/10.24057/2071-9388-2024-3511

ACKNOWLEDGMENTS: This research is extracted from the dissertation of the Ph.D student (Mr. Mohammad Reza Salami) in Environmental Engineering and Science, Islamic Azad University of Ardabil Branch. Therefore, the authors appreciate the esteemed president, educational and research deputies of Ardabil Islamic Azad University for their cooperation in facilitating the implementation of this project.

Conflict of interests: The authors reported no potential conflict of interest.

INTRODUCTION

The water crisis, such as water scarcity, water pollution and other water-related issues, has been ranked fifth among the world's top 10 risks according to the Global Risk Report 2020 (Yang et al. 2022). Recent centuries have increasingly experienced various erosions and corresponding effects on surface water and soil at the local, national, continental and international policy levels. As a result, many studies have focused on soil erosion process, sediment dynamics, sediment assessment, reservoir sediment and environmental aspects of suspended sediment transport and subsequently special measures to reduce soil erosion (De Girolamo et al. 2015). Sediment transport and sedimentation lead to consequences such as the formation of sediment islands in the river course and as a result reducing the flood flow transfer capacity, reducing the lifespan of dams and storage capacity of reservoirs, corrosion of river structures and damage to water structures and fields, and sedimentation in the canal. The sediment load in rivers is mainly composed of suspended sediment load (SSL) and sediment bed load (SBL). The SSL consists of suspended particles transported due to river turbulence, and the SBL contains coarser particles that flow on the river bed. Suspended sediment concentration (SSC) is one of the main factors of disrupting the natural flow of water (Efthimiou 2019). Spatial and temporal changes of SSC are related to anthropogenic and natural factors (Sa'ad et al. 2021), so that population growth along with climate change leads to overexploitation of land, thus affecting the quantity and quality of water in dam reservoirs (Mazhar et al. 2022). The annual reduction in the storage capacity of dams in the world following the sedimentation is approximately 0.5 to 1% of the reservoir volume, which is more than 4 to 5% for many dams; therefore, most dams lose the main part of their water storage capacity within 25 to 30 years (Verstraeten et al. 2003). Suspended sediments are continuously transported and accumulated in a river system, thereby affecting river morphology and biological services (Martinez and Cox 2023; Jangjoo 2021). About 20 billion tons of suspended sediments enter the oceans annually because of erosion and transport of sediments in

river systems (Abbasi et al. 2021; Dos Santos et al. 2018). In general, suspended sediment accounts for 70-90% of the total annual river sediment (Pavanelli & Cavazza 2010; Regüés & Nadal-Romero 2013; Khan et al. 2021). In addition, suspended sediments, especially fine particles, are considered as physical pollutants due to the transport of chemicals (Safizadeh et al. 2021; Aires et al. 2022; Khoram Nejadian et al. 2023). Several studies reported a close relationship between SSC and heavy substances such as nitrate and phosphate (Endreny & Hassett 2005; Edwards and Withers 2008; Horowitz 2008; Cao et al. 2011; Wang et al. 2015).

In recent years, two methods of water sampling and the use of satellite spectrum have been employed to monitor the SSCs (Sa'ad et al. 2021). Water sampling is both time-consuming and more expensive (Sa'ad et al. 2021). In fact, the use of these conventional methods for water quality monitoring is challenging due to limited resources in terms of capital and available labor, especially in developing countries (Adjovu et al. 2023). On the other hand, SSC is very different in terms of time and space (Du et al. 2021), so that this natural heterogeneity makes it difficult to obtain a synoptic view of suspended sediments through in situ SSC sampling (Lei et al. 2021). Therefore, in recent years, indirect techniques, especially those that use satellite images, have become popular to investigate SSC in large rivers. These methods, which have been tested since early in the 21st century, are more cost- and time-effective (dos Santos et al. 2018). Sa'ad et al. (2021) in the east coast of Malaysia, by examining the statistical correlation of total suspended sediment (TSS) with Landsat 8 bands, concluded that TSS had a correlation coefficient (R^2) of 0.79 with the green, near-infrared (NIR), and short-wavelength (SWIR) bands. Jally et al. (2021) investigated the correlation of Landsat-8 Operational Land Imager (OLI) satellite data and SSC in Chilika Lake in eastern India and found that the multiband linear regression model ($R^2 = 0.6$) could explain SSC changes better than the single-band regression model ($R^2 = 0.39$). Cremon et al. (2020) used Top-of-Atmosphere (ToA) and Landsat 5 surface reflectance data in the Araguaia River in west-central Brazil, and showed that multiple regression models with ToA reflectance using VNIR bands, band ratios, SWIR band 5 could better explain SSC changes (adjusted $R^2 = 0.87$, normalized root mean square error (NRMSE) = 10.09%) compared to the models with surface reflectance (adjusted $R^2 = 0.6$, NRMSE = 15.43%). Wen et al. (2022) investigated the total suspended matter (TSM) of Chinese lakes using Landsat data and showed that the red band had a correlation with TSM ($R^2 = 0.76$). Aires et al. (2022) used the spectral data of Landsat 8 and Sentinel-2 satellites, and found a strong regression relationship between the NIR band of both satellites and surface sediment concentration. Martinez and Cox (2023) investigated SSC in the Middle-Mississippi and Lower-Missouri rivers in the United States using Landsat 8, 7, and 5 data, and reported that the R^2 value of the developed regression model was 0.72, 0.71 and 0.75 for the spectral reflectance of the mentioned satellites, respectively.

In addition to using single bands and band ratios for SSC monitoring, previous studies used satellite indices such as normalized difference water index (NDWI), normalized difference turbidity index (NDTI) and TSM to monitor water quality (Toming et al. 2017; Zhu et al. 2020; Meena et al. 2021; Das et al. 2021; Mazhar et al. 2022; Adjovu et al. 2023). Despite the fact that the majority of the aforementioned studies reported a high correlation coefficient for the regression models used, the efficiency of these regression models and their preference to SRCs are challenging and controversial. For this reason, in the present study, the effectiveness of Sediment rating curves (SRCs) and satellite spectral information to estimate of suspended sediment concentration (SSC). In an innovative approach at the same time and in a single location was analyzed and investigated. Accordingly, the present study aimed to estimate SSC in Sefidroud river in northern Iran using SRCs and satellite images and to validate the efficiency of the regression models of both methods using real field samples measured.

MATERIALS AND METHODS

Study area

The Sefidroud watershed is one of the largest watersheds in Iran and a subset of the Caspian Sea watershed, about 73% of which is located in the mountainous areas of the Alborz and Zagros mountain ranges and the rest in the plains and foothills (Othman et al. 2013). The area of this basin is 59,217 km^2 and its main river is Sefidroud (Ghaffari et al. 2022). As the second largest river in Iran, Sefidroud is formed by joining the Shahrood River (from the southeast side) and the Ghezel Ozan River (from the northeast side) near the city of Manjil (Khosravi et al. 2019) and is introduced to the Caspian Sea near Astaneh-ye Ashrafiyeh County after crossing the width of Gilan province. The mean annual discharge (MAD) of this river is 3998 million cubic meters. Manjil dam is located on Sefidroud in Manjil city, which was put into operation in 1963 with an initial storage capacity of 1.76 billion cubic meters at the normal level of the reservoir. This dam was built with the purpose of civil and economic development, flood control, organizing Sefidroud river, creating a suitable and reliable water source for supplying water to 24,000 hectares of agricultural lands in Gilan province and using hydroelectric potential energy (Othman et al. 2013). Climate changes and human interventions have greatly reduced the capacity of the lake behind this dam, so that reservoir siltation leads to the formation of a total of 32 million tons of sediment inside the lake every year; and now the volume of the reservoir has reached half of that during construction (the volume of the lake was 1.8 billion cubic meters at the time of construction and has reached 900 million cubic meters now) (Kavian et al. 2016). This study has used information from four regional sediment monitoring stations in Gilan. The Gilvan station is located on Ghezel Ozan River, the Lowshan station on Shahrood River, the Rudbar station on Sefidroud River after Manjil Dam, and the Astaneh-ye Ashrafiyeh station in Astaneh-ye Ashrafiyeh County near the shores of the Caspian Sea on the Sefidroud River. Fig. 1 shows the location of the studied stations.

Data analyzed in the study

The SSC of Sefidroud River water was monitored using data collected between 2013 and 2020 from four sediment monitoring stations of Gilvan, Lowshan, Rudbar and Astaneh-ye Ashrafiyeh affiliated to Gilan Regional Water Authority. At each station, the SSC and corresponding discharge data have been measured at least 10 times per year, so that a total of 122 data sets were recorded at Gilvan, 174 at Lowshan, 80 at Rudbar, and 140 at Astaneh-ye Ashrafiyeh stations during the eight-year period. After quality control for qualitative parameter data in terms of outliers, the SRCs were drawn for each of the stations based on eight years of data. The present research used the data of spectral bands of Level-1 Precision and Terrain (L1TP) Landsat 8 images. TP is the highest quality level-1 product suitable for pixel-level time series analysis (Sa'ad et al. 2021). To

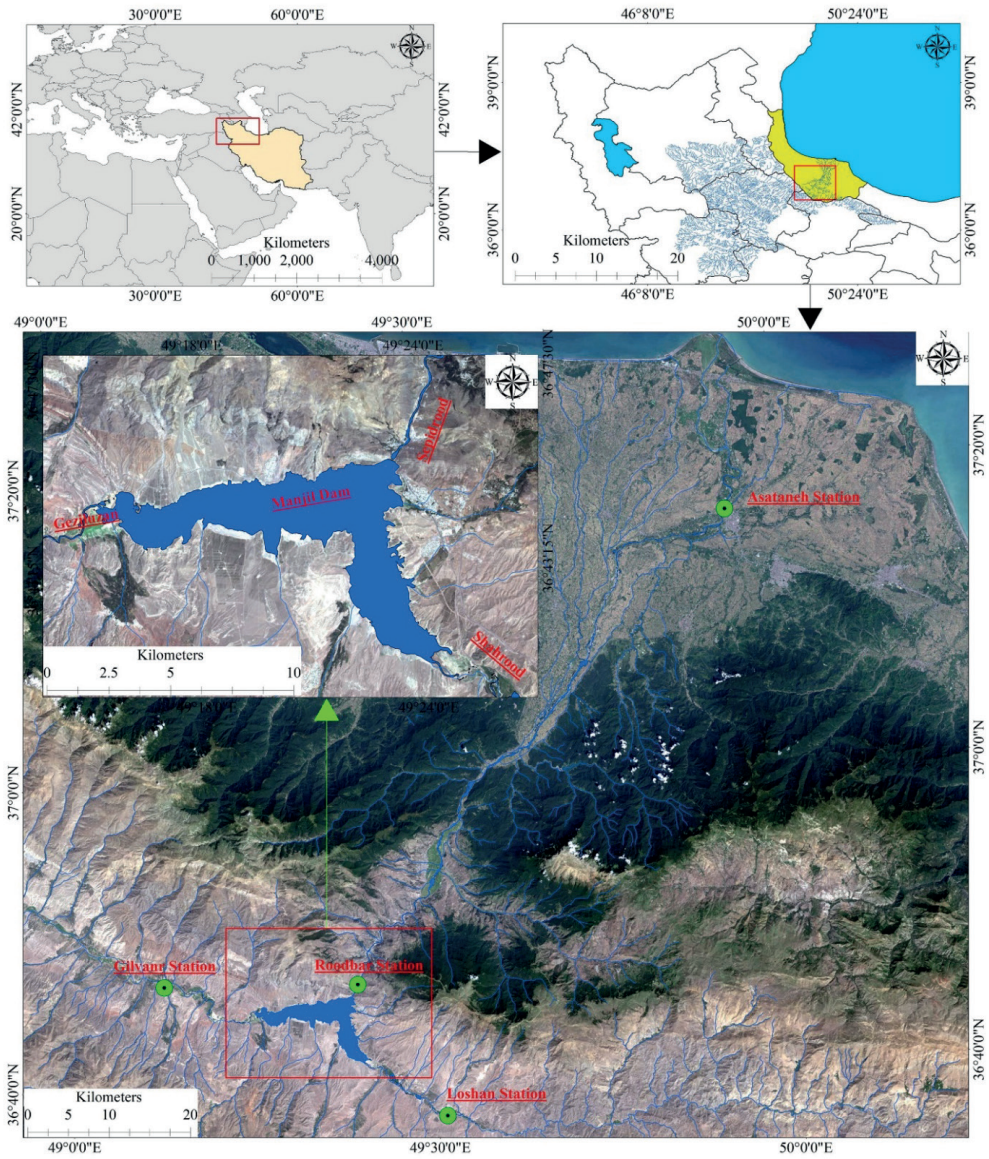

Fig. 1. Location of Sefidroud River and studied hydrometric stations, Gilan province, Iran

this end, 46 images captured by the Operational Land Imager (OLI; path: 166, row: 34) between 2013 and 2020 were acquired from the United States Geological Survey (USGS). The images were extracted at the same time as the SSC samples were taken (on the same day), and the criteria for selecting these images were based on the level of cloudiness and appropriate quality.

Drawing sediment rating curves

Normally, methods of sampling suspended sediment of water resources include interpolation and extrapolation procedures (Walling and Webb 1981, 1988; Walling 1994). The interpolation method assumes that the concentration or discharges obtained from the samples taken are representative of a long-term period (for example, days and weeks) and requires regular sampling. The extrapolation method estimates river sedimentation through more limited field measurements and establishing a relationship between the sediment discharge and the corresponding flow discharge; sediment rating curves (SRCs) are a typical example of the extrapolation method (Efthimiou 2019). the SRC method, the relationship between discharge and SSC is usually obtained according to Equation 1 (Asselman 2000; Efthimiou 2019; Khan et al. 2021; Azadi et al. 2020).

$$Q_s = \alpha Q_w^b \quad (1)$$

Where, Q_s stands for the sediment concentration or suspended sediment discharge in milligrams per liter (mgL^{-1}) or tones per day, Qw for the flow rate in cubic meters per second (m^3s^{-1}), and α and b for the constant coefficients of the regression equation.

The most common way to get the SRC is to pass a line through the point cloud of flow discharge and SSC, called single-linear SRC (Asselman, 2000; Azadi et al. 2020). Sometimes the distribution of point cloud is such that it needs to pass more than one line, which is called the broken line interpolation or bi-linear SRC (Zarris et al. 2011; Efthimiou 2019). In this method, first, the cumulative curve of SSC data versus flow discharge values is drawn in a log-polar coordinate system. Then, the amount of flow discharge at the point of abrupt change of slope and cumulative curvature is used as a base or initial guess for the separation of the data series (point cloud).

To draw bi-linear SRC, after drawing the graph of SSC cumulative curve and normal flow discharge data, the most suitable abrupt change point of SSC cumulative curve slope and the corresponding flow discharge was used as a base or initial guess to separate the data series (point cloud). In order to achieve the optimal flow discharge value of the data separator, different flow discharge values around the initial value were also tested by trial and error, and finally, the best result (flow discharge) was identified for the optimal separation of the initial series of data. Thus,

flow charges smaller and larger than 10, 45, 15 and 10 m3s-1 were used for Gilvan, Lowshan, Rudbar, and Astaneh-ye Ashrafiyeh stations, respectively, for data separation and bi-linear SRC drawing.

Jansson (1996) suggested that flow discharges should be divided into a number of classes with a certain trend, and for the mean discharge of each class, the mean SSC of the same group should be determined and the SRC should be drawn using these new data. This method is called middle-class SRC (Khaleghi & Varvani 2018). In order to determine the classes for drawing middle-class SRC, the discharge range smaller than 2 m^3/s for Gilvan and Lowshan stations, and the discharge range smaller than 5 $m^3s^{-1}$for Rudbar and Astaneh-ye Ashrafiyeh stations were considered as the first class. Then, the range of discharge changes in each class gradually increased, so that the range of changes of the last class of Gilvan, Lowshan, Rudbar and Astaneh-ye Ashrafiyeh stations was considered to be greater than 200, 130, 280 and 240 m^3s^{-1}, respectively. The reason is that the number of discharge episodes captured in larger discharges is limited. For example, the number of recorded episodes of the last class at Rudbar station (200 < m^3s^{-1}) was only 1, while the number of first-class episodes (5 > m^3s^{-1}) was 19. Therefore, 19, 18, 19 and 20 classes were determined for Gilvan, Lowshan, Rudbar and Astaneh-ye Ashrafiyeh stations, respectively, and middle-class SRC was drawn by calculating the mean SSC and flow discharge of each class.

Satellite image preprocessing

Remote sensing techniques to measure SSC use surface reflectance measured by multispectral sensors on satellites or cameras. Surface reflectance can be correlated with SSC to provide an indirect measure of SSC by creating SSC-surface reflectance models (Martinez and Cox 2023). in the present research, after receiving the mentioned satellite images, the data quality was controlled based on atmospheric, geometric and radiometric errors using ENVI 5.3 program. Since the majority of received images had a coordinate system, there was no need for geometric correction. One of the important challenges of remote sensing data in the investigation of water zones is the resolution and atmospheric correction of satellite images (Yang et al. 2022). Earth's atmosphere consists of liquid, solid and gas particles, many of which cause optical absorption, diffusion and scattering. The signal received by the satellite is emergent radiation from the earth's surface and atmosphere, which is recorded directly through the sensor. The radiation measured in the sensor is known as top of atmosphere (ToA). The purpose of atmospheric corrections is to convert the ToA radiation of objects into reflection from the Earth's surface. Therefore, the radiometric correction was first done by calibrating the digital numbers (DN) of the image to radiance (Cremon et al. 2020; Jally et al. 2021; Adjovu et al. 2023). Then, the atmospheric correction was performed using Fast Line-of-sight Atmospheric Analysis of Spectral Hypercubes (FLAASH) module. This module can correct wavelengths in the visible, NIR and SWIR regions up to 3 micrometers (Kantakumar and Neelamsetti 2015). The parameters required for the atmospheric correction were extracted from the MTL text file data as well as the Advanced Spaceborne Thermal Emission and Reflection Radiometer (ASTER) 30-meter DEM.

Fusion the images

Remote sensing studies are more interested in pixel-level image fusion (Xu and Ehlers 2017). Pixel-based satellite image fusion algorithms use the geometric details of a high-resolution panchromatic (PAN) image and spectral information from a multispectral (MS) image with low spatial resolution to generate a high spatial resolution MS image (Xu and Ehlers 2017; Pushparaj and Hegde 2017; Zhang et al. 2016). In recent years, many efforts have been made to provide algorithms suitable for fusion spectral and spatial information of satellite images (Kavzoglu and Colkesen 2009, Im et al. 2008, Yia et al. 2012; Liao et al. 2014). The current research used the Gram-Schmidt algorithm, in which a PAN band is simulated using the MS image spectral bands. Generally, in this algorithm, the simulated PAN band is obtained by averaging the MS image bands, and is considered as the first band. Then, the Gram-Schmidt transformation is conducted for the simulated PAN band and the MS bands. Next, the PAN band of the high-resolution image is replaced with the first Gram-Schmidt band (Sarp 2014; Pushparaj and Hegde 2017).

Correlation between spectral reflectance and suspended sediment concentration

After preliminary processing on satellite images, the correlation of SSC and spectral reflectance changes was analyzed. To this end, using random sampling in SPSS program, first 30% of the information of 46 satellite images and SSC (15 samples) were selected and left out of the data set; 70% of the data (spectral information of 31 satellite images) was used for the analysis of regression models, and the 30% left out was used in the stage of checking the efficiency of regression models of spectral information and SSC. It should be noted that in SPSS software, for random sampling of data, the percentage defined for sampling in the program environment is applied in a limited way. That is, to sample 30% of the data, the range of 25 to 35% of the data may be randomly sampled. For this reason, in the current research, about 30% defined in SPSS program, finally 33% (15 samples) and the rest (70%) finally 67% (31 samples) were sampled. In order to investigate the spectral reflectance of the runoff of Sefidroud, Ghezel Ozan and Shahrood rivers, first, five fixed 15-meter pixels were considered in all images from the location of the stations to 150 meters upstream of the station, followed by calculating the average values of spectral reflectance of seven image bands in these five pixels. It seemed that the average spectral reflectance of 5 fixed pixels at the closest point to the hydrometric stations compared to the spectral reflectance of one pixel was more suitable for SSC analysis due to the possibility of errors caused by the geometric and radiometric characteristics of the images. After extracting the spectral reflectance values of the image bands, the correlation between SSC and spectral reflectance of 7 bands and 21 band ratios was investigated. In such studies, the criterion is usually the ratio of the larger band to the smaller band. The band ratio B4/B3 is one of the most important spectral information in water pollution investigations, that is why this ratio is referred to as the TSM index, which is used in many studies to monitor water quality (Toming et al. 2017; Zhu et al. 2020; Das et al. 2021).

A total of 28 spectral parameters including bands and band ratios were used to check the correlation between qualitative parameters and spectral reflectance of the images. In choosing the most appropriate correlation equation in Excel, among the four regression equations, exponential, linear, logarithmic and power, the equation with higher correlation coefficients was selected as the best one.

Efficiency criteria of regression models

After analyzing SRCs and checking the correlation between SSC and 28 spectral reflectance parameters of 70% of the data, the models with the highest correlation coefficients were selected. Using the discharge values in the regression equations of SRCs and spectral reflectance, the SSCs were calculated in 30% of the left out data. Then, the estimated values from SRCs and satellite images were compared with the actual measured values. In order to evaluate the efficiency of the regression models, the percent error criterion was first used to get an overview of the error values of each of the correlation equations. For this purpose, first percent bias (PBIAS) was calculated according to Equation 2. The optimal value of this error is zero, and positive and negative values indicate overestimation and underestimation of the estimated data compared to the observed data, respectively (Jung et al. 2020). Its optimal value is zero and acceptable values are ±15% (Khan et al. 2021).

$$PBIAS = \frac{\sum_{i=1}^{n}\left(Qs_{obs} - Qs_{est}\right)}{\sum_{i=1}^{n} Qs_{obs}} \quad (2)$$

Where, Qs_{obs} is the sum of the observed SSC values in the desired period (30% of the total data), Qs_{est} is the sum of the estimated SSC values in the desired period (30% of the total data) and n is the number of observed and estimated data (equal to 15 in this research).

The estimated percent error provides an overview of the error values of each method, so other statistical criteria were also used to select the appropriate method. Thus, the statistical tests including mean absolute error (MAE), root mean square error (RMSE), Nash-Sutcliffe efficiency (NSE) and general standard deviation (GSD) were applied to evaluate, compare and validate each of the SRCs. These statistical criteria were calculated through Equations 3 to 6, respectively.

$$MAE = \frac{\sum_{i=1}^{n}\left|Qs_{obs} - Qs_{est}\right|}{N} \quad (3)$$

$$RMSE = = \sqrt{\frac{\sum_{i=1}^{n}\left(Qs_{obs} - Qs_{est}\right)^2}{N}} \quad (4)$$

$$NSE = 1 - \frac{\sum_{i=1}^{n}\left(Qs_{obs} - Qs_{est}\right)^2}{\sum_{i=1}^{n}\left(Qs_{obs} - \overline{Qs}_{obs}\right)^2} \quad (5)$$

$$GSD = \frac{RMSE}{\overline{Qs}_{est}} \quad (6)$$

Where, Qs_{obs} is the observed SSCs (in tons per day or mg/L), Qs_{est} is the estimated SSCs, and N is the number of observed samples.

The RMSE shows the distribution of the average difference between observed and estimated values, but it cannot provide information about overestimation and underestimation of the model (Farhadi et al. 2020; Ghadim et al. 2020). Like RMSE, the MAE is a common measure to show the average difference between observed and estimated values, but it is less sensitive to the output than RMSE, and one of its advantages is that it is preferred for smaller data sets (Efthimiou 2019). The NSE evaluates the residual variance of the estimated value compared to the variance of the measured data (Jung et al. 2020) and R2 describes the degree of collinearity among the observed and calculated data (Azadi et al. 2020). The value of NSE and R2 varies between zero and 1, and the higher the value, the lower the error, so that a value above 0.5 is acceptable for the model (Khan et al. 2021; Mackialeagha et al. 2022). The optimal equation was selected using the Simple Addition Ranking of the values of the evaluation indices. Thus, the closest values of MAE, NSE and R2 to the number 1 and the closest values of RMSE and GSD to the number zero in the desired station, which represents the smallest difference between the estimated and observed SSCs (Azadi et al. 2020; Ghadim et al. 2020; Adjovu et al. 2023), were assigned rank 1 and the next values were assigned rank 2. Then, the sum of the rank values of each method was compared to each other, and any method that had the lowest total rank was introduced as the optimal method. If the total ranks in two or more methods were equal, the priority was given to the equation of the method that had the highest R^2 value based on the correlation coefficient between the observed and estimated SSCs.

RESULTS

Drawing sediment rating curves

After quality control of sediment data measured at four sediment monitoring stations, a simple linear sediment curve was drawn for each station (Figure 2). The results showed that the R^2 value of the exponential correlation between SSC and the corresponding discharge in Gilvan, Lowshan, Rudbar and Astaneh-ye Ashrafiyeh stations was 0.67, 0.50, 0.79 and 0.81, respectively. The fitted line of exponential regression also revealed that suspended sediment discharge (Q_s) started from lower water discharges (Q_w) in Gilvan, Lowshan and Astaneh-ye Ashrafiyeh stations, but Astaneh-ye Ashrafiyeh station had lower Q_s compared to Gilvan and Lowshan stations, per corresponding water discharge (Q_w), while in Rudbar station, compared to Gilvan, Lowshan, and Astaneh-ye Ashrafiyeh stations, Q_w for Q_s initiation was more, and compared to Astaneh-ye Ashrafiyeh station, Q_s was more for Q_w.

Fig. 3 shows bi-linear SRCs drawn for the studied stations. The results indicated that, apart from Rudbar station, the R^2 value of at least one of the regression equations increased in three other stations. The R^2 value was 0.31, 0.56, 0.06 and 0.73 for the discharges lower than Astaneh-ye Ashrafiyeh station and 0.64, 0.12, 0.43 and 0.30 for the discharges higher than Astaneh-ye Ashrafiyeh station at Gilvan, Lowshan, Rudbar and Astaneh-ye Ashrafiyeh stations, respectively.

Fig. 4 shows middle-class SRCs drawn for the studied stations. The results showed that the R^2 value of middle-class SRCs in all four studied stations was higher than that of both single-linear and bi-linear SRCs, so that it was 0.85, 0.65, 0.56 and 0.83 for Gilvan, Lowshan, Rudbar and Astaneh-ye Ashrafiyeh stations, respectively. These results indicated that middle-class SRCs were more accurate in predicting flow discharge and SSC values compared to single-linear and bi-linear SRCs due to the highest value of R^2.

The results obtained from the regression models of suspended sediment concentration and spectral bands

The results showed that among 28 spectral parameters (including 7 bands and 21 band ratios), four band ratios B4/B3, B4/2, B6/B5 and B7/B5 had an exponential and power correlation with the R^2>0.35 (Fig. 4). The R^2 value of band ratios B4/B3 and B4/2 with exponential and power correlation was 0.74 and 0.43, respectively, and the R^2 value of band ratios B6/B5 and B7/B5 with exponential correlation was 0.46 and 0.39, respectively. The band ratios B4/B3 and B4/2 had a direct relationship with Q_s, so that the increase in the values of these band ratios was accompanied by the increase in Q_s, but the relationship of band ratios B6/B5 and B7/B5 with Q_s was inverse, so that the increase of these ratios was associated with the decrease of Q_s.

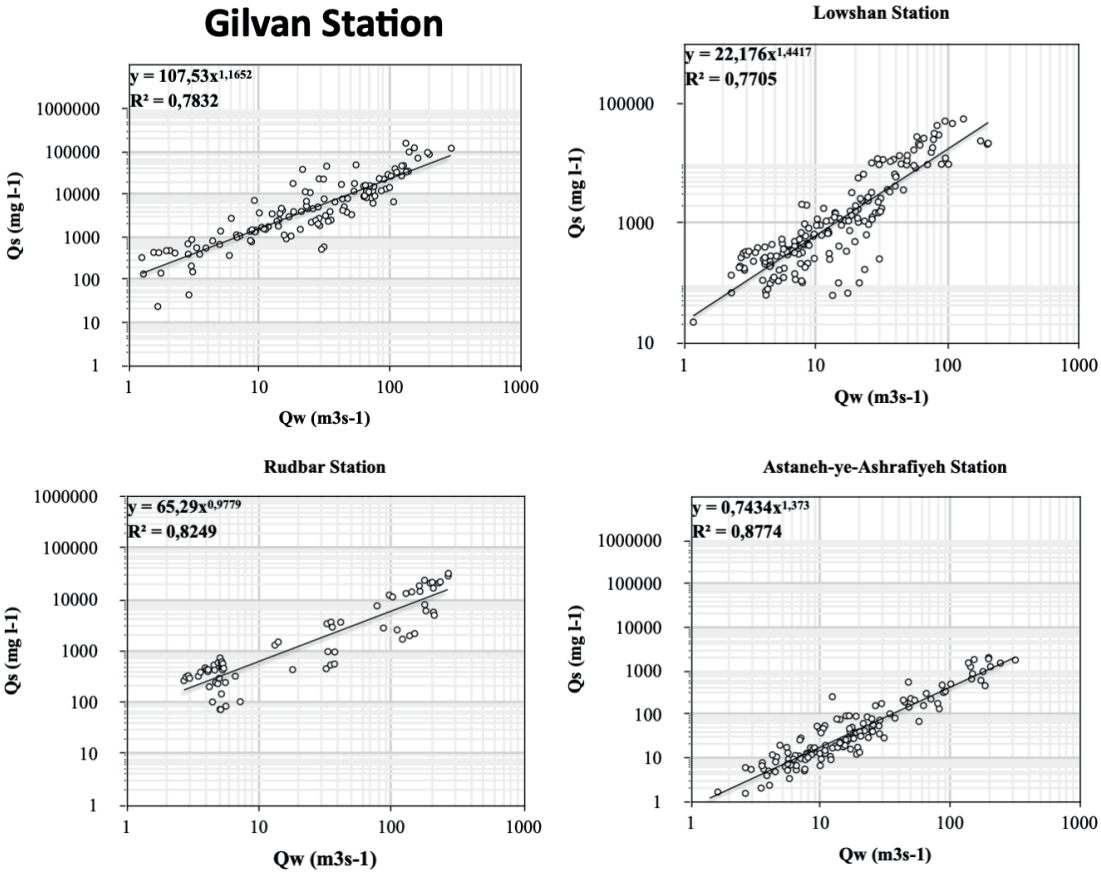

Fig. 2. Single-linear sediment rating curves drawn for the studied stations

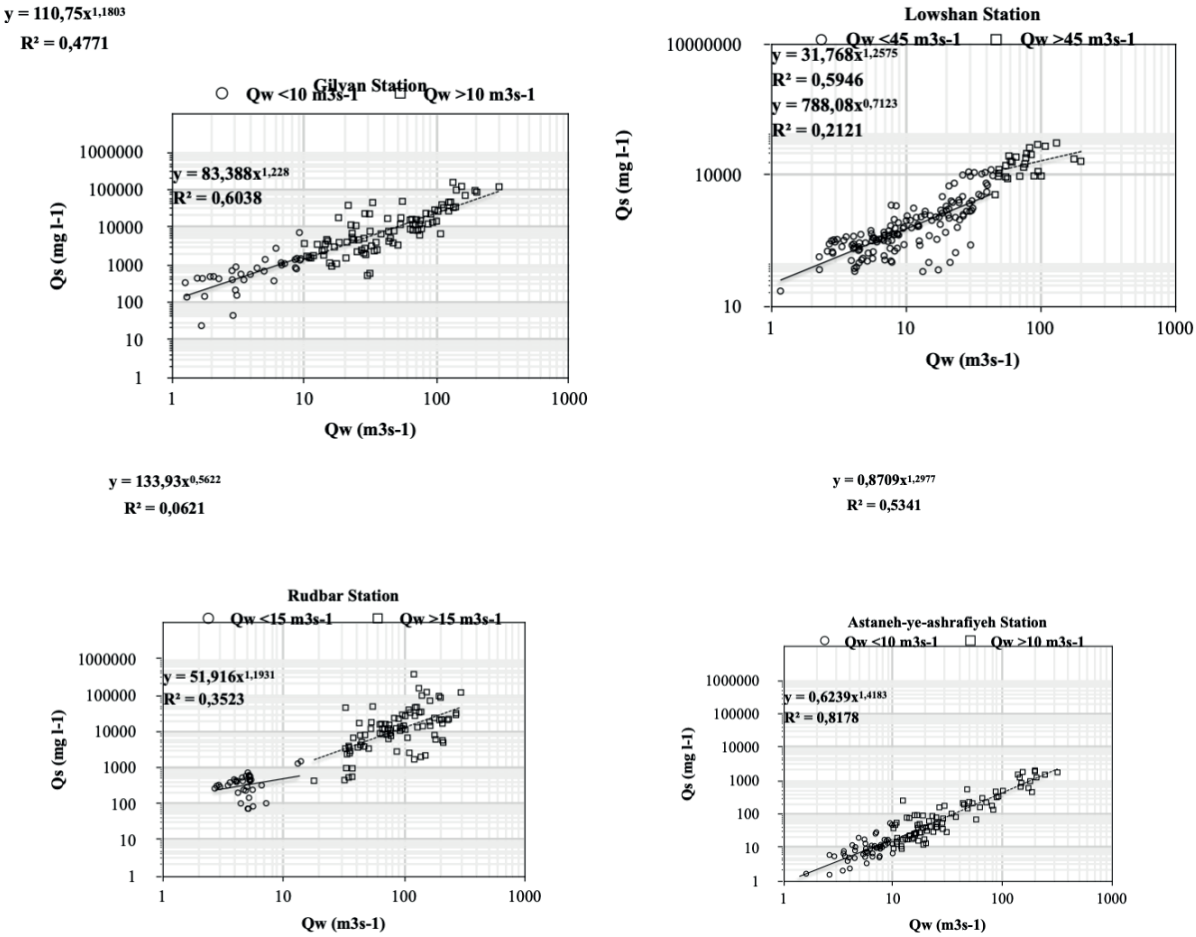

Fig. 3. Bi-linear sediment rating curves drawn for the studied stations

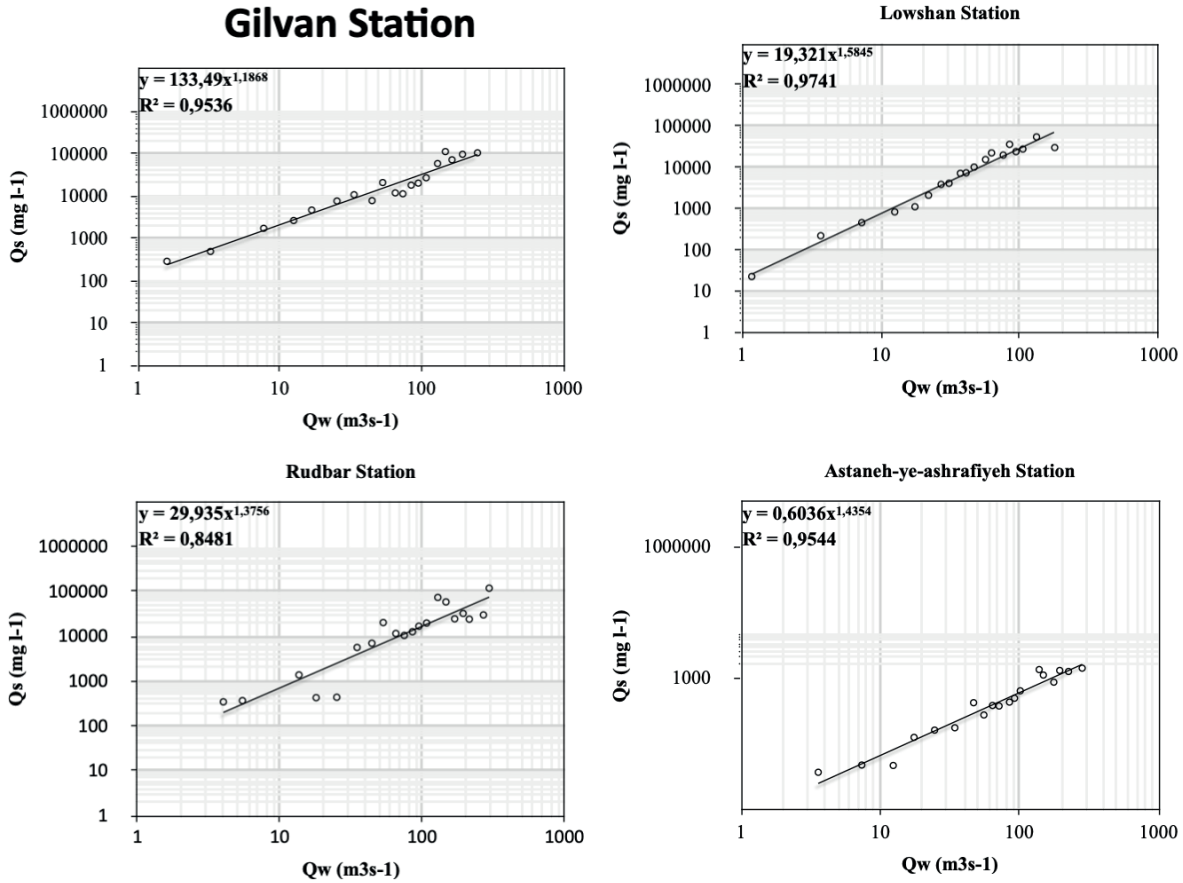

Fig. 4. Middle-class sediment rating curves drawn for the studied stations

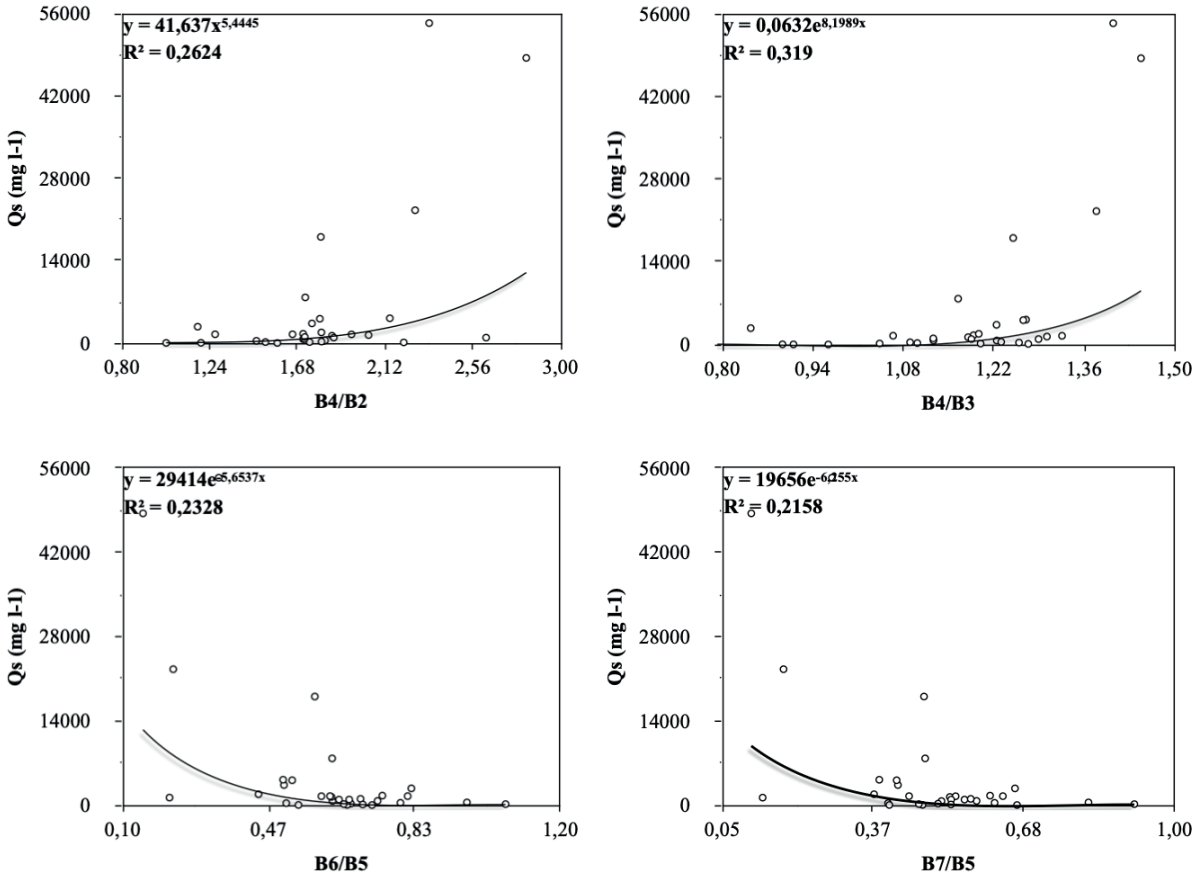

Fig. 5. Regression model of satellite spectral bands versus suspended sediment discharge (Q_s)

Determining the efficiency of regression models

The results revealed that the middle-class SRCs in the three stations of Gilvan, Lowshan and Astaneh-ye Ashrafiyeh had higher R^2 values. In addition, at Rudbar station, single-linear SRC had the highest R^2 value. Among the regression relationships of Q_s versus satellite band ratios, the B4/B3 band ratio had the highest R2 value. Therefore, to check the efficiency of the mentioned regression models, the values of the statistical criteria were calculated using 30% of the data (15 samples) (Table 1). The results showed that the regression equation B4/B3 versus Q_s was underestimated and the SRC equations were overestimated, so based on the PBIAS index, using the B4/B3 band ratio, the total Q_s in 15 samples was underestimated by about 51%, while using SRCs, the total Q_s was estimated to be around 15% more. However, the Q_s values estimated from B4/B3 band ratio had lower MAE, RMSE and NSE (2723 and 6055 mg/L and 46%, respectively), while the Qs values estimated from SRCs had higher MAE, RMSE and NSE (4198, 9125 mg/L and 22%, respectively). In addition to lower PBIAS, the Q_s values estimated from SRCs also had lower GSM (2.24). However, considering the impact of all efficiency criteria on the accuracy of regression models, the ranking of error values and total rankings showed that Q_s values estimated from B4/B3 band ratio with a total rank of 7 compared to Q_s values estimated from SRCs with a total rank of 8 were in the first priority (Table 2).

Investigating the regression relationship of Q_s values estimated from the band ratio B4/B3 and SRCs with the observed values of Q_s based on four exponential, linear, logarithmic and power correlation equations showed that the values of Q_s estimated from the band ratio B4/B3 had an exponential relationship and the values of Q_s estimated from SRCs had a logarithmic relationship. The findings of the present study indicated that the R2 value of the Q_s estimated from the band ratio B4/B3 was much higher compared to the Q_s estimated from SRCs (86% versus 14%). Therefore, both the total ranking of the efficiency criteria of the regression model and R_2 of the estimated to observed Q_s values showed that the regression equation of band ratio B4/B3 had better efficiency for Q_s estimation.

DISCUSSION AND CONCLUSION

Sediment concentration (SSC)

During the period of 2013 to 2020, the present study monitored suspended sediment concentration (SSC) using single-linear, bi-linear and middle-class sediment rating curves (SRCs) as well as Landsat 8 images in four sediment monitoring stations on Sefidroud river in northern Iran. The results indicated that the middle-class SRCs predominantly had higher coefficient of determination (R_2, exponential) at all stations. The middle-class SRCs were invented by Jansson (1996) in a study of the Reventzon river basin in Costa Rica by sampling and using the data of the Palomo sediment monitoring station to reduce the logarithmic retransformation bias of the single linear sediment rating curve. The results of Jansson (1996) showed that the estimate of sediment concentration using middle-class SRC was very close to the observed values, while single-linear SRC showed a lower estimate. One of the important advantages of using middle-class SRC can be neutralizing the effect of having more samples in low discharges in the calendar statistics method; because by averaging the data in flow classes, the large number of observations in the base discharges will no longer have an effect on the

Table 1. Efficiency criteria of regression models of sediment rating curves and B4/B3 band ratio based on suspended sediment discharge

Regression model	PBIAS	MAE	RMSE	NSE	GSD
Sediment rating curves	14.51	4197.95	9125.25	-0.22	2.24
Band ratio B4/B3	-51.48	2722.96	6054.81	0.46	3.51

Table 2. Ranking of efficiency criteria and priority of regression models of sediment rating curves and B4/B3 band ratio based on suspended sediment discharge

Regression model	PBIAS	MAE	RMSE	NSE	GSD	Total ranks	Priority
Sediment rating curves	1	2	2	2	1	8	2
Band ratio B4/B3	2	1	1	1	2	7	1

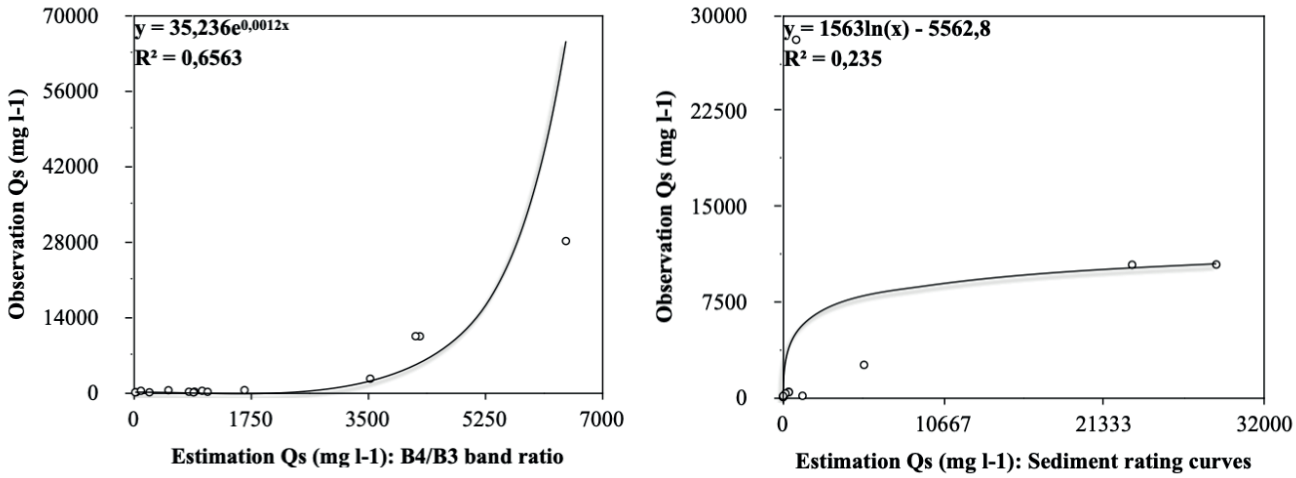

Fig. 6. The regression relationship of suspended sediment discharge estimated from the band ratio B4/B3 and sediment rating curves with observed suspended sediment discharge

SRC. Walling and Webb (1981 and 1988) and Walling (1994) suggested that the quality of the SRC can be improved by giving more weight to higher discharges that have higher sediment concentrations. Accordingly, in middle-class SRCs, due to the reduction of the effect of low points, the estimation of sediment in high discharges is improved, and also in this method, the distribution of points is reduced and the error caused by logarithmic transformation is minimized. On the other hand, the results related to the bilinear SRC indicated that in three of the four studied sediment monitoring stations, the R2 value of at least one of the bilinear regression equations increased compared to the single linear one. These results are consistent with the findings of Efthimiou (2019) and Zarris (2019), so that Efthimiou (2019) in a research on the suspended sediments of the Venetikos River in northern Greece and Zarris (2019) in the Nestos River on the border between Greece and Bulgaria showed that the bi-linear SRC had better efficiency for estimating SSC than the single linear one.

Spectral reflectance

The results of investigating the correlation between SSC and spectral reflectance of 7 single bands and 21 band ratios, 31 Landsat 8 satellite images, showed that four band ratios B4/B3, B4/2, B6/B5 and B7/B5 had exponential and power correlations with Q_s so that the band ratio B4/B3 (R^2= 0.74, exponential) had the highest correlation with Q_s. In the studies related to the relationship between satellite spectral information and suspended sediment, many researchers have focused on the green (B3: Green), red (B4: Red), near infrared (B5: NIR) and short wave infrared (B7 and B6: SWIR) bands. Sa'ad et al. (2021) found the R^2 value of 79% between the TSS and the green, near-infrared and short-wave infrared spectral bands of Landsat 8 on the east coast of Malaysia. Jally et al. (2021) also obtained 60% correlation between Landsat 8 spectral bands in Chilika Lake in eastern India. Cremon et al. (2020) improved the correlation coefficient of near-infrared and short-wave infrared bands and band ratios of Landsat 5 with SSC to about 87% in the Araguaia River in west-central Brazil. Wen et al. (2022) also showed in Chinese lakes that Landsat red band had a correlation coefficient of 0.76 with TSM. Aires et al. (2022) also reported a strong regression relationship between the NIR band of both Landsat 8 and Sentinel-2 satellites and suspended sediments. Martinez and Cox (2023) showed the correlation of Landsat 8, 7 and 5 spectral bands with SSC (R^2 = 0.72, 0.71 and 0.75, respectively) in the Mississippi and Missouri rivers in the United States of America.

The results related to the investigation of SRC efficiency and regression model between band ratio B4/B3 and Q_s using 15 measured land samples showed that although the SRCs compared to the regression model between the band ratio B4/B3 and Q_s had lower errors of PBIAS (15 versus -51%) and GSM (3.5 versus 2.2), the regression model between the band ratio B4/B3 and Q_s with lower MAE, RMSE and NSE errors (2723 and 6055 mg/L and 46% respectively) compared to SRCs (4198, 9125 mg/liter and 22%, respectively) was able to better estimate Q_s values in general. , the ranking of the overall efficiency criteria is actually the ranking of the validation criteria used in the current research. Any validation criterion that has more accuracy has been assigned a lower rank, and finally, any method with a lower numerical value has been selected as a more efficient method. In this research, the results showed that the band ratio B4/B3 has a lower rank.

In addition, the correlation coefficient between the estimated and observed Q_s showed that the Q_s estimated from the band ratio B4/B3 with the exponential regression model had a much higher R^2 (86% versus 24%) compared to the Q_s estimated from the SRC. This result is in line with the findings of Zhu et al. (2020), as the aforementioned researchers also investigated the regression relationship between Qs values observed and estimated from the B4/B3 band ratio of Landsat 8 in West Lake, Zhejiang Province, China, and came to the conclusion that there was an exponential relationship (R^2=82%) between the observed and estimated values.

In general, the results of the present study showed that satellite spectral information, especially the B4/B3 band ratio, had a very favorable capability for estimating suspended sediments. Considering that recording SSC data in sediment monitoring stations requires manpower and laboratory work, and in addition, more time is spent on sampling, laboratory work, and setting sediment data, free access to satellite images can effectively reduce costs and save time. On the other hand, sample collection in sediment monitoring stations is in the form of point and in situ sampling, while SSC varies according to the conditions of the river, in different regions and during different intervals (Du et al. 2021). Therefore, it is impossible to monitor the spatial changes of SSC along the river or water zones using SRCs (Lei et al. 2021), because it is impossible to sample all water zones due to financial and time constraints, and in some cases, easy access to all points is impossible due to the topographical conditions of the rivers and water areas. Meanwhile, one of the advantages of satellite images, regardless of its accuracy in estimating suspended sediments, is that satellite data captures ground information in a raster form in a wide area at the same time. Therefore, access to this raster information with spectral value and applying regression models on the spectral information of that zone easily provides the possibility of monitoring the spatial changes of phenomena, including water pollution, in all zones, even areas with difficult access. This helps water resource managers and decision makers to prepare a map of water pollution changes along the watershed and identify critical areas of water pollution and its causes in order to make appropriate decisions.

REFERENCES

Abbasi A, Taghavi L, Sarai Tabrizi M (2021) Qualitative Zoning of Groundwater to Assessment Suitable Drinking Water Using GIS Software in Mohammad Shahr, Meshkinshahr, and Mahdasht in Alborz Province. Anthropogenic Pollution. doi: 10.22034/ap.2021.1907787.1076

Adjovu GE, Stephen H, James D, Ahmad S (2023) Overview of the Application of Remote Sensing in Effective Monitoring of Water Quality Parameters. Remote Sensing 15(7):1938

Aires URV, da Silva DD, Fernandes Filho EI, Rodrigues LN, Uliana EM, Amorim RSS, de Melo Ribeiro CB, Campos JA (2022) Modeling of surface sediment concentration in the Doce River basin using satellite remote sensing. Journal of Environmental Management 323:116207

Asselman NEM (2000) Fitting and interpretation of sediment rating curves. Journal of hydrology 234(3-4):228-248

Cao Z, Zhang X, Ai N (2011) Effect of sediment on concentration of dissolved phosphorus in the Three Gorges Reservoir. International Journal of Sediment Research 26(1):87-95

Cremon ÉH, da Silva AMS, Montanher OC (2020) Estimating the suspended sediment concentration from TM/Landsat-5 images for the Araguaia River–Brazil. Remote Sensing Letters 11(1):47-56

Das S, Kaur S, Jutla A (2021) Earth observations-based assessment of impact of COVID-19 lockdown on surface water Quality of Buddha Nala, Punjab, India. Water 13(10):1363

De Girolamo AM, Pappagallo G, Lo Porto A (2015) Temporal variability of suspended sediment transport and rating curves in a Mediterranean river basin: The Celone (SE Italy). CATENA 128:135-143

dos Santos ALMR, Martinez JM, Filizola Jr NP, Armijos E, Alves LGS (2018) Purus River suspended sediment variability and contributions to the Amazon River from satellite data (2000–2015). Comptes Rendus Geoscience 350(1-2):13-19

Du Y, Song K, Liu G, Wen Z, Fang C, Shang Y, Zhao F, Wang Q, Du J, Zhang B (2020) Quantifying total suspended matter (TSM) in waters using Landsat images during 1984–2018 across the Songnen Plain, Northeast China. Journal of environmental management, 262:110334

Edwards AC, Withers PJA (2008) Transport and delivery of suspended solids, nitrogen and phosphorus from various sources to freshwaters in the UK. Journal of Hydrology 350(3–4):144-153

Efthimiou N (2019) The role of sediment rating curve development methodology on river load modeling. Environmental monitoring and assessment 191:1-19

Endreny Th, Hassett J (2005) Robustness of pollutant loading estimators for sample size reduction in a suburban watershed. Intl. J. River Basin Manage, (IAHR & INBO) 3(1):53-66

Farhadi H, Fataei E, Kharrat Sadeghi M (2020) The Relationship Between Nitrate Distribution in Groundwater and Agricultural Landuse (Case study: Ardabil Plain, Iran). Anthropogenic Pollution. doi: 10.22034/ap.2020.1885788.1059

Ghadim HB, Salarijazi M, Ahmadianfar I, Heydari M, Zhang T (2020) Developing a Sediment Rating Curve Model Using the Curve Slope. Polish Journal of Environmental Studies 29(2):1151–1159

Ghaffari A, Nasseri M, Pasebani Someeh A (2022) Assessing the economic effects of drought using Positive Mathematical Planning model under climate change scenarios. Heliyon 8:e11941

Horowitz AJ (2008) Determining annual suspended sediment and sediment-associated trace element and nutrient fluxes. Science of The Total Environment 400(1–3):315-343

Im J Jensen, Tullis J (2008) Object-based change detection using correlation image analysis and image segmentation, International Journal of Remote Sensing 29:399-423

Jangjoo MR (2021). Modelling fuzzy multi-criteria decision-making method to locate industrial estates based on geographic information system. Anthropogenic Pollution. doi: 10.22034/ap.2021.1933630.1111

Jally SK, Mishra AK, Balabantaray S (2021) Retrieval of suspended sediment concentration of the Chilika Lake, India using Landsat-8 OLI satellite data. Environmental Earth Sciences 80:1-18

Jansson MB (1996) Estimating a sediment rating curves of the Reventzon river at Palomo using logged mean loads within discharge classes, Journal of Hydrology, 183(4):227-241

Jung BM, Fernandes EH, Möller Jr OO, García-Rodríguez F (2020) Estimating suspended sediment concentrations from flow discharge data for reconstructing gaps of information of long-term variability studies. Water 12(9):2382

Kavian A, Dodangeh S, Abdollahi Z (2016) Annual suspended sediment concentration frequency analysis in Sefidroud basin, Iran. Modeling Earth Systems and Environment 2:1-10

Kavzoglu T, Colkesen I (2009) A Kernel function analysis for support vector machines for land cover classification. International Journal of Applied earth observation and Geoinformation 11:352-359

Khaleghi MR Varvani J (2018) Sediment rating curve parameters relationship with watershed characteristics in the semiarid river watersheds. Arabian Journal for Science and Engineering 43(7):3725-3737

Khan MA, Stamm J, Haider S (2021) Assessment of soft computing techniques for the prediction of suspended sediment loads in rivers. Applied Sciences 11(18):8290

khoram nejadian S, Esmaili A, Asemi S, Shams-Esfandabad B (2023) Determining heavy metal and developing model for concentration in the feathers of house sparrow (Ni, Pb,Cd) in Tehran. Anthropogenic Pollution. doi: 10.22034/ap.2023.1983320.1154

Khosravi K, Rostaminejad M, Cooper JR, Mao L, Melesse AM (2019) Dam break analysis and flood inundation mapping: The case study of Sefid-Roud Dam, Iran. In Extreme hydrology and climate variability 395-405

Lei S, Xu J, Li Y, Li L, Lyu H, Liu G, Chen Y, Lu C, Tian C, Jiao W (2021) A semi-analytical algorithm for deriving the particle size distribution slope of turbid inland water based on OLCI data: A case study in Lake Hongze. Environmental Pollution 270:116288

Liao K, Xu S, Wu J, Zhu Q, An L (2014) Using support vector machines to predict cation exchange capacity of different soil horizons in Qingdao City, China. J. Plant Nutrition Soil Science 177(5):775-782

Mackialeagha M, Salarian MB, Behbahaninia A (2022) The use of multivariate statistical methods for the classification of groundwater quality: a case study of aqueducts in the east of Tehran, Iran. Anthropogenic Pollution. doi: 10.22034/ap.2022.1965587.1134

Martinez MJ, Cox AL (2023) Remote-Sensing Method for Monitoring Suspended-Sediment Concentration on the Middle-Mississippi and Lower-Missouri Rivers. Journal of Contemporary Water Research & Education 177(1):17-30

Mazhar N, Javid K, Akram MAN, Afzal A, Hamayon K, Ahmad A (2023) Index-Based Spatiotemporal Assesment of Water Quality in Tarbela Reservoir, Pakistan (1990– 2020). Geography, Environment, Sustainability 15(4):232-242

Meena SR, Chauhan A, Bhuyan K, Singh RP (2021) Chamoli disaster: pronounced changes in water quality and flood plains using Sentinel data. Environmental earth sciences 80(17):601

Othman F, Sadeghian MS, Ebrahimi F, Heydari M (2013) A study on sedimentation in sefidroud dam by using depth evaluation and comparing the results with USBR and FAO methods. Int. Proc. Chem. Biol. Environ. Eng 51(9):6

Pavanelli D, Cavazza C (2010) River suspended sediment control through riparian vegetation: a method to detect the functionality of riparian vegetation. Clean Soil Air Water 38(11):1039-1046

Pushparaj J, Hegde AV (2017) Evaluation of pan-sharpening methods for spatial and spectral quality. Applied Geomatics:9(1):1-12

Regüés D, Nadal-Romero E (2013) Uncertainty in the evaluation of sediment yield from badland areas: Suspended sediment transport estimated in the Araguás catchment (central Spanish Pyrenees). CATENA 106:93-100

Sa'ad FNA, Tahir MS, Jemily NHB, Ahmad A, Amin ARM (2021) Monitoring total suspended sediment concentration in spatiotemporal domain over Teluk Lipat utilizing Landsat 8 (OLI). Applied Sciences 11(15):7082

Safizadeh E, Karimi D, Gahfarzadeh HR, Pourhashemi SA (2021) Investigation of physicochemical properties of water in downstream areas of selected dams in Aras catchment and water quality assessment (Case study: Aras catchment in the border area of Iran and Armenia). Anthropogenic Pollution. doi: 10.22034/ap.2021.1912491.1082

Sarp G (2014) Spectral and spatial quality analysis of pan-sharpening algorithms: A case study in Istanbul. European Journal of Remote Sensing 47(1):19-28

Toming K, Kutser T, Uiboupin R, Arikas A, Vahter K, Paavel B (2017) Mapping water quality parameters with sentinel-3 ocean and land colour instrument imagery in the Baltic Sea. Remote Sensing 9(10):1070

Verstraeten GJ, Poesen JDV, Koninckx X (2003) Sediment yield variability in Spain: a quantitative and semiqualitative analysis using reservoir sedimentation rates. Geomorphology 50(4): 327-348

Walling DE, Webb BW (1988) The reliability of rating curve estimates of suspended sediment yield: some further comments. In: Proceedings of the Porto Alegre Symposium BSediment budgets, 11–15 December, Porto Alegre, Brazil. IAHS Publication 174:337–350. Wallingford, UK: IAHS Press.

Walling DE, Webb BW (1988) The reliability of rating curve estimates of suspended sediment yield: Some further comments, In Sediment Budgets. Proc. Of Porto Symp. Dec. 1988, IAHS Publ, (174): 337 - 350.

Walling DE (1994) Measuring sediment yield from river basins, in: R. Lal (Edd), Soil erosion Research Methods. Soil and Water Conservation Society pobl, 2nd eddition: 39-83

Wang X, Liu Z, Miao J, Zuo N (2015) Relationship between nutrient pollutants and suspended sediments in upper reaches of Yangtze River. Water Science and Engineering 8(2):121-126

Wen Z, Wang Q, Liu G, Jacinthe PA, Wang X, Lyu L, Tao H, Ma Y, Duan H, Shang Y, Zhang B (2022) Remote sensing of total suspended matter concentration in lakes across China using Landsat images and Google Earth Engine. ISPRS Journal of Photogrammetry and Remote Sensing 187:61-78

Xu S, Ehlers M (2017) HYPERSPECTRAL IMAGE SHARPENING BASED ON EHLERS FUSION. International Archives of the Photogrammetry, Remote Sensing and Spatial Information Sciences, XLII-2/W7: 941-947

Yang H, Kong J, Hu H, Du Y, Gao M, Chen F (2022) A review of remote sensing for water quality retrieval: progress and challenges. Remote Sensing 14(8):1770

Yia L, Binga L, Qian-lia L, Chenc P, Yuana L (2012) A Change Detection Method for Remote Sensing Image Based on Multi-Feature Differencing Kernel Svm,» ISPRS Annals of Photogrammetry, Remote Sensing and Spatial Information Sciences 1:227-235

Zarris D, Vlastara M, Panagoulia D (2011) Sediment Delivery Assessment for a Transboundary Mediterranean Catchment: The Example of Nestos River Catchment. Water Resources Management 25(14):3785-3803

Zhang J, Yang J, Reinartz P (2016) The optimized block-regression-based fusion algorithm for pan sharpening of very high-resolution satellite imagery. The International Archives of the Photogrammetry, Remote Sensing and Spatial Information Sciences, Volume XLI-B7, 2016 XXIII ISPRS Congress, 12–19 July 2016, Prague, Czech Republic.

Zhu W, Huang L, Sun N, Chen J, Pang S (2020) Landsat 8-observed water quality and its coupled environmental factors for urban scenery lakes: A case study of West Lake. Water Environment Research 92(2):255-265

Check for updates

CC BY

RESEARCH PAPER

MODELLING OF POTENTIAL IMPACT OF CLIMATE CHANGE ON WATER REGIME AND CHANNEL PROCESSES IN THE RIVER LENA NEAR CITY YAKUTSK: POSSIBILITIES AND LIMITATIONS

Inna N. Krylenko[1,2*], Ekaterina D. Pavlyukevich (Kornilova)[1,2], Aleksandr S. Zavadskii[1], Pavel P. Golovlyov[1], Eugenia A. Fingert[1], Natalya M. Borisova[2], Vitaly V. Belikov[2]

[1] Lomonosov Moscow State University, Faculty of Geography, Moscow, 119991, Russia

[2] Water Problems Institute of the Russian Academy of Sciences, Moscow, 119333, Russia

***Corresponding author:** krylenko_i@mail.ru**

Received: May 12th 2024 / Accepted: November 22nd 2024 / Published: December 31st 2024

https://doi.org/10.24057/2071-9388-2024-3723

ABSTRACT. STREAM_2D software package was applied for retrospective and predictive simulations of the Lena River hydraulic and channel changes during ice-free period near the city of Yakutsk. The modelling results indicate significant correspondence of simulated water discharges distribution and water levels with observed one, the model also has captured main erosion and accumulation zones, according to the 2009–2016 years observations. Runoff hydrographs of the ECOMAG runoff model simulations based on the global climate model MIROC-ESM-CHEM data were used as input for the hydrodynamic model with daily time step for two climate scenarios RCP2.6 and RCP8.5.

Comparison of scenario, based on modern hydrographs, and two scenarios, based on climate projections, have shown the changes in the range of channel-forming discharges and their duration. According to the results of 20-year simulation of channel evolution for three scenarios, the position of the main areas of erosion and deposition under scenario RCP2.6 and RCP8.5 retained the same as under actual scenario, but some additional new local areas of erosion can be formed during peak flows near the banks. Erosion can increase by up to 1 - 2 meters and even more in some areas, but the shifting of some large erosion-accumulative forms is slower than according to the scenario, based on the modern hydrographs, due to the reduced duration of channel-forming flood discharges.

KEYWORDS: hydrodynamic modeling, channel processes, STREAM 2D, climate change, ECOMAG, runoff change

CITATION: Krylenko I. N., Pavlyukevich (Kornilova) E. D., Zavadskii A. S., Golovlyov P. P., Fingert E. A., Borisova N. M., Belikov V. V. (2024). Modelling Of Potential Impact Of Climate Change On Water Regime And Channel Processes In The River Lena Near City Yakutsk: Possibilities And Limitations. Geography, Environment, Sustainability, 4(17), 112-120

https://doi.org/10.24057/2071-9388-2024-3723

ACKNOWLEDGEMENTS: The authors are grateful to the participants of fieldwork, including the team of the Makkaveev laboratory of Soil Erosion and Fluvial Processes of the geographical faculty of Moscow State University. The authors express their gratitude to the Academy of Sciences of the Republic of Sakha (Yakutia) for scientific and information assistance in conducting research.

The study was carried out under the Governmental Order to the Water Problems Institute of RAS, subject FMWZ-2022-0001 (flow dynamic estimation) and under the state assignment of Faculty of Geography, Lomonosov Moscow State University part 1.10, CITIS 121051100166-4 (bathymetric survey), 121051400038-1 (Lena river regime data collection), the part of research, concerning Lena runoff modeling was supported by RSF project №24-17-00084, transport of sediments was analyzed with support by the Ministry of Science and Higher Education of Russian Federation under the Agreement 075-15-2024-614, date 13.06.2024.

Conflict of interests: The authors reported no potential conflict of interest.

INTRODUCTION

The analysis of flow hydraulics at sites with complex topography, taking into account the large number of structures in the channel (incisions, diversion dams, water intakes) and in the floodplain (bridge crossings, flood protection dams, etc.) has been carried out last decades using hydrodynamic modeling methods (Jodhani, 2021). Calibration and validation of the hydraulics at different flow rates (e.g. with and without floodplain inundation) is mandatory for such modeling. Although nowadays there are some examples of models for long sections of large rivers such as the Parana (Guererro et al., 2015), Mississippi (Scott et al., 2008), Nile (Saeed et al., 2020), usually due to their complexity, moving-bottom hydrodynamic models are mainly used for non-extended channel reaches and/or for non-extended time periods (Sloff et al, 2012; Horvat

et al., 2015; Zhang et al., 2014). Moving-bottom simulations are very computationally demanding, so there is a difficulty to perform calculations for complex computational meshes for long periods. Often the data on real channel changes are not available for the validation of the modeled channel evolution for long periods or for all modeling area.

At the same time, the need for prospective long periods modeling of channel evolution is driven by the requirement of comparative hydromorphological processes analyzing in the river section both under modern conditions and in the future, in order to assess the degree of anthropogenic impact on the water and channel regimes. Mathematical modelling has becoming one of the powerful tools in this case, which, combined with traditional hydrological and morphological approaches, gives opportunity for the rate and direction of channel changes assessment and developing of medium and long-term channel evolution forecasts, both in existent conditions and also taken into consideration various feasible infrastructure projects in river channels and on the floodplains.

An important issue in predictive modelling is the choice of computational scenarios. The most traditional approach to the problem is to use schematic hydrographs based on modern runoff series as input, sometimes taking into account discharges of low repeatability (for example, 1% probability discharge) (Vijay et al.,2007; Golovlyov et al., 2019). However, in the climate changes context, this approach does not allow to consider the impact of expected changes on the water regime and channel deformation, which is particularly relevant for the areas, where modern trends are clearly expressed and further runoff growth is projected. At the same time, demand on the assessments of the possible climate changes impact on water regime and channel processes is very high and such tasks require the development of new approaches, based on mathematical modelling methods.

Runoff is one of the key factors determining the intensity of channel evolution. Estimation of runoff changes based on runoff formation models grounded on global climate model data is now widespread (Gelfan et. al., 2021). A number of studies has also demonstrated the possibility of combining flow generation models with other types of models, including hydrodynamic ones (Grimaldi et al., 2019, Krylenko, 2023), to assess changes in the hydrodynamic characteristics of flow and flooding. The including of hydrodynamic models with channel bottom deformation module in this model chains is not so often, for example (Nones et al., 2014) due to complexity of the task. Thus, it is possible to perform scenario calculations taking into account runoff changes for the period of the climate forecast if the block of channel deformations is included.

The possibilities and limitations of this approach are considered in our paper on the example of the Lena River near Yakutsk city. The city of Yakutsk (which is administrative, culture and industrial center of the North East of Russia) is situated on the left bank of the Lena River. The city has faced with many problems, concerning intensive channel processes last decades. Sediment accumulation near the main water intake structure, supplying Yakutsk city by the drinking water, and deterioration in conditions of navigation roots to the main city ports are the most dramatic problems. This region is characterized by a significant increase in annual runoff volumes and growing anthropogenic pressures, including the bridge construction and floodplain development projects.

This study is performed on the base of STREAM 2D hydrodynamic model (Belikov and Aleksyuk, 2020), adapted for the 75 km long River Lena section near Yakutsk. The first task was to perform detailed model hydraulic calibration and validation to apply the model for a complex channel and floodplains system of the Lena River near Yakutsk. Validation of the channel deformation modeling through continuous simulation for the period between repeated channel surveys of 2009 and 2016 was the next goal in order to assess the quality of the model's reproduction of the main trends in vertical channel changes. The final parts of the research consider the possible channel changes for 20-year forecast period taking into account projected the Lena River runoff changes under the RCP2.6 and RCP 8.5 climate scenarios, especially regarding the difficult situation with the city's water supply due to the shallowing of the Adamovskaya channel, which is closest to Yakutsk city.

STUDY AREA

The city of Yakutsk, which is now the administrative center of the Sakha Republic, is an old Russian city (founded in the 17th century) located in the Lena River valley in the area under study. The city's population is about 300 thousand people. Three hydrological gauges are in operation within the considered section of the Lena River near Yakutsk city. The measuring discharges and water levels gauge in the village of Tabaga is located in the upper part of the studied reach. The Lena River basin area for the Tabaga gauge is 897 000 km^2. The water level measuring gauge of the Yakutsk city is situated in the middle part of the study area, and Kangalassy gauge (Fig. 1) is located at the lower boundary of the area. The river section under study is characterized by numerous ramifications, and is located between the Tabaginsky cliff at upstream and the Kangalassky cliff in the lower reaches (which limit the spread of the left bank floodplain) and low terraces above the floodplain, as they are rocky capes. The width of the main channel of the Lena River in this section is 3.5-4 km.

Numerous engineering and water facilities exist in the city of Yakutsk on the Lena River, so it is necessary to take into account the peculiarities of the water and channel regime of the river for their safe operation. An unfavourable situation has been created in recent years for the entire water infrastructure of the city in the territory, due to the fact that the river channel near the left bank, where the city is located, grows shallower, while the right branch develops and large forms of the channel topography also shift (Chalov et al., 2016). The above-mentioned re-formations of the channel lead to the displacement of the navigable fairway, which complicates the work of the port, leads to failure of the city water intake, and complications associated with the ferry crossing. The adverse channel changes effect on this section of the Lena River was discovered for the first time as early as the 1970s by the expedition of the Lomonosov Moscow State University, and even then forecasts, according to which the shallowing of the branches near the city was expected, were made (Zaitsev and Chalov, 1989; Chalov et al., 2012). Different projects were performed for the preserving of the main flow in the city area in connection with the existing problems of water use, including hydrodynamic model application (Belikov et al., 2002).

MATERIALS AND METHODS

Hydrodynamic modeling

STREAM 2D software package, based on the numerical solution of two-dimensional Saint-Venant equations in the "shallow water" approximation and widespread in Russia, was used for modeling. Hybrid computational grids of irregular structure and original topography interpolation algorithms have been applied for the task. This software showed high efficiency in modelling both for flow hydraulics and channel changes, including those for different key

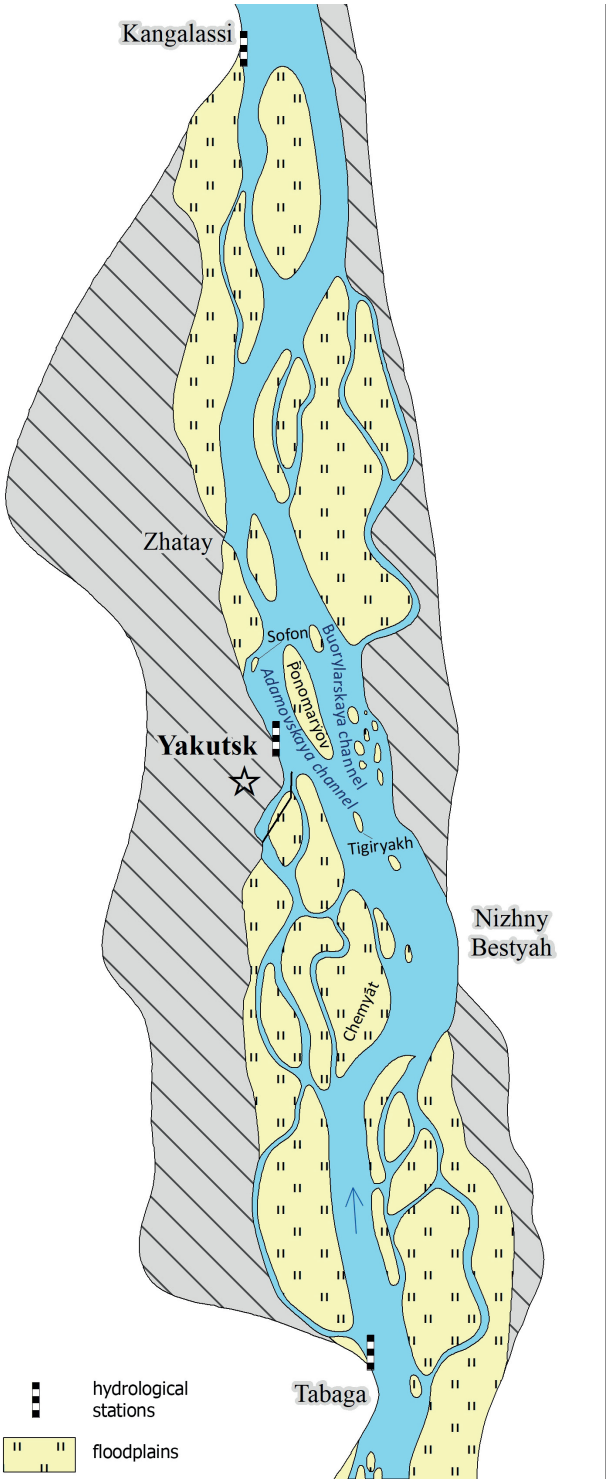

Fig. 1. Study area

area in Russia (Volga, Ob, Lena, Kolyma, Vilyuy, Yana, Amur etc.) (Belikov and Aleksyuk, 2020; Belikov et al, 2023). The description of the mathematical equations included in the numerical scheme of the model is presented, for example, in (Aleksyuk and Belikov, 2017). When modelling, a block of channel changes was involved, taking into account the convective transport of soil particles by flow, soaking up and sedimentation of sediments in an uneven flow, changing the bottom levels over time, taking into account the effect of flattening (transverse diffusion) of the underwater slope in a direction orthogonal to the velocity vector.

Model area is cover 75 km of the Lena River valley including branched channels and wide floodplain from Tabaga to Kangalassy gauge cites. Data of these stations were used for model boundary conditions assigning. Data of Yakutsk city gauge station as well as measured during field campaign water levels and flow velocities was taken into account for model calibration and validation. Model based on irregular hybrid curvilinear quadrangular and triangular mesh, which includes more than 50 thousands sells.

The initial data for the application of the hydrodynamic model were the materials of field researches of the soil erosion and channel processes laboratory at the Geography Faculty of Moscow State University, including the results of repeated bathymetric surveys, measurements of water discharges, water levels and water slopes and daily regime observation data of hydrological gauges on the Lena rivers - Tabaga, Yakutsk, Kangalassi. The bathymetric survey data for 2009, 2016, 2021 were integrated with the digital model of the floodplain topography to create the integrated digital topography models. The map of jam-hazardous part of river

channels was compiled on the basis of historical data and satellite images to set the places of ice jams formation, the dates of the ice jams formation were taken according to the hydrological gauges data.

The field data obtained during the expedition researches in 2016 was used to set the parameters of the channel-forming sediments fractions. Mainly the channel sediments are represented by the sand with an average diameter of 0.36 mm, so the average diameter of the channel sediments was taken into account in the simulations. Initial model hydraulic calibration was performed based on data of the same field campaign. Model calibration and validation was done on the second step, based on long-term data of hydrological gauges Tabaga and Yakutsk from 2001 up to 2016 year. Due to the presence of multi-temporal bathymetric surveys, actual and modelled bottom evolution for the period 2009-2016 were compared for validation of channel deformation block.

Input runoff scenarios for the channel evolution forecast

Modeling of flow dynamics and channel changes was performed for the 20-year forecast period with a daily step. Modern bottom topography from 2021 year was used as a starting point. To save computation time, the modelling was carried out only for the warm period from May 1 to October 1 of each year, which covered the passage of the most important for the formation and displacement of the main channel forms, winter periods were excluded from the simulations.

As the base scenario 1, we used combination of modern hydrographs for the last years 2010 - 2020, repeated twice, to represent the modern conditions of channel formations. On the peak of one flood, 1% probability discharge was added.

We used outputs of ECOMAG runoff model (Motovilov, 2016) based on the data of the global climate models with daily time step to take into account possible runoff change at the 21st century. Ensemble of five models and different climate scenarios for the Lena River - for Tabaga gauge were considered during flooding characteristic modeling at separate research (Krylenko, 2023). We examined in detail the results of scenario modeling based on data from the MIROC-ESM-CHEM climate model (Nozawa et al., 2004) in this study, because the estimates of the runoff characteristics of the Lena River using this model as climate forcing well correspond to observed ones for the historical period and are closest to the ensemble average.

Climate projections for two greenhouse gas emission scenarios were taken into account, "soft" scenario rcp2.6 and "hard" scenario rcp8.5. Projected long-term flow hydrographs for the period from 2046 to 2065 from ECOMAG runoff model, forced by data of the MIROC-ESM-CHEM climate model, for the scenarios RCP2.6 and RCP8.5 were used as input data for the STREAM 2D hydrodynamic model. As result, three input runoff scenarios for the Lena River bottom change simulations was considered: 1. modern runoff input; 2. runoff change according scenario RCP2.6; 3. runoff change according scenario RCP8.5.

RESULTS

Results of model calibration and validation

Calibration and validation of hydraulic characteristics based on field data

The calibration and verification of the model was originally carried out based on data from 2016 field surveys, including a comparison of the water level marks along the longitudinal profiles and the distribution of the water discharges along the branches for various water discharges. When the roughness coefficients equal to 0.015–0.017 for the channels and 0.05 for the floodplain, a good compliance between the measured and calculated water levels at the control points was reached. The difference between the modelled and observed water levels at the Yakutsk gauge was 1–4 cm. The difference between the values obtained during special expeditionary surveys (instantaneous water level measurements) and the results of modelling at control points did not exceed 10–18 cm on the average along the length of the study section.

The model reproduces well the distribution of water discharges among the main branches. In the main branching point near the Yakutsk city, which determines the water situation of the city, the Adamovskaya channel, closest to the city, receives 37-39 % of the input water discharge in the flow range from 9560 to 30000 m^3 s-1 according to measurement data, the right Buorylarskaya channel gets up to 55 % of the input flow, which reproduces the model. The remaining 7 % of the input water flow goes along the Khatykhstakhaya channel, and the model slightly underestimates the water discharge in it (modelling value is 5 % of the total water flow), due to the small detailing of the computational grid in this channel because of its insignificant width in comparison with the main channel.

Calibration and validation of hydraulic characteristics based on long-term data of hydrological gauges

Additional refinement of the roughness coefficients for the ice jams periods at the hazardous sections according to the data for 2009-2015 was made to simulate water flow dynamics for the flood periods, and it was found that the best compliance of the water levels is provided with the roughness coefficients of the ice jams sections equal to 0.073.

The simulation, based on data for the period from 2001 to 2015, showed that the hydrodynamic model, adapted according to the field and regime observations data for 2009-2015, provides a steady good quality of water levels modelling over a long-term period, which confirms both by visual match of the graphs of the observed and simulated water levels (Fig. 2), and high values of the simulation quality criterion. The criterion of Nash-Sutcliffe (NSE) for the studied periods for the Lena River gauge in Yakutsk was 0.90 for 2001–2008 and 0.93 for 2009–2015 years (it is assumed that the results with NSE> 0.75 can be considered as good in the hydrological modelling practice).

Validation of inundation zones based on data of satellite images

An additional validation of the model was carried out by comparing the simulated flooding boundaries with the flooding boundaries provided by satellite images (more than 20 images). It was found that the relative error for the divergence of flooded areas does not exceed 10 % during floods and high waters and the maximum divergence reaches 18 % during ice jams when comparing the real hydrological situations observed by modeling and interpreting satellite images (Kornilova et al., 2018).

Validation of channel changes modeling results for the historical period

Due to the presence of multi-temporal bathymetric surveys, both actual and model bottom evolution were evaluated for the period 2009-2016. Despite some limitations of model simulations (only the warm period

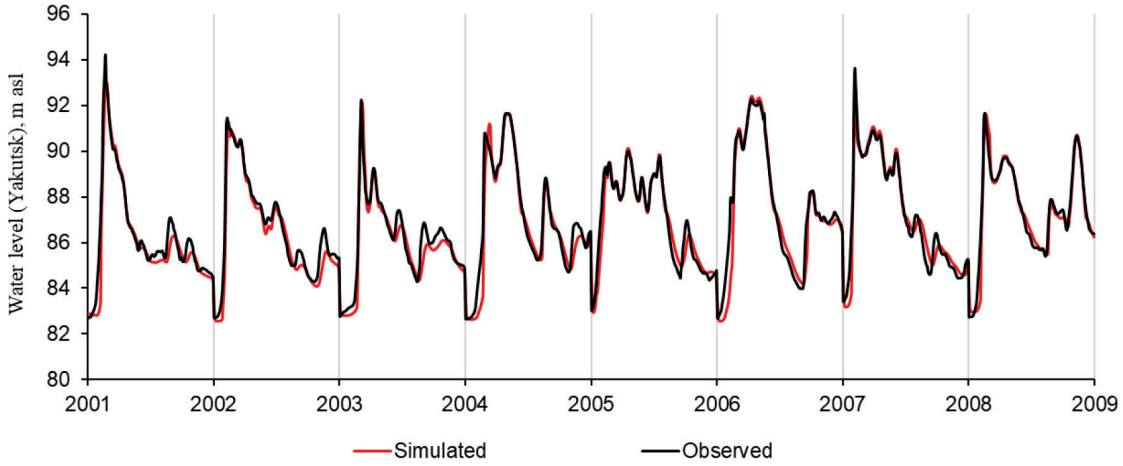

Fig. 2. Observed and modelled water levels at the Yakutsk gauge at 2001-2008 (ice-free periods)

of the years were modelled, sediments were considered as homogenous), the main positive result was the correspondence of the simulated and observed main zones of erosion and deposition (Fig. 3). Totally, in the 70 % of modeling sells inside the channels deposition or erosion zones coincide with estimated according bathymetry surveys. But one can notice some alternation of sections with almost complete coincidence of the situation of the simulated and actual changes and areas, where the model reproduced not so good.

The model adequate showed the channel changes in the upstream part of the studied section from the Tabaga until the Chemyat island. The model indicated erosion zone near the right steep bank downstream from this part of the channel, but in reality there are deposition zone. The possible reason of this discrepancy can be that the model is underestimated planform channel changes, which took more flow energy. There is the vast deposition zone near the Tigiryakh island. The stable two-stream system has formed near this island in the last decade, which is of decisive importance for the channel processes within the Yakutsk. The model again showed a situation close to reality in this area. The obtained distribution of water flow along the branches corresponds to that observed in the 2016 year (the flow discharge was distributed equally among the right and left main branches). In the next section from the Tigiryakh island to Ponomarev island, which is the most difficult for modelling because of the diversity channel processes factors, the simulation results can only be called partially successful. The model showed erosion along the left bank, but did not identify it in the central part of the channel. Despite the strong

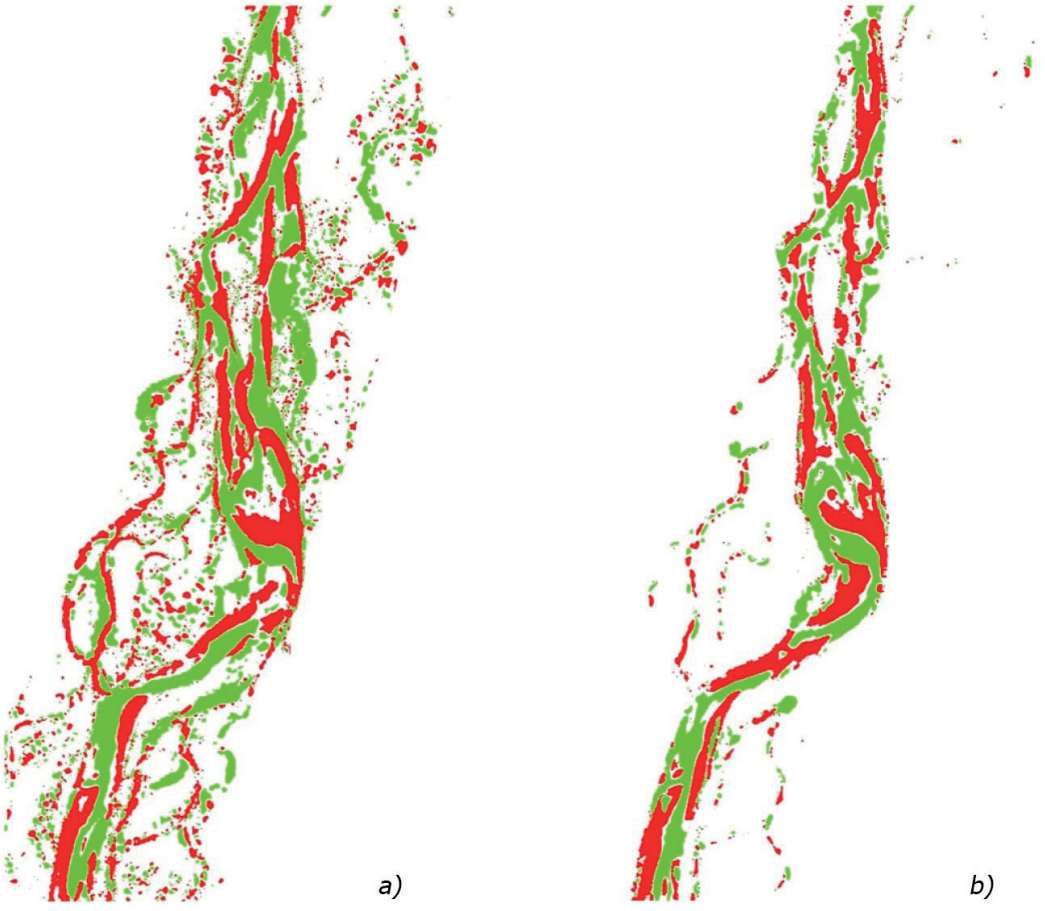

Fig. 3. Deposition (shown in green colour) and erosion (shown in red colour) zones in the Lena River channel for the period 2009 – 2016 year according observation data (a) and modelling (b)

discrepancy between the actual and model data, the distribution of water flow between Adamovskaya and Buorylarskaya branches coincides with the observed (39 % and 51 % correspondingly). Along the Adamovskaya and Buorylarskaya channels, the model has demonstrated quite realistic results. In the downstream section of the Lena River near Zhatay 75 % of the flow is going in the main stream. Modelling on this section showed a result that is different from the observed one. This section is characterized by the maximum rate of planform changes.

Water regime and channel processes under climate change scenarios

According to the analysis of the input hydrographs, it is expected that both the annual and peak runoff of the Lena River will increase during the 21st century, under both "soft" and "hard" climate scenarios (Fig. 4a). The increase in annual runoff could be up to 18% by the middle of the century and 19% at the end of the century under a "soft" scenario. Under a "hard" scenario, the increase could be as high as 23%. A significant increase in maximum discharges and a shift of floods to earlier dates are expected (Figure 4b). Thus, the maximum discharge during the second half of the 21st century under the RCP2.6 scenario could reach 57 000 $m^3 s^{-1}$, and under the RCP8.5 scenario, it could reach 72 000 $m^3 s^{-1}$. This would be by 7% and 35% higher, respectively, than the present-day 1% probability discharge, which is estimated based on a long-term series of observations at 53 100 $m^3 s^{-1}$. This increase in water discharge would lead to a corresponding increase in the depths and areas of flooding in riverine territories. In addition to an increase in the maximum discharge during snow-melt flood, the predicted hydrographs are characterized by a decrease in the discharge during the rain flood period, which is particularly pronounced for the hardest scenario RCP8.5.

Changes in runoff hydrographs are reflected in changes in the channel-forming discharge curve for the climate projection period. The channel-forming water discharges are those which have the most significant impact on the channel over a multi-year period (20-25 years) and at which the greatest sediment discharge is observed. They correspond to the maximums of the function $f(P*Q^2)$. The calculated product $(P*Q^2)$ for determining channel-forming discharge accounts for changes in water content of a river through the recurrence P of observed water discharges (Borshchenko, Chalov, 2010; Chalov, 1987). According analysis of modelled discharges, the main channel-forming discharge shifts from a range of 26000-27000 $m^3 s^{-1}$ to a range of 36000-40000 $m^3 s^{-1}$ even under the mild climate scenario, and two peaks in the range of 38000-42000 $m^3 s^{-1}$ are observed under the RCP8.5 scenario (fig. 5).

The main Adamovskaya and Buorylarskaya branches, which determine the situation near Yakutsk city, under RCP2.6 scenario, develop similarly to the trends shown in the current channel forecasts. The water content of the Adamovskaya branch increases significantly relative to the

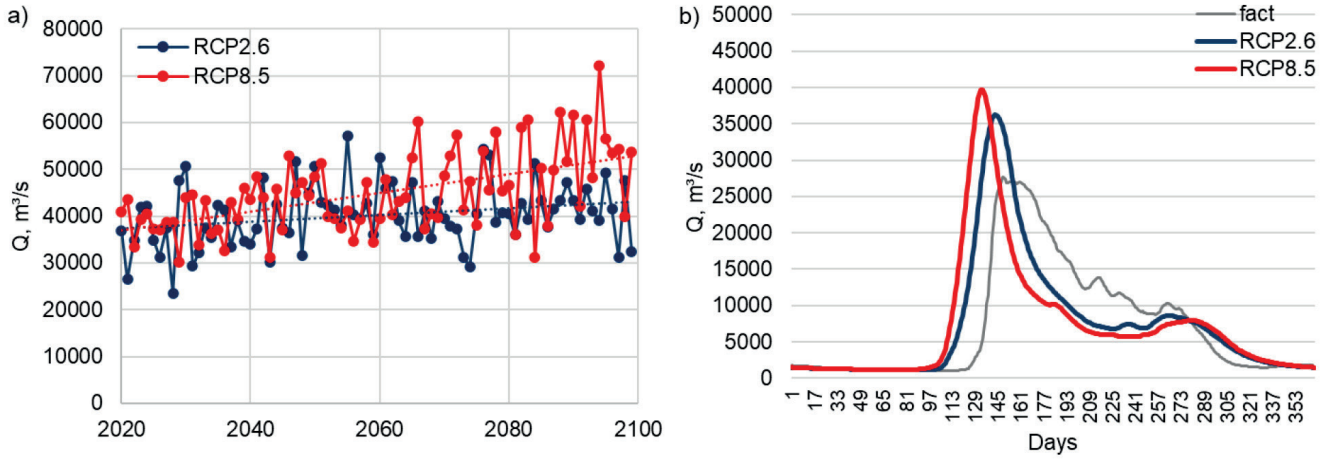

Fig. 4. Maximum discharge based on modeling results (a) and multiyear averaged predicted runoff hydrographs obtained from the ECOMAG model using data from the global climate model MIROC-ESM-CHEM for the middle of the XXI century (b), Lena River (Tabaga) for two climatic scenarios

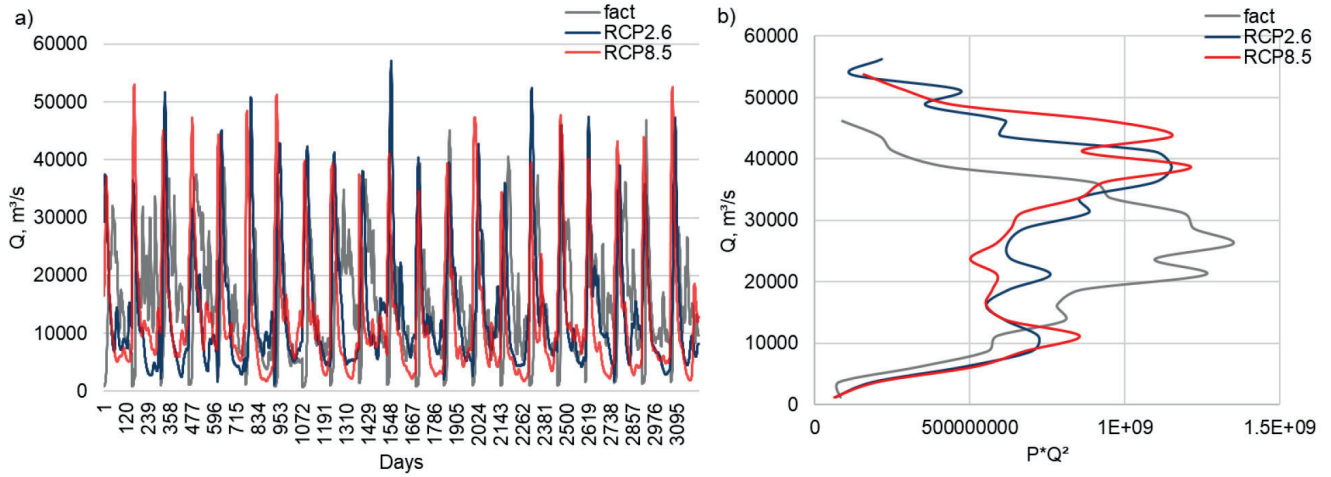

Fig. 5. Predicted runoff hydrographs derived from the ECOMAG model using data from the global climate model MIROC-ESM-CHEM, used as input data for assessing trends in changes in channel reshapes (a); channel-forming water discharge in the present period and under climate change under RCP2.5 and RCP8.5 scenarios simulated with MIROC-ESM-CHEM climate model data (b)

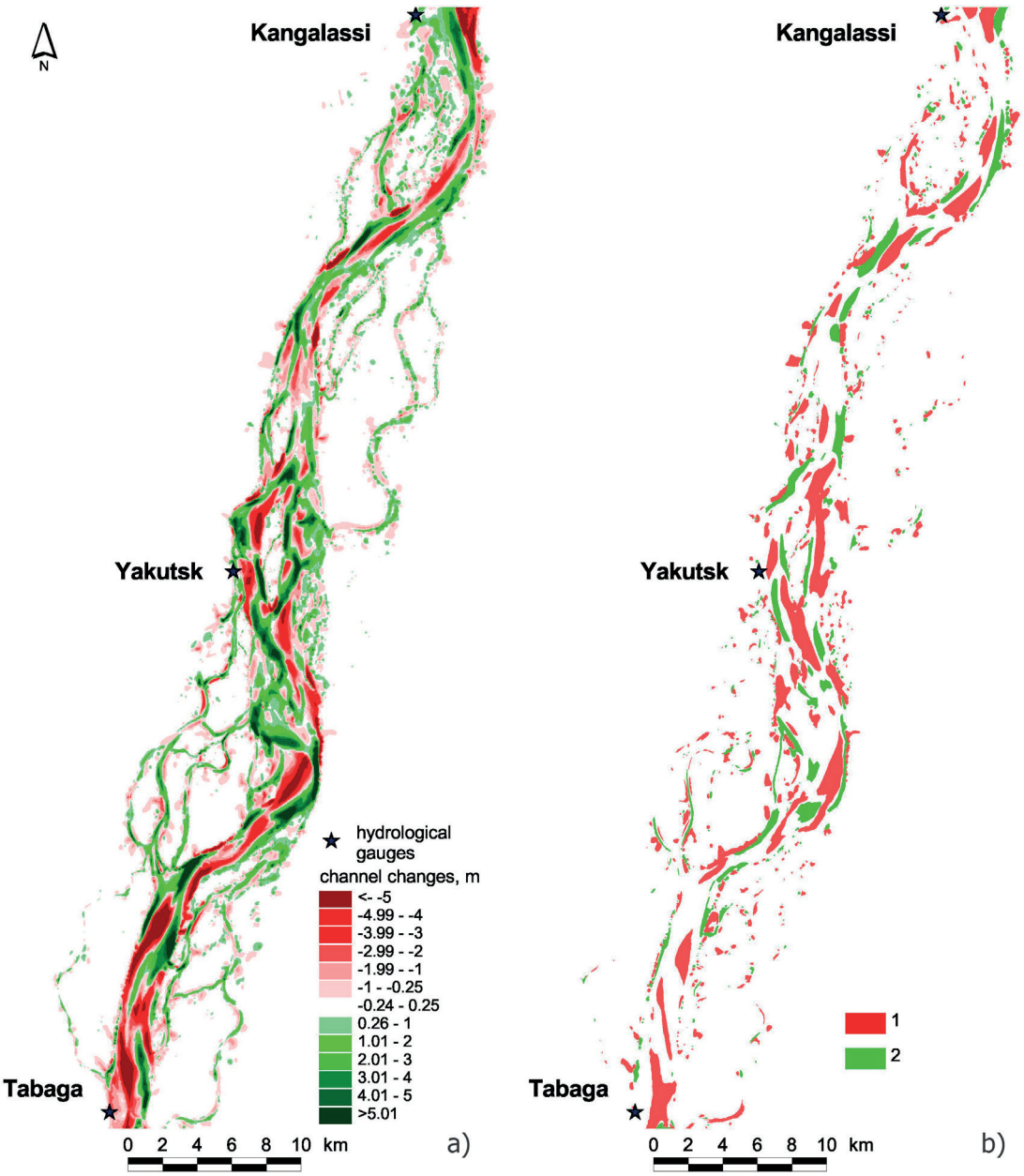

Fig. 6. Projected channel changes for scenario 3 (under RCP8.5 runoff input) (a); zones of negative (1) and positive (2) differences (more than 1 m) between final channel bottom from scenario 3 (under RCP8.5 runoff input) in comparison with scenario 1 based on modern runoff after 20-year period of channel deformations (b)

Buorylarskaya branch by the end of the 20-year forecast period (Fig. 7a). Under scenario RCP8.5, the Adamovskaya and Buorylarskaya branches retain almost equal water capacity under the maximum discharge during the whole forecast period. However, there is a positive trend is the growth of low-water discharge in the Adamovskaya branch (Fig. 7b), which will favourably affect the situation with water supply in Yakutsk.

DISCUSSIONS

Comparison of modelled bottom changes with the observed ones for the period 2009-2015 has demonstrated that in the 70 % of channel grid sells model adequately reproduce the erosion and deposition trends. In connection with the novelty of such studies for large sections of lowland rivers, these results should be considered as positive. At the same time, the use of a hydrodynamic model to reproduce channel evolution has a number of limitations. In general, the accuracy of channel changes estimates based on modelling methods is determined by a number of objective factors. The most important factors are:

- Accuracy of hydrometeorological scenarios selection for the period under study (including annual runoff hydrographs), taking into account the peculiarities of ice phenomena passage, etc;
- Variability of the river channel evolution process itself (occurrence of so-called bifurcations of the solution). It is well known that repeated replication of the same physical experiment with a deformable bed under identical initial and boundary conditions can lead to different results;
- Difficulty in taking into account in the modelling, for objective and subjective reasons (inadequacy and inaccuracy of the initial data, complexity of a number of physical processes, etc.), a number of factors that significantly influence the process of evolution of the river channel (heterogeneity of the bed materials; presence in some areas of an underlying surface that is difficult to erode; presence of various types of vegetation that hinder erosion; presence of permafrost and frozen ground after winter);
- Difficulty in accounting for bank erosion and planform changes.

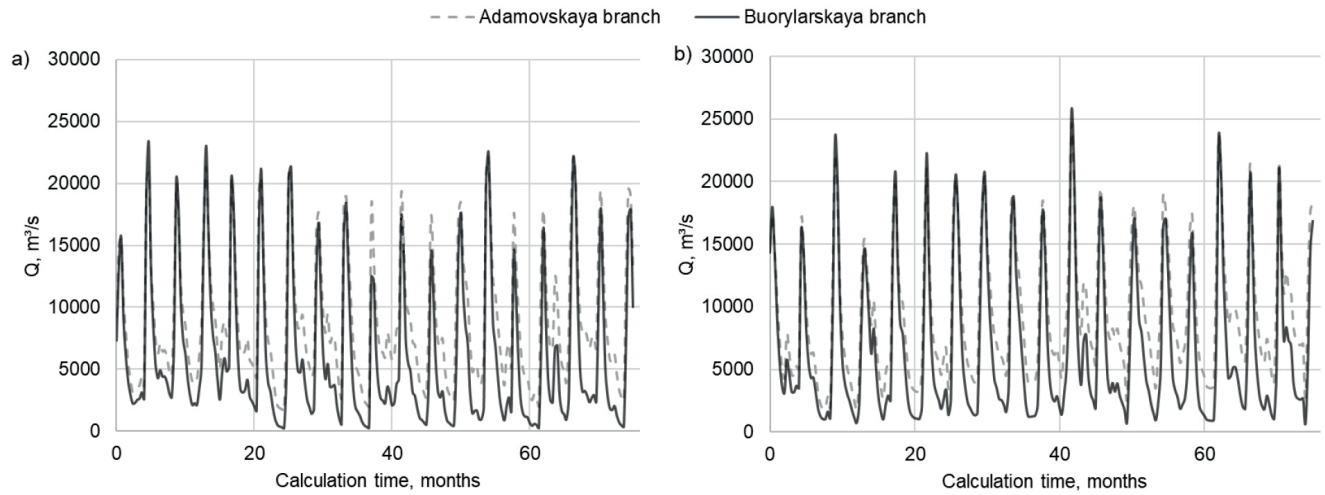

Fig. 7. Discharge in the Adamovskaya and Buorylarskaya branches under modeling based on predicted hydrographs: a) under the RCP2.6 scenario, b) under the RCP8.5 scenario

For the Lena River section under study discrepancies of simulation results with observed one in some sections is connected with the determining role of planform changes there. The further development of the model should take into account planform channel deformation block improvement. More attention should be pay also for the ice-covered period and ice jams periods, for which channel bottom changes have not been investigated enough.

In case of climate projection, the complex consideration of mentioned above factors, in particular planform changes due to bank erosion and permafrost degradation, is currently difficult to implement in practice. Long-term simulations of channel evolution (over a period of more than 50 years) without accurate estimations of planform changes can lead to unrealistic results.

Possibility to consider changing of the input hydrographs due to climate change is demonstrated in this work. The obtained estimates of changes in the hydrographs of the Lena River at Tabaga gauge for the period of climate forecast have shown, that simple extrapolation on the basis of existing trends does not give an idea of changes in the shape of hydrographs and, as a consequence, changes in the range of channel-forming discharges. It is also shown, that due to the change of channel-forming discharges, new local areas of erosion occur during peak flows, especially near the banks.

Also it will be important to take into considerations further the contribution of the catchment component of sediment load, to improve the modelling approach for simulation of the river channel evolution. Economic development of the area and intensification of erosion due to thawing permafrost under different climate warming scenarios will increase the contribution of sediment inflow from the catchment to the Lena River channel. According to (Maltsev and Ivanov, 2022), soil erosion losses in the catchment near the city of Yakutsk have increased by 4% over the last decade. This additional material may influence channel incision and redistribution of runoff along the branches.

CONCLUSION

The numerical two-dimensional hydrodynamic model of the Lena River near Yakutsk city was developed, calibrated, and verified using field data. The model successfully reproduce the distribution of water discharges among the channels, the water level regime for a long-term period and zones of inundation.

Comparison of modelled bottom changes with the observed ones for the period 2009-2016 has demonstrated that in the 70 % of channel grid sells model adequately reproduce the erosion and deposition trends. The aim of the future directions of the study is further improving of modeling, taking into account planform changes, ice cover, permafrost and contribution of the catchment component of sediment load.

The obtained estimates of changes in the hydrographs of the Lena River at Tabaga gauge for the period of climate forecast have shown, that simple extrapolation on the basis of existing trends does not give an idea of changes in the range of channel-forming discharges and consequently in the channel evolution over long-term period. In this case, an integrated approach, described in the paper, using input hydrographs from the runoff formation model offers a number of advantages for a better-grounded choice of simulations scenarios.

REFERENCES

Aleksyuk, A.I. and Belikov, V.V. (2017). Simulation of shallow water flow with areas and bottom discontinuities, Computational Mathematics and Mathematical Physics, Vol. 57, no. 2, p. 318–339. DOI: 10.1134/s0965542517020026, 2017.

Belikov, V.V. and Aleksyuk, A.I. (2020). Modeli melkoi vody v zadachakh rechnoi gidrodinamiki (Shallow-Water Models in Problems of River Hydrodynamics), Moscow: RAN, ISBN 978-5-907036-22-2, 346p.

Belikov, V.V., Aleksyuk, A.I., Borisova, N.M., Vasil'eva E. S. and Glotko A.V. (2023). Experience in Numerical Hydrodynamic Simulation of Long River Reaches. Water Resour 50, 465–481. https://doi.org/10.1134/S0097807823040036

Belikov, V.V., Zaitsev, A.A. and Militeev, A.N. (2002). Mathematical modeling of complex sections of large rivers channels, Water resources, V. 29, № 6, p. 698–705. (in Russian)

Borshchenko E., Chalov R. (2010). Channel-forming water flow rates and morphodynamics of river channels in the Russian part of the Amur basin. Geography and Natural Resources. 31. 148-158. 10.1016/j.gnr.2010.06.010.

Chalov R.S. (1987). Channel-forming water discharges and their significance for the study of channel processes in rivers. Dynamics of channel flows. Collection of scientific papers (interuniversity). LPI named after M.I. Kalinin Leningrad, p 103-108

Chalov, R.S., Kirik, OM., Ilyasov, A.K. and Botavin D.V. (2012).Yakutsk water junction on the Lena river: problems of channel processes, history, modern times, prospects, management possibilities, Water Industry of Russia: problems, technologies, management, № 3, p. 44–56 (in Russian).

Chalov, R.S., Zavadsky, A.S., Ruleva, S.N., Kirik, O.M., Prokop'ev, V.P., Androsov, I.M. and Sakharov, A.I. (2016). Morphology, deformations, temporary changes in the channel of the Lena river and their influence on the economic infrastructure in the Yakutsk region, Geomorphology, № 3, p. 22–35 (in Russian).

Gamal H. El Saeed, Neveen A. Badway, Hossam M. Elsersawy and Fatma S. Ahmed (2020). Evaluate the Nile River Confluence Morphological Changes on the Shear Layer// Journal of Scientific and Engineering Research, 7(2):220-229

Gelfan, A.N., Frolova, N.L., Magritskii, D.V., Kireeva, M.B., Grigor'ev, V.Yu., Motovilov, Yu.G. and Gusev, E.M.(2021) Effect of climate changes on the annual and maximal runoff of the Russian rivers: assessment and forecasts, Fundam. Prikl. Klimatol., vol. 7, no. 1, pp. 36–79.

Golovlyov, P., Kornilova, E., Krylenko, I., Belikov, V., Zavadskii, A., Fingert, E., Borisova, N., and Morozova, E.(2019) Numerical modeling and forecast of channel changes on the river Lena near city Yakutsk, Proc. IAHS, 381, 65–71, https://doi.org/10.5194/piahs-381-65-2019.

Grimaldi, S., Schumann, G. J.-P., Shokri, A., Walker, J. P. and Pauwels, V. R. N. (2019). Challenges, opportunities and pitfalls for global coupled hydrologic-hydraulic modeling of floods. Water Resources Research, 55, 5277–5300. https://doi.org/10.1029/2018WR024289

Guerrero, M., Latosinski, F., Nones, M., Szupiany, R. N., Re, M. and Gaeta, M. G. (2015). A sediment fluxes investigation for the 2-D modelling of large river morphodynamics. Advances in Water Resources, 81, 186–198. Doi:10.1016/j.advwatres.2015.01.017

Horvat, Z, Horvat, M. and Spasojevic, M. (2015). Two dimensional river flow and sediment transport model. Environmental Fluid Mechanics. 15. 595-625. 10.1007/s10652-014-9375-y.

Jodhani, K. H., Patel, D. and Madhavan, N. (2021). A review on analysis of flood modelling using different numerical models. Materials Today: Proceedings. doi:10.1016/j.matpr.2021.07.4

Kornilova, E.D., Krylenko, I.N., Golovlyov, P.P., Sazonov, A.A. and Nikitsky, A.N. (2018). Verification of the two-dimensional hydrodynamic model of the Lena River near Yakutsk according to time-based space imagery data, Modern problems of remote sensing of the Earth from space, V. 15, № 5, p. 169 - 178. (in Russian). DOI: 10.21046/2070-7401-2018-15-5-169-178

Krylenko, I.N. (2023) Evaluating Inundation Characteristics under Climate Changes. Water Resour 50, 577–582. https://doi.org/10.1134/S0097807823040152

Maltsev, K. and Ivanov, M. (2022). Comparative Study on Sediment Delivery from Two Small Catchments within the Lena River, Siberia. Water. 14, 3055. https://doi.org/10.3390/w14193055

Motovilov Y.G. (2016) Hydrological simulation of river basins at different spatial scales: 1. Generalization and averaging algorithms. Water Resour 43(3):429-437. https://doi.org/10.1134/S0097807816030118

Nones, M., Guerrero, M. and Ronco, P. (2014). Opportunities from low-resolution modelling of river morphology in remote parts of the world, Earth Surf. Dynam., 2, 9–19, https://doi.org/10.5194/esurf-2 9-2014.

Sloff, K. and Mosselman, E. (2012). Bifurcation modelling in a meandering gravel-sand bed river. Earth Surface Processes and Landforms, 37(14), 1556–1566. doi:10.1002/esp.3305

Vijay, R., Sargoankar, A. and Gupta, A. (2007). Hydrodynamic Simulation of River Yamuna for Riverbed Assessment: A Case Study of Delhi Region. Environ Monit Assess 130, 381–387. https://doi.org/10.1007/s10661-006-9405-4

Zaitsev, A.A. and Chalov, R.S. (1989). Channel processes and regulation of the river Lena in the area of Yakutsk, Water resources, № 5, pp. 75-81 (in Russian).

Zhang, W., Xu, Y., Wang, Y. and Peng, H. (2014) Modeling Sediment Transport and River Bed Evolution in River System. Journal of Clean Energy Technologies, Vol. 2, No. 2

Check for updates

CC BY

RESEARCH PAPER

LEVELS, D,S-PATTERNS AND SOURCE IDENTIFICATION OF METALS AND METALLOIDS IN RIVER WATERS OF THE GAS-PRODUCING REGION IN THE NORTH OF WESTERN SIBERIA (PUR RIVER BASIN)

M. Lychagin*, S. Porsheva, D. Sokolov, O. Erina, E. Krastyn, V. Efimov, T. Dubrovskaya, D. Kotov,N. Kasimov

Lomonosov Moscow State University, GSP-1, Leninskie Gory, Moscow, 119991, Russian Federation

***Corresponding author:** lychagin@geogr.msu.ru

Received: November 21st 2024 / Accepted: November 22nd 2024 / Published: December 31st 2024

https://doi.org/10.24057/2071-9388-2024-3741

ABSTRACT. The study aimed to determine the levels, spatial and temporal variability of the concentrations, and forms of migration of metals and metalloids in the Pur River basin, which is one of the most important oil and gas producing areas in the north of Western Siberia. The study is based on the results of hydrological and geochemical studies conducted in 2021-2023 during the summer low water and spring flood periods. We found generally low content of dissolved metals and metalloids in water of the Pur River and its tributaries, not exceeding the world average values, except for Fe and Zn. Levels of metals and metalloids in the suspended matter were also lower than the global averages, except for Fe and Mn. Changes in the content of dissolved and suspended forms of metals caused by hydroclimatic factors and anthropogenic impact were determined. Near cities, the maximum concentrations of Zn, Cd, Cu and other metals in suspended matter are 3-5 and more times higher than the baseline values. Analysis of EF values for median contents allowed to identify the association of elements with considerable and high enrichment in suspended matter: Fe, Mn, Sb, As, Cd and Zn. The maximum EF values ranged from 25 to 45, which corresponds to very high degree of enrichment. Three groups of chemical elements were identified on the basis of D,S-analysis.

KEYWORDS: Arctic, hydrological and geochemical research, surface water, dissolved, suspended, pollution, enrichment, sources, natural, anthropogenic

CITATION: M. Lychagin*, S. Porsheva, D. Sokolov, O. Erina, E. Krastyn, V. Efimov, T. Dubrovskaya, D. Kotov, N. Kasimov (2024). Levels, D,S-Patterns And Source Identification Of Metals And Metalloids In River Waters Of The Gas-Producing Region In The North Of Western Siberia (Pur River Basin). Geography, Environment, Sustainability, 4(17), 121-145
https://doi.org/10.24057/2071-9388-2024-3741

ACKNOWLEDGEMENTS: This study was supported by the Russian Science Foundation (Project no. 22-17-00102). The results of field studies obtained under the Russian Geographical Society grant "Yamal Meridian" were used.

Conflict of interests: The authors reported no potential conflict of interest.

INTRODUCTION

Over recent years, attention to the ecological state of rivers in the Arctic basin has been growing due to climate change and increasing human impact. Climatic changes contribute to a significant increase in river runoff, which in turn leads to an increase in chemical fluxes into the seas of the Arctic Ocean (Chalov et al., 2023; Chupakov et al., 2020; Demina et al., 2010; Gebhardt et al., 2004; Gordeev et al., 2024; Hartwell et al., 2020). Industrial mining, urban development, the construction of roads and other infrastructures often has a negative impact on the state of river basins. Arctic river ecosystems are particularly vulnerable to anthropogenic impacts in comparison to temperate rivers (Barker et al., 2014; Garnier et al., 1996; Krickov et al., 2019).

Metals and metalloids (MMs) can enter the environment from natural sources such as the weathering of soil and bedrock, as well as through human activities such as mining, industry and agriculture. Generally, metals enter aquatic systems through washout from surface soils, diffuse inflow from groundwater, polluted sediments, leaching from agricultural areas and waste ponds, failure of waste ponds, and discharge of industrial and mining effluents (Hudson-Edwards, 2003; Inam et al., 2011; Macklin et al., 2006; Mighanetara et al., 2009). Natural factors, including the mobilization of sediment material through bank and channel erosion can dominate over pollutant transport in certain conditions (Chalov et al., 2015). Due to their inability to biodegrade, metals in the aquatic environment can threaten ecosystems long after their initial input.

An increasing number of studies confirm that the migration patterns of metals largely determine their mobility, bioavailability and toxicity in the aquatic environment (Ali et al., 2019; de Paiva Magalhães et al., 2015; Fytianos, 2001; Landner and Reuther, 2005; Miranda et al., 2021; Violante et al., 2010; Wu et al., 2016). Understanding the processes that control the migration patterns and

transport of metals in a river basin is key to managing this ecosystem. For example, aquatic migration of metals adsorbed on suspended sediments can be significantly slower than metals in dissolved form (S. Chalov et al., 2020; Thorslund et al., 2012).

In recent decades, the number of publications on the content of metals and metalloids in dissolved and suspended forms in river waters has increased dramatically, which is largely due to the development of analytical methods, especially the use of ICP-MS method, which allows the high accuracy determination of a wide range of chemical elements in microquantities. The average content of dissolved (Gaillardet et al., 2014) and suspended forms of elements in the world's rivers has been assessed (V. Savenko, 2006; Viers et al., 2009). There is increasing attention being paid to the ratio of dissolved to suspended forms of metals and metalloids. At the basin level, using the example of the Selenga River, the largest tributary of Lake Baikal, it has been shown that the ratio of element migration forms is determined mainly by the properties of the elements themselves, hydroclimatic conditions and anthropogenic load (Kasimov et al., 2020).

Over the last few decades, an extensive database on the major ions composition and ionic runoff of the world's rivers (Meybeck, 2003) and the Arctic Ocean basin (McClelland et al., 2023) has been collected. However relatively few data on the content and forms of trace elements in Arctic rivers are still available. The paper (Gordeev et al., 2024) summarizes the results of the studies carried out on the largest rivers of the Russian Arctic (Ob, Yenisei, Lena, Kolyma) in 2004-2006. It was concluded that the content of most elements in Arctic rivers is significantly lower than the global average. The assessment of the fluxes of dissolved substances based on the average content of elements and the average annual water flow showed that the Lena River is characterized by the largest flow into the Arctic Ocean, followed by the Yenisei, Ob and Kolyma.

A review on the dissolved forms of chemical elements in the rivers of the Russian Arctic is presented in the paper of (Savenko and Savenko, 2024), who summarized the results of river water analysis obtained by ICP-MS over the last 30 years. The study, which covered rivers in both the Asian and European parts of the Russian Federation, confirmed that the content of most elements in Arctic rivers is close to or significantly below the global average. In the northern part of Western Siberia there is still a lack of data on dissolved forms of elements in most rivers except for the Ob River (Kolesnichenko et al., 2021; Pokrovsky et al., 2015, 2016). The content of metals and metalloids in suspended form in the rivers of this region has been still poorly studied. In one of the few works (Soromotin et al., 2022) it was noted that the content of metals and metalloids in the river sediments of the Ob River estuary is low due to their low content in peat horizons of soils in the catchment areas.

The key factors determining the features of spatial and temporal variability of metal contents and fluxes at the river basin level have been still poorly understood. The lack of detailed information at the basin level makes it impossible to assess the anthropogenic impact on the natural environment and to predict the response of the water system to future climatic changes and the industrial development in the Arctic region. It is difficult to solve these problems at the basin level of the largest Arctic rivers, so in this study the Pur River basin, located between the Ob River in the west and the Yenisei River in the east, was chosen as a model object.

The Pur River basin is one of the most important oil and gas producing areas in the north of Western Siberia with the Urengoy field located on its territory. This field is the world's third largest in terms of explored natural gas reserves, as well as more than 10 other large oil and gas fields. The rivers in the Pur River basin have been experiencing significant anthropogenic impacts over the past few decades due to the influence of the fields themselves, as well as the settlements that are centers of water pollution, oil and gas infrastructure and refining industry, and diffuse pollution during snowmelt and rainfall. The impact of the oil and gas complex on river systems is complex and includes transformation of the catchment area, erosion, input of pollutants from atmospheric deposition, etc. (Moskovchenko, 1998).

The first task of the study was to determine the levels, spatial and temporal variability of dissolved and suspended forms of metals and metalloids in the Pur River and its tributaries. A particular attention was given to the studying of the Evoyakha River, a left tributary of the Pur River, which flows through Novy Urengoy, the largest center of anthropogenic impact in the basin. The second task was to identify the predominant forms of metal and metalloid migration and their variability on the basis of D,S – analysis. The third task was to assess human-induced changes in content of metals and metalloids in river waters and identify their main natural and anthropogenic sources. The study is based on the results of 5 field campaigns conducted in 2021-2023 during the summer low water and spring flood periods (Fig. 1).

STUDY AREA

The Pur River basin is a lowland plain with altitude less than 50 meters a.s.l. The river channels are weakly incised and highly sinuous, flow among low banks, meander in wide valleys, forming branches and channels (Fig. 2). The lithology is formed by siltstones, clays and marls of the Permian system overlain by Quaternary alluvial-marine, lake-alluvial and alluvial Quaternary sediments of different grain size. The weak erosional dissection of the watershed combined with the close occurrence of permafrost results in waterlogging of soils (Kolesnichenko et al., 2021).

The climate of the Pur River basin is continental subarctic, with long winters (up to 8 months), short summers, strong winds, and shallow snow cover. The average annual air temperature is about -5°C. The annual amplitude of temperatures is 35-40°C. The natural features of the territory are largely determined by permafrost, which is mainly discontinuous, but in the north of the basin becomes continuous (Pokrovsky et al., 2015). The topography is extremely flat, and lithology is fairly homogeneous (peat, sand and silt). Soils are presented mainly by Histosols and Histic Gleysols, in the southern areas Gleyic Albic Podzols are predominant. Northern taiga landscapes prevail in the southern part of the basin, while forest-tundra landscapes prevail in the northern part. The most common trees are dwarf birches, polar willows, spruce, fir and larch. Mosses and lichens are common, as well as small shrubs.

The Pur River is 389 km long and has a basin area of 112,000 km^2. The Pur is formed at the confluence of the Pyakupur and Aivasedapur rivers, which flow from the northern slope of the Siberian Uvals. In its lower reaches, the river forms a 21 km wide delta and flows into the Taz Bay of the Kara Sea. The Pur has a large number of tributaries, among which the Evoyakha River, which flows through the Urengoyskoye field and the urban area of Novy Urengoy, is the most affected by anthropogenic pressure.

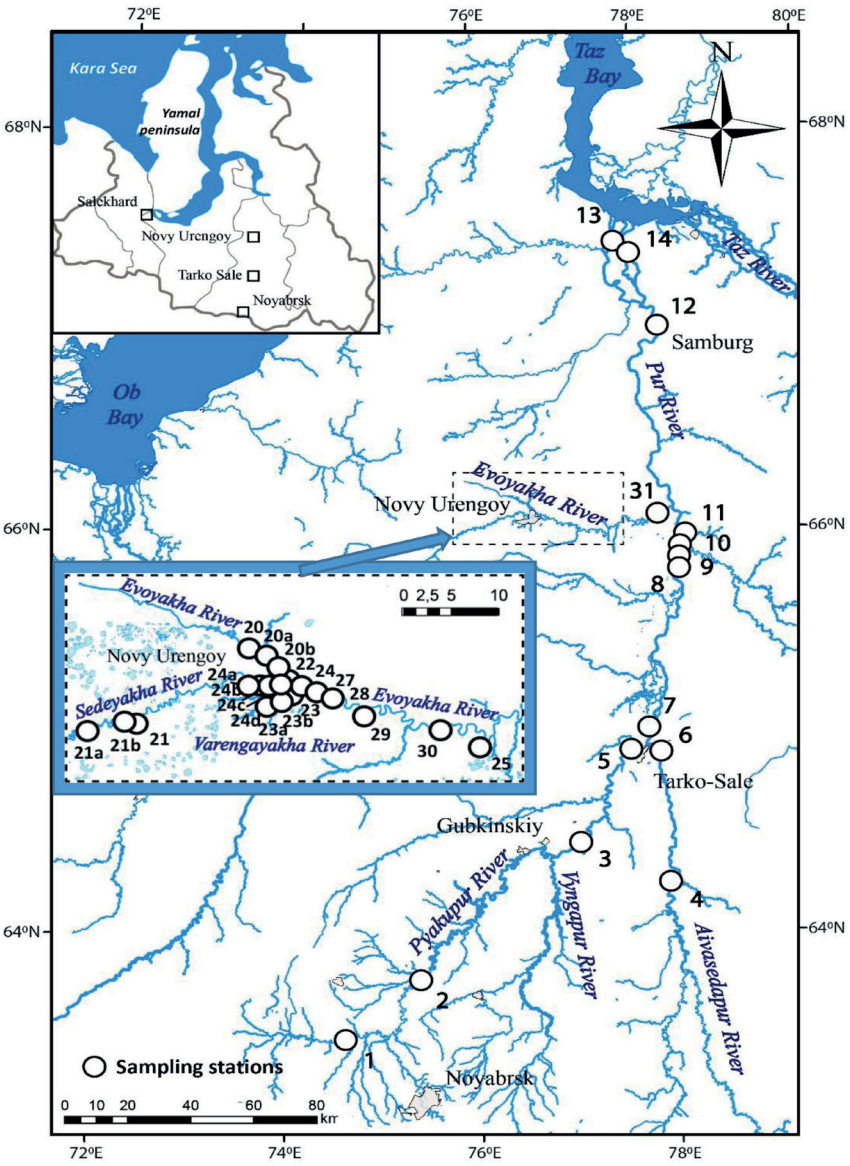

Fig. 1. Study area

Fig. 2. Pur River during snowmelt flood, June 2022

There are a large number of rivers and lakes in the Pur River basin. The density of the river network is 0.38 km/km^2. The total number of lakes exceeds 85,000. Many lakes are directly connected with the river network. The rivers of the Pur basin have mixed feeding with the predominance of ground and marsh feeding, with runoff mainly in the warm season. The rivers of the Pur basin are covered with ice for most of the year. The period of open water even in the warmest years does not exceed 5 months in the upper reaches and 4.5 months in the lower reaches. The appearance of stable ice cover occurs at the end of the first or beginning of the second part of October. The ice cover on the Pur River breaks up in late May to early June. After the ice drift, the water temperature rises rapidly and with the end of the spring level rise, is higher than the air temperature; this remains until the following spring (Popov, 2013).

The rivers of the area feature consistent annual runoff. The flow is formed with sufficient (more than 600 mm) annual precipitation and low evaporation. High wet-land (50%) and lacustrine (10%) areas have an important impact on the runoff and its variability both within a year and in the multi-year dynamics. The average annual flow rate of the rivers into the basin is 9-10 l/sec·km^2. The coefficient of variation of annual runoff decreases from south to north from 0.15 to 0.10 (Agbalyan et al., 2016).

The main flow (57-63% of the annual runoff) occurs in spring and summer, 21-25% in autumn, and 18-20% in winter, depending on the year's water availability. Highest flow occurs during the spring flood, which starts in May-June and lasts for 40-50 days in small rivers. The highest discharge is observed during this period, and lasts for between 1-5 days. Floods sharply intensify all channel processes, ice drift, an increase in river turbidity, and an increase in sediment runoff, and the flushing of pollutants from catchments, while stagnant and heavily polluted old lakes, on the contrary, are washed out, only flowing for a short period. Rain floods are observed almost every year. The volume of total runoff of the largest rain floods is 5-40%, in some years - up to a volume of 73% during the spring runoff. Maximum discharges reach 10-50% of the magnitude of spring maxima. Periods of low flow are common for both summer-autumn and winter seasons. The period of low flow from the end of the flood to the beginning of ice events is recognized as the summer-autumn low-water period. The winter low-water period is stable and continuous, much lower than the summer period.

The Pur River waters have low turbidity, ranging from 9 to 28 mg/l. The sediment flux is 6.5 tons/year from 1 km^2 of the catchment area. The runoff of dissolved substances in water is almost 2.5 times greater than the particulate runoff (Uvarova, 2011).

The main sources of river water pollution in the Pur basin are oil and gas production facilities and cities, including Novy Urengoy, which is the center of a large gas-producing region. The area of the city is surrounded by developed oil and gas fields, the nearest one - Urengoyskoye - is located about 10 km away from the city. The Novourengoy Gas Chemical Complex is located 30 km south-east of the city. Its production infrastructure includes a liquefied gas storage facility, flare units, reagent warehouses, and a waste utilization complex. The city also has 15 heating plants, various food industry facilities, public utilities and transportation facilities.

Field sampling and laboratory processing

The study is based on the results of 5 field campaigns conducted in 2021 - 2023 during different phases of the water regime: in August 2021 during the summer low flow, in 2022 and 2023 during the spring flood (May-June) and summer-autumn low flow period (August-September). Samples were taken along the entire length of the Pur River from its head at the confluence of the Pyakupur River and the Ayvasedapur River to its mouth. Sampling stations were located upstream and downstream the urban areas of Tarko-Sale, Korotchaevo settlement, Samburg, Urengoy, as well as upstream and downstream of major tributaries (Fig. 1). A special attention was given to the Evoyakha River impacted by the of Novy Urengoy. In total, the measurements covered more than 30 sites, and 140 water and river sediment samples were collected (Supplementary 1).

Water discharge and velocities were measured using a SonTek M9 acoustic Doppler current profiler mounted on a PVC raft, from motorized PVC boat, or wading if the depth was less than 0.8 m. Water samples were taken from the surface layer into pre-prepared 1.5-liter bottles. Measurement of the vertical distribution of physicochemical parameters of the water column at several stations showed the absence of significant gradients resulting from turbulent mixing, thus allowing the surface samples to be considered representative. Electrical conductivity, pH and dissolved oxygen content were also measured in situ. River water samples were filtered on a vacuum system using "Millipore" membrane filters with a pore diameter of 0.45 μm. After filtration, all filters were dried and reweighed for further determination of the amount of suspended material.

The particle size distribution of the suspended matter was determined in the laboratory of the Department of Landscape Geochemistry and Soil Geography, Faculty of Geography, Moscow State University using a laser particle analyzer "Fritsch Analysette 22 MicroTec Plus". The concentration of major ions Ca^{2+}, Mg^{2+}, Na^{+}, K^{+}, HCO_3^{-}, Cl^{-}, SO_4^{2-} in river water was determined by capillary electrophoresis using the KAPEL®-105M system (Lumex Group of Companies).

The concentration of chemical elements in river water and suspended matter was determined on an Elan-6100 inductively coupled plasma mass spectrometer and an OPTIMA 4300 inductively coupled plasma optical emission spectrometer (Perkin Elmer) at the All-Russian Research Institute of Mineral Raw Materials named after N.M. Fedorovsky (Moscow). In this work we used the results of analysis of Al, Fe, Mn, Ni, Co, V, Cr, Cu, Zn, Pb, Cd, As, Sb, Sn, Bi, U, Sr, Ba, and Rb.

Data analysis

Statistical analysis of the obtained dataset included calculation of median values, standard deviations and coefficients of variation. Due to the high variability of the contents for a number of elements, the regional geochemical features of the river basins were studied on the basis of mean and median values. Calculations were carried out separately for the Pur River and its main tributary Evoyakha River, which is caused by the specific natural conditions and significant anthropogenic load in its basin. The results of replicate river water sampling were used to calculate mean and median values in each hydrological season for both rivers.

The features of MMs accumulation in dissolved forms were identified on the basis of concentration factors Cf - ratios of element contents in the studied sites to average

contents in rivers of the world (Gaillardet et al., 2014) and rivers of the Kara Sea basin (Savenko et al., 2020). For suspended matter, Cf values were calculated relative to global average values according to (Viers et al., 2009).

The Enrichment factor (EF) was calculated to assess the contamination of river sediment. EF calculation allows to compensate for differences in the content of rare elements in rocks, soils and sediments caused by differences in their mineralogical composition and grain size (Horowitz, 1986) and to assess the anthropogenic contribution to pollution of solid phase components of the environment - soils, road dust, bottom sediments and suspended matter (Barbiery, 2016; Ediagbonya et al., 2015; Ryan and Windom, 1988; Vlasov et al., 2020). EF is calculated as the ratio of the metal content in the studied sample to a certain metal (reference) in the same sample, to a similar ratio in the Earth's crust:

$$EF = (Ci/Cref)_{Sample} / (Ci/Cref)_{UCC}$$

where *Ci* and *Cref* are the contents of the studied and reference elements, respectively, *UCC* – upper continental crust (Rudnick and Gao, 2013).

D,S-pattern of river waters was determined basing on the DS coefficient, which is a ratio of the volumetric concentration of suspended forms Cvs of an element to the total concentration of suspended and dissolved Cvd forms: *DS =Cvs/(Cvs+Cvd)*, % (Kasimov et al., 2020). The elements were ranking by decreasing DS ratio (%), grouping into quartiles (<25%, 25-50%, 50-75%, >75%) and presented in a matrix form. The prevalence of undissolved forms of the element is characterized by DS > 50 %, dissolved forms < 50 %.

The identification of major factors controlling MMs content in suspended matter and their contribution to the total values was performed using PCA/APCS-MLR. Two data sets for the Pur and Evoyakha rivers were used in the analysis, they included concentrations of 20 metals and metalloids at all sampling points. Z-normalization was applied prior to analysis:

$$Z_{ik} = \left(C_{ik} - \overline{C}_i\right) / \sigma_i$$

where C_{ik} is the concentration of the i-th chemical element in sample *k*, $\overline{C}_i$ is the average concentration of the i-th element for all samples, and σi is the standard deviation of the i-th element.

The Varimax rotation method was used to simplify factor interpretation and reduce the number of items with high factor loadings. Only principal components (PCs) that explain more than 5% of the total variance of the data set with eigenvalues > 1 (Kaiser criterion) were used as factors. We used the PCA method with calculation of absolute principal component scores (APCS) and further application of multiple linear regressions (MLR) to estimate the contribution of sources to elemental concentrations. PCA/ APCS-MLR is a valuable method for identifying independent factors using eigenvector decomposition of the matrix of pairwise correlations between compound concentrations (Thurston et al. 2011). APCS allows the total mass of each element to be distributed among the PCA-derived components, i.e., among the different sources. Detailed methodology can be found in (Liang et al. 2019; Chen et al. 2021). The main steps of the approach are summarized below.

Since the factor scores obtained by PCA are normalized, with the mean equal to zero and the standard deviation equal to one, the true value for each factor score was calculated by introducing an artificial sample with concentrations equal to zero for all variables. For this additional sample, the normalized values of the PTE concentrations would be as follows:

$$\left(Z_o\right)_i = \frac{0 - \overline{C}_i}{\sigma_i} = -\frac{\overline{C}_i}{\sigma_i}$$

The APCs for each component are then estimated by subtracting the coefficients for this artificial sample from the coefficients for each of the true samples. Regression of elemental concentration data to APC provides estimates of coefficients that convert APC to the mass source contribution of contaminants from each source for each sample. Source contributions to Ci can be calculated using MLR:

$$C_i = \varepsilon_{0i} + \sum \left(APCS_p \times \varepsilon_{pi}\right),\ p = 1, 2, \ldots, n$$

where ε_{0i} is the multiple regression crossover point for the i-th element, εpi is the multiple regression coefficient of source *p* for pollutant *i*, and $APCS_p$ is scaled value of the rotated coefficient p for the sample under consideration. $APCSp \times \varepsilon_{pi}$ represents the contribution of source *p* to C_i. Mean value of $APCSp \times \varepsilon_{pi}$ for all samples represents the average contribution of sources (Ma et al., 2021). APCS uncertainty (UNC, %) was calculated as follows:

$$UNC = \left(C_{meas} - C_{model}\right) / C_{meas} \times 100\,\%$$

where C_{meas} is measured concentration, C_{model} is the predicted concentration of the element based on the results PCA / APCS-MLR (Song et al., 2006).

RESULTS AND DISCUSSION

Hydrogeochemical conditions

The first field campaign was conducted in 2021 during the summer low water period from August 16 to August 30. In 2022, the expedition timed to the spring flood phase took place from May 23 to June 16, and to the summer-autumn low water period - from August 2 to 23. During the spring 2023 field campaign we managed to cover the period shortly after spring flood peak (Fig. 3). At the Urengoy station, the flood peak was observed during the first days of the survey, with initial measurements made on the day after its passing at a water level 2 cm below the peak, and final measurements made 8 days later at a water level 39 cm below the peak. The measured water discharges at the beginning and end of this period were 4440 and 3730 m³/s. The water discharge of the Pur River during the study period decreased in this station by 16% with a 37 cm drop in level.

During the 2023 summer expedition, there was a summer low flow. In mid-August, the water level at all three Roshydromet stations reached the minimum values. The exception is the Pur River - Samburg, where level increases (up to 1 m) were observed due to the steady wind. Discharge of the Pur River naturally increased from 24 m³/s in the upper reaches of the basin (Pyakupur River near Muravlenko) to 280 m³ /s in the Purpe district, 414-428 m³/s in the town of Tarko-Sale, 550-590 m³/s in the area between Korotchaevo and Urengoy, and 721 m³/s near the town of Samburg. Flow rates during the period of field campaigns at the flood recession in 2023 were close to those during the same period in 2022. Discharges during the low flow period in 2023 were on average 10-15% lower than in 2022. This is explained by weather conditions of the year and the later period of the expedition.

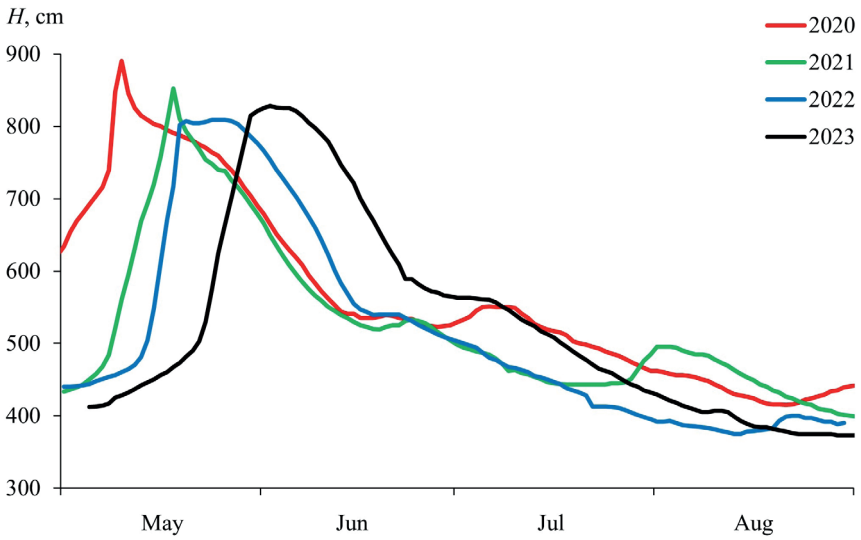

Fig. 3. Water level fluctuations (H, cm) in the station of the Pur River - Urengoy according to the Roshydromet gauging station

Rivers in the north of Western Siberia in general have low *mineralization*, which is due to the cold humid climate, widespread permafrost and fluvioglacial deposits of sandy and sandy loam composition. According to our data, the average mineralization of the Pur River water in the spring flood was 11 mg/l, during the summer low flow - 49 mg/l, which corresponds to the estimates for other large rivers of the region in the spring flood and summer-autumn low flow: Nadym River - 12 and 49 mg/l, Taz River - 35 and 62 mg/l, respectively.

During the spring flood of 2023, the Pur River mineralization was influenced by melt water inflow from the catchment and varied insignificantly along the river (Fig. 4). During the summer low flow period it increased approximately 4 times due to predominantly groundwater-derived baseflow. The maximum mineralization of 75 mg/l was observed downstream of Urengoy settlement near the right bank of the river (station 11b), where it is one and a half times higher than at the left bank (station 11a). It is caused by the impact of ship repair facilities, fuel and oil storage of the river port Urengoy, which is located on the right bank of the river above this station.

In the Evoyakha River, during the flood period mineralization of water was below 10 mg/l (average – 7.4 mg/l) and varied slightly from source to mouth This river catchment is dominated by permafrost soils, which do not thaw by the beginning of the flood, which defines the predominant role of snowmelt water in the hydrochemical runoff in this period. During low flow, the average mineralization increased to 26 mg/l due to rise of groundwater feeding. The highest mineralization up to 32 mg/l was observed downstream of Novy Urengoy due to the discharge of wastewater from the city sewage treatment plants and storm water from industrial sites.

For Na, K, Ca and Mg, a latitudinal distribution trend was established, consisting in a general decrease of their concentrations to the north (Supplementary 2). The lowest levels of major ions were observed in the Evoyakha River. This latitudinal trend is caused by a decrease in the share of groundwater supply and an increase in the share of snowmelt feeding as the area increases and the depth of permafrost decreases, as previously noted (Pokrovsky et al., 2015). The average pH value of river water during low flow periods is 7.3, while during floods it decreases to 5.5 due to a significant inflow of snowmelt water.

The particle size distribution of suspended matter in the Pur River basin is mainly dominated by sand particles larger than 50 μm, with an average share of 46%, while for fine particles smaller than 10 μm it is 21% (Fig. 5). The share of sand particles decreases to 40% during low water and increases to 54% during floods. In contrast, the share of PM_{10} particles increases to 23% during low water and decreases to 17% during floods. Changes in the particle size distribution of river suspended

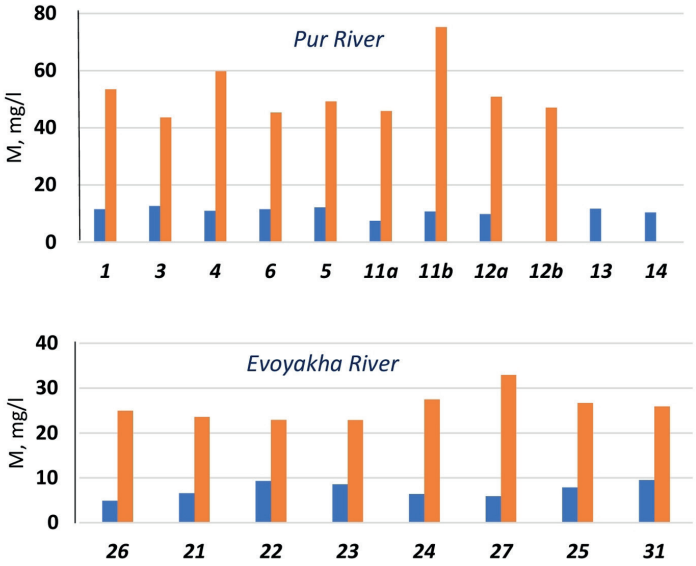

Fig. 4. Changes in water mineralization along the Pur River and Evoyakha River during spring flood (blue) and low flow (orange) periods in 2023; numbers of sampling stations correspond to the numbers in the Fig. 1

sediment naturally reflect changes in flow velocity and suspending capacity of the stream in different hydrological seasons. The average suspended matter diameter in the Pur River basin is about 70 μm, which is slightly less than the average size (83 μm) in rivers of different natural areas (Chalov and Efimov, 2021). This is explained by the lower ability of the Pur River to transport suspended material due to the small amplitude of altitude in its basin.

Dissolved forms of metals and metalloids in river waters

The Pur River and its main tributary, the Evoyakha River, are generally characterized by low levels of dissolved forms of metals and metalloids (Table 1), which is due to their low content in Quaternary sediments of predominantly light texture that comprise the catchments. Compared to global averages (Gaillardet et al., 2014), Fe and Zn contents are elevated in both rivers. The average Fe content in the Pur and Evoyakha rivers (140 μg/l) is 2 times higher than the global average and close to the average Fe content in the rivers of the Kara Sea basin - 180 μg/l (Savenko and Savenko, 2024). Iron accumulation in surface waters is a distinctive feature of Western Siberia (Gordeev et al., 2024; Kolesnichenko et al., 2021; Romanova and Samarin, 2019). The source of iron is peatland waters, feeding small rivers and streams in the study area. The average Zn content in the Pur River (3.1 μg/l) is 5 times higher than the global average (Gaillardet et al., 2014), but generally corresponds to the average for the rivers of the Kara Sea basin - 2.2 μg/l (Savenko and Savenko, 2024) and the lower reaches of the Ob and Taz Rivers - 4-7 μg/l (Pokrovsky et al., 2016; Soromotin et al., 2022). The levels of Ni, Co, Sb, Pb and Cd in the Pur River waters are close to the world average, while V, Cu, As, U, Ba and Rb are several times lower. Statistical analysis of the data revealed the highest variability (v>100%) for the content of Al, Fe, Mn, Co, Cu, Zn, Pb and Cd, caused apparently by the seasonal changes and anthropogenic impact.

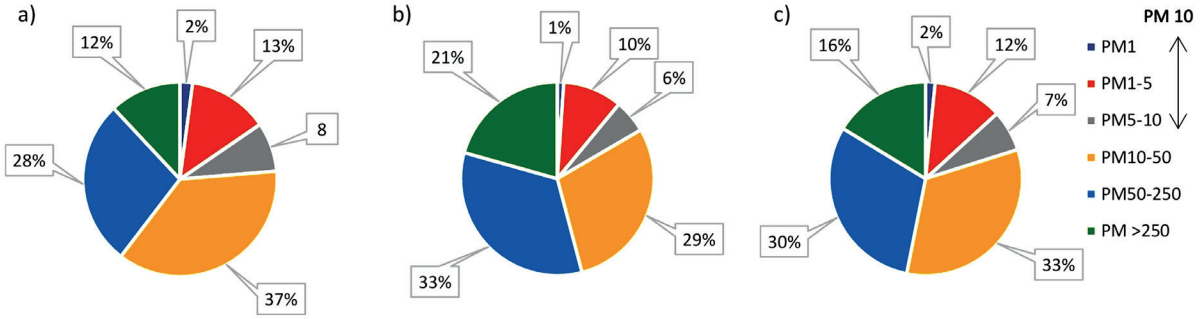

Fig. 5. The grain size distribution of river suspended matter in the Pur River basin: a) low flow; b) flooding; c) annual average

Table 1. Levels of dissolved forms of metals and metalloids in the Pur and Evoyakha rivers compared to the global average and regional background, μg/L

MMs	Pur River, n= 43					Evoyakha River, n=85					World Rivers[1]	Kara Sea Basin[2]	Pur River[3]
	median	mean	min	max	v%	median	mean	min	max	v%			
Al	4,5	25,3	0,35	**82**	118	23,5	27,8	1,6	**157**	85	32	17,7	35,6
Fe	**86***	141	3,0	**510**	110	**117**	**144**	10	**681**	93	66	180	568
Mn	1,4	20,4	0,12	**108**	165	8,0	41,6	0,3	**282**	123	34	22,2	52,4
Ni	0,54	0,65	0,23	**3,60**	79	1,3	1,43	0,06	**14,4**	107	0,8	1,03	1,04
Co	0,04	0,08	0,04	**0,37**	100	0,04	0,36	0,04	**3,74**	148	0,15	0,08	0,10
V	0,13	0,14	0,03	0,28	54	0,15	0,15	0,03	**1,06**	102	0,71	0,93	-
Cu	0,6	1,14	0,10	**11,0**	164	0,93	1,67	0,10	**19,0**	156	1,48	1,54	0,8
Zn	**2,6**	**3,09**	0,20	**21,0**	125	**3,8**	**4,66**	1,19	**19,4**	81	0,6	2,2	-
Pb	0,04	0,11	0,09	**1,20**	186	0,058	0,141	0,01	**2,90**	235	0,08	0,099	0,157
Cd	0,003	0,01	0,002	**0,096**	163	0,003	0,011	0,003	**0,094**	153	0,08	0,007	0,005
As	0,3	0,32	0,20	0,49	22	0,31	0,34	0,09	**0,93**	44	0,62	0,56	0,31
Sb	0,075	0,075	0,036	0,240	43	0,073	0,067	0,011	**0,143**	48	0,07	0,066	-
U	0,003	0,005	0,001	0,013	68	0,007	0,008	0,000	0,026	66	0,37	0,242	-
Sr	27,5	22,6	6,2	42,0	50	7,8	10,8	2,2	**75,0**	92	60	129	17,4
Ba	6,3	6,4	4,3	9,3	20	5,1	9	1,7	**242,7**	293	23	12,1	17,8
Rb	0,54	0,64	0,41	2,6	51	0,79	0,81	0,36	**2,21**	34	1,63	0,61	-

n - number of samples
v% - coefficient of variation

[1] Gaillardet et al., 2014;
[2] Savenko, Savenko, 2024
[3] Pokrovsky et al., 2016

In bold are values higher than the World average

According to the seasonal variability in the waters of the Pur River (Table 2), a group of elements with a maximum in the high-water period is distinguished: Al, Fe, Mn, Ni, Co, Cu, Zn, Pb, and Cd. The variability is especially distinct for Al, Fe and Mn, whose contents are tens of times more in the high-water than in the low-water period. The increase in the contents of Al and Fe is associated with their lateral input in the form of organo-mineral colloids from the seasonally thawed soil layer of watersheds (Krickov et al., 2019). In addition, Fe and Mn are mobile in a reducing environment and in the lowest oxidation degree of 2+ may come from water-saturated mineral gley soil horizons. Mn, Ni, Co, Cu, and Zn come to the river water from organic soil horizons mainly in spring in the form of organo-mineral complex compounds (Pokrovsky et al., 2016). For these metals, as well as for Pb and Cd, technogenic supply with atmospheric deposition may be of great importance. The other group is formed by elements, whose contents slightly differ in high and low-water periods, or the maximum occurs in low-water periods. It includes anionic elements such as As, Sb, U, V, and Sr. They are brought into rivers mainly by groundwater in ionic form.

In the waters of the Evoyakha River during floods, the average contents of Al, Fe and Mn are 2-3 times lower than in the Pur River. This is probably explained by more severe climatic conditions of its basin, located in the forest tundra zone. Soil thawing depth in the north of Western Siberia is one of the main factors of dissolved organic matter and associated metals entering river waters (Pokrovsky et al., 2015). It determines a higher Fe content in the Evoyakha River during low-water periods than in the Pur River. According to (Opekunova et al., 2020), in peat-gley soils of northern taiga landscapes occupying the southern part of the Pur River basin, the thickness of the seasonally thawed layer can reach 2 m. This promotes iron deposition on the complex geochemical barrier in the upper soil horizons and a decrease in its input into rivers with the surface runoff. In forest-tundra and tundra landscapes in the northern part of the basin, the thickness of the seasonally thawed layer is less (0.2-0.9 m), which prevents the formation of geochemical barriers and promotes active migration of Fe and other metals. The average contents of Ni, Co, Cu, Zn, Pb, Cd in the Evoyakha River in the high-water period slightly, and in the low-water period significantly higher than in the Pur River, which is obviously associated with the anthropogenic impact of N. Urengoy. The median values of Fe, Mn, Co, Cu, Zn, Pb, Cd contents in the waters of the Pur and Evoyakha rivers are distinctly lower than the mean values. For Fe and Mn this is due to seasonal factor, for other metals - to the anthropogenic one, manifested in local maxima of contents in some river sections.

In the Pur River waters (Fig. 6), relatively high metal contents were also observed in areas subject to anthropogenic impact. In the low-water period of 2023, in the upper reaches of the river (Pyakupur River) downstream of Muravlenko, Zn content increased to 21, Cu - 4.5, Ni - 3.6, Pb - 1.2 µg/l, which is many times higher than the background levels for this hydrological period. Increased Cu and Zn contents during low water periods were also observed in the waters of the Pur River near Korotchaevo and downstream near Urengoy settlement and Samburg village.

In the basin of the Evoyakha River (Fig. 7) a section polluted with heavy metals was identified in the area of the industrial zone in the eastern part of N.Urengoy, where the content of Cu increases up to 4-8, Zn - 16-19, Pb - 0.4-0.6 µg/l. Maximum concentrations exceed the background values by 5-7 times. The metal contents are similar during both low and high-water periods, which indicates the permanent pollution of river water, probably caused by urban or industrial sewage. In the same area, we found an increase of Ba content up to 10-15 µg/l, and in some samples more than 50 µg/l, which is an order of magnitude higher than background levels. Apparently, drilling operations were previously carried out in the adjacent area. Elevated Ba concentrations in natural waters of oil and gas production areas are usually associated with drilling wells, where barite is used as a weighting agent for drilling fluids.

Table 2. Seasonal differences in the content of dissolved forms of metals and metalloids in the Pur and Evoyakha rivers in 2021-2023, µg/l

River	Pur		Evoyakha	
Season (n)	High water (18)	Low water (25)	High water (44)	Low water (41)
Al	58	1,9	32	11
Fe	268	20	90	138
Mn	54,6	0,6	15,0	4,2
Ni	0,81	0,45	1,10	1,45
Co	0,19	<0,09	0,75	0,64
V	0,17	0,13	0,16	0,18
Cu	0,82	0,45	1,04	0,94
Zn	3,05	0,85	3,50	3,90
Pb	0,11	<0,02	0,23	0,08
Cd	0,011	<0,006	0,023	0,030
As	0,34	0,29	0,28	0,32
Sb	0,085	0,074	0,072	0,080
U	0,007	0,003	0,007	0,005
Sr	11,0	30,0	5,4	18,2
Ba	6,8	6,2	4,7	6,0
Rb	0,59	0,58	0,76	0,81

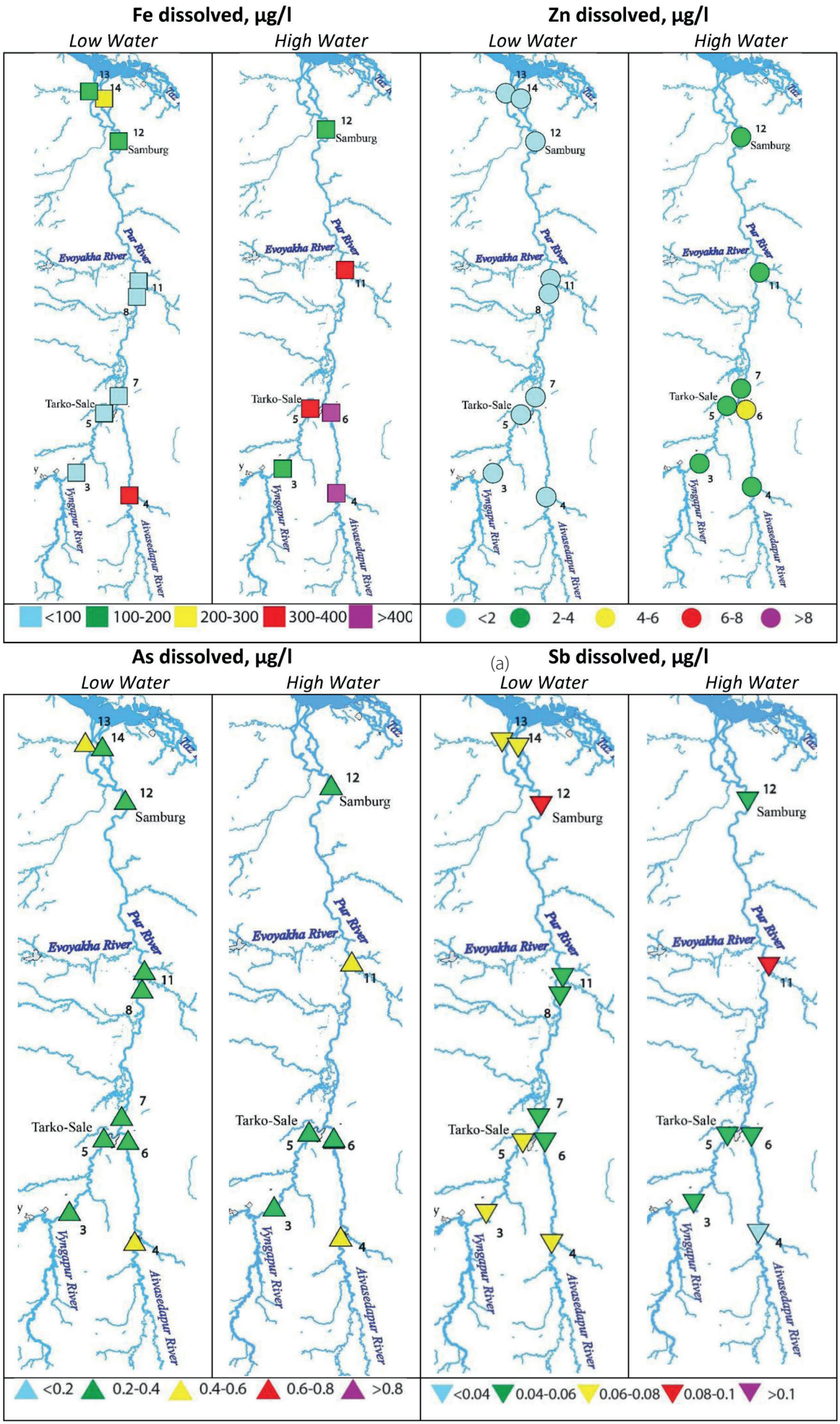

Fig. 6. Dissolved metals and metalloids in the Pur River water

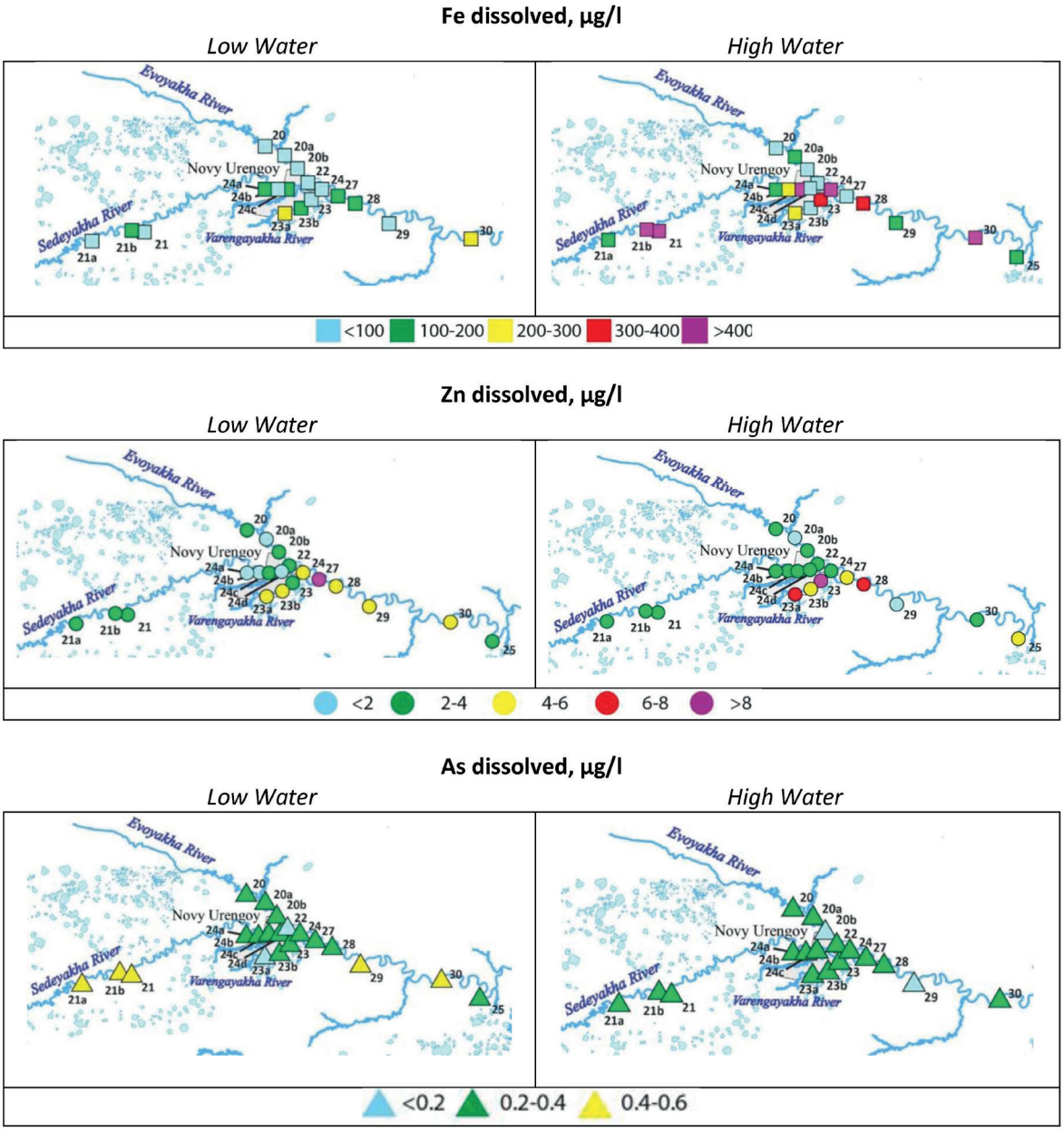

Fig. 7. Dissolved metals and metalloids in the Evoyakha River water

Thus, the river waters in the Pur River basin are characterized by generally low contents of metals and metalloids, not exceeding the world average values, except for Fe and Zn. A high variability of Al, Fe, Mn, Co, Cu, Zn, Pb and Cd contents was observed, caused by seasonal factor and anthropogenic impact. For some metals mean content significantly differs from the median values. It is caused by significant increase in their concentrations at a few river sections. Therefore, it is reasonable to use median values to characterize the regional hydrogeochemical background of the study area.

Suspended forms of metals and metalloids

Median levels of metals and metalloids in the suspended matter of the Pur River (Table 3) are in most cases lower than the global averages (Viers et al., 2009). First of all, this is characteristic of Al, whose content is 3.3 times less than the world average during flood and 6.7 times less than in low-water season. The low content of Al is due to grain-size and mineralogical composition of the suspended matter with the predominance of quartz-rich sandy particles larger than 50 microns, and also active migration of Al in colloidal organo-mineral compounds (see above). The greatest dispersion is characteristic of Cu: in low water it is 75 times less than the world average, in high water - 25 times less. The contents of Ni, Co, V, Cr, Cr, Zn, Cd, Pb, Sn, U, Bi, Rb, Ba, Sr are 2-5 times lower than the world averages. Only Fe and Mn levels exceed the world averages: 1.5 times in the high water and 2 - 4 times in the low water. Enrichment of the Western Siberian rivers with these metals in dissolved and suspended forms was determined earlier by (Agbalyan et al., 2016; Babushkin et al., 2007). Their source is anoxic ground and swamp waters where Mn and Fe have increased mobility. Entering river waters with oxic conditions, they can be precipitated hydroxides and adsorbed on solid suspended particles. The Sb content is slightly higher than the global average. It is anionogenic element that can be deposited together with Fe by adsorption and coprecipitation.

According to seasonal dynamics two groups of elements can be distinguished in suspended matter of the Pur and Evoyakha rivers (Table 4). The first group - iron group elements (Fe, Mn, Ni, Co), as well as As, Sb, Cd, Sr and Ba - is characterized by an increase in concentrations during low-water, the second group - Al, V, Pb, Sn, Bi, U and Rb - during high-water seasons (Fig. 8). The increase of Fe and Mn concentrations in summer period is obviously

Table 3. Levels of metals and metalloids in the Pur and Evoyakha suspended matter compared to global and regional background, μg/g

MMs	Pur River, n=45					Evoyakha River, n=80					World Rivers[1]	UCC[2] (Clarke)
	median	mean	min	max	v%	median	mean	min	max	v%		
Al	16100	19400	8300	43650	49	25300	30800	2665	65962	55	87200	80500
Fe	**105100**	**106400**	52275	**192720**	34	**117700**	**138200**	10462	**287074**	61	58100	46500
Mn	**5988**	**5466**	872	**10000**	51	**3043**	**4660**	206	**32336**	108	1679	1000
Ni	23	25	10	46	36	69	**85**	24	**434**	76	74,5	47
Co	14	13	7	22	27	**36**	**51**	5	**353**	109	22,5	17
V	40	41	17	78	37	104	105	23	**164**	23	129	97
Cr	53	51	25	73	24	108	136	66	**379**	84	130	92
Cu	1,1	4,4	0,4	30,6	162	17	31	0,7	**182**	138	75,9	28
Zn	95	107	19	**393**	61	171	192	59	**582**	62	208	67
Pb	11,2	13,8	5,5	**78,9**	84	14,8	15,4	5	42	31	61	17
Cd	0,38	0,40	0,10	1,04	50	0,49	0,58	0,1	**3,24**	82	1,55	0,09
As	19	19	7	36	41	21	25	6	61	61	36	5
Sb	**2,87**	**2,92**	0,80	**6,02**	40	**2,98**	3,7	0,48	**16,1**	113	2,2	0,4
Sn	1	1,6	0,14	**16,0**	170	2,12	3,41	0,40	**6,48**	273	4,6	2,1
Bi	0,17	0,18	0,09	0,40	44	0,23	0,38	0,09	**2,10**	106	0,85	0,16
U	0,6	0,67	0,30	1,3	37	1,08	1,08	0,25	1,98	31	3,3	2,7
Sr	115	119	84	**225**	23	91	92	24	175	26	187	320
Ba	403	433	281	**1153**	33	319	356	49	**3030**	90	522	624
Rb	20	24	10	50	44	28	34	5	72	57	78,5	84

n*- number of samples
[1] Viers et al., 2009;
[2] Rudnick, Gao, 2003 - Upper Continental Crust
* In bold are values higher than the World average

caused by deposition of their mobile compounds, added with groundwater to river waters with oxidizing conditions. Accumulation of other metals and metalloids during low water may be related to the processes of sorption and coprecipitation with Fe and Mn hydroxides. Al and other metals of the second group enrich suspended solids in rivers during floods due to increased erosion processes.

Iron accumulation in the suspended matter of the Evoyakha River during low-water season is even stronger – up to 21.6% (Cf 3.5). Cf values for Mn, Co and Sb exceed 1.5, for As, Ni, Cr, and Zn they are close to 1.0. Mean contents of metals in suspended matter of the Evoyakha River in summer are close to the global averages, but they are higher than in the Pur River. This is probably due to the significant spread of permafrost in the Evoyakha River catchment, which prevent leaching of elements. During thawing of permafrost, soil solutions interact with mineral soil horizons, thus ensuring active leaching and removal of metals and metalloids. Their highest levels occur in the late summer low-water period, when the maximum thawing of the active layer is reached, and as a consequence, the flow of acidic soil solutions enriched with colloids into the river network increases (Krickov, 2017). Additional confirmation of this hypothesis is the increase in water turbidity in the Evoyakha River during the summer low-water period compared to the spring flood.

Anthropogenic impact can have even more significant effects on the metal contents. Near cities, the maximum concentrations of Zn, Cd, Cu and other metals in suspended matter are 3-5 and more times higher than median (baseline) values. For example, during both seasons baseline content of Zn in the Pur River is about 100 μg/g, however below Tarko-Sale town and Samburg settlement it increases to 200-300 μg/g (Fig. 9). Zn content in the suspended matter of the Evoyakha River and its tributaries upstream of Novy Urengoy is 60-70 μg/g in high water, 90-100 μg/g in low water, and increases to 200-300 and 500-600 μg/g, respectively, downstream of the city (Fig. 10).

A number of indices is used to assess the magnitude of human-induced change in the aquatic environments. G. Birch (2023) examined 11 indices and found the Enrichment Factor (EF) to be most capable to produce high quality enrichment determinations.

EF is calculated as the ratio of the metal content in the studied sample to a certain element (reference) in the same sample, to the same ratio in the Earth's crust:

$$EF = (Ci/Cref)_{Sample} / (Ci/Cref)\,UCC$$

where *Ci* and *Cref* are the contents of the studied and reference elements, respectively, *UCC* – upper continental crust (Rudnick and Gao, 2014).

Table 4. Seasonal differences in metal and metalloid contents in the Pur and Evoyakha suspended matter (2021 – 2023)

River	Pur		Evoyakha	
Season (n)	HW (19)	LW (26)	HW (37)	LW (43)
Al	26110	13000	42460	18640
Fe	91220	111000	58140	216300
Mn	2371	7165	1614	3175
Ni	22	26	39	98
Co	11	15	32	44
V	51	32	105	103
Cr	54	50	83	149
Cu	3,1	1,1	15,4	27,5
Zn	98	93	99	216
Pb	15	9	15	15
Cd	0,3	0,4	0,2	0,8
As	16	20	13	36
Sb	2,6	3,0	2,1	4,0
Sn	1,3	0,9	2,0	2,2
Bi	0,20	0,12	0,23	0,22
U	0,74	0,53	1,21	0,96
Sr	106	121	93	90
Ba	378	425	348	286
Rb	31	18	50	20

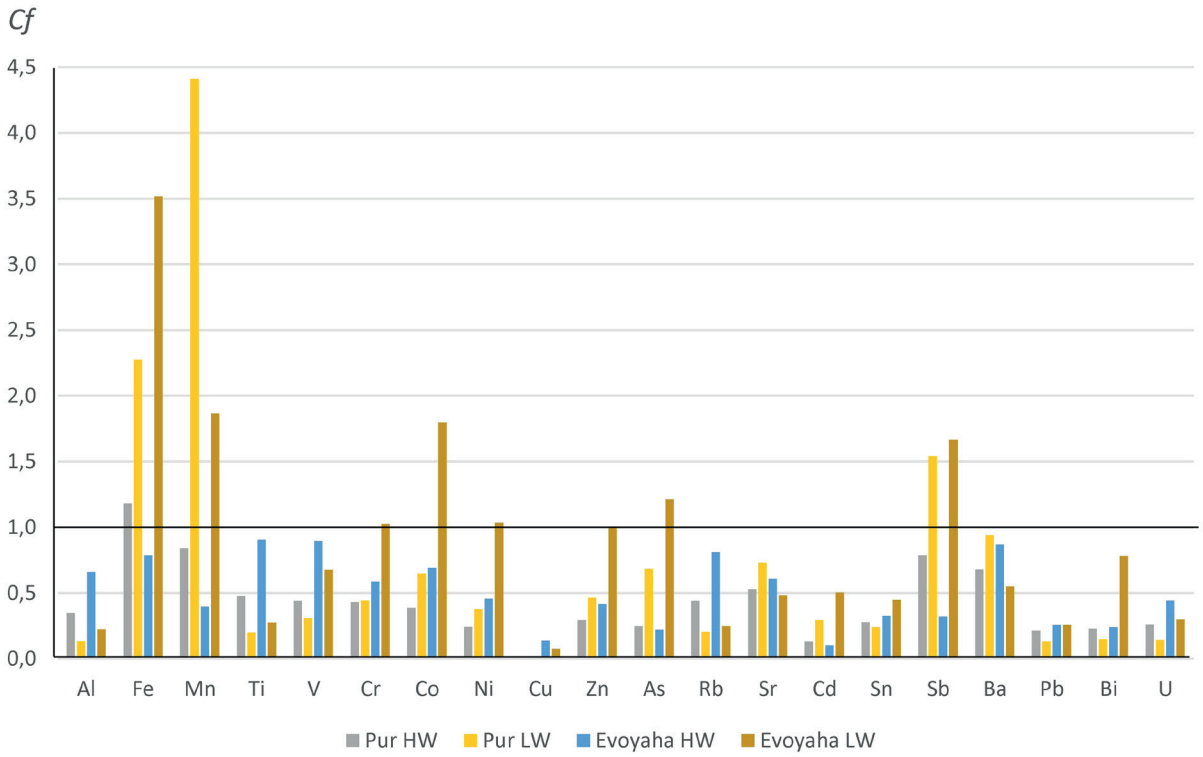

Fig. 8. Concentration factors relative to the world average (according to Viers et al., 2009) in suspended matter of the Pur and Evoyakha rivers during high water (HW) and low water (LW) seasons

(b)

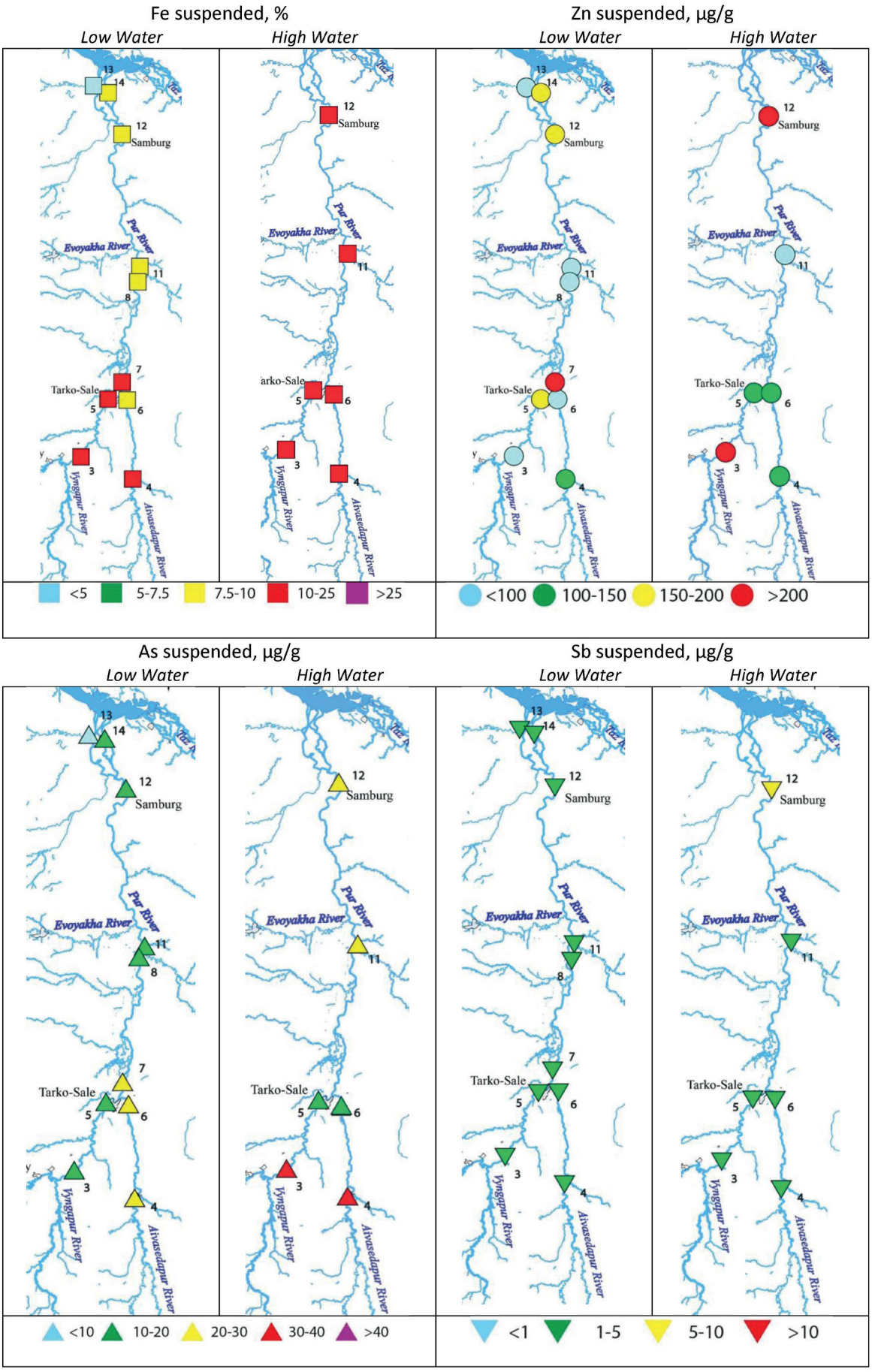

Fig. 9. Metals and metalloids in suspended matter of the Pur River

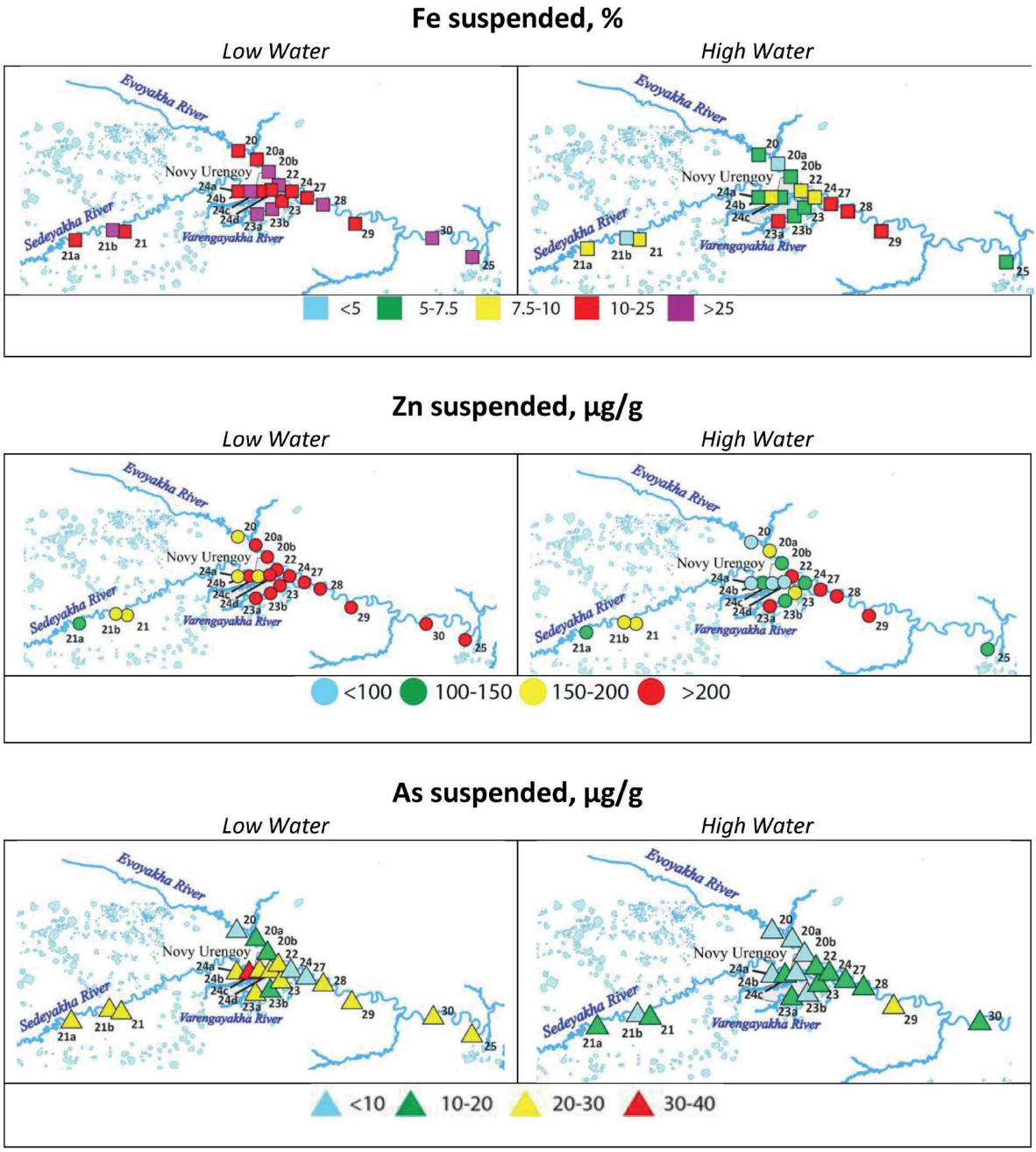

Fig. 10. Metals and metalloids in suspended matter of the Evoyakha River

Al, Fe, Mn, Sc, and La are commonly used as reference elements (Azoulay et al., 2001; Schiff and Weisberg, 1999). In the Pur River basin Al, Fe and Mn show high variability of content and diversity of migration forms, therefore, the EF values obtained on their basis are questionable. That is why we used Sc as a reference element.

For sediments the following categories of enrichment are most commonly used: 1-3 – low, 3-5 - moderate, 5-10 – considerable, 10-25 – high, 25-50 - very high, > 50 - extremely high (Birch, 2020).

Analysis of EF values for median contents of MMs allowed to identify the association of elements with considerable and high enrichment of suspended matter: Fe, Mn, Sb, As, Cd and Zn. In low water it is characteristic of both rivers, in high water it is characteristic only of the Pur River (Fig. 11).

The enrichment of suspended particles by Fe and Mn can be explained by the natural process of precipitation of their hydroxides in the oxidizing environment of river waters. However, enrichment by Sb, As, Cd and Zn is most likely of anthropogenic origin. This association of elements is typical for urban soils and road dust and is mainly due to the impact of motor vehicles. Particulate matter enriched with these elements enters rivers with urban stormwater and snowmelt runoff and contributes significantly to the deterioration of surface waters quality (Müller et al., 2020). EF elements of this association strongly increase in suspended particles of the Pur and Evoyakha rivers below the settlements (Tarko-Sale, Urengoy, Novy Urengoy). The maximum values range from 25 to 45, which corresponds to very high degree of enrichment.

Forms of migration of metals and metalloids

The ratio of element migration forms in water flows is determined by the DS coefficient, which characterizes the distribution of chemical elements between suspended (S) and dissolved (D) forms. Until relatively recently, it was considered in geochemistry that suspended forms of element migration prevail distinctly in river runoff (Gordeev et al., 2024; V. Savenko, 2006). The results of our studies in the Selenga, Volga, Don and other rivers showed that for a number of elements the role of dissolved forms was underestimated. On the basis of D,S-analysis (Kasimov et al., 2020a; Kasimov et al., 2020b; Kuryakova, 2011; Lychagin et al., 2017, etc), we identified three groups of chemical elements: D-elements with the predominance

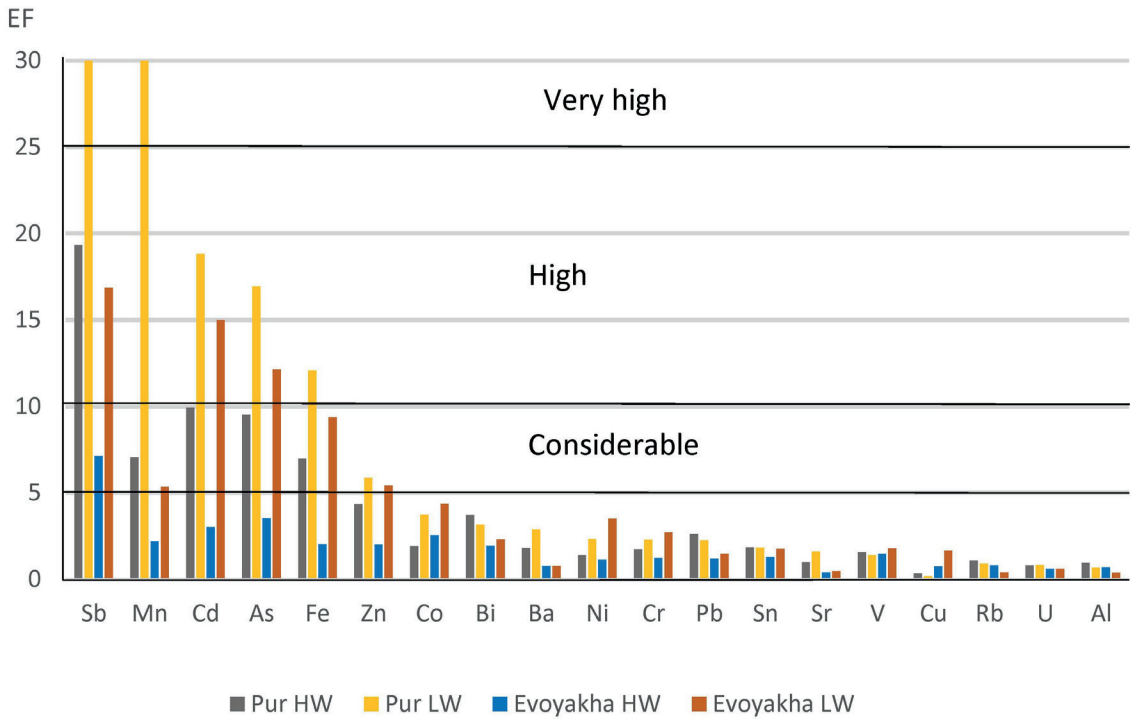

Fig. 11. EF for median values of chemical elements referenced to Sc in suspended matter of the Pur and Evoyakha rivers for high water (HW) and low water (LW) seasons

of dissolved form of migration, S-elements, the main form of migration of which is suspended, and a transitional group of D,S-elements, for which the ratio of suspended and dissolved forms varies widely. The position of chemical elements within a particular group is determined by internal migration factors (properties of the elements themselves), while their behavior within groups (change in DS value) is determined by external factors, mainly hydroclimatic and anthropogenic.

In the Pur and Evoyakha rivers the D-element group includes Ca, Sr, Cu, Mo, Rb (Fig. 12). Ca, as well as Mg, Na and K are among the main cations of natural waters, for which the dissolved form is almost always predominant. Sr is a typical cationic element, many of its compounds are well soluble. In terms of water migration rate, it is close to Ca. Mo migrates in natural waters in the form of anions, it is also characterized by the predominance of dissolved forms of migration, which we have previously reported for other rivers. The appearance of Cu among the D-elements is a specific feature of the Pur River. This is due to the very low Cu content in its suspended matter, where the median value (1.1 μg/g) is 70 times lower than the global average (Table 3). In the Evoyakha River, the median Cu content is 17 μg/g, which is only 4 times lower than the global average, so Cu moves to the group of D,S-elements, which is more usual (Fig. 12b) .

The group of D,S-elements includes Sb, As, Ba, Ni, Cd, Zn, and U. Almost all of them are the priority pollutants of the environment. For these elements, seasonal differences in the proportion of migration forms are most pronounced in the Evoyakha river, where the share of suspended forms increases during floods. This is caused by a significant increase in turbidity during the flood period - up to 20-30, and in some places up to 50-70 mg/l, while during low season it is 8-10 mg/l. Spring flooding on the Evoyakha River is short and high, while on the Pur River it is lower and longer lasting. The turbidity of the Pur River water is 15-20 mg/l and almost does not change seasonally. Therefore, the anthropogenic factor is more important for the ratio of different migration forms in the Pur River. Below cities, the share of suspended forms tends to increase. This is especially noticeable for Urengoy, where at the site downstream of the river port the share of suspended forms of not only DS but also D-elements, Mo and Rb, increases.

The group of S-elements includes lithophilic elements firmly bound to mineral particles – Al, Fe, Mn, Ti, Bi, Co, V, Pb. For them the share of suspended forms may change quantitatively, but always remains predominant.

Source identification of suspended forms of MMs

The PCA/APCS-MLR method was applied for two data sets, the first one included the data on MMs contents in 63 samples collected during 2021-2023 in the Evoyaha River, and the second one comprised the chemical data on 40 samples collected during the same period in the Pur River. In the first step of the analysis, the data were normalized and then principal component analysis was applied.

The Evoyaha River

For the dataset from the Evoyaha River, four factors (F1-F4) were identified. They explained 78% of the total variance (Supplementary 3). The first factor (F1) had the largest contribution (40%) to the total variance. According to APCS-MLR results, this factor explained more than 50% of the mass input of Fe, As, Cr, Ni, Zn, Cd, Sb (Fig. 13), and probably related to the sorption of elements by iron hydroxides. The EF values ranging from 5 to 10, as well as the coefficient of variation (60-70%) suggest a mixed origin of these elements - natural and anthropogenic. The human-induced contribution of As, Cr, Zn and Ni is probably related to oil and gas production ((Xu et al., 2018; Saravanan et al., 2022).

The second factor (F2) explained 23% of the total variance. Large proportions of Sr, V and Pb (more than 80%) and U, Ba, Rb, Al, Ti and Cu (60-80%) inputs were associated with this factor. The contents of these elements varied little along the river course and did not depend on the season (Cv 20-50%), the EF values were also low. So, the F2 factor was interpreted as a lithogenic factor. The third (F3) and the fourth (F4) factors accounted for 8 and 7% of the total variance, respectively. The F3 contributed to 50% of Mn and 45% of Co. Mn is considered to be one of the main markers of oil pollution (Saravanan et al., 2022). The F4 explains the partial input of Bi, Sn, Cu, Pb and Co. These metals are markers of emissions from vehicles

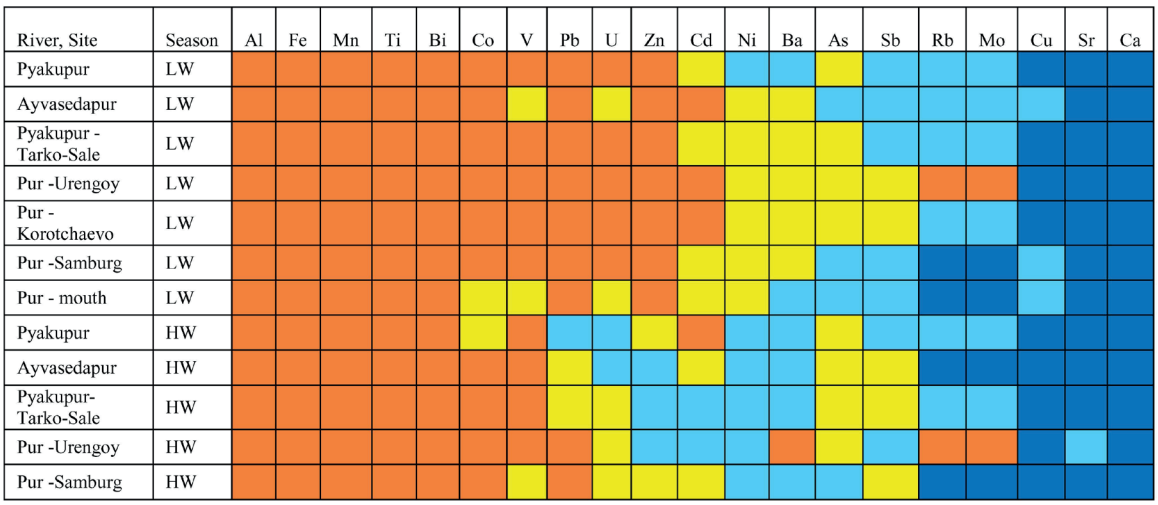

Fig. 12. Matrix of MMs migration forms in Pur (a) and Evoyakha (b) Rivers

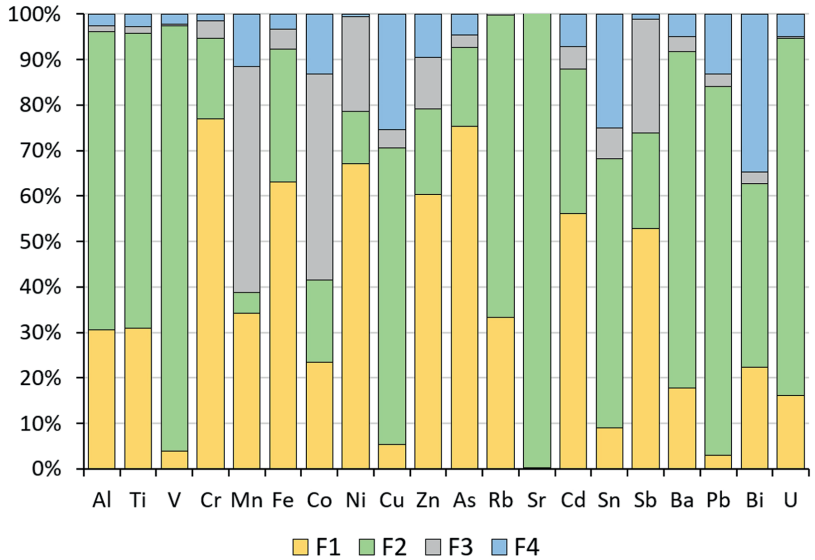

Fig. 13. Relative contribution of sources for suspended matter of the Evoyakha River, according to APCS-MLR model calculations: F1 – iron deposition, F2 – lithogenic, F3 – oil and gas production, F4 – vehicles emission

(Thorpe, Harrison, 2008). The coefficient of variation for some metals was close to or greater than 100%, and the maximum contributions of factors F3 and F4 were observed within the city and downstream. This confirms the input of MMs with F3 and F4 as anthropogenic. Thus, 4 main factors of MMs input into suspended particles were identified for the Evoyakha River. The greatest contribution is made by a mixed natural-anthropogenic factor associated with iron. The second source of MMs input is lithogenic. The third and fourth factors are caused by anthropogenic input and are defined as the influence of oil and gas production and vehicle emissions, respectively.

The Pur River

Four factors (F1-F4) were also identified for the Pur River dataset. They explained 74% of the total variance in MMs content (Supplementary 3). The first factor F1 accounted for 36% of the total variance. It was responsible for the input to

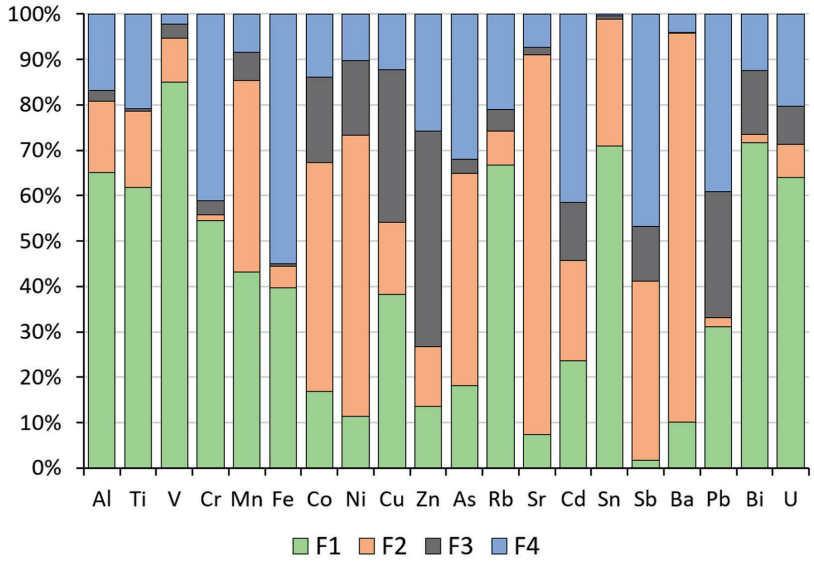

Fig. 14. Relative contribution of sources for suspended matter of the Pur River, according to APCS-MLR model calculations: F1 – lithogenic, F2 – oil and gas production, F3 and F4 – vehicles emission (F3 – wear of tires, F4 – wear of brake pads)

the suspended particles of 85% of the total mass of V, more than 60% of Rb, Al, U, and Ti. The similar association of elements was noted for the lithogenic factor in Evoyakha, suggesting a regional bedrock influence. The coefficient of variation of the MMs did not exceed 50%, in addition, these elements had the lowest EF values, hence factor F1 can be interpreted as a lithogenic factor.

The factor F2 accounted for 22% of the total variance. It contributed more than 80% of Ba and Sr, and most of the mass of Ni, Co, As, Mn and Sb. This factor is most likely related to the sorption of the elements by Mn (hydr)oxides (Zheng et al., 2020). For all the elements associated with the F2 factor, a high correlation was displayed particularly by Mn (0.6-0.8). This association of MMs is similar to the F3 group for the Evoyakha River, which we linked to oil and gas production. The significant contribution of Ba and Sr may be due to their use in drilling fluids. Each of the two factors F3 and F4 contributed 8% to the total variance. Factor F3 was responsible for the input of Zn, Cu and small portions of Pb (Fig. 14). Zn is one of the markers of car tires abrasion, with Cu and Pb often found with it (Thorpe, Harrison, 2008; Alves et al., 2020). The factor F4 accounted for half of the Fe, Sb, Sn and Pb input. This association of elements may be due to the wearing of the vehicles brake pads (Pant, Harrison, 2013). High EF values for the elements associated with factors F3 and F4 (EF>5), indicate the anthropogenic nature of these factors. In addition, the maximum contribution of both factors was observed at sites within cities. Hence, it can be assumed that these metals enter the urban environment through motor vehicles and are transported to rivers by storm water drainage systems.

Thus, 4 factors of MMs input were determined for suspended particles of the Pur River waters. The first factor explains the lithogenic input, the second one is related to oil and gas production. The third and fourth factors are defined as the vehicle influence, at that, the third factor is related to input from wear of tires, the fourth factor - with wear of brake pads.

CONCLUSIONS

1. Waters of the Pur River and its tributaries are characterized by generally low content of dissolved metals and metalloids, not exceeding the world average values, except for Fe and Zn. A high variability of Al, Fe, Mn, Co, Cu, Zn, Pb and Cd contents was observed, caused by seasonal factor and anthropogenic impact. The median contents of metals can be used as the baseline values.

2. Median levels of metals and metalloids in the suspended matter of the Pur River are lower than the global averages, except for Fe and Mn. According to the seasonal dynamics two groups of elements can be distinguished: the first group - Fe, Mn, Ni, Co, As, Sb, Cd, Sr and Ba - is characterized by an increase in concentrations during low-water, the second group - Al, V, Pb, Sn, Bi, U and Rb - during high-water seasons. Near cities, the maximum concentrations of Zn, Cd, Cu and other metals in suspended matter are 3-5 and more times higher than the baseline values. Analysis of EF values for median contents of MMs allowed us to identify the association of elements with considerable and high enrichment of suspended matter: Fe, Mn, Sb, As, Cd and Zn.

3. On the basis of D,S-analysis, we identified three groups of chemical elements in the Pur River basin: D-elements – Ca, Sr, Cu, Mo, Rb; D,S-elements – Sb, As, Ba, Ni, Cd, Zn, and U; S-elements – Al, Fe, Mn, Ti, Bi, Co, V, Pb. The position of chemical elements within a particular group is determined by properties of the elements themselves, while their behavior within groups is determined by external factors, mainly hydroclimatic and anthropogenic.

4. On the basis of PCA/APCS-MLR method, we determined 4 main factors with different contributions to the total content of metals and metalloids in river sediment: lithogenic, iron oxidation, urban wastewaters, and motor vehicle emissions.

REFERENCES

Agbalyan E. V., Shinkaruk E. V. and Khoroshavin V.Y. (2016). Characteristics of water quality indicators in the Tazovsky district of the Yamalo-Nenets Autonomous Okrug (in Russian). Scientific Bulletin of the Yamalo-Nenets Autonomous Okrug, 2, 22–29.

Ali H., Khan E. and Ilahi I. (2019). Environmental chemistry and ecotoxicology of hazardous heavy metals: Environmental persistence, toxicity, and bioaccumulation. In: Journal of Chemistry , Vol. 2019. DOI: 10.1155/2019/6730305

Alves C.A., Vicente A.M.P., Calvo A.I., Baumgardner D., Amato F., Querol X., Pio C., Gustafsson M. / Physical and chemical properties of non-exhaust particles generated from wear between pavements and tyres // Atmospheric Environment, Volume 224, 2020, 117252, ISSN 1352-2310, https://doi.org/10.1016/j.atmosenv.2019.117252.

Azoulay A., Garzon P. and Eisenberg M.J. (2001). Comparison of the mineral content of tap water and bottled waters. Journal of General Internal Medicine, 16(3). DOI: 10.1111/j.1525-1497.2001.04189.x

Babushkin A.G., Moskovchenko D. and Pikunov S. V. (2007). Hydrochemical monitoring of surface waters of the Khanty-Mansiysk Autonomous Okrug - Yugra (in Russian).

Barker A.J., Douglas T.A., Jacobson A.D., McClelland J.W., Ilgen A.G., Khosh M.S., Lehn G.O. and Trainor T.P. (2014). Late season mobilization of trace metals in two small Alaskan arctic watersheds as a proxy for landscape scale permafrost active layer dynamics. Chemical Geology, 381. DOI: 10.1016/j.chemgeo.2014.05.012

Birch G.F. (2020). An assessment of aluminum and iron in normalisation and enrichment procedures for environmental assessment of marine sediment. Science of the Total Environment, 727. DOI: 10.1016/j.scitotenv.2020.138123

Chalov S., Moreido V., Sharapova E., Efimova L., Efimov V., Lychagin M. and Kasimov N. (2020). Hydrodynamic controls of particulate metals partitioning along the lower selenga river-main tributary of the Lake Baikal. Water (Switzerland), 12(5). DOI: 10.3390/W12051345

Chalov S., Prokopeva K., Magritsky D., Grigoriev V., Fingert E., Habel M., Juhls B., Morgenstern A., Overduin P.P. and Kasimov N. (2023). Climate change impacts on streamflow, sediment load and carbon fluxes in the Lena River delta. Ecological Indicators, 157. DOI: 10.1016/j.ecolind.2023.111252

Chalov S.R. and Efimov V.A. (2021). Mechanical composition of suspended sediments: classification, characteristics, spatial variability (in Russian). Bulletin of Moscow University. Series 5: Geography, 4, 91–103.

Chalov S.R., Shkolny D.I., Promakhova E.V., Leman V.N. and Romanchenko A.O. (2015). Formation of sediment runoff in regions of placer deposit development (in Russian). Geography and Natural Resources, 2, 22–30.

Chen L., Zhang H., Ding M. et al (2021) Exploration of the variations and relationships between trace metal enrichment in dust and ecological risks associated with rapid urban expansion. Ecotoxicol Environ Safety 212:111944. https://doi.org/10.1016/j.ecoenv.2021.111944

Chupakov A. V., Pokrovsky O.S., Moreva O.Y., Shirokova L.S., Neverova N. V., Chupakova A.A., Kotova E.I. and Vorobyeva T.Y. (2020). High resolution multi-annual riverine fluxes of organic carbon, nutrient and trace element from the largest European Arctic river, Severnaya Dvina. Chemical Geology, 538. DOI: 10.1016/j.chemgeo.2020.119491

de Paiva Magalhães D., da Costa Marques M.R., Baptista D.F. and Buss D.F. (2015). Metal bioavailability and toxicity in freshwaters. In: Environmental Chemistry Letters , Vol. 13, Issue 1. DOI: 10.1007/s10311-015-0491-9

Demina L.L., Gordeev V. V., Galkin S. V., Kravchishina M.D. and Aleksankina S.P. (2010). The biogeochemistry of some heavy metals and metalloids in the Ob River estuary-Kara Sea section. Oceanology, 50(5). DOI: 10.1134/S0001437010050103

Ediagbonya T.F., Nmema E., Nwachukwu P.. and Teniola O.D. (2015). Identification and quantification of heavy metals, coliforms and anions in water bodies using enrichment factors. Journal of Environmental Analitic Chemistry, 2(146), 2380–2391.

Fytianos K. (2001). Speciation analysis of heavy metals in natural waters: A review. In: Journal of AOAC International , Vol. 84, Issue 6. DOI: 10.1093/jaoac/84.6.1763

Gaillardet J., Viers J. and Dupré B. (2014). Trace Elements in River Waters. In Treatise on Geochemistry; : , 2014; pp. 225–272. Elsevier Science: Amsterdam, The Netherlands, 225–272.

Garnier J.M., Martin J.M., Mouchel J.M. and Sioud K. (1996). Partitioning of trace metals between the dissolved and particulate phases and particulate surface reactivity in the Lena River estuary and the Laptev Sea (Russia). Marine Chemistry, 53(3–4). DOI: 10.1016/0304-4203(95)00094-1

Gebhardt A.C., Gaye-Haake B., Unger D., Lahajnar N. and Ittekkot V. (2004). Recent particulate organic carbon and total suspended matter fluxes from the Ob and Yenisei Rivers into the Kara Sea (Siberia). Marine Geology, 207(1–4). DOI: 10.1016/j.margeo.2004.03.010

Gordeev V. V., Pokrovsky O.S., Zhulidov A. V., Filippov A.S., Gurtovaya T.Y., Holmes R.M., Kosmenko L.S., McClelland J.W., Peterson B.J. and Tank S.E. (2024). Dissolved Major and Trace Elements in the Largest Eurasian Arctic Rivers: Ob, Yenisey, Lena, and Kolyma. Water (Switzerland), 16(2). DOI: 10.3390/w16020316

Hartwell S.I., Lomax T. and Dasher D. (2020). Characterization of sediment contaminants in Arctic lagoons and estuaries. Marine Pollution Bulletin, 152. DOI: 10.1016/j.marpolbul.2019.110873

Horowitz A.J. (1986). A primer on trace metal-sediment chemistry. US Geological Survey Water-Supply Paper, 2277.

Hudson-Edwards K.A. (2003). Sources, mineralogy, chemistry and fate ofheavy metal-bearing particles in mining-affected river systems. Mineralogical Magazine, 67(2). DOI: 10.1180/0026461036720095

Inam E., Khantotong S., Kim K.W., Tumendemberel B., Erdenetsetseg S. and Puntsag T. (2011). Geochemical distribution of trace element concentrations in the vicinity of Boroo gold mine, Selenge Province, Mongolia. Environmental Geochemistry and Health, 33(SUPPL. 1). DOI: 10.1007/s10653-010-9347-1

Kasimov N., Shinkareva G., Lychagin M., Chalov S., Pashkina M., Thorslund J. and Jarsjö J. (2020). River water quality of the Selenga-Baikal Basin: Part II-metal partitioning under different hydroclimatic conditions. Water (Switzerland), 12(9). DOI: 10.3390/W12092392

Kasimov N., Shinkareva G., Lychagin M., Kosheleva N., Chalov S., Pashkina M., Thorslund J. and Jarsjö J. (2020). River water quality of the Selenga-Baikal Basin: Part i-spatio-temporal patterns of dissolved and suspended metals. Water (Switzerland), 12(8). DOI: 10.3390/W12082137

Kolesnichenko I., Kolesnichenko L.G., Vorobyev S.N., Shirokova L.S., Semiletov I.P., Dudarev O. V., Vorobev R.S., Shavrina U., Kirpotin S.N. and Pokrovsky O.S. (2021). Landscape, soil, lithology, climate and permafrost control on dissolved carbon, major and trace elements in the ob river, western siberia. Water (Switzerland), 13(22). DOI: 10.3390/w13223189

Krickov I. V. (2017). Geochemical features of river suspension of the meridional profile of Siberia (in Russian). West Siberian Peatlands of the Cycle and Cycle: Past and Present, 147–148.

Krickov Ivan V., Pokrovsky O.S., Manasypov R.M., Lim A.G., Shirokova L.S. and Viers J. (2019). Colloidal transport of carbon and metals by western Siberian rivers during different seasons across a permafrost gradient. Geochimica et Cosmochimica Acta, 265. DOI: 10.1016/j.gca.2019.08.041

Landner L. and Reuther R. (2005). Speciation, mobility and bioavailability of metals in the environment. Springer Netherlands, 139–274.

Liang S-Y, Cui J-L, Bi X-Y et al (2019) Deciphering source contributions of trace metal contamination in urban soil, road dust, and foliar dust of Guangzhou, southern China. Sci Total Environ 695:133596. https://doi.org/10.1016/j.scitotenv.2019.133596

Lychagin M., Chalov S., Kasimov N., Shinkareva G., Jarsjö J. and Thorslund J. (2017). Surface water pathways and fluxes of metals under changing environmental conditions and human interventions in the Selenga River system. Environmental Earth Sciences, 76(1). DOI: 10.1007/s12665-016-6304-z

Ma Y., Mummullage S., Wijesiri B. et al (2021) Source quantification and risk assessment as a foundation for risk management of metals in urban road deposited solids. J Hazard Mater 408:124912. https://doi.org/10.1016/j.jhazmat.2020.124912

Macklin M.G., Brewer P.A., Hudson-Edwards K.A., Bird G., Coulthard T.J., Dennis I.A., Lechler P.J., Miller J.R. and Turner J.N. (2006). A geomorphological approach to the management of rivers contaminated by metal mining. Geomorphology, 79(3–4). DOI: 10.1016/j.geomorph.2006.06.024

McClelland J.W., Tank S.E., Spencer R.G.M., Shiklomanov A.I., Zolkos S. and Holmes R.M. (2023). Arctic Great Rivers Observatory. Water Quality Dataset. Version 20230314. https://arcticgreatrivers.org/data

Meybeck M. (2003). Global Occurrence of Major Elements in Rivers. In: Treatise on Geochemistry , Vols. 5–9. DOI: 10.1016/B0-08-043751-6/05164-1

Mighanetara K., Braungardt C.B., Rieuwerts J.S. and Azizi F. (2009). Contaminant fluxes from point and diffuse sources from abandoned mines in the River Tamar catchment, UK. Journal of Geochemical Exploration, 100(2–3). DOI: 10.1016/j.gexplo.2008.03.003

Miranda L.S., Wijesiri B., Ayoko G.A., Egodawatta P. and Goonetilleke A. (2021). Water-sediment interactions and mobility of heavy metals in aquatic environments. Water Research, 202. DOI: 10.1016/j.watres.2021.117386

Moskovchenko D. V. (1998). Oil and gas production and the environment: ecological and geochemical analysis of the Tyumen region (in Russian).

Müller A., Österlund H., Marsalek J. and Viklander M. (2020). The pollution conveyed by urban runoff: A review of sources. In: Science of the Total Environment , Vol. 709. DOI: 10.1016/j.scitotenv.2019.136125

Opekunova M.G., Opekunov A.Y., Kukushkin S.Y. and Lisenkov S.A. (2020). Elemental composition of soil waters in northern Siberia and its change under the influence of oil and gas production (in Russian). Fourth Vinogradov Readings. Hydrology from Knowledge to Worldview, 750–755.

Pant P., Harrison R.M., / Estimation of the contribution of road traffic emissions to particulate matter concentrations from field measurements: A review // Atmospheric Environment, Volume 77, 2013, Pages 78-97, https://doi.org/10.1016/j.atmosenv.2013.04.028.

Pokrovsky O.S., Manasypov R.M., Loiko S.., Krickov I.A., Kopysov S.., Kolesnichenko L.G., Vorobyev S.N. and Kirpotin S.N. (2016). Trace element transport in western Siberian rivers across a permafrost gradient. Biogeosciences, 13(6), 1877–1900.

Pokrovsky O.S., Manasypov R.M., Loiko S., Shirokova L.S., Krickov I.A., Pokrovsky B.G., Kolesnichenko L.G., Kopysov S.G., Zemtzov V.A., Kulizhsky S.P., Vorobyev S.N. and Kirpotin S.N. (2015). Permafrost coverage, watershed area and season control of dissolved carbon and major elements in western Siberian rivers. Biogeosciences, 12(21). DOI: 10.5194/bg-12-6301-2015

Popov P.A. (2013). Fishes of the Subarctic of Western Siberia: habitat conditions, structure of ichthyocenoses, ecology (in Russian).

Romanova T.I. and Samarin V.A. (2019). Features of the chemical composition of surface waters and bottom sediments of rivers and lakes of the Khanty-Mansi Autonomous Okrug - Yugra. International Scientific Journal, 12–1(90), 154–163.

Rudnick R.L. and Gao S. (2013). Composition of the Continental Crust. In: Treatise on Geochemistry: Second Edition , Vol. 4. DOI: 10.1016/B978-0-08-095975-7.00301-6

Ryan J.D. and Windom H.L. (1988). A geochemical land statistical approach for assessing metal pollution in coastal sediments. Metals in Coastal Environments of Latin America. Berlin Heidelberg: Springer.

Saravanan A., Senthil Kumar P., Hemavathy R.V., Jeevanantham S., Harikumar P., Priyanka G., Rebekah Angelina Devakirubai D. / A comprehensive review on sources, analysis and toxicity of environmental pollutants and its removal methods from water environment // Science of The Total Environment, Volume 812, 2022, 152456, ISSN 0048-9697, https://doi.org/10.1016/j.scitotenv.2021.152456.

Savenko V. (2006). World rivers' suspended sediment chemical composition (In Russian). GEOS.

Savenko A.V., Savenko V.S. and Pokrovsky O.S. (2020). New data on the content of dissolved trace elements in the waters of Russian Arctic rivers (in Russian). Reports of the Russian Academy of Sciences. Earth Sciences, 491(2), 82–88.

Savenko A.V. and Savenko V.S. (2024). Trace Element Composition of the Dissolved Matter Runoff of the Russian Arctic Rivers. In: Water (Switzerland), Vol. 16, Issue 4. DOI: 10.3390/w16040565

Schiff K.C. and Weisberg S.B. (1999). Iron as a reference element for determining trace metal enrichment in Southern California coastal shelf sediments. Marine Environmental Research, 48(2). DOI: 10.1016/S0141-1136(99)00033-1

Song Y, Xie S, Zhang Y et al (2006) Source apportionment of PM2.5 in Beijing using principal component analysis/absolute principal component scores and UNMIX. Sci Total Environ 372:278–286. https://doi.org/10.1016/j.scitotenv.2006.08.041

Soromotin A., Moskovchenko D., Khoroshavin V., Prikhodko N., Puzanov A., Kirillov V., Koveshnikov M., Krylova E., Krasnenko A. and Pechkin A. (2022). Major, Trace and Rare Earth Element Distribution in Water, Suspended Particulate Matter and Stream Sediments of the Ob River Mouth. Water (Switzerland), 14(15). DOI: 10.3390/w14152442

Thorpe A., Harrison R.M. Sources and properties of non-exhaust particulate matter from road traffic: a review // Sci.Total Environ. 2008. V. 400. №. 1–3. P. 270–282.

Thorslund J., Jarsjö J., Chalov S.R. and Belozerova E. V. (2012). Gold mining impact on riverine heavy metal transport in a sparsely monitored region: The upper Lake Baikal Basin case. Journal of Environmental Monitoring, 14(10). DOI: 10.1039/c2em30643c

Thurston G.D., Ito K., Lall R. (2011) A source apportionment of U.S. fine particulate matter air pollution. Atmos Environ 45:3924–3936. https://doi.org/10.1016/j.atmosenv.2011.04.070

Uvarova V.I. (2011). Assessment of the chemical composition of water and bottom sediments of the Nadym River. Bulletin of Ecology, Forestry and Landscape Science, 11, 143–153.

Viers J., Dupré B. and Gaillardet J. (2009). Chemical composition of suspended sediments in World Rivers: New insights from a new database. Science of the Total Environment, 407(2), 853–868.

Violante A., Cozzolino V., Perelomov L., Caporale A.G. and Pigna M. (2010). Mobility and bioavailability of heavy metals and metalloids in soil environments. Journal of Soil Science and Plant Nutrition, 10(3). DOI: 10.4067/S0718-95162010000100005

Wu Q., Zhou H., Tam N.F.Y., Tian Y., Tan Y., Zhou S., Li Q., Chen Y. and Leung J.Y.S. (2016). Contamination, toxicity and speciation of heavy metals in an industrialized urban river: Implications for the dispersal of heavy metals. Marine Pollution Bulletin, 104(1–2). DOI: 10.1016/j.marpolbul.2016.01.043

Xu T., Wang L., Wang X., Li T., Zhan X. / Heavy metal pollution of oil-based drill cuttings at a shale gas drilling field in Chongqing, China: A human health risk assessment for the workers // Ecotoxicology and Environmental Safety, Volume 165, 2018, Pages 160-163, ISSN 0147-6513, https://doi.org/10.1016/j.ecoenv.2018.08.104.

Zheng Q., Hou J., Hartley W., Ren L., Wang M., Tu S., Tan W. / As(III) adsorption on Fe-Mn binary oxides: Are Fe and Mn oxides synergistic or antagonistic for arsenic removal? // Chemical Engineering Journal, Volume 389, 2020, 124470, ISSN 1385-8947, https://doi.org/10.1016/j.cej.2020.124470.

SUPPLEMENTARY 1

Table 1. Sampling points in 2021-2023 (numbering corresponds to Fig. 1)

N	River	Description	2021	2022		2023	
			Aug	Jun	Aug	Jun	Aug
1	Pyakupur	upper reaches (30 km south of Muravlenko, 50 km north-west of Noyabrsk)			+	+	+
2	Pyakupur	at the latitude of Muravlenko and Khanymey					+
3	Pyakupur	at the latitude of Purpe and Kharampur		+	+	+	+
4	Ayvasedapur	at the latitude of Purpe and Kharampur		+	+	+	+
5	Pyakupur	near Tarko-Sale (above the confluence with the Ayvasedapur)		+	+	+	+
6	Ayvasedapur	near Tarko-Sale (above the confluence with the Pyakupur)		+	+	+	+
7	Pur	near Tarko-Sale (below the confluence of the Pyakupur and the Ayvasedapur)			+		+
8	Pur	above Korotchaevo (left branch)			+		+
9	Pur	above Korotchaevo (right branch)			+		+
10	Pur	between Korotchaevo and Urengoy			+		+
11	Pur	below Urengoy		+	+	+	+
12	Pur	below Samburg		+	+	+	+
13	Pur	15 km from the mouth, left branch			+	+	
14	Pur	15 km from the mouth, right branch			+	+	
15	Khanto (lake)	northern boundary of Noyabrsk			+		+
16	Khanayakha	0.2 km from the source			+		+
17	Khanayakha	0.6 km from the source			+		+
18	Khanayakha	1.1 km from the source			+		+
19	Nankpyokh	mouth			+		+
20	Evoyakha	above Novy Urengoy	+	+		+	+
21	Sedeyakha	above Novy Urengoy	+	+		+	+
22	Evoyakha	confluence with the Sedeyakha	+	+		+	+
23	Sedeyakha	confluence with the Yevoyakha	+	+		+	+
24	Evoyakha	below the confluence with the Sedeyakha	+	+		+	+
25	Evoyakha	below Novy Urengoy	+	+		+	+
26	Sedeyakha	upper reaches	+	+		+	+
27	Evoyakha	Novy Urengoy, eastern industrial zone	+	+		+	+
28	Evoyakha	eastern border of Novy Urengoy town	+	+			+
29	Evoyakha	7 km below Novy Urengoy	+	+			+
30	Evoyakha	21 km below Novy Urengoy	+	+			+
31	Evoyakha	10 km from the mouth	+	+		+	+

SUPPLEMENTARY 2

Table 1. Hydrochemical characteristics and content of major ions in water bodies of the Pur River basin during the 2023 flood

Station	Date	River	HCO_{3-}	SO_4^{2-}	Cl^-	Ca2+	Mg^{2+}	Na^+	K^+	M,mg/l
			mg/l							
1	04.06.2023	Pyakupur	7,57	0,25	0,60	1,17	0,68	0,98	0,30	12
3	05.06.2023	Pyakupur	6,96	0,97	1,32	0,87	0,56	1,52	0,45	13
4	05.06.2023	Ayvasedapur	7,94	0,42	0,20	1,06	0,50	0,64	0,23	11
5	04.06.2023	Pyakupur	6,58	0,57	1,20	0,74	0,48	1,47	0,44	11
6	05.06.2023	Ayvasedapur	8,73	0,31	0,34	1,20	0,73	0,52	0,40	12
11a	03.06.2023	Pur	4,76	0,49	0,58	0,58	0,36	0,51	0,20	7
11a	10.06.2023	Pur	5,98	0,37	0,33	0,85	0,58	0,81	0,27	9
11b	03.06.2023	Pur	7,38	0,42	0,40	0,78	0,55	0,79	0,35	11
11b	10.06.2023	Pur	7,81	0,54	1,03	1,04	0,64	0,99	0,25	12
12a	10.06.2023	Pur	6,35	0,50	0,64	0,70	0,49	0,84	0,32	10
13	10.06.2023	Pur	7,93	0,47	0,56	0,87	0,60	0,86	0,40	12
14	10.06.2023	Pur	6,71	0,50	0,73	0,70	0,48	0,87	0,37	10
21	02.06.2023	Sedeyakha	3,66	0,39	0,71	0,44	0,24	0,67	0,45	7
21	07.06.2023	Sedeyakha	3,60	0,90	0,38	0,61	0,34	0,81	0,35	7
22	01.06.2023	Evoyakha	5,98	1,00	0,19	0,75	0,35	0,61	0,38	9
22	08.06.2023	Evoyakha	5,49	1,78	0,31	1,00	0,54	0,62	0,23	10
23	01.06.2023	Sedeyakha	4,15	1,12	0,63	0,57	0,27	1,12	0,69	9
23	08.06.2023	Sedeyakha	2,87	1,20	0,29	0,65	0,39	0,77	0,33	6
24	01.06.2023	Evoyakha	3,30	0,82	0,38	0,49	0,23	0,80	0,38	6
24	08.06.2023	Evoyakha	2,75	1,67	0,61	0,79	0,37	0,91	0,43	8
25	02.06.2023	Evoyakha	2,14	1,07	0,49	0,54	0,32	0,78	0,57	6
25	08.06.2023	Evoyakha	2,93	1,58	0,74	0,71	0,41	1,02	0,56	8
26	31.05.2023	Sedeyakha	2,81	0,53	0,35	0,35	0,17	0,46	0,26	5
31	03.06.2023	Evoyakha	5,19	0,63	0,81	0,90	0,39	1,01	0,62	10
27a	06.06.2023	Evoyakha	2,99	1,57	0,50	0,54	0,25	0,58	0,40	7
27b	06.06.2023	Evoyakha	4,15	1,30	0,50	0,51	0,27	0,59	0,52	8
27c	06.06.2023	Evoyakha	2,93	1,49	0,75	0,51	0,30	0,81	0,40	7

Table 2. Hydrochemical characteristics and content of major ions in water bodies of the Pur River basin during the 2023 low-water season

Station	Date	River	HCO_3^-	SO_4^{2-}	Cl^-	Ca^{2+}	Mg^{2+}	Na^+	K^+	M, mg/l
			mg/l							
1	21.08.2023	Pyakupur	37	0,60	2,63	7,79	2,78	2,32	0,38	53
2	20.08.2023	Pyakupur	35	0,84	4,34	7,41	3,23	4,62	1,20	57
3	21.08.2023	Pyakupur	29	0,97	1,32	6,08	2,66	2,73	0,45	44
4	22.08.2023	Ayvasedapur	42	0,56	1,19	10,18	3,63	1,77	0,32	60
5	22.08.2023	Pyakupur	34	0,58	3,01	5,66	2,54	2,70	0,59	49
6	22.08.2023	Ayvasedapur	33	0,44	1,16	6,21	2,76	1,74	0,25	45
7	22.08.2023	Pur	33	0,76	3,49	6,13	2,68	2,90	0,37	49
8	23.08.2023	Pur	17	0,86	1,65	2,50	1,21	0,89	0,18	24
9	23.08.2023	Pur	17	0,81	1,70	2,08	1,88	0,69	0,17	25
10	23.08.2023	Pur	16	0,86	0,63	3,07	1,54	1,11	0,23	23
11a	23.08.2023	Pur	31	1,58	2,03	5,94	2,79	1,90	0,50	46
11b	23.08.2023	Pur	51	1,23	4,13	7,62	3,36	6,07	2,31	75
12a	29.08.2023	Pur	35	1,48	3,10	6,19	2,80	2,12	0,36	51
12b	29.08.2023	Pur	31	1,17	2,98	6,63	3,16	2,22	0,36	47
20	18.08.2023	Evoyakha	15	5,85	0,28	2,89	1,64	0,85	0,35	27
21	18.08.2023	Sedeyakha	13	5,28	0,50	2,44	1,40	0,87	0,28	24
22	16.08.2023	Evoyakha	11	6,58	0,56	2,38	1,42	0,74	0,24	23
23	16.08.2023	Sedeyakha	13	4,53	0,91	2,39	1,41	0,79	0,24	23
24	16.08.2023	Evoyakha	13	7,26	0,78	2,88	1,72	1,11	0,29	27
25	19.08.2023	Evoyakha	13	4,48	1,70	3,51	1,93	1,23	0,41	27
26	25.08.2023	Sedeyakha	14	3,77	0,62	3,47	1,43	1,18	0,42	25
27	25.08.2023	Evoyakha	19	4,38	0,82	4,64	2,22	1,58	0,40	33
28	25.08.2023	Evoyakha	14	2,28	1,55	2,39	1,26	2,31	0,80	25
29	25.08.2023	Evoyakha	12	2,84	0,92	2,54	1,25	1,51	0,47	21
30	25.08.2023	Evoyakha	16	3,58	2,81	3,76	1,78	3,19	1,52	33
31a	25.08.2023	Evoyakha	16	4,51	2,80	2,75	1,53	1,60	0,60	30
31b	25.08.2023	Evoyakha	17	2,61	1,09	2,39	1,39	1,15	0,22	26
15	21.08.2023	Lake Hanto	53	1,17	1,33	8,22	3,52	1,63	0,29	69
18	21.08.2023	Khanayakha	49	7,60	0,88	8,80	3,69	1,27	0,34	71
19	21.08.2023	Nankpyokh	50	1,88	1,34	10,18	3,59	1,95	0,32	69

MAJOR ION CONTENT

Hydrochemical studies during flood and low-water seasons in 2023 made it possible to determine the content of the main ions (HCO^{3-}, SO_4^{2-}, Cl^- anions and Ca^{2+}, Mg^{2+}, Na^+, K^+ cations) in the waters of the Pur River and its tributaries, as well as to trace their seasonal dynamics. A total of 57 water samples were processed. Chemical analyses were made according to the methods set out in (Komarova, Kamentsev, 2006; RD 52.24.493, 2020).

During the study period the average mineralization of the Pur River water was 10.8 mg/l in spring, and increased to 49 mg/l during the summer low water period, that corresponds to literature studies for other large rivers in the Arctic region (Geoecological ..., 2007). The maximum values of mineralization (75 mg/l) at this time were observed in the area of the village of Urengoy. Average mineralization of the water of the tributary of the Pur River – Evoyakha River during flood is 7.4 mg/l and in summer low water period - 26 mg/l. Meltwater and rainwater share in water supply plays an important role in mineralization and major ions content formation.

According to Alekin's classification (1970), all samples of water of the studied area belonged to the bicarbonate class and mixed type. During the flooding in the Pur River the proportion of Mg^{2+} among the cations was slightly increased (by 1-2%-eq.). Samples from Evoyakha River also belonged to bicarbonate class. They have an increased share of sulfates (8-13%-eq.). An increased proportion of sodium was observed among the cations (12-21%-eq.). During the autumn period the share of SO_4^{2-} uprise to 9-22%-eq. Ca^{2+} prevailed among the cations, but the share of Mg^{2+} was also relatively high, which makes it impossible to distinguish the predominant type.

The major ions content changes along the rivers reflect the sources of water supply. The relative content of Na^+, Mg^{2+}, Cl^- was increased in the water of the Pyakupur River (stations 1, 3) during the flooding period. These elements come from atmospheric precipitation of marine origin and enter into rivers with meltwater. The share of HCO3$^-$ and Ca^{2+} was reduced in comparison to the low-water season, since there was a strong dilution of river water by meltwater from the catchment area. In the samples of the Ayvasedapur River (stations 4 and 6), the proportion of HCO^{3-} was higher by 6-8%-eq., which indicates a lower amount of meltwater in the water runoff. On Pyakupur River in the Tarko-Sale area, increased shares of Na^+ and Cl^- were found, which may indicate the presence of human-made pollution. Downstream, the ratio between the main ions changed slightly.

I n the Evoyakha River basin during the flooding, smaller proportions of HCO^{3-} were observed in comparison with the Pur River. The river is mainly fed by meltwater, as well as the waters of lakes and swamps, which are gradually thawing. The intake of swamp waters in the upper reaches contributes to an increase in the share of SO_4^{2-} as well as K^+. In the middle and lower reaches of the river. The third factor that increased the amount of Na^+, Cl^-, SO_4^{2-} in the ion composition of water is the anthropogenic influence of the city of Novy Urengoy, from where these chemical elements come from wastewater and from storm sewers. The influence of the city weakened in the lower reaches of the river (station 31) as a result of dilution by tributaries.

During the low water period, an increase in the content of HCO^{3-} and Ca^{2+} was observed in the Pur River as a result of the predominant supply of groundwater to water bodies, in particular, as a result of melting of permafrost. The share of Mg^{2+} changed slightly. The SO_4^{2-} and K+ ions content accounted for 1-3%-eq, which indicated a weak contribution of swamp waters to the total water runoff. The increase in Na^+ content observed in station 11b water is probably due to the influence of the river port of the settlement Urengoy.

In the Evoyakha River basin more heterogeneous macro-component composition was observed in the low water period. Compared with the flooding, the share of HCO^{3-} has changed slightly, but the amount of SO_4^{2-} has increased significantly, especially in the upper reaches of the Evoyakha and Sedeyakha Rivers (up to 23%-eq). This may occur due to the intensive flow of water from the swampy part of the river basin. Close to the sampling station 27 (below the treatment facilities and industrial sites of Novy Urengoy city), an increase in the share of Na^+ and Cl^- was observed, which can be attributed to human influence, which can be traced throughout the entire middle and lower reaches of the river.

SUPPLEMENTARY 3

Table 1. Source contributions of MMs (%) by the MLR-APCS model in suspended matter of the Evoyakha River

Factor	F1	F2	F3	F4	R^2
Al	31	**65**			0,97
Ti	31	**65**			0,97
V		**94**			0,74
Cr	77	18			0,72
Mn	34		**50**	11	0,88
Fe	**63**	29			0,93
Co	23	18	**45**	13	0,81
Ni	**67**	12	21		0,90
Cu		**65**		25	0,49
Zn	**60**	19	11	9	0,80
As	**75**	17			0,60
Rb	33	**67**			0,97
Sr		**97**			0,69
Cd	**56**	32		7	0,54
Sn	9	**59**	7	25	0,64
Sb	**53**	21	25		0,46
Ba	18	**74**			0,88
Pb		**81**		13	0,66
Bi	22	**40**		35	0,62
U	16	79			0,89
Eigenvalue	7,9	4,6	1,5	1,4	
% Total	39,7	22,9	7,7	7,1	

Check for updates

CC BY

RESEARCH PAPER

PHYSICAL-GEOGRAPHICAL CHARACTERISTICS OF THE UNA RIVER BASIN – CONTRIBUTION TO THE ANALYSIS OF THE STATE AND POSSIBILITIES OF RADIOACTIVE WASTE DISPOSAL IN THE BORDER ZONE

Aida Korjenić[1*]

[1] University of Sarajevo, Faculty of Science, Zmaja od Bosne 33-35, Sarajevo, 71000, Bosnia and Herzegovina

***Corresponding author:** aida.k@pmf.unsa.ba

Received: November 21st 2024 / Accepted: November 22nd 2024 / Published: December 31st 2024

https://doi.org/10.24057/2071-9388-2024-3306

ABSTRACT. The selection of a location for the disposal of radioactive waste, used sources and spent nuclear fuel in the Republic of Croatia began to be considered as early as 1988. However, in the last 10 years, intensive activities have been undertaken regarding the selection of this location. One possible location is Čerkezovac in the Trgovska Gora area, which is located in the Una River basin and less than 1 km away from the border with Bosnia and Herzegovina. It is planned to establish a Radioactive Waste Management Center in Čerkezovac, where all spent radioactive sources located at two sites in Croatia, all institutional waste owned by Croatia, as well as low and intermediate level radioactive waste from the Krško Nuclear Power Plant, would be accommodated. According to the ESPOO Convention (Art. 1, paragraph VIII), transboundary impact implies any impact, not exclusively of a global nature, within the jurisdiction of the signatory state caused by a planned activity, whose physical origin is wholly or partially within the jurisdiction of another signatory state. The majority of the influential surface area of the radioactive waste disposal site (assuming a distance of 5 km from the Čerkezovac site in the Trgovska Gora area) is located within the territory of Bosnia and Herzegovina. This influence could have negative implications on the natural values and protected areas in the Una River valley in Bosnia and Herzegovina, as well as the life of the population.

In this paper, based on the analytical-synthetic research approach, the basic physical-geographical characteristics of the Una River basin have been determined. During the analysis, it was concluded that the connection of physical-geographic components within the Una River basin created a series of natural values that formed the basis for the designation of protected areas. This refers to the fluvial and karst landforms that dominate this area, as well as phytogeographic formations, which stand out for their uniqueness and irreplaceability, morphography and morphometry, and the degree of preservation of physical-geographic phenomena and processes. The results of the research can contribute to a better understanding of the potamological characteristics of the Una, its hydrological significance, as well as the need for environmental protection in the context of the possibility of nuclear waste disposal in the border zone of the Una basin. The processing of all parameters relevant to the study and cartographic representation in this paper were performed in the ArcGIS software package.

KEYWORDS: Una River basin, physical-geographical characteristics, nuclear waste, border area

CITATION: Korjenić A. (2024). Physical-Geographical Characteristics Of The Una River Basin – Contribution To The Analysis Of The State And Possibilities Of Radioactive Waste Disposal In The Border Zone. Geography, Environment, Sustainability, 4(17), 146-158

https://doi.org/10.24057/2071-9388-2024-3306

Conflict of interests: The authors reported no potential conflict of interest.

INTRODUCTION

The presence of radioactive nuclides generated by nuclear power plants or diverse civilian and military applications constitutes a substantial environmental challenge in the contemporary era (Delić et al. 2016) and the optimal approaches to handle radioactive waste and spent nuclear fuel progresses together with advancements in engineering knowledge and technologies (Veinović, 2016). Radioactive waste includes a range of materials that maintain heightened levels of radioactivity even after being used and disposal, while spent nuclear fuel comprises the leftover radioactive substances utilized as fuel within nuclear power plant reactors. According to (Đurić et al. 2021), the lifetime of radioactive waste repositories is 60 years, while the period for the cessation of radioactive impact extends beyond 250 years.

Following the assessment of Croatian territories in 1993, seven locations with potential for the disposal of radioactive waste were identified: Petrova gora, Trgovska gora, Zrinska gora, Moslavačka gora, Bilogora, Papuk-Krndija, Psunj, and Požeška gora. At a subsequent phase, utilizing the PROMETHEE analysis (Preference ranking organization method for enrichment evaluations) dating back to 1997, four potential sites for establishing the repository were identified: Moslavačka gora, Trgovska gora, Papuk, and Psunj. According to (Lalić et al. 2023), research on the construction of a radioactive waste repository in Croatia was conducted based

on studies by various authors (Jurković et al. 2000; Trontl et al. 2010; Trontl et al. 2020; Mostečak et al. 2012; Pevec et al. 2017; Jakić and Filipin, 2018). Ultimately, as per official strategic documents regarding radioactive waste management, the Government of the Republic of Croatia designated the Čerkezovac site on Trgovska gora as the exclusive preferred location. This indicates that it is the sole site where additional investigations will be carried out to evaluate the possibility of building and establishing a repository and disposal site for radioactive waste (Samardžić et al. 2021).

Radioactive waste, mostly low and medium-level radioactive waste from the Krško nuclear power plant, as well as spent nuclear fuel, should be placed at this location. In addition to this, all radioactive waste (RAW II) generated in medical institutions, industry and research institutes for which the Republic of Croatia is responsible will be stored. Based on the quantities generated so far, it is estimated that the amount of low and medium-level radioactive waste produced by the Krško nuclear power plant until 2043. It is considered that the total volume of this waste that should be stored and then disposed of at the Čerkezovac site is about 5,000 m^3. According to the Strategy for the Disposal of Radioactive Waste, Used Sources and Spent Nuclear Fuel of Croatia, the surface type of disposal is preferred, whereby the contents of the disposal site are isolated from people and the environment by a system of barriers (Fund, 2015).

Trgovska gora is located in the Una River basin, which mostly covers the territory of Bosnia and Herzegovina. In Bosnia and Herzegovina, there are 594 settlements with 339,790 inhabitants in this basin according to the 2013 census. The territory of 12 municipalities within the Una River basin belongs either entirely or partially to the entity of Republika Srpska, where 164,498 inhabitants reside, while 10 municipalities belong to the Federation of Bosnia and Herzegovina with 175,292 inhabitants, which is about 10% of the total number of inhabitants of Bosnia and Herzegovina. Research on the impact of the construction of radioactive waste disposal sites on Bosnia and Herzegovina by authors from Bosnia and Herzegovina, published in scientific journals and professional conferences (Delić et al. 2016; Samardžić et al. 2021; Đurić et al. 2021; Mandžić et al. 2021; Trbić and Đorđević, 2021; Lalić et al. 2023), nevertheless showed that the location in Trgovska Gora does not meet ecological and safety standards. According to (Mandžić et al. 2021), the previous assessment of the available documentation upon which the location of Trgovska gora was chosen indicates that the designated criteria for site selection were not sufficiently respected. Also, the cross-border impact on Bosnia and Herzegovina was superficially addressed, although about 70% of potential negative impacts could affect the territory of Bosnia and Herzegovina. Lalić et al. (2023) analyzed the impact on seven areas of human security in the local community of Novi Grad in Bosnia and Herzegovina. The research showed that potential disposal of radioactive waste in Trgovska Gora in the Republic of Croatia, in the border area near the Una River and without the consent of the neighboring state would have negative implications and set a dangerous precedent. All mentioned researches indicate, among other things, to the fact that there are still unknown characteristics of the terrain, which are essential for the construction of facilities for the disposal of radioactive waste. In this regard, it is necessary to conduct adequate additional research in the territories of the Republic of Croatia and Bosnia and Herzegovina.

This paper is also a contribution to the analysis of the physical-geographical characteristics in the Una River basin, particularly in terms of their influence on the water balance regime of the Una. Tsang et al. (2015) emphasize that significant progress has been made in hydrology, especially in subsurface flow and transport of dissolved substances, in the last 35 years due to continued interest in assessing the impacts of proposed nuclear waste repositories. Research has been conducted in various geological formations to explore the effectiveness and safety of these potential disposal sites. Progress in hydrological research can find application in other areas as well, particularly in environmental protection and spatial planning. Almost all hydrological characteristics fundamentally depend on physical-geographical factors, and they are considered the main factors of the creation, existence, maintenance, and nourishment of a watercourse (Korjenić, 2020). Certainly, separate physical-geographical entities form a component structure of factors, in the formation and development of a watercourse. These characteristics are mainly expressed through geological, geomorphological (morphographic and morphometric), climatic, hydrographic, pedological and phytogeographic peculiarities of the observed basin.

The study area

The Una River system and its catchment area is the object of research in this paper. The basin of the Una River extends mostly over the territory of Bosnia and Herzegovina, while a smaller area includes part of the neighboring Republic of Croatia. The Una River system drains water from the area, partly or entirely, 22 municipalities in Bosnia and Herzegovina, while in neighboring Croatia, this area includes 8 municipalities. Trgovska gora, i.e. the Čerkezovac site, designated by the Republic of Croatia for the disposal of radioactive waste, is located in the Sisak-Moslovačka County and the municipality of Dvor (Fig. 1). The location of the planned landfill is a former military storage complex, occupying an area of about 0.6 km^2 (60 hectares). It is situated at an altitude of 319.4 meters, in the eastern part of the Trgovska Gora massif, not far from the valley of the Una River and the state border with Bosnia and Herzegovina (mingor.gov.hr). Although there are indications for postponement, the start of construction of the center is planned for 2025, while the planned start of work is scheduled for 2026.

Analysis of the river system and morphometric indicators were obtained using Arc GIS software, from topographic maps at a scale of 1:25,000. According to (Korjenić, 2018), considering all permanent and the largest intermittent streams, the total length of the watercourses in the area of the Una basin is 10,190.6 km. The length of the intermittent streams is 6,012.8 km, and the permanent 4,177.8 km.

From its source, where it is formed by numerous karst springs all the way to Bihać, the Una flows in the Dinaric direction, i.e. from southeast to the northwest. Then the river's course turns towards the northeast directions and continues to flow through a deeply incised, wide and spacious valley. It maintains this direction all the way to Kostajnica, from where it flows eastward to Kozarska Dubica. From that part to its mouth in Jasenovac, the Una River takes a meridian direction. The spring of the Una, has typical karst characteristics, which is why the upper part of its stream is classified as karstic. From its spring to Adrapovci, the Una flows through karst terrain and has the hydrographic characteristics of karst, i.e. the absence of a large number of tributaries and sparsely branched tributary valleys. The springs mostly appear near the contact of water-permeable Cretaceous limestones and impermeable Miocene clastites, they are of a concentrated type and have an ascending-overflow mechanism of emergence (Institute for Water Management, 2009). From the Bihać to Bosanska Krupa, the Una flows through a canyon and there are no major tributaries in this part. From Bosanska Krupa towards Rudice, the Una receives larger tributaries from

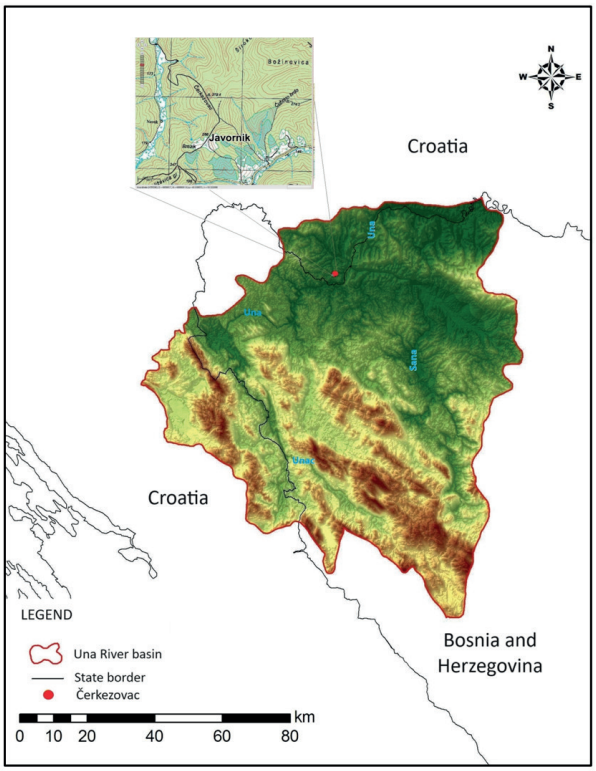

Fig. 1. The location of the Una River basin and Čerkezovac site

the right side: Krušnica, Bukovska and Vranovina, and from the left: Ljusina, Baštra and Glodina, as well as other smaller streams. Downstream towards Novi Grad, the Una receives Vojskova and Vidorija on the right side and Javornik, Crni Potok and Svinjica on the left, as well as numerous smaller streams. In this lower part of the basin, the tributaries of the Una are widely branched in their upper courses.

The southern part of the Čerkezovac location drains through local stream valleys, both east and west of the main ridge, into the aforementioned Crni Potok. At Novi Grad, on its right side, receives its largest tributary, the Sana. In this catchment area, significant accumulations of groundwater have formed, which discharge at the karst springs of the Sana, Ribnik, Okašnica, Sanica, Korčanica, Dabar and Zdena. After the confluence with the Sana, from Novi Grad towards Kostajnica, Una receives the water of several larger and smaller streams. Tunjica, Strižna and Strigova flow into the Una on the right, while tributaries Žirovnica near Dvor, Divuša, Lorić and Volinja on the left side of basin. Going further downstream towards Kozarska Dubica and the confluence of the Una and the Sava, several tributaries can be distinguished that feed Una in its lower course. Vučijak and Petrinjica with narrow and deep, and Slabinja, Mlječanica and Binjacka with wide valleys on the right side, while on the left side Krivaja and Ivančevac flow into Una.

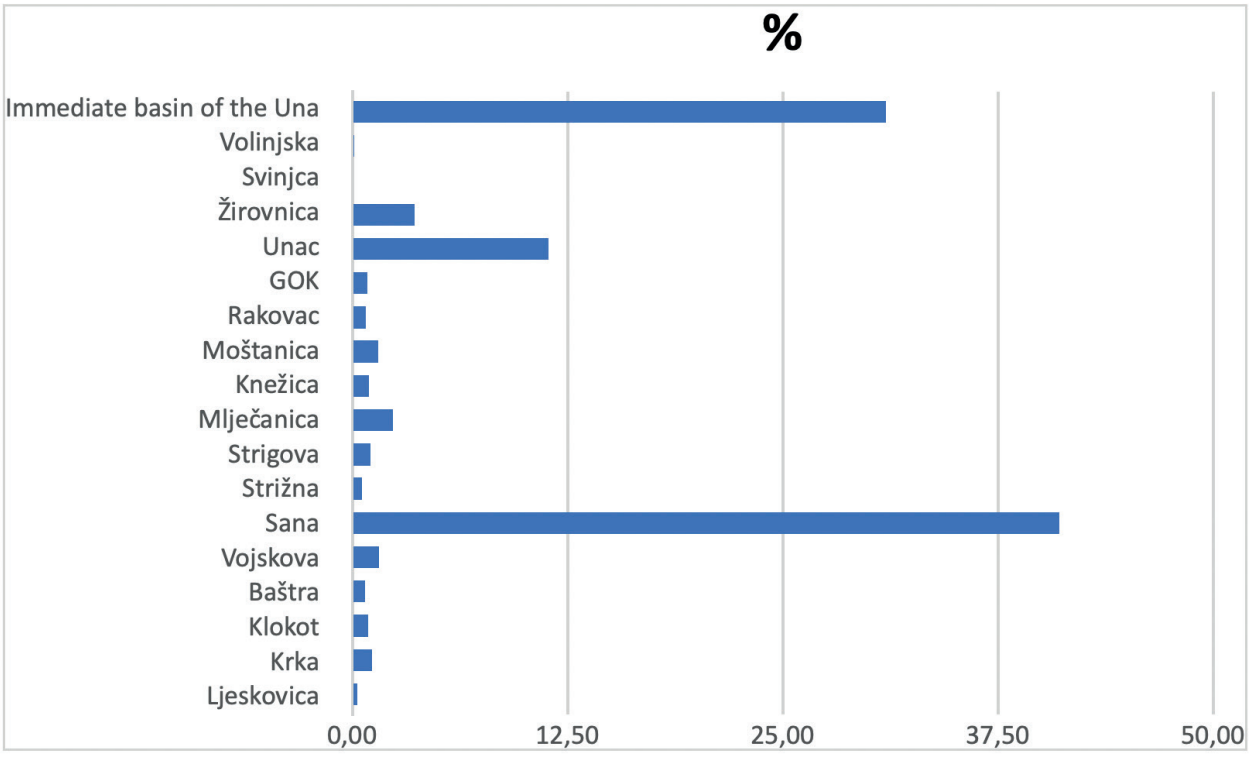

Diagram 1. Percentage participation of the larger tributary basin in the total Una basin

MATERIALS AND METHODS

The study involves synthesizing various component research along with additional field studies of the given area. To determine the general hydrographic characteristics of the area of the Una basin, phase surveys were used, which sought to determine quantitative-qualitative features in the spatio-temporal dynamics of the main elements of the river regime and water balance. In the first phase of the work, it was necessary to determine and separate, and then thoroughly analyze the identified physical-geographical factors. All considerations were directed towards the mechanism of modifying influences on the hydrographic specificities of the Una River basin. For this purpose, various thematic maps were created, which, in addition to visualization, further contributed to a better understanding of the presented theoretical positions. During the second phase of the work, basic meteorological and hydrographic-statistical data were collected, obtained on the basis of direct instrumental measurements of meteorological and elements of the river regime in the Una River basin. The classification and methods of processing these data are based on the established criteria of meteorological and hydrographic statistics and adapted for the realization of the goals and objectives of this study. All data were brought to the same length of the time observation series of thirty years for the period 1961–1990. This period was taken into consideration due to the fact that meteorological stations and measurements were interrupted during the war in Bosnia and Herzegovina during the 90s of the last century, so that the next climatological series 1991-2020 is not complete and continuous. By applying the analytical-synthetic method, in the third phase, a quantitative-qualitative comparison of the above-mentioned characteristics was made between all water-meter stations, and based on them, the physical-geographic regularities in the temporal and spatial dynamics of each element of the river regime were determined. In this regard, thematic maps were created for visual representation of the spatial distribution of analyzed hydrological parameters.

During the work, various computer programs were used for cartographic processing, graphic, tabular and textual representation. Morphometric measurements and cartographic analyzes in the Una River basin were performed by computer, using the ArcGIS software, on geocoded and digitized topographic maps at a scale 1:25,000 for the Una River basin. According to (Medeiros et al. 2023), landscape cartography facilitates the evaluation of geosystemic units by considering their environmental, social, economic, and cultural roles. Overexploitation of these functionalities can lead to environmental issues and irreversible impacts on the natural system.

RESULTS AND DISCUSSION

Physical-Geographical Characteristics of the Una River Basin

Various data can be found in the professional literature regarding the surface area covered by the Una River basin. It is mostly reported that the basin covers 9640 km^2 (Spahić, 1991), 9368 km^2 in the territory of Bosnia and Herzegovina, of which 5020 km^2 is within the territory of the Federation of Bosnia and Herzegovina (Žigić et al. 2010). Most of the data is related to the orographic or topographic watershed, which, due to the predominant terrains with aquifers of fissure-cavernous porosity, does not constitute a real watershed between the neighboring basins and the Una basin, so they should be taken with caution. It is difficult to determine the concrete and precise watershed, and thus the area of the basin, until direct hydrogeological research is carried out in the area of the entire basin. In recent times, such research has been conducted in the area of the western and southwestern parts of the watershed. The geological structure of the terrain, diversity of rocks with different permeability, and tectonic characteristics of this area have resulted in a surface watershed that separates in the northwest, north, and northeast, and in the southern part of the basin near Bosansko Grahovo. The watershed further extends into the interior and does not coincide with the orographic watershed. At the same time, it should be noted that the majority of the territory covered by the watershed is made of carbonate, water-permeable rocks, and that the area is abundant in fault-line fractures, which has influenced the mismatch between surface and underground watershed. According to (Bošnjak, 1938), the upper part of the Una valley is cut into a series of Mesozoic limestones, i.e. a deep karst between Grmeč in the east and Plješevica in the west. The area of deep karst descends towards the north and near Bihać transitions into an area of shallow karst that belongs to the rim of the Pannonian basin. The middle course of the Una up to Arapovac (downstream from Novi Grad) is developed in the karst plane, while the lower part of the Una course is in the Paleozoic and flysch zone. The area around the mouth of the Una River into the Sava River is of the youngest origin and was formed during the Diluvium, constructed from diluvial and alluvial sediments. The polymorphism and polygenetic structure of the Una valley are reflected through a series of smaller and larger valley interconnected by gorges and canyons. The valley represents tectonic depressions lowered along faults, formed in the middle of the Tertiary period during the Oligo-Miocene uplift of the Dinaric system (Spahić, 1988).

The canyons in the valley of the Una River were formed by the erosion of the lake islands, at the end of the Pliocene, during the drainage of the lake from the Pannonian Basin. Fluvial and lacustrine terraces are represented along the entire length of the Una River and generally maintain the same relative height along the river's course, while their absolute height increases upstream. The polyphasic nature of the Una valley is also indicated by travertine barriers, which have divided the longitudinal profile of the Una into sections.

In the Una River basin, the presence of 5 deep faults and a series of first and second-order fractures has been determined. According to the seismotectonic map (Fig. 2), the deep faults are: Una, the Novi Grad - Banja Luka (Olovo - Višegrad), Kozara, Kozara - Spreča and Sava faults. By comparing these faults with the surface geological formations and structures, it is noted that they generally coincide with the paleogeographic and larger tectonic units in the Dinarides, as pointed out by numerous authors (Herak, 1986). First-order faults, both longitudinal and transverse, are young (neotectonic) faults with lengths exceeding 10 km, and they are associated with the epicenters of previous earthquakes.

Trgovska gora is located approximately 1 km from the active fault zone. The tectonic conditions indicate the existence of an assumed fault running almost west-east. According to (Delić et al. 2016), the fault trace is about 450 m south of the Čerkezovac military facility. The geological structure significantly influences on the maintenance of rainwater on the surface and its absorption into underground. It determines the depth of erosion processes and the incision of river valleys. Geological factors also play a significant role in the movement of underground water. They determine the conditions for groundwater formation, its position, flow velocity, depth of hydrological isolator and the character of the hydrological collector. Among other things, hydrogeological relations also influence the density of the river network.

The area of the Una River basin considering its spatial

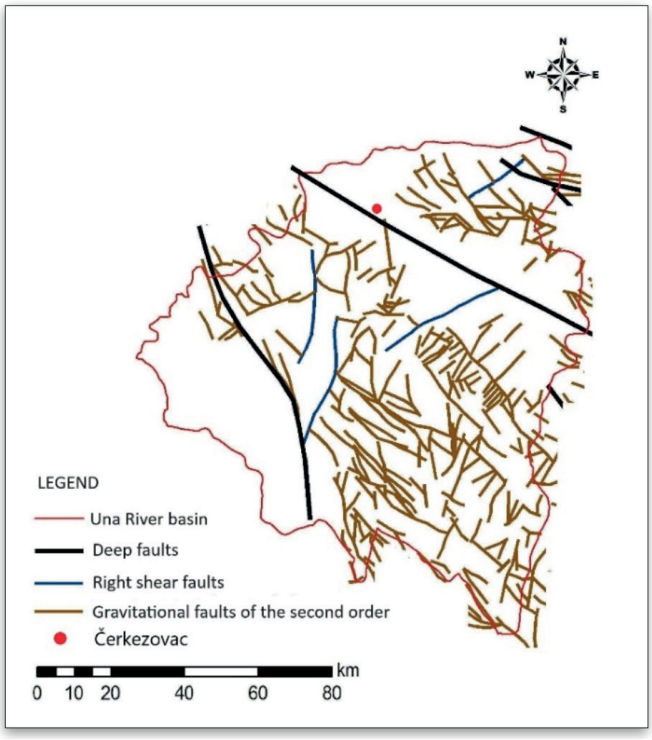

Fig. 2. Location of faults in the Una basin

Source: GIS database of FB&H Spatial Vulnerability Studies

extent, directionality, and significant differences in altitude, is characterized by a complex geological structure and lithological composition. This is a direct consequence of a long and complex geological past as well as complex geotectonic movements. In the preparation of this study, during the analysis of the geological composition of the terrain, the geological map a scale 1:500 000 was used, as well as 1:100 000, sheets Bihać, Kostajnica, Bosanska Krupa, Prijedor, Banja Luka, Ključ, Drvar, Glamoč, Udbina and their interpreters. Paleozoic rocks, as the oldest, are part of the Sana - Una and Paleozoic of Ključ. In the Una River basin, the rocks of the Sana-Una Paleozoic extend from the right tributaries of the Una: Vojskove, Čađavica and Vidorija in the northwest, and within the area of Piskavica – Bronzani Majdan – Kozica valley – Sanski Most – Budimlić Japra – Rudice (Una valley) – Novi Grad. A part of the Una basin in the northwest, specifically the right side of the Žirovnica basin, belongs to the Banija Paleozoic. The border between the Banija and Sana - Una Paleozoics is formed by the river Una. The oldest Paleozoic rocks of this basin belong to the Lower and Middle Carboniferous. Carboniferous deposits are represented by sandstones, conglomerates and shales, and interlayers of dolomite and ankeritic limestones.

Trgovska Gora is mainly composed of clastic Paleozoic deposits of the Lower Devonian - Carboniferous period, represented mainly by shales (clay shale), marls, sandstones, less often conglomerates, limestones and dolomites.

The Lower Triassic formations, in their classic facies development of verfen layers, are widespread in all structural-facies units. The composition of the Lower Triassic deposits mainly includes clastic rocks: sandstones, marls and clays, and carbonate rocks: limestones and less often dolomites. All these rocks are affected by metamorphic processes of a lower degree, so they represent, in fact, semi-metamorphic rocks. The Middle and Upper Triassic formations, in some parts of the observed area, could not be separated, and as undivided, these formations are represented by limestones, dark gray cherts and marls.

The tectonized ophiolitic mélange is part of the Central Ophiolitic Zone, and in the area of the Una River basin it is registered on the geological map, sheets Kostajnica and Prijedor. The formations of this mélange represent a paleo-relief in younger Tertiary sediments, tectonically separated from Eocene flysch and Triassic deposits, often overlain discordantly by Miocene sediments. They consist mainly of sandstones, clays, marls and cherts. Along with these rocks, conglomerates occur, as well as igneous rocks with serpentinites, diabases, gabbros, and occasionally granites.

The Paleogene is represented in the Una River basin by formations from all three of its epochs: Paleocene, Eocene and Oligocene. The Paleocene and Eocene are characterized by the carbonate type of sediments, initially freshwater sheet and layered marly limestones (Paleocene, lower Eocene), followed by marine bank foraminiferal limestones. Towards the end of the Eocene, clastites of the typical flysch series dominate the sedimentation, while during the Oligocene layered conglomerates, sandstones and marls play a leading role. Flysch deposits are also registered in the northwestern part of the basin, in the area of Zrinjska Gora, and form a watershed in this area of the basin.

The Quaternary is represented by various clastic sediments in the area of the Una River basin. These deposits are identified across fields, their peripheries, and river valleys. They consist of deluvial slope sediments, proluvium, scree and slope breccias, quartz sand, marsh and lake sediments, river terraces, alluvial deposits and travertine.

Over 40 different stratigraphic units can be distinguished in the area of the Una basin, indicating the complexity and specificity of the terrain, and therefore the complexity of geological, hydrogeological and hydrological relations in this area (Korjenić et al. 2017). The lithological composition of the rocks, their position and the depth of aquifer layers largely influence the conditions of accumulation in the basin and the outflow of groundwater, which feeds the main flow of the Una River. The greatest influence of the geological structure on precipitation runoff occurs in basins whose larger or smaller surfaces are exposed to the process of karstification, as is the case in the Una River basin. Such influence is most intense in the upper part of the basin, where there are no large number of surface watercourses.

In catchments constructed of hydrological isolators, precipitation water is retained on the surface, thus, among other favorable conditions, influencing surface runoff, whereas in catchment areas constructed of hydrological collectors, surface runoff is limited and transferred into the groundwater (Spahić, 2013). This mainly refers to the karstified carbonate part of the catchment, which affects the disorganization of surface runoff into underground drainage.

Based on the previous analysis, seven hydrogeological units of different permeability and transmissivity can be distinguished in the area of the Una basin:

1. aquifers of fissure-caverous porosity,
2. highly karst aquifers,
3. hydrogeological complexes predominantly without aquifers,
4. aquifers of intergranular porosity,
5. aquifers of fissure porosity,
6. non-aquiferous rocks,
7. hydrogeological complexes with aquifers of mixed porosity.

Geomorphologically, Trgovska gora is a separate unit of Zrinjska gora, the larger part of which is composed of Eocene flysch and volcanogenic-sedimentary layers of the "ophiolitic mélange" type (sandstones, clayey and argillaceous shales, breccias, conglomerates, limestones, eruptives, cherts and serpentine).

According to (Samardžić et al. 2021), the complexity of the geological structure in the area of Trgovska gora primarily manifests in the fact that it is located at the forefront of a large regional nappe, where Paleozoic rocks, with poorly water permeability, overlay Triassic carbonates. Triassic carbonates represent the main groundwater aquifers in the lower course of the Una River, thus artesian and possibly thermal waters can be expected in this area. The mentioned authors consider that the geological structure and the proximity of the Una River represent unfavorable circumstance from the aspect of hydrogeology for the storage and disposal of radioactive waste at the Čerkezovac location. The Trgovska gora area and the Čerkezovac locality belong to the grouped water body of the Una groundwater (lower course of the Una).

The Una River basin is predominantly hilly - mountainous in character. If hypsometric zones are analyzed as geomorphological categories, it can be concluded that all levels are represented in this area. Of the total area of the Una basin, the lowest, flattened hypsometric levels cover 1157.73 km^2. The slightly undulating and hilly relief, with its area, participates with 36.23% of the total. When it comes to the area above 500 m above sea level, which refers to foothill steps and mountainous dissected structures, this area encompasses 52.17% of the basin area. The largest share in the area, 3632.88 km^2, has structures from 500 to 1000 m above sea level.

Zrinjska Gora, where the locality Čerkezovac is situated, is intersected by faults of various orientations and likely represented a structural axis in the geological past, extending either E - W or NE - SW. It belongs to the category of remobilized fault-folded rock massive structures of Paleozoic-Tertiary orogeny. It consists of relatively low-medium mountain masses of highly heterogeneous geological composition. Zrinjska gora rises between the Glinska Depression and the Sava Basin. It is located between the rivers Kupa, Sava, Una, Glina and Glinica. The highest peak, Piramida, is 616 meters above sea level. The relief of Zrinska Gora is branched out with several relatively separate units: Zrinska Gora, the hills of Trgovska Gora or Bužimska and the hills of Hrastovička Gora.

By analyzing the basic meteorological parameters in this study, a fundamental picture of the climatic characteristics in the basin area was obtained, which significantly affects the river regime of the Una. The lowest average monthly temperature for a multi-year period in this area is -1.1ºC (January), indicating that it belongs to the C climate or a moderately warm climate, because this climate includes areas with the lowest average monthly temperature ranges between 18 ºC and -3 ºC. The annual air temperature fluctuation is 20.4 °C, which is another characteristic of this climate because, according to Spahić M (2002), in the interior of the continents (areas with a Cfb climate), the fluctuations increase to 18.7 °C, or 22.2 °C. If we consider the highest average monthly temperature of 19.3 ºC (July), and the fact that as many as 6 months have temperatures above 10 ºC (May, June, July, August, September, and October), we can determine the subtype of climate. In this case it is

Table 1. Percentage participation of aquifer types on the of the Una River basin surface

Type of aquifer	Water permeability	%
Aquifers of fissure-caverous porosity	Well permeable rocks	34.1
Highly karst aquifers	Impermeable rocks	19.6
Hydrogeological complexes predominantly without aquifers	Well permeable rocks	10.3
Aquifers of intergranular porosity	Poorly permeable to impermeable rocks	5.7
Aquifers of fissure porosity	Well permeable rocks	20.4
Non-aquiferous rocks	Impermeable rocks	8.3
Hydrogeological complexes with aquifers of mixed porosity	Permeable rocks	1.6

Korjenić i dr. 2017.

Table 2. Surface areas of represented morphogenetic relief types and their proportions in the total area of the surveyed terrain

Morphogenetic type of relief	Area (km^2)	Participation (%)
Karst relief	4429,2	44,4
Fluviokarst relief	665,9	6,7
Fluvial denudation relief	3368,1	33,7
Fluvial accumulation relief	1516,3	15,2

b-subtype climate or climate with warm summer. Analyzing the distribution of precipitation, it is noticed that precipitation occurs throughout the year. There is no dry period in this area, which is precisely characteristic of the f-type climate or humid climate. A larger amount of precipitation occurs in the warmer part of the year, while it is less in the colder period. This is also one of the regularities of the Cfb climate, and it depends on cyclone activity.

The modification of the climate occurs with the increase in altitude, which caused the formation of a submountainous (Cfbx) and mountainous (Df) climate in the south of the basin, specifically in the regions of Grmeč, Osječenica and Plješevica. The humid climate is further confirmed by the analysis of the rainfall factor for the Una River basin area, which amounts to 118.2. According to (Lang, 1915), humid areas are those where the rainfall factor ranges from 100 to 160. By comparing the data on the average annual precipitation and temperatures, data on the drought index according to (De Marton, 1926) were obtained, based on which it is concluded that the entire area of the Una basin has an index greater than 40, specifically 58.2. This value corresponds to areas with extremely good humidity and abundant runoff. All four seasons are clearly expressed. The annual temperature cycle expressed by seasons shows that the average winter temperature is 1.8°C, and the summer temperature is 18.5°C. In addition to warmer summers and colder winters, transitional seasons can also be felt.

The dynamics of the pluviometric regime is greatly influenced by the intensity and frequency of high and low-pressure barometric fields of large and medium scales. In relation to their influence are the characteristics of the thermal regime, relative humidity, cloudiness and windiness, which directly affect precipitation. The total amount of precipitation in the area of the Una River basin of 1273.77 mm was obtained based on the isohyet method, and for the purposes of this study, a map of the average annual precipitation according to the Atlas of Climate of the SFRY was used. The average amount of precipitation between two isohyets multiplied by the area between them is calculated for all isohyets on the basin surface, and the sum of the these obtained multiplications gives the average amount of precipitation in the basin.

Inflow from the basin is also significantly affected by the intensity of precipitation. Heavy rains impact rivers with smaller basins, causing them to rise very quickly and intensively increase the water level in the bed. Steady rains gradually raise water levels and such water levels can last for days, which is very favorable from the point of view of the hydrological balance. Heavy rains, in hydrological practice, usually mean intense precipitation lasting from a minute to 24 hours. The average intensity of precipitation

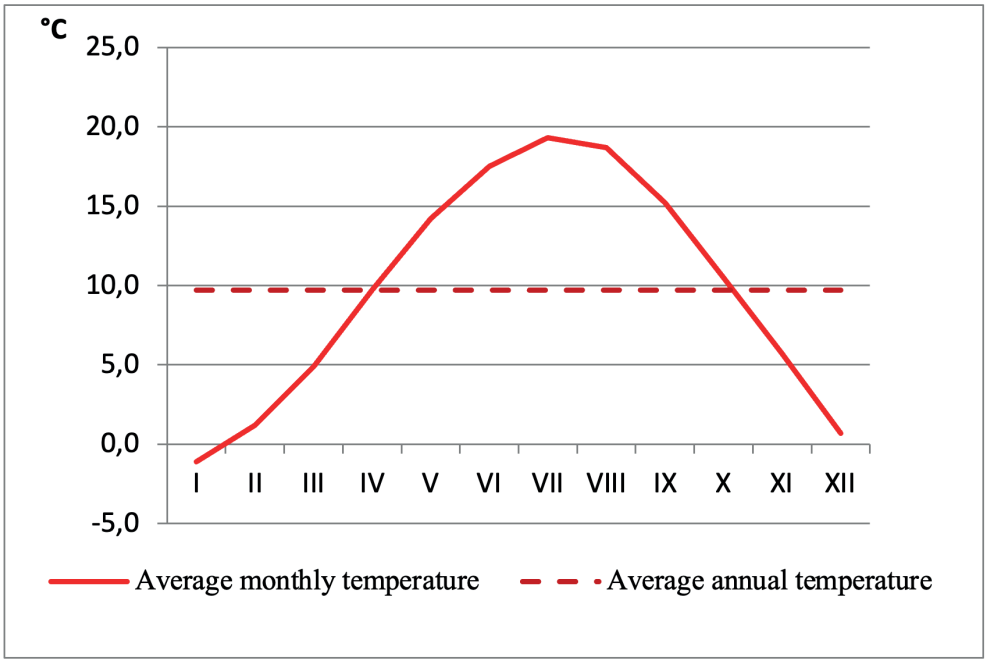

Fig. 3. The graph of the annual course of average temperatures for the Una River basin

Table 3. The annual amount of precipitation in the Una River basin by the isohyetal method

Isohyet in Una River basin	a_i (km^2)	$P = \sum_{i=1}^{n} \frac{\alpha i P i}{A}$
800 - 900	11,9	1,02
900 - 1000	700,6	66,50
1000 - 1250	4844,2	540,00
1250 – 1500	2999,8	412,50
1500 – 1750	1055,7	178,75
1750 – 2000	367,3	75,00
Σ		1273,77

**P - average amount of precipitation, ai - surface area between two isohyets, Pi – the average precipitation that corresponds to the elemental surface ai, and is determined as the mean value of the height of two isohyets, A- total area of the basin, n- total number of elementary surfaces ai Korjenić i dr. 2017.*

is the result of the relationship between the average height of precipitation and the average number of days with precipitation.

Local showers during the summer are of high intensity and can deliver over 5 l/h/m2 of surface area within one hour. Although cyclone activity is significantly weaker in summer, in the northern half of the Una basin it has a significant impact and accounts for approximately half of the total amount of summer precipitation. Unlike the northern part, cyclonic activities in the southern part of the basin pass almost unnoticed. The probability of rain occurring during the summer is below 50%, which is consistent with predominantly clear weather. At the beginning of autumn, cyclonic activity begins to dominate, and over 50% of the total number of cyclones, in this period, affects the catchment area from the southern side. Autumn precipitation is extremely frontal in nature: the rain is usually moderate and long-lasting. The maximum duration of autumn rains, especially in the western parts, can reach up to 20 days. Considering that, autumn has only about 40 rainy days, it follows that half of the total number of days can have consecutive occurrence of rainfall. Regarding the activity of baric centers during the winter, the polar atmospheric front reaches the Mediterranean region, and its baric depressions strongly influence the Una River basin from the south, about 65% of the total number of depressions. Winter cyclone activity noticeably changes the character of the pluviometric regime. The amounts of winter precipitation gradually decrease from the southern parts of the basin towards the northern ones. Winter precipitation, like autumn ones, is frontal, often long-lasting and moderate. Unlike autumn, winter precipitation comes in the form of snow, making this season considerably poorer in terms of precipitation quantity compared to autumn. Spring precipitation is extremely frontal, and local precipitation is observed only in the second half of the season.

Trbić and Đorđević (2021), through an analysis of three five-day indices of extreme precipitation, have determined that they show positive anomalies for the periods 2021-2050. and 2071-2100. By the end of the analyzed period, it is expected that the number of episodes with a five-day precipitation accumulation exceeding 60 mm will increase by three more events in these two periods. According to their research, accumulations during individual precipitation episodes will increase, with a maximum increase of 40% expected during the period 2071-2100. The northwestern parts of Bosnia and Herzegovina, near Trgovska gora, will be particularly exposed to these changes. One of the consequences of the increase in intense rainfall could be the occurrence of flash floods.

A very significant climatic factor influencing the river regime is the snow cover. According to (Spahić, 2013), in combination with spring rains, snowfall can increase the runoff coefficient above 100%. Therefore, monitoring snowfall is of great importance in determining the river regime. Snow and its occurrences are related to the winter half of the year. Therefore, the maximum number of days with a snow cover ≥10 cm in the area of the Una River basin occurs during the winter period, on average 7.2 days. Spring and autumn have an average of 1.4 such days. Heavy precipitation mainly occurs on the southern mountain slopes, and decreases towards the northern parts of the basin. The maximum height of the snow cover usually occurs in January and February, in the range of about 100 to 120 cm for inhabited areas, while at higher altitudes in the conditions of a mountain climate, it can be significantly higher, and snowdrifts can reach a height of over 200 cm.

Elimination criteria in selecting a location for radioactive waste disposal includ, among other things, natural floodplains as well as areas with increased erosion caused by the lithological composition or dynamic relief, areas with landslides and terrains prone to landslides (Conclusion of the Government of the Republic of Croatia, 1992), all of which may occur in the area of Trgovska gora in the event of increased intense precipitation and the formation of flash floods.

In the area of the Una basin, the pluviometric regime is characterized by two distinct maxima, in June and November, and two minima, in February and September. The months in which maximum precipitation occurs differ in individual areas of the basin, depending on a number of factors. Maximums may also occur during May or April, while another, secondary maximum occurs, besides November, also occurs in December. Rainfall minimums also vary in certain parts of the Una basin. They are mostly observed during January or March and then in October.

Looking at the Una River basin in general, it can be concluded that this area belongs to a continental, and a transitional continental pluviometric regime.

Table 4. Average, maximum, and absolute rainfall intensity per season (mm)

	summer	autumn	winter	spring
Average intensity / 1 rain day	11	> 12	< 9	> 11
Maximum intensity	28	30	20	26
Absolute intensity	> 60	60	50	> 50

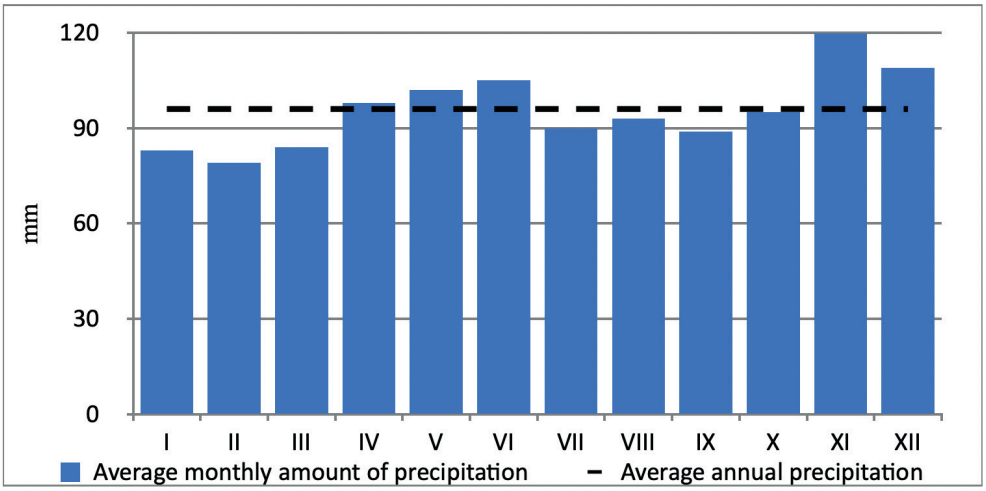

Fig. 4. Graph of the average annual flow of the rainfall regime

The southern and southeastern part of the catchment area is developed in the area dominated by karst, that is, where there is a discrepancy between the surface and underground drainage. In order to explain the impact of karst retention on water flow into the Una River, graphs of the intensity of changes in precipitation and runoff for certain gauges were created. For comparison, the water gauges in the upper and lower part of the Una River were presented and analyzed. Different values and obtained graphs, according to the data for individual gauges, result from different altitudes, geological substrate, or aquifer types represented in the catchment area up to these gauges, as well as monitoring of the annual precipitation regime characteristic for each hydrological station. When determining the relationship between precipitation, air temperature and runoff, the value specific precipitation intensity (i) was used, which indicates how many liters of precipitation are excreted, on average, per second over an area of 1 km^2 of the basin. The correlative value to the specific precipitation intensity is the specific runoff. The following graphs illustrate the dependence of average monthly runoff values on precipitation in the Una catchment area. According to the graph constructed based on the the water gauge data in Kozarska Dubica, in the lower course of the Una River, two phases of increasing and decreasing runoff are observed. The first phase of increased runoff lasts from January to April, and the second from August to December. The phases of reduced runoff last from December to January and from April to August. The positions of points 1, 2, 3 and 4 show that during these months the runoff coefficient is greater than the amount of precipitation.

Two phases of increase and decrease of runoff are clearly observed and in the upper course of the Una River. The coefficient of runoff higher than the amount of precipitation is recorded in March and April. The water meter stations record a similar annual trend, as well as an increase in runoff during the first four months. The significant increase in runoff during April indicates the occurrence of karst and snow retention, which, with a delay, brings water from melted snow and water from very rich underground karst recipients into the streams. This particularly applies to the upper and middle parts of the Una River basin, where waters often flow directly from karst without the gradual formation of a river network.

Through the mutual influence of geological structure, climate, relief, hydrological conditions, vegetation, and human activities, creates a loose surface layer of the earth - soil. The analysis of individual soil types was conducted using the ArcGIS program, based on the pedological maps of Bosnia and Herzegovina and Croatia at a scale of 1:500,000. The highest taxonomic levels of soil classification are divided, and in the area of the Una River basin, the most represented soils are from automorphic division or automorphic soils and hydromorphic division or hydromorphic soils. Different types of soils occur independently but also within a complexes or mosaics. Automorphic soils individually constitute 38.8% of the total area, hydromorphic soils 10.5%, while the largest area is covered by mosaics of different soil types, accounting for 50.6% of the total area of the Una River basin.

Vegetation and land use in the Una River basin area were analyzed using data from the digital database CLC (Corine Land Cover), for Bosnia and Herzegovina and Croatia. This database on land cover status and changes and land use was created under the CORINE program (COoRdination of INformation on the Environment). In the Una River basin area, out of a total of 22 categories identified, deciduous forest vegetation covers the largest area, approximately 3648 km^2. Mixed deciduous and coniferous vegetation accounts for 11% of the total basin area, while coniferous forests account for only 2.5%. Cultivable plots and agricultural areas have a significant share, 27% of the total area, unlike orchards and grainy fruit plantations, which cover only 2.5 km^2. The moderate continental climate, relief, as well as pedogeographic characteristics in the Una River basin area, have caused to the high production of phytogeographic resources in this area. Biogeographically, the basin belongs to the Eurosiberian region and within it to the Illyrian province. The most widespread biome in this area is the ecosystem of temperate moist deciduous forests of sedge oak and common hornbeam (Carpinion betuli illyricum), the ecosystem of beech-fir forests (Abieto-fagetion moesiacae) and the ecosystem of dark coniferous forests (Abieti - piceion illyricum). In the upper Una River area, there also exists the ecosystem of Mediterranean-montane forests of ceris (Quercion cerris), while in the area of Plješevica and the northwestern slopes of Grmeč, mountain beech forests (Fagetion moesiacae montanum) are encountered. Fragmentarly, in the valleys of the rivers Una and Sana, the floodplane forest ecosystem (Populetalia albae)

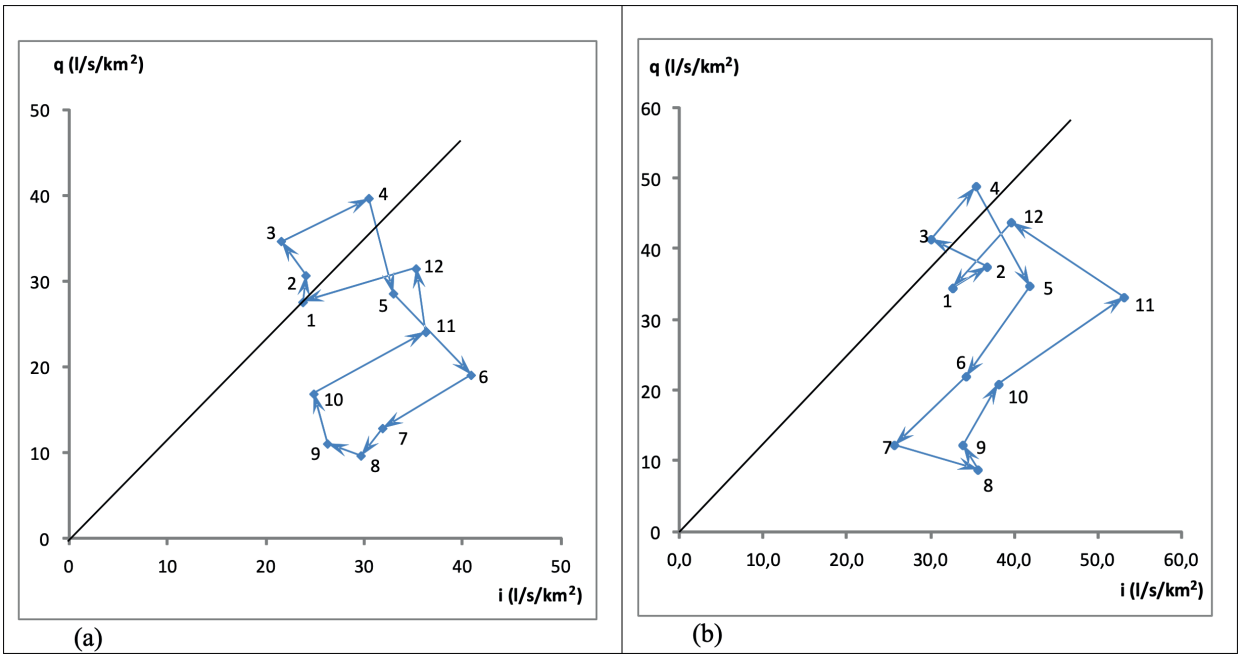

Fig. 5. Graph of precipitation change (*i* = liters per sec/km^2) and runoff (*q* = liters per sec/km^2) at the Una River in a) Bosanska Dubica, altitude *h* = 97.14 m a.s.l, b) in Kulen Vakuf, *h* = 298,8 m a.s.l

can be observed, and on Osječnica, ecosystem of conifer scrub close to the tree limit (Pinion mughi illyricum). The highest zones of the Grmeč and Osječenica belong to the ecosystem of mountainous limestone terrains (Oxytropidion dinaricae). Moderately moist forests are modified by altitude according to the highest hypsometric positions of Plješevica and Grmeč into the type of subalpine forests and pastures. Climatic conditions, primarily air temperature decreasing and the amount of precipitation that increases with the increase in altitude, the geological structure, as well as relief characteristics, slope inclination and the exposure, have largely influence on the spatial distribution of individual phytocenoses. Chestnut forests are characteristic of the basin area, especially its northwestern part. They mix with the downy oak ecosystem at the lower boundary and with beech forests at the upper boundary. The highest zones of Grmeča and Osječenica belong to the ecosystem of mountainous limestone areas (Oxytropidion dinaricae). Moderately moist forests are modified by altitude towards the highest hypsometric positions of Plješevica and Grmeč into the type of subalpine forests and pastures. Climatic conditions, primarily the air temperature which decreases and the amount of precipitation that increases with rising altitude, the geological structure, as well as relief characteristics, slope inclination and exposure, have largely influenced the spatial distribution of individual phytocenoses.

The mosaic of all physical-geographical determinants has influenced the development, shape and size of the catchment area. Through concrete and direct measurements of some basic parameters, indicators have been obtained from which more complex elements of the basin and the Una River course itself have been derived. By measuring the length of the main course as well as all unclassified courses, on the analyzed topographic maps marked as Una, the total length is obtained, which is much greater than the length of the main stream and amounts to 282.2 km.

The Una River basin is asymmetric in favor of the right basin surface, which is greatly contributed by the basin of its tributary, the Sana River. The intensity of flood waves along the entire longitudinal profile can be explained by analyzing the coefficient of basin fullness. This coefficient is always < 1, and the higher and closer to 1 it is, the greater the flood waves and floods on the river. Analyzing the slope in the river flow by sector, it is concluded that the upper course of the Una, from its spring to Bihać, is characterized by significant slopes over short distances, with an average gradient of 2.5°/$_{oo}$. The middle course of the Una, up to Novi Grad, also characterized by considerable falls (1.4°/$_{oo}$), while in the lower course down to the mouth of the Sava, a balanced profile predominates with minimal average gradients, only 0.34°/$_{oo}$. Results should be clear and concise.

CONCLUSIONS

The results of the analysis of the physical-geographical characteristics of the basin surface can be applied in solving water management problems, environmental protection, spatial planning, economic planning and other forms of economic activity. Also, these results can find their practical application in the determination of average water levels for rivers without hydrological monitoring and measurements, in the determination of water balance components and forecasting of hydrological quantities. In this case, they contribute to a better understanding of the physical-geographical conditions in the Una River basin, where the construction of a radioactive disposal site is planned. The interrelationship of the physical-geographical components within the Una River basin has created a series of natural values that formed the basis for distinguishing protected areas.

According to the spatial plan of Bosnia and Herzegovina from 1980, various sections within the valley of the Una River were included in different protection categories:

- the Una River course up to Ripač was included in the regional nature parks of Bosnia and Herzegovina of zero value, and since 2008 it has been designated as a National Park,
- the Una Valley from Ripač to Bosanski Novi (Novi Grad) was categorized as recreational and other natural areas of national importance with protection levels II-IV. Since 2019, it

Table 5. Basic morphometric characteristics

Morphometric characteristics	Value	Unit
Length of the basin	129, 4	km
Maximum width of the basin	127, 3	km
Average width	77, 1	km
Degree of asymmetry	74,7:25,3	(%)
Coefficient of basin fullness	0,63	
Maximum height (Hmax)	1961	m
Minimum height (Hmin)	92	m
Index relief of basin	1869	m
Average height of the basin	598,98	m
Length of the main stream	221,8 km	
Stream development coefficient	1,93	
Total slope of the stream	307	m
Average slope of the stream	1,4	°/$_{oo}$
Watershed incision depth	376,18	m

has been declared a protected landscape known as the "Una Nature park", which includes the lower course of the river Una and the area of the municipalities of Krupa na Uni, Novi Grad, Kostajnica and Kozarska Dubica.

The uniqueness of the Una River primarily consists of hydrological and geomorphological phenomena such as travertine barriers that create waterfalls, river islands, cascades, smaller waterfalls, as well as numerous rare and endemic species of plants. In addition to these, in the Una River basin are protected to a certain degree: Kozara Mountain as a National Park, the primeval forests area of Plješevica and Lom, sites on the Grmeč Mountain abundant with natural, untouched primordial values, primarily geomorphological and biogeographical, than the Sanica River Valley, the springs of the Sana River and the valley of the Sana River to Sanski Most and Bliha waterfall. In the Una River basin, there are registered sites within the Natura 2000 network. This ecological network consists of areas important for the conservation of endangered species and habitats of the European Union, with the aim of ensuring favorable conditions for them and their long-term survival. In the lower course of the Una River, in the territory of Bosnia and Herzegovina, among others, Acidophilic beech forests (Luzulo-Fagion), Illyrian beech forests of the Aremonio-Fagion association, Illyrian oak-hornbeam forests of the Rythronio-Carpinion association and sweet chestnut forests can be distinguished (Milanović et al. 2011). Natura 2000 also protects the area along the left bank of the Una River in the Republic of Croatia, which is located near the locality of Čerkezovac. Although the Una River basin abounds in physical-geographical (natural) values, this area is also characterized by exceptional cultural and historical value.

In this regard, there is justified concern about the potential threat to parts of the territory of Bosnia and Herzegovina and the negative consequences that the construction of this disposal site may have on the life of the population in the Una River valley and its tributaries.

Also, Delić et al. (2016) conducted an analysis of comparative criteria for a low and intermediate-level radioactive waste repository at the Trgovska Gora site. The criteria were grouped into four categories based on prevailing characteristics: technical-technological aspects, facility safety, safety and acceptability of the immediate location, and acceptability of the wider location. The valuation of comparative criteria was performed based on a Preliminary Hazard Analysis (PHA), assuming that each comparative criterion could be considered a hazard. The authors concluded that 22 criteria (79%) are expected to have high-risk levels due to the hazards arising from the selected criteria, and that the Trgovska Gora is an unacceptable location according to most comparative criteria due to the high level of risk.Lalić et al. (2023), state that the construction of a radioactive waste disposal site could cause significant pressure on the public and the population living in that area, leading to a potential emigration. Eliminating criteria according to the Conclusion of the Government of the Republic of Croatia (1992), include, among others, areas in the zone of nominal active faults, areas with intensified erosion caused by the lithological composition or dynamic relief, areas designated for the protection of drinking water sources, special purpose areas and their protective zones, areas of national parks, nominal nature parks and other significant nature reserves.

By analyzing the physical-geographical characteristics in the Una River basin and in part of Trgovska gora, it is clear that this area has a series of eliminating criteria when choosing a location for radioactive waste disposal, which need to be taken into account, leading to planning the construction of disposal sites in another location.

Additionally, a surface disposal facility is planned, which, unlike an underground one, has a lower level of safety and protection. In underground disposal facilities, any contact of people, plants and animals with waste is prevented for a much longer period.

Examples of underground disposal facilities can be found in Switzerland, where the project plans a tunnel disposal facility with a capacity of 80,000 m^3 for low and medium radioactive waste. The disposal tunnel units are lined with concrete, and after being placed in the tank, they are filled with special cement. The closure of the landfill includes the complete filling and sealing of all access tunnels and utility rooms (Levant, 2000).

The Olkiluoto underground disposal facility for low and medium-level radioactive waste in Finland is located at the location of the nuclear power plant, i.e. in the immediate vicinity of the generation of radioactive waste, and was put into operation in 1992. The disposal facility consists of two silos at a depth of 60 to 95 m in tonalites. Depending on the type of waste, the silos differ from each other in that the walls of the silo intended for the disposal of LRW are built of shotcrete, while the silo for bitumenized MRW has thick concrete walls, while both silos are surrounded by solid impermeable rock (Veinović, 2013).

Germany started the process of licensing RAW disposal facility with negligible heat emissions back in 1982. According to its characteristics, this RAW corresponds to the waste classified as low and medium radioactive waste in the Republic of Croatia. According to German legislation, all RAW must be disposed of in underground disposal facility (Commission of the European Communities, 1984).

In Croatia, due to the incomparably lower financial cost, the construction of a surface disposal site for low and medium-level radioactive waste was planned instead of an underground one, without sufficiently taking into account the interests of the local community as well as the long-term and better protection of people and the environment.

REFERENCES

Atlas of the climate of the SFRY 1931-1960. Federal Hydrometeorological Institute of Yugoslavia (in Serbian).

Bošnjak R. (1938). Una Valley, Gazette of the Serbian Geographical Society, Vol. XXIV, Beograd (in Serbian).

Commission of the European Communities (1984). Research project for the determination of the suitability of the mine 'Konrad' as a final repository for radioactive waste products, Luxembourg

Convention on Environmental Impact Assessment in a Transboundary Context (Espoo Convention), https://unece.org/environment-policyenvironmental-assessment/text-convention#article1

De Martonne E. (1926). Aresime et indice d'aritile. Comptes Rendus de L'AcadSci, 182, 1395-1398.

Delić E., Dizdarević E., Softić A., Nukić E. (2016). Comparative Analysis of Site Characterization for Storrage and Deposition of Radio Active Waste on Location Trgovska Gora: What Went Wrong?, 3rd International Scientific Meeting on Civil Engineering and Environmental Engineering E-GTZ, Volume: 3, Tuzla. https://www.researchgate.net/publication/302581310,

Đurić N., Mandžić K., Samardžić N. (2021). Review of the selection of Trgovska Gora for the disposal site for low and medium radioactive waste in the Republic of Croatia, Round table Radioactive waste disposal site at Trgovska Gora in Croatia, Department of Natural, Mathematical and Technical Sciences ANURS, Banja Luka (in Serbian).

Eliminating RAW criteria according to the Conclusion of the Government of the Republic of Croatia (1992), http://narodne-novine.nn.hr/clanci/sluzbeni/257537.html (in Croatian).

Fund for financing the decommissioning and disposal of radioactive waste and spent nuclear fuel of the Krško Nuclear Power Plant (in text: Fund), 2015, Brochure: 10 answers to 10 possible questions about the disposal of radioactive waste in the Republic of Croatia

Geological map of Yugoslavia, sheets Sarajevo, Zagreb, Dubrovnik, R 1:500,000, Federal Geological Institute, Beograd 1971.

Geological map sheets: Banja Luka, Bihać, Bosnia. Krupa, Bosanski Novi, Drvar, Glamoč, Ključ, Kostajnica, Prijedor, R 1:100,000, Federal Geological Institute, Beograd 1975.

Herak M. (1986). Geotectonic frame of karst plains, Acta Carsologica 14/15, Ljubljana

Institute for Water Management (2009). Groundwater bodies in the territory of the Federation of Bosnia and Herzegovina, vol. I, Sarajevo (in Bosnian).

Jakić I., Filipin R. (2018). Analysis of public opinion survey Nuclear energy - thepresent and the future (2000-2017). In: Proceedings of the 12th International Conference of the Croatian Nuclear Society, Zagreb, pp. 166.1–166.11. https://inis.iaea.org/search/search.aspx?orig_q=RN:46136388

Jurković I. A., Prah M., Ječmenica R., Matanić R., Lebegner J. (2000). Public opinion survey Nuclear energy - the present and the future. In: Proceedings of the 3rd International Conference Nuclear Option in Countries with Small and Medium Electricity.

Komatina M. i dr. (1980). Hydrogeological map of Yugoslavia, sheets Sarajevo, Zagreb, Dubrovnik, R 1:500 000, Beograd

Korjenić A. (2018). Spatial Flow and Outflow Distribution in the Una Basin. Hydrology. Vol. 6, No. 2, 2018, pp. 53-60. DOI:10.11648/j.hyd.20180602.12

Korjenić A. (2020). River Una – physical-geographical conditions of hypsometric zoning of waters in the basin. Thesis (PhD), Faculty of Science, University of Sarajevo (in Bosnian).

Korjenić A., Sivac A., Okerić Š. (2017): Geological Characteristics and Density of the Una Water System as a Factor of Spatial Planning, B&H, Journal of International Environmental Application & Science, Vol. 12, No. 1, p. 63 – 72.

Korjenić A., Temimović E., Banda A., Sivac A. (2018). Basic Characteristics of the Pluviometric Regime in the Una River Basin. International Journal of Research, 6(2), 234-245. https://doi.org/10.5281/zenodo.1194665.

Lalić V., Ćeranić P., Baškalo D. (2023). A Radioactive Waste Repository in the Border Area Between the Republic of Croatia and Bosnia and Herzegovina: Human Security Perspective. Security Dialogues, 14 (2). pp. 115-133, DOI:10.47054/SD23142115l

Lang R. (1915) Versuch einer exakten Klassifikation der Boden in klimatischer und geologischer Hinsicht. Internationale Mitteilungen für Bodenkunde, 5, 312.

Levanat, I., 2000. Radioactive waste, APO, Zagreb (in Croatian).

Mandžić K., Đurić N., Samardžić N, Ćerimagić Đ. (2021). Necessary level of field research in the part of Bosnia and Herzegovina, immediately next to Trgovska Gora (site of radioactive waste disposal site in Croatia), Round table Radioactive waste disposal site at Trgovska Gora in Croatia, Department of Natural, Mathematical and Technical Sciences ANURS, Banja Luka (in Serbian).

Medeiros R. B., dos Santos L. C. A., Bezerra J. F. R., Marques A. R., dos Santos G. I. F. A. (2023). Landscape Cartography in the Maranhense Amazon: The Case of the Lower Course of the Pindaré River Basin. Geography, Environment, Sustainability, 4(16), pp. 39-51https://DOI-10.24057/2071-9388-2023-2706

Milanović Đ., Drešković N., Đug S., Stupar V., Hamzić A., Lelo S., Muratović E., Lukić Bilela L., Kotrošan D. (2011). Natura 2000 - Bosnia and Herzegovina, Center for Environmentally Sustainable Development, Sarajevo (in Bosnian).

Mostečak A., Ciglenečki T., Veinović Z. (2012). Public opinion on the need to build a radioactive waste disposal site in the Republic of Croatia. In: Mining-Geological-Oil Proceedings 24, pp. 73–80. https://www.researchgate.net/publication/305215849 (in Croatian).

Orientation Water Management Basis of the Una River Basin/book 5, Energoinvest, Sarajevo 1961. (in Bosnian).

Pevec D., Baće M., Trontl K., Matijević M., Ječmenica R., Dučkić P., Holjak A., Jakić I. (2017). National survey on nuclear energy and radioactive waste in Croatia. In: Proceedings of the 26th International Conference Nuclear Energyfor New Europe NENE2017 (Bled, Slovenia, 11-14 September 2017), Ljubljana, pp.1105.1–1105.18. https://arhiv.djs.si/proc/nene2017/html/pdf/NENE2017_1105.pdf

Samardžić N., Đurić N., Jahić M., (2021). Hydrogeological characteristics of the wider area of Trgovska Gora with reference to the issue of disposal of radioactive waste at the preferential location Čerkezovac in Dvor (Republic of Croatia), Round table Radioactive waste disposal site at Trgovska Gora in Croatia, Department of Natural, Mathematical and Technical Sciences ANURS, Banja Luka (in Serbian).

Spahić M. (1988). Natural values of Una - Sana, Project «Natural and social values of Una - Sana», Institute for Spatial Planning of the Faculty of Civil Engineering in Sarajevo, (in Bosnian).

Spahić M. (1991). The Una River, potamological considerations, Bulletin of the Association of Ecologists of Bosnia and Herzegovina, Series B, No. 6, Sarajevo (in Bosnian).

Spahić M. (2002). General Climatology, Geographical Society of the Federation of Bosnia and Herzegovina, Sarajevo (in Bosnian).

Spahić M. I. (2013). Hydrology of the land, Sarajevo Publishing, Sarajevo (in Bosnian).

Spatial Vulnerability Studies of FB&H (2008). Institute of Hydrotechnics of the Faculty of Civil Engineering in Sarajevo, IPSA Institut, Sarajevo (in Bosnian).

Trbić G., Đorđević V. (2021). Projected intense precipitation in the Trgovska Gora region and its possible impact on the territory of the Republic of Srpska and Bosnia and Herzegovina. Round table Radioactive waste disposal site at Trgovska gora in Croatia, Department of Natural, Mathematical and Technical Sciences ANURS, Banja Luka (in Serbian).

Trontl K., Pevec D., Jakić I., Matijević M. (2020). Radioactive waste management in Croatia-public opinion, legal framework, and policy. Energy Policy, 146.

Trontl K., Pevec D., Ječmenica R. (2010). Public opinion survey - energy - thepresent and the future - 2009/10. In: Proceedings of the 8th International Conference Nuclear Option in Countries with Small and Medium Electricity Grids. https://inis.iaea.org/collection/NCLCollectionStore/_Public/41/086/41086813.pdf

Tsang C.F., Neretnieks I., Tsang Y. (2015). Hydrologic issues associated with nuclear waste repositories, Water Resources Research, 51, 6923–6972, doi:10.1002/2015WR017641

Veinović Ž. (2016). Disposal of radioactive waste - world practice and Croatian challenges, Environmental Protection, Chem. Ind. 65 (7-8), pp. 420–423 (in Croatian).

Veinović, Ž. (2013). Deep Geological Repositories, lecture: Underground waste repositories. Zagreb: Rudarsko-geološko-naftni fakultet (in Croatian).

Request for the issuance of instructions on the content of the study on the environmental impact, Task: Center for the disposal of radioactive waste, (2023). Ekonerg d.o.o., Zagreb. https://mingor.gov.hr/UserDocsImages/UPRAVA-ZA-PROCJENU-UTJECAJA-NA-OKOLIS-ODRZIVO-GOSPODARENJE-OTPADOM/Puo/24_02_2023_Zahtjev_Cerkezovac.pdf (in Croatian).

Žigić I., Skopljak F., Hrvatović H., Pašić-Škripić D. (2010). Hydrogeological regionalization of terrain in the Una River basin on the territory of the Federation of Bosnia and Herzegovina, Proceedings of Faculty of Mining, Geology and Civil Engineering, University of Tuzla, Tuzla (in Bosnian).

Check for updates

CC BY

RESEARCH PAPER

INTERNAL RESERVES OF CITIES: A NEW APPROACH TO ASSESSING THE TRANSFORMATION OF URBAN SPACE UNDER THE INFLUENCE OF BROWNFIELDS

Andrei M. Dregulo[1,2*]

[1] Herzen State Pedagogical University of Russia, 48 Moika Embankment, Saint-Petersburg, 191186, Russia

[2] Institute for Problems of Regional Economics RAS, 38 Serpukhovskaya, Saint-Petersburg, 190013, Russia

***Corresponding author:** adregulo@bk.ru

Received: February 19th 2024 / Accepted: July 25th 2024 / Published: October 1st 2024

https://doi.org/10.24057/2071-9388-2024-3263

ABSTRACT. The disadvantage of the traditional approach to territorial planning of the past years is associated with an underestimation of the essence and multifaceted social brownfields and their importance in the sustainable development of urban areas in post-industrial society. The prospects for the development of the inner space of the city and the quality of life of people largely depend on the presence of brownfields since most of the brownfields can have a negative impact on the environment. This is especially noticeable in large cities and agglomerations. In this paper, we analyze the spatial distribution of brownfields in the largest agglomeration of Russia, comparing their prospects for redevelopment with the analysis of 10 dominant criteria of local priority affecting the transformation of the urban area. The article discusses in detail the reasons for making decisions about the nature of the impact of brownfields and the priority tasks of their elimination: the environmental situation and the economic interests of stakeholders. The study shows that the practice of making decisions on the liquidation of brownfields largely depends on their inclusion in the state register of objects of accumulated environmental damage, which makes it possible to accumulate environmental damage in the near future. However, the entry of accumulated environmental damage into the state register of objects is (1) a practiced procedure because it implies co-financing of the brownfield liquidation project by the federal authorities and (2) an insufficiently objective procedure for assessing the impact (lack of local priority criteria). Based on the conducted research, we believe that the elimination or urbanization of brownfields should be based on the analysis of local priorities in the transformation of urban areas (different from the criteria of modern practice of introducing the state register of brownfields), including the features of the territorial organization of public space, ecological and geographical environment, and public opinion.

KEYWORDS: brownfields, transformation of urban space, internal reserves, pollution, adaptation, redevelopment, accumulated environmental damage, comfortable city

CITATION: Dregulo A. M. (2024). Internal Reserves Of Cities: A New Approach To Assessing The Transformation Of Urban Space Under The Influence Of Brownfields. Geography, Environment, Sustainability, 4(17), 159-170
https://doi.org/10.24057/2071-9388-2024-3236

Conflict of interests: The authors reported no potential conflict of interest.

INTRODUCTION

The territorial aspects of the emergence of brownfields in cities are due to the economic development of the past few years. In the industrial era, many industrial facilities and often residential buildings for workers of these enterprises were located in the historical center of cities. In the post-industrial era, as urbanization processes intensified due to global migration and other factors, the issue of brownfields became increasingly prominent, impacting both the development of inner urban space and the social adaptation of objects and territories back into economic circulation. The spatial distribution of brownfields often depends on the economic specifics of the region and national environmental and sectoral legislation, which causes differences in the types of brownfields and approaches to their elimination. For example, in China, the industrial type of brownfields was the most dominant compared to the mining type, while the eastern part of China was the most "vulnerable" to the abundance of brownfields compared to its western part (Zhang et al. 2022). In the European Union, the dominant part of brownfields is associated with degraded agricultural land and municipal and industrial buildings (Van Liedekerke et al. 2013). In Russia, in the post-Soviet period, so many ruined and abandoned facilities appeared, a number of political decisions were taken to eliminate brownfield "hot spots": especially large landfills, oil and sludge storage facilities (Dregulo and Khodachek 2022). Nevertheless, the modern practice of inventorying of objects with signs of accumulated environmental damage in Russia is not effective enough (Dregulo 2023). Firstly, because it is largely based on the criteria for the spread of Brownfield influence at a high spatial level: 1. The territory's area measured in hectares per square meter;; 2. The number of individuals residing in the territory negatively impacted by the presence of brownfields, expressed in thousands; 3. The number of individuals living in the territory at risk of negative impact due to the brownfields'

location, expressed in thousands. In our opinion, it is ineffective at the local (municipal level) because it does not take into account the local priorities of the development of the city (municipality). At the same time, the inventory procedure is highly bureaucratic and requires significant funding already at the initial stage. The purpose of the article is to develop practices for the inventory of objects of accumulated environmental damage based on correlation signs of the significance of their impact on the transformation of urban space, subsequent clustering (ranking) and project preparation of measures to eliminate them. The novelty of this study lies in the author's new approach to identifying brownfields of accumulated environmental damage – identifying key and socially significant brownfields (high redevelopment potential) and their factors of influence on the transformation of urban space based on local urban development priorities. The local priority of urban development is understood as factors influencing the decision to recognize an object as an object of accumulated environmental harm, based on primary indicators directly or indirectly indicating the object as a source of accumulated environmental harm.2.

MATERIALS AND METHODS OF RESEARCH

Problem statement

The study was conducted on the territory of the St. Petersburg agglomeration, one of the largest in Russia with high rates of urbanization processes (Korshunov 2023; Solodilov 2021). A special place in the development of the St. Petersburg agglomeration as the largest economic hub in the Baltic region is occupied by the "quality of life economy" (Okrepilov 2021). This concept includes the whole spectrum of urban problems that are solved through key areas: the development of the transport network (Sokolova and Starshov 2022), the regional fuel and energy complex (Bondar 2021), including issues of ensuring the health of senior citizens (Safarova and Safarova 2022) and the digital transformation of urban governance and development (Kuznetsov and Gorin 2022). All of these aspects of regional development are closely related to the territorial structure of urban interior space. This causes the problems that have become increasingly obvious with the appearance of brownfields on the territory of the city and its periphery due to past economic (economic) activity. Industrial enterprises play an important role in this. After the extensive privatization of the 1990s, it became obvious that industrial enterprises make the greatest contribution to the negative development of environmental processes that change a favorable urban environment into an unfavorable one. Nevertheless, the studies conducted (Zamyatina et al. 2021) have shown that the enterprise management strives to implement the Sustainable Development Goals and intends to work with city authorities for this, which is likely to be a favorable basis for adapting the inner urban space burdened with industrial and other brownfields.

Understanding Distinction Designations

In the national Russian legislation, the term "objects of accumulated environmental damage" (AED) is used, which does not have the same meaning as Brownfield (B) the term is accepted in Western countries, but still has a fairly close similarity:

- "A brownfield is a property, the expansion, redevelopment, or reuse of which may be complicated by the presence or potential presence of a hazardous substance, pollutant, or contaminant" (Overview of EPA's Brownfields Program);
- "AED – territories and water areas where accumulated environmental damage has been identified, capital construction facilities and waste disposal facilities that are a source of accumulated environmental damage" (Federal Law "On Environmental Protection").

In the further text, we will use the abbreviation B/AED to designate these objects while implying all aspects inherent in both one term and the second.

Design research

Data collection and preparation for the study were carried out in several stages (Fig. 1). At the first stage, the spatial factors of the location of B/AED were determined (a map of the distribution of B/AED was compiled) in the inner and historical part of the city, the peripheral part of the city, and in remote territories included in the metropolitan agglomeration – defining projects in relation to the urban environment and transformational – referring projects to the category of transforming the urban environment, and the matrix B/AED is based on local significance criteria (determinants). Each object (B/AED) was assigned a designation number and a brief description of its location (Table 1).

Table 1. Designation and description of the B/AED location

Brownfield designation	Description
B1	MSW landfill (located in the northern part of Saint-Petersburg)
B2	Landfill of sewage sludge (located in the northern part of Saint-Petersburg)
B3	The territory of 'Tuchkov buyan' (the historical center of Saint-Petersburg)
B4	Territory 'Okhtinsky Cape' (St. Petersburg) (historical center of Saint-Petersburg)
B5	'Krasny Bor' landfill, Leningrad Region (Saint-Petersburg Agglomeration)
B6	MSW landfill Leningrad region, 'Sosnovy Bor' (Saint-Petersburg agglomeration)
B7	MSW landfill on the territory of the state nature reserve of regional significance 'Lake Shchuchye', Zelenogorsk (Saint-Petersburg agglomeration)
B8	Landfill of sewage sludge (located in the southern part of Saint-Petersburg)
B9	Open pits (St. Petersburg agglomeration)
B10	Landfill (in the North-western part of Saint-Petersburg)
B11	Hydro-ash dump (North-eastern part of Saint-Petersburg)

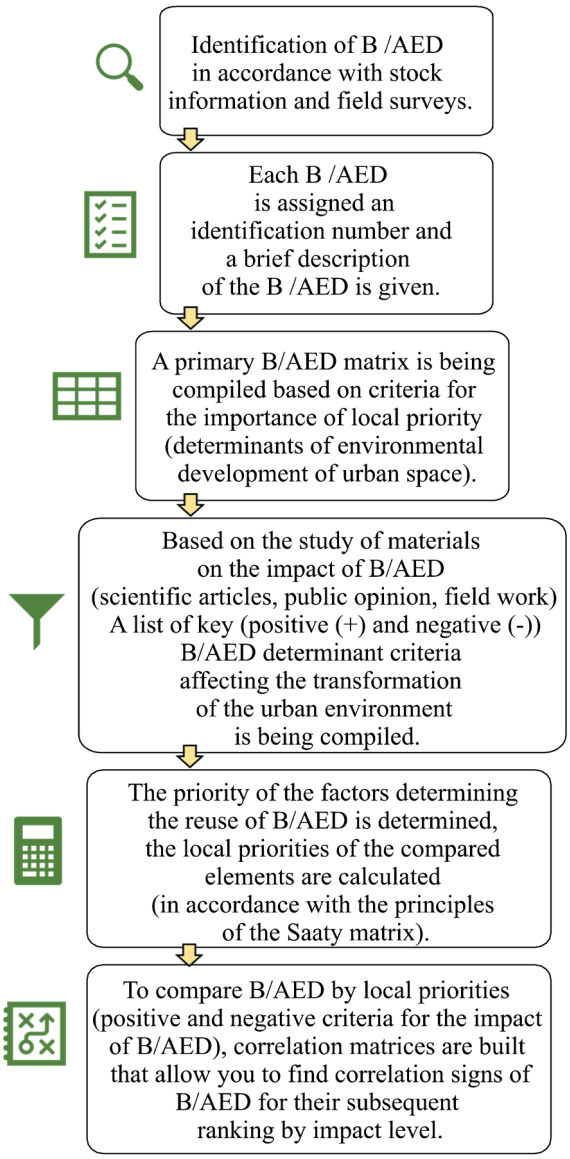

Fig. 1. A flowchart describing the methodology of the study

Table 2. Criteria B/AED impact on the urban environment transformation

Designation of criteria	The value of the criterion	Determinant criteria
C1	-	Has signs of accumulated environmental damage
C2	+	Included in the state register of Brownfields for subsequent liquidation/redevelopment
C3	-	Risks associated with soil pollution
C4	-	Risks associated with water pollution
C5	-	Risks associated with air pollution
C6	+	State property
C7	-	Private property
C8	+	Redevelopment | New (intended) use
C9	+	Public response
C10	+	Measures to eliminate / minimize harm

Among the positive criteria determining the possibilities of economic use of B/AED as a positive factor (+) of influence on the transformation of the urban environment, we included: C2, C6, C8, C9, and C10. Thus, the following criteria were attributed to the negative factors (-) B/AED: C1, C3, C4, C5, and C7. A description of all the criteria is given below.

• Criterion 1. Has signs of accumulated environmental damage. An object localized within the boundaries of a city or its periphery (B/AED). Only redevelopment projects

in certain urban areas, that is, projects related to the occurrence of potential environmental harm/damage, fall under consideration. Projects affecting the territories of the gray belt were not considered.

• Criterion 2. Included in the State register of objects of accumulated environmental damage. Inclusion in the register implies (1) recognition of B/AED as an object dangerous to the natural environment and humans; and (2) guarantees its liquidation.

• Criterion 3. Risks associated with soil pollution. The greatest contribution to this process is made by such types of B/AED as degraded industrial and agricultural enterprises, and MSW landfills. Heavy metals (arsenic, cadmium, zinc, copper, lead, chromium, mercury) get into the soil. Excessive content of these elements leads to diseases in humans, animals, and plants. In addition, soil contaminated with organic substances contributes to the development of rodents that are sources and carriers of pathogens for particularly dangerous infections (rabies, tularemia, plague and hemorrhagic fever with renal-pulmonary syndrome).

• Criterion 4. Risks associated with water pollution. Often, B/AEDs are located in the peripheral part of the city near water sources (rivers, lakes, streams). The increasing climatic risks associated with an increase in the average annual precipitation may provoke the entry of pollutants from surface runoff into reservoirs.

• Criterion 5. Risks associated with air pollution. This aspect is very important for B/AEDs where waste is accumulated or buried. Over a long period of time, the surface solid layers of waste form an isolated (anoxic) structure. The waterlogging of waste contributes to their rapid decay, which in turn is accompanied by the formation and emission of hydrogen sulfide, carbon dioxide, methane, and other greenhouse gases.

• Criteria 6,7. Affiliation. This criterion considers the affiliation of B/AED. This aspect is quite important to consider in light of the fact that, according to many B/AEDs in the post-Soviet space, after privatization, they became conditionally ownerless. The environmental damage caused by the brownfields as a result of the past years' economic activities became an encumbrance for the new owner. And as practice has shown, many were in no hurry to eliminate this environmental damage, as a result of which a new name appeared in the national legislation – "objects of accumulated environmental damage".

• Criterion 8. Redevelopment (changes in the functional purpose of a spatial object in the process of redevelopment). One possible solution is to change the project's concept during implementation. The most significant examples of environmental transformation projects are those that, due to circumstances, do not find a final result for a long time, even in the case of intervention by higher authorities. Such projects are able to form an assessment of the quality of urban environment management (adaptation or transfer of the project to a new location), arising in the process of conflict communication among various actors.

• Criterion 9. Public response. The public response in public discourse, mass media, and Internet media was considered. Increased attention to the problems of environmental safety and the quality of life of the population living in the vicinity or in the zone of impact of B/AED is associated with an increase in the number of publications in social networks, regional media, in which discussions are held related to the possible implementation of B/AED redevelopment projects.

• Criterion 10. Measures to eliminate / minimize damage or harm. This criterion considers that at the time of the study, measures were carried out (in whole or in part) at the B/AED facilities to reduce the negative impact on the environment (reclamation).

Data processing and formalization

In order to determine the priority of the determinants of the reuse of B/AED, an author's summary matrix of B/AED objects was compiled to assess the impact on the transformation of the urban environment, and a summary review was compiled in two areas – positive and negative determinants by the method (Šimková et al. 2020). For each matrix, the local priorities of the compared elements were calculated (assuming a generally acceptable condition). The values of the weights were quantified in terms of the principles of the Saaty matrix (Saaty 1987) with dimensions where m = 1...*i* and n = 1...*j*, given by the number of rows and columns subject to the condition m = n. This symmetric matrix also corresponds to the fact that the method is based on an interactive comparison of all predefined determinants of the same rank with an estimate (Table 3).

Values equal to 1 were taken on the diagonal of the matrix on the principle of comparing the same determinant, that is, their equivalence, and identified pairwise comparisons of individual factors. If the determinant was preferable to the determinant in the column, it was assigned the opposite value. Estimates of a single determinant were determined by the values of factors – partial positions – in accordance with as products of the values of all determinants. To each row of the matrix, and, consequently, to the corresponding element, we

Table 3. Evaluation of negative and positive criteria-determinants in the Saati matrix

The value of the determinant criterion	Description of the compared values of the criteria-determinants
1	Equal importance of the compared elements of the hierarchy. Both the compared elements *i* and *j* have the same significance for a higher-level element
3	Moderate superiority of the *i* element of the hierarchy over O. Previous experience and evaluation suggest that one element is slightly more important than the other.
5	Substantial or strong superiority of the *i* element. Previous experience and evaluation indicate a higher significance of one element compared to another.
7	Significant superiority of the *I* element.
9	The very high importance of the element has clearly manifested itself in the past.
2,4,6,8	A very significant superiority of the *I* element. We are talking about the maximum possible difference between the two elements.

associate the geometric mean of its elements. The values of the factors of partial positions were determined by the Eq. (1):

$$S_i = \sum C_i \quad (1)$$

In addition, the values for each criterion *i* (a finite number of criteria-determinants *c*, where *c*=5) were quantified by the Eq. (2):

$$R_i = (S_i)^{\frac{1}{c}} \quad (2)$$

Based on the calculations performed, the amount was determined by which the final value of the individual weights (local priority) of the criteria-determinants was calculated according to the Eq. (3):

$$a_i = \frac{R_i}{\sum R_i} \quad (3)$$

As a result, we obtained local priorities of the corresponding compared numerical values of weight (local priority of the determinant criterion) reflecting the interaction of various criteria for the influence of B/AED on the transformation of the urban environment and their priority in the process of restoring internal urban reserves. To compare B/AED, correlation matrices were constructed based on the binomial distribution (positive and negative criteria for the influence of B/AED), which allow us to find correlation signs of significance characteristics for their subsequent clustering (ranking) and project preparation of measures to eliminate them. Statistical data processing (construction of correlation matrices based on the Pearson correlation coefficient, which measures the linear relationship between variables of positive and negative criteria for the influence of B/AED on the transformation of the urban environment) was carried out using Seaborn libraries: statistical data visualization[1].

RESULTS

The results of the spatial inventory of B/AED have shown that currently eleven B/AED with different types of economic specifics can be distinguished on the territory of the St. Petersburg agglomeration. The main part of the B/AED is located on the peripheral part of the borders of St. Petersburg and its agglomeration (Fig. 2).

To systematize the criteria-determinants identified, a summary matrix B/AED was compiled that characterizes the potential impact on the transformation of the urban environment (Table 4).

The two brownfields B3 and B4 were among the most discussed objects to be renovated, causing widespread discussion in the community. We pay special attention to them because the public opinion and public response that they received allowed them to subsequently adopt a public point of view on the new functional purpose of these B/AEDs. Objects B3 and B4 are located in the historical part of St. Petersburg (objects B3 and B4). The territory on which object B3 was located was an archipelago of small islands, on one of which a marina was built in the first half of the 15th century.

In the 19th century, a nursery of ornamental plants appeared here, followed by wine warehouses and a vodka factory. The channels between the islands gradually filled up. In the first half of the 20th century, architects repeatedly presented concepts for the development of this place: from the construction of a museum complex to the construction of a city park. At the turn of the 1950s and 1960s, buildings of the State Institute of Applied Chemistry were built here.

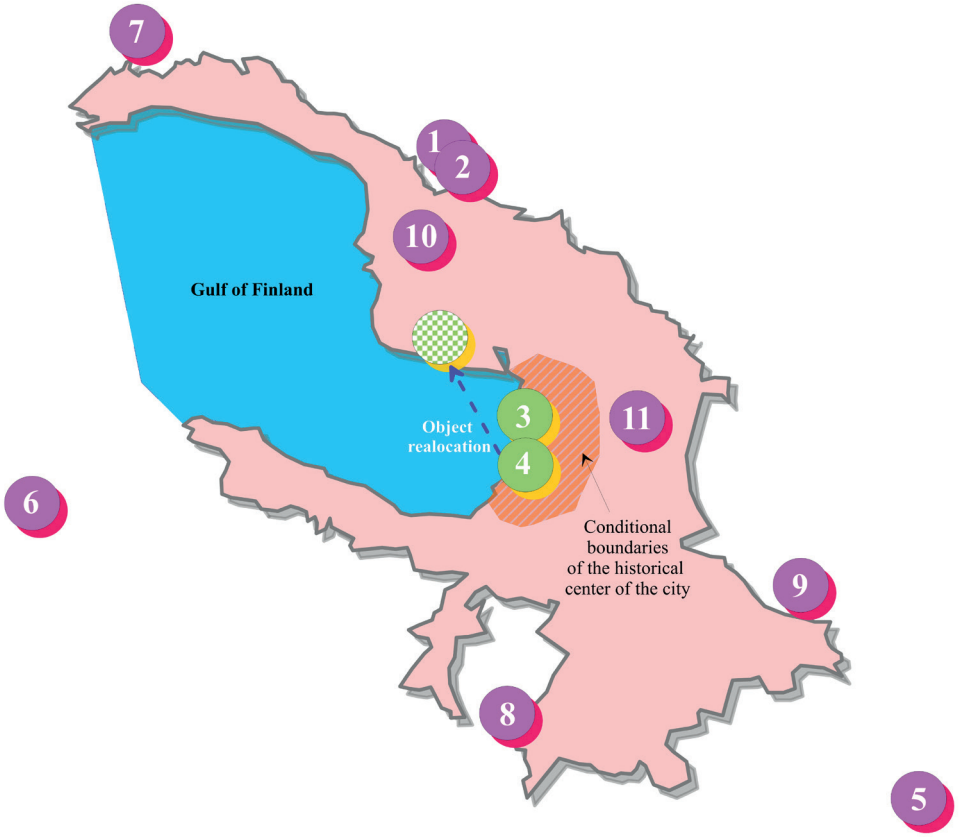

Fig. 2. Location of B/AED in the Saint-Petersburg agglomeration

[1] https://seaborn.pydata.org/

Table 4. Summary matrix of the B/AED impact on the transformation of the urban environment

Object designation	Has the signs of AED	Included in the state register of objects AED	Risks associated with soil contamination	Risks associated with water pollution	Risks associated with air pollution	Affiliation	Redevelopment H-high potential/ L-low potential
B1	yes	no					L (conservation/ reclamation backfilling with soil)
B2	yes	no					L (conservation/ reclamation backfilling with soil
B3							H
B4							H
B5	yes						L (conservation)
B6	yes						L (reclamation)
B7	yes						H
B8	yes	no					L
B9	yes	no					L
B10	yes						H
B11	yes						H
	Pollution risks (which were observed before the redevelopment or are currently being observed)						
	Public response						
	Measures to eliminate / minimize harm						
	State property						
	Private property						
	New (intended) use						
	There is no information / or there is no negative impact						

The rune buildings of the Institute (a redevelopment project involving a new function of urban public space. During the dismantling of buildings, a significant portion of the chemicals that were not removed (or stored for a long time on the institute's territory) contaminated the soil. Significant excavation was required to eliminate environmental damage and achieve environmental safety in public spaces. A full-scale development of cultural and leisure buildings, as well as a park area, is currently being carried out on the facility's territory.

Object B4 is in development after paleogeographic discoveries. During excavations carried out in 1993, artifacts of human habitation from the Bronze Age, the Early Iron Age, and the Neolithic era were found, dating from the end of the fifth millennium BC. This object was of great geographical importance for the defense and development of the northwest. At various times, 'The Landskrona' fortress was located here, built in 1300, and in 1611 the bastions of 'The Nienschanz' fortress were erected. Subsequently, the shipbuilding plants of the 'Okhtinsky Cape' were organized here. In the twentieth century, shipbuilding enterprises were repurposed for the production of technological equipment, and in the post-perestroika (difficult economic time for the country), the territories were planned to be sold for development for business or residential construction purposes.

In 2019, 'Gazprom Neft' acquired this site (1) and developed a new architectural concept for its development. Initially, the plan was to build the Gazprom Tower on this site (2); however, a long public outcry with the participation of many prominent figures of science and culture changed the new building project (3), leading the Gazprom Tower project on the shore of the Gulf of Finland in the northwestern part of Saint-Petersburg.

The situation is more complicated with other objects. Firstly, a significant part of B/AED has high risks

of contamination with environmental components. The vast majority of B/AEDs are located in the Gulf of Finland's catchment area. In particular, these include landfills of solid municipal waste and sewage sludge, which were put into operation in the 1970s and 1980s . Since then, the city's borders have expanded significantly, including as a result of urbanization (construction of residential buildings and the opening of industrial enterprises, including foreign capital). At the same time, a significant part of the B/AED is not included in the state register, while all of them have signs of environmental harm (effects on soil, water bodies and atmospheric air).

It is important to note that only 4 of the submitted objects (B5, B6, B7, B10) are included in the state register of objects of accumulated environmental damage. Half of the studied objects have low redevelopment potential, both in terms of the implementation of engineering and technical measures and in terms of the lack of interested parties. For such facilities, the most likely design solution would be their conservation. At the same time, it should be noted that for some of them there was a public outcry due to the various negative environmental impacts felt by citizens (pollution of soils, water bodies, or atmospheric air) (B1, B2, B5, B6, B8, B9, and B10) (with the exception of objects B3 and B4, the public outcry was caused by location, architecture, including building height restrictions in the historical center). Using the comparative characteristics of brownfields according to the above criteria based on the binomial distribution (yes = 1/no = 0) (Table 5).

• Objects B3 and B4 were intentionally removed from the list after the redevelopment. Based on the comparative characteristics of the binomial distribution, a correlation matrix was formed (Fig. 3), which allows us to identify the most similar objects (B/AED).

The similarity of B/AED can be divided into 3 potential groups: (1) high similarity, a correlation value of 0.8 and more; (2) average similarity, a correlation value of 0.79 to 0.6, and (3) slight similarity, a correlation value less than 0.6. According to the obtained correlation values, in (1) group objects B1-B2, B5; B2-B8; B6-B10; B9-B7, B8. A characteristic feature that unites these objects is waste management activities (burial, warehousing, processing):

• Objects B1, B2. The facilities are located near the nearest "neighbor" of the sewage sludge landfill 'Severny' was commissioned in 1986. The total area of B1, and B2 is more than 150 hectares. In the draft general plan of St. Petersburg approved in 2005, in the period up to 2010, the municipal

Table 5. Comparative characteristics of B/AED according to local criteria based on binomial distribution

Designation of local priority	B1	B2	B5	B6	B7	B8	B9	B10	B11
C1	1	1	1	1	1	1	1	1	1
C2	0	0	1	1	1	0	0	1	1
C3	1	1	1	1	1	1	1	1	1
C4	1	1	1	0	1	1	1	0	1
C5	0	0	0	0	1	0	1	0	0
C6	1	1	1	1	1	1	1	1	1
C7	0	0	0	0	0	0	0	0	0
C8	0	0	0	0	0	0	0	0	1
C9	1	1	1	1	0	0	0	0	0
C10	1	0	1	0	0	0	0	0	0

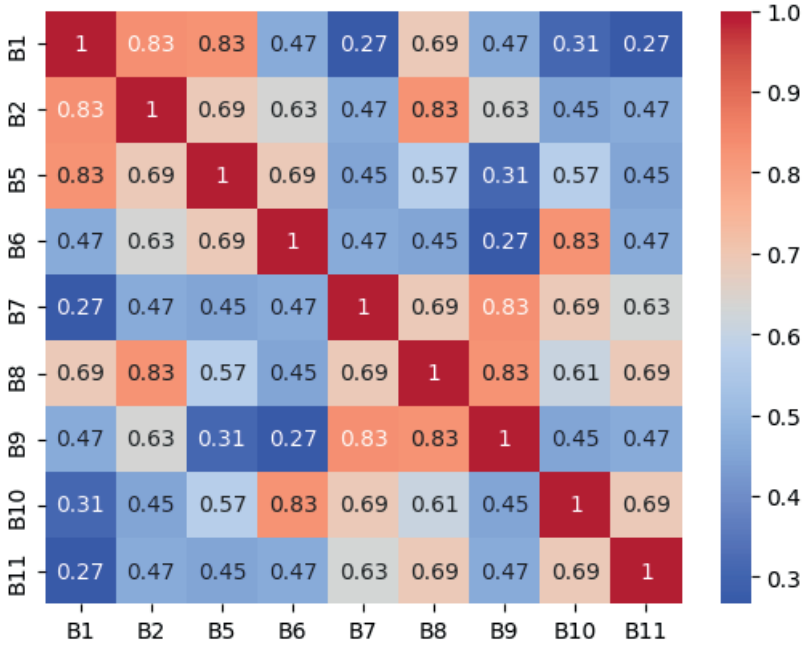

Fig. 3. Correlation matrix of positive and negative criteria-determinants of B/AED based on binomial distribution

authorities had to carry out the reclamation of landfills. However, to date, Facility B1 has been managed, Facility B2 is currently in operation, and there are clear signs of accumulated environmental damage (Dregulo et al. 2022; Dregulo and Bobylev 2021, 2021a). Over the years, there have been a significant number of complaints from the public about the smell of landfills. However, the "neighborhood" of these objects was often used by the management of the objects in blaming each other. Considering the high anthropogenic load in this part of the city, the city authorities have provided for the organization of a specially protected natural area. 'Levashovsky forest', which should be implemented by 2025. The question of how, when, and by whom the procedure for the rehabilitation/ reclamation of landfills is envisaged and what status these territories will have remains open. To date, changes in the law "On the General Plan of St. Petersburg" are "migrating" from one version of the law to another, but there is still no comprehensive solution to the problem.

• Object B5. The 'Krasny Bor' landfill, where waste of the 1st hazard class was buried. The territory of the landfill is subject to reclamation in order to completely eliminate the negative impact on the environment. During the period of operation, the waste in the depths of the landfill mixed and not only did not reduce their danger, but it also turned into a set of decomposition products and the transformation of the original highly toxic substances. This mass of toxicants is located in open maps (partially overgrown with grass and shrubs (1)), not protected from atmospheric precipitation. During the rainy and floody periods, there is intense flooding of waste, which causes the maps to overflow. To date, part of the work has been carried out to cover several maps (2). The general unfavorable situation is further aggravated by the fact that the existing storm water treatment facilities are not operating normally. Currently, the facility has been mothballed and included in the state register of objects of accumulated environmental damage for subsequent reclamation.

• Object B6. Landfill of municipal solid waste. It has been in operation for about 40 years. The work included land restoration; the surface of the landfill was covered with a special insulating membrane; a protective mineral layer and a layer of vegetable soil were laid, followed by the sowing of perennial grasses. The reclamation area spanse 9 hectares. To date, the landfill has been reclaimed.

• Object B7. The dump was formed in the 1960s. The landfill in the reserve appeared on the site of a former sand quarry. In the early 1980s, it was closed and covered with soil. Now the dump is overgrown with bushes and grass. In 2011, the state nature reserve of regional significance 'Lake Shchuchye' was established, the boundaries of which included the territory where the landfill of the former landfill is located. 'Druzhinnoye Lake' is located near the landfill. Twenty years later, the territory was closed, covered with soil, and used an area of 1.2 hectares for snow removal after cleaning the territories in winter. The composition of the landfill is soil, sand screenings, and construction waste. At the same time, the landfill masses contain polyethylene, plastic, cardboard, and textiles, as is stated in the draft. The total volume of waste disposed of is more than 80 thousand m3. The facility is planned to be reclaimed within several years.

• Object B8. A sewage sludge landfill located in the southern (peripheral) part of the St. Petersburg agglomeration. This facility has been operating since the 1980s and is practically identical to the B2 facility in terms of technology. Unfrozen sewage sludge from the southern aeration station was exported to the landfill. Since the late 2000s, raw (unfrozen) sewage sludge has not been exported to landfills, but ash (1) from the combustion of sewage sludge has been disposed of. Prolonged accumulation of sediment flooding at landfill sites (2) provoked the entry of pollutants into the surface layers of soil and groundwater. The facility is an operating landfill and is not included in the register of state facilities for accumulated environmental damage.

• Object B9. A complex of small sand mining facilities located in the border zone of the southeastern part of St. Petersburg in the catchment area of the Neva River. In the 1980s and 1990s, the practice was widely used after the extraction of minerals, solid municipal waste was buried in the "bowl" of the dump. According to data (Kulibaba et al. 2016), about 200 such objects have been identified in the Neva River catchment area, many of which are flooded, which poses a threat of pollution entering groundwater and surface waters. At the reclamation sites, foci of soil pollution and highly toxic drainage runoff (heavy metals, ammonia, nitrites, nitrates, petroleum products and other organic pollutants) arise from dumps similar to the filtrate from MSW landfills flowing through the local hydrographic network into the Neva River. The objects are not included in the state register of objects with accumulated environmental damage.

• Object B10. A large, closed landfill with a height of up to 30 m, located in the northwestern part of St. Petersburg, has a total area of more than 20 hectares. The landfill operated from 1933 to 1977. Even after the closure, construction, household, and industrial waste was taken to the landfill. In 1993, the landfill was localized, and the garbage was collected in a separate landfill that was sheltered and mothballed in the early 2000s. Since 2008, it was planned to reclaim the landfill and build a business complex on the vacated territory, but the project was not implemented due to detected chemical (radiation) contamination. The developer refused to implement the project due to the impossibility of completely eliminating pollution and, as a result, a lack of liquidity for future housing commissioning in this area. In 2010, the Government of St. Petersburg discussed the possibility of selling the land at auction for construction, but it was never implemented. In accordance with the general plan of Saint-Petersburg, this landfill belongs to the zone of recreational facilities, with the inclusion of engineering infrastructure facilities related to the maintenance of the zone. Since 2021, the facility has been included in the state register of objects with accumulated environmental damage. It is assumed that the liquidation will be carried out in two stages: (1) the accumulated waste will be taken to the existing landfill; (2) and after that, reclamation works will be carried out at the landfill site (restoration of a fertile soil layer, planting of grass, trees and shrubs).

• Object B11. The decommissioned hydro-ash dump B11 is located in the southeastern part of St. Petersburg, with a total area of 28 hectares. In the 1930s of the last century, ash from locomotive furnaces at the nearest railway stations was brought to this territory. As a result, the hydro-ash dump received ash from several thermal power plants in the city. In 1977, the facility was decommissioned. After the closure of the hydro-ash dump, its territory was used as a snow dump. Since the decommissioning of the ash dump, a layer of turf has formed on its surface (1), trees and shrubs have grown (2), and a reservoir has formed in the southeastern part (3). According to materials published on the official websites of the city authorities and local media, object B11 has been included in the state register of objects of accumulated environmental damage since

2021. However, in the materials of the official list of objects of accumulated environmental damage, object B11 was not found (is not listed) in the register.

Another dominant factor for all these objects is the presence of signs of accumulated environmental damage/harm. They are all included in the pool of state-owned objects; there was a public outcry for almost every one of them, but not all of them are included in the state register of objects of accumulated environmental harm. For some facilities, measures have been taken to minimize environmental harm, but it is not possible to completely eliminate environmental harm. This determines the need to consider in more detail the influence of positive and negative criteria and their significance and usefulness (hierarchical significance) in solving urban development problems. Among the negative factors, the most significant was the factor of influence on atmospheric air (C5 = 0.227) (Table 6).

The significance of C3 and C4 turned out to be slightly less; the value of local priority 0.223 and 0.204, respectively. However, these criteria are highly variable, as their value heavily depends on the specifics of the economic activity of the object B/AED. This is true only for the proposed list of objects considered B/AED, and it may not be the same for other objects in a different city. This is evidenced by the low indicator of the local priority of criterion C1 (the object has signs of accumulated environmental damage). The criterion (C7) of the ownership of B/AED that is not in state ownership has a low local priority of determination. In the case when the object is of particular interest to stakeholders (investors-developers), the process of its renovation causes more confidence that this object will acquire a new function in the urban space because the expected result for them will be the benefit received after the introduction of the object into economic turnover (sale, leasing, etc.). Regarding the value of positive criteria, we see that the inclusion of B/AED in the state register is the most important determinant criterion (C2 = 0.22) affecting the further transformation of urban space (Table 7).

This is understandable due to the fact that inclusion in the register guarantees subsidies to the federal government for measures to eliminate accumulated environmental damage, which, in fact, is confirmed by their equal value with the criterion C10 = 0.22. At the same time, we note that objects B3 and B4 have never been included in the state register of objects with accumulated environmental damage. Nevertheless, their importance in the formation of urban space was of particular importance for the city, primarily in terms of their historical and location aspects. As a result, the decision to redevelop these facilities was made based on other criteria than those mentioned above, particularly political and social factors. Criterion C8 had an average value of local priority among the list of positive determinants. The local priority of public resonance (C9) and the affiliation of B/AED under state jurisdiction (C6) had the lowest indicators of 0.19 and 0.17, respectively. The correlation between criteria (determinants) influencing the transformation of urban space (Fig. 4) shows that there is a strong correlation between such factors as the sign of accumulated environmental damage (C1) and the risks of environmental impact (C3, C4, and C5) which are equal to 0.81, 0.72, 0.59, respectively. And therefore, the environmental factor is a top priority.

The value of the C5 criterion of influence on atmospheric air is still more correlated with the C4 criterion (0.96), compared with C3 (0.86). The higher local priority of the C5 factor is probably due to the public resonance of the past years, when uncontrolled emissions of landfill gases reached residential areas, which caused a high number of complaints from the population to regional authorities, including on social networks. This mainly concerns peripherally located B/AEDs. This indicates that when making decisions about the nature of the impact of B/AED, and the priorities for their elimination are more determined by the environmental situation and the economic interests of stakeholders. Criterion C7 showed a negative correlation with the "ecological" criteria C7 – C5, C4, at the same time C7 – C3 weak correlation, C7 – C1 average correlation.

Table 6. Quantitative assessment of negative criteria (determinants) of the impact of B/AED on the transformation of urban space

Criteria	C1	C3	C4	C5	C7	S_i	R_i	a_i	Weight coefficients (%)
C1	1	1/5	1/5	1/3	1/3	2.06	1.156	0.149	14.9
C3	5	1	1/2	1/2	9	16.0	1.74	0.223	22.3
C4	5	2	1	2	1/4	10.2	1.59	0.204	20.4
C5	5	2	1/2	1	9	17.5	1.77	0.227	22.7
C7	3	1/9	4	1/9	1	8.22	1.52	0.195	19.5
Total	19	4.51	4.64	4.78	19.58	53.98	7.776	1	100

Table 7. Hierarchical significance of positive criteria-determinants of B/AED influencing the transformation of urban environment

Criteria	C2	C6	C8	C9	C10	S_i	R_i	a_i	Weight coefficients (%)
C2	1	7	9	5	1/3	22.33	1.86	0.22	22.0
C6	1/7	1	5	1/9	1/9	6,362	1.45	0.17	17.0
C8	1/9	1/5	1	5	7	13.31	1.68	0.2	20.0
C9	1/5	9	1/5	1	1/9	10.51	1.6	0.19	19.0
C10	3	9	1/7	9	1	22,14	1,86	0.22	22.0
Total	4.45	26.20	15.34	20.11	8.55	139.48	8.45	1	100

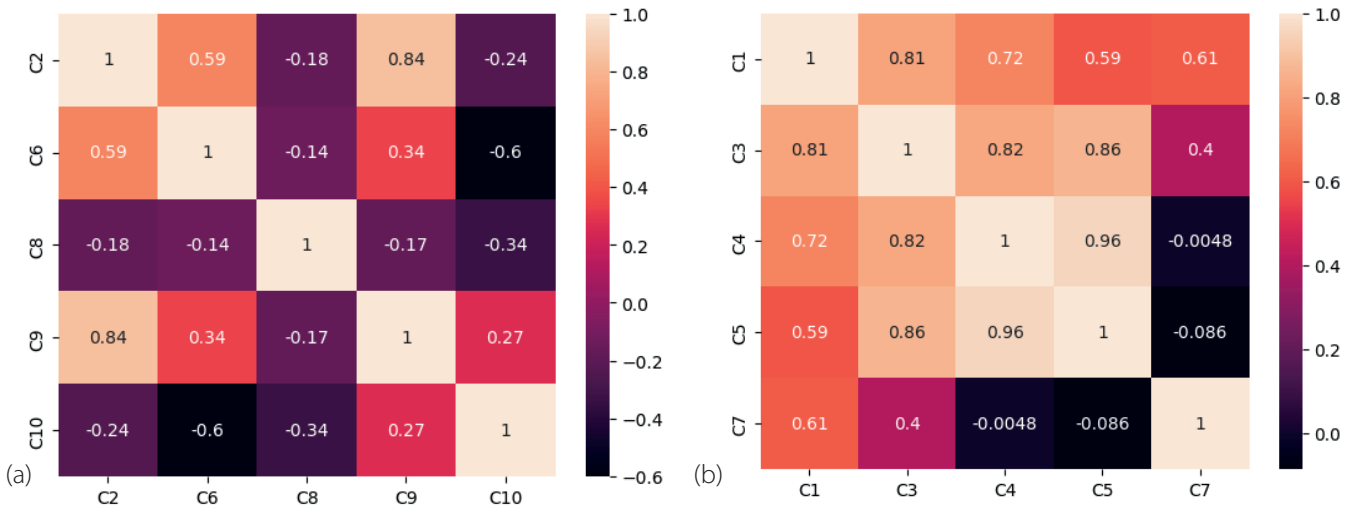

Fig. 4. The ratio of positive and negative criteria-determinants of B/AED influencing urban environment transformation

DISCUSSION

In this study, we have addressed the important problem of considering local priorities in urban space development. B/AED – how historical imprints of past economic activity and the gradual development of territories associated with cleaning processes become protracted problems affecting the transformation of urban space. Decision-making tools for the B/AED inventory are ineffective and require expanding the list of local priorities for sustainable development and public control (expression of opinion, discussion, etc.) to make decisions in shaping a new look of urban space after the elimination of B/AED. For example, in India, the problem of eliminating B/AEDs has not yet been fully understood in terms of what they are essentially B/AEDs, and which are identified by the criterion of "state of the earth" (Verma and Banerji 2023). For many countries, the problem of B/AED renovation turns out to be not a financial but a mental component of the market (Trouw et al. 2020). Developers often do not want to risk being "pioneer enthusiasts", although this factor is probably the driving force (example) for other developers. It is important to understand not only the benefits for the authorities but also the commercial benefits that will be possible if B/AEDs become socially (socially) attractive objects after renovation / elimination of environmental harm. Thus, studies (Vojvodíková et al. 2021) show that the most important criterion for the restoration of B/AED territories is their departmental affiliation. The participation of public investments may not always be enough for the redevelopment of B/AED. In fact, we have seen from this study that the criteria for the ownership of an object (private / state property) have a low weight of local priority in making decisions on their liquidation. Nevertheless, we know that the B/AED redevelopment projects that have been implemented in a number of the most developed countries in the world, including China, the USA, Canada, Germany, and England (Lin et al. 2019) are quite successful, but at the same time, they differ in key aspects and may often not be economically feasible for other countries. This means that there is no single approach to solving the problem. The ranking of B/AED into categories does not always coincide for different authors, depending on the central focus: "fast or slow renovation", "technical or environmental aspects", "urban or agricultural", "public or private", etc. (Ray et al. 2021). The elimination of B/AED, and therefore, there is a need for research on a combination of best practices based on considering the interests of all groups of the population (government-business-citizens). We also pay particular attention to the fact that public response is one of the most important factors to consider. Our research on B/AED assessments and rankings based on local priorities helps identify the most important aspects of priority actions for spatial needs. At the same time, we note that this approach will have an optimal effect only in synthesis with other practices, which determines further research in this direction (comparative, predictive, etc.).

CONCLUSION

In this study, the author proposed a new approach to B/AED inventory based on the identification and comparison of local priorities (criteria-determinants) of urban space transformation under the influence of B/AED for environmentally balanced urban development. The pilot implementation of this approach allowed us to formulate some final theses:

• The practice of inventory and inclusion of potential B/AED objects in the state register of objects of accumulated environmental damage (hereinafter the register) for subsequent liquidation is ineffective at the municipal level in terms of further development of urban space. Of the eleven objects with B/AED signs, only 4 are included in the register. Probably, this is largely due to the political will of the state authorities (landfills on the territory of specially protected natural areas, for example), the economic interests of large investors (the territory of 'Tuchkov Buyan' and 'Okhtinsky Cape'), or the lack of necessary resources ('Krasny Bor' landfill, etc.). Most of the discovered B/AED have low redevelopment potential (landfills, landfills waste), and therefore, it is not possible to attract stakeholders for the further development of these territories;

• The proposed criteria of local priority allowed us to identify the dominant factors (their weight values) influencing the transformation of St. Petersburg's the urban space. Of the five negative criteria for local priority:
1. Impact on the atmosphere (22.7%); >
2. Risks associated with soil pollution (22.3%); >
3. Risks associated with water pollution (20.4%); >
4. Ownership of the facility (private property) (19.5%); >
5. The facility has signs of accumulated environmental damage (14.9%). Positive criteria: there were two criteria in the first place. 1 The object is included in the state register (22%) = 1. Measures have been taken at the facility to eliminate/minimize damage (22%) ;> 2. Possibility of redevelopment (20%); > 3. Public response (19%); > 4. Ownership of the object (private/public) (17%). The weight values of local priorities show that the most

important positive factor (the local priority of the territory's development) is the fact that the object is included in the B/AED register. This is obvious because funds from the federal budget will be allocated for its liquidation. The effect on the atmosphere was the most significant negative priority. This negative impact factor is most easily detected and causes a public outcry, therefore increasing attention to the problem of eliminating B/AED;

• It is advisable to make predictive estimates of the impact of B/AED by identifying similarities of B/AED. The study shows that even with a characteristic feature combining these objects (waste management activities), local priorities have different "weights": (1) high similarity, correlation value from 0.8 and more, (2) average similarity, correlation value from 0.79 to 0.6, and (3) slight similarity, correlation value correlations are less than 0.6. And therefore, approaches to the elimination of objects of the same type of B/AED should not be universal;

• Subjectivization of the perception of local priorities and forecast estimates in the transformation of urban space (which are taken into consideration for the B/AED inventory) is one of the key factors in making decisions to eliminate them, and therefore, for the selection of local priorities, territorial development plans should be guided, starting from the municipal level, considering public opinion (including in the preparation of an inventory plan B/AED public hearings). Despite the fact that the criterion of public resonance is not dominant, it cannot be ignored (the history of public resonance in St. Petersburg with the objects 'Tuchkov Buyan', 'Okhtinsky Cape' clearly testifies to its effectiveness, including for redevelopment purposes).

Thus, the study shows that the proposed approach can be successfully used for the inventory of objects and their subsequent liquidation in order to effectively search for factors of spatial development in inner urban areas (on a local level). Nevertheless, the author notes that the effectiveness of this approach can be significantly higher if it is used in conjunction with current practices, but this requires further research in this direction (comparative, predictive, etc.).

Funding. This research was funded by the Russian Science Foundation No. 23-27-00034, https://rscf.ru/en/project/23-27-00034/.

REFERENCES

Ahmad, N., Zhu, Y., Shao, J., Lin, H. (2020). Stakeholders' perspective on strategies to promote contaminated site remediation and brownfield redevelopment in developing countries: empirical evidence from Pakistan. Environmental Science and Pollution Research, 27(13), 14614–14633DOI:10.1007/s11356-020-07990-3

Axenov, K. E., and Galustov, K. A. (2023). Urban regimes and socially significant projects of the urban environment transformation in the Russian Federation. Vestnik of Saint Petersburg University. Earth Sciences, 68(1),4-28 DOI:10.21638/spbu07.2023.101

Bondar, E. G. (2022). The current state and prospects of the fuel and energy complex of St. Petersburg and the Leningrad region. The Economy of the North-West: Problems and Prospects of Development, 2(69), 71–77DOI:10.52897/2411-4588-2022-2-71-77

BenDor, T. K., Metcalf, S. S., Paich, M. (2011). The Dynamics of Brownfield Redevelopment. Sustainability, 3(6), 914–936DOI:10.3390/su3060914

Chen, I.-C., and Yang, B.-C. (2022). Developing decision model and sustainable mapping to screen the efficiency of brownfield redevelopment based on socioeconomic open data. Sustainable Environment Research, 32(1).DOI:10.1186/s42834-022-00139-6

Dregulo, A. M. (2023). Brownfields, Environmental Stability and Renewable Energy: Pathways to Overcome the Imperfection of Cumulative Effect Assessment. Energies, 16(17), 6218 DOI:10.3390/en16176218

Dregulo, A. M. and Khodachek, A. M. (2022). Waste Management Reform In Regions Of The Russian Federation: Implementation Issues On The Way To Sustainable Development. Geography, Environment, Sustainability, 15(1), 6–13DOI:10.24057/2071-9388-2021-078

Dregulo, A. M., Shapkin, V. M., Kichko, A. A. (2022). Microbial analysis of sewage sludge shows closer monitoring needed for landfill waste. Proceedings of the Institution of Civil Engineers - Waste and Resource Management, 175(2), 57–63DOI:10.1680/jwarm.21.00023

Dregulo, A. and Bobylev, N. (2021). Integrated Assessment of Groundwater Pollution from the Landfill of Sewage Sludge. Journal of Ecological Engineering, 22(1), 68–75DOI:10.12911/22998993/128872

Dregulo, A. and Bobylev, N. (2021a). Heavy Metals and Arsenic Soil Contamination Resulting from Wastewater Sludge Urban Landfill Disposal. Polish Journal of Environmental Studies, 30(1), 81–89DOI:10.15244/pjoes/121989

Federal Law «On Environmental Protection» dated 10.01.2002 N 7-FZ https://www.consultant.ru/document/cons_doc_LAW_34823/ (accessed 30.10.2023)

Green, T. L. (2018). Evaluating predictors for brownfield redevelopment. Land Use Policy, 73, 299–319.DOI:10.1016/j.landusepol.2018.01.008

Jian, H., Hao, H., Haize, P., Chuan, L., Xiaoqin, L., Yan, W., Haidan, J., & Changliang, Z. (2022). Research on brownfield redevelopment based on Wuli-Shili-Renli system theory and catastrophe progression method. PLOS ONE, 17(11), e0277324DOI:10.1371/journal.pone.0277324

INTERREGVB Central Europe 2014 – 2020 http://ec.europa.eu/regional_policy/en/atlas/programmes/2014-2020/austria/2014tc16rftn003 (accessed 04.10.2023)

Kim, H., Woosnam, K. M., & Kim, H. (2022). Urban gentrification, social vulnerability, and environmental (in) justice: Perspectives from gentrifying metropolitan cities in Korea. Cities, 122, 103514 DOI:10.1016/j.cities.2021.103514

Krejčí, T., Navrátil, J., Martinát, S., Frazier, R. J., Klusáček, P., Pícha, K., Škrabal, J., Osman, R. (2021). Spatial Unevenness of Formation, Remediation and Persistence of Post-Agricultural Brownfields. Land, 10(3), 325. DOI:10.3390/land10030325

Klusáček, P., Navrátil, J., Martinát, S., Krejčí, T., Golubchikov, O., Pícha, K., Škrabal, J., Osman, R. (2021). Planning for the future of derelict farm premises: From abandonment to regeneration? Land Use Policy, 102, 105248 DOI:10.1016/j.landusepol.2020.105248

Kulibaba V. V. Petukhov V.V., Zinatulina E.I., Merinova E. S. (2016) Assessment of past ecological damage open pits in the Neva lowland. Regional ecology, 1(43),108-114

Kuznetsov, S. V. and Gorin, E. A. (2022). Digital transformation of St. Petersburg industry: common problems and system solutions. The Economy of the North-West: Problems and Prospects of Development, 4(71), 67–75DOI:10.52897/2411-4588-2022-4-67-75

Korshunov, I. V. (2023). The problems of sustainable development in regional strategies of the northwest federal district. The Economy of the North-West: Problems and Prospects of Development, 1(72), 8–17 DOI:10.52897/2411-4588-2023-1-8-17

Lin, H., Zhu, Y., Ahmad, N., Han, Q. (2019). A scientometric analysis and visualization of global research on brownfields. Environmental Science and Pollution Research, 26(17), 17666–17684DOI:10.1007/s11356-019-05149-3

Navrátil, J., Krejčí, T., Martinát, S., Frazier, R. J., Klusáček, P., Pícha, K., Škrabal, J., Osman, R. (2021). Variation in brownfield reuse of derelict agricultural premises in diverse rural spaces. Journal of Rural Studies, 87, 124–136DOI:10.1016/j.jrurstud.2021.09.004

Okeyinka O.M., Khan R., Pathirage C., Mahammedi C.E.D., West A. (2023) A Critical Review of Developers' Decision Criteria for Brownfield Regeneration: Development of the BRIC Index. Sustainability. 15(9):7105 DOI:10.3390/su15097105

Okrepilov, V. V. (2021). Experience in creating strategic documents for the development of the economy of St. Petersburg, aimed at improving the quality of life. The Economy of the North-West: Problems and Prospects of Development, 1(64), 4–13DOI:10.52897/2411-4588-2021-1-4-13

Overview of EPA's Brownfields Program. Available online: https://www.epa.gov/brownfields/overview-epas-brownfields-program (accessed on 31.10.2023).

Patnayaka, R. (2018). Brownfield Development Scenario in India and Prospective Challenges. International Journal of Innovation and Scientific Research, 37, 1-12

Rey, E., Laprise, M.,Lufkin, S. (2021). Urban Brownfields: Origin, Definition, and Diversity. The Urban Book Series, 7–45 DOI:10.1007/978-3-030-82208-8_2

Saaty, R. W. (1987). The analytic hierarchy process—what it is and how it is used. Mathematical Modelling, 9(3–5), 161–176DOI:10.1016/0270-0255(87)90473-8

Safarova, A. A., & Safarova, G. L. (2022). Life expectancy at older ages in the regions of the northwestern federal district of Russia. The Economy of the North-West: Problems and Prospects of Development, 3(70), 176–186DOI:10.52897/2411-4588-2022-3-176-186

Šimková, Z., Seňová, A., Divoková, A., Očenášová, M., Varga, P., & Tyulenev, M. A. (2020). Is it possible to use brownfields at the end of mining and processing of minerals? Economics and Innovation Management, 3, 59–67DOI:10.26730/2587-5574-2020-3-59-67

Sokolova, E. V. and Starshov, E. D. (2022). Infrastructural challenges of global cities: the case of st. Petersburg transportation system. The Economy of the North-West: Problems and Prospects of Development, 3(70), 120–132 DOI:10.52897/2411-4588-2022-3-120-132

Solodilov, V. V. (2023). THE urbanization perspectives of the northern part of the lomonosovsky district of the Leningrad region. The Economy of the North-West: Problems and Prospects of Development, 3(74), 173–183 DOI: 10.52897/2411-4588-2023-3-173-183

Song, Y., Lyu, Y., Qian, S., Zhang, X., Lin, H., Wang, S. (2022). Identifying urban candidate brownfield sites using multi-source data: The case of Changchun City, China. Land Use Policy, 117, 106084/DOI:10.1016/j.landusepol.2022.106084

Sun, Y., Li, H., Lei, S., Semple, K. T., Coulon, F., Hu, Q., Gao, J., Guo, G., Gu, Q., & Jones, K. C. (2022). Redevelopment of urban brownfield sites in China: Motivation, history, policies and improved management. Eco-Environment & Health, 1(2), 63–72 DOI:10.1016/j.eehl.2022.04.005

Trouw, M., Weiler, S., Silverstein, J. (2020). Brownfield Development: Uncertainty, Asymmetric Information, and Risk Premia. Sustainability, 12(5), 2046DOI:10.3390/su12052046

Verma, N. S. and Banerji, H. (2023). Defining the term "Brownfield" in India. Remediation Journal. Portico.DOI:10.1002/rem.21768

Vojvodíková, B., Fojtík, R., Tichá, I. (2021). Design and Verification of a Simple Approach to Brownfields Categorization. Sustainability, 13(20), 11206DOI:10.3390/su132011206

Wang, Z., Chen, X., Huang, N., Yang, Y., Wang, L., Wang, Y. (2022). Spatial Identification and Redevelopment Evaluation of Brownfields in the Perspective of Urban Complex Ecosystems: A Case of Wuhu City, China. International Journal of Environmental Research and Public Health, 19(1), 478DOI:10.3390/ijerph19010478

Zamyatina, M. F., Gorin, E. A., & Fesenko, R. S. (2022). The main directions for achieving the goals of sustainable production and consumption and their perception by enterprises (St. Petersburg case). The Economy of the North-West: Problems and Prospects of Development, 1(68), 67–80DOI:10.52897/2411-4588-2022-1-67-80

Zhang, X., Song, Y., Qian, S., Wang, S., Wu, D. (2022). Exploring Spatial Distributions and Formation Factors of Brownfields in China: From Macro-Scales. Frontiers in Environmental Science, 10 DOI:10.3389/fenvs.2022.918621

Check for updates

CC BY

RESEARCH PAPER

ASSESSMENT OF SEAWATER QUALITY AND ENVIRONMENTAL SUSTAINABILITY FOR SHIPWRECK DIVING TOURISM: A CASE STUDY OF MV BOELONGAN NEDERLAND IN MANDEH BAY, INDONESIA

Aprizon Putra[1], Dedi Hermon[2], Yulius[1], Widya Prarikeslan[2], Azhari Syarief[2*], Nia Naelul Hasanah Ridwan[3], Taslim Arifin[1], Febriandi[1], Harfiandri Damanhuri[4], Teguh Widodo[1], Andri Dermawan[2]

[1] National Research and Innovation Agency (BRIN), Cibinong, Bogor, 16911, Indonesia
[2] Universitas Negeri Padang (UNP), Air Tawar, Padang, 25131,Indonesia
[3] Ministry of Maritime Affairs and Fisheries (KKP), Gambir, Jakarta, 10110,Indonesia
[4] Universitas Bung Hatta (UBH), Ulak Karang, Padang, 25133,Indonesia
***Corresponding author:** azharief@fis.unp.ac.id
Received: June 24th 2024 / Accepted: November 27th 2024 / Published: December 31st 2024
https://doi.org/10.24057/2071-9388-2024-3469

ABSTRACT. The purpose of this research is to model the condition of seawater quality based on Government Regulation No. 22/2021 about «Implementation of Protection and Environmental Management», the results of which can later be used as a basis for reference for the concept of environmental conservation. The research was conducted at the MV Boelongan Nederland shipwreck site, focusing on seawater quality measurements including physical, chemical, and pollutant parameters. Sampling was performed at various locations near the shipwreck and nearby estuaries using purposive sampling. Parameters such as pH, temperature, turbidity, dissolved oxygen (DO), biological oxygen demand (BOD), salinity, and concentrations of pollutants like phenol, polyaromatic hydrocarbons (PAH), and pesticides were measured and analyzed using geographic information system (GIS) tools. Data analysis revealed that despite some variations, seawater quality parameters generally met regulatory standards, supporting marine life and tourism activities. However, localized pollution was observed, particularly near estuary areas, emphasizing the need for targeted conservation efforts. The research results indicate that the estuarine areas experience light pollution due to land-based runoff, which could affect the long-term sustainability of the shipwreck site. However, the overall seawater quality at the shipwreck location remains favorablefor marine tourism and conservation. The findings suggest that a zoning system could be beneficial for managing underwater heritage sites, thereby supporting both environmental preservation and the economic development of the region. Furthermore, the research emphasizesthe potential of shipwrecks as tourism assets, suggesting their role as artificial reefs and underwater museums thatcontributeto visitors' recreational and educational experiences.

KEYWORDS: environmental sustainability, Mandeh bay, MV Boelongan Nederland shipwreck, seawater quality, tourism development

CITATION: Putra A., Hermon D., Yulius, Prarikeslan W., Syarief A., Nia N. H. Ridwan, Arifin T., Febriandi, Damanhuri H., Widodo T., Dermawan A. (2024). Assessment Of Seawater Quality And Environmental Sustainability For Shipwreck Diving Tourism: A Case Study Of Mv Boelongan Nederland In Mandeh Bay, Indonesia. Geography, Environment, Sustainability, 4(17), 171-182
https://doi.org/10.24057/2071-9388-2024-3469

ACKNOWLEDGEMENTS: The authors express their sincere gratitude to the Government of Pesisir Selatan Regency, West Sumatra Province, for their invaluable assistance in providing data facilities, accompanying staff, and permits for conducting this research. Their support and collaboration were instrumental in the successful completion of this research.

Conflict of interests: The authors reported no potential conflict of interest.

INTRODUCTION

The sinking ship site is considered to have historical, scientific, and economic value. The sunken ship site can be used as an object of research to explore the knowledge connected to it, which is closely related to the development of regional and national character to strengthen national identity and also to serve as an object of marine tourism in the form of shipwreck diving, the implication of which is to preserve the sunken ships while developing them so that they can provide opportunities for sustainable management (such as environmental conservation, cultural heritage preservation, and sustainable tourism development) and community welfare (such as improving the local economy, improving quality life, and preservation of local culture).

Pesisir Selatan Regency is one of the regencies in West Sumatra Province thatis a leading destination for tourism activities, especially marine tourism (Such as Carocok Painan Beach, Cingkuak Island, Mandeh Bay, Langkisau Beach, and Batu Kalang Beach) and cultural tourism (Such as Rumah Gadang Mandeh Rubiah, Langkisau Festival, and Nagari Seribu Rumah Gadang in Koto Baru) (Stanford et al. 2012; El Silisna and Susanti 2020). This is in line with the establishment of

West Sumatra Province as one of the main tourist destinations in Indonesia along with 9 other provinces, including North Sumatra, Bali, West Nusa Tenggara, and others which were declared in the "Visit Indonesia Year" by the Ministry of Culture and Tourism in January 2011, the "Visit Indonesia" brand was discontinued and was replaced with the campaign "Wonderful Indonesia" which was mentioned by the rebranding to increase tourism appeal, increase competition in the global tourism industry, expand the scope of promotion, modernize and adjust to global trends, and respond to evaluation/feedback (Adams 2018; Lemy et al. 2019; Nabhan et al. 2023).

The region of Mandeh Bay is a leading tourist region in the Pesisir Selatan Regency, which is located in the sub-district of Koto XI Tarusan. The type of tourism offered is marine ecotourism (Alhadi, 2018; Triyatno et al. 2020). This is because theregion has many islands, bays, and capes with beautiful panoramas. In this region of Mandeh Bay, the sinking ship MV Boelongan Nederland is also a shipwreck diving tourist location. The waters of Mandeh Bay contain several large estuaries, contributing to the increased sedimentation in the region.. Therefore, it is necessary to carry out an experimental analysis of the sedimentation rate in the waters of the sinking site of the MV Boelongan Nederland (Ridwan 2015). Hermon et al. (2022) add simulated tidal currents and their effects on sediment distribution in the region of Mandeh Bay waters. Therefore, it is important to research sediment accumulation and seawater quality.

In the policy framework for managing underwater heritage, the Regulation of the Minister of Maritime Affairs and Fisheries No. 28/2021 about "Organization of Marine Spatial Planning" mentions the existence of a vision for the management of underwater heritage in the future as stated in Law No. 17/2007 concerning "the Development Plan". Regional Long-Term Development Plan (RLTDP), especially related to the 7th mission, namely "Making Indonesia Become an Archipelagic State that is Independent, Advanced, Strong, and Based on National Interest" by generating maritime insight and culture (Ali and Sulistiyono, 2020; Safitri 2020).

The purpose of this research is to model the condition of seawater quality based on Government Regulation No. 22/2021 about "Implementation of Protection and Environmental Management", the results of which can later be used as a basis for reference for the concept of environmental conservation in region of Mandeh Bay, Pesisir Selatan Regency - West Sumatra, Indonesia. Meanwhile, the urgency of the research is as a basis for determining the sustainability of the maritime conservation area by Regulation of the Minister of Maritime Affairs and Fisheries No. 17/2008 about "Conservation Areas of Coastal and Small Islands" to support regional development in an integrated and sustainable manner.

METHODS

The research location is at the MV Boelongan Nederland shipwreck, the estuary of the Mandeh River, and the Nyalo River in

Table 1. Forms of analysis for measuring physical, chemical, and pollutant seawater parameters and the tools used

Parameter types	Parameters	Units	Data results obtained		Tools
			Field results	Labor results	
Physical parameters of seawater	Degree of Acidity (pH)		✓		Litmus Paper/Universal pH Paper
	Temperature	°C	✓		Water Quality Meter AZ Instrument 86031: Digital Sampling System
	Turbidity	ntu	✓		YSI ProDSS: Digital Sampling System
	Brightness	m	✓		Secchi Disk: Standard for measuring water transparency
Chemical parameters of seawater	Dissolved Oxygen (DO)	mg/L	✓		Water Quality Meter AZ Instrument 86031: Multiparameter Meter with Optical DO Probe
	Biological Oxygen Demand (BOD)	mg/L		✓	Hach HQ440D: Dual Input Multi-Parameter Meter
	Salinity	‰	✓		Water Quality Meter AZ Instrument 86031: Digital Sampling System
	Nitrate (NO3-N)	mg/L	✓		YSI ProDSS: Digital Sampling System
	Ammonia (NH3-N)	mg/L	✓		YSI ProDSS: Digital Sampling System
	Phosphate (PO4-P)	mg/L		✓	Hach DR3900: Spectrophotometer
	Sulfide Compounds (H_2S)	mg/L		✓	Hach DR3900: Spectrophotometer
Pollutant parameters of seawater	Phenol Compounds	mg/L		✓	Agilent 7890B GC System: Gas Chromatography
	Polyaromatic Hydrocarbons (PAH)	mg/L		✓	Agilent 7890B GC System with 5977B MSD: GC-MS System
	Polychlor Biphenyl (PCB)	mg/L		✓	Agilent 7890B GC System with 5977B MSD: GC-MS System
	Surfactants (detergents)/ MBAs	mg/L		✓	Agilent 1260 Infinity II LC: Liquid Chromatography
	Oils and Fats	mg/L		✓	Agilent 7890B GC System: Gas Chromatography
	Pesticides	mg/L		✓	Agilent 7890B GC System with 5977B MSD: GC-MS System

the region of Mandeh Bay waters. The research was conducted in the waters of the MV Boelongan Nederland shipwreck as a diving tourism area. Purposive sampling, which considers various water conditions and conditions thought to affect seawater quality, determines the seawater quality measurement stations (Septiariva and Suryawan, 2021; Brown et al. 2020; Isdianto and Luthfi, 2020). Measurement/observation and laboratory testing for seawater quality are shown in the following Table 1 below.

The results of this test of the seawater quality can have an effect on the MV Boelongan Nederland sinking site, either directly or indirectly. This is because of the conditions of the seawater quality, especially the temperature, pH, and salinity. This can be known sooner or later, as the metal hull of the ship could be damaged by corrosion (Ridwan 2019).

The results can later be used as a basis for taking action to reduce the corrosion rate of the sunken shipwreck as partof the preservation efforts. The geographic information system (GIS) software used in this study is ArcGIS Desktop 10.8 and GAT software. The operating system used is Windows 10 on a computer based on Intel® Core™ i5 Processor. One of the advantages of ArcGIS software is that it provides a means for customizing applications with the Avenue language (Kennedy 2013; Dewata and Putra, 2021; Putra et al. 2023). The avenue script runs interpolation, changing the values for each created interpolation model. For the Inverse Distance Weighted (IDW) method, 8 simulations were carried out with the number of samples. Meanwhile, for the IDW method, 13 simulations were performed by changing the interval parameters, type, and several samples. The resulting grid data has a resolution of 100 m, and the interpolated file size is about 277 kilobytes. Fig. 1 below provides more details.

RESULTS

Seawater Quality parameter values

Seawater quality parameters that can support research in diving tourism areas are related to physical, chemical, and pollution factors. The water area of the research site is often used as a diving tourist destination, a stop for fishers, and is famous for fishing. Since this water area has quite important biological and non-biological resources, it is necessary to carry out a series of sampling activities and measure seawater quality conditions so that they can be implemented in case of significant and negative changes in the environment and seawater quality can be recognized and anticipated in time. Seawater quality measurements are divided into physical, chemical, and seawater pollution measurements. These measurements are crucial to ensuring the sustainability of marine life and the continued attractiveness of the area for tourism and fishing activities. By monitoring the physical properties, chemical composition, and potential pollutants in the seawater, researchers can identify any shifts that might affect the health of the marine ecosystem. The results of the laboratory tests are presented in Table 2 below.

Results of IDW Interpolation for the Physical Parameters of Seawater Quality

Physics of Seawater Quality for pH

From Table 2, it can be seen that the pH range at the observation locations ranges from 7.12-7.61 using the Litmus Paper/Universal pH Paper. The lower values tend to be closer to the estuary (locations 2-3 and 4-5), while the pH values increase towards the sea. This phenomenon aligns with the findings of Hall et al. (2021), which observed a similar trend of decreasing pH near freshwater inputs and estuarine regions. This isbecause the estuary areas (the Mandeh River and the Nyalo River) receive a higher supply of fresh water, thus lowering the pH. The mixing of fresh and saltwater creates a gradient, affecting the buffering capacity of seawater and its ability to maintain pH stability (Christensen 2023). The research by Hammer et al. (2014) showed that the closer to the sea, the pH value usually has a pH of more than 8. The condition of the pH value is caused by the influence of freshwater from the river that reaches the location due to high precipitation in June-July 2023, thereby increasing the volume of river water. Additionally, the impact of rainfall and river water on pH variation has been widely observed in tropical regions, where high precipitation often leads to significant pH fluctuations in coastal waters (Rahman et al. 2023). The pH range above the observation locations in the research areais still the natural pH of marine waters. It is known that the pH of the waters in

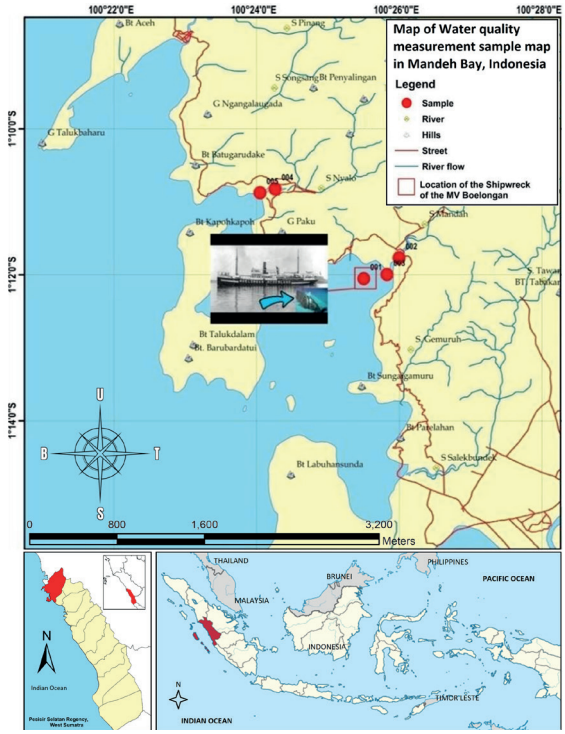

Fig. 1. Map of seawater sampling locations

Table 2. Values of seawater quality parameters from laboratory analysis

No	Parameter	Quality standards the Government Regulation No. 22/2021		Unit	Locations		
		Biota	Tourism		1	2-3	4-5
Physics							
1	pH	7-8,5[(d)]<0,2 unit of change pH	7-8,5[(d)]		7,61	7,21	7,12
2	Temperature	natural [3(c)]	natural[3(c)]	°C	30,3	29,1	29,1
3	Turbidity	<5	5	ntu	4,2	6,2	6,5
4	Brightness	coral: >5 <10% changes in the euphotic depth of mangroves: -seagrass: >3	<6	m	8	3	3
Chemistry							
1	DO	>5>6 (>80-90% saturation)	>5	mg/L	4,8	5,6	5,2
2	BOD	20	10	mg/L	3,67	2,72	2,42
3	Salinity	natural[3(e)]	natural[3(e)]	‰	33,3	32,2	32,9
4	NO_3-N	0,008-0,002	0,008	mg/L	1,15	1,3	1,3
5	NH_3-N	0,3	nothingl	mg/L	0,05	0,1	0,11
6	PO_4-P	0,015	0,015	mg/L	0,13	0,21	0,33
7	H_2S	0,01 Pesticide (acrolein) = 0,0002	nothing[l]	mg/L	0,005	0,05	0,09
Pollutants							
1	Phenol Compound	0,002	nothingl	mg/L	0,0035	0,0151	0,0239
2	PAH	0,003	0,003	mg/L	ttd*)	0,0007	0,00111
3	PCB	0,01	nothingl	mg/L	ttd*)	ttd*)	ttd*)
4	Surfactant (detergent)/MBAS	1	0,001	mg/L	0,2	7	7
5	Oil and fat	1	1	mg/L	0,305	0,823	0,959
6	Pesticide	0,01	nothingl(f)	mg/L	ttd*)	0,025	0,03

*) ttd = not detected

Indonesia ranges from 6.0 to 8.5. Government Regulation No. 22/2021 stipulates that the pH value for marine tourism is in the range of 7-8.5 (Putra et al. 2023). The rise and fall of pH are mainly influenced by freshwater input. Seawater can buffer very large changes in pH to prevent changes in pH.

Physics of Seawater Quality for Temperature

The seawater temperature at the observation locations, which ranged from 29.1-30.3°C using the Water Quality Meter AZ Instrument 86031. This temperature value includes the natural value in the seawater quality standard for marine biota and marine tourism according to Government Regulation No. 22/2021, where the water temperature in Indonesia generally ranges from 27-32°C (Junaidi et al. 2019). According to Tortell (2005),temperature is one of the limiting factors for marine ecosystems and biota, where temperature changes can affect physical, chemical, and biological processes in water bodies. Hemraj et al. (2023) found in similar research that small temperature fluctuations can influence nutrient cycling and the metabolic rates of marine organisms. An increase in water temperature from the natural temperature range can cause a decrease in the solubility of gases in water such as O_2, CO_2, N_2, and CH_4. Judging from the measurement results obtained, the water temperature is natural so that it does not interfere with the ecosystem, the biota that lives in it, and the preservation of the remains of the sinking ship. According to Candra et al. (2024), stable sea temperatures within the natural range help maintain biodiversity and the health of coral reefs, which are crucial for supporting marine life in tropical regions. Prarikeslan et al. (2020) added that high temperatures can cause the death of marine biota, so an increase in temperature from the threshold can disrupt the physiology of marine biota. The vulnerability of marine species to temperature changes is heightened in tropical ecosystems where many species are already near their thermal tolerance limits (Beaty et al. 2019). Temperatures in the ocean vary depending on depth, water masscirculation, turbulence, geographical conditions, and distance from heat sources such as underwater volcanoes. The sea surface temperature is highly dependent on the amount of heat it receives from the sun.

Physics of Seawater Quality for Turbidity

The measurement results had a turbidity range of 4.2 to 6.5 ntu at the observation locations. Turbidity ranges between 0 and 4.2 mg/L using the YSI ProDSS. The further into the river from the estuary, the higher the turbidity value,

namely 6.2 mg/L. The turbidity value specified according to Government Regulation No. 22/2021 for marine tourism is 5 ntu and for marine biota is <5. The turbidity value is still below the quality standard value threshold in Government Regulation No. 22/2021, so it is still suitable for marine tourism purposes. However, according to the research by Yi et al. (2024), prolonged exposure to elevated turbidity levels, even if they are within the regulatory limits, can still have detrimental effects on marine organisms by reducing the light penetration necessary for photosynthesis. In the research of Butler and Ford (2018), turbidity and total dissolved solids (TDS) are interrelated:if the TDS is high, the turbidity will be high and the brightness low. This will affect the penetration of sunlight into the waters, which then continues in the process of photosynthesis. The research by Mills et al. (2023) also confirmed that high turbidity can significantly reduce the photosynthetic efficiency of coral reefs, impacting their resilience against environmental stressors. The existing river flow, which empties into the observation locations, produces the mixed sandy silt substrate that causes the turbidity. . This causes high turbidity and sedimentation, which can block the growth of marine life in the region's waters, as well as the development of access revitalization connecting roads in the observation locations. It has been noted by MacIntosh et al. (2023) that increased sedimentation not only harms marine flora and fauna but also disrupts the ecological balance of coastal areas by altering habitats and nutrient cycles. The mangroves at that location in the Mandeh Bay region have transformed into built-up areas, specifically roads. The turbidity also has a very large impact, especially the silting of the sea surface.

Physics of Seawater Quality for Brightness

The brightness level and visibility at the observation locations ranged from 3-8 m using the Secchi Disk. This variation in water brightness and visibility is most likely due to the influence of sedimentation and tide times. The existence of several rivers (Mandeh and Nyalo) that empties into the observation locations will carry mud particles and wastes from land to sea waters. At high tide, which is in the morning until around 10 am, the brightness of the water is high because the sediment from the river has not entered the sea, as it is held back by the rising tide. The brightness level will decrease during the day because, at low tide, there will be sediment input carried by river water that enters the sea. This phenomenon is consistent with the findings of Figueroa and Son (2024), which showed that tidal cycles have a significant impact on water clarity, especially in areas with high sediment influx from river sources. For marine tourism, the quality standard value for brightness is >6 m,according toGovernment Regulation No. 22/2021. When brightness falls below this threshold, it can negatively affect marine tourism activities, particularly those involving snorkeling or diving, where water clarity is crucial for visibility (Baker et al. 2019). Furthermore, sedimentation not only impacts water clarity but also affects the health of benthic ecosystems, as sediments can smother habitats and reduce light availability for photosynthetic organisms like seagrass and corals (Ajwang 2024). The ongoing influx of sediments from rivers and the resuspension caused by tidal movements create a fluctuating environment that challenges both the marine ecosystem and the tourism industry,which relieson clear waters.

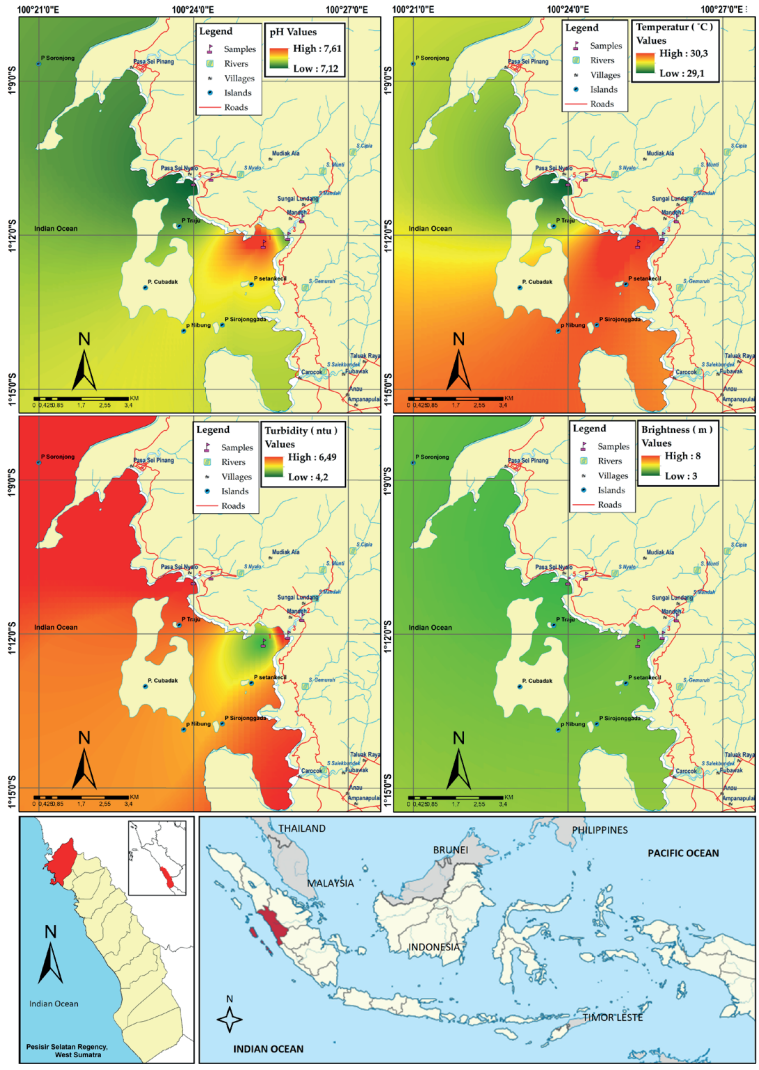

Fig. 2. Map of IDW interpolation for physical parameters of seawater quality: 1) pH, 2) temperature, 3) turbidity, and 4) brightness in the region of Mandeh Bay waters

Based on the analysis of seawater quality's physical parameters, it is evident that factors such as pH, temperature, turbidity, and brightness play a significant role in influencing the marine environment at the observation sites. These interconnected variables provide insight into the overall health and suitability of the water for marine biota and tourism activities. For more details, see Fig. 2 below for the distribution of the value of physical parameters of seawater quality (pH, temperature, turbidity, and brightness) at the observation locations.

Results of IDW Interpolation for the Chemical Parameters of Seawater Quality

Chemical of Seawater Quality for DO

The next parameter is DO, or dissolved oxygen, which marine biota, including microorganisms, use for their metabolismwhere this oxygen is then utilized by marine biota, including microorganisms, for their metabolism (Davis 1975). Under natural conditions, DO balance will be maintained through a continuous process. However, human activities such as agricultural runoff or wastewater discharge can introduce excess nutrients into the water, leading to eutrophication, which depletes dissolved oxygen levels over time (Dewata et al. 2024). If there is a disturbance, such as the entry of excessive organic matter, it will trigger an increase in microorganisms. This riseis followed by an increase in the need for dissolved oxygen. With a steady supply of oxygen but an increase in demand, the amount of oxygen content will automatically decrease. The ideal DO value for marine biota considered good enough for marine tourism according to Government Regulation No. 22/2021 is above 5 mg/L using the Water Quality Meter AZ Instrument 86031. The DO values measured at the observation sitesranged from 5.6 to 4.6 mg/L. This means that the DO content in the research location is high enough to support marine life and benefit marine tourism. The research results by Yu et al. (2023) have indicated that DO levels above 5 mg/L are typically sufficient to sustain diverse marine ecosystems and prevent hypoxic conditions that can harm marine organisms. The observation locations fall into the lightly polluted category when compared to the pollution criteria issued by Lee et al. (1978); Kenney et al. (2009) based on DO. .This classification suggests that while the water quality is still relatively good, continuous monitoring and management are needed to prevent further degradation that could affect both marine biota and tourism activities. More details can be seen in

Chemical of Seawater Quality for BOD

BOD, or biological oxygen demand, is the amount of dissolved oxygen needed by marine microorganisms to oxidize organic matter in water. This BOD value is usually used to see the level of seawater quality degradation through a decrease in dissolved oxygen levels (Jin et al. 2010). A high BOD indicates that microorganisms use a lot of oxygen to break down organic material. According to Lee et al. (2023), elevated BOD levels can lead to oxygen depletion, which severely impacts aquatic life, especially in areas with limited water circulation. BOD is usedto determine the standard BOD level. According to Dasgupta and Yildiz (2016), this BOD shows the dissolved oxygen level used by microorganisms in breaking down organic material within 5 days in a certain volume of water at a temperature of 20°C. According to Government Regulation No. 22/2021 for marine biota,the highest BOD value specified is 20 mg/L,and for marine tourism, it is10 mg/L. If this maximum limit is compared with the measurement results, then the value in the observation locations is still far below the value suggested by the Decree of the Minister of Environment, which is in the range of 2.42-3.67 mg/L using laboratory analysis with the Hach HQ440D. These values indicate that the water quality is relatively good and suitable for marine tourism and biota, as low BOD levels reflect minimal organic pollution (Weis., 2023). However, the observation locations fall into the lightly polluted category when compared to the classification values of Lee et al. (1978); Kenney et al. (2009), the observation locations are included in the lightly polluted category. This suggests that while pollution levels are low, continuous monitoring is necessary to ensure that BOD levels remain within safe limits, especially as nearby human activities increase. More details can be seen in Table 4 below.

Chemical of Seawater Quality for Salinity

The results of the measurement of salinity values tend to show characteristics of seawater salinity that are not affected by freshwater, although lower salinity is measured at the estuary location. Salinity values ranged from 33.3-32.2‰ with successive values of 33.3 at location 1; 32.2 at location 2-3, and 32.9 at location 4-5 including the

Table 3. Seawater quality based on DO content

mg/L	Status
>6,5	Not polluted until very lightly polluted
4,5-6,4	light polluted
2,0-4,4	Medium polluted
<2	heavy polluted

Source: (Lee et al. 1978; Kenney et al. 2009)

Table 4. Seawater quality based on BOD content

mg/L	Status
≥2,9	Not polluted until very lightly polluted
3,00-5,00	light polluted
5,10-14,90	Medium polluted
≤15	heavy polluted

Source: (Lee et al. 1978; Kenney et al. 2009)

impact of the revitalization of the connecting road access in the research location using the Water Quality Meter AZ Instrument 86031. Salinity describes the concentration of the total ion contained in water with the main constituent ions, such as sodium, potassium, magnesium, and chloride (Millero 2013). Salinity will vary vertically and horizontally depending on the input of freshwater, rainwater, and evaporation. Research by Duan et al. (2018) highlights that salinity variations are critical in influencing the distribution and health of marine ecosystems, as sudden changes can lead to stress in sensitive species. Salinity playsan important role in marine organisms'livesas well asthe solubility of gases in seawater. When compared with the standard value for seawater quality for biota according to Government Regulation No. 22/2021, the pH range is still within normal limits for marine life such as coral, seagrass, and mangroves. In terms of salinity, some marine biota, such as mangroves, can adapt to very low salinity conditions. Mangroves are known for their unique ability to thrive in brackish water, making them highly adaptable to fluctuating salinity levels (Meera et al. 2023). The salinity of coral reef waters in Indonesia is generally 31‰. Where is the salinity condition at the research location with a value of with a value of 33.3‰ is still natural salinity where salinity in Indonesian marine waters generally ranges from 30-35‰.This meansthat the salinity levels at the observation sitesare well within the range thatlocal marine life can handle.This protects important ecosystems like coral reefs and seagrass beds.

Chemical of Seawater Quality for NO3-N

NO_3-N is a form of nitrogen compound that is important for the metabolism of autotrophic organisms (Kamp et al. 2015). The formation of nitrate occurs through the oxidation of ammonia compounds to nitrite, followed by the conversion of nitrite to nitrate, a process commonly referred to as nitrification (Paśmionka et al. 2021). The measured nitrate value in the observation locations is 1.15-1.3 mg/L using the YSI ProDSS. The highest value was measured at the mouth of the river, while the lowest was at the research location. This demonstratesthe impactof organic matter input from land to water. High NO3-N levels, especially near river mouths, are often caused by agricultural runoff or sewage discharge, which adds to the amount of nutrientsin coastal waters (Jiang et al. 2023). According to Government Regulation No. 22/2021, the NO_3-N value is 0.008 mg/L. This discrepancy suggests that the NO_3-N levels in the observation locations are significantly higher than the threshold, potentially indicating nutrient pollution that could lead to eutrophication if left unmanaged. Elevated NO_3-N levels can lead to excessive growth of algae, which depletes oxygen and disrupts marine ecosystems. Nutrient pollution from sources such as agriculture and urban runoff is a growing concern in many coastal regions, as highlighted by Röthig et al. (2023), where long-term accumulation of nutrients has led to detrimental effects on water quality and biodiversity.

Chemical of Seawater Quality for NH_3-N

In addition to NO_3-N, NH_3-N is also a typeof nitrogen compound found in the sea. NH_3-N is formed from the fixation of nitrogen gas and ammonification of organic nitrogen during the decomposition process of organic matter. In addition, NH_3-N comes from the secretions of organisms as well as the input of organic waste from land (domestic waste, industry, and fertilizers). This form of nitrogen is particularly relevant in coastal ecosystems, where nutrient-rich runoff from agriculture and urban areas contributes to elevated NH3-N levels, leading to potential eutrophication (Sarma and Kumar, 2024). NO_3-N is toxic to marine biota because it interferes with the process of binding oxygen in the blood (Sánchez et al. 2017). The maximum limit value of NH_3-N for marine biota according to Government Regulation No. 22/2021 is 0.3 mg/L. The value of the measurement results in the research location showed that the NH_3-N level was at a low level with a range of 0.05-0.12 mg/L using the YSI ProDSS. These levels are well below the regulatory threshold, indicating that the waters in the research location are still safe for marine organisms and do not pose a significant risk of toxicity (Luo et al. 2023). Thus, the levels of NH_3-N in the research location are not toxic to the existing biota. However, it is essential to continue monitoring NH_3-N levels, as prolonged exposure to even low levels of NH_3-N can lead to chronic stress in sensitive marine species, potentially affecting biodiversity and ecosystem health.

Chemical of Seawater Quality for PO_4-P

One form of PO_4-P compound that exists in water is orthophosphate. Phosphate playsan important role in the metabolic process of biota through the process of protein formation and energy transfer (Hamal et al. 2024). Orthophosphate is a vital nutrient for marine organisms, as it plays a key role in cell growth, reproduction, and overall ecosystem productivity. But when present in excess, it can lead to serious ecological imbalances, particularly in coastal areas (Devlin and Brodie, 2023).According to the Ministry of Environment, 0.015 mg/L is a good PO_4-P content for marine biota. This highconcentration suggests not only the influence of external pollutants, but also a potential risk of long-term ecological degradation if these inputs continue unchecked. The measured PO_4-P value in the research location is above the value set according to Government Regulation No. 22/2021 in the range of 0.13-0.35 mg/L using laboratory analysis with the Hach DR3900: Spectrophotometer. This indicates the useof industrial waste or agricultural runoff as fertilizer. Such inputs are often associated with nutrient pollution, where excess phosphorus, along with nitrogen compounds, can significantly alter water quality (Devlin and Brodie, 2023). High levels of PO_4-P in the waters can trigger eutrophication. This process leads to overgrowth of algae, which blocks sunlight and diminishes oxygen levels, creating dead zones that are inhospitable to most marine life. If left unmanaged, this condition could result in hypoxic zones, severely impacting marine biodiversity and threatening local fisheries.In the long term, such nutrient pollution can also lead to changes in species composition, favoring those that can tolerate lower oxygen levels and reducing the overall resilience of marine ecosystems.

Chemical of Seawater Quality for H_2S

H_2S in water are usually the result of anaerobic bacterial respiration in addition to methane (CH_4). Anaerobic bacteria increase when there is a decrease in DO in the water, which causes a decrease in aerobic bacteria. Like aerobic bacteria, anaerobic bacteria also break down organic components in the absence of oxygen (Dhanaraj 2024). This process typically occurs in nutrient-rich environments where organic matter accumulates and depletes oxygen, creating favorable conditions for anaerobic activity. The presence of H_2S is a key indicator of hypoxic or anoxic conditions in aquatic environments, often signaling significant organic pollution and low oxygen levels (Hao et al. 2023). The H2S is not only toxic to marine organisms but also contributes to the characteristic foul odor in stagnant or polluted water bodies, further emphasizing its role as a sign of water quality deterioration. According to Government Regulation No. 22/2021, the recommended H_2S value is 0.01 mg/L. The H_2S content in the region of Mandeh Bay waters ranges from 0.005-0.09 mg/L using laboratory analysis

with the Hach DR3900: Spectrophotometer. High H_2S levels were measured at two locations in the estuary with values of 0.05 mg/L and 0.09 mg/L, respectively, indicating localized areas of potential concern, particularly near sources of nutrient runoff or organic matter deposits. Two other locations, some distance from the estuary, have low levels of H_2S. Elevated levels of H_2S can be harmful to marine life, particularly in estuarine areas where nutrient loading and organic matter accumulation are more common (Bastami et al. 2023). This condition, if left unaddressed, could lead to severe ecological disturbances, including fish kills and the degradation of benthic habitats. Long-term monitoring and management efforts are essential to mitigate the effects of H_2S and improve water quality in such vulnerable areas.

After analyzing several chemical parameters affecting seawater quality at the observation locations, including DO,BOD, salinity, NO3-N, NH_3-N, PO_4-P, and H_2S, we can conclude that the water quality in the area is still relatively good to support marine life and tourism activities. However, the elevated levels of certain parameters, such as NO_3-N and PO_4-P, indicate the influence of agricultural and industrial runoff, which could potentially trigger eutrophication if not properly managed. Similarly, the higher H_2S values at the estuary locations suggest anaerobic processes driven by elevated organic matter content. Continuous monitoring is essential to maintain the ecological balance and prevent further environmental degradation due to changes in these chemical parameters. Fig. 3 below provides a detaileddistribution of the value of chemical parameters of seawater quality (DO,BOD, salinity, NO_3-N, NH_3-N, PO_4-P, andH_2S) at the observation sites.

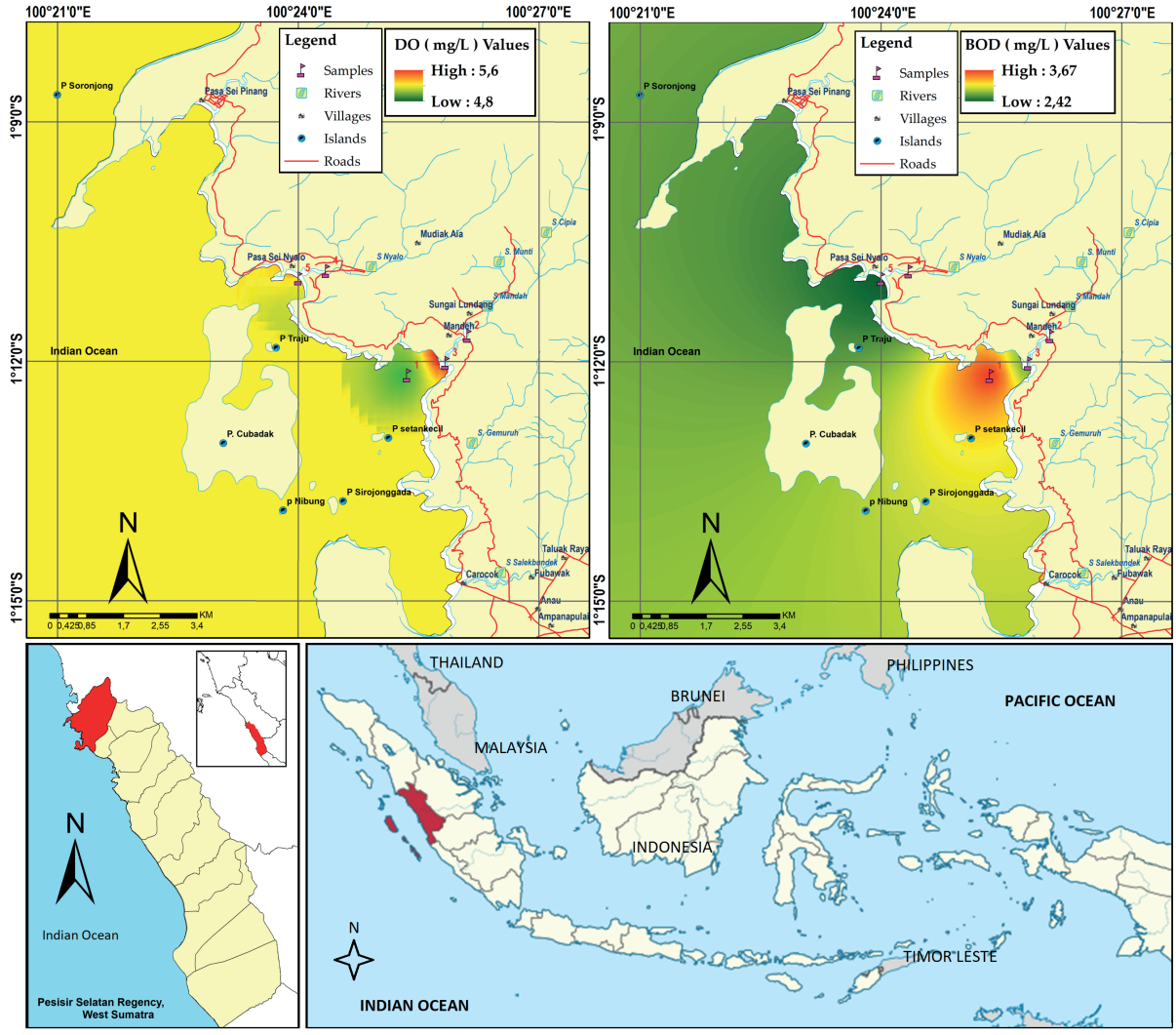

Fig. 3. Map of IDW interpolation for chemical parameters of seawater quality:1) DO; 2) BOD_5; 3) salinity; 4) NO_3-N; 5) NH_3-N; 6) PO_4-P; and 7) H_2S of seawater in region of Mandeh Bay waters

Table 5. Seawater quality standards for marine biota

Parameters	Unit	Quality standards
Phenol Compound	mg/L	0,002
PAH	mg/L	0,003
PCB	mg/L (ppm)	0,01
Surfactant (detergent)/MBAS	mg/L	1
Oil and fat	mg/L	1
Pesticide	mg/L (ppm)	0,01

Results of Pollutant Parameters of Seawater Quality

Some of the water pollutants that are often used as indicators of seawater quality are phenol compounds, PAH, PCB, surfactants (detergents), oils and fats, and pesticides. For the threshold value, the Minister of Environment'sDecreehas determined the quality standard value. More details can be seen in Table 5 below.

Phenol compounds, also known as carbolic acid or benzenol, are aromatic hydrocarbon compounds that are acidic and toxic. This compound is widely used in industry, both as a base material and as a material needed in the production process (Stich 1991). An example of the use of phenol is in the pharmaceutical industry, such as for antiseptics, aspirin drugs, and so on. The remaining compounds from industrial products can be transported into the water. These compounds are easily soluble in water, which can reduce seawater quality. The compound hasnegativeeffects on health issuessuch as lung, kidney, liver function, and cancer-causing substances.

The range of phenolic compounds at the sampling location was from the smallest to 0.0035 mg/L at location 1; 0.0151 mg/L at location; 0.0153 mg/L at location 2; and 0.0239 at location 3 using laboratory analysis with the Agilent 7890B GC System: Gas Chromatography. Compared to the quality standard value, the highest content of phenolic compounds at location 1 already exceeded the threshold value of 0.002 mg/L. Other water pollutants are known as PAH and PCB. PAHs are a large group of compounds that have many aromatic rings in their structure. Examples of PAH compounds include naphthalene, fluorene, pyrene, and others. These compounds are toxic, carcinogenic, or cancer-causing. Sources of PAH compound pollution are usually from industry, motor vehicles, or oil spills from transport ships and oil refineries. In the observation locations, no PCB compounds were identified, while the PAH was measured to be very low with a range of 0.0007 mg/L at location 2 and 0.00111 mg/L at location 3 using laboratory analysis with the Agilent 7890B GC System with 5977B MSD: GC-MS System. Even at location 1 (shipwreck), PAH was not identified. This value is very low when compared to the Minister of Environment's Decree'squality standard value of 0.003 mg/L.

Surfactants are chemical compounds that are widely used in detergents or other cleaning agents.The composition of surfactants can reach 15-40% of the total material used. Besides being able to damage the skin, this compound also has a carcinogenic effect. In waters, high concentrations of detergents can cause eutrophication. The amount of surfactant (detergent) in the observation sites was 0.2 mg/L at sites 1, 2, and 3. This was found using the Agilent 1260 Infinity II LC: Liquid Chromatography in a laboratory. The detergent concentration was much higher than the quality standard value. This suggeststhat there is pollution in the estuary that comes from the mainland. Meanwhile, the oil and fat content in the observation locations is 0.305 mg/L, respectively, at location 1; 0.823 mg/L at location 2; and 0.959 mg/L at location 3,according tolaboratory analysis with the Agilent 7890B GC System: Gas Chromatography. At location 3,the concentration was almost the same as the quality standard value. Using laboratory analysis with the Agilent 7890B GC System and the 5977B MSD: GC-MS System, the pesticide content was 0.025 mg/L in location 2, respectively; and 0.03 mg/L at location 3 using laboratory analysis. Apart from site1, all locations had higher pesticide content than the quality standard.

DISCUSSIONS

According tothe description above, seawater quality lower in estuary locations than in locations further away from estuary areas. The value of the content of several pollutants shows that the estuary location is lightly polluted. This indicates the input of water pollutants from the mainland through river water to the sea. The measurements and analysis of hydrological conditions reveal that the average temperature, average salinity, DO, PO_4-P, NO_3-N, pH, and brightness at the observation locations remain relatively suitable for various purposes,adhering to the criteria outlined in Government Regulation No. 22/2021. In general, the seawater quality conditions (brightness, pH, and temperature) at the wreck site of the observation locations do not indicate extreme natural conditions that could lead to rapid weathering or chemical destruction of the sinking site. Until now, Indonesia has not developed a zoning system that can be used as a guideline to clarify the potential land use of an area or area for the development of historical heritage sites (e.g., shipwrecks) for the development of marine tourism.

Shipwrecks, like the renowned Liberty Wreck in Tulamben, Bali, are captivating sites for diving enthusiasts, serving as prime attractions for diving tourism. These submerged relics typically serve as focal points for marine biodiversity, fostering vibrant and distinct ecosystems akin to artificial reefs. According to Paxton et al. (2023), shipwrecks contribute significantly to the proliferation of marine life, offering habitat complexity that supports a diverse range of species. This ecological role enhances the attractiveness of shipwrecks for divers and researchers alike, as these sites not only provide thrilling underwater experiences but also offer unique opportunities for studying marine ecosystems in artificially created environments. Moreover, shipwrecks are increasingly recognized for their cultural and historical value, serving as underwater time capsules that preserve artifacts and structures from past eras. Tzanakis (2024) highlights that these sunken vessels have the potential to evolve into underwater museums, offering recreational excursions while simultaneously serving as educational platforms. This dual role is crucial in promoting the conservation of underwater cultural heritage, as noted by Brooks et al. (2023), who argue that the integration of cultural heritage preservation with tourism can lead to sustainable management practices that benefit both the environment and local communities.

In addition to their ecological and cultural significance, shipwrecks also contribute to the economic development of coastal regions. The tourism revenue generated by diving activities around shipwrecks can provide substantial financial support for local economies. As Islami (2024) discusses, the economic impact of shipwreck tourism extends beyond direct income, as it also fosters the development of related industries, such as hospitality, guiding services, and marine conservation initiatives. Furthermore, the potential of shipwrecks as training venues for aspiring divers cannot be understated. Shipwrecks offer unique challenges and learning opportunities that are essential for developing advanced diving skills. According to Ababneh (2024), training in shipwreck environments enhances divers' proficiency in navigation, buoyancy control, and underwater problem-solving, making these sites invaluable for both recreational and professional diver training programs. Overall, shipwrecks are multifaceted assets that contribute to marine biodiversity, cultural heritage preservation, economic growth, and diver education. The integration of these aspects into a cohesive management strategy, as suggested by Barianaki et al. (2024), can ensure that shipwrecks continue to provide ecological, cultural, and economic benefits while promoting sustainable tourism practices.

CONCLUSIONS

Conclusions from research results regarding seawater quality in diving tourism areas include physical, chemical, and water pollutants, namely: 1) the pH ranged from 7.12 to 7.61, with lower values near estuaries due to higher freshwater input. Despite fluctuations, the pH remains within the natural range for marine waters in Indonesia; 2) temperature ranged from 29.1 to 30.3°C, falling within the acceptable range for marine biota and tourism activities according to environmental standards; 3) turbidity ranged from 4.2 to 6.5 ntu, with values below the quality standard for marine tourism. However, increased turbidity near estuaries poses challenges to marine life due to sedimentation; 4) DO ranged from 4.6 to 5.6 mg/L, indicating adequate oxygen levels to support marine life and tourism activities. The locations fall within the lightly polluted category based on DO criteria; 5) BOD ranged from 2.42 and 3.67 mg/L, indicating relatively low levels and falling within acceptable limits for marine biota and tourism; 6) Salinity ranged from 32.2 to 33.3‰, with variations influenced by freshwater input but remaining suitable for marine life; 7) NO_3-N ranged from 1.15 to 1.3 mg/L, while NH^3-N ranged from 0.05 to 0.12 mg/L, both within acceptable ranges for marine biota; 8) PO_4-P ranged from 0.13 to 0.35 mg/L, indicating potential water pollutants from industrial or agricultural runoff and warranting monitoring to prevent eutrophication; 9) H_2S ranged from 0.005 to 0.09 mg/L, with higher concentrations near estuaries, indicating anaerobic bacterial activity but remaining within acceptable limits; 10) various water pollutants such as phenol compounds, PAH, PCB, surfactants, oils and fats, and pesticides were identified, with some locations exceeding quality standard values, particularly near estuaries. Overall, while the seawater quality parameters generally meet regulatory standards for marine biota and tourism, there are localized water contamination concerns, especially near estuaries. Continued monitoring and management efforts are essential to maintain and improve seawater quality, particularly in sensitive marine ecosystems like diving tourism areas. Additionally, the research highlights the potential of shipwrecks as diving tourism attractions and emphasizes the need for appropriate management and preservation of such sites for recreational and educational purposes. Sedimentation is, in general, the most important natural phenomenon to be studied in more detail in the future around the Mandeh Bay waters.

REFERENCES

Ababneh, A. (2024). Review Future Technologies in Underwater Cultural Heritage. Journal of the General Union of Arab Archaeologists, 9(2), 1-19. https://doi.org/10.21608/JGUAA2.2024.251548.1157

Adams K M. (2018). Tourism, economy, and society. Routledge Handbook of Contemporary Indonesia.

Ajwang V. (2024). Impact of Pollution on Coral Health in Coastal Reef Ecosystems. American Journal of Natural Sciences, 5(1), 33-43. https://doi.org/10.47672/ajns.2043

Alhadi Z. (2018). Community-based tourism development viewed from economic, social culture and environment aspects in Mandeh's integrated marine tourism area. MATEC Web of Conferences. 229, 01006. https://doi.org/10.1051/matecconf/201822901006

Ali I., and Sulistiyono S.T. (2020). A Reflection of "Indonesian Maritime Fulcrum" Initiative: Maritime History and Geopolitical Changes. Journal of Maritime Studies and National Integration, 4(1), 12-23. https://doi.org/10.14710/jmsni.v4i1.8081

Bastami K.D., Manbohi A., Mehdinia A., Hamzehpour A., Haghparast S., and Taheri M. (2024). Distribution of hydrogen sulfide, nitrogen, and phosphorus species in inshore and offshore sediments of the south Caspian Sea. Marine Pollution Bulletin, 202, 116330. https://doi.org/10.1016/j.marpolbul.2024.116330

Barianaki E., Kyvelou S.S., and Ierapetritis D.G. (2024). How to Incorporate Cultural Values and Heritage in Maritime Spatial Planning: A Systematic Review. Heritage, 7(1), 380-411. https://doi.org/10.3390/heritage7010019

Beaty F., Gehman A.L.M., Brownlee G., and Harley C.D. (2023). Not just range limits: Warming rate and thermal sensitivity shape climate change vulnerability in a species range center. Ecology, 104(12), e4183. https://doi.org/10.1002/ecy.4183

Brown A.R., Webber J., Zonneveld S., Carless D., Jackson B., Artioli Y., and Tyler C.R. (2020). Stakeholder perspectives on the importance of water quality and other constraints for sustainable mariculture. Environmental Science & Policy, 114, 506-518. https://doi.org/10.1016/j.envsci.2020.09.018

Brooks, C., Waterton, E., Saul, H., and Renzaho, A. (2023). Exploring the relationships between heritage tourism, sustainable community development and host communities' health and wellbeing: A systematic review. PloS one, 18(3), e0282319. https://doi.org/10.1371/journal.pone.0282319

Butler B.A. and Ford R.G. (2018). Evaluating relationships between total dissolved solids (TDS) and total suspended solids (TSS) in a mining-influenced watershed. Mine water and the environment, 37(1), 18-30. https://doi.org/10.1007/s10230-017-0484-y

Candra O., Putra A., Priyambodo D.G., Revina R., and Elfizon (2024). Variability between wind and sea waves based on environmentally friendly as renewable energy in Pariaman City. Journal of Sustainability Science and Management, 19(10), in press.

Christensen J.P. (2023). The roles of carbonate, borate, and bicarbonate ions in affecting zooplankton hatching success under ocean acidification. Marine Chemistry, 256, 104269. https://doi.org/10.1016/j.marchem.2023.104269

Dasgupta M., and Yildiz Y. (2016). Assessment of biochemical oxygen demand as indicator of organic load in wastewaters of Morris County, New Jersey, USA. Journal of Environmental & Analytical Toxicology, 6(3), 378. https://doi.org/10.4172/2161-0525.1000378

Davis J.C. (1975). Minimal dissolved oxygen requirements of aquatic life with emphasis on Canadian species: a review. Journal of the Fisheries Board of Canada, 32(12), 2295-2332. https://doi.org/10.1139/f75-268

Devlin M., and Brodie J. (2023). Nutrients and eutrophication. In Marine Pollution: Monitoring, Management, and Mitigation. Springer Nature Switzerland. 75-100.

Dewata I., Hamdi, Putra, A., Hasmira M.H., Driptufany D.M., Fajrin., Yulius, H., Hidayat, M., Yusran, R., and Arman, A. (2024). Water quality of Batang Merao watershed and implementation of Landsat 8 OLI/TIRS for the transparency of Lake Kerinci waters. Journal of Sustainability Science and Management, 19(4), 110-121. http://doi.org/10.46754/jssm.2024.04.009

Dewata I., and Putra A. (2021). Kriging-GIS model for the spatial distribution of seawater heavy metals. Periodicals of Engineering and Natural Sciences (PEN), 9(2), 629-637. http://dx.doi.org/10.21533/pen.v9i2.1851

Dhanaraj, C. J. (2024). Harmful Effects of Water Pollution. Handbook of Water Pollution, Wiley, 123-148. https://doi.org/10.1002/9781119904991.ch5

Duan C., Yang M., Wang Q., Xue J., Yuan L., and Wu H. (2023). Impacts of salinity stress caused by ballast water discharge on freshwater ecosystems. Regional Studies in Marine Science, 65, 103079. https://doi.org/10.1016/j.rsma.2023.103079

El Silisna B., and Susanti R. (2020). Sport Tourism Event of Tour De Singkarak to Support Destination Management in West Sumatera, Indonesia. Journal of Tourism, 7(1), 55-72. https://doi.org/10.24922/eot.v7i1.58742

Figueroa S.M., and Son M. (2024). Transverse variability of residual currents, sediment fluxes, and bed level changes in estuaries with an estuarine dam: Role of estuarine type, dam location, and discharge interval. Continental Shelf Research, 274, 105196. https://doi.org/10.1016/j.csr.2023.105196

Hall N., Testa J., Li M., and Paerl H. (2023). Assessing drivers of estuarine pH: A comparative analysis of the continental USA's two largest estuaries. Limnology and Oceanography, 68(10), 2227-2244. https://doi.org/10.1002/lno.12345

Hamal R., Jaya A.A., Ratnasari R., and Walinono A.R. (2024). The Influence Of Source, Seed Weight And Scattering Distance On The Growth Of Seaweed (Kappaphycus Alvarezii) In Mandale Waters Pangkep District, South Sulawesi. International Journal of Economics, Business and Innovation Research, 3(01), 211-224. https://doi.org/10.70799/ijebir.v3i01.570

Hammer K., Schneider B., Kuliński K., and Schulz-Bull D.E. (2014). Precision and accuracy of spectrophotometric pH measurements at environmental conditions in the Baltic Sea. Estuarine, Coastal and Shelf Science, 146, 24-32. https://doi.org/10.1016/j.ecss.2014.05.003

Hao Y., Shen J., Zhang Y., Xie P., and Liu Y. (2023). Assessing the pollution level of a subtropical lake by using a novel hydrogen sulfide fluorescence technology. Environmental Research, 229, 115916. https://doi.org/10.1016/j.envres.2023.115916

Hemraj D.A., Falkenberg L.J., Cheung K., Man L., Carini A., and Russell B.D. (2023). Acidification and hypoxia drive physiological trade-offs in oysters and partial loss of nutrient cycling capacity in oyster holobiont. Frontiers in Ecology and Evolution, 11, 1083315. https://doi.org/10.3389/fevo.2023.1083315

Hermon D., Gusman M., Putra A., and Dewata I. (2022). Value estimating of the sedimentation rate at the shipwreck sites (MV Boelongan Nederland) the Mandeh Bay Region-Pesisir Selatan Regency. IOP Conference Series: Earth and Environmental Science, 967(1), 012007. https://doi.org/10.1088/1755-1315/967/1/012007

Isdianto A., and Luthfi, O.M. (2020). The Relation of Water Chemical Quality to Coral Reef Ecocsystems in Damas. Journal of Environmental Engineering and Sustainable Technology, 7(2), 26-34. http://dx.doi.org/10.21776/ub.jeest.2020.007.02.3

Islam M.S. (2024). Blue Economy, Complex Challenges: the Future of Marine Tourism in Bangladesh. Safran Kültür Ve Turizm Araştırmaları Dergisi, 7(1), 42-68. https://dergipark.org.tr/tr/pub/saktad/issue/84368/1443733

Jiang L., Lu X., Wang G., Peng M., Wei A., Zhao Y., and Soetaert K. (2023). Unraveling seasonal and interannual nutrient variability shows exceptionally high human impact in eutrophic coastal waters. Limnology and Oceanography, 68(5), 1161-1171. https://doi.org/10.1002/lno.12294

Jin X.L., Jing M., Chen X., Zhuang Z.X., Wang X.R., and Lee F.S. (2010). A study on the relationship between BOD and COD in a coastal seawater environment with a rapid BOD measurement system. Water science and technology, 61(6), 1499-1503. https://doi.org/10.2166/wst.2009.810

Junaidi M., Azhar F., Diniarti N., and Lumbessy S.Y. (2019). Estimation of organic waste and waters carrying capacity for lobster cage culture development in North Lombok District, West Nusa Tenggara Province. Aquaculture, Aquarium, Conservation & Legislation, 12(6), 2359-2370.

Kuroda T., Takai R., Kobayashi Y., Tanaka Y., and Hara S. (2008). Corrosion rate of shipwreck structural steels under the sea. OCEANS 2008-MTS/IEEE Kobe Techno- Ocean, 1-6. http://dx.doi.org/10.1109/OCEANSKOBE.2008.4531052

Kamp A., Høgslund S., Risgaard-Petersen N., and Stief P. (2015). Nitrate storage and dissimilatory nitrate reduction by eukaryotic microbes. Frontiers in microbiology, 6, 1492. https://doi.org/10.3389/fmicb.2015.01492

Kennedy M.D. (2013). Introducing geographic information systems with ARCGIS: a workbook approach to learning GIS. John Wiley &Sons.

Kenney M.A., Sutton-Grier A.E., Smith R.F. and Gresens S.E. (2009). Benthic macroinvertebrates as indicators of water quality: The intersection of science and policy. Terrestrial Arthropod Reviews, 2(2), 99. https://doi.org/10.1163/187498209X12525675906077

Lee Y.W., Oh Y.H., Lee S.H., Kim D., and Joung D. (2023). Assessment of water quality in a coastal region of sea dike construction in Korea and the impact of low dissolved oxygen concentrations on pH changes. Journal of Marine Science and Engineering, 11(6), 1247. https://doi.org/10.3390/jmse11061247

Lee C., Wang S.B., and Kuo C.L. (1978). Benthic Macroinvertebrate and Fish as Biological Indicators of Water Quality, With Reference of Community Diversity Index. Bangkok. International Conference on Water Pollution Control in Development Countries. Bangkok. Thailand.

Lemy D.M., Teguh F., and Pramezwary A. (2019). Tourism development in Indonesia. Delivering Tourism Intelligence. 11, 91-108. https://doi.org/10.1108/S2042-144320190000011009

Luo H.W., Lin M., Bai X.X., Xu B., Li M., Ding J.J., Hong W.J., and Guo L.H. (2023). Water quality criteria derivation and tiered ecological risk evaluation of antifouling biocides in marine environments. Marine Pollution Bulletin, 187, 114500. https://doi.org/10.1016/j.marpolbul.2022.114500

MacIntosh A., Dafforn K., Penrose B., Chariton A., and Cresswell T. (2023). Assessing the ecological impacts of NORM-contaminated scale on marine infauna using sediment microcosms. Chemosphere, 340, 139939. https://doi.org/10.1016/j.chemosphere.2023.139939

McGeady R., Runya R.M., Dooley J.S., Howe J.A., Fox C.J., Wheeler A.J., Summer G., Callaway A., Beck S., Brown L.S., Dolly G., and McGonigle C. (2023). A review of new and existing non-extractive techniques for monitoring marine protected areas. Frontiers in Marine Science, 10, 1126301. https://doi.org/10.3389/fmars.2023.1126301

Millero F.J. (2013). Chemical Oceanography (4thed.). CRC Press. https://doi.org/10.1201/b14753

Mills K., John E.H., Muir D.D., Santodomingo, N., Johnson K.G., Hussein M.A.S., and Sosdian S. (2023). Growth responses of mixotrophic giant clams on nearshore turbid coral reefs. Coral Reefs, 42(2), 593-608. https://doi.org/10.1007/s00338-022-02259-9

Meera S.P., Bhattacharyya M., and Kumar A. (2023). Dynamics of mangrove functional traits under osmotic and oxidative stresses. Plant Growth Regulation, 101(2), 285-306. https://doi.org/10.1007/s10725-022-00817-3

Nabhan F., Bangkara B.A., Sugiarti S., Tuhuteru L., and Siagawati M. (2023). Identification of HR management best practices in marketing tourism production and services: scientific proof of progress in tourism destinations in several provinces in Indonesia. Enrichment: Journal of Management, 13(1), 313-322. https://doi.org/10.35335/enrichment.v13i1.1211

Paśmionka I.B., Bulski K., and Boligłowa E. (2021). The Participation of Microbiota in the Transformation of Nitrogen Compounds in the Soil—A Review. Agronomy, 11(5), 977. https://doi.org/10.3390/agronomy11050977

Paxton A.B., McGonigle C., Damour M., Holly G., Caporaso A., Campbell P.B., Meyer-Kaiser K.S., Hamdan L.J., Mires C.H., and Taylor J.C. (2023). Shipwreck ecology: Understanding the function and processes from microbes to megafauna. Bioscience, 74(1), 12–24. https://doi.org/10.1093/biosci/biad084

Prarikeslan W., Syah N., Barlian E., Suasti Y., and Putra A. (2020). A potential locations of marine tourism in Pasumpahan island, Padang city-Indonesia. International Journal of GEOMATE Journal, 19(72), 123-130. https://doi.org/10.21660/2020.72.ICGeo5

Putra A., Triyatno., Darwis R., Dewata I., Tanto T.A., Mustapha M.A., Razi P., and Zainul R. (2023). Suitability of Mangrove Ecosystems as a Protected Zone Based on Land-Use Changes. Physical Oceanography, 30(5), 866-881.

Putra A., Dewata I., Hermon D., Barlian E., Umar G., Widodo T., and Damanhuri H. (2023). Activity Recommendations Based on an Environmental Approach in Zoning of Marine Protected Areas (MAPS) Pariaman City-Indonesia. EnvironmentAsia, 16(3), 57-67. http://dx.doi.org/10.14456/ea.2023.35

Rahman M.H., Pandit D., Begum, N., Sikder M.N.A., Preety Z.N., and Roy T.K. (2023). Fluctuations of physicochemical parameters in the waters of the Chattogram Coastal Area, Bangladesh. Marine Science and Technology Bulletin, 12(4), 530-539. https://doi.org/10.33714/marstecbull.1246432

Ridwan N.N.H. (2015). Maritime Archaeology in Indonesia: resources, threats, and current integrated research. Journal of Indo-Pacific Archaeology, 36, 16-24. https://doi.org/10.7152/jipa.v36i0.14911

Ridwan N.N.H. (2019). Vulnerability of shipwreck sites in Indonesian waters. Current Science, 117(10), 1623-1628. https://www.jstor.org/stable/27138522

Röthig T., Trevathan-Tackett S.M., Voolstra C.R., Ross C., Chaffron S., Durack P.J., Warmuth L.M., and Sweet M. (2023). Human-induced salinity changes impact marine organisms and ecosystems. Global Change Biology, 29(17), 4731-4749. https://doi.org/10.1111/gcb.16845

Sánchez Ó.J., Ospina D.A., and Montoya S. (2017). Compost supplementation with nutrients and microorganisms in composting process. Waste Management, 69, 136-153. https://doi.org/10.1016/j.wasman.2017.08.012

Safitri M. (2021). Indonesia's Marine and Fishery Genetic Resource Conservation by Means of Intellectual Property. International Conference on Sustainable Development Goals (ISCIS). 1(1), 89-98.

Sarma, D., and Kumar, D. (2024). Eutrophication in freshwater and its microbial implications. In Chapter books of Handbook of Aquatic Microbiology, 194, Routledge.

Septiariva I.,. and Suryawan I.W.K. (2021). Development of water quality index (WQI) and hydrogen sulfide (H2S) for assessment around suwung landfill, Bali Island. Journal of Sustainability Science and Management, 16(4), 137-148. http://doi.org/10.46754/jssm.2021.06.0012

Stanford R.J., Wiryawan B., Bengen D.G., Febriamansyah R., and Haluan J. (2012). Identification Of Poor Fishing-Dependent Communities In Mainland West Sumatra. Buletin PSP, 20(1), 15-34.

Stich H.F. (1991). The beneficial and hazardous effects of simple phenolic compounds. Mutation Research/Genetic Toxicology, 259(3-4), 307-324. https://doi.org/10.1016/0165-1218(91)90125-6

Tortell P.D. (2005). Dissolved gas measurements in oceanic waters made by membrane inlet mass spectrometry. Limnology and Oceanography: Methods, 3(1), 24-37. https://doi.org/10.4319/lom.2005.3.24

Triyatno., Bert I., Idris., Hermon D., and Putra A. (2020). Hazards and morphometry to predict the population loss due of landslide disasters in Koto XI Tarusan-Pesisir Selatan. International Journal of GEOMATE, 19(76), 98-103. https://doi.org/10.21660/2020.76.ICGeo12

Tzanakis M. (2024). Underwater Phantasmagoria: The Touristization of Scuba Diving. In Scuba Diving Practices in Greece: A Historical Ethnography of Technology, Self, Body, and Nature, 139-176. Cham: Springer International Publishing. https://doi.org/10.1007/978-3-031-48839-9_6

Villatoro M.M., Amos C.L., Umgiesser G., Ferrarin C., Zaggia L., Thompson C.E., and Are D. (2010). Sand transport measurements in Chioggia inlet, Venice lagoon: Theory versus observations. Continental Shelf Research, 30(8), 1000-1018. https://doi.org/10.1016/j.csr.2009.06.008

Weis, J.S. (2024). Marine Pollution: What Everyone Needs to Know®. Oxford University Press. https://doi.org/10.1093/oso/9780197556372.001.0001

Yi Y., Zhao F., Hou C., Zhang C., and Tang C. (2024). Mechanism and threshold of environmental stressors on seagrass in high-turbidity estuary: Case of Zostera japonica in Yellow River Estuary, China. Frontiers in Marine Science, 11, 1432106. https://doi.org/10.3389/fmars.2024.1432106

Yu H., Fang G., Rose K.A., Lin J., Feng J., Wang H., Cao Q., Tang Y., and Zhang, T. (2023). Effects of habitat usage on hypoxia avoidance behavior and exposure in reef-dependent marine coastal species. Frontiers in Marine Science, 10, 1109523. https://doi.org/10.3389/fmars.2023.1109523

Check for updates

CC BY

RESEARCH PAPER

URBAN GREEN INFRASTRUCTURE ASSESSMENT: IDENTIFICATION OF PUBLIC GREEN SPACES MISUSE

Maria E. Skachkova[1]

[1] Empress Catherine II Saint Petersburg Mining University, 2, 21st Line, St. Petersburg, 199106, Russia

***Corresponding author:** Skachkova_ME@pers.spmi.ru

Received: June 19th 2024 / Accepted: November 27th 2024 / Published: December 31st 2024

https://doi.org/10.24057/2071-9388-2024-3458

ABSTRACT. Assessment of urban green infrastructure is a task of strategic planning and tactical implementation of decisions taken in the context of sustainable development of urban territories. One of the directions of such an assessment is to identify instances of land misuse within cities' public green areas. It reflects the legal fairness of the use of urban green spaces, but currently has a weak scientific justification. Therefore, it is pertinent to develop a methodology for evaluating urban green infrastructure in order to pinpoint areas with inappropriate usage Critical analysis and synthesis allowed us to justify the assessment of the misuse of land within urban green zones as an equal element of the urban green infrastructure assessment system. A geospatial database was created to assess public green spaces. Using the results of remote sensing of territories, as well as the «boxplot» method in combination with the Python programming, the NDVI was calculated, and a classification of vegetation elements and artificial objects located within public green spaces in cities was carried out. Based on the obtained classification categories, a mechanism for identifying «green» areas with misuse of land was proposed, and a list of public green areas with similar violations in St. Petersburg was determined. The practical results of the study include: technology for assessing urban green infrastructure to identify public green spaces with misuse; geospatial databases of public green spaces for St. Petersburg; identified public green spaces with obvious violations of their use, including unauthorized parking, littering, sand dumps, unauthorized placement of industrial, warehouse, retail, transport, or other non-recreational facilities within the boundaries of PGS, vehicle collisions with «green» areas; erroneous inclusion of residential buildings and adjacent courtyards, non-residential facilities, as well as organized parking spaces within PGS's boundaries.

KEYWORDS: greening, territory assessment, sustainable development, misuse of land, boxplot, NDVI, GIS

CITATION: Skachkova M. E. (2024). Urban Green Infrastructure Assessment: Identification Of Public Green Spaces Misuse. Geography, Environment, Sustainability, 4(17), 183-197
https://doi.org/10.24057/2071-9388-2024-3458

Conflict of interests: The authors reported no potential conflict of interest.

INTRODUCTION

Urban green spaces (UGS) are a natural and ecological basis of urbanized areas, play a key role in the formation of a sustainable environment, and perform a number of significant functions: ecological, which includes environment-forming, sanitary-hygienic, environmental, protective (barrier); aesthetic, including decorative and architectural; recreational; transit; specialized; engineering and technical (Ma et al. 2019; Vidal et al. 2022; Jian and Yang 2024). UGS ecosystem services, as a consequence of these functions, provoke socio-economic transformations of the urban environment (Gagarina 2023). For example, the availability and quality of UGS affect the value of real estate in cities by increasing the attractiveness and psychological comfort of territories, reducing noise pollution, and improving the microclimate (Bykowa et.al. 2024). Assessing the potential of multifunctional green infrastructure is an crucial strategic task for environmental protection, socio-economic development, and spatial planning in the region , considering the concept of sustainable development (Cherepovitsyn et al. 2021), an integrated ecosystem approach, and the promotion of social and environmental justice (Enssle and Kabisch 2020; Klimanova et al. 2022; Skachkova and Guryeva 2023).

The global community's experience in assessing UGS is extensive and relates to the various ecosystem services provided by green spaces. Several enlarged groups can help identify the main areas of urban green infrastructure assessment.

UGS spatial accessibility

To assess the quality of public green spaces, taking into account spatial differentiation, Stessens et al. developed a GIS-based proximity sub-model based on the concept of theoretical functional levels (TFL), as well as a quality model based on the example of Brussels (Stessens et al. 2017). The authors understand classification by theoretical functional levels, where green spaces of a certain size have a specific radius of attraction for the population. Together, these models make it possible to assess which TFLs and what level of green space quality is available to residents of each city block in Brussels.

Schindler et al. used a survey of respondents in Brussels, Luxembourg, and Rouen to create models of the spatial movement of respondents from their place of residence to their preferred urban green space. Models are classified as centrifugal and centripetal based on their type of use. It is also concluded that the size of UGS has little effect

on the distance respondents travel to them. Accordingly, the size of the landscaping does not affect the choice of a recreation place by residents. Residents can travel to the popular UGS not the standard distance of 300-500 m but 1.4-1.9 km (Schindler et al. 2022). Work by Jang et al. is devoted to the development of an index of urban green spaces accessibility, which shows the features of the green spaces' distribution at the citywide or local level (Jang et al. 2020).

Many researchers write in their publications about the well-known "3-30-300" concept (Schindler et al. 2022; Rakhmatullina et al. 2023; Browning et al. 2024), which provides three rules. Firstly, every resident should be able to see at least three trees from their home. This fact has a positive impact on mental health and well-being. Secondly, every urban area must have 30 percent tree canopy coverage. Barcelona, Bristol, Seattle, Canberra, and Vancouver, for example, set this goal for themselves[1]. Thirdly, a maximum distance of 300 m to the nearest green area must be maintained. This distance appears in many studies (Rakhmatullina et al. 2023; Bolkaner and Asilsoy 2023). Russian legislation normalizes the radius of public green area accessibility: for multi-storey residential buildings, 400 m; for low-rise residential buildings, 800 m (Set of rules 476.1325800.2020). These indicators correspond to a time interval of 5-10 minutes and correlate with the Chinese concept of "city in 15 minutes", "city in 10 minutes" and "city in 5 minutes" (Luo et al. 2022).

Residents' provision of UGS

Usually, the green spaces provision of the population, including public green spaces, is characterized by the "green area per inhabitant" indicator (Grunewald et al. 2019). The World Health Organization defines the maximum parameters for the green space provision per person: the minimum value is 9 m^2, the optimal value is 50 m^2. However, green space provision varies greatly across countries. For example, in Belgium, Australia, and Germany the provision reaches 200 m^2 per person, while for Spain and Macedonia the indicator is only 4 m^2 (Pouya and Aghlmand 2022). For Russian cities, minimum standards for providing green space to the population have been established. For St. Petersburg, these parameters vary from 6 to 18 m^2 depending on the administrative region.

This direction of urban green infrastructure assessment has a qualitative component and may include alternative studies in various aspects: studying the relationship between the green space amount and the mental well-being of children of different ethnicities (McEachan et al. 2018), as well as indicators of the residents' health (general poor health, depression, severe mental illness, etc.) (Mears et al. 2020).

Assessment of the ecological state of green spaces

Assessment of the ecological state of the urban environment includes studies of soil and vegetation cover. Cover is "an integral indicator of environmental well-being and at the same time a potential source of secondary pollution of the natural environment" (Pashkevich et al. 2020; Mityakova et al. 2023). During this assessment, an individual assessment of trees can be carried out according to a set of dendrometric indicators on trial plots; the state of different types of vegetation (trees, shrubs, flower beds, lawns) is determined, as well as a score (coefficient, category) of the ecological state of public green spaces (Shchasnaya and Rondak 2024). The remote sensing approach is also popular for assessing the environmental quality of cities. Giofandi et al. used four indices (NDBI - Build-up Index, NDSI - Soil Index, SAVI - Vegetation Index, NDNI - Moisture Index) and revealed an environmental quality decrease of Pekanbaru city (Riau province, Indonesia) (Giofandi et al. 2024).

Environmental inequality assessment

The concept of environmental justice asserts that all people have the right to benefit from the UGS barrier function (e.g., protection from noise, vibration, pollution) as well as other UGS ecosystem services. Environmental inequality refers to the link between environmental quality and social class divisions. Environmental stratification suggests an uneven distribution of UGS among urban residents. At the same time, the UGS quality varies depending on the socioeconomic status of residents, which means that areas with high incomes tend to have higher qualitative and quantitative indicators of greening (Luo et al. 2022; Wang et al. 2021; Kurniawan 2023). A study by Nesbitt et al. in this area also shows that, in addition to population income, a strong correlation is observed between the presence of higher education among residents and the distribution of urban vegetation (Nesbitt et al. 2019).

However, the results of Chinese colleagues are discordant with the above conclusions, saying that "the provision of green space does not strongly discriminate against people's socioeconomic levels in China". High levels of vegetation quality may apply to different social groups (including migrants and marginalized groups) (Wu et al. 2022). Tehran Research (Iran) shows an intermediate result: areas with higher socioeconomic status in Tehran receive more ecosystem services from UGS. However, in underdeveloped areas, a similar trend is observed (Roodsari and Hoseini 2022). The Paris study is devoted to the relationship between social inequality and the availability of green spaces using the example of Paris (Ile-de-France region). Again, this is an environmental justice concept that raises the issue that in many cities, access to green space is stratified by income and ethnicity (Liotta et al. 2020).

Aesthetic assessment of green spaces (assessment of attractiveness / comfort)

This type of assessment can be carried out in different directions. Brindley et al. consider the cleanliness of greenspace. Their unsatisfactory level negatively has a negative impact on the health of nearby residents. The authors see possible reasons for this in psychological discomfort, which prevents people to visit green spaces and to receive required ecosystem services (Brindley et al. 2019). Stessens et al. investigate the biological value, land cover composition, area, and form of green spaces as key indicators of the quality of public green spaces (PGS), a measure of visitor perception. How people perceive green spaces and their quality is relevant for urban area management purposes (Stessens et al. 2020).

The above list of assessment aspects is not exhaustive. For example, Kuklina et al. assessed green spaces according

[1] *C. Konijnendijk van den Bosch (2021). Promoting health and wellbeing through urban forests – Introducing the 3-30-300 rule. [online] The IUCN Urban Alliance. Available at: https://iucnurbanalliance.org/promoting-health-and-wellbeing-through-urban-forests-introducing-the-3-30-300-rule/*

to the criterion of urban sustainability in the Arctic (Nadym, Russia) (Kuklina et al. 2021). The Klimanova's study includes the assessment of ecosystem services (Klimanova et al. 2021). In particular, the ecosystem service associated with air purification, taking into account the absorption capacity of trees by a method developed for cities in Canada and America using the iTree tool, is of interest (Nowak et al. 2018). Works devoted to urban heat islands are also related to the assessment of urban infrastructure from the point of view of microclimate regulation by UGS (Kirschner et al. 2023; Murtinová et al. 2024; Pan et al. 2023).

Our study contributes to assessments related to the legal regime of the public green areas used in cities. The misuse placement of objects in public green areas that do not comply with legally established regulations and requirements forcibly reduces urban "green zones". The issue of their preservation, as noted by Klimanova, "is a hot topic among decision-makers and citizens in the largest cities" (Klimanova et al. 2021). It is extremely important that "gray" spaces, which include "anthropogenic, sealed, non-permeable, paved surfaces made of asphalt, concrete, and other durable materials", did not suppress "green" and "blue" spaces in the urbanization processes (Noszczyk 2023).

Unfortunately, there are very few scientific works devoted to the assessment of misuse of public green spaces in cities. These studies are often associated with socio-legal research. A particular example is "green" criminology, which raises issues of environmental damage due to criminal actions of citizens, companies, authorities and their representatives. The "green crime" reason is the desire to achieve economic gain, as well as the undeveloped environmental consciousness of citizens (Ignjatović 2023).

According to Russian legal practice the following violations as typical of the green infrastructure use regime: illegal formation and disposal of land plots; illegal construction; illegal extraction of natural resources. Often, these violations are recorded in the field of use and protection of specially protected natural areas (Berdinskikh 2021). Environmental prosecutors identify more than 3,000 violations in protected areas' territories every year. Government and administrative bodies, as well as citizens and legal entities, violate the law. (Solovyeva et al. 2020). For example, at present (2024), the Russian Investigative Committee is conducting a procedural check regarding the illegal construction of a large sports facility on the territory of the landscape park "Krylatskie Hills" (part of the regional specially protected natural area "Natural and Historical Park "Moskvoretsky", Moscow)[2]. In 2017, a criminal case was opened in St. Petersburg regarding illegal construction on the territory of the Gladyshevsky nature reserve[3]. Unauthorized construction of a cottage village was discovered on the territory of the state natural landscape reserve "Baidarsky" (Rezervnoye village, Sevastopol)[4]. Unfortunately, there are many similar examples throughout Russia. Moreover, such actions lead to both the degradation of the ecosystem and the inability of the green infrastructure to perform ecosystem functions. In particular, illegal actions lead to limited physical access to those green areas that are public by status and, accordingly, have open access. PGS may also be inaccessible due to erroneous decisions made by officials, as well as insufficient social support for the preservation of green spaces (Biernacka and Kronenberg 2019).

To suppress violations related to the organization of unauthorized parking in green areas, control and supervisory measures are carried out in Russia (as part of municipal control in the field of improvement in accordance with the Federal Law of July 31, 2020 No 248-FZ "On State Control (Supervision) and Municipal Control in Russian federation"). These events, which take the form of raids and on-site inspections, involve the examination of the planned territory. The choice of the survey area may be planned or justified by residents' complaints. However, the residents do not always have an active civil legal position, so control and supervisory measures may not be comprehensive and may not reflect the full scale of the problem. Accordingly, it is necessary to introduce additional technologies that allow automatic or semi-automatic assessment of the urban area and then carry out a control and surveillance raid. Spiridonov notes that promising ways to improve control and supervisory activities are the introduction of remote control technologies using services that allow "to use modern digitalization achievements to increase the efficiency and convenience of practical control (supervision)" (Spiridonov 2023). For complex spatiotemporal analysis, it is necessary to use modern geographic information systems, among which QGIS is currently the leader (Stessens et al. 2017; Tempa et al. 2024: Baltyzhakova and Romanchikov 2021).

Summarizing the scientific review, a system of assessment of urban green infrastructure is proposed. It is based on the global concept of sustainable development (Gagarina 2023; Pashkevich and Danilov 2023) (Fig. 1). It is obvious that legal justice, which involves assessment of urban green infrastructure based on its (legal) illegal use, as well as social provision, environmental stability, and economic efficiency, should become a mandatory element of the sustainable development concept of urban areas. In this regard, the goal of this study was formulated: to develop a methodology for assessing urban green infrastructure in order to identify green areas that are not being used for their legal purpose.

MATERIALS AND METHODS

St. Petersburg green fund

St. Petersburg is a million-plus city of federal significance, the second most populous city in Russia, and the largest cultural, economic, scientific, and transport center. It is located (Fig. 2) in the north-west of the Russian Federation (59º57′ N, 30º19′ E), its area is more than 1.4 thousand km2; the population is 5.5 million people. St. Petersburg's administrative-territorial division is made up of 18 administrative districts.

The city's green fund includes a system of green areas that perform various functions:

1. Public green space territories are green areas used for recreational purposes by an unlimited number of people. They are divided into three categories: citywide significance, local significance, and landscaping reserve. The main difference between these groups is which department they belong to: activities of the first and third

[2] *Borisova V. and Bondarev D. (2024) Development of the Krylatskie Hills Park in the Krylatskoye District: Residents came to a meeting with State Duma Deputy Dmitry Kuznetsov over the improvement of the Krylatskie Hills. Available at: https://msk1.ru/text/gorod/2024/08/20/73983644/?ysclid=m02rr75b5398485376.*

[3] *An attempt to build in the Gladyshevsky nature reserve resulted in a criminal case. (2017). Available at: https://www.fontanka.ru/2017/03/13/102/?ysclid=m02sfg84vh566552018.*

[4] *Khruleva I. (2023) An illegal cottage village was found in the reserve «Baidarsky». Available at: https://sevastopol.press/2023/11/30/v-zakaznike-bajdarskij-nashli-nezakonnyj-kottedzhnyj-poselok/?ysclid=m02t34vplh184460060.*

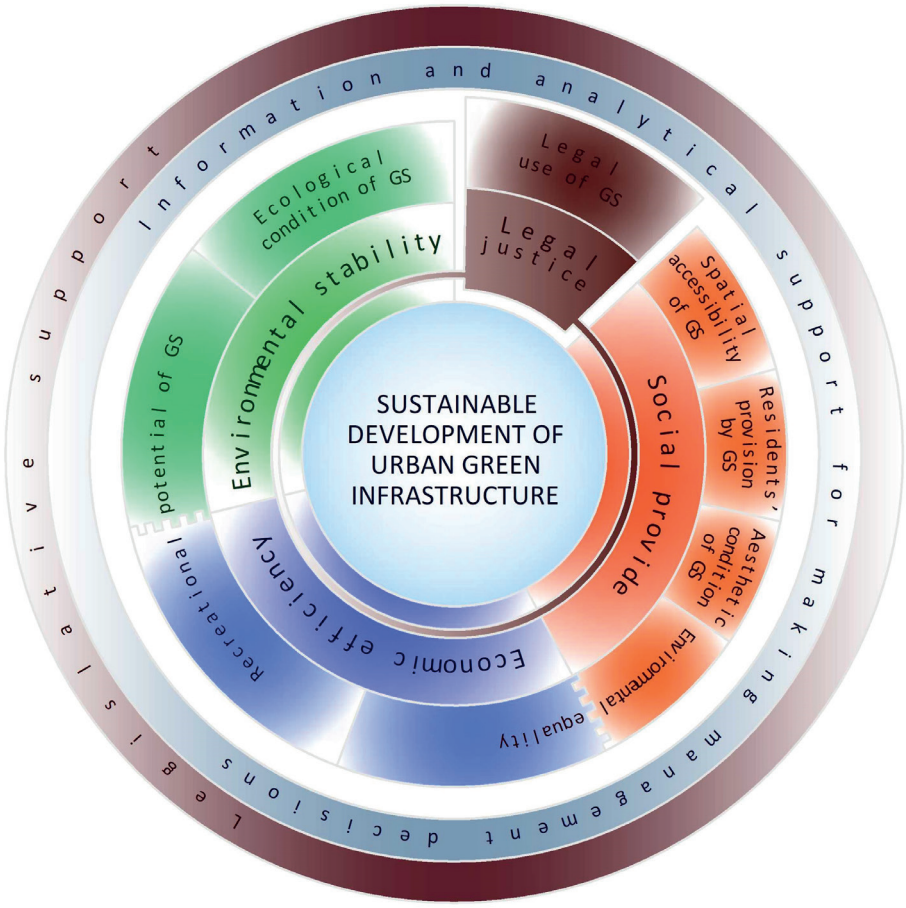

Fig. 1. System of urban green infrastructure assessment as part of the sustainable development concept of urban areas (compiled by the author): GS – green spaces

Fig. 2. Location of Saint Petersburg (compiled by the author)

categories are provided by the St. Petersburg authorized executive body of state power; green territories with local significance are managed by the local authorities of intra-city municipalities of the city; landscaping reserves are undeveloped areas potentially intended for landscaping.

2. Special-purpose green areas are intended for landscaping areas with special use conditions and perform the function of protective landscaping.

3. Green territories with limited use - these land plots are owned by St. Petersburg, and access to green spaces on them may be restricted by the copyright holder.

4. Protected forest areas include urban forests and forest park areas within the city boundaries.

5. Specially protected natural areas (SPNA) within the borders of St. Petersburg.

The author's research is devoted to the analysis and assessment of the first group of territories, which are further designated as territory of PGS or PGS.

As of 01/05/2024, the St. Petersburg PGS has an area of 8,383.4 ha, including citywide significance PGS - 6,078.0 ha, local significance PGS - 1,843.4 ha, landscaping reserve PGS - 462.0 ha (St.-Petersburg Law dated 10/08/2007 No. 430-85 "On public green spaces"). The distribution of PGS by the city administrative districts is presented in Fig. 3, 4.

PGS are represented by parks, gardens, squares, boulevards, alleys and forest parks (Table 1).

In the PGS system, public gardens predominate in number, and their area often does not exceed 1 ha. This indicates the fragmentation of the city's green fund - a negative anthropogenic process associated with the

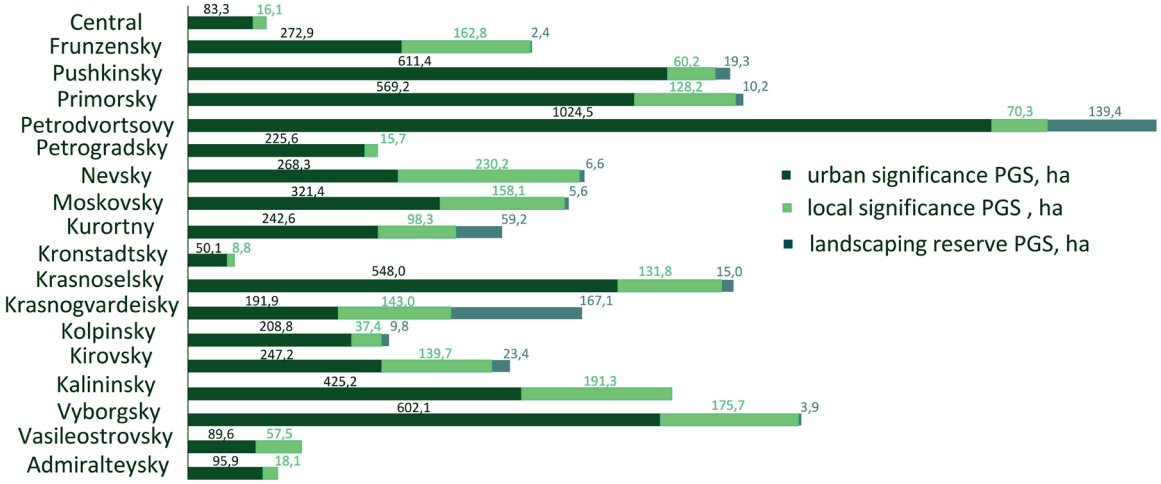

Fig. 3. PGS area of St. Petersburg administrative districts (ha) as of 02/01/2024 (compiled by the author)

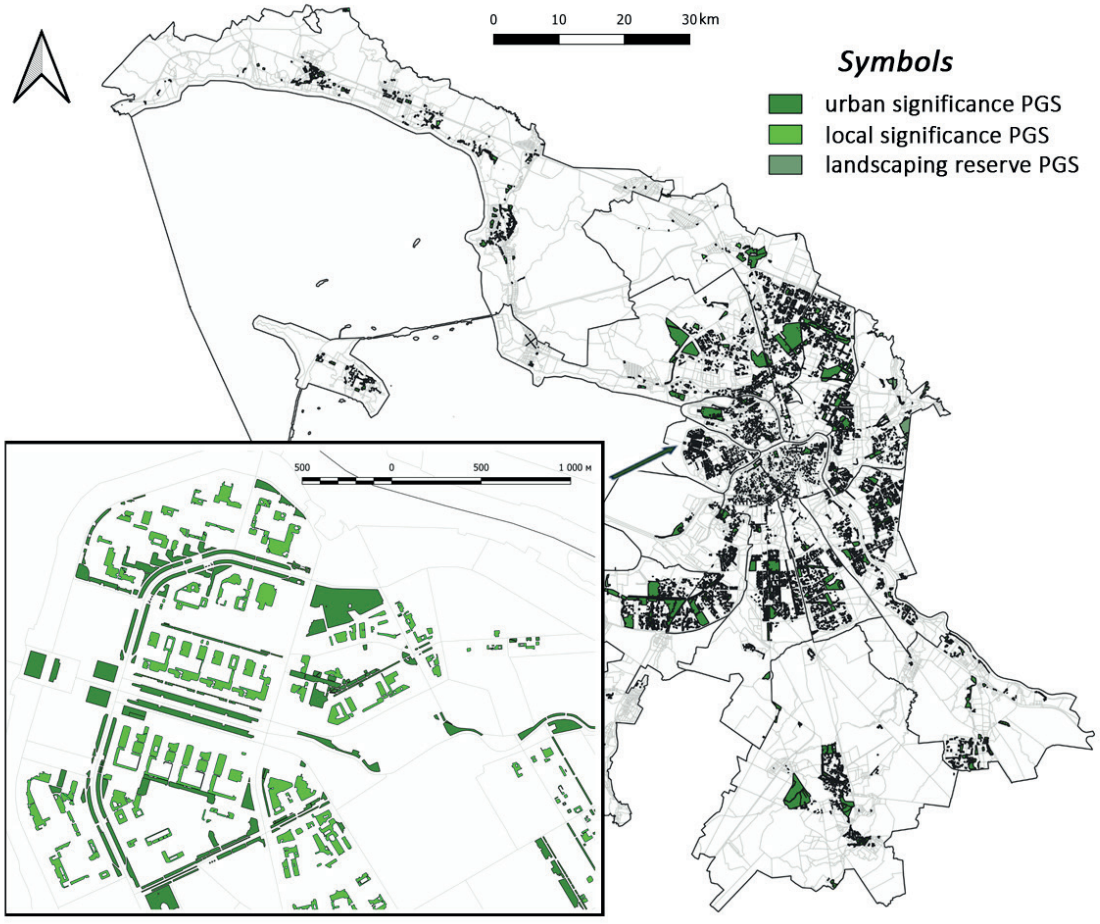

Fig. 4. PGS system of St. Petersburg: citywide significance, local significance, and landscaping reserve (compiled by the author)

Table 1. Distribution of St. Petersburg PGS by landscaping objects (compiled by the author)

PGS category	Parks	Gardens	Squares	Boulevards	Alleys	Forest parks	SUM
	in the numerator – area, ha; in the denominator – quantity, units						
citywide significance	3671.7 / 95	485.1 / 138	1400.7 / 1688	344.8 / 134	1.9 / 1	173.8 / 1	6078.0 / 2057
local significance	6.6 / 2	0.5 / 1	1824.3 / 5604	10.0 / 11	2.0 / 2	0 / 0	1843.4 / 5620
landscaping reserve	124.3 / 7	0 / 0	243.6 / 79	3.5 / 3	0 / 0	90.5 / 1	462.0 / 90
TOTAL	3802.6 / 104	485.6 / 139	3468.5 / 7371	358.3 / 148	3.9 / 3	264.3 / 2	8383.4 / 7767

destruction of continuous habitat. Reducing the average area of green areas increases their permeability and sensitivity to degradation and also increases environmental pressure on these spaces (Nasehi and Namin 2020; Nazombe and Nambazo 2023).

Creation of a geospatial database of St. Petersburg PGS using QGIS

The creation of a geospatial database, as the best way to systematize and visualize semantic and spatial data (Kolesnik et al. 2022), was carried out in the free cross-platform geographic information system Quantum GIS 3.34.0. The project coordinate system was adopted as WGS 84.

For the purposes of the study, a Sentinel-2 multispectral image (the European Space Agency (ESA)) was used. Image resolution is 10 m, and image coverage is the territory of St. Petersburg as of June 15, 2023 (image ID: S2B_MSIL2A_20230615T092559_N0509_R136_T35VPG_20230615T120159). Cloud cover was less than 3%. Such images are widely used to assess vegetation by researchers around the world (Wu et al. 2023; Giuliani et al. 2021). The image was processed at level 2A; accordingly, radiometric, geometric, and atmospheric corrections were performed for it. The summer survey season is justified by the active growing season of plants, which is necessary to determine the normalized difference vegetation index (NDVI). The earliest reference to the use of NDVI is given in the study by Rouse et al. (Rouse et al. 1974).

At the first stage, two raster layers B04 and B08 were loaded into the GIS project, corresponding to the red (Red) and infrared (NIR) spectral channels.

The QGIS raster calculator (Toolbar - Data Analysis - Raster Analysis - Raster Calculator) allowed us to calculate the NDVI (Eq.(1)), which is based on the unique spectral response of anthropogenic objects, vegetation, and water bodies (Kumar et al. 2023; Jin et al. 2024):

$$NDVI = \left(\frac{\rho_{NIR} - \rho_{RED}}{\rho_{NIR} + \rho_{RED}} \right) \quad (1)$$

where:

ρ_{NIR} – reflection in the near-infrared region of the spectrum (spectral channel B08); ρ_{RED} – reflection in the red (visible) region of the spectrum (spectral channel B04).

The second stage involved using QGIS to download data from the Regional Geographic Information System of St. Petersburg[5]. A new connection to the RGIS server was created by adding the WFS layer, which made it possible to add to the GIS project a layer of PGS boundaries in St. Petersburg, as well as layers of cadastral districts and blocks in vector form. The attribute information of the PGS layer encompasses the administrative district where the PGS is situated, its legal PGS number, its name and location, its area, and the number of the scheme that approved the PGS boundaries. The listed data is publicly available, and if it is not possible to use the RGIS St. Petersburg server, you can use the cartographic application of the St. Petersburg Law "On Green Spaces for Public Use" and manual digitization methods.

In the third stage, a grid of 10×10 m squares was created over the entire city territory using a separate vector layer ("pixel-by-pixel" grid). In the process of spatial analysis and assessment of territories, a similar approach is common (Raguzin et al. 2023; Kovyazin et al. 2021: Kopylova et al. 2023). The grid square was the same size as the pixels in the multispectral image channels that had already been loaded, and the edges of the grid square lined up with the edges of the pixels in the red and NIR raster images. Subsequently, such an overlay of vector and raster layers made it possible to perform a "pixel-by-pixel" analysis, transferring the data obtained from a raster multispectral image to the vector square of the grid.

To reduce the vector mesh layer's data volume (the file size was initially more than 25 GB), it was trimmed to the PGS layer. The QGIS Zonal Statistics tool allowed us to create an additional vector layer that included NDVI values for each grid square within the PGS boundaries only.

Classification of objects within the PGS territory

In addition to vegetation (trees, shrubs, flower beds, lawns), buildings, structures, artificial surfaces for various purposes, as well as water bodies, can be located on the PGS territory (Bolkaner and Asilsoy 2023).

For forests, the issue of classifying forest vegetation according to the NDVI values has been widely studied (Tempa et al. 2024; Kovyazin et al. 2023). In particular, in the absence of forest vegetation, NDVI values are in the range of 0-0.2, for low vegetation - 0.2-0.4, for high vegetation - 0.4-0.6, for closed and very dense vegetation the values NDVI are 0.6-1.0 (Kovyazin et al. 2021). The index values are also known for various types of tree and shrub vegetation. For example, a deciduous forest is characterized by an average NDVI value of 0.83, and shrubby vegetation – 0.68 (Priya et al. 2023).

For urban conditions, the NDVI values of green spaces may differ due to the aggressive anthropogenic load on the natural environment. Also, green areas of cities are not always represented by a closed tree stand. Rather, on the contrary, in gardens, squares, and boulevards, a sparse tree

[5] *https://rgis.spb.ru/*

stand predominates with the presence of parterres, garden and meadow lawns, shrubs, artificial objects, and surfaces.

To test this hypothesis, a comparison method ("pixel-by-pixel" analysis) was used. A Yandex Satellite base layer was added to the GIS project using the QuickMapServices plugin. This layer was superimposed on a grid of squares within the PGS boundaries, created at stage 2.2. The NDVI values of the "single-digit" squares were visually compared with the RGB image of the same area of the Yandex Satellite image. "Single-digit" squares were defined as those squares that contained only one type of vegetation, cover, or object within their boundaries. The set of analyzed squares met the condition of representativeness.

Classification of vegetation, coverings or objects located in the PGS territory, using NDVI value, was performed using the "Boxplot" method in the Python programming environment. The program code is available[6].

Identification of PGS areas that potentially conflict with their standard functions

Based on the NDVI interval corresponding to areas without vegetation (step 2.3), we identified squares of the "pixel-by-pixel" grid that could potentially be used for incorrect purposes (in the QGIS project they were highlighted in red, which made it possible to visualize the result). A SQL query was used to trim the data.

Subsequent analysis of "suspicious" squares was carried out using a visual comparison of the corresponding Yandex Satellite area with legal types of economic activity within the PGS territory. Field surveys were also done, which made it possible to clarify the results of remote sensing methods.

Technology of assessing urban green infrastructure to identify misuse green areas

Fig. 5 presents a schematic representation of the technology for assessing urban green infrastructure to identify misused green areas.

RESULTS

Calculation of the NDVI

After loading two raster layers (B04 and B08) of a multispectral image of St. Petersburg territory into the GIS project, using the QGIS "Raster Calculator" function a raster image (separate layer) was obtained containing NDVI values for each pixel of the study area. The vegetation index calculation's graphical result was displayed in panchromatic color. To obtain a color image, in the properties of the raster layer, the image rendering was changed to "Single-channel pseudo-color" and a color map (palette) was added (Fig. 6). The palette can be created manually or loaded from an already created .txt file. The resulting images and palette file are available[7].

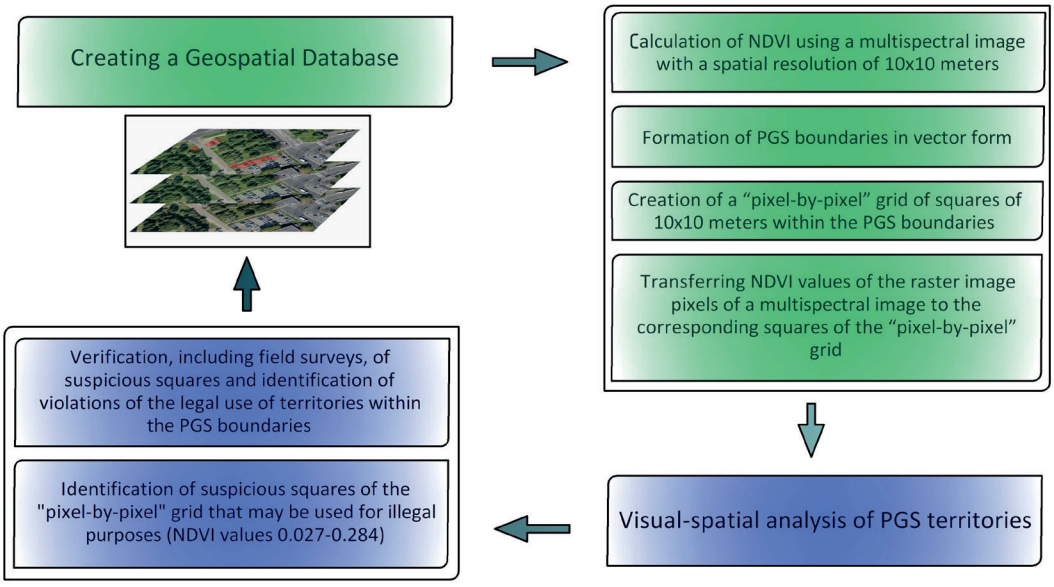

Fig. 5. Technology of assessing urban green infrastructure to identify misused green areas (compiled by the author)

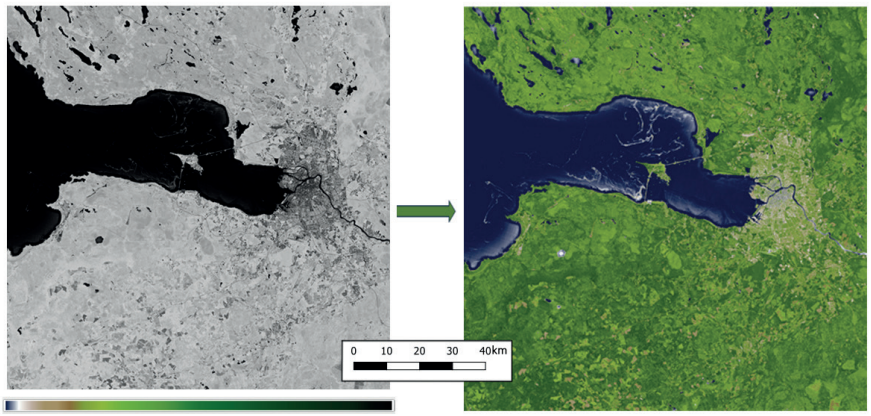

Fig. 6. Calculation and visualization of NDVI as of June 15, 2023 (compiled by the author)

[6] *https://drive.google.com/drive/folders/1RUKMATPKbchYFyWESVPNkZyzBhndu93X?hl=ru*
[7] *https://drive.google.com/drive/folders/1KkXxfYQoEVkS4p_8iHSq-uq_AENFcfb3?hl=ru*

Uploading RGIS data

The result of downloading data from the RGIS of St. Petersburg was five vector layers: citywide significance PGS; local significance PGS; landscaping reserve PGS; boundaries of cadastral areas; boundaries of cadastral blocks. The boundaries of cadastral districts and blocks correspond to the cadastral division of the Russian Federation territory.

Creating a grid of squares ("pixel-by-pixel" grid) and determining NDVI values for squares within the PGS boundaries

A grid of 10×10 m squares was created using a separate vector layer (Vector – Analysis – Create Grid). Next, it was trimmed along the boundaries of the layer containing the St. Petersburg PGS (Vector – Geoprocessing – Crop). Using zonal statistics (Analysis Tools - Raster Analysis - Zonal Statistics), an NDVI value was calculated at stage 3.1, for each square within the PGS boundaries (Fig. 7).

Comparison of NDVI values and Yandex Satellite images within the boundaries of the PGS square ("pixel-by-pixel" analysis)

The obtained NDVI values of PGS squares within the borders of St. Petersburg range from -0.0809 to 0.7166. For further "pixel-by-pixel" analysis citywide significance PGS located in different areas of the city were selected (Fig. 8). The condition of mandatory analysis of squares with minimum and maximum NDVI values was also taken into account.

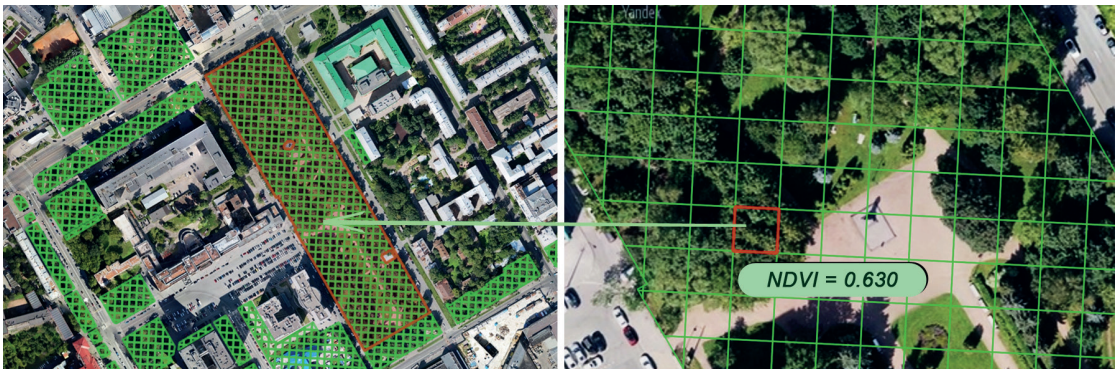

Fig. 7. Garden «Vasileostrovets» - citywide significance PGS No. 2005 (compiled by the author)

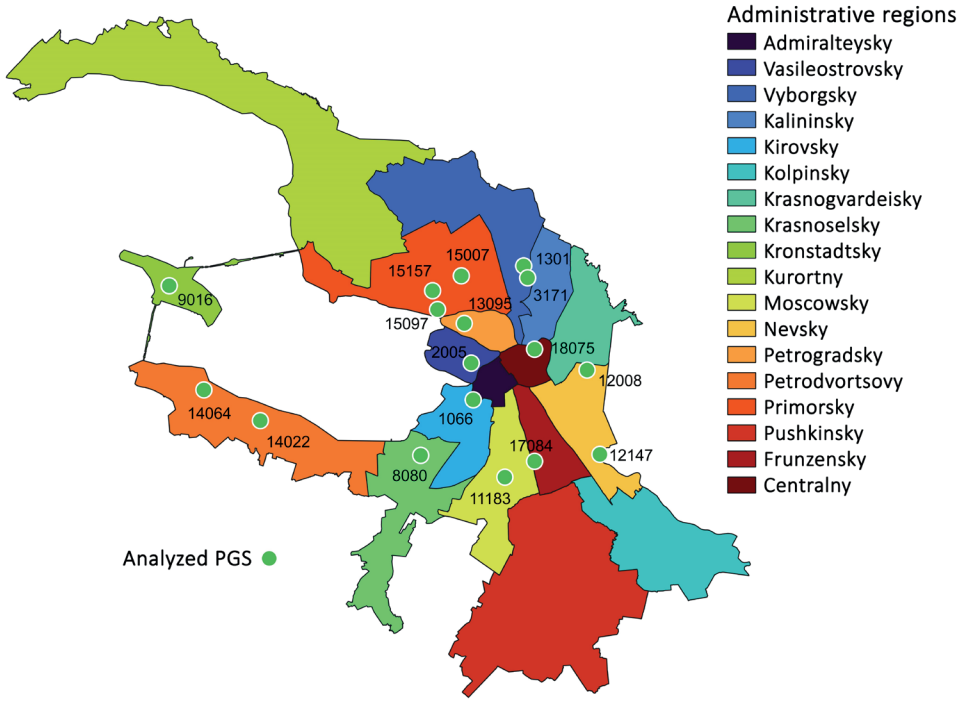

Fig. 8. Location of the PGS for comparing NDVI values and the Yandex Satellite image within the boundaries of the PGS squares. Map key: No 1066 – Ekateringof Park on Ekateringof Island; No 11183 - square w/num., Pulkovskoye Highway near house 15, bldg. 2; 12008 - Yablonovsky garden between the Okkervil Riv., Voroshilov Str. and Latvian Riflemen Str.; No 12147 - Spartak Garden between Obukhovskaya Oborony Ave., Rybatsky Ave. and the Neva Riv.; No 13095 - Primorsky Victory Park between Grebny Canal, Ryukhin St. and the Malaya Nevka R.; No 14022 - English Park between St. Petersburg Ave., Red Cadets Blvd. and Blan-Menilskaya Str.; No 14064 – square w/num. between Dvortsov Prospect and Aleksandrovskaya Str.; No 15007 – boulevard w/num. on Dolgoozernaya Str. from Planernaya Str. to Korolev Ave.; No 15097 - Park named after the 300th anniversary of St. Petersburg between the Gulf of Finland and Primorsky Prospect; No 15157 – square w/num. on Shuvalovsky Prospect from Furniture Str. to Bogatyrsky Ave.; No 17087 - Rescuers Square northeast of the intersection of Bukharestskaya Str. and Fuchik Str.; No 18075 - Tavrichesky Garden between Kirochnaya Str., Tavricheskaya Str., Shpalernaya Str. and Potemkinskaya Str.; No 2005 - Vasileostrovets garden between Sredny Ave. V.I., 25th Line V.I., Bolshoy Ave. V.I. and Club Lane.; No 3001 - Sosnovka Park between Northern Ave., Tikhoretsky Ave., Svetlanovsky Ave., Torez Ave. and Vitkovsky Str.; No 3171 – park w/num. near Olginsky pond; No 8080 - South Primorsky Park on Peterhofskoye Highway, bounded by the Valor Str. And Marshal Zakharov Str.; No 9016 – square w/num. at the intersection of Citadel highway and Hydrobuilders Str. (compiled by the author).

In total, more than 7.5 thousand "single-digit" squares were analyzed (Fig. 9), within the boundaries of which NDVI values and a visual image of the corresponding section of the PGS according to Yandex Satellite were compared.

The classification of vegetation, surfaces, and other objects in the PGS was carried out using the boxplot method, which made it possible to determine the NDVI ranges for three types of vegetation, buildings, artificial road surfaces, sports grounds, beaches, and water surfaces, as well as to cut off outliers (Fig. 10).

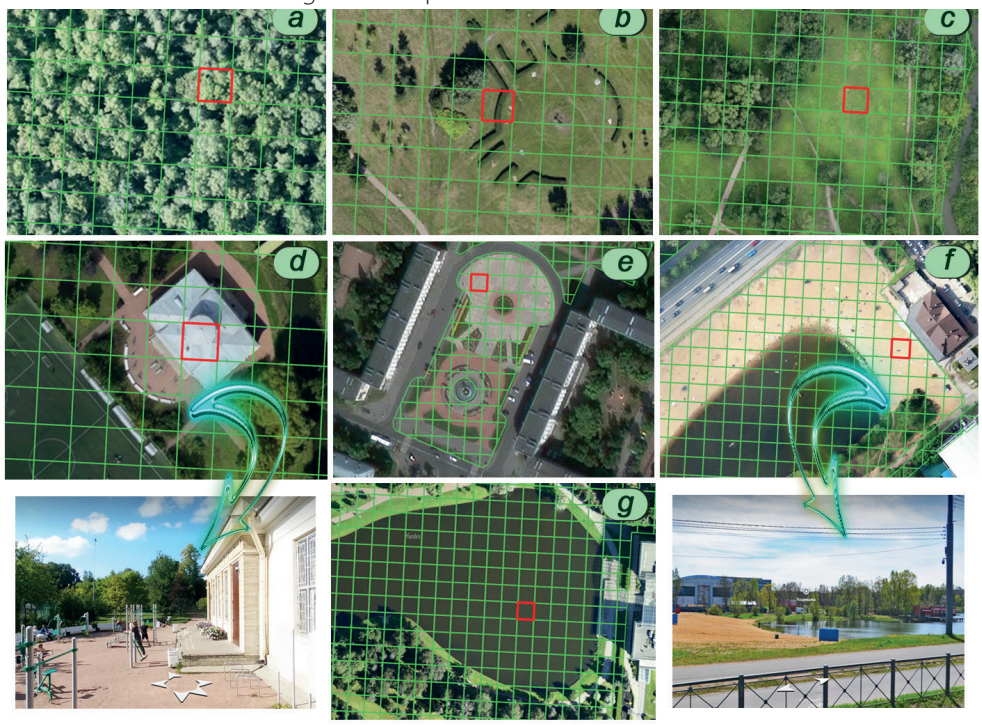

Fig. 9. Types of vegetation, coverings and other objects in the territory of the PGS. Map key: (a) Trees; NDVI = 0.513; No 3001 - Sosnovka Park between Northern Ave., Tikhoretsky Ave., Svetlanovsky Ave., Torez Ave. and Vitkovsky Str.; (b) Shrub vegetation; NDVI = 0.445; No 17087 - Rescuers Square northeast of the intersection of Bukharestskaya Str. and Fuchik Str.; (c) Herbaceous vegetation (lawn); NDVI = 0.524; No 12147 - Spartak Garden between Obukhovskaya Oborony Ave., Rybatsky Ave. and the Neva Riv.; (d) Buildings; NDVI=0.053; No 18075 - Tavrichesky Garden between Kirochnaya Str., Tavricheskaya Str., Shpalernaya Str. and Potemkinskaya Str.; (e) Artificial surfaces; NDVI=0.038; No 14064 – square w/num. between Dvortsov Prospect and Aleksandrovskaya Str.; (f) Beaches; NDVI = 0.083; No 3171 – park w/num. near Olginsky pond; (g) Water (incl. blooming water and water with algae); NDVI = 0.004; No 13095 - Primorsky Victory Park between Grebny Canal, Ryukhin St. and the Malaya Nevka R. (compiled by the author, including using Yandex Maps images).

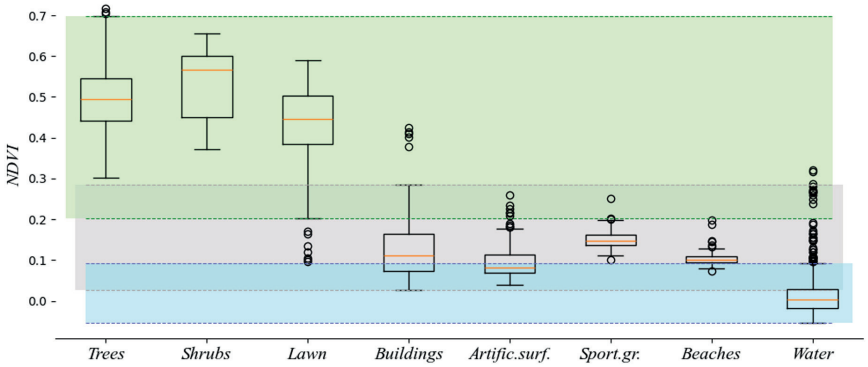

Boxplot parameters	Trees	Shrubs	Lawn	Buildings	Artific.surf.	Sport.gr.	Beaches	Water
Quantity	6402	78	224	93	158	102	78	372
Average	0,497	0,534	0,433	0,131	0,097	0,151	0,105	0,021
Max value	0,717	0,656	0,591	0,425	0,259	0,251	0,198	0,322
Min value	0,302	0,373	0,097	0,027	0,038	0,100	0,074	-0,053
Upper mustache	0,698	0,656	0,591	0,284	0,177	0,200	0,129	0,092
Lower mustache	0,302	0,373	0,203	0,027	0,038	0,100	0,078	-0,053

Fig. 10. Boxplot method for classifying vegetation, coverings and other objects on the territory of the PGS (compiled by the author)

As a result, three consolidated categories of objects located within the territories of the PGS were identified (Table 2).

The research by Klimanova (2021), which determines NDVI intervals for a surface without vegetation (0.18-0.30) and a surface with vegetation (more than 0.30), demonstrates the comparability of the results in Table 3.

During the "pixel-by-pixel" analysis, several patterns were also identified:

1. NDVI of water bodies decreases with increasing depth;
2. on the shallows, the vegetation index takes on a positive near-zero value;
3. for blooming water or water with a lot of algae, NDVI reaches values of 0.3. It is obvious that the index responds to an increase in chlorophyll in aquatic vegetation. The boxplot method allows you to cut off such inflated values, highlighting them as outliers.

Identification of violations within the boundaries of the St. Petersburg PGS

According to the St. Petersburg legal zoning, PGS are located in various territorial zones: recreational (TR0-2, TR2, TR3-2, TR4, TR5-2), residential (T1ZH2-2, T2ZH1, T3ZH1, T3ZH2, T3ZhD3), public-business (TD1-1_1, TD1-1_2, TD2_1, TD1-2_2), multifunctional (T3ZhD3), external transport facilities (TI4_1), road network (TU), agricultural use (TR2/TS1). For PGS with citywide importance, the most common zones are TP2 (preservation and arrangement of open green spaces during their active use) and TP4 (preservation and arrangement of recreational territories of palace and park complexes and other historically valuable city-forming objects and spaces), for PGSwith local significance, different types of residential areas.

Also, according to the Law of St. Petersburg "On Administrative Offenses in St. Petersburg", the placement of vehicles in PGS, green spaces performing special functions, restricted green spaces, lawns is prohibited and entails administrative liability.

Taking into account the consolidated categories of objects located within the territories of the PGS (Table 2), an SQL query was executed. Its result was the "gray" zones within the PGS territories, where the vegetation index NDVI lies in the range of 0.027-0.284, which corresponds to artificial objects (Fig. 11).

The resulting "gray" zones are represented by different categories of objects and surfaces:

1. areas without vegetation (trampled or with artificial coverings);
2. areas occupied by parking, cluttered areas;
3. areas occupied by temporary facilities (underground metro facilities under construction that require temporary operation of green areas (Volokhov and Mukminova 2021));
4. water bodies;
5. areas occupied by structures and objects that do not conflict with the recreational function of the PGS.

Of the entire set of citywide significance PGS, the identified PGS with the presence of "gray" zones account for more than 50% (more than 1000 PGS). And at this stage, the task arises of differentiating "gray" zones according to compliance (not compliance) with the functions of PGS.

Identifying "gray" areas, which include cluttered areas or areas occupied by unauthorized parking or buildings, can be done in several ways:

- non-automated analysis of PGS by comparing the location of "gray" zones with Yandex Satellite (or other image of the territory with sufficient resolution), as well as with field survey data, if necessary;
- application of neural networks, including convolutional (Shestakov et al. 2023) for automatic classification.

In this study, the first method was used. The implementation of the second method is a promising direction for future research.

During the analysis, citywide significance PGS were identified, economic activities on the territory of which

Table 2. NDVI intervals for consolidated categories of objects located within the territories of the PGS (compiled by the author)

Consolidated categories	Minimum NDVI value	Maximum NDVI value
Landscaping	0.203	0.698
Artificial objects	0.027	0.284
Water	-0.053	0.092

Fig. 11. SQL query result: red squares have NDVI values in the range 0.027-0.284 (compiled by the author)

completely or partially do not comply with urban planning regulations and regional legislation (Fig. 12, 13). Within the boundaries of the identified PGS, there are buildings with an obvious non-recreational function, such as spontaneous parking, litter, sand dumps, and so on.

The list of PGS with identified inconsistencies with their intended purpose, including photographic documentation, is available[8].

Thus, the problems identified during the "pixel-by-pixel" comparative analysis boil down to the following aspects:

- unauthorized placement within the PGS boundaries of objects of production, storage, trade, transport or other non-recreational purposes, implementation of related economic activities that do not comply with urban planning regulations;
- spontaneous parking prohibited by regional legislation;
- discrepancy between the purpose of PGS and legal zoning, which provokes a contradiction between the Law of St. Petersburg "On Rules of Land Use and Development of St. Petersburg" and the Law of St. Petersburg "On Administrative Offenses in St. Petersburg".

DISCUSSION

The total official area of St. Petersburg PGS is 8383.4 ha, and the permanent population of St. Petersburg is more than 5.5 million people (as of 01/01/2024). Taking these indicators into account, the average PGS provision of city residents is about 15 m^2/person, while the established norm is 10 m^2/person. (Urban Development. Urban and Rural Planning and Development. Code of Practice 42.13330.2016; Ministry of Construction and Housing and Communal Services of the Russian Federation: Moscow, Russia, 2016. (In Russian)). PGS occupy 6% of the city's total area.

In 2024, the area of citywide significance PGS of St. Petersburg increased by more than 75 ha (1.2%) due to the assignment of PGS status to a number of green areas, as well as the clarification of their boundaries. Obviously, this method of increasing greenery is of a formal nature and does not actually increase the number and area of green spaces. PGS status should be a mechanism for protecting green areas from illegal use, but in practice this mechanism does not work satisfactorily.

In addition to PGS status, green areas must have clearly defined boundaries, information about which must be entered into the Real Estate Cadastre in accordance with the state cadastral registration procedure. Currently, only a small part of PGS is registered. At the same time, during the author's research, discrepancies in the area of individual PGS according to the real estate cadastre data and according to the RGIS data (according to the Law of St. Petersburg dated October 8, 2007 No. 430-85 "On public

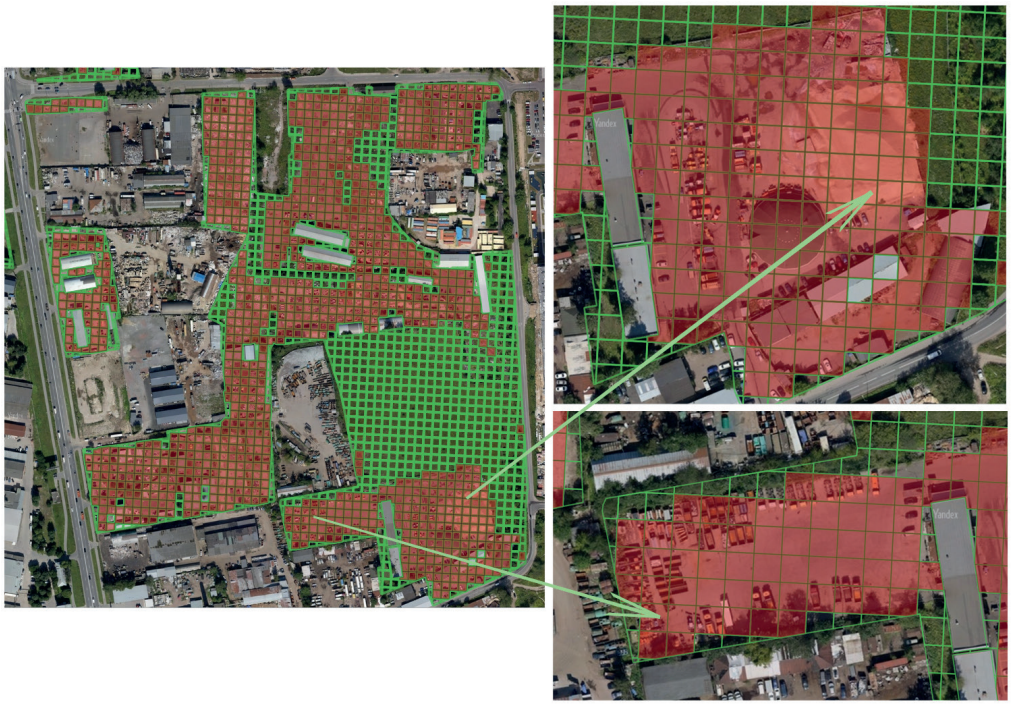

Fig. 12. No. 11243 – The square is northeast of the intersection of M. Mitrofanievskaya Str. and Mitrofanyevskoe Highway (compiled by the author)

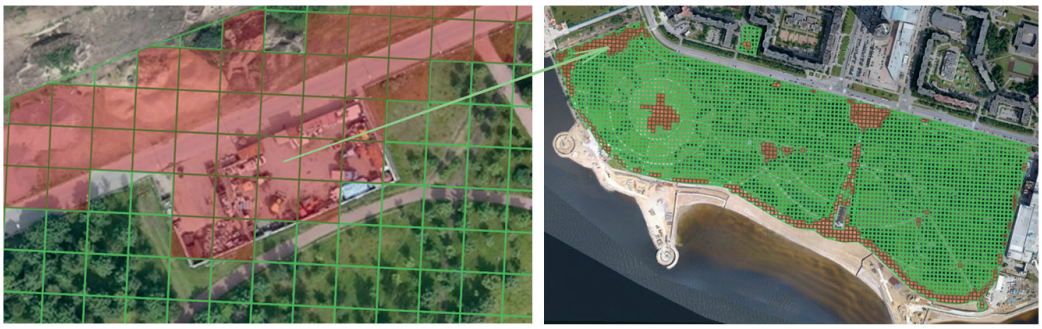

Fig. 13. No. 15097 – Park named after the 300th anniversary of St. Petersburg between the Gulf of Finland and Primorsky Prospect (compiled by the author)

[8] *https://docs.google.com/spreadsheets/d/1JGcYRlafaNKDQlbEtu3WdJ_zT2QrSwrldHDjgg5qxOk/edit#gid=0*

green spaces use") were identified. For specific examples, we can cite citywide significance PGS No. 1028 (a public garden at the intersection of 7th Krasnoarmeyskaya Str. and Egorov Str.) and No. 5090 (Leningradsky Square on Stachek Avenue at 114a; Fig. 14). Such inconsistencies indicate unregulated interdepartmental interaction between the Rights Registration Authority (Rosreestr) and the Property Relations Committee of St. Petersburg.

The solution to these problems should be a concept adopted at the state level that defines the principles, methodological foundations, and methods of accounting, assessment, and monitoring of urban green infrastructure (Slovic et al. 2023), and its result will be a mechanism of information and analytical support for making management decisions.

The authors Klimanova et al. rightly note that forms of green areas transformation can be changes when woody or non-woody vegetation is replaced by built-up or other "non-green" areas (Klimanova et al. 2021). To quickly respond to such actions with minimal labor and financial costs, remote methods are optimal. Many researchers use multispectral Landsat imagery with a spatial resolution of 30×30 m. But such spatial resolution provokes inaccurate results (Klimanova et al. 2021). This work uses Sentinel-2 images with a spatial resolution of 10×10 m, which increases the reliability of the results. It is also worth noting that an alternative to high-resolution satellite images can be the results of shooting from unmanned aerial vehicles, which allow increasing the resolution to tens of centimeters. However, in relation to the largest city territories, this option requires additional financial investments, time, and labor resources.

Moving on to the discussion of the misuse problem of territories within the PGS boundaries, it is worth noting that violations are associated with several reasons:

- firstly, the lack of landscaping, including fencing or side stones along the PGS border, provokes collisions of vehicles with "green" areas (No. 17157);
- secondly, the implementation of necessary temporary construction work, in connection with the creation of socially significant infrastructure, reduces the total area of the PGS for the construction period, which can last more than one year (No. 2015, No. 2019);
- thirdly, the initially incorrect establishment of the PGS boundaries leads to the erroneous inclusion of residential buildings and adjacent courtyard areas (No. 13174), non-residential objects (No. 5150), as well as organized parking spaces in landscaping areas (No. 17010, No. 5090, No. 5211);
- fourthly, the lack of an effective and operational mechanism of monitoring the PGS legal use and the lack of systematic environmental education lead to systematic violations in the form of unauthorized parking (ZNOP No. 15062, No. 3134, No. 4179).

These reasons result in an actual decrease in the area of greenery, which is confirmed by the authors (Klimanova et al. 2021), noting the "loss of green infrastructure" in Russian cities of about 6%. At the same time, formal indicators of green space "on paper" are overestimated, and, accordingly, when the indicator of the population's provision of green space is calculated, the official results cannot be considered reliable. According to the author's calculations, for citywide significance PGS, the area of green areas with misuse was more than 20 ha (0.3% of the area of citywide significance PGS in St. Petersburg according to official statistics (Fig. 2)). Accordingly, there will be a similar decrease in the population's PGS provision for the city in general. Differentiation by city administrative districts may differ from the citywide result.

The study has some limitations, among which the following can be highlighted: the original cartographic material; technical means of data processing; restrictions related to seasonality of observations.

When using multispectral satellite images, resolution plays an important role. The author's study used publicly available Sentinel-2 images with a resolution of 10 m. Even higher resolution images (for example, from unmanned aerial vehicles) will improve the accuracy of the assessment results of green areas. But, in this case, the cost of such cartographic material for the entire city, taking into account the time dynamics, will be disproportionately high. Potential consumers of the proposed technology may not have the opportunity to purchase ultra-high-resolution images due to budgetary constraints. In our opinion, poor funding of urban landscaping is a deep problem of sustainable urban development, and to improve the life quality of citizens, it is necessary to increase investment in this area (Aram 2024).

Additionally, the spatial resolution of images directly determines the pixel size. As a result, the vegetation index's calculated value is assigned to a 10×10 m area. If the PGS area is less than 100 m^2, or the area is linear and less than 10 m wide, the NDVI is erroneously influenced by the objects and coverings surrounding the green area, thereby underestimating its value. Increased demands are placed on computer hardware because data spatial analysis of a vast metropolitan area requires increased RAM, a sufficiently powerful video card, as well as a capacious HDD for storing images, the size of which is usually about 1 GB. To determine vegetation indices, satellite images taken exclusively during the growing season of active plant growth are used (and season depends on the climatic characteristics of the region).

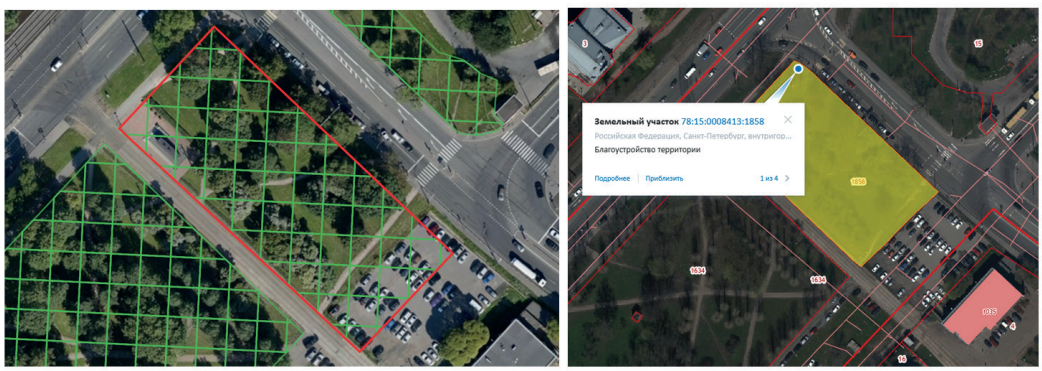

Fig. 14. Leningradsky Square on Stachek Ave. at 114a. Map key: on the left - the PGS boundaries according to the RGIS of St. Petersburg (area 3.9310 ha); on the right - the PGS boundaries according to the Real Estate Cadastre (3.7945 ha) (compiled by the author, including according to data[9])

[9] *https://pkk.rosreestr.ru/*

CONCLUSIONS

The study is scientifically unique because it confirms the ranges of NDVI values for different types of vegetation, coverings, and objects in the PGS. The NDVI values in the city and in the forest have a different upper threshold. For metropolitan conditions, the maximum value is 0.7, while forest plantations can have an index of up to 1.0. The poor ecology of urbanized areas and the sparseness of urban vegetation primarily explain this. Also, the concept of sustainable development of urban green infrastructure based on its assessment system has scientific significance.

The following results have practical significance: (1) technology of urban green infrastructure assessment to identify public green spaces with misuse; (2) geospatial database PGS of St. Petersburg, which includes vector layers: citywide significance PGS; local significance PGS; landscaping reserve PGS; "pixel-by-pixel" grid of squares, as well as layers with calculated NDVI values, including values indicating misuse of public green areas; (3) identified PGS areas with obvious violations of the use of green areas.

REFERENCES

Aram F. (2024). Resources of Urban Green Spaces and Sustainable Development. Resources, 13, 10. DOI: 10.3390/resources13010010.

Baltyzhakova T. and Romanchikov A. (2021). Spatial analysis of subway passenger traffic in Saint Petersburg. Geodesy and Cartography, 47(1), 10-20. DOI: 10.3846/gac.2021.11980.

Berdinskikh S. (2021). On Typical Violations of Legislation in the Field of Use and Protection of Specially Protected Natural Areas. Actual Problems of Russian Law, 16, 205-213. DOI: 10.17803/1994-1471.2021.126.5.205-213.

Bolkaner M.K. and Asilsoy B. (2023). Reinventing the Urban Neighborhood Green Index in the Context of Urban Ecology as a Conceptual Framework in NorthernNicosia, Cyprus. Sustainability, 15, 13880. DOI: 10.3390/su151813880.

Brindley P., W. Cameron R., Ersoy E., Jorgensen A., Maheswaran R. (2019). Is more always better? Exploring field survey and social media indicators of quality of urban green space, in relation to health. Urban For Urban Green, 39, 45-54. DOI: 10.1016/j.ufug.2019.01.015.

Browning M.H.E.M., Locke D.H., Konijnendijk C., Labib S.M., Rigolon A., Yeager R., Bardhan M., Berland A., Dadvand P., Helbich M., Li F., Li H., James P., Klompmaker J., Reuben A., Roman L.A., Tsai W.-L., Patwary M., O'Neil-Dunne J., Ossola A., Wang R., Yang B., Yi L., Zhang J., Nieuwenhuijsen M. (2024). Measuring the 3-30-300 rule to help cities meet nature access thresholds. Sci. Total Environ, 907, 167739. DOI: 10.1016/j.scitotenv.2023.167739.

Bykowa E., Banikevich T., Zalivatskaya N., Pirogova O. (2024). Modeling the Cadastral Value of Land Plots of Gardening and Horticultural Non-Profit Partnerships Taking into Account the Influence of Local Factors of the Territory. Land, 13(7), 1004. DOI: 10.3390/land13071004.

Cherepovitsyn A., Rutenko E., Solovyova V. (2021). Sustainable Development of Oil and Gas Resources: A System of Environmental, Socio-Economic, and Innovation Indicators. J. Mar. Sci. Eng, 9, 1307. DOI: 10.3390/jmse9111307.

Enssle F. and Kabisch N. (2020). Urban green spaces for the social interaction, health and well-being of older people - An integrated view of urban ecosystem services and socio-environmental justice. Environ Sci Policy, 109, 36-44. DOI: 10.1016/j.envsci.2020.04.008.

Gagarina E.S. (2023). Green infrastructure, and ecosystem services in sustainable urban development. AMIT, 1(62), 228-247. DOI: 10.24412/1998-4839-2023-1-228-247.

Giofandi E.A., Syahzaqi I., Sekarjati D., Putri A. M., Marta H., Sekarrini C. E. (2024). Assessment Of Remote Sensing Approach For Urban Ecological Quality Evaluation In Pekanbaru City, Riau Province Indonesia. Geography, Environment, Sustainability, 1(17), 28-35. DOI: 10.24057/2071-9388-2023-2640.

Giuliani G., Petri E., Interwies E., Vysna V., Guigoz Y., Ray N., Dickie I. (2021). Modelling Accessibility to Urban Green Areas Using Open Earth Observations Data: A Novel Approach to Support the Urban SDG in Four European Cities. Remote Sens, 13, 422. DOI: 10.3390/rs13030422.

Grunewald K., Richter B., Behnisch M. (2019). Multi-Indicator Approach for characterising urban green space provision at city and city-district level in Germany. Int. J. Environ. Res. Public Health, 16(13), 2300. DOI: 10.3390/ijerph16132300.

Ignjatović Đ. (2023). Green criminology and crime control. Crimen (Beograd), 14(1), 24-63. DOI: 10.5937/crimen2301024I.

Jang K.M., Kim J., Lee H.-Y., Cho H., Kim Y. (2020). Urban Green Accessibility Index: A Measure of Pedestrian-Centered Accessibility to Every Green Point in an Urban Area. ISPRS Int. J. Geo-Inf, 9, 586. DOI: 10.3390/ijgi9100586.

Jian M. and Yang J. (2024). Unveiling the adaptation strategies of woody plants in remnant forest patches to spatiotemporal urban expansion through leaf trait networks. Forest Ecosystems, 11, 100186. DOI: 10.1016/j.fecs.2024.100186.

Jin Y., Wang F., Zong Q., Jin K., Liu Ch., Qin P. (2024). Spatial patterns and driving forces of urban vegetation greenness in China: A case study comprising 289 cities. Geogr. Sustain, 5(3), 370-381. DOI: 10.1016/j.geosus.2024.03.001.

Kirschner V., Macků K., Moravec D., Maňas J. (2023). Measuring the relationships between various urban green spaces and local climate zones. Sci. Rep, 13, 9733. DOI: 10.1038/s41598-023-36850-6.

Klimanova O.A., Bukvareva E.N., Illarionova O.A., Kolbovsky E.Yu. (2022). Assessment of ecosystem services at the municipal level and its possible integration into territorial planning. Proceedings of the Russian Academy of Sciences. Geographical series, 86(4), 605-620. DOI: 10.31857/S2587556622040069.

Klimanova O., Illarionova O., Grunewald K., Bukvareva E. (2021). Green infrastructure, urbanization, and ecosystem services: The main challenges for Russia's largest cities. Land, 10(12), 1292. DOI: 10.3390/land10121292.

Kolesnik O.A., Demidova P.M., Sannikova A.P. (2022). Creation of a geospatial database of particularly valuable productive agricultural land taking into account geodetic data in order to provide land monitoring. Vestnik of the Siberian State University of Geosystems and Technologies (SSUGT), 6, 39-48. DOI: 10.33764/2411-1759-2022-27-6-39-48.

Kopylova N.S., Grigoriev K.V., Slobodkin S.M., Romanchikov A.Yu, Pavlov N.S. (2023). Working at the concept of an interactive atlas "The history of the engineering geodesy department development". Geodesy and Cartography, 84(5), 9-17. DOI: 10.22389/0016-7126-2023-995-5-9-17.

Kovyazin V.F., Kitcenko A.A., Shobairi S.O.R. (2021). Cadastral valuation of forest lands, taking into account the degree of development of their infrastructure. Journal of Mining Institute, 249, 449-462. DOI: 10.31897/PMI.2021.3.14.

Kovyazin V.F., Nguyen T.A., Nguyen T.T. (2023). Monitoring the forest fund lands of Kon Tum province, Vietnam using remote sensing data of Earth. Geodesy and cartography = Geodezia i Kartografia, 84(8), 57–64. (In Russ.) DOI: 10.22389/0016-7126-2023-998-8-57-64.

Kuklina V., Sizov O., Fedorov R. (2021). Green Spaces as an Indicator of Urban Sustainability in the Arctic Cities: Case of Nadym. Polar Sci, 29, 100672. DOI: 10.1016/j.polar.2021.100672.

Kumar A., Upreti M., Pandey A.C., Saikia P., Khan M.L. (2023). Contribution of Landscape Transformation in the Development of Heat Islands and Sinks in Urban and Peri-Urban Regions in the Chota–Nagpur Plateau, India. Resources, 12, 58. DOI: 10.3390/resources12050058.

Kurniawan H.B., Roychansyah M.S. (2023). The Social Equity Of Public Green Open Space Accessibility: The Case Of South Tangerang, Indonesia. Geography, Environment, Sustainability, 1(16), 45-54. DOI: 10.24057/2071-9388-2022-124.

Liotta C., Kervinio Y., Levrel H., Tardieu L. (2020). Planning for environmental justice - reducing well-being inequalities through urban greening. Environ Sci Policy, 112, 47-60. DOI: 10.1016/j.envsci.2020.03.017.

Luo J., Zhai S., Song G., He X., Song H., Chen J., Liu H., Feng Y. (2022). Assessing inequity in green space exposure toward a «15-minute city» in Zhengzhou, China: Using deep learning and urban big data. Int. J. Environ. Res. Public Health, 19(10), 5798. DOI: 10.3390/ijerph19105798.

Ma B., Zhou T., Lei S. et al. (2019). Effects of urban green spaces on residents' well-being. Environ Dev Sustain, 21, 2793–2809. DOI: 10.1007/s10668-018-0161-8.

Mears M., Brindley P., Jorgensen A., Maheswaran R. (2020). Population-level linkages between urban greenspace and health inequality: The case for using multiple indicators of neighborhood greenspace. Health Place, 62, 102284. DOI: 10.1016/j.healthplace.2020.102284.

Mityakova I.I., Ivanova R.R., Shvedova T.E. (2023). Assessment of the ecological state of the urban environment in the «soil-plant» system of the city of Yoshkar-Ola. Bulletin of Udmurt University Series Biology Earth Sciences, 33(4), 403-412. DOI: 10.35634/2412-9518-2023-33-4-403-412.

Murtinová V., Gallay I., Olah B. (2022). Mitigating Effect of Urban Green Spaces on Surface Urban Heat Island during Summer Period on an Example of a Medium Size Town of Zvolen, Slovakia. Remote Sens, 14, 4492. DOI: 10.3390/ rs14184492.

Nasehi S. and Namin A.I. (2020). Assessment of urban green space fragmentation using landscape metrics. Modeling Earth Systems and Environment, 6(1). DOI: 10.1007/s40808-020-00809-7.

Nazombe K. and Nambazo O. (2023). Monitoring and assessment of urban green space loss and fragmentation using remote sensing data in the four cities of Malawi from 1986 to 2021. Scientific African, 20, e01639. DOI: 10.1016/j.sciaf.2023.e01639.

Nesbitt L., J. Meitner M., Girling C., R.J. Sheppard S., Lu Yu. (2019). Who has access to urban vegetation? A spatial analysis of distributional green equity in 10 US cities. Landsc Urban Plan. 181, 51-79. DOI: 10.1016/j.landurbplan.2018.08.007.

Noszczyk T. (2023). Detecting changes in green and blue spaces: Modeling based on statistical approach. Ecol. Indic, 154, 110878. DOI: 10.1016/j.ecolind.2023.110878.

Nowak D.J., Hirabayashi S., Doyle M., McGovern M., Pasher J. (2018). Air pollution removal by urban forests in Canada and its effect on air quality and human health. Urban For Urban Green, 29, 40–48. DOI: 10.1016/j.ufug.2017.10.019.

Pan T., He S., Liu Z., Jiang L., Zhao Q., Hamdi R. (2023). Analyzing Changes in Urban Green Spaces and Their Effect on Land Temperature from the Perspective of Surface Radiation Energy Balance in Rizhao City, the Central Coast of China. Remote Sens, 15, 4785. DOI: 10.3390/rs15194785.

Pashkevich M.A., Beck K., Matveeva V.A., Alekseenko A.V. (2020). Biogeochemical assessment of soil and vegetation cover condition in industrial, residential and recreational zones of St. Petersburg. Journal of Mining Institute, 241, 125–130. DOI: 10.31897/PMI.2020.1.125.

Pashkevich M.A. and Danilov A.S. (2023). Ecological security and sustainability. Journal of Mining Institute, 260, 153-154.

Pouya S. and Aghlmand M. (2022). Evaluation of urban green space per capita with new remote sensing and geographic information system techniques and the importance of urban green space during the COVID-19 pandemic. Environ. Monit. Assess, 194, 633. DOI: 10.1007/s10661-022-10298-z.

Priya M.V. et al. (2023). Monitoring vegetation dynamics using multi-temporal Normalized Difference Vegetation Index (NDVI) and Enhanced Vegetation Index (EVI) images of Tamil Nadu. Journal of Applied and Natural Science, 15(3), 1170-1177. DOI: 10.31018/jans.v15i3.4803.

Raguzin I.I., Bykova E.N., Lepikhina O.Yu. (2023). Polygonal Metric Grid Method for Estimating the Cadastral Value of Land Plots. Lomonosov Geography Journal, (3), 92-103. (In Russ.) DOI: 10.55959/MSU0579-9414.5.78.3.8.

Rakhmatullina I., Rakhmatullin Z., Zaitsev G., Davydychev A., Gilmanova G., Komissarov M. (2023). The Green Space Availability in Ufa City Metropolis. Forests, 14, 1297. DOI: 10.3390/f14071297.

R.C. McEachan R., C. Yang T., Roberts H., E. Pickett K., Arseneau-Powell D., J. Gidlow Ch., Wright J., Nieuwenhuijsen M. (2018). Availability, use of, and satisfaction with green space, and children's mental wellbeing at age 4 years in a multicultural, deprived, urban area: results from the Born in Bradford cohort study. Lancet Planet. Health, 2(6), e244-e254. DOI: 10.1016/S2542-5196(18)30119-0.

Roodsari E.N. and Hoseini P. (2022). An assessment of the correlation between urban green space supply and socio-economic disparities of Tehran districts - Iran. Environ. Dev. Sustain, 24, 12867–12882. DOI: 10.1007/s10668-021-01970-4.

Rouse J.W, Haas R.H., Scheel J.A., Deering D.W. (1974). Monitoring Vegetation Systems in the Great Plains with ERTS. Proceedings, 3rd Earth Resource Technology Satellite (ERTS) Symposium, 1, 48-62. Available at: https://ntrs.nasa.gov/citations/19740022614.

Schindler M., Le Texier M., Caruso G. (2022). How far do people travel to use urban green space? A comparison of three European cities. Appl Geogr, 141, 102673. DOI: 10.1016/j.apgeog.2022.102673.

Set of rules 476.1325800.2020. Territories of urban and rural settlements. Rules for planning, development and improvement of residential districts (2020). Ministry of construction and housing and communal services of the Russian Federation. Available at: https://docs.cntd.ru/document/565322506.

Shchasnaya I. and Rondak U. (2024). Green spaces system analysis and assessment of plantings' ecological state in Minsk city applying geoinformation technologies. E3S Web of Conferences. II International Scientific and Practical Conference «Energy, Ecology and Technology in Agriculture» (EEA2023). 480, 02016. DOI: 10.1051/e3sconf/202448002016.

Shestakov A.K., Petrov P.A., Nikolaev M.Y. (2023). Automatic system for detecting visible emissions in a potroom of aluminum plant based on technical vision and a neural network. Metallurgist, 66, 1308 – 1319. DOI: 10.1007/s11015-023-01445-z.

Skachkova M. and Guryeva O. (2023). Monitoring of the State of Saint Petersburg Green Spaces by Remote Sensing Data. Ecol. Ind. Russ, 27(5), 51-57. (In Russ.) DOI: 10.18412/1816-0395-2023-5-51-57.

Slovic A.D., Kanai C., Marques Sales D., Carnavalli Rocha S., de Souza Andrade A.C., Martins L.S. et al. (2023). Spatial data collection and qualification methods for urban parks in Brazilian capitals: An innovative roadmap. PLoS ONE, 18(8), e0288515. DOI: 10.1371/journal.pone.0288515.

Solovyeva N., Shinkaruk V., Fantrov P., Kakhhorov D. (2020). Features of prosecutorial supervision over the implementation of legislation on specially protected natural territories in modern Russia. IOP Conference Series: Materials Science and Engineering, 828, 012025. DOI: 10.1088/1757-899X/828/1/012025.

Spiridonov A.A. (2023). Features of the Model of Control and Supervisory Activities in the Context of Public Administration Development Mechanisms in Russia: Constitutional Law Context. Lex russica, 76(1), 63-75. DOI: 10.17803/1729-5920.2023.194.1.063-075.

Stessens P., Canters F., Huysmans M., Khan A.Z. (2020). Urban green space qualities: An integrated approach towards GIS-based assessment reflecting user perception. Land Use Policy, 91, 104319. DOI: 10.1016/j.landusepol.2019.104319.

Stessens P., Z. Khan A., Huysmans M., Canters F. (2017). Analysing urban green space accessibility and quality: A GIS-based model as spatial decision support for urban ecosystem services in Brussels. Ecosyst. Serv, 28(C), 328-340. DOI: 10.1016/j.ecoser.2017.10.016.

Tempa K., Ilunga M., Agarwal A., Tashi. (2024). Utilizing Sentinel-2 Satellite Imagery for LULC and NDVI Change Dynamics for Gelephu, Bhutan. Appl. Sci, 14, 1578. DOI: 10.3390/app14041578.

Vidal D.G., Dias R.C., Teixeiram C.P., Fernandes C.O., Filho W.L., Barros N., Maia R.L. (2022). Clustering public urban green spaces through ecosystem services potential: A typology proposal for place-based interventions. Environ Sci Policy, 132, 262–272. DOI: 10.1016/j.envsci.2022.03.002.

Volokhov E.M. and Mukminova D.Z. (2021). Deformations assessment during subway escalator tunnels construction by the method of artificial freezing of soil for the stage of ice wall formation. Journal of Mining Institute, 252, 826-839. DOI: 10.31897/PMI.2021.6.5.

Wang R., Feng Z., Pearce J., Yao Y., Li X., Liu Y. (2021). The distribution of greenspace quantity and quality and their association with neighborhood socioeconomic conditions in Guangzhou, China: A new approach using deep learning method and street view images. Sustain. Cities Soc, 66, 2210-6707. DOI: 10.1016/j.scs.2020.102664.

Wu L., Kim S.K., Lin C. (2022). Socioeconomic groups and their green spaces availability in urban areas of China: A distributional justice perspective. Environ Sci Policy, 131, 26–35. DOI: 10.1016/j.envsci.2022.01.008.

Wu Sh., Yu W., An J., Lin Ch., Chen B. (2023). Remote sensing of urban greenspace exposure and equality: Scaling effects from greenspace and population mapping. Urban For Urban Green, 90, 128136. DOI: 10.1016/j.ufug.2023.128136.

Check for updates

CC BY

RESEARCH PAPER

MODELING OF THE 50-YEAR DYNAMICS OF THE RECLAIMED LANDS VULNERABILITY TO WIND SOIL EROSION IN THE REGION OF PRIPYAT POLESYE

Aliaksandr N. Chervan[1*], Yury S. Davidovich[1], Arkadzy L. Kindeev[1]

[1] Belarusian State University, Nezavisimosti av., 4, 220030, Minsk, Belarus

***Corresponding author:** ChervanAlex@gmail.com

Received: March 15th 2024 / Accepted: November 27th 2024 / Published: December 31st 2024

https://doi.org/10.24057/2071-9388-2024-3290

ABSTRACT. Environmentally unsafe agricultural use of soil and land resources is caused by the high share of reclaimed land in the Pripyat Polesye region and global climate change. The research aims to evaluate the long-term vulnerability of the soil cover, utilizing the example of a large agricultural enterprise spanning over 9,200 hectares in a zone of hydro-technically drained peat-bog and alluvial soils in the central and terraced floodplain of the Pripyat River (Belarus). The assessment of the degree of vulnerability is expressed on the basis of the genetic characteristics of soils in accordance with the soil-hydrological constants: the moisture content of the capillary fringe rupture and the limiting field capacity. The dynamics of spatial and temporal changes in soils by groups of vulnerability to wind erosion is controlled in geoinformation software based on specialized spectral brightness indices according to satellite data for plant vegetative season. Dependences of the degree of vulnerability on heterogeneity of soil cover structure and intensity of agricultural use of soils by types of land have been established. The obtained patterns can be used to develop adaptive landscape farming systems in the Polesye region and to forecast degradation processes of agricultural lands.

KEYWORDS: erosion, soil cover, Pripyat Polesye, GIS, TVDI

CITATION: Chervan A. N., Davidovich Y. S., Kindeev A. L. (2024). Modeling Of The 50-Year Dynamics Of The Reclaimed Lands Vulnerability To Wind Soil Erosion In The Region Of Pripyat Polesye. Geography, Environment, Sustainability, 4(17), 198-204
https://doi.org/10.24057/2071-9388-2024-3290

Conflict of interests: The authors reported no potential conflict of interest.

INTRODUCTION

Unfavorable meteorological phenomena due to global climate change annually cause significant damage in the most weather-dependent sector of the economy – crop farming. Over the past 50 years, droughts in Belarus have doubled in frequency, leading to wind erosion of soils (Chervan et al. 2022), with the region of drained peat-bog soils – Pripyat Polesye – carrying the greatest risk.

Active reclamation works began in the second half of the 20th century in the Belarusian Polesye territory in the Pripyat River valley, with the goal of regulating the water regime of peat-bog soils for their use in agricultural processes. Land reclamation has led to a significant reduction in the area of natural landscapes, primarily large swamps. Thus the area of swamps before the start of land reclamation in the 1960s (Bakarasov 2015) comprised 2.9 million hectares, or 14.2% of the territory of Belarus. Only 0.7 million hectares out of 2.2 million hectares of all drained lands (~30%) are occupied by ameliorative systems with bilateral regulation of the water regime. It predetermines high environmental risks of wind erosion of automorphic and semi-hydromorphic soils in the zone of influence of the drainage network against the background of global climate change and the close relationship of agroecosystems with meteorological conditions.

Currently, 863 thousand hectares of swamps (29.3% of the original area) have been preserved in Belarus as a result of widespread, often excessive, drainage and extensive extraction of peat in a natural or close to natural state. 630 thousand hectares are located within the boundaries of specially protected natural areas; about 313 thousand hectares require the establishment of a special protection regime; and 314 thousand hectares of swamps have international protection status. Belarus uses more than 2.8 million hectares of drained land (34%) for agricultural purposes in 2021; each administrative region of Belarus accounts for an average of 24.2 thousand hectares, with the Polesye region accounting for even more. The share of drained agricultural landscapes in Polesye exceeds 26% which is almost 3 times more than in the rest of the country (Meerovsky & Filippov 2022).

A number of state programs have been approved to restore disturbed lands in the Belarus providing for cultural and technical measures on sandy and sandy loamy soils left after peat extraction due to the reduction in the area of arable land on drained lands in accordance with the regional measures of the European Union ("Climate change adaption" 2019). However, it necessitates a thorough examination of the natural environment, which is already in a vulnerable state: changes in soil levels, groundwater levels, and soil-forming processes have led to a radical transformation of the main types of vegetation. Sedimentation of alluvial deposits occurs throughout the territory, primarily in the central floodplain against the background of wind erosion, given that the majority of

Polesye territory is situated on the floodplain of the river Pripyat. Combined with drainage reclamation, it constitutes a regional environmental problem (Gusev 2022).

Currently, termination of the service period of reclamation systems (50-70 years) makes it necessary to modernize and/or eliminate them. Conducting a retrospective analysis of changes in Polesye landscapes, particularly their vulnerability to current wind erosion of soils, is necessary to determine the most natural and environmentally-friendly development policy.

Thus, the purpose of the research presented in the article is to GIS-model the 50-year dynamics of reclaimed land vulnerability to wind soil erosion using remote sensing data. An assessment of changes in the heterogeneity of the soil cover, structure, and land use types on selected pilot polygons of a large agricultural land user is given over a 50-year period. The degree of vulnerability of the soil cover and its dynamics have been established, and the optimal use of land in the future was determined on the basis of a geosystem approach to the soil cover structure.

Different models are used to figure out how vulnerable the soil cover is. These models use geoinformation systems and remote sensing data (Elyagoubi & Mezrhab 2022) and machine learning (Zhao et al. 2022). The morphometric indicators of terrain, granulometric composition, and hydrological regime of soils are interpreted as the basis for modeling soil vulnerability in most of these models (Lohani et al. 2020). Belarusian scientists also note the importance of considering the hydrological state of soils when determining adaptation measures and mitigating the consequences of droughts, particularly on agricultural lands (Meerovsky et al., 2021). Simultaneously, the assessment of soil vulnerability serves as an initial yet crucial step in the scientific validation and practical application of these measures, which should rely on the geosystem approach.

MATERIALS AND METHODS

The methodological stages of the research carried out include the soil cover vulnerability assessment before and after a reclamation regulation of the water regime taking into account the agricultural use of soils of different genesis. The study object is the territory of a large agricultural enterprise, with a high proportion of reclaimed land – the unitary enterprise "Agrocomplex Polesie", in the Pinsk district of the Republic of Belarus. The dynamics of composition and soil cover structure, and types of land on cultivated areas were spatially analyzed in the GIS environment based on the interpretation of multi-temporal (1974, 1986, 1989–1990, 2000–2003, 2018–2022) aerial photography and satellite data.

The overlay operations and calculation of summary statistics of geodata were performed using the ArcToolBox toolkit in the ArcGIS software environment – Geospatial Analyst and Geostatistical Analyst modules. Automated interpretation of multi-temporal multispectral images was performed in the ENVI software package with the selection of reliable spectral brightness channels in accordance with actual land use.

The vulnerability (predisposition) of soils to wind erosion was assessed on the basis of taking into account soil-hydrological constants in accordance with the genetic classification position of each soil variety: the limited field moisture (LFM) and capillary rupture moisture (CRM). In the Belarusian Polesye region, waterlogged conditions genetically predetermine the productivity of agricultural soils, making its use during the growing season especially important and indicative (Romanova 2015). The number of days per year or during the growing season was taken during which the moisture content in the 0–20 cm layer exceeds the LFM level and is below the CRM (significant soil-hydrological constants). It is used as the measure of assessment of the moisture supply of soil of a certain genesis and granulometric composition. Spatial consideration of the soil function of mitigating meteorological droughts due to internal predisposition makes it possible to identify the degree of risk of agricultural land degradation due to global climate change (Chervan & Melnik 2022).

The dynamics of the soil cover formation of the studied reclamation system "Parokhonskoe" of the agricultural complex "Polesye" (total area more than 9,200 ha) was studied in accordance with the geosystem approach to the soil cover structure – changes were analyzed not in individual soil taxons but in their combinations in homogeneous geomorphological, orographic and lithological conditions. This principle makes it possible to diagnose significant (irreversible) changes in soil cover in terms of probable land degradation due to economic use. We measured the amount of heterogeneity within the boundaries of soil combinations in dynamics by looking at both the coefficients of soil contrast and complexity, which is a number that shows how different and complicated the soil cover is, and the degree to which the soil is vulnerable to deflation.

The inventory of geosystems by soil combinations is based on the teachings of V.M. Friedland on the soil cover structure (Chervan et al. 2016). This approach has not found wide distribution in studies of Western Europe, USA, and Australia but has been actively developed in Belarus both for analyzing the suitability of agricultural land (Chervan et al. 2016; Chervan 2021) and assessing the biodiversity of protected areas (Romanova & Andreeva 2003; Kindeev & Mudragelova 2022). At this point, the fast growth of GIS technologies has made it possible to create adaptive landscape farming systems that are based on a multiscale analysis of the different types of soil cover. Geostatistics and pedometrics have grown in popularity recently thanks to the availability of quantitative data on the properties and indicators of the soil cover. These methods, along with a geosystem assessment, allow the soil to be shown as a discrete-continuum body (Chervan et al. 2022). Tasks for using remote sensing data are set to obtain operational information on qualitative and quantitative indicators of the state of disturbed geosystems in general and soil cover in particular (Savin 2022). The classical measures for assessing the heterogeneity of the soil cover structure developed by Yu.K. Yuodis (Yuodis 1967) are the coefficient of complexity, contrast, and heterogeneity as a complex indicator of soil cover heterogeneity used in the cadastral assessment of agricultural land and the calculation of bio- and pedodiversity (Chervan et al. 2022, Kindeev & Mudragelova 2022). The development of geoinformation systems made it possible to use the developed indicators for a comprehensive geosystemic assessment of the landscapes stability to anthropogenic impact and the development of recommendations for anti-erosion measures (Chervan et al. 2016). This allows us to determine the feasibility of utilizing these values to evaluate the changes in Polesye's soil cover due to land reclamation.

The identified soil combinations (SC) are individualized in terms of their component composition and their share in participation in the soil cover structure. Qualitative (soil genetic type) and quantitative (share of soil in combination) diversity of land use conditions are encoded through the SC formula.

The area calculation of soil contours or land plots, vector-raster transformations, and cartographic algebra were performed in the geodatabase through the ArcGIS 10.7 software package.

The degree of anthropogenic impact on the soil cover was determined by the composition of land types with

an assessment of the dynamics of the land use structure simultaneously with the analysis of soil cover for the period 1974–2022. The nine arrays of representative plots with a total area of more than 2,800 hectares were selected for the purpose of increasing the reliability of the results of the geostatistical analysis. The choice of these arrays was made on the basis of different dynamics of the soil cover structure and the composition of land types over a 50-year period to confirm the hypothesis of an increase in the vulnerability of the soil cover of agricultural lands under the conditions of intensification of agrolandscapes.

Aerial photography and satellite images were used to analyze land use dynamics. Multi-temporal satellite images for each of the studied periods were used to take into account the phenology of agricultural crops and detect different phases of land use. It was combined into one composite for subsequent classification using a trainable non-parametric classifier – the support vector machine method (SVM). High-resolution remote sensing standards QuickBird and Ikonos, detailed land plans, and field survey results were used to train the classifier on the study territory.

Soil vulnerability is based on its hydrological regime, so the main thing that is monitored from afar is moisture. This is done by analyzing at radar images (Dubois et al. 1995; Meng et al. 2018; Zeyliger et al. 2020; Kang et al. 2021; Ondieki et al. 2023), as well as different normalized vegetation indices (Sadeghi et al. 2017; Colliander et al. 2017; Suk Lee et al. 2019; Wang et al. 2020; Santi et al. 2020). The temperature-vegetation dryness index (TVDI) was used to study soil moisture in addition to the traditional use of the red (red), near infrared (NIR), short-wave infrared (SWIR) wavelength ranges (Sadeghi et al. 2017; Twumasi et al. 2021) and less often the blue range (Zhang et al. 2013), reflecting the relationship between the temperature of the earth's surface and NDVI index designed to study the surface moisture of the soil and vegetation cover (Sandholt 2002). By using these indices made, we were able to learn about how soil moisture changed over 50 years and, as a result, how dangerous the soil cover was in pilot areas.

The data of multispectral and aerial photography were subjected to visual and automated interpretation to determine the structure of land use by land types and soil moisture conditions according to the NDVI and TVDI indices in accordance with the previously developed methodology (Sandholt 2002; Sadeghi et al. 2017). Remote sensing materials were selected according to the principle of similarity of shooting time during the growing season, image quality, and a single geometric and spectral (radiometric and atmospheric) correction at the post-processing stage in the ENVI 5.5 software package. Multispectral satellite images of the Landsat-5 TM, Landsat-7 ETM+, and Landsat-8 OLI/TIRS systems with a spatial resolution of 30 to 120 m for March–May 1986, 1989, 1991, 1999, 2000, 2001, 2003, 2018 and 2022 were used as a basis for the analysis in GIS. The satellite images used were selected in such a way that the shooting dates in different years did not differ by more than 2 weeks in accordance with a similar ratio of natural and cultivated vegetation. The use of these systems is due to the wide time coverage as well as the presence of a thermal infrared channel, which is necessary for calculating the TVDI index.

RESULTS AND DISCUSSION

The amount of available water that is due to the balance of rainfall, soil moisture, evaporation, and different types of water runoff is what the value of moisture reserves in soil combinations is. Belarussian approaches to genetic soil classification enable spatial differentiation based on the degree of hydromorphism, from automorphic to hydromorphic (mineral moistened and organogenic peat-bog soils). The parameterization of moisture supply was carried out in the range between LFM and CRM ranges for each element in the formulas of SC on the territory of 9 arrays of representative plots. The group most vulnerable to deflation includes soils where the range of available moisture during the growing season is below the CRM constant for more than 130 days per year (Romanova 2015). The indicators assigned to the groups of strongly-, medium-, and weakly-vulnerable soils were 101-130, 71-100, and 51-70 days, respectively. The group of the least vulnerable includes soil varieties with a moisture content below the CRM in the root layer during the growing season, less than 50 days per year.

A distinctive feature of the agricultural enterprise under consideration is the predominance of soddy waterlogged and peat-bog soils of different thicknesses and the peculiarity of the occurrence of lowland peat. It should be noted the changing dynamics of land use in agrolandscapes, from traditional farming (1960–1990) to modern intensive agricultural use in the form of saturation of crop rotations with tilled crops within the boundaries of arable and improved meadow land plots. The analyzed data for 1974 included the soil cover characteristics of agricultural lands, which were based on the first round of soil-geobotanical survey materials in Belarus. Additionally, the analysis considers the land use structure of various land types, which are identified using panchromatic aerial photography data at a scale of 1:10,000.. The results in Table 1 illustrate the relative importance of the elements of SC and land type composition in determining the susceptibility of soils to wind erosion, ranging from the least vulnerable soils (I) to the group with the highest risk of deflation (V). At the same time, the soil-hydrological constants were additionally differentiated according to the conditions for the presence of moisture resistance within the soil profile in accordance with the granulometric composition of the soil-forming and underlying rock.

Over the 50-year period, there have been significant changes in the soil cover structure caused by the intensification of agricultural use, as shown in Table 1 and Fig. 1. The spatial accuracy of the original and modeled geodata at a scale of 1:10,000 – the most detailed level for land cadastral information in Belarus – limits the measurements and calculations error. According to the first round of soil-geobotanical surveys in Belarus in the 1960s (Romanova 2015), plots 1–4 had a lot of waterlogged peat-bog and paleo-floodplain silt-gley soils. However, these plots also had soils that were breaking down because peat deposits were being actively mineralized in these agrocenoses as early as 1974. The continuing intensity of agricultural impact within arrays № 5-6, which include arable and meadow improved types of land, has led to an increase in heterogeneity of the soil cover structure over the entire period under consideration. The cultivated areas within the boundaries of arrays № 8–9 are currently characterized by less intensive inclusion in agricultural production. However, in 2022, the predominance of semi-hydromorphic (temporarily excessively moist and gleyic) soil combinations replaced the predominance of hydromorphic soils in 1974.

It should be noted all representative land plots are characterized by an increase in the heterogeneity coefficient (K_h) over a 50-year period in soil cover structure (Table 2) which simultaneously takes into account the contrast (Kc) and dissection (Kr) of elements in the soil

combination formula. The areas with the most crop production and the more complex soil cover structure at the start—sample arrays № 1-4 and № 8–9 in Table 1—have a greater increase in soil heterogeneity.

The results of automated interpretation of remote sensing data for each sample array were normalized in the GIS according to the TVDI index by the method of equal intervals for 5 groups for the entire survey period. According to remote sensing data (spectral index TVDI), active reclamation and agricultural impact have increased in the proportion of soils susceptible to deflation, leading to a complex soil cover structure over a 50-year period. It should be taken into account that this spectral index is sensitive to significant meteorological changes within the vegetative season. It is planned to replace the "triangle method" used to calculate the TVDI index with the "trapezoid method" in further scientific research using data from the optical short-wave infrared wavelengths of the Sentinel-2 system due to more high spatial resolution.

The calculation of the intergroup percentage ratio allowed to determine the TVDI value for each survey date within the boundaries of each array of representative

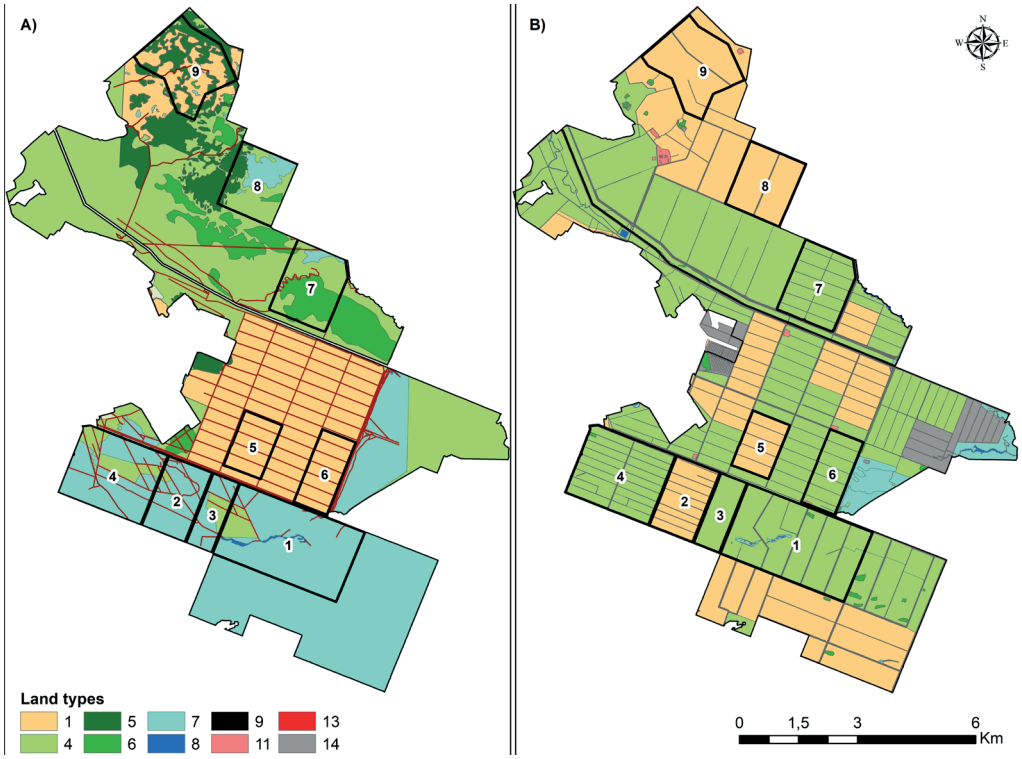

Fig. 1. Types of land of the agricultural complex «Polesye» A) 1974 year; B) 2022 year:
1 – arable; 4 – meadow improved; 5 – under shrubs; 6 – forests; 7 – swamps; 8 – water bodies; 9 – under roads; 11 – under construction; 13 – unused; 14 – other

Fig. 2. Degree of soil vulnerability A) 1974 year; B) 2022 year:
1 – the least vulnerable; 2 – weakly vulnerable; 3 – moderately vulnerable; 4 – vulnerable; 5 – the most vulnerable

plots for the period 1986–2022 (Fig. 3). Attention is drawn to the fact that most of the arrays of the agrolandscapes under consideration were characterized by a high degree of susceptibility to deflation due to reclamation and then active agricultural development. It led to the complication of soil cover structure already after 10–15 years of the reclamation system operation – they are located in the range of 3–4.5 vulnerability groups on the chart. Separate extremes (arrays № 3, 9 in May 2000; arrays № 3, 8 in May 2001) are caused by a change in the use of agrocenoses or significant meteorological differences during the plant growing season. It should be noted a significant difference in the present situation with the risk of deflation in representative areas: the greatest danger of wind erosion due to insufficient amount of productive moisture in the root layer of soils is for arrays № 2, 3, 8. It is possible that the transfer of some of them to fallow land is a forced organizational measure in connection with the loss of the productive capacity of soils on these lands. Array № 9 is also represented by fallow lands, since unfavorable phenomena in cultivated areas due to the initially more heterogeneous soil cover structure (Table 1) appeared even earlier. Arrays № 6, 7 with composed soil cover of thicker organogenic soils are currently less at risk of deflation and are used as meadow-improved lands with intensive crop rotations

CONCLUSIONS

During the review period, varying degrees of agricultural land use intensification caused significant changes in soil cover structure, which we registered through research. The heterogeneity coefficient, which is the best way to show how complex the soil cover structure is, went up by 5–10 times for most of the main soil combinations over a 50-year period. In some cases, it went up by more than 100 times (No. 6 and 7). The significant combination area from 133 to 645 indicates the significance of the studies conducted and the regional nature of changes in the soil cover structure under the influence of agricultural activity. According to the materials of ground studies and interpretation data of archival remote sensing data, it can be seen that the key area soils at the very beginning of the time period

Table 1. Dynamics of vulnerability of soil cover of representative plots taking into account of land use structure

Sample array of plots	Square, hectares	Soil combination*		Land use structure**		Vulnerability	
		1974	2022	1974	2022	1974	2022
1	645	$PB^{65}+SS_3^{25}+PBd^{10}$	$PB^{65}+SS_3^{20}+PBd^{10}+SS_2^{5}$	$Ms^{90}+S^{10}$	$M_i^{95}+O^{5}$	$II^{65}+III^{25}+IV^{10}$	$II^{35}+I^{30}+III^{25}+IV^{10}$
2	224	$PBd^{50}+PB^{45}+SS_2^{5}$	$PB^{50}+PBd^{40}+SS_2^{10}$	$S^{95}+Ms^{5}$	$FL^{95}+O^{5}$	$II^{45}+IV^{45}+V^{5}+III^{5}$	$IV^{30}+II^{30}+I^{20}+III^{15}+V^{5}$
3	133	$PBd^{55}+PB^{35}+SS_3^{10}$	$PBd^{50}+PB^{40}+SS_2^{5}+SS_3^{5}$	$S^{75}+Ms^{25}$	M_i^{100}	$IV^{50}+II^{35}+III^{10}+V^{5}$	$II^{30}+IV^{30}+V^{20}+III^{10}+I^{10}$
4	428	$PB^{70}+PBd^{20}+SS_2^{10}$	$PB^{70}+PBd^{15}+SS_3^{10}+SS_2^{5}$	$S^{80}+Ms^{20}$	$M_i^{95}+O^{5}$	$II^{75}+V^{15}+III^{5}+IV^{5}$	$I^{60}+III^{25}+II^{10}+IV^{5}$
5	150	PB^{100}	$PB^{80}+SS_3^{10}+PBd^{10}$	A^{100}	M_i^{100}	$II^{95}+IV^{5}$	$I^{60}+II^{20}+III^{10}+IV^{10}$
6	180	PB^{100}	$PB^{90}+SS_3^{10}$	A^{100}	M_i^{100}	II^{100}	$I^{75}+II1^{5}+III^{10}$
7	290	$FSS^{60}+PB^{40}$	$FSM^{60}+PB^{30}+FSS^{5}+PBd^{5}$	$Ms^{50}+US^{45}+S^{5}$	M_i^{100}	II^{100}	$I^{70}+II^{20}+III^{5}+V^{5}$
8	260	$PB^{65}+SS_3^{20}+PBd^{15}$	$PB^{55}+SS_3^{20}+PBd^{20}+SS_2^{5}$	$Ms^{65}+S^{30}+US^{5}$	FL^{100}	$II^{65}+III^{20}+V^{15}$	$I^{40}+III^{25}+II^{20}+IV^{15}$
9	341	$SS_3^{45}+SS_2^{20}+PB^{15}+SPS_2^{10}+FSS^{10}$	$PBd^{20}+PB^{20}+SS_3^{20}+SS_2^{15}+SPS_2^{15}+SPS_1^{10}$	$O^{55}+Ms^{45}$	FL^{100}	$III^{75}+II^{15}+IV^{5}+V^{5}$	$III^{50}+IV^{20}+II^{10}+I^{10}+V^{10}$

*Soils: SPS – sod-podzolic swampy (SPS1 – temporarily over-hydrated, SPS2 – gleyic), SS – soddy swampy (SS1 – temporarily over-hydrated, SS2 – gleyic, SS3 – gley), PB – peat-bog low-lying type, FSS – floodplain soddy swampy, FSM – floodplain silt-marsh, PBd – degropeat mineral residual-peaty.

**Land types: A – arable, Mi – meadow improved, Ms – meadow swampy, S – swamps, US – under shrubs, FL – fallow land, O – other (water bodies, under construction, unused lands

Table 2. Cartometric assessment of the soil cover structure of representative plots

Sample array of plots	1974			2022		
	K_k	K_c	K_h	K_k	K_c	K_h
1	9.56	0.07	0.7	10.6	0.5	5.32
2	21.53	0.09	1.89	21.9	0.48	10.6
3	18.68	0.12	2.29	20.6	0.73	15.1
4	10.49	0.05	0.53	11.5	0.43	4.94
5	2.02	0.08	0.16	6.32	0.66	4.18
6	0.13	0.04	0.01	3.3	0.51	1.68
7	0.35	0.04	0.01	3.12	0.53	1.68
8	10.83	0.05	0.55	15.6	0.46	7.22
9	7.93	0.06	0.48	12.7	0.81	10.3

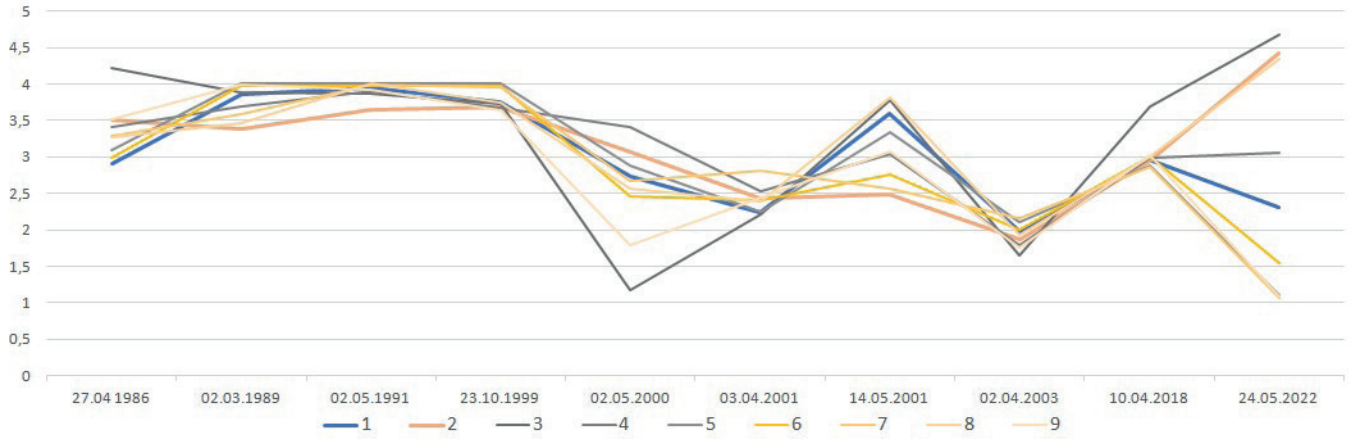

Fig. 3. Dynamics of soil vulnerability groups in sample arrays over a 40-year period

under consideration are in a state of degradation due to active peat extraction. The increasing of soil cover structure heterogeneity is observed as a result of the high intensity of agricultural production, and the proportion of automorphic soils vulnerable to deflation increases. The predominance of hydromorphic soils has been replaced by the prepotency of semi-hydromorphic soils in most of the agrolandscapes, which is noted for the entire Polesye region.

An effective measure of adaptive landscape use of the assessed lands during the review period was defined by the transformation it to a category of fallow lands, which significantly reduce the risk of wind erosion and homogenize the soil cover by increasing the role of meadow vegetation formations.

The methodology applied on the example of a key agricultural enterprise can also be applied in other physical and geographical regions of the Polesye region characterized by alluvial sedimentation in the zone of the central and terraced floodplains of the river basin. The hard-to-reach areas of the southern part of the Brest, Pripyat and Gomel Polesye are of particular interest because of "conserved" as a result of the consequences of the Chernobyl nuclear accident but also differed in the dynamics of the soil cover structure.

REFERENCES

Bakarasov V. (2015) Geoecological destabilization of the natural environment of reclamation ecotone territories of the Republic of Belarus: BSU Press. (In Russian)

Chervan A. (2021). Typification of the structure of the soil cover using GIS tools to assess the productive potential of agricultural landscapes (on the example of the Republic of Belarus) // Bulletin of the Udmurt University. Series "Biology. Earth Sciences", Vol. 31, Issue. 3. 280-289. (In Russian)

Chervan A. et al. (2016). Geosystem approach to the organization of nature management in waterlogged agrolandscapes (on the example of the APC «Lovzhansky» of the Vitebsk region of Belarus). Scientific statements of the Belgorod State University. Natural Sciences, № 25 (239), Vol. 37. 143-155. (In Russian)

Chervan A., Kindeev A., Sazonov A. (2022). Soil cover structure, pedo- and biodiversity of the Berezinsky Biosphere Reserve. Eurasian Soil Science, № 10, 1215-1227.

Chervan A., Melnik V. (2022). Assessment and intra-regional differences in the vulnerability of soils of agricultural lands of the Belarusian Polesye to droughts in the context of climate warming. Reports of the National Academy of Sciences of Belarus, V. 66. № 4. 444-453. https://doi.org/10.29235/1561-8323-2022-66-4-444-453. (In Russian)

Climate change adaptation in the agricultural sector in Europe. EEA, Luxemburg, 2019. 110 p. https://doi.org/10.2800/537176.

Colliander, A. et al. (2017) Spatial Downscaling of SMAP Soil Moisture Using MODIS Land Surface Temperature and NDVI during SMAPVEX15. IEEE Geoscience and Remote Sensing Letters, 14, 2107-2111. https://doi.org/10.1109/LGRS.2017.2753203

Dubois, P., Zyl, J. and Engman, T. (1995) Measuring Soil Moisture with Imaging Radars. IEEE Transactions on Geoscience and Remote Sensing, 33, 915-926. https://doi.org/10.1109/36.406677

Elyagoubi S., Mezrhab A. (2022). Using GIS and remote sensing for mapping land sensitivity to wind erosion hazard in the middle Moulouya Basin (North-Eastern Morocco). Journal of Arid Environments. https://doi.org/10.1016/j.jaridenv.2022.104753.

Gusev A. (2022). Risk assessment of negative climatogenic reactions in Polesye landscapes. Russian Journal of Applied Ecology, (4), 13–19. https://doi.org/10.24852/2411-7374.2022.4.13.19. (In Russian)

Kang, C. et al. (2021) Global Soil Moisture Retrievals from the Chinese FY-3D Microwave Radiation Imager. IEEE Transactions on Geoscience and Remote Sensing, 59, 4018-4032. https://doi.org/10.1109/TGRS.2020.3019408

Kindeev A., Mudragelova Yu. (2022). Quantitative characteristics of soil heterogeneity in geosystems of the Berezinsky Biosphere Reserve. Land of Belarus, № 1, 49-58. (In Russian)

Lohani S. et al. (2020). Performance of the Soil Vulnerability Index with respect to slope, digital elevation model resolution, and hydrologic soil group. Journal of Soil and Water Conservation, Vol. 75, № 1, 12-27.

Meerovsky A., Filippov V. (2022). Western Expedition to Drain Swamps in the History of Land Reclamation in Belarus. Reclamation, №. 4, 52-57. (In Russian)

Meerovsky A., Melnik V., Yacsuhno V. (2021). Vulnerability of soils of agricultural lands to droughts in the conditions of climate warming in Belarusian Polesye. Reclamation, №. 2, 29-36. (In Russian)

Meng Q. et al. (2018). Combined use of GF-3 and Landsat-8 satellite data for soil moisture retrieval over agricultural areas using artificial neural network. Advances in meteorology, 2018, № 5, 1–11. https://doi.org/10.1155/2018/9315132

Ondieki J. et al. (2023) Enhancing Surface Soil Moisture Estimation through Integration of Artificial Neural Networks Machine Learning and Fusion of Meteorological, Sentinel-1A and Sentinel-2A Satellite Data. Advances in Remote Sensing, 12, 99-122. doi: 10.4236/ars.2023.124006.

Romanova M., Andreeva V. (2003). The structure of the soil cover and geosystem of the Berezinsky Biosphere Reserve. Eurasian Soil Science, № 5, 543-549.

Romanova T.A. (2015). Water regime of soils in Belarus. Minsk: IVC Minfina. 144 p. (In Russian)

Sadeghi M., Babaeian E., Tuller M., Jones S. (2017). The optical trapezoid model: A novel approach to remote sensing of soil moisture applied to Sentinel-2 and Landsat-8 observations. Remote Sensing of Environment, 198, 52-68.

Sandholt I., Rasmussen K., Anderson J. (2002). A simple interpretation of the surface temperature/vegetation index space for assessment of the surface moisture status. Remote Sensing of Environment, Vol. 79, 213-224.

Santi E. et al. (2020) Soil Moisture and Forest Biomass Retrieval on a Global Scale by Using CyGNSS Data and Artificial Neural Networks. 2020 IEEE International Geoscience and Remote Sensing Symposium, Waikoloa, 26 September-2 October 2020, 5905-5908. https://doi.org/10.1109/IGARSS39084.2020.9323896

Savin I. (2022). Prospects for the development of soil mapping and monitoring based on interpolation of point data and remote methods. Bulletin of Moscow University. Series 17. Soil science, № 2, 13-19. (In Russian)

Suk L. et al. (2019) Estimation of Soil Moisture Using Deep Learning Based on Satellite Data: A Case Study of South Korea. GIScience & Remote Sensing, 56, 43-67. https://doi.org/10.1080/15481603.2018.1489943

Twumasi Y. et al. (2021). Estimation of land surface temperature from Landsat-8 OLI thermal infrared satellite data. A comparative analysis of two cities in Ghana. Advances in remote sensing, № 10, 131–149. https://doi.org/10.4236/ars.2021.104009

Wang Q. et al. (2020). Comparative analysis of Landsat-8, Sentinel-2, and GF-1 data for Retrieving soil moisture over wheat farmlands. Remote sensing, 1–16. https://doi.org/10.3390/rs12172708

Yuodis Yu. (1967). On the structure of the soil cover of the Latvian SSR. Eurasian Soil Science, № 11, 50-55. (In Russian)

Zeyliger A., Muzalevsky K., Zinchenko E., Ermolaeva O., Melihov V. (2020). Field testing of the method of cartographic modeling of the moisture reserves of the surface layer of the soil cover, based on the data of the Sentinel-1 radar survey and the digital elevation model. Modern Problems of Remote Sensing of the Earth from Space, Vol. 17, № 4, 113-128.

Zhang, N., Hong, Y., Qin, Q., Liu, L. (2013). VSDI: a visible and shortwave infrared drought 920 index for monitoring soil and vegetation moisture based on optical remote 921 sensing. International Journal of Remote Sensing, 34 (13), 4585-4609.

Zhao Y. et al. (2022). Assessing the influencing factors of soil susceptibility to wind erosion: A wind tunnel experiment with a machine learning and model-agnostic interpretation approach. Catena, Vol. 215. https://doi.org/10.1016/j.catena.2022.106324.

Check for updates

CC BY

RESEARCH PAPER

AGRICULTURAL TERRACES OF DAGESTAN: ANCIENT LEGACY FOR CLIMATE CHANGE ADAPTATION AND BUILDING RESILIENCE OF MOUNTAIN COMMUNITIES

Raisa G. Gracheva[1,2*], Vera V. Vinogradova[1,2], Alexander V. Sheludkov[1,2], Shakhmardan S. Muduev[3]

[1] Institute of Geography, Russian Academy of Sciences, Staromonetniy lane. 29, Moscow, 119017, Russia

[2] HSE University, Pokrovsky boulevard 11, Moscow, 109028, Russia

[3] Research Institute of Management, Economics, Politics and Sociology of DSUNE, Ataeva 5, Makhachkala, 367008, Russia

***Corresponding author:** gracheva@igras.ru

Received: March 15th 2024 / Accepted: November 27th 2024 / Published: December 31st 2024

https://doi.org/10.24057/2071-9388-2024-3410

ABSTRACT. In agricultural mountain regions, changes in weather patterns force people to look for new agricultural activities, shift from agriculture to tourism services, or even leave the mountains. This study discusses the role of Dagestan's agricultural terraces as a potential resource for mountain people to adapt agricultural activities to climate change, thereby demonstrating the community resilience grounded on local traditional practices. We selected eight mountainous administrative districts of Dagestan as a case study area and tracked the changes of average annual, summer, and winter temperatures and precipitation for different altitudes in 2011–2020 compared to 2000–2010. We also conducted 30 informal exploratory interviews with local farmers and officials (purposive sampling) aiming at revealing common local narratives regarding climate change and its impact on agricultural activities, including the use of terraces. According to our results, respondents perceive the warming and drying of the Dagestan mountains as a growing water scarcity due to decreased precipitation and reduced snow cover, and as an opportunity to expand agricultural activities to higher altitudes. Agricultural terraces are seen as a prime land resource, preventing erosion and conserving soil moisture. Including terraces as a tourist attraction could increase interest in the local landscape and its history and may also indirectly serve to strengthen the resilience of local communities. While climate change may make it difficult to farm in the mountains, tourism becomes an additional source of income for farmers and supports agriculture.

KEYWORDS: North Caucasus, mountains, climate change perception, agriculture, historical heritage

CITATION: Gracheva R. G., Vinogradova V. V., Sheludkov A. V., Muduev S. S. (2024). Agricultural Terraces Of Dagestan: Ancient Legacy For Climate Change Adaptation And Building Resilience Of Mountain Communities. Geography, Environment, Sustainability, 4(17), 205-216
https://doi.org/10.24057/2071-9388-2024-3410

ACKNOWLEDGEMENTS: The article was prepared in the framework of a research grant funded by the Ministry of Science and Higher Education of the Russian Federation (grant ID: 075-15-2022-325).

Conflict of interests: The authors reported no potential conflict of interest.

INTRODUCTION

The spatial diversity of climate change and its impacts on the environment and human activities requires a differentiated approach to assessing the adaptation measures needed on a particular territory. The IPCC reports specifically highlight mountain regions, as the increasing impacts of climate change on people and ecosystems here are reducing the resilience of mountain communities (Hock et al. 2019; Adler et al. 2022). Complex relief and altitude differences create a wide range of landscapes and biological diversity of mountain regions. However, they also make life hard for people because mountain areas tend to have fewer cities and people, making it harder to get to places and making them more vulnerable to extreme weather and slow-onset events.

All these challenges are also characteristic of the mountainous regions of the Caucasus. Over the past 30–40 years, the Caucasus has seen an increase in annual and seasonal temperatures, especially in summer, by an average of 0.5–0.7°C, a drier climate, and a growing frequency and intensity of meteorological extremes (Assessment 2022; Kozachek et al. 2017; Shvarev et al. 2021; Tashilova et al. 2019). Rapid glacier retreat (Solomina et al. 2024; Tielidze et al. 2022; Toropov et al. 2019) has cut off a lot of water in places where it is already scarce, such as the South Caucasus and the eastern flank of the North Caucasus. Overall, the environmental impacts of climate change are already posing a threat to the Caucasus population and its economic activities (Ahouissoussi et al. 2014; Sheludkov and Vinogradova 2024).

Many studies (Kohler et al. 2010; Ponce 2020; Salukvadze and Backhaus 2020; Gracheva et al. 2023) have reported that changes in weather patterns and their impact on agroecosystem productivity force people in agricultural mountain regions to look for new agricultural activities,

shift from agriculture to tourism services, or even leave the mountains. In seeking opportunities for building resilience of mountain communities, we argue that, alongside the new agricultural activities, a wide range of local practices and centuries-old experience can help mountain people to adapt to climate change (Gruneis et al. 2018). In particular, climate challenges are driving interest in revitalization of terrace farming (Stanchi et al. 2012; Birthal and Hazrana 2019; Cicinelli et al. 2021).

Terrace farming ensures soil conservation, water runoff regulation, and the possibility of using different crops along the altitudinal gradient (Ponce 2020). The loose substrate of the terraces retains the infiltrating water; thus, terraced slopes reduce peak flows in mountain rivers and store water in areas with a lack of moisture (FAO 2000). For centuries, these agricultural landscapes have been the basis of the resilience of mountain communities (e.g. Stanchi et al. 2012; Tarolli et al. 2014; Kiesow and Bork 2017; Gauci and Schembri 2019). Currently, farmers continue to use and modernize some terraces for the cultivation of high-quality crops, primarily grapes (Birthal and Hazrana 2019; Zoumides et al. 2022).

Among the terraced mountains, the terraces of the Caucasus and, in particular, of the North Caucasus are much less known in the world. Stretching along the mountain ranges from west to east, they form an almost continuous network of mountain-terrace complexes, which are the densest and most diverse in the Eastern Caucasus, primarily in Dagestan ('mountain country') (Gracheva and Idrisov 2021). Partially abandoned, these ancient terraces still form a primary base for local agriculture, serving as places for vegetable and fruit growing, viticulture, and livestock grazing.

This study discusses the role of Dagestan's agricultural terraces as a potential resource for mountain people to adapt agricultural activities to climate change, thereby demonstrating the community resilience grounded on local traditional practices. Resilience is considered the persistence, adaptability, and transformability of socio-ecological systems in the face of dynamic changes (Folke 2016; Wyss et al. 2022) and needs to be combined with United Nations Sustainable Development Theory (Vlasova et al. 2021). We will only talk about adaptation actions in agriculture here, but we will show that mountain communities' ability to be resilient comes from many places and things, such as local traditions, local government, and the sharing of knowledge across communities.

We start with a short discussion of the terraced farming phenomena, focusing on the terraced complex of Mountainous Dagestan and its links to other well-known cases of terraced farming in the world. Then we give a brief description of the study area and our research design. In the results section, we show the current trends of climate parameter change in the selected mountain districts of Dagestan and discuss the results of informal surveys of mountain residents and other stakeholders in the context of climate change. We consider the adaptation actions of the rural population to climate change from the point of view of the use of terraces as a land resource. Finally, we propose to include ancient agricultural terraces in the list of tourist sites in Dagestan as a unique cultural and historical heritage and human-shaped mountain landscapes.

TERRACE FARMING IN BUILDING RESILIENCE OF MOUNTAIN COMMUNITIES

Terrace farming is an ancient invention for farmers to adapt to local environmental conditions. One of the best examples of such adaptation is the Andean agriculture, with its 5,000-year history, where soil conservation is a part of the local culture. The Andean mountain agriculture shows how strengthening the identity and resilience of a community and a territory as a whole is achieved through traditional agriculture. The growing influence of modern technologies is eroding these traditions, but the outflow of young people and the loss of traditional knowledge can cause much more devastating consequences (Inbar and Llerena 2000).

The terraced agricultural landscapes of Southern Europe also reflect the efforts of people in supporting land resources and strengthening stability during centuries. Since the 15th century, the island of Madeira, Portugal, has served as an example of an almost perfectly adapted agricultural system of intensive farming (Kiesow and Bork 2017). The history of the terraces of the Maltese Islands, constructed on rocky slopes, goes back more than five thousand years. Grapes, which occupied the terraces over time, became the main crop of the island for many centuries (Gauci and Schembri 2019). Since the 1960s, the tourism industry has rapidly replaced the rural lifestyle, transforming the remains of grandiose Mediterranean terracing systems into tourist sites that serve as evidence of the region's distinctive culture (Gauci and Schembri 2019; Grove and Rackman 2003; Kiesow and Bork 2017). In some regions, land abandonment and growing tourism pressure lead to the destruction and disappearance of terraces and, in fact, to the collapse of the historical landscapes (Tarolli et al. 2014).

Dagestan is considered one of the centers of ancient terrace technologies, which emerged in the Bronze – Early Iron Ages and flourished in the Middle Ages (Vavilov 1936; Spenser and Hale 1961; Skripnikova 2007; Aglarov 2016). In conditions of extreme land shortage in the mountains, diverse terrace farming became widely used and highly advanced in Dagestan. One can find here almost all types of agricultural terraces characteristic of the Middle East, the Andes, the Mediterranean, and other regions with developed terrace farming (Aglarov 2016; Magomedkhanov et al. 2022). Terrace soils helped to maintain the stability of agriculture in a vulnerable environment, and terrace farming constituted an integral part of the socio-ecological system, created over centuries and supporting the resilience of mountain communities.
According to the remote sensing data, agricultural terraces in Dagestan cover an area of more than 3500 km, rising up the slopes to 2100–2400 m above sea level (Pinskoy et al. 2023). That is approximately 7% of the total area, or approximately 14% of the mountainous area of the republic.

The main area of terraces is located in the central limestone part of Mountain Dagestan at altitudes from 1000 to 1800–2100 m (Borisov et al. 2021). In the past, narrow strip terraces with retaining walls on steep slopes were planted with vineyards and orchards. Wide terraces without retaining walls with grassy slopes constructed on valley slopes and sloping plateaus were used for high-intensity, three-layer farming, with grain, legumes, and melons growing in one field and fruit trees on the edges of the terraces; grassy slopes were first-class hayfields (Aglarov 2016). Now, bushes and trees have overgrown the narrow terraces (Fig. 1a), while cabbage, potatoes, and other vegetables occupy the wide terraces (Fig. 1b).

In the southern part of Mountain Dagestan, terraces rise to 2400 m; here, soils of terraces built on the easily destroyed shale and slate rocks are suitable for cultivation with modern technology. Some researchers think that over 50–60 years, the amount of loose soil material on such terraces increased by 2-3 times on average (Borisov et al. 2016; Pinskoy et al. 2023).

Fig. 1a. Abandoned narrow-strip terraces. Interior Dagestan (Photo courtesy of I. Idrisov.)

Fig. 1b. Terraces with cabbage fields. Levashinsky district, Dagestan (Photo courtesy of Sh. I.Sharipov. After Gracheva, Idrisov, 2021)

In the 1930s, the Soviet authorities initiated the construction of new terrace complexes, however many of the old terraces had already been abandoned by that time. From the 1960s to the end of the 1980s, terrace farming ceased in many mountainous areas of Dagestan. According to experts from the Ministry of Agriculture of Dagestan, no more than 20% of terraced lands are currently used in crop production, and only those located near villages and roads no higher than 1500–1800 m above sea level. Many terraces serve only as pastures. At the same time, in the areas of cabbage farming and in the southern areas of horticulture and viticulture, especially in the Derbent area, more than 30% of terraced land is used[1].

While the old terraces of Dagestan are mostly well preserved and show no signs of destruction, a new cycle of terrace construction has begun in recent years for vineyards and intensive orchards (Gracheva et al. 2023). However, when comparing ancient and modern terraces, it turned out that ancient terraces, built by hand and carefully cultivated over centuries, are much more resistant to erosion than bulldozer and excavator terraces (Boziev 2008). The same results were obtained from a study of terraces built for vineyards using machinery in one of the provinces of Spain. It turned out that one heavy rain was enough for the terrace to slide and destroy the plantings of the lower third of the slope (Ramos et al. 2007).

Currently, the terraced lands of Dagestan and the remaining knowledge about terrace farming are not fully used. We seek to answer if the abandoned terraced lands will be in demand with new agricultural trends driven by the need to adapt to climate change.

STUDY AREA AND METHODS

Study area. The Republic of Dagestan lies on the eastern end of the northern flank of the Greater Caucasus along the western shore of the Caspian Sea. With an area of 50,300 km^2, Dagestan is the largest of the seven republics of the North Caucasus; it extends from north to south for 405 km and a latitude of about 213 km (Fig. 2).

[1] *Estimates from our field observations confirmed by local authorities.*

Fig. 2. Dagestan. Key study districts of Mountain Dagestan: 1 – Khunzakhsky, 2 – Gunibsky, 3 – Levashinsky, 4 – Akushinsky, 5 – Charodinsky, 6 – Laksky, 7 – Kulinsky, 8 – Agulsky (map content prepared by authors[2])

The southern half of Dagestan lies in the Caucasus Mountains, and the southern border runs along the Main Caucasus Range. The highest peak here is Mount Bazarduzu (4466 ma.s.l.) on the border with the Azerbaijan Republic. In the north lies a huge territory of steep mountain ranges and plateaus with deep river canyons, called Mountain Dagestan, or Inland Dagestan. In central and southern parts, heights are from 900–1000 m to 3000 and more than 4000 m. In the northwest, the ridges with heights greater than 2000 m separate Dagestan from the mountains of Chechnya. To the north and northeast, mountains decrease to 600–1000 m, forming a chain of foothills. The vast dry steppe and semi-desert Caspian Lowland extend to the north of the Sulak River.

The climate of Dagestan as a whole is temperate continental, dry and semi-dry in the lowlands, semi-dry in the inner valleys, and with a gradual increase in humidity with height. According to Akaev et al. (1996), the highlands with permanent snow cover have a cold climate without a dry season. These characteristics coincide with the Köppen-Geiger classification (Peel et al. 2007), according to which the climate of Dagestan belongs to two classes, moderate and cold. Foothill ridges, creating a "rain shadow" from the Caspian Sea and northern moisture-containing air currents, protect Inland Dagestan in the east and northeast; from the south and southwest it is fenced off by the spurs of the Greater Caucasus (Akaev et al. 1996). Some climatic data for Eastern Caucases obtained by ERA5-Land reanalysis are shown in Table A.1 in Appendix A.

The total population size of Dagestan exceeds 3,2 million people. Compared to other regions of the North Caucasus, Dagestan is distinguished by high population density in the mountainous areas[3] (about 50 people/km2); more than half of the region's rural population lives here (Imangulov & Safronov 2023). 70% of all Dagestan settlements are mountain villages; most of them – about 800 – are located at the altitudes between 1000 and 2000 m (Muduev 2022).

About 42% of Dagestan's agricultural land lies in the mountains. More than half of them are pastures and hayfields; the rest are arable lands and perennial plantations – orchards and vineyards. About 80% of agricultural production comes from small family farms, the share of which in the mountains is more than 90%[4]. In addition to livestock farming, which increases with altitude, crop farming plays a significant role. The most common crops in Mountain Dagestan are traditional horticulture, which includes apricot, peach, plum, and cherries, as well as the cultivation of cabbage, potatoes, and, in recent years, tomatoes. It is known that back in the mid-19th century

[2] *Map source: Russia_Dagestan_location_map.svg, https://commons.wikimedia.org/w/index.php?curid=14036356*

[3] *Territories above 500 m above sea level are considered mountainous, according to the Mountain Law of Dagestan (2010). https://docs.cntd.ru/document/895279692 (accessed 17.05.2024).*

[4] *Rosstat. (2022). Agricultural Micro Census 2021. https://rosstat.gov.ru/folder/75792 (accessed 17.05.2024) (in Russian).*

there were about 1,500 orchards in the Derbent area (Basiev et al. 2016). Crop production is concentrated mainly on agricultural terraces, currently used, as mentioned above, near roads and villages, in an altitude range not exceeding 1800 m above sea level.

Methods. We conducted our study in 2022-2023, which involved investigating climatic trends, conducting field observations, and conducting exploratory surveys with local residents and officials (purposive sampling). We chose eight Dagestan administrative districts (see Fig. 2) as case study areas because they are in the middle of Mountain Dagestan and have different average elevations, areas, populations, and main crops: Khunzakhsky, Levashinsky, Laksky, Charodinsky, Gunibsky, Akushinsky, Kulinsky, and Agulsky.

Climate change investigation. We relied on our previous study of climate change in the Eastern Caucasus (41°–45° N, 45°–49° E) over the past 20 years (Gracheva et al. 2023) by extending it with four other mountain districts. Based on high-resolution (0.1° × 0.1°) reanalysis data from ERA5-Land (Hersbach et al. 2023), we looked at how average annual, summer, and winter temperatures and precipitation changed at different elevations from 2011 to 2020 compared to 2000 to 2010. Since the article focuses on the population adaptation to modern climate change, a shorter period (2000–2020 – 21) was chosen, divided into 2 decades. We paid special attention to the sum of average daily temperatures exceeding 10°C (the so-called active temperatures), which characterizes the biological minimum temperature required for plant growth (Losev 1994).

Field observations and exploratory surveys. Our field observations included several car trips in July 2022 and September 2023 which covered selected districts and adjacent mountain areas. Particular attention was paid to possibly new agricultural activities and the use of agrarian terraces.

During the field trips, we conducted 30 informal exploratory interviews with local residents and administrations (purposive sampling). The interviews aimed at obtaining first insights relating to local stakeholders' views on climate change, its impact on agricultural activities including the use of terraces, possible adaptation options, and growing tourism activities. Conversations took place in four districts differing in altitude (Khunzakhsky, Levashinsky, Laksky, and Charodinsky) with representatives of local authorities (9) and local residents (21) including farmers (17), schoolteachers (2), street fruit sellers, and guesthouse employees. The age of the participants ranged from 30 to 55; there were 20 men and 10 women. All respondents had their own land plots and were involved in farming.

We also sought information on agricultural development from municipal authorities in four other districts, namely Gunibsky, Akushinsky, Kulinsky, and Agulsky. Additionally, we participated in a working meeting of the Public Chamber of Dagestan in July 2022, where representatives from 33 mountain municipalities discussed the social and economic issues facing these areas. Valuable information on adaptation to climate change in agriculture was obtained during informal meetings with government officials and two businesspersons who produced greenhouse equipment and represented a seed company. We also analyzed official documents and information from official websites of the Dagestan government, municipalities, and regional media.

RESULTS AND DISCUSSION

Observed trends in changing climate. Our previous assessment of the trends in climate parameters in the eastern part of the North Caucasus showed an increase in summer, winter, and average annual temperatures over the period of 2000–2020 while precipitation had negative annual and seasonal trends, especially noticeable recently (2011–2020) (Gracheva et al. 2023). The most marked increase in temperatures was in the middle mountains, at altitudes from 500 to 2000 m above sea level, in the most populated and developed areas (Table 1). In general, the mountains of the Eastern Caucasus and Dagestan in particular are becoming warmer and drier, as it is happening in many other mountain regions of the world (Beniston and Stoffel 2014, 2016).

In our study area, average annual temperatures were increasing by approximately 0.4–0.5°C per 10 years, while annual precipitation was noticeably decreasing: by 50–60 mm in 10 years (Table 1). At all altitudes, we observed an increase in the sum of active temperatures: by 89°C per decade above 3500 m above sea level and by 148–155°C at altitudes of 500–2000 m above sea level (see also Table A.1). The increase in this parameter with altitude indicates the possibility of expanding the areas of some agricultural crops.

Local views on climate change and adopted adaptation strategies: mountain terraces as a land resource. Much to our surprise, we had very similar responses to the questions in the interviews, which made it easier to reconstruct common local opinions regarding climate change, its impacts on living in the mountains, and the future of agricultural terraces. These narratives are summarized in Table A.2 in Appendix A. They reveal climate-induced risks, although not always explicitly linked to climate change, as well as the adopted adaptation strategies by respondents. Notably, the answers from the officials were in line with those from farmers: many members of the administration came from mountain villages and knew the local reality well.

According to the interviews, the most visible and crucial effect of climate change in Mountain Dagestan is the growing water scarcity caused by both the decrease in precipitation and the reduction of the snow cover. For example, 160 springs that fed the vegetable gardens, orchards, and livestock have disappeared in the Khunzakhsky district alone. Water deficit forces farmers to drill deep wells and even to purchase and transport water in tanks from the canal running through the Caspian Lowland. Farmers also note a shift in seasons, with a delay in autumn and spring and a shorter winter season overall. Due to the unpredictability of the weather, especially in spring and early summer, it is often impossible to apply traditional planting dates.

Previously, we identified three adaptation strategies adopted by farmers: switching to more resistant crops, intensive orchards, and greenhouse construction (Gracheva et al 2023). Mountain terraces are seen as a major land resource to support existing agricultural activities as well as to expand agriculture to new areas and to higher altitudes. Excavators made it easier to build new terraces, even though they could only restore and use terraces close to roads.

Temperature fluctuations and lack of moisture force farmers to switch to new, more resistant crop varieties. The challenge has required the cooperation of farmers with breeding institutes and seed enterprises, and they responded effectively due to the support of the

Table 1. Some data on the study municipal districts (official data) and differences in climate characteristics in 2011–2020 compared to 2000–2010, Dagestan (author's calculations using ERA5-Land data, Hersbach et al. 2023)

Municipal district	Altitude range, m.a.s.l.	Area sq.km	Population people (2021)	Agri cultural land, ha	Cropland, ha	Δt °C*	Δp mm**	ΔΣT>10 °C ***	ΔHTC****	Main crops
Khunzakhsky	1500–2000	552	31000	108200	9000	0.39	–56	157	–0.02	Fruits, legumes, vegetables
Gunibsky	1500–2100	609	25800	158300	7000	0.40	–59	155	–0.05	Fruits, vegetables
Levashinsky	1200–1500	813	80400	78526	14200	**0.53**	–65	**181**	–0.06	Cabbage, fruits, vegetables
Akushinsky	1300–2500	622	59000	62300	20600	0.43	–59	144	–0.08	Cabbage, potatoes, vegetables
Laksky	1400–2200	700	12000	104800	4400	0.33	–52	112	–0.07	Potatoes, vegetables, fruits
Charodinsky	2000–3000	894	13600	131300	760	0,34	–47	138	–0.03	Potatoes, vegetables
Kulinsky	2000–3000	651	10400	120924	2909	0,44	–82	151	–0.07	Potatoes, vegetables
Agulsky	2000–3000	793	10400	70500	1200	0,36	–65	132	–0.04	Potatoes, vegetables

Significant changes are highlighted in bold.
* Δt – the difference in annual temperature values between the periods 2000–2020 and 2011–2020 at altitudes of 1000–2000 m a.s.l.
** Δp – the difference in annual precipitation values between the periods 2000–2020 and 2011–2020 at altitudes of 1000-2000 m a.s.l.
*** ΔΣT >10 – the difference in annual sum of temperatures >10°C between periods 2000–2020 and 2011–2020 at altitudes of 1000–-2000 m a.s.l.
**** ΔHTC – the difference in hydrothermal coefficient (HTC = p × 10 / ∑ t>10) between the periods 2000–2020 and 2011–2020 at altitudes of 1000-2000 m a.s.l.

administration[5]. Selected resistant varieties and hybrids, including local varieties, have made it possible to preserve and expand terrace cabbage plantations, although the problem of water supply remains tense.

The need for greenhouses has arisen in recent years due to the increasing unpredictability of spring and early summer weather and the increasing frequency of spring frost and summer hail. In a short time, greenhouses occupied more than 700 hectares in the mountains, located on terraces near villages, especially on the southern mountain slopes (Dagpravda 2022), and this area is growing every year. The demand for greenhouses caused a sharp emergence of industry producing modern greenhouse equipment.

Some farmers are starting to look for additional opportunities to maintain income and are turning to intensive orchards (see Table A.2; personal communications). Development of intensive and super-intensive orchards is a direct response to climate change and a way to support mountain agriculture. Intensive orchards are especially relevant for the Eastern Caucasus and the Lesser Caucasus with a water scarcity. A case in point is Armenia, where planting intensive orchards is considered one of the ways to increase the resilience of rural areas in the face of climate change[6]. Intensive orchard technologies were developed primarily to maximize yields due to planting density (Barritt and Van Dalfsen 1992). In recent decades, such a property of intensive planting as reducing the vulnerability of trees to lack of moisture and sudden temperature changes has become very important (Palese et al. 2010; Aznar-Sánchez et al. 2011). Although intensive orchards require large investments in infrastructure and plant nurseries (Shakhmirzoev et al. 2017), interest in them quickly spread widely among small family farms in Mountain Dagestan. In response, nurseries and training centers for farmers appeared (Muduev 2022) (Fig. 3). Currently the area of intensive and super-intensive orchards in the region is more than 4000 ha and grows rapidly due to the renewal of old terraces and newly built ones (official reports[7]). The area of intensive orchards is expanding due to the conversion of the part of cabbage plantations to fruit production (information from a regional administration expert). The scale of these transfers has not yet been assessed, and there is no data on the area of new terraces.

Currently, in addition to the orchards, vineyards are being restored and planted on the terraces. New terraces are built using excavators, usually on accessible mountain slopes near roads. As mentioned, new terraces may not be resistant to erosion and sliding. Strengthened control will

[5] Riadagestan. (2022). White cabbage seed production is revived in Dagestan. https://riadagestan.ru/news/the_government_of_the/v_dagestane_vozrozhdaetsya_semenovodstvo_belokochannoy_kapusty/ (accessed 5.11.2022) (in Russian).
[6] MRD Talk1. (2022). Climate Change Adaptation in Mountains. https://www.mrd-journal.org/?mrd-talks=climate-change-adaptation-in-mountains-how-to-close-the-gap-between-policies-and-local-realities (accessed 30.06.2022).
[7] Fertilizer Daily (2022). Horticulture is developing intensively in Dagestan. https://www.fertilizerdaily.ru/20220531-v-dagestane-intensivno-razvivaetsya-sadovodstvo/ (accessed 11.11.2022) (in Russian).

Fig. 3. Agronomist (left) trains farmers in planting intensive orchards (Photo courtesy of Sh. Muduev)

be required, including over the safety of adjacent roads, especially as natural processes become extreme.

Adaptation to climate change includes not only actions taken to reduce existing or potential risks but also taking advantage of opportunities associated with climate change[8]. This opportunity could be the expansion of orchard areas above the altitude limits of their usual growth due to an increase in heat supply and, above all, an increase in the sum of active temperatures (Losev 1994). The Botanical Garden of Dagestan has already planted local fruit varieties on terraces up to 2000 m above sea level (Asadulaev and Magomedmirzaev 2018).

Adaptation initiatives of the rural mountain population are supported by the Program for the Socio-Economic Development of Mountain Territories developed by scientists of Dagestan and adopted by authorities. The Program includes financial support of small mountain farms by subsidies and grants[9]. This is an effective example where initiatives from below ("bottom-up") were supported by decisions from above ("top-down") (Eicken et al. 2021). However, the program does not include the revival of terraces, leaving it to the discretion and responsibility of farmers. To introduce the huge land resource of terraces into the economy, a program for inventorying terraces and determining the possibility of their use for different crops is necessary.

Agricultural terraces as cultural heritage and tourist sites. Among the views on the mountain terraces, there is the idea of terraces as the cultural heritage of mountain peoples. In our interviews, this issue was raised primarily by officials and public figures (see Table A.2).

Tourism in Dagestan has been booming in recent years: in 2022, more than 1.5 million tourists visited the republic (Mintourism 2023). In addition to popular tourist sites, agricultural terraces can be a "calling card" of Dagestan (Fig. 4). Educational and scientific tourist programs should incorporate the history of their creation, their role in the resilience of mountain communities, and their value as sources of scientific information. The construction and further maintenance of the terraces was a labor-intensive and lengthy process, requiring the joint efforts of many people. Thus, terraces are witnesses to the solidarity of community, concern for its stable existence, the transfer of knowledge and skills from generation to generation, and respect for the achievements of predecessors (Aglarov 1986; Magomedkhanov et al. 2022).

While climate change, i.e., water scarcity, may make it difficult to farm in the mountains, tourism becomes an additional source of income for farmers and supports agriculture by adapting agricultural products to the requirements of tourism, as it has been seen in other parts of the world (Debarbieux et al. 2014).

Agricultural terraces are sources of scientific information about natural changes and the history of society (Aglarov 1986; Kiesow, Bork 2017). During the construction of the terraces, wood remains and roots were burned or buried, and thus a valuable paleoarchive was created, storing information about the natural conditions at the time of the terrace building. Unfortunately, this archive is still almost unclaimed in Dagestan. Moreover, some methods of terrace formation have caused scientific confusion. To compact the terrace, a mountain stream was sometimes directed onto it; the water leveled and compacted the soil, left sand and small pebbles in it, and filled the retaining wall with stone material, strengthening it (Aglarov 2016). For researchers, the presence of pebbles sometimes serves as a reason to classify such terraces as river or lake terraces, which significantly confuses the natural history of the region (according to discussions at scientific conferences).

Agricultural terraces have become special multifunctional landscapes, integral elements of geodiversity, influencing spatial patterns and the functioning of modern natural ecosystems in Dagestan, and forming a unique aesthetic appearance of mountain slopes. Including terraces as a tourist attraction could increase interest in the local landscape and its history and may also indirectly serve to strengthen the resilience of local communities.

[8]*UNFCC. (2023). United Nations Framework Convention on Climate Change. Introduction. https://unfccc.int/topics/adaptation-and-resilience/the-big-picture/introduction (accessed 17.05.2024).*

[9]*Program. (2020). On approval of the state program of the Republic of Dagestan «Socio-economic development of mountain territories of the Republic of Dagestan». https://docs.cntd.ru/document/561752993 (accessed on 8 August 2022) (in Russian).*

Fig. 4. Old agricultural terraces in Khunzakhsky district, Dagestan. Photo by A. Sheludkov

CONCLUSION

Climate changes add new risks to the vulnerable mountain environment and livelihood of mountain communities and reduce the resilience of mountain territories. In the Eastern Caucasus and, in particular, in Dagestan, trends in climate parameters show gradual warming and aridization. The population response to these processes in the mountains of Dagestan is almost the same as is observed in many mountain regions of the world (Adler 2022; Debarbieux et al 2014; Hussein et al 2021; Ponce 2020). People are adapting to climate change by changing agricultural ways, trying to solve water problems, and combining farming with tourism.

In the face of climate change, there is a noticeable trend in Dagestan toward the involvement of agricultural terraces as a land resource. Restoring terrace farming is in line with mountain agriculture by preventing erosion and conserving soil moisture while water resources are gradually reduced (FAO 2000; Dorren and Rey 2004). Terraces regulated the relationship between the mountain community and the environment, maintaining land productivity, protecting from dangerous natural processes, and limiting land conflicts that were inevitable due to a shortage of land resources in the mountains.

Building resilience in mountain communities in the face of climate change involves multiple actors. Horizontal knowledge transfer plays a huge role here. It enables the dissemination of best practices among farmers, involves scientific organizations such as the experimental stations for new varieties of agricultural plants, and gives impetus to the development of supporting industries such as producing greenhouse equipment. Yet there is also a great role for local and regional authorities, which can support local initiatives. By now, the Dagestan authorities have not yet included terrace farming in the supporting programs, and this issue remains the responsibility of farmers. Researchers are facing increasing importance in inventorying terraces, assessing the agronomic value of soils, and determining the economic feasibility of terrace reclamation.

The agricultural terraces of many mountainous regions can be considered as genius loci, the "genius of the place", which created life-supporting environment and the unique appearance of the territory. The inclusion of terraces in the list of tourist sites, as in many mountainous regions of the world, will increase interest in scientific tourism and, in general, the interest in the local landscape that stores information about the history of nature and societies of the mountains of Dagestan.

REFERENCES

Adler C., Wester P., Bhatt I., Huggel C., Insarov G.E., Morecroft M.D., Muccione V., Prakash A. (2022). Cross-Chapter Paper 5: Mountains. In: Climate Change 2022: Impacts, Adaptation and Vulnerability. Contribution of Working Group II to the Sixth Assessment Report of the Intergovernmental Panel on Climate Change. Cambridge, UK and New York, NY, USA: Cambridge Univ. Press, 2273-2318, DOI: 10.1017/9781009325844.022.

Aglarov M.A. (1986). Terrace Agriculture of Dagestan (Issues of Origin, Cultural Typology and Social Role of the System). Studia Praehistorica, 8, 50-62 (in Russian).

Aglarov M.A. (2016). Once More about Agricultural Terraces of Dagestan. Vestn. Dagest. Nauch. Tsentr., 62, 30–53 (in Russian).

Ahouissoussi N., Neumann J.E., Jitendra P.S., editors. (2014). Building Resilience to Climate Change in South Caucasus. Agriculture. Washington, DC, USA: The World Bank, 9–11.

Akaev B.A., Ataev Z.V., Gadzhieva Z.Kh. et al. (1996). Physical Geography of Dagestan: Textbook. Moscow: Shkola Publ. (in Russian).

Asadulaev Z.M., Magomedmirzaev M.M. (2018). Mountain Botanical Garden of the Dagestan Scientific Center of the Russian Academy of Sciences. Makhachkala: ALEF Publ. (in Russian).

Assessment. (2022). Third Assessment Report on Climate Change and Its Consequences on the Territory of the Russian Federation. General Summary. St. Petersburg, Russia: Naukoemkie Tekhnologii Publ. (in Russian).

Aznar-Sánchez J.A., Emilio Galdeano-Gómez E., Juan C., Pérez-Mesa J.C. (2011). Intensive Horticulture in Almería (Spain): A Counterpoint to Current European Rural Policy Strategies. Journal of Agrarian Change, 11(2), 241-261.

Barritt B.H., Van Dalfsen K.B. (1992). Intensive Orchard Management : A Practical Guide to the Planning, Establishment, and Management of High Density Apple Orchards. Yakima, WA, USA: Good Fruit Grower.

Basiev S.S., Bekuzarova S.A., Chshieva M.Ch., Ayskhanova E.S. (2016). Agriculture History in the North Caucasus. Vestnik Vladikavkazskogo Nauchnogo Tsentra, 16(1), 43-50 (in Russian with English summary).

Beniston M, Stoffel M. (2014). Assessing the Impacts of Climatic Change on Mountain Water Resources. Sci. Total. Environ., 493, 1129-1137, DOI: 10.1016/j.scitotenv.2013.11.122.

Beniston M, Stoffel M. (2016). Rain-on-Snow Events, Floods and Climate Change in the Alps: Events May Increase with Warming up to 4 °C and Decrease thereafter. Sci. Total. Environ., 571, 228-236.

Birthal P.S., Hazrana J. (2019). Crop Diversification and Resilience of Agriculture to Climatic Shocks: Evidence from India. Agricultural Systems, 173, 345-354, DOI: 10.1016/j.

Borisov A.V., Kashirskaya N.N., El'tsov M.V., Pinskoy V.N., Plekhanova L.N., Idrisov I.A. (2021). Soils of Ancient Agricultural Terraces of the Eastern Caucasus. Eurasian Soil Science, 54(5), 665-679, DOI: 10.1134/S1064229321050045.

Boziev T.Kh. (2008). Terrace Farming in the Mountain Conditions of Kabardino-Balkaria. International Agricultural Journal, 4, 66-67 (in Russian with English summary).

Cicinelli E., Caneva G., Savo V. (2021). A Review on Management Strategies of the Terraced Agricultural Systems and Conservation Actions to Maintain Cultural Landscapes around the Mediterranean Area. Sustainability, 13, 4475, DOI: 10.3390/su13084475.

Dagpravda (2022). Opening of the closed ground. Available at: https://dagpravda.ru/ekonomika/otkrytie-zakrytogo-grunta-3/ [Accessed 17 May 2024] (in Russian).

Debarbieux B., Oiry Varacca M., Rudaz G., Maselli D., Kohler T., Jurek M., editors. (2014). Tourism in Mountain Regions: Hopes, Fears and Realities. Sustainable Mountain Development Series Geneva, Switzerland: UNIGE, CDE, SDC.

Dercon G., Deckers J., Govers G., Poesen J., Sanchez H., Vanegas R., Ramirez M., Loaiza G. (2003). Spatial Variability in Soil Properties on Slow-Forming Terraces in the Andes Region of Ecuador. Soil Tillage Res., 72, 31-41.

Dorren L., Rey F. (2004). A review of the effect of terracing on erosion. In: Briefing papers of the 2nd SCAPE Workshop, Cinque Terre Italy. Citeseer, 97–108.

Eicken H., Danielsen F., Sam J.M., Fidel M., Johnson N., Poulsen M.K. (2021). Connecting Top-Down and Bottom-Up Approaches in Environmental Observing. BioScience, 71, 467-483.

FAO. (2000). Manual on Integrated Soil Management and Conservation Practices. FAO Land and Water Bulletin 8, Rome, Italy.

Folke C., Carpenter S., Elmqvist T., Gunderson L., Holling C.S., Walker B. (2002). Resilience and Sustainable Development: Building Adaptive Capacity in a World of Transformations. AMBIO: A Journal of the Human Environment, 31(5), 437-440, DOI: 10.1579/0044-7447-31.5.437.

Gauci R., Schembri J.A., editors. (2019). Landscapes and Landforms of the Maltese Islands. Springer, Cham.

Gracheva R.G., Idrisov I.A. (2021). Agricultural terrace complexes of mountainous regions: cultural and historical heritage and an integral element of the landscape. Voprosy Geografii, 153, 69-89 (in Russian).

Gracheva R.G., Vinogradova V.V., Muduev Sh.S. (2023). Adaptation of the Activities of the Population of the Mountain Territories of Dagestan to Climate Change: Trends in Agriculture. Reg. Res. Russ., 13, S127-S140, DOI: 10.1134/S2079970523600191.

Grove A.T., Rackham O. (2003). The Nature of Mediterranean Europe. An Ecological History. London: Yale University Press.

Gruneis H., Penker M., Höferl K.M., Schermer M., Scherhaufer P. (2018). Why do We not Pick the Low-Hanging Fruit? Governing Adaptation to Climate Change and Resilience in Tyrolean Mountain Agriculture. Land Use Policy, 79, 386-396. DOI: 10.1016/j.landusepol.2018.08.025.

Hersbach H., Bell B., Berrisford P., Biavati G., Horányi A., Muñoz Sabater J., Nicolas J. et al. (2023). ERA5 monthly averaged data on single levels from 1940 to present. Copernicus Climate Change Service (C3S) Climate Data Store (CDS). DOI: 10.24381/cds.f17050d7.

Hock R., Rasul G., Adler C., Cáceres B., Gruber S., Hirabayashi Y., Jackson M. et al., editors. (2019). IPCC Special Report on the Ocean and Cryosphere in a Changing Climate, 133–202.

Imangulov L.R., Safronov S.C. (2023). Rural Dagestan: All-Russian Trends and Regional Features of Development. Izv. Akad. Nauk, Ser. Geogr., 87(7), 963-976 (in Russian with English summary), DOI: 10.31857/S2587556623070099.

Inbar M., Llerena C.A. (2000). Erosion Processes in High Mountain Agricultural Terraces in Peru. Mt. Res. Dev., 20(1), 72-79, DOI: 10.1659/0276-4741(2000)020[0072:EPIHMA]2.0.CO;2

Kiesow S., Bork H.-R. (2017). Agricultural Terraces as a Proxy to Landscape History on Madeira island. Portugal Historia, 71, 127-152.

Kohler Th., Giger M., Hurni H., Ott C., Wiesmann U., von Dach S.W., Maselli D. (2010). Mountains and Climate Change: A Global Concern. Mt. Res. Dev., 30(1), 53-55, DOI: 10.1659/MRD-JOURNAL-D-09-00086.1.

Kozachek A., Mikhalenko V., Masson-Delmotte V., Ekaykin A., Ginot P., Kutuzov S., Legrand M., Lipenkov V., Preunkert S. (2017). Large-Scale Drivers of Caucasus Climate Variability in Meteorological Records and Mt El'brus Ice Cores. Clim. Past, 13, 473-489, DOI: 10.5194/cp-13-473-2017.

Losev A.P. (1994). Practicum on Agrometeorological Support of Crop Production. St. Petersburg: Gidrometeoizdat Publ. (in Russian).

Magomedkhanov M.M., Sadovoy A.N., Ataev Z.V., editors. (2022). Ethnoculture of Mountain Development: North Caucasus. Makhachkala, Russia: Alef Publ. (in Russian).

Mintourism. (2023). Results of Activities. Available at: https://mintourismrd.ru/itogi-dejatelnosti-ministerstva-po-turizmu-i-narodnym-hudozhestvennym-promyslam-za-2020-2022-gody-i-za-1-e-polugodie-2023-goda/ [Accessed 11 Sep. 2023] (in Russian).

Muduev Sh S. (2022). Results of the Implementation of the State Program "Socio-Economic Development of Mountain Territories of the Republic of Dagestan» for 2019–2021 and Prospects for Expanding State Support". MEPS: Management, Economics, Politics, Sociology, 1, 53-59 (in Russian with English summary), DOI: 10.24412/2412-2025-2022-1-53-59.

Palese A.M., Nuzzo V., Favati F., Pietrafesa A., Celano G. et al. (2010). Effects of Water Deficit on the Vegetative Response, Yield and Oil Quality of Olive Trees (Olea europaea L, cv Coratina) Grown under Intensive Cultivation. Sci. Horticulturae, 125, 222-229.

Peel M.C., Finlayson B.L., McMahon T.A. (2007). Updated World Map of the Köppen-Geiger Climate Classification. Hydr. Earth Syst. Sci., 11, 1633-1644.

Pinskoy V.N., Idrisov L.A., Kashirskaya N.N., Eltsov M.V., Borisov A.V. (2023). Soils of Agricultural Terraces on Clay Shales in the Mid-Mountain Zone of the Eastern Caucasus. Eurasian Soil Sci., 5, 695-704, DOI: 10.1134/S1064229323600227.

Ponce C. (2020). Intra-Seasonal Climate Variability and Crop Diversification Strategies in the Peruvian Andes: A Word of Caution on the Sustainability of Adaptation to Climate Change. World Dev., 127, 104740, DOI: 10.1016/j.worlddev.2019.104740.

Ramos M.C., Cots-Folch R., Martínez-Casasnovas J.A. (2007). Sustainability of Modern Land Terracing for Vineyard Plantation in a Mediterranean Mountain Environment – the Case of the Priorat Region (NE Spain). Geomorphology, 86(1-2), 1-11, DOI: 10.1016/j.geomorph.2006.08.004.

Salukvadze G., Backhaus N. (2020). Is Tourism the Beginning or the End? Livelihoods of Georgian Mountain People at Stake. Mt. Res. Dev., 40(1), R28, DOI: 10.1659/MRD-JOURNAL-D-19-00078.1

Shakhmirzoev R.A., Dogeev G.D., Shakhmirzoev A.R. (2017). Development of intensive horticulture in the Republic of Dagestan. Sb. Nauch. Tr. GNBS, 144(2), 51-54 (in Russian with English summary).

Sheludkov A., Vinogradova V. (2024). Population Exposure to Heat Waves in Russian Regions, According to Climate Change Scenarios for the Mid-21 Century. Geo Journal, 89, 47, DOI: 10.1007/s10708-024-11057-y.

Shvarev S.V., Kharchenko S.V., Golosov V.N., Uspenski M.I. (2021). A Quantitative Assessment of Mudflow Intensification Factors on the Aibga Ridge Slope (Western Caucasus) over 2006–2019. Geogr. Nat. Resour., 42, 122-130, DOI: 10.1134/S1875372821020128.

Skripnikova M.I. (2007). Man-Made Terraced Agroecosystems of Eurasian Mountain Landscapes. Vestn. Altai. Gos. Agrar. Univ., 37(10), 35-45 (in Russian with English summary).

Solomina O., Jomelli V., Bushueva I.S. (2024). Holocene Glacier Variations in the Northern Caucasus, Russia. In: European Glacial Landscapes, Chapter 19, 353-365.

Spenser J.E., Hale G.A. (1961). The Origin, Nature, and Distribution of Agricultural Terracing. Pacific Viewpoint, 2(1), 1-40. DOI: 10.1111/apv.21001.

Stanchi S., Freppaz M., Agnelli A., Reinsch T., Zanini E. (2012). Properties, Best Management Practices and Conservation of Terraced Soils in Southern Europe (from Mediterranean areas to the Alps). A Review. Quat. Int., 265, 90-100.

Tarolli P., Preti F., Romano N. (2014). Terraced Landscapes: From an Old Best Practice to a Potential Hazard for Soil Degradation due to Land Abandonment. Anthropocene, 6, 10-25.

Tashilova A.A., Ashabokov B.A., Kesheva L.A., Teunova N.V. (2019). Analysis of Climate Change in the Caucasus Region: End of the 20th–Beginning of the 21st Century. Climate, 7(1), 11. DOI: 10.3390/cli7010011.

Tielidze L.G., Nosenko G.A., Khromova T.E., Paul F. (2022). Strong Acceleration of Glacier Area Loss in the Greater Caucasus Between 2000 and 2020. Cryosphere, 16, 489-504. DOI: 10.5194/tc-16-489-2022.

Toropov P.A., Aleshina M.A., Grachev A.M. (2019). Large-Scale Climatic Factors Driving Glacier Recession in the Greater Caucasus, 20th-21st century. Int. J. Climatol., 39(12), 4703-4720. DOI: 10.1002/joc.6101.

Vavilov N.I. (1936). World Experience in Agricultural Development of Highlands. Priroda, 2, 74-84 (in Russian).

Vlasova T., Petrov A.N., Volko, S. (2021). Rethinking Sustainability Monitoring in the Arctic by Linking Resilience and Sustainable Development in Socially-Oriented Observations: A Perspective. Sustainability, 13, 177, DOI: 10.3390/su13010177.

Wyss R., Luthe T., Pedoth L., Schneiderbauer S., Adler C. et al. (2022). Mountain Resilience: A Systematic Literature Review and Paths to the Future. Mt. Res. Dev., 42(2), A23-A36, DOI: 10.1659/MRD-JOURNAL-D-21-00044.1.

Zoumides C, Bruggeman A, Giannakis E, Kyriakou N. (2022). A Future for Mountain Terraces: Experiences from Mediterranean Wineries. Mt. Res. Dev., 42(3), R35-R49, DOI: 10.1659/MRD-JOURNAL-D-21-00031.

APPENDIX A

Table A.1. Changes in temperature (T) and precipitation (P) in 2011–2020 compared to 2000–2010 at different altitudes according to ERA-5 reanalysis data (Hersbach et al. 2023). Eastern Caucasus 41–45° N 45–49° E.

H, m	T average annual, °C			T average summer, °C			T average winter, °C			Σ T > +10°C,			P average annual, mm			P average summer, mm			P average winter, mm		
	2000–2010 1	2011–2020 2	ΔT 2–1	2000–2010 1	2011–2020 2	ΔT 2–1	2000–2010 1	2011–2020 2	ΔT 2–1	2000–2010 1	2011–2020 2	ΔT 2–1	2000–2010 1	2011–2022 0	ΔP 2–1	2000–2010 1	2011–2020 2	ΔP 2–1	2000–2010 1	2011–2020 2	ΔP 2–1
0–500	13.2	13.6	0.4	24.7	25.5	0.7	2.5	2.6	0.1	4240	4360	120	440	397	–43	94	87	–7	97	95	–2
500–1000	10.2	10.7	0.5	20.9	21.5	0.7	–0.6	0.1	0.7	3351	3498	148	876	815	–61	266	248	–18	111	115	4
1000–2000	5.5	6.0	0.4	15.7	16.3	0.6	–4.9	–4.3	0.6	2037	2192	155	1099	1039	–60	426	407	–19	107	110	2
2000–2500	2.8	3.2	0.4	13.0	13.6	0.6	–7.4	–7.0	0.4	1349	1480	130	1051	998	–53	416	395	–21	104	106	2
2500–2800	1.4	1.8	0.4	11.6	12.2	0.6	–8.9	–8.5	0.4	1014	1126	112	1001	959	–42	394	380	–14	104	105	1
2800–3000	0.9	1.3	0.4	11.1	11.8	0.7	–9.3	–8.9	0.4	897	1017	120	946	893	–53	348	324	–24	106	108	2
3000–3500	0.7	1.1	0.4	10.8	11.4	0.6	–9.2	–8.8	0.4	834	936	102	1008	951	–57	384	361	–24	106	107	1
3500–5000	–0.5	–0.1	0.4	9.5	10.2	0.6	–10.5	–10.1	0.4	571	660	89	1063	1002	–62	431	402	–29	102	104	2

Table A. 2. Exploratory interviews: questions and most common opinions

Questions	Most common opinions
Do you/people notice climate change? If yes, which ones?	- "In recent years, farming has become hard. The seasons have shifted, fall is late, little snow, and spring weather is unpredictable". - "The hardest thing is that there is less and less water. Previously, wells were drilled up to 50 m, now up to 250 m and even deeper". - "There is often intense heat. Apricots and apples began to ripen where they had not even bloomed before".
What are you doing to overcome climate challenges? How do you/people adapt?	- "Cabbage requires water. We are forced to buy and transport water in tanks from the Caspian lowland, from the canal". - "I replaced the water supply system with a drip irrigation system, and many people do this". -"We have to change the varieties of cabbage and other vegetables. Now it is possible to buy new varieties or hybrids, they are better than others in temperature changes. There are demonstration sites; you can buy new seeds". - "Now many people are switching to intensive orchards, it is profitable, and they are more resistant to heat. I will wait and see; they say you can get subsidies". -"I have an orchard, it's a family tradition. We have a plot with an intensive orchard, still very young. Indeed they are resistant, but you need to keep a close eye on the spring weather". -"Greenhouses are saving us. You have to invest money, but you don't have to worry about the weather".
Terraces: are they necessary? Do you use them? For what? Do old terraces need to be restored?	-"You see what mountains we have. Many villages stand on old terraces. Cabbage, potatoes, orchards - all on the terraces". -"Where to put greenhouses? On the terraces. Now we are building new terraces for the orchards, using excavators, my family does it". -"I'll plant an intensive orchard on part of the terrace land under cabbage; it's more profitable". -"Not all old terraces can now be used. They are overgrown and expensive to restore. Only those that are close. Not everywhere there are roads". -"These are good pastures; let them remain so, thanks to our ancestors".
Does agriculture provide a sufficient livelihood?	(This is the only question that is answered without much desire). -"If cabbage is bad, potatoes or fruit may be good. Everyone has livestock". -"You can always earn extra money if something goes wrong; in transport, in warehouses..." -"The youth? They will always find money, tourism is nearby".
What is more important for you: tourism or agriculture? For mountainous areas? For Dagestan?	-"There can only be one answer: the main thing in the mountains is agriculture". -"We welcome tourism and welcome tourists. However, we live by agriculture". -"I cannot say the same about my children..."

[5] Riadagestan. (2022). White cabbage seed production is revived in Dagestan. https://riadagestan.ru/news/the_government_of_the/v_dagestane_vozrozhdaetsya_semenovodstvo_belokochannoy_kapusty/ (accessed 5.11.2022) (in Russian).
[6] MRD Talk1. (2022). Climate Change Adaptation in Mountains. https://www.mrd-journal.org/?mrd-talks=climate-change-adaptation-in-mountains-how-to-close-the-gap-between-policies-and-local-realities (accessed 30.06.2022).
[7] Fertilizer Daily (2022). Horticulture is developing intensively in Dagestan. https://www.fertilizerdaily.ru/20220531-v-dagestane-intensivno-razvivaetsya-sadovodstvo/ (accessed 11.11.2022) (in Russian).

Check for updates

CC BY

RESEARCH PAPER

GAMMA-EMITTING ISOTOPES SPECIATION IN FLOODPLAIN SOILS OF THE BALCHUGOVSKAYA CHANNEL TEMPORARY STREAM (THE YENISEI RIVER)

Marya Y. Kropacheva[1*], Anna V. Repina[1], Yulia S. Vosel[1]

[1] Sobolev Institute of Geology and Mineralogy SB RAS, 3, Koptuga ave, Novosibirsk, 630090, Russian Federation

***Corresponding author:** marya@igm.nsc.ru

Received: April 8th 2024 / Accepted: November 27th 2024 / Published: December 31st 2024

https://doi.org/10.24057/2071-9388-2024-3339

ABSTRACT. The paper presents the first data on the ratio of gamma-emitting isotopes (^{137}Cs, ^{152}Eu, ^{154}Eu, ^{60}Co) speciation in the floodplain soil and rhizosphere of floodplain plants in the Balchugovskaya channel. This channel is located in the near impact zone of the Krasnoyarsk Mining and Chemical Combine alongside the Yenisei River. The formation of a temporary stream during high floods affects the spatial distribution of isotope specific activities in the soil and rhizosphere of this area. The gross specific activities of isotopes vary in a very wide range. The highest ones are recorded in the lower outlet of the temporary stream (up to 800 Bq kg^{-1}). The procedure of sequential extraction was applied to obtain data on isotope speciation. The hydrological regime characterized by high floods in this section of the Yenisei River, as well as the biological activity of plants, exerts a noticeable influence on the spatial distribution of isotope specific activities and their speciation ratios. Lower percentages or the absence of mobile forms of isotopes in the plant rhizosphere, as compared to the bulk soil, provide evidence for this. In general, isotopes in the soil and rhizosphere tend to accumulate in the organic and residual fractions. There are noticeably different distributions of isotope speciation in central areas and sides of the temporary stream entrance and outlets. The most diverse speciation patterns were observed for ^{152}Eu and ^{154}Eu isotopes, but under different hydrological conditions.

KEYWORDS: speciation, gamma-emitting isotopes, soil, rhizosphere, the Yenisei floodplain

CITATION: Kropacheva M. Y., Repina A. V., Vosel Y. S. (2024). Gamma-Emitting Isotopes Speciation In Floodplain Soils Of The Balchugovskaya Channel Temporary Stream (The Yenisei River). Geography, Environment, Sustainability, 4(17), 217-222
https://doi.org/10.24057/2071-9388-2024-3339

ACKNOWLEDGEMENTS: This work was supported by a grant from the Russian Science Foundation (project No 23-27-00364). The analytical studies of samples were performed in the Analytical Center for multi-elemental and isotope research SB RAS.

Conflict of interests: The authors reported no potential conflict of interest.

INTRODUCTION

The Yenisei floodplain has been significantly impacted by the Krasnoyarsk Mining and Chemical Combine (KMCC) located in the town of Zheleznogorsk. The main source of this impact were two direct-flow reactors that produced weapons-grade plutonium. The impact on the floodplain biogeocoenosis was significant and was traced all the way to the Kara Sea, where the content of ^{137}Cs in the bottom sediments exceeded global fallout by 4-8 fold (Vakulovsky et al. 1995). When the KMCC direct-flow reactors were turned off in 1991 and 1992, the specific activities of isotopes in the water decreased by a factor of 1000 (Nosov 1996; Nosov et al. 2010). However, the amounts of isotopes in the sediments of the floodplain remained quite high (Linnik et al., 2004; Sukhorukov et al., 2000, 2004).

Radioecological studies in this territory have been conducted over more than 30 years. Part of the research focused on the study of isotope distribution in the Balchugovskaya channel, located in the so-called MCC near impact zone. The floodplain area from the MCC reactor cooling discharge outlet to the Kan River influx into the Yenisei River (~30 km) is considered the latter. The channel has a complex geomorphological structure and hydrological regime (Linnik et al., 2005). Both along the entire Yenisei floodplain and in the Balchugovskaya channel, the riverside zone 5-50 m wide, flooded during floods, exhibits the highest level of isotope contamination (Nosov et al., 1993; Stukin et al., 2002). The isotope distribution in this riverbed section correlated with parameters of hydrological and sedimentation regimes in the 1960-1990s, in particular after the Krasnoyarsk hydroelectric power plant constructed in 1967 (Linnik et al., 2005). Numerous studies have focused on the distribution of isotopes in bottom sediments (Bolsunovsky, 2011; Bolsunovsky and Bondareva, 2007; Bolsunovsky et al., 2021; Bondareva and Bolsunovskii, 2008; Semizhon et al., 2010; Zotina et al., 2014, 2019) of the Balchugovskaya channel.

There were noticeably fewer studies of isotope distribution in floodplain soils. Favorable conditions for the deposition of silt and large amounts of organic matter along the river banks, resulting in a sharp increase in isotope content in floodplain soils, were observed in the Balchugovskaya channel (Korobova et al., 2016; Kuznetsov et al., 1999; Linnik et al., 2005; Linnik et al., 2004). The results of sampling and radiometric mapping at the channel cape led

to the identification of various landscape-radiation sections in this part of the floodplain (Linnik et al., 2004; Sukhorukov et al., 2004). The profiles showed that a noticeable amount of radioactive contamination was contained both in the surface deposits and distributed throughout the soil profile, including the underlying gravel layer. The isotope ratios in floodplain sediments were also used to determine the chronology of floodplain contamination (Linnik et al., 2005; Linnik et al., 2004). Several studies have focused on the distribution of isotopes in the granulometric fractions of floodplain soils (Korobova et al., 2014; Kropacheva et al., 2013; Linnik et al., 2004). Thus, the Balchugovskaya channel represents a complex floodplain segment, which is part of the area where the floodplain biogeocenosis continues to be influenced by the nuclear fuel cycle plant.

In models of isotope migration, the main parameter is the proportion of exchange forms of the isotope in the soil or bottom sediment (Bulgakov et al., 2002; Konoplev, 2020; Mikhaylovskaya et al., 2002). Moreover, studies on isotope migration typically treat the soil as a single entity (Tajima et al., 2022; Tsuji et al., 2016). The soil that is part of the plant's rhizosphere and the soil outside the rhizosphere have different conditions for isotope accumulation, as shown by our monitoring studies in 2003-2016 (Kropacheva et al., 2021; Kropacheva et al., 2011; Kropatcheva et al., 2012). However, samples for them were taken at only one site of the Balchugovskaya channel (Fig. 1a, point 1). The remaining territory has not been covered by studies on the distribution of artificial isotopes in the rhizosphere of floodplain plants.

The aim of the study is the determination of isotope speciations in surface sediments (floodplain soil and plant rhizosphere) of the Balchugovskaya channel. The isotopes ^{137}Cs, ^{152}Eu, ^{154}Eu, and ^{60}Co are analyzed in this study because they are the main gamma-emitting contaminants of the Yenisei River floodplain. The procedure of sequential extraction was applied to obtain data on isotope speciation. Determination of the percentage of mobile speciations of isotopes will allow the assessment of isotope removal from floodplain soil and plant rhizosphere during floods of different intensityintensities. The obtained data can be used in the assessment of secondary isotope pollution of the Yenisei floodplain and modeling of isotope migration in the river system.

MATERIALS AND METHODS

Sampling

The Balchugovskaya channel is an anabranch between the Yenisei eastern bank and Berezovy Island. At a distance of 3.5 km from the entrance to the channel, the riverbed rounds a ledge on the eastern bank (Linnik et al., 2005). During high floods, the water flow goes straight through the ledge, forming two temporary streams (Fig. 1b).

In August 2019 floodplain soils were sampled at nine points: at the entrance to the temporary streams (points 1, 6, 7) and at two outlets, the upper (points 2, 3, 8) and lower (points 4, 5, 9). The depth of sampling (~30 cm) was chosen to capture the entire layer of sedge roots. At each point, a cube of soil with sedge roots (~30 cm^3) was extracted and manually disassembled into plant roots with adjacent rhizosphere and bulk soil. The part of the soil that remained adhered to the roots after shaking the sample was considered a rhizosphere; the rest of the soil was taken as bulk soil (Séguin et al., 2004). The rhizosphere was separated from the roots after drying.

Sequential chemical fractionation

To study the association of isotope to different speciation, sequential extraction procedure were applied to soil and rhizosphere samples using a five-step procedure (Table 1). The procedure has previously been applied in other research projects on floodplain soils and bottom sediments in the KMCC near impact zone. (Bondareva, 2012; Semizhon et al., 2010). However, this is the first case of its application to floodplain soils of the Balchugovskaya channel temporary streams.

The point 7 rhizosphere sample wasn't fractionated because it was already being used to find out ^{90}Sr-specific activities by β-radiometry with radiochemical preparation.

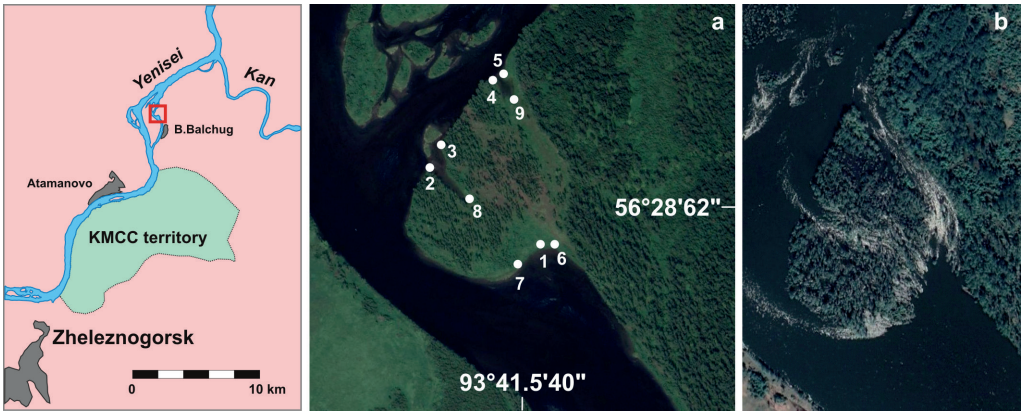

Fig. 1. Balchugovskaya channel: a) sampling scheme (August 2019); b) same place in high flood (June 2021)

Table 1. Schemes of sequential extraction of isotopes from a soil and a rhizosphere

fraction		chemical reagents	mobility	
I	exchangeable ions	CH_3COOH_4 (1M) pH=7	decrease	↓
II	carbonates	CH_3COOH_4 (1M) and HNO_3 pH=5		
III	Fe, Mn oxides and hydroxides	NH_4OH·HCl (0,2M) in CH_3COOH (25%)		
IV	organic matter	H_2O_2 (35%) + HNO_3 (1M) pH 1.5, 85°C		
V	residual solids	-		

Measuring procedure

The specific activity of isotopes was measured by semiconductor gamma spectrometry with lead and tungsten shields on an IFTP DGDK-100V coaxial Ge(Li) detector (Dubna, Russia). The data were processed using the AnGamma software SPC "Aspect", (Dubna, Russia) (SPC "Aspect" 2000). The following gamma-lines were used for isotope detection: 661.66 keV (^{137}Cs), 1173 and 1332 keV (^{60}Co); 344 and 778 keV (^{152}Eu), 1274 keV (^{154}Eu). Measurements lasted from 1 to 24 hours, depending on isotope activity level, to provide a photopeak area accuracy to within 5–10%. The detection limit for ^{137}Cs was from 2 to 5 Bq kg^{-1}. All sample activities were recalculated according to the date of sampling.

The Analytical Center for Multi-Elmental and Isotope Research SB RAS conducted the analytical studies of the samples.

RESULTS AND DISCUSSION

The bulk isotopes specific activities vary in a wide range. The ^{137}Cs exhibit the highest values, ranging from 200 to 800 Bq/kg. The levels of isotopes specific activity in the upper outlet are approximately equal to the ones at the entrance to the temporary stream (^{137}Cs) and in some cases exceed them (^{152}Eu and partially ^{60}Co). The lower outlet has significantly higher bulk isotopes specific activities for almost all isotopes than the upper outlet. This outlet has a higher bed at the turning point, which obviously causes less frequent flooding and no isotope leaching. Higher isotope levels have also previously been recorded at this site, although less contamination corresponded to the higher terrain (Linnik et al., 2005). In general, isotopes in the soil and rhizosphere gravitate toward organic and residual fractions.

The ratio of speciation isotope patterns in soils and rhizospheres at the side points of the temporary stream outlets is about the same. Points 2 and 4 on the left side of the temporary stream outlets are more similar than points 3 and 5 on the right side. The distribution of speciation ^{154}Eu isotope forms in the soil and rhizosphere of the central areas of temporary stream outlets (points 8 and 9) is significantly different. In the upper outlet, the isotope is associated with a significant proportion of carbonates (24-34%). In the lower outlet, it is linked to Fe oxides and hydroxides (30%). The ratio of speciation isotopes on the right side of the temporary stream entrance (point 6) is also noticeably different from typical. Obviously, favorable conditions for sediment accumulation are formed here even at high floods, as indicated by the distribution of the speciation ^{154}Eu isotope. This isotope is equally present in the exchangeable and carbonate fractions in soil, in the exchangeable fraction, the Fe and Mn oxides and hydroxides fraction, and the organic fraction in the rhizosphere. Earlier studies have reported markedly higher densities of isotope contamination at this site (Linnik et al., 2005) than the center (point 1) and left side (point 7) of the entrance to the temporary stream.

Lower levels or lack of isotopes in exchangeable fraction in the rhizosphere compared to bulk soil may be a consequence of uptake of these forms by plant roots. The mobile forms of Eu isotopes in these three points (6, 8, and 9) result from the absence of two typical processes for other points and isotopes: 1) the mobile forms of the isotope are not washed out at low floods; 2) Eu isotopes are not uptaken by plants (Kropatcheva et al. 2012). The lack of ^{60}Co in soil or rhizosphere fractions when its total activities are present (points 1, 5, 6, and 7) indicates that the total activities were measured for an active particle that did not fall into the weighed quantity for sequential extraction technique.

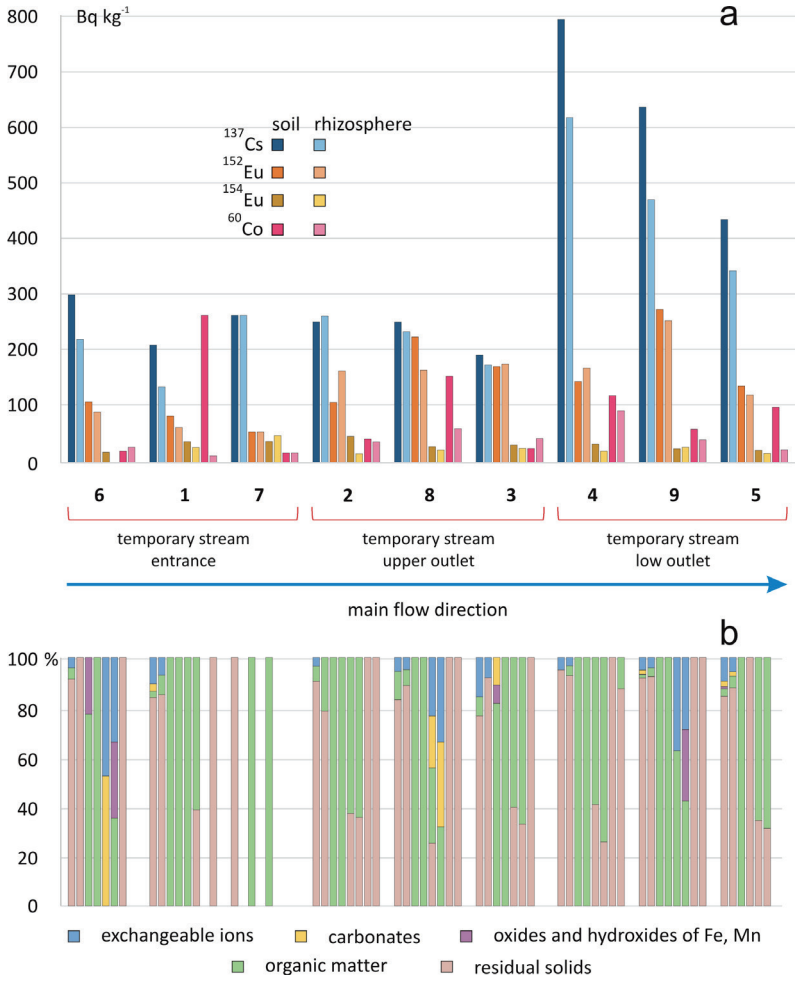

Fig. 2. Isotope specific activity in soil and rhizosphere bulk samples (a) and isotope speciation distribution in the samples (b)

A statistical analysis was conducted based on the obtained data to identify possible correlations between the specific activities of isotopes and their speciation. Since the data samples are not normally distributed, the Spearman rank-order correlation coefficient ρ was used to calculate the correlation coefficient.

The total specific activities of some isotopes had very strong positive (0.75–1.00) and statistically significant ($p<0.05$) correlations with each other. These are ^{137}Cs in the soil and the rhizosphere, ^{152}Eu in the soil and the rhizosphere, ^{152}Eu in the soil and ^{154}Eu in the rhizosphere, ^{154}Eu in the soil, and ^{60}Co in the rhizosphere (Fig. 3). The other ratios, although quite high, are not statistically reliable.

Table 2 shows statistically significant correlations between the specific activities of isotopes in soil and rhizosphere and the percentage of speciation isotopes in soil and rhizosphere.

Very high positive correlations (0.75-1.00) are observed between the specific activities of isotopes in the soil and rhizosphere, between fractions I of soil and rhizosphere, and between fractions IV of soil and rhizosphere (Table 2, Nos. 1, 3, 6). A large R^2 value (0.7436-0.8998) is also characteristic for all these correlations. The R^2 values for many of the ratios (Table 2, Nos. 4, 8–11, and 14) are much lower (0.4094-0.5543), but the correlations are high positive or negative (|0.50 - 0.75|). The remaining ratios (Table 2,

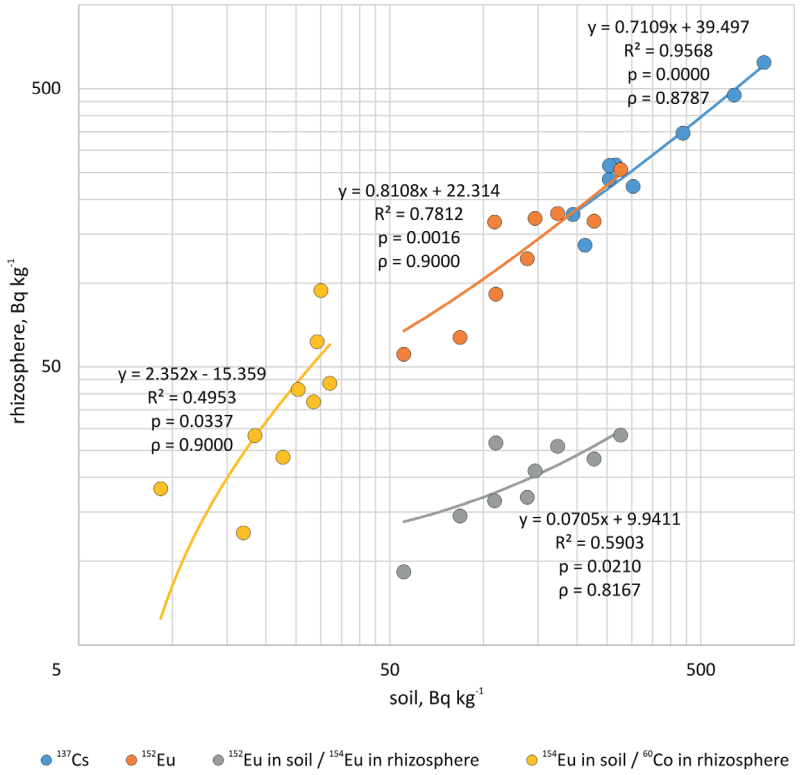

Fig. 3. Correlations between the isotope specific activities in soil and rhizosphere

Table 2. Statistically significant ($p<0.05$) correlations between the specific activities of isotopes and their speciation

No.	Ratios	ρ	R^2	p
1	soil, Bq kg^{-1} vs. rhizosphere, Bq kg^{-1}	0.8657	0.8998	0.0000
2	soil, Bq kg^{-1} vs. V fraction of rhizosphere, %	0.4156	0.2242	0.0062
3	I fraction of soil, % vs. I fraction of rhizosphere, %	0.9345	0.8956	0.0000
4	II fraction of soil, % vs. I fraction of rhizosphere, %	0.6179	0.5409	0.0000
5	I fraction of soil, % vs. III fraction of rhizosphere, %	0.4954	0.7646	0.0000
6	IV fraction of soil, % vs. IV fraction of rhizosphere, %	0.7625	0.7436	0.0000
7	IV fraction of soil, % vs. V fraction of rhizosphere, %	-0.4132	0.3031	0.0011
8	V fraction of soil, % vs. IV fraction of rhizosphere, %	-0.6109	0.4859	0.00001
9	V fraction of soil, % vs. V fraction of rhizosphere, %	0.5320	0.4094	0.00008
10	I fraction of soil, % vs. II fraction of soil, %	0.5660	0.5543	0.00000
11	IV fraction of soil, % vs. V fraction of soil, %	-0.6689	0.5437	0.00000
12	I fraction of rhizosphere, % vs. II fraction of rhizosphere, %	0.4609	0.3299	0.0006
13	I fraction of rhizosphere, % vs. III fraction of rhizosphere, %	0.4939	0.5598	0.00000
14	IV fraction of rhizosphere, % vs. V fraction of rhizosphere, %	-0.6558	0.4916	0.00001

Nos. 2, 5, 7, 12, 13) have medium positive or negative (|0.25 - 0.49|) correlations, with low R^2 values (0.2242-0.5598), except for ratio No. 5 ($R^2 = 0.7646$).

Positive correlations between the states of isotopes in the soil and rhizosphere (specific activities and speciation) indicate similar migration paths of isotopes in these states. According to correlation ratios 1, 3, and 6, it can be asserted that the total migration of isotopes is primarily determined by the behavior of isotopes in exchangeable and organic fractions. The proportions of isotopes found in V fractions (correlation ratio No. 9) determine the isotope migration pattern, which is significantly weaker.

CONCLUSION

The first data on the distribution of ^{137}Cs, ^{152}Eu, ^{154}Co, and ^{60}Co isotopes in the soil and rhizosphere of floodplain plants in the Balchugovskaya channel temporary streams have been obtained. The sequential extraction technique was employed for the first time in the study of these floodplain soils, with the aim of determining isotope speciation in both the soil and the rhizosphere of floodplain plants. The hydrological regime formed during flooding affects the total specific activities of isotopes and isotope speciation. Migration properties of isotopes are determined mainly by their behavior in exchangeable and organic fractions of soil and rhizosphere.

REFERENCES

Bolsunovsky A. (2011). Radionuclide speciation in sediments of the Yenisei River. Radioprotection, 46(6), S195–S198. DOI: 10.1051/RADIOPRO/20116457S

Bolsunovsky A. and Bondareva L. (2007). Actinides and other radionuclides in sediments and submerged plants of the Yenisei River. Journal of Alloys and Compounds, 444–445(SPEC. ISS.), 495–499. DOI: 10.1016/j.jallcom.2007.01.146

Bolsunovsky A.Y., Dementyev D.V. and Vakhrushev V.I. (2021). Transport of Artificial Radionuclides over Long Distances Downstream along the Yenisei River during the 1966 Extreme Flood Event. Doklady Earth Sciences, 498(2), 514–518. DOI: 10.1134/S1028334X21060052

Bondareva L. (2012). The relationship of mineral and geochemical composition to artificial radionuclide partitioning in Yenisei river sediments downstream from Krasnoyarsk. Environmental Monitoring and Assessment, 184(6), 3831–3847. DOI: 10.1007/s10661-011-2227-z

Bondareva L.G. and Bolsunovskii A.Y. (2008). Speciation of artificial radionuclides ^{60}Co, ^{137}Cs, ^{152}Eu, and ^{241}Am in bottom sediments of the Yenisei river. Radiochemistry, 50(5), 547–552. DOI: 10.1134/s1066362208050196

Bulgakov A.A., Konoplev A.V., Kanivets V.V. and Voitsekhovich O.V. (2002). Modelling the long-term dynamics of radionuclides in rivers. Radioprotection, 37(C1), C1-649. DOI: 10.1051/RADIOPRO/2002182

Konoplev A.V. (2020). Radiocesium wash-off from contaminated catchments to rivers: Chernobyl and Fukushima. In: G. V. Kucherik and Y. A. Omelchuk eds., Ecological, Industrial and Energy Safety - 2020 , 295–300. CevSU.

Korobova E.M., Linnik V.G. and Brown J. (2016). Distribution of artificial radioisotopes in granulometric and organic fractions of alluvial soils downstream from the Krasnoyarsk Mining and Chemical Combine (KMCC), Russia. Journal of Soils and Sediments, 16(4), 1279–1287. DOI: 10.1007/s11368-015-1268-2

Korobova E.M., Linnik V.G., Chizhikova N.P., Alekseeva T.N., Shkinev V.M., Brown J. and Dinu M.I. (2014). Granulometric and mineralogic investigation for explanation of radionuclide accumulation in different size fractions of the Yenisey floodplain soils. Journal of Geochemical Exploration, 142, 49–59. DOI: 10.1016/j.gexplo.2014.02.030

Kropacheva M., Melgunov M. and Makarova I. (2013). Radiocesium and radiostrontiun in alluvial soil and riverside plants rhizosphere (near impact zone of Krasnoyarsk MCC). Central European Geology, 56(2–3), 153–159. DOI: 10.1556/ceugeol.56.2013.2-3.1

Kropacheva M., Melgunov M., Makarova I., Chuguevsky A. and Vosel Y. (2021). Monitoring and assessment of ^{137}Cs and ^{90}Sr radioactive isotopes in the 'soil – rhizosphere – sedge' system of the Yenisei River floodplain (near impact zone of Krasnoyarsk MCC, Russia). Environmental Monitoring and Assessment, 193(8), 473. DOI: 10.1007/s10661-021-09260-2

Kropacheva M.Y., Chuguevskii A. V., Mel'gunov M.S. and Bogush A.A. (2011). Behavior of ^{137}Cs in the soil-rhizosphere-plant system (by the example of the Yenisei River floodplain). Contemporary Problems of Ecology, 4(5), 528–534. DOI: 10.1134/S1995425511050134

Kropatcheva M., Chuguevsky A. and Melgunov M. (2012). Distribution of ^{152}Eu and ^{154}Eu in the 'alluvial soil–rhizosphere–plant roots' system. Journal of Environmental Radioactivity, 106, 58–64. DOI: 10.1016/j.jenvrad.2011.10.021

Kuznetsov Y.V., Legin V.K., Shishlov A.E., Stepanov A.V., Savitsky Y.V. and Strukov V.N. (1999). A study of ^{239,240}Pu and ^{137}Cs behavior in the system Yenisey river–Kara Sea. Radiokhimiya, 41(2), 181–186.

Linnik V.G., Brown J.E., Dowdall M., Potapov V.N., Surkov V. V., Korobova E.M., Volosov A.G., Vakulovsky S.M. and Tertyshnik E.G. (2005). Radioactive contamination of the Balchug (Upper Yenisey) floodplain, Russia in relation to sedimentation processes and geomorphology. Science of the Total Environment, 339(1–3), 233–251. DOI: 10.1016/j.scitotenv.2004.07.033

Linnik V.G., Volosov A.G., Korobova E.M., Borisov A.P., Potapov V.N., Surkov V. V., Borghuis A., Brown J. and Alekseeva T.A. (2004). Distribution of technogenic radionuclides in alluvial sediments and among fractions of the soil in the near zone of the Krasnoyarsk mining and chemical combine. Radiochemistry, 46(5), 508–514. DOI: 10.1007/s11137-005-0020-y

Mikhaylovskaya L.N., Molchanova I. V. and Pozolotina V.N. (2002). ^{90}Sr and ^{137}Cs in flood-plain soils of the Techa river. Radioprotection, 37(C1), C1-717. DOI: 10.1051/RADIOPRO/2002193

Nosov A.V. (1996). Analysis of the radiation environment on the Enisei river after decommissioning of straight-through reactors at the Krasnoyarsk mining—Chemical complex. Atomic Energy, 81(3), 670–674. DOI: 10.1007/bf02407062

Nosov A.V., Ashanin M.V., Ivanov A.B. and Martynova A.M. (1993). Radioactive contamination of the R. Enisey due to discharges from Krasnoyarsk Mining and Chemical Corporation. Atomic Energy, 74(2), 139–144. DOI: 10.1007/BF00760357

Nosov A.V., Krylov A.L., Kiselev V.P. and Kazakov S.V. (2010). Modelling of Migration of Artificial Radionuclides in Surface Waters. Nauka.

Séguin V., Gagnon C. and Courchesne F. (2004). Changes in water extractable metals, pH and organic carbon concentrations at the soil-root interface of forested soils. Plant and Soil, 260(1/2), 1–17. DOI: 10.1023/B:PLSO.0000030170.49493.5f

Semizhon T., Röllin S., Spasova Y. and Klemt E. (2010). Transport and distribution of artificial gamma-emitting radionuclides in the River Yenisei and its sediment. Journal of Environmental Radioactivity, 101(5), 385–402. DOI: 10.1016/j.jenvrad.2010.02.012

Stukin E., Kvasnikova E. and Golosov V. (2002). Global radioactive deposition on the Yenisey-river catchment and its contribution to the summary contamination of the valley. Radioprotection, 37(C1), C1-17. DOI: 10.1051/RADIOPRO/2002035

Sukhorukov F.V., Degermendzhy A.G., Belolipetsky V.M., Bolsunovsky A.Y., Kovalev S.I., Kosolapova L.G., Melgunov M.S. and Raputa V.F. (2004). Distribution and migration of radionuclides in the Yenisei plain. Publ. House of SB RAS, Department "Geo".

Sukhorukov F.V., Melgunov M.C. and Kovalev S.I. (2000). The main traits of distribution of technogenous radionuclides in alluvial soils and bottom sediments of the Yenisei River. Contemporary Problems of Ecology, 1, 39–50.

Tajima S., Yoshida S., Fukui T., Nihei N. and Kobayashi N.I. (2022). Cesium-137 stored on and discharged from banks of an agricultural canal in Iitate, Fukushima. Journal of Environmental Radioactivity, 241(November 2021), 106775. DOI: 10.1016/J.JENVRAD.2021.106775

Tsuji H., Nishikiori T., Yasutaka T., Watanabe M., Ito S. and Hayashi S. (2016). Behavior of dissolved radiocesium in river water in a forested watershed in Fukushima Prefecture. Journal of Geophysical Research: Biogeosciences, 121(10), 2588–2599. DOI: 10.1002/2016JG003428

Vakulovsky S.M., Kryshev I.I., Nikitin A.I., Savitsky Y.V., Malyshev S.V. and Tertyshnik E.G. (1995). Radioactive contamination of the Yenisei River. Journal of Environmental Radioactivity, 29(3), 225–236. DOI: 10.1016/0265-931X(95)00033-7

Zotina T.A., Trofimova E.A., Alexandrova Y.V. and Anishchenko O.V. (2019). Assessment of the Quality of Bottom Sediments in the Middle Reaches of the Yenisei River by Allium test. Contemporary Problems of Ecology, 12(3), 265–274. DOI: 10.1134/S1995425519030120

Zotina T.A., Trofimova E.A., Bolsunovsky A.Y. and Anishenko O. V. (2014). Experimental estimation of the possible use of submersed macrophytes for biotesting bottom sediments of the Yenisei River. Contemporary Problems of Ecology, 7(4), 410–421. DOI: 10.1134/S1995425514040131

Check for updates

CC BY

RESEARCH PAPER

SURFACE OZONE IN THE INDUSTRIAL CITY OF CHELYABINSK, RUSSIA

Tatyana G. Krupnova*[1], Olga V. Rakova[1], Valeria I. Simakhina[1], Ekaterina A. Vykhodtseva[2], Valeriy M. Kochegorov[2]

[1] Institute of Natural Sciences and Mathematics, South Ural State University, 76 Prospect Lenina, Chelyabinsk, 454080, Russia

[2] Chelyabinsk Center for Hydrometeorology and Environmental Monitoring, Federal Service for Hydrometeorology and Environmental Monitoring (Rosgidromet), 15 Vitebskaya st., Chelyabinsk, 454080, Russia

*Corresponding author: krupnovatg@susu.ru

Received: April 21st 2024 / Accepted: November 27th 2024 / Published: December 31st 2024

https://doi.org/10.24057/2071-9388-2024-3364

ABSTRACT. This work studies the variations in daily and seasonal concentrations of surface ozone (O_3), and nitrogen oxides (NO and NO_2) as its precursors in Chelyabinsk, a large industrial city in Russia. A monitoring station located outside the zone of influence of large industrial and transport local sources of air pollution was chosen for the research. The research was carried out during 2019, which can also be considered as a "background" period, because in 2020, during the COVID-19 lockdown, there was a decrease in concentrations of precursors. However, in 2022–2024 concentrations of precursors increased due to increased production capacity. Daily O_3 variations are characterized by three peaks that correlate with changes in concentrations of nitrogen oxides (NO_x) determined by peak loads and emission intensity of thermal power stations. There are two seasonal peaks of surface O_3 concentrations. The spring peak in March is caused by natural processes. In March 2019, an advection of an air mass with different properties and gas composition was observed from areas with powerful sources of precursor gases or saturated with O_3 from the south (areas in Kazakhstan). During episodes of high O_3 levels, Chelyabinsk was located on the crest of a cyclone, in the warm sector, where low-level jets formed. The summer maximum of surface O_3 in June was caused by photochemical reactions during anticyclones and prolonged inversions.

KEYWORDS: surface ozone, nitrogen oxides, temperature inversion, low-level jets

CITATION: Krupnova T. G., Rakova O. V., Simakhina V. I., Vykhodtseva E. A., Kochegorov V. M. (2024). Surface Ozone In The Industrial City Of Chelyabinsk, Russia. Geography, Environment, Sustainability, 4(17), 223-234
https://doi.org/10.24057/2071-9388-2024-3364

ACKNOWLEDGEMENTS: This study was supported by grant from the Russian Science Foundation, project 24-27-20017 and Chelyabinsk oblast.

Conflict of interests: The authors reported no potential conflict of interest.

INTRODUCTION

Surface ozone (O_3) is one of the most dangerous urban air pollutants, having caused several hundred thousand premature deaths and tens of millions of asthma attacks worldwide (Zhang et al. 2019). O_3 is necessary in the stratosphere but undesirable in the troposphere because it reacts with many compounds to form oxygen-containing organic substances and particles. Humans are exposed to O_3 mainly through inhalation, but cutaneous reactions have also been reported (Salonen et al. 2018). Being highly reactive, it can cause a 25% increase in the rates of skin cancer (Rawat and Matta 2021). In the troposphere, O_3 is categorized as a secondary pollutant because it is not emitted directly but is synthesized through chemical reactions from precursors (Nuvolone et al. 2018). Its sources in urban air are debated. Despite the large number of studies on surface O_3 in cities, there is practically no research focusing on O_3 concentrations in Russian industrial cities.

Complex photochemical reactions between nitrogen oxides (NO_x) ($NO+NO_2$) and volatile organic compounds (VOCs) form ozone (Belan 2010; Nguyen et al. 2022). Changes in VOCs, NO, and NO_2 concentrations, as well as weather conditions, influence surface O_3 concentrations (Ouyang et al. 2022; Di Bernardino et al. 2023; Wang et al. 2023). Industry, transport, and power plants produce NO_x.The contribution of different sources to VOCs varies considerably from city to city and region to region; these can be vehicle and industrial emissions as well as emissions from urban vegetation.

Isoprene (McGenity et al. 2018) and terpenes (Rosenkranz et al. 2021) are the main VOCs produced by plants. The effect of isoprene emissions on O_3 formation in cities is well known (Watson et al. 2006). Studies showed that some types of trees emit significantly more isoprene (e.g., poplar, oak) (Simon et al. 2019). In south Shanghai, biogenic VOCs are the major precursors of O_3. This mechanism is defined as O_3 production in the area leeward of the isoprene source in forests (Geng et al. 2011). The increase in O_3 concentration in the Seoul metropolitan area is also largely due to biogenic isoprene emissions (Lee et al. 2014; Kim et al. 2016). However, the major sources of VOCs are coal combustion and coking. For example, a study from Taiyuan, Shanxi Province, China, showed that the main sources of VOCs included coal and biomass combustion (33%) and coking sources (28%). Vehicle

and biological emissions were 14% and 7%, respectively (Ren et al. 2021). In some large industrial cities, without oil and coke production, transport is the main source of VOCs (Xie et al. 2021).

There is no doubt that O_3-VOC-NO_x concentrations are closely interrelated. VOCs are oxidized in the troposphere forming O_3. However, the more NO_x released, the less O_3 produced, since NO_x titrates O_3. Thus, we increase O_3 by reducing NO_x emissions. Recent data, however, have shown that even if all anthropogenic VOC emissions are reset to zero, the amount of O_3 will still be significant (Colombi et al. 2023). According to Colombi et al. (2023), decreasing VOC emissions would reduce the amount of O_3 in South Korea, but concentrations would remain above 80 ppbv even if all anthropogenic emissions from South Korea and China were zeroed out. The East Asian atmospheric background, determined by zeroing out all anthropogenic emissions over East Asia, is very high at 55 ppbv, which means that the 60 ppbv air-quality standard in South Korea is out of reach without dealing with the cause, which is still not clear.

Surface O_3 concentrations and their relationship with meteorological conditions, inversion layers, and heat islands should be studied to improve the understanding of the physicochemistry of these phenomena and to develop and evaluate strategies for improving air quality. Recent studies have shown that traditional greening strategies (Knight et al. 2021) and white roofs (Fallmann et al. 2016) have little efficacy.

Until recently, the concentration of surface O_3 has been the subject of little attention in Russian cities. In recent years, the ongoing economic digitalization and the implementation of smart cities have led to the emergence of online air quality monitoring systems in many large cities in Russia, including the monitoring of surface O_3 concentrations. Several Russian research groups are working on surface O_3 monitoring (Berezina et al. 2020; Simakina et al. 2020; Chubarova et al. 2021; Thorp et al. 2021; Andreev et al. 2021; Virolainen et al. 2023). One of the latest reviews (Andreev et al. 2022) showed that during 2021, the average daily O_3 concentration exceeded the maximum permissible concentration (MPC) for most of the year for all observation sites (17 stations), and at some stations it is double or even triple the MPC. Anticyclonic conditions in summer observe the maximum concentration in Moscow and St. Petersburg, while some stations, like Obninsk, observe maximum concentrations in March and even December, a phenomenon that remains unexplained (Andreev et al. 2022).

A study of the background O_3 concentration in Siberia in an area devoid of anthropogenic influence by Moiseenko et al. (2021) was conducted at the Zotino Tall Tower Observatory (ZOTTO) at a remote station in Central Siberia, commissioned in October 2006 as part of a joint project of the Max Planck Institute for Biogeochemistry, Jena, Germany, and the Sukachev Institute of Forestry, Siberian Branch of the Russian Academy of Sciences, Krasnoyarsk (Russia). In March and April, ZOTTO recorded the highest amount of O_3 in background conditions with low-pollution. This amount dropped significantly in May and reached a plateau by June for the observation period from 2006 to 2014. There is data on spring maxima from at least seven more stations in Russia, which are usually background or suburban stations (Andreev et al. 2022).

A more comprehensive analysis of O_3 formation in specific cities in Russia is required. Russian industrial cities are unique urban ecosystems. The vast concentration of industrial enterprises defines their development and ecological peculiarities. This paper studies, for the first time, the patterns of annual and daily variation of surface O_3 concentrations in a typical Russian industrial city, Chelyabinsk.

METHODOLOGY

Study area and observation station

Chelyabinsk is located on the geological boundary of the Urals and Siberia, in the Asian part of Russia, on the eastern slope of the Ural Mountains, on both banks of the Miass River (the Tobol River basin). The city's relief is mildly hilly. The climate is moderately continental.

Chelyabinsk is the administrative center and largest city of the Chelyabinsk region, Russia. It is the seventh-largest city in Russia with a population of over 1.1 million people. Chelyabinsk is a typical Russian industrial city, with an area of 530 km^2. It contains several of the largest metallurgical enterprises in Russia, including the country's only zinc plant, the largest steel foundry, coke and chemical enterprises, a pipe-rolling plant, a steel smelter for the production of ferro-manganese, ferro-chrome, and electrodes, and several enterprises for the production of mineral wool. Chelyabinsk is a major transport hub, with an international airport, a railway station, and several state highways. In addition to cargo and personal transport (many families in the city have more than one car), Chelyabinsk has a well-developed public transport network, including bus, tram, and trolleybus fleets, and a new metro is under construction. For the analysis, we used the data from the official monitoring station of the Russian Federal Service for Hydrometeorology and Environmental Monitoring (Roshydromet). The service operates independently from the local city authorities, and all laboratories have accreditation certificates for chemical and analytic measurements and the monitoring of air conditions. O_3 content monitoring has been conducted in the city since 2019, but measurements of surface O_3 content were not mandatory until recently and were experimental; therefore, data were not available for all monitoring stations and not for all time periods.

Monitoring stations can only be categorized roughly. In Russian industrial cities, there is no division into residential, industrial, and commercial zones. As a result, industrial enterprises can be found in the city center, and one of the world's largest zinc plants is located in the central area of Chelyabinsk. In the north of the city, there is an industrial area with Russia's largest steel smelting plant.. Many employees prefer to live close to work, so there are large residential areas in the neighborhood, which are interspersed with commercial property. The monitoring stations have been described in detail by Krupnova et al. (2020).

Direct emissions have minimal impact on two background monitoring stations.However, one of them is adjacent to a large urban forest with relic pine trees and exposed to a busy nearby highway. So, we chose the other as the urban background (UBG) station (Fig. 1).

We chose 2019 as the conditional background year for this paper because it best reflects the city's ecosystem, characterized by stable traffic flows and the work of industrial enterprises throughout the year. From 2020, the city was affected by social and political issues and was marked by COVID-19 lockdowns, which caused remote work and studies in 2021, and therefore, changes in the traffic flows of personal and public transport. In 2022, Russia came under sanctions, which led to a temporary decrease in production and consequently a decrease in emissions of dust and NO_x. In response, the economy was oriented toward domestic markets, which was followed by an increase in production to record levels. All these processes are difficult to take into account when analyzing the situation. Production volumes are classified information, as the enterprises in the city are related to national security. These social and economic processes in 2020–2022 had

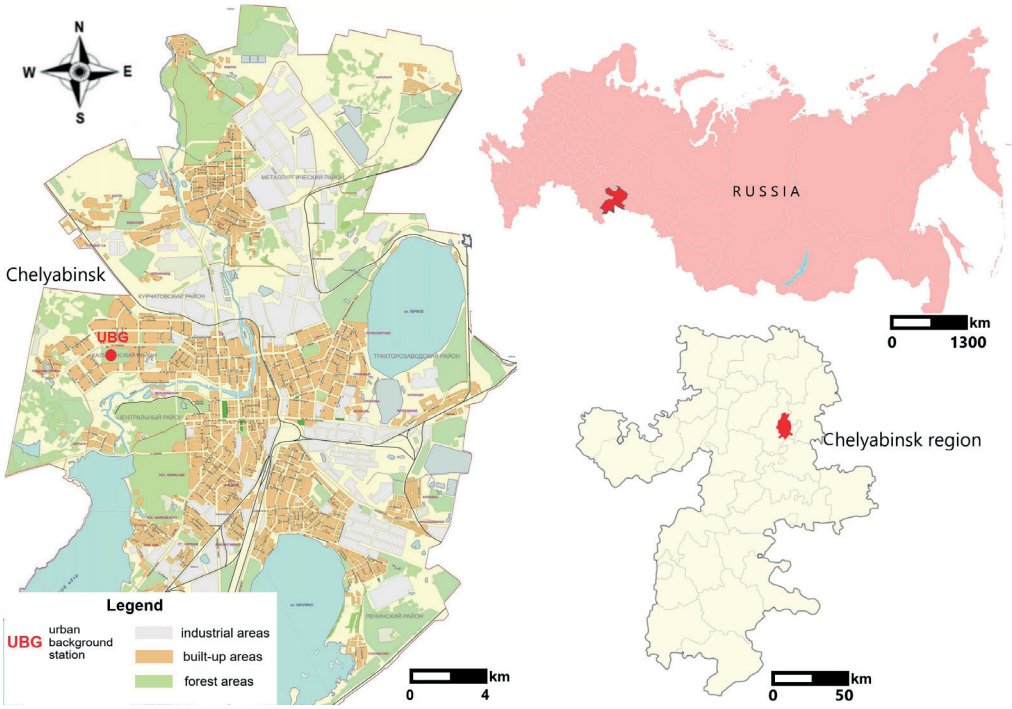

Fig. 1. Map of study area and observation station location

a significant impact on NO_x and dust emissions affecting the surface O_3 cycle. Therefore, we chose 2019 to analyze typical daily and seasonal O_3 variations for Chelyabinsk, as well as correlations with NO_x and meteorological conditions. We used data from the Roshydromet server. Pollution monitoring is continuous with measurements every 20 minutes (72 per day). In addition, we analyzed episodes of high O_3 concentrations at the background station.

Description of the data and instrumentation

Hourly averaged meteorological parameters were captured by a meteorological station (Davis Instruments Vantage Pro2, USA). Gases were measured by a set of commercial instruments. O3 was measured by an ultraviolet photometric analyzer (OPTEC, F-105, Russia), with detection limit of 1 ppbv (10 s average). We performed calibration checks using NIST-traceable O_3 standards.

NO and NO_2 were monitored using a chemiluminescent analyzer (OPTEC, R-310 A, Russia). We calibrated this analyzer weekly with certified NO compressed gas standards and dynamic dilution calibrators, as well as monthly with NO gas standard dilution and gas phase titration. The results were processed using Microsoft Excel 2013 and IBM SPSS 27.0 software.

Measurements with the altitude temperature profiler MTP-5 (Russia) provided the parameters for temperature inversions.

The analysis of synoptic situations during episodes of increased O_3 concentrations was carried out by analyzing charts of the absolute and relative topography at the level of 300, 850, 925 hPa (at observation times of 00:00 and 12.00 UTC), maps of surface analysis, and annular weather maps (at 00:00, 03:00, 06:00, 09:00, 12:00, 15:00, 18:00 UTC) available in the archive of the Chelyabinsk Central Hydrometeorological Service. To assess large-scale atmospheric circulations, data from a report by the Russian Hydrometeorological Center on the main features of atmospheric and weather conditions in the northern hemisphere was used.

RESULTS AND DISCUSSION

Dependence of surface O_3 concentrations on season

Fig. 2 shows monthly variation of O_3, NO, NO_2 concentrations in 2019.

Fig. 2 shows that the concentration of O_3 increases from January to March. The first local maximum is observed in March, followed by slow growth, and the main maximum is observed in June. Then the concentration of O_3 gradually decreases, reaching a minimum in December. The concentration of NO is maximum in February–March, and then it gradually decreases. There is a NO minimum in July. After that, NO gradually increases until December. Similarly, NO_2 reaches its peak in February. In June-August, there is a NO_2 minimum. After that, NO_2 gradually increases until December. The main sources of NO_x are metallurgy, thermal power plants, and motor transport. Most metallurgical production is year-round; therefore, they do not affect seasonal changes in NO_x emissions. The central heating season begins in October and ends in April in Chelyabinsk. The coldest days are often in January and February when heating capacities are at maximum. This is the likely reason for the observed seasonal change in NO_x concentrations. In addition, in recent years, during the winter, people have often used remote ignitions to turn on and warm up car engines — often for 15–20 minutes several times a day. This leads to an increase in NOx emissions. In new residential districts of Chelyabinsk there are local central heating systems that can be used at any time, even on cold summer days, with an uncomfortable decrease in temperature in rainy weather in early autumn. O_3 synthesis begins to increase from March, reaching a maximum in July along with an increase in solar radiation activity (Fig. 3).

The March local maximum is counterintuitive since solar radiation is not yet very high (Fig. 3), but the amount of NO_x remains high. As noted in the introduction, the spring maximum described in a large number of works is typical for the entire Eurasian territory. It is not associated with local sources, but rather reflects natural processes. There is convincing evidence that, unlike the summer maximum, which is associated with photochemical O_3 generation, the spring maximum is associated with atmospheric dynamics. During the periods under study, advection of an air mass with different properties and gas composition was observed from areas with

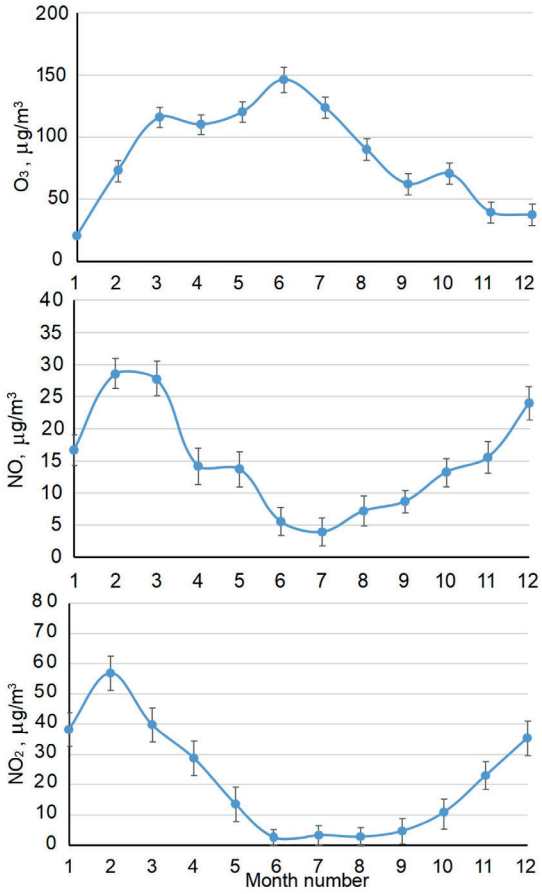

Fig. 2. Monthly variation of O_3, NO, NO_2 concentrations (µg·m^{-3}) in 2019

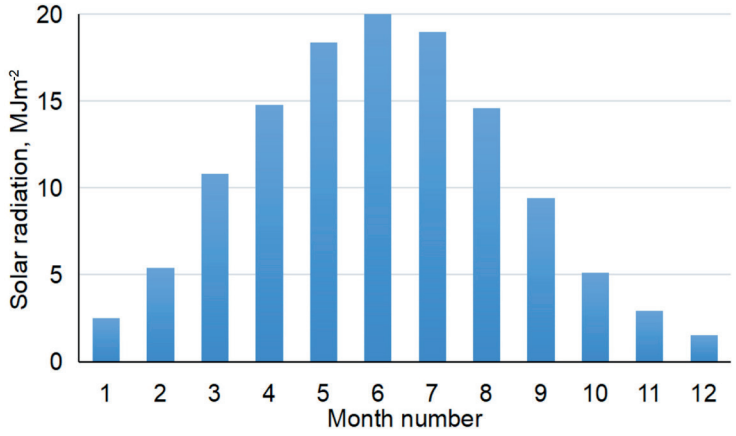

Fig. 3. Monthly values of solar radiation (MJ·m^{-2}) in 2019

powerful sources of precursor gases or saturated with O_3 from the south (areas of Kazakhstan, Central Asia), or from the west, which is transferred by a southwest flow enveloping the Ural Mountains from the south. As an atmospheric front passes, the thermal structure of the atmosphere changes, as does the gas composition. Similar phenomena have been described by Antokhin et al. (2020). Below we consider in more detail two episodes of increased O_3 concentrations in March 2019, caused by the formation of cyclone-induced low-level jets (LLJs).

Dependence of surface O_3 concentrations on the time of day

Fig. 4 shows that NO and NO_2 concentrations are negatively correlated. At 7 a.m., 1 p.m., and 7 p.m., there is a maximum of NO_2 and a minimum of NO. In January and February, at the same times, three O_3 maxima are observed; starting in March, the morning and evening maxima become minima, the daytime maximum persists in all seasons, and a nighttime O_3 maximum appears, which in December is larger than the daytime one. The main peak in the afternoon hours is associated with solar radiation.

In January and February, long-term surface inversions were almost constant (Table 1), while there was no movement of the air in the inversion layer or air with pollutants circulating under the inversion layer. The upper atmosphere had no vertical supply of O_3. Almost the entire mass of O_3 was formed as a result of photochemical reactions. The predominant sources of NO_x and VOCs are emissions from thermal power plants and boilers. The fact that NO_x extremes do not align with vehicle peak hours (in Chelyabinsk, 9 a.m. and 8 p.m.) supports this. At 7 a.m., 1 p.m., and 7 p.m., peak loads and emissions from thermal power stations are associated with nitrogen dioxide extremes (Fig. 5).

In March, there was a morning and afternoon O_3 maximum, as well as an evening minimum. In addition to the photochemical mechanism, conditions exist for the vertical supply of O_3 from the upper layers of the atmosphere. Gradually, the daytime maximum becomes

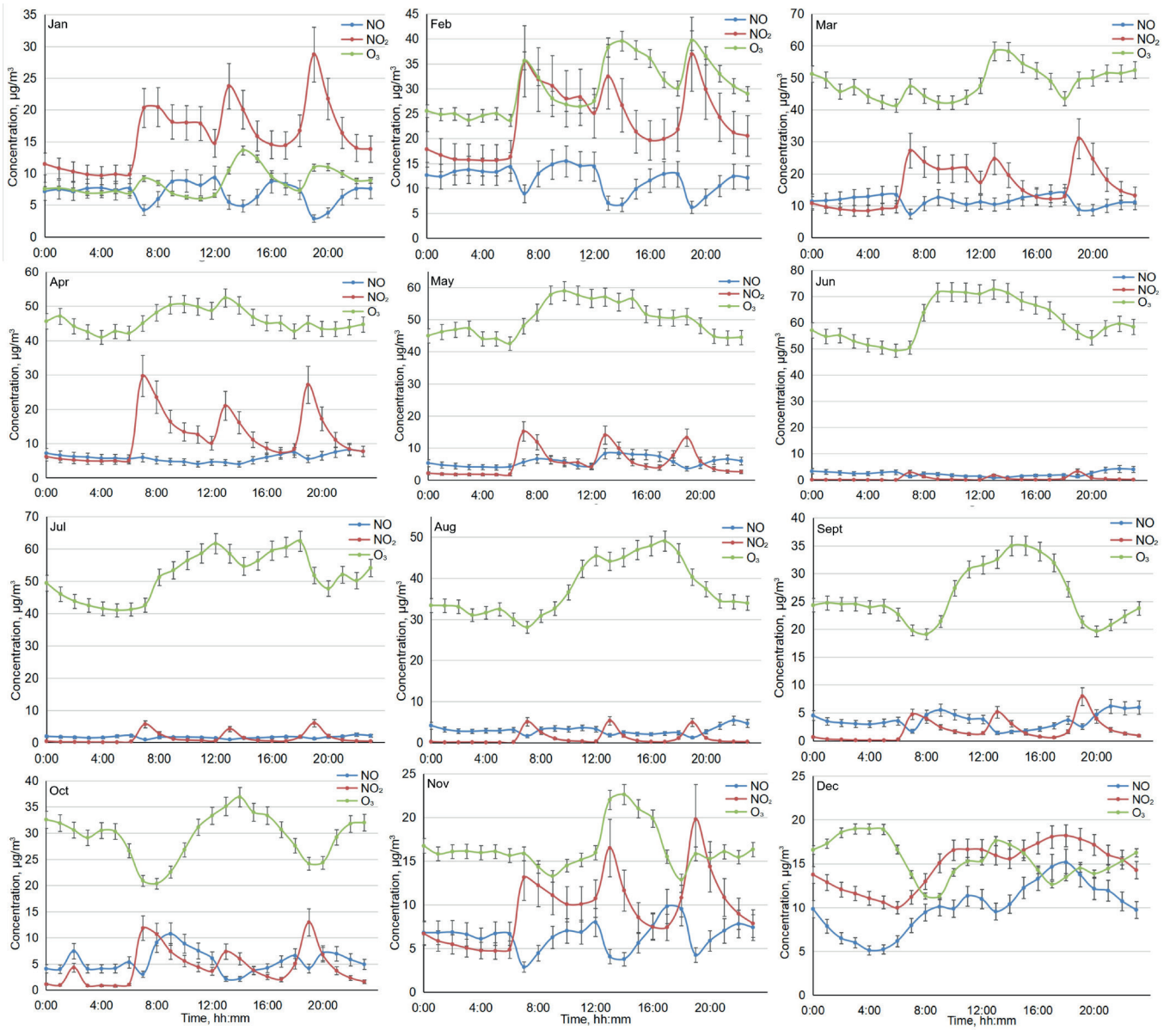

Fig. 4. Hourly variation of NO, NO_2, and O_3 concentrations (μg·m^{-3}) during the year

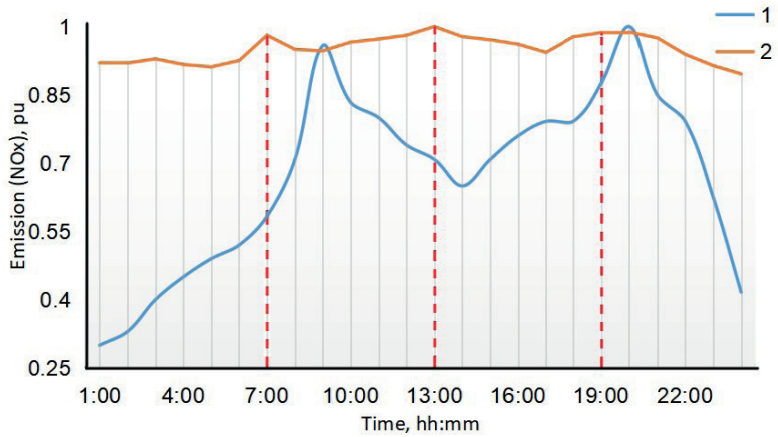

Fig. 5. Relative intensity of emissions from (1) motor vehicles[1] and (2) thermal power stations[2]

[1] *https://aims.susu.ru*
[2] *https://purchase.frwd.energy/monitoring-chtec/*

Table 1. Average duration of inversions in different months

Month	Average duration of inversions, h
January	12
February	13
March	8
April	6
May	6
June	6
July	5
August	5
September	6
October	6
November	7
December	8

more pronounced; in April, a morning minimum and nocturnal increases in O_3 concentration appear. The nocturnal maximum becomes most pronounced from October to December. Nocturnal O_3 enhancement is caused mainly by atmospheric processes, including horizontal transport and vertical mixing. Horizontal transport connects with follow phenomena. At night, the intensity of vehicle traffic decreases, and air masses gradually move into the city, where ground-level O_3 has not been destroyed by anthropogenic emissions. Low-level jet streams include vertical mixing. The O_3 produced by the photochemical reactions during the day provides an abundant O_3 source in the nocturnal residual layer, and atmospheric mixing causes the ozone-rich air in the residual layer to mix into the nocturnal boundary layer, triggering the nocturnal O_3 increase. Low-level jets' turbulence decouples the residual layer from the stable boundary layer, resulting in a decrease in the residual layer's O_3 concentration and an increase in the surface O_3 concentration. By morning, there is a decrease in the concentrations of terrestrial O_3 due to the fact that its supply from the troposphere is minimal since the atmosphere at this time is as stable as possible.

Episodes of high O_3 concentrations

Episode 1

Fig. 6 shows that the surface O_3 concentrations were 90–115 μg·m^{-3} on March 6 from 3 p.m. to 7 p.m. and 100–120 μg/m^{-3} on March 7 from 1 a.m. to 9 a.m.

At the 300 hPa level (≈9 km), Chelyabinsk region and Chelyabinsk city were located at the periphery of an extensive trough of a near-field cyclone. Flows were observed in a western, southwestern direction of 27–31 m/s^{-1} (97–112 km/h^{-1}). At the level of 850 hPa (≈1.5 km), Chelyabinsk was located on the southeastern periphery of a vast trough of a cyclone. The map (Fig. 6) clearly shows the passage of a warm atmospheric front through Chelyabinsk and the Chelyabinsk region, as well as LLJs in the warm sector of the cyclone. At the same time, a sharp increase in air temperature was observed from a night temperature of -12 to a daytime temperature of +4 according to the profile on March 6 and +5.3 ºC on March 7 (at night on March 7, the minimum temperature was about 0 ºC). In the evening of March 7, with the passage of a cold front (Fig. 6), the air mass changed again; a decrease in temperatures, an increase and change in wind direction, and a resulting decrease of the O_3 concentration in the surface layer were observed. The high O_3 level in the evening and at night on March 6 and in the morning of March 7 is not the result of local O_3 formation, but is of an advective nature. A warm air mass saturated with O_3 was brought from Central Asia by southwesterly flows. The cyclone-induced LLJs transport O_3 to the ground, where it accumulates. No inversions were observed on March 6 and 7, and there were no obstacles to O_3 penetration into the surface layers.

Episode 2

Another episode of high O_3 concentrations was observed on March 11–12 (Fig. 7). In the two episodes, the synoptic situation is almost identical. At the 300 hPa level (≈9 km), the Chelyabinsk region and Chelyabinsk city were on the eastern periphery of the trough of an extensive cyclone, the maximum development of which occurred on March 12. At the level of 850 hPa (≈1.5 km) Chelyabinsk, as in episode 1, was located on the south-eastern periphery of a vast trough. Heat was spreading in the atmosphere by south-western flows, a warm front was observed on the 11th and an occlusion front on March 12, and LLJs were also observed in the warm sector. At night, the air temperature was from -2.2 to +1.5 ºC, and during the day it warmed up to +4, +6 ºC. High O_3 concentrations were 115–130 μg·m^{-3} and 80–135 μg·m^{-3} from 2 p.m. to 7 p.m. on March 11 and from 8 a.m. to 2 p.m. on March 12, respectively. The inversions were characteristic only for the early morning of March 12 and quickly collapsed. The LLJs transported O_3 to the ground.

Episode 3

Tropospheric O_3 concentrations of up to 210 μg/m^{-3} were recorded during the day from May 8 to 9 (Fig. 8). At the 300 hPa level (≈9 km), from May 8, the Chelyabinsk region and Chelyabinsk city were at the crest of increased geopotential; the leading flow was southward from 21–24 m/s^{-1} (76–86 km/h^{-1}), due to the pushing of the high-altitude trough near the polar cyclone and the displacement of the ridge to the west. On May 9, the study area was in a low-gradient field, while the flow changed to a northern, relatively

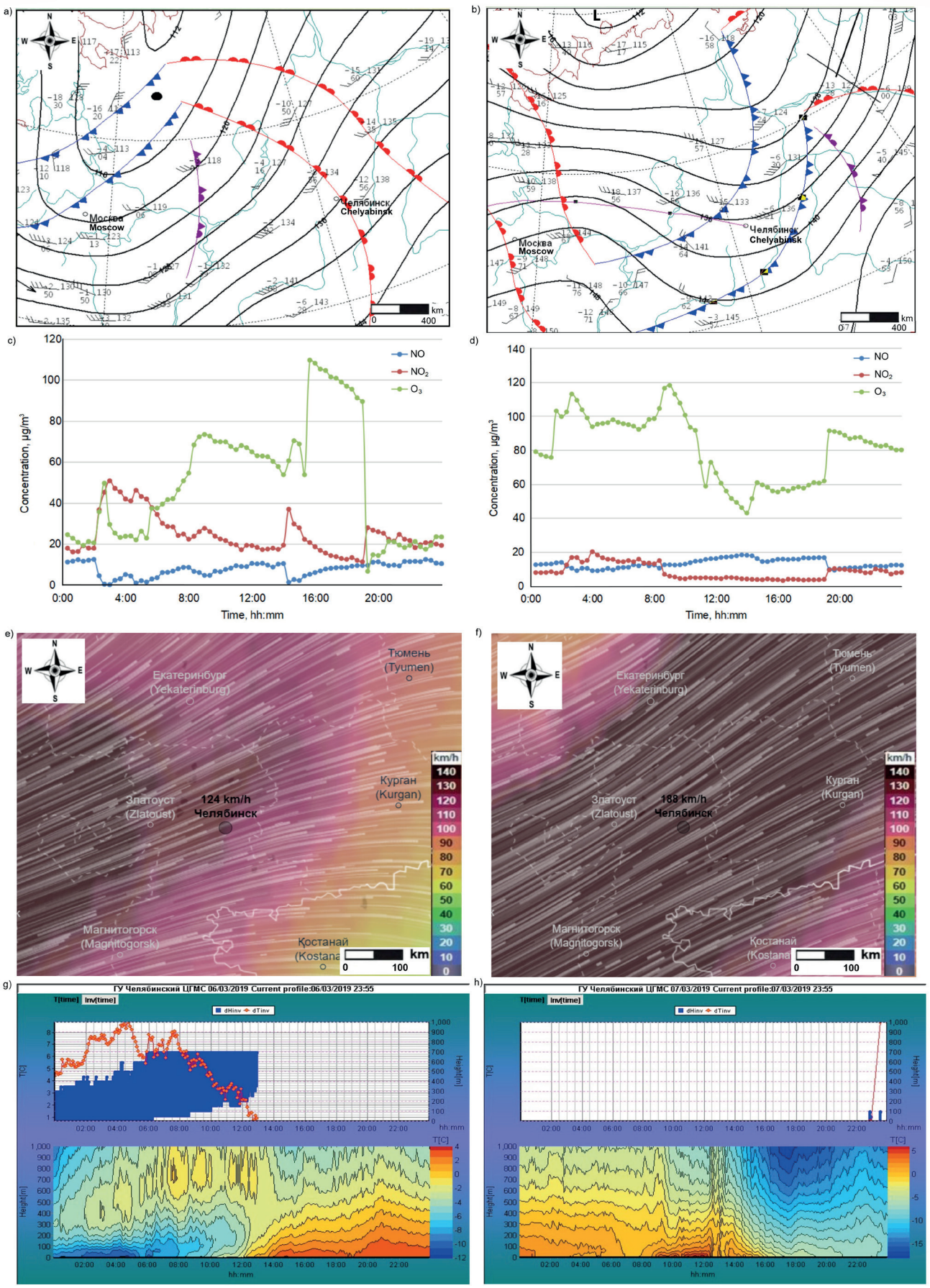

Fig. 6. Weather charts at 850 hPa; hourly variation of NO, NO_2 and O_3 concentrations (μg·m^{-3}); 300 hPa charts with wind speed and wind vectors; and temperature profiles on March 6 (left) and March 7 (right)

weak 9–16 m·s^{-1} (32–58 km·h^{-1}). The crest corresponded to an extensive Siberian anticyclone at ground level and up to 1.5 km on May 8. On May 9, a local cyclone formed in Bashkiria on the wave of the polar front, which brought rain to the Chelyabinsk region. The temperature background remained almost unchanged, then the pressure increased again and Chelyabinsk found itself on the crest of an anticyclone. The wind at the ground was weak: calm or variable 1–3 m·s^{-1}; only on May 9 gusts of up to 15 m·s^{-1} were observed. Abnormally hot weather was observed with a deviation of average daily

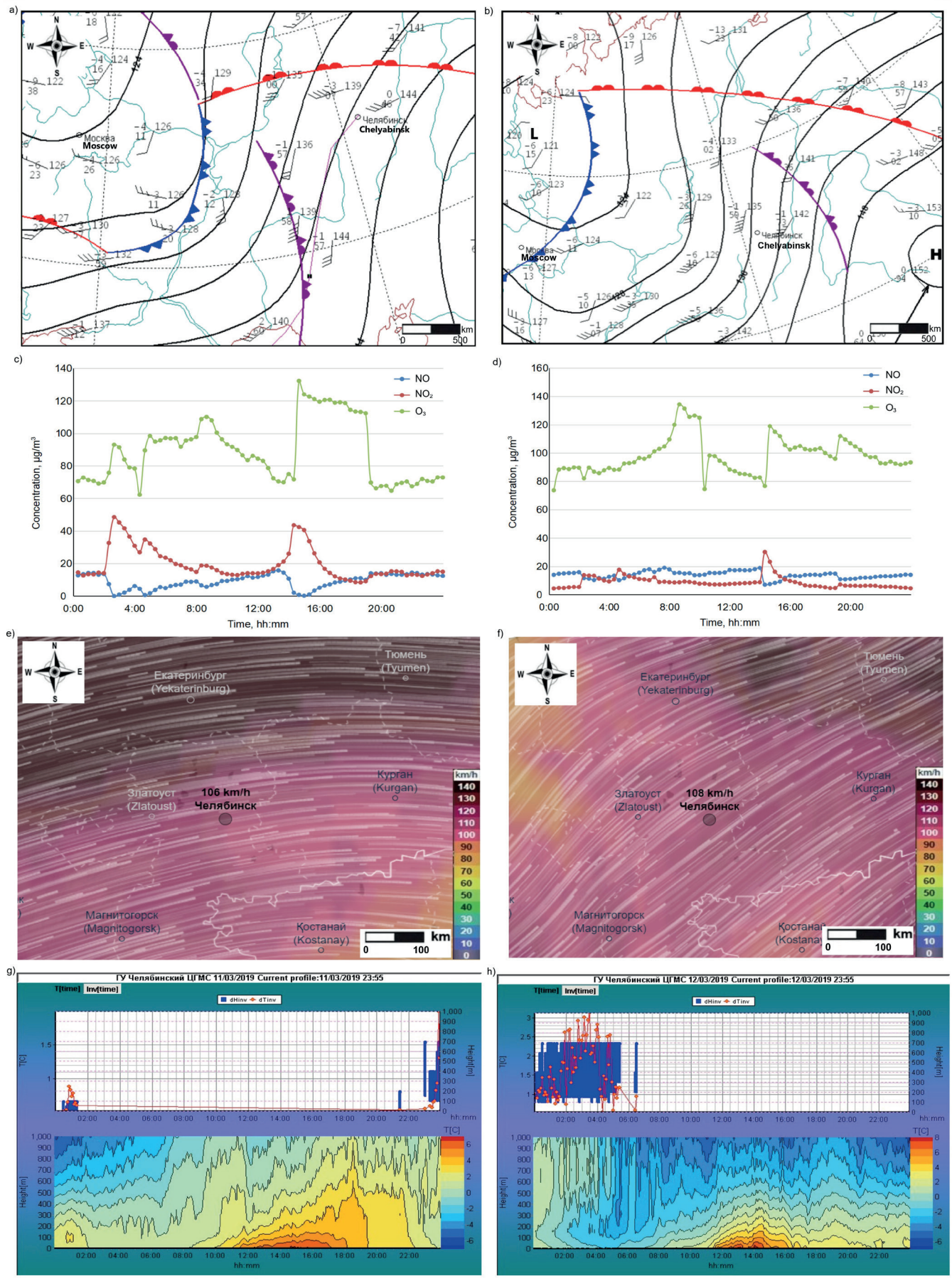

Fig. 7. Weather charts at a level of 850 hPa, hourly variation of NO, NO_2, and O_3 concentrations (μg·m^{-3}), 300 hPa charts with wind speed and wind vectors and temperature profiles on March 11 (left) and 12 (right)

temperatures from the norm by 7–12 °C; the maximum air temperature in the city reached +28 °C. Nighttime and daytime inversions were also observed.

There were days with strong sunlight and low winds, which favored the photochemical production of O_3 and the accumulation of O_3 and its precursors. Photochemical O_3 formation is the cause of the observed high concentration of O_3.

Episode 4

On June 10–11, high O_3 concentrations of up to 160 μg·m^{-3} were recorded throughout the day. At the level of 300 hPa (≈9 km) at the beginning of the period, the Chelyabinsk region was on the northeastern periphery of the altitudinal ridge; by the end of the period, an extensive tropospheric trough was spreading from the territory of the island of Novaya Zemlya and the Kara Sea and covered the Chelyabinsk region. The flows were northwest 12–16 m·s^{-1} (43–58 km·h^{-1}). At the level of 850 hPa (≈1.5 km),

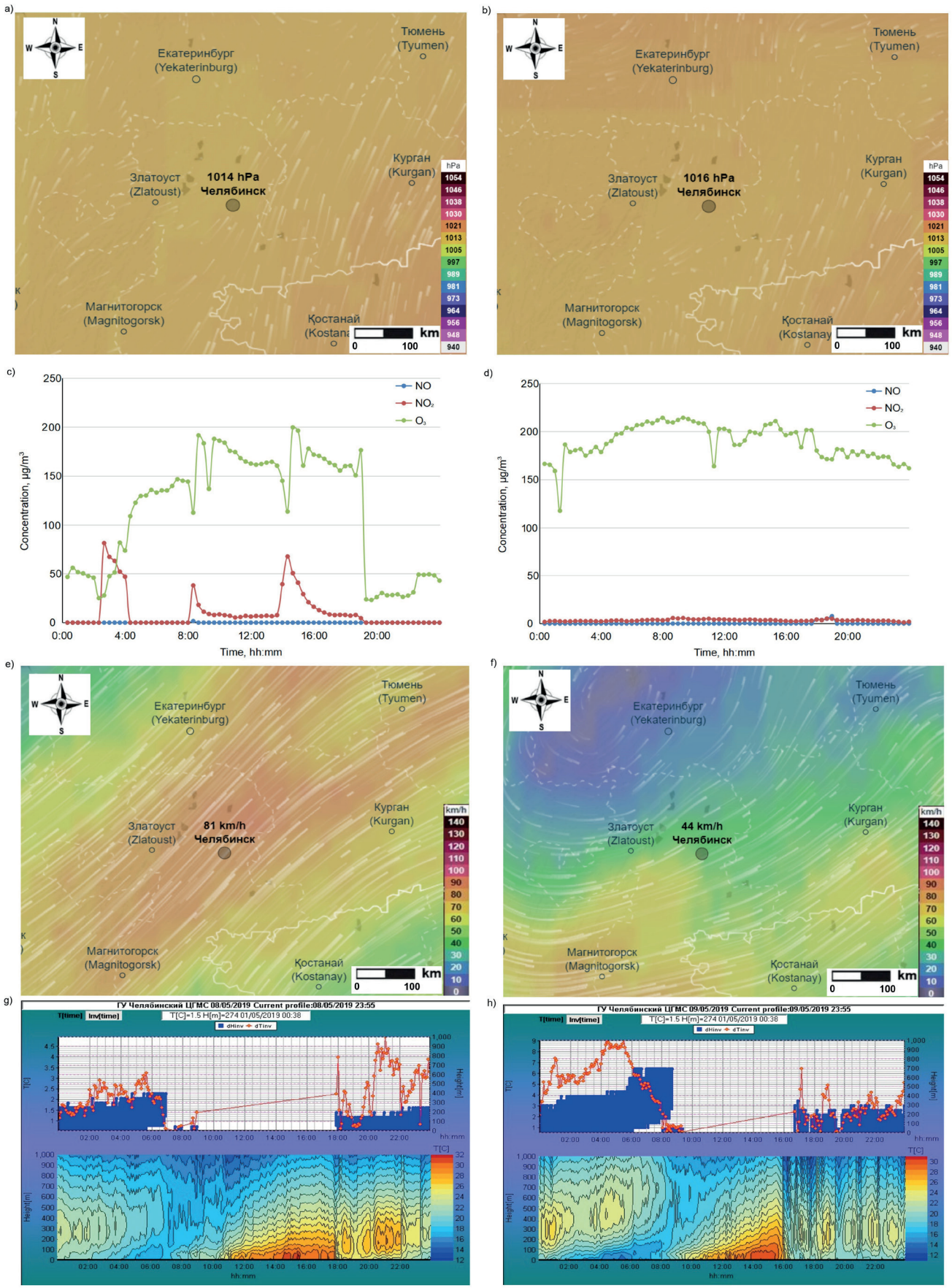

Fig. 8. Synoptic weather charts with the surface air pressure and wind vectors, hourly variation of NO, NO², and O³ concentrations (μg·m^{-3}), 300 hPa charts with wind speed and wind vectors, and temperature profiles on May 8 (left) and May 9 (right)

the territory was in the warm sector of the crest of a vast anticyclone with its center south of Moscow. There was an occlusion front and a cold front in the warm sector, so there were heavy rains in the Chelyabinsk region on June 10–11. During this period, the temperature background in Chelyabinsk was high; maximum air temperatures reached 26–28 °C; night inversions were also observed. The night was calm; during the day, there was a west/northwest wind of 3–5 m·s^{-1}, with isolated gusts of 11–12 m·s^{-1}. At the level of 925 hPa, a moderate wind of a western, northwestern direction of 7–10 m·s^{-1} was observed (Fig. 9).

In hot, windless weather on the afternoon of June 10, a photochemical accumulation of O_3 occurred. At 4 p.m., after the passage of a cold front and local rainfall, a sharp decrease in O_3 concentration in the air occurred in the area of the monitoring station. On the night of June 10–11, warm, windless weather returned. Under nighttime inversion conditions, air from O_3-rich areas on the outskirts

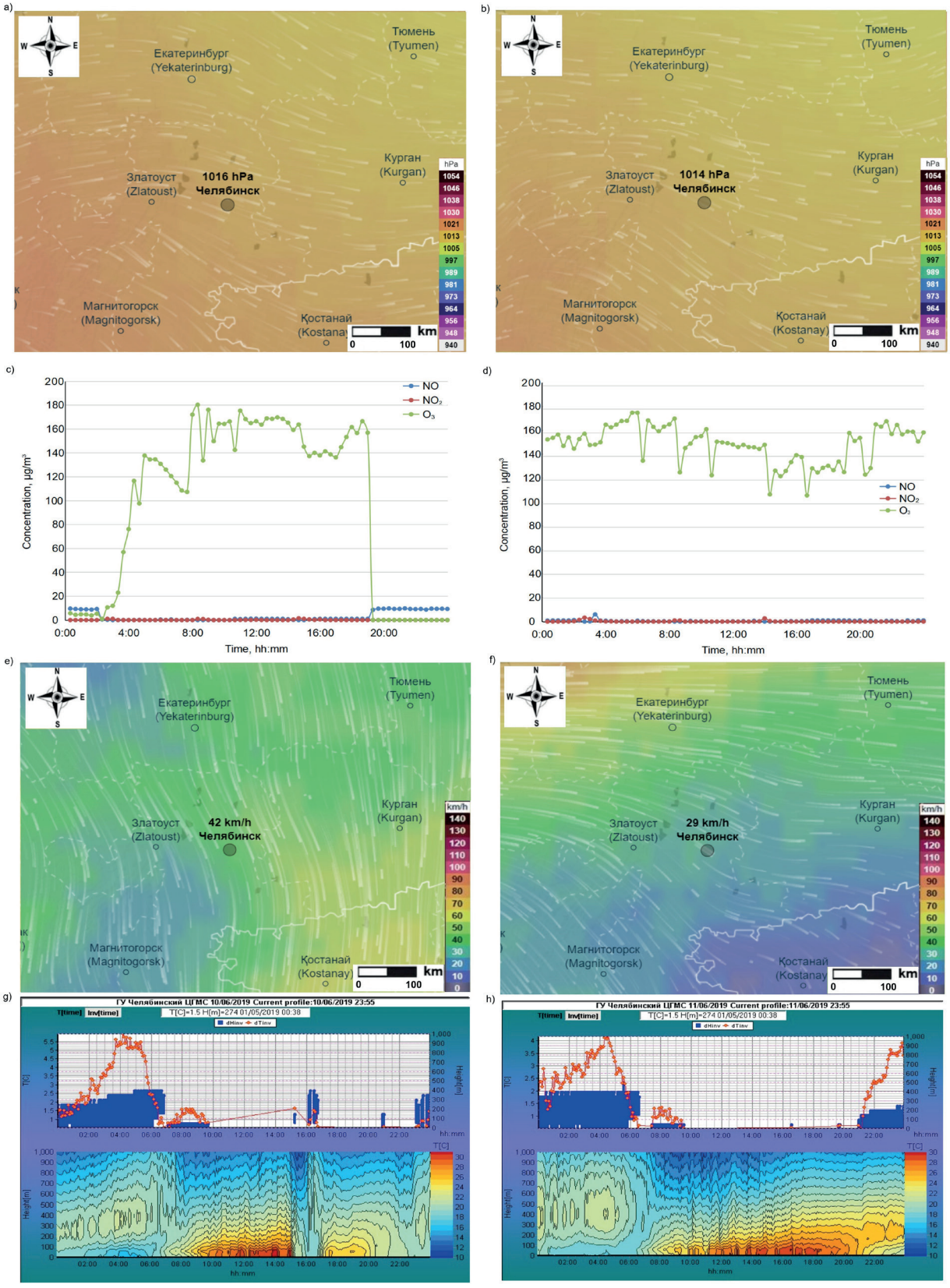

Fig. 9. Synoptic weather charts with the surface air pressure and wind vectors, hourly variation of NO, NO_2 and O_3 concentrations (µg·m^{-3}), 300 hPa charts with wind speed and wind vectors, and temperature profiles on June 10 (left) and June 11 (right)

entered the center, causing the O_3 concentration to increase again. With the anticyclone on June 11, hot weather set in, which contributed to the photochemical accumulation of O_3. High concentrations of surface O_3 were observed throughout the entire day on June 11.

CONCLUSION

This study investigates the processes associated with ground-level O_3 in a typical Russian industrial city, Chelyabinsk, including O_3 content and its relationship with atmospheric dynamics and chemical processes. We offer the following conclusions and recommendations:

• The data clearly show severe O_3 pollution in the city at a background station. To obtain a complete picture of pollution, data from other (in particular industrial and transport) monitoring stations is needed. In this regard, the expansion of the city's air monitoring network is strongly recommended.

• Measurements and studies have shown that O_3 production is correlated with NO_x. However, strategies need to be developed to control O_3 precursors, particularly VOCs. It is recommended to accelerate the implementation of VOC and NO_x control measures.

• It has been established that vertical mixing and transport by LLJs is one factor in the increase in O_3 in the spring (the March maximum). In summer (the June maximum), it is due to photochemical reactions. It is recommended that control measures be taken to reduce emissions from the energy and vehicle industries.

• Global transport appears to be an important cause of the high O_3 levels in Chelyabinsk, highlighting the need for precursor controls in other major cities as well as control of transboundary transport, including from Kazakhstan.

• Additional vertical measurements of chemical and meteorological parameters are needed to understand processes throughout the boundary layer and exchanges with the free troposphere.

• Further research on the effects of O_3 on human health and crops is recommended.

REFERENCES

Andreev V.V., Arshinov M.Y., Belan B.D., Davydov D.K., Elansky N.F., Zhamsueva G.S. et al. (2021). Surface ozone concentration over Russian territory in the first half of 2020. Atmospheric and Oceanic Optics, 33(6), 671-681, DOI: 10.1134/S1024856020060184.

Andreev V.V., Arshinov M.Y., Belan B.D. et al. (2022). Tropospheric ozone concentration on the territory of Russia in 2021. Atmospheric and Oceanic Optics, 35(6), 741-757, DOI: 10.1134/S1024856022060033.

Antokhin P.N., Antokhina O.Yu., Antonovich V.V., Arshinova V.G., Arshinov M.Yu., Belan B.D., Belan S.B., Davydov D.K., Dudorova N.V., Ivlevв G.A. , Kozlov A.V. , Pestunov D.A., Rasskazchikova T.M., Savkin D.E., Simonenkov D.V. , Sklyadneva T.K., Tolmachev G.N., Fofonov A.V. (2020). Correlation between the dynamics of atmospheric composition and meteorological parameters near Tomsk. Atmospheric and Oceanic Optics, 33(7), 529-537. DOI: 10.15372/AOO20200705

Belan B.D. (2010). Ozone in the troposphere. Tomsk: Publishing House of the Institute of Atmospheric Optics SB RAS.

Berezina E., Moiseenko K., Skorokhod A., Pankratova N.V., Belikov I., Belousov V. and Elansky N.F. (2020). Impact of VOCs and NOx on ozone formation in Moscow. Atmosphere, 11, 1262, DOI: 10.3390/atmos11111262.

Chubarova N.Ye., Androsova Ye.Ye., and Lezina Ye.A. (2021). The dynamics of the Atmospheric pollutants during the Covid-19 Pandemic 2020 and their relationship with meteorological conditions in Moscow. Geography, Environment, Sustainability, 14(4), DOI: 10.24057/2071-9388-2021-012.

Colombi N.K., Jacob D.J., Yang L.H., Zhai S., Shah V. et al. (2023). Why is ozone in South Korea and the Seoul metropolitan area so high and increasing? Atmospheric Chemistry and Physics, 23, 4031-4044. DOI: 10.5194/acp-23-4031-2023.

Di Bernardino A., Mevi G., Iannarelli A.M., Falasca S., Cede A., Tiefengraber M. and Casadio S. (2023). Temporal variation of NO2 and O3 in Rome (Italy) from Pandora and in situ measurements. Atmosphere, 14(3), 594, DOI: 10.3390/atmos14030594.

Fallmann J., Forkel R. and Emeis S. (2016). Secondary effects of urban heat island mitigation measures on air quality. Atmospheric Environment, 125, 199-211, DOI: 10.1016/j.atmosenv.2015.10.094.

Geng F., Tie X., Guenther A., Li G. et al. (2011). Effect of isoprene emissions from major forests on ozone formation in the city of Shanghai, China. Atmospheric Chemistry and Physics, 11, 10449-10459, DOI: 10.5194/acpd-11-18527-2011.

Kim S., Sanchez D., Wang M., Seco R. et al. (2016). OH reactivity in urban and suburban regions in Seoul, South Korea - an East Asian megacity in a rapid transition. Faraday Discussions, 18(189), 231-51, DOI: 10.1039/c5fd00230c.

Knight T., Price S., Bowler D. et al. (2021). How effective is 'greening' of urban areas in reducing human exposure to ground-level ozone concentrations, UV exposure and the 'urban heat island effect'? An updated systematic review. Environmental Evidence, 10, 12, DOI: 10.1186/s13750-021-00226-y.

Krupnova T.G., Rakova O.V., Plaksina A.L., Gavrilkina S.V., Baranov E.O. and Abramyan A.D. (2020). Effect of urban greening and land use on air pollution in Chelyabinsk, Russia. Biodiversitas, 21, 2716-2720. DOI: 10.13057/biodiv/d210646.

Lee K.-Y., Kwak K.-Y., Ryu Y.-H., Lee S.-H. and Baik J.-J. (2014). Impacts of biogenic isoprene emission on ozone air quality in the Seoul metropolitan area. Atmospheric Environment, 96, 209-219, DOI: 10.1016/j.atmosenv.2014.07.036.

McGenity T.J., Crombie A.T. and Murrell J.C. (2018). Microbial cycling of isoprene, the most abundantly produced biological volatile organic compound on Earth. International Society for Microbial Ecology, 12, 931-941, DOI: 10.1038/s41396-018-0072-6.

Moiseenko K.B., Vasileva A.V., Skorokhod A.I., Belikov I.B., Repin A.Yu. and Shtabkin Yu.A. (2021). Regional impact of ozone precursor emissions on NO_x and O_3 levels at ZOTTO tall tower in central Siberia, Earth Space Sci, 8, 2021EA001762, DOI: 10.1029/2021EA001762.

Nuvolone D., Petri D. and Voller F. (2018). The effects of ozone on human health. Environmental Science and Pollution Research, 25(5), DOI: 10.1007/s11356-017-9239-3.

Nguyen D.-H., Lin Ch., Vu C.-T., Cheruiyot N.K., Nguyen M.K., Le T.H., Lukkhasorn W., Vo T.-D.-H. and Bui X.-T. (2022). Tropospheric ozone and NO_x: A review of worldwide variation and meteorological influences. Environmental Technology and Innovation, 28, 102809, DOI: 10.1016/j.eti.2022.102809.

Ouyang S., Deng T., Liu R. et al. (2022). Impact of a subtropical high and a typhoon on a severe ozone pollution episode in the Pearl River Delta, China. Atmospheric Chemistry and Physics, 22, 10751-10767, DOI: 10.5194/acp-22-10751-2022.

Rawat K. and Matta G. (2021). Ozone: Risk assessment, environmental, and health hazard. In: Singh J(ed) Hazardous Gases: Risk Assessment on Environment and Human Health, Academic Press, 301-312.

Ren X., Wen Y., He Q., Cui Y. et al. (2021). Higher contribution of coking sources to ozone formation potential from volatile organic compounds in summer in Taiyuan, China. Atmospheric Pollution Research, 12(6), 101083, DOI: 10.1016/j.apr.2021.101083.

Rosenkranz M., Chen Y., Zhu P. and Vlot A.C. (2021). Volatile terpenes - mediators of plant-to-plant communication. Plant, 108(3), 617-631, DOI: 10.1111/tpj.15453.

Salonen H., Salthammer T. and Morawska L. (2018). Human exposure to ozone in school and office indoor environments. Environment International, 119, 503-514, DOI: 10.1016/j.envint.2018.07.012.

Simakina T.E. and Kryukova S.V. (2020). Spatio-temporal distribution of surface ozone in Saint Petersburg, Gidrometeorologiya i Ekologiya. Hydrometeorology and Ecology, 61, 407-420 (In Russian), DOI: 10.33933/2074-2762-2020- 61-407-420.

Simon H., Fallmann J., Kropp T., Tost H. and Bruse M. (2019). Urban trees and their impact on local ozone concentration-a microclimate modeling study. Atmosphere, 10(3), 154, DOI: 10.3390/atmos10030154.

Thorp T., Arnold S.R., Pope R.J., Spracklen D.V. et al. (2021). Late-spring and summertime tropospheric ozone and NO_2 in Western Siberia and the Russian Arctic: regional model evaluation and sensitivities. Atmospheric Chemistry and Physics, 21, 4677-4697, DOI: 10.5194/acp-21-4677-2021.

Virolainen Ya.A., Ionov D.V. and Polyakov A.V. (2023). Analysis of long-term measurements of tropospheric ozone at the St. Petersburg State University Observational site in Peterhof, Izvestiya, Atmospheric and Oceanic Physics, 59(3), 287-295, DOI: 10.1134/S000143382303009X.

Wang J., Dong J., Guo J., Cai P., Li R., Zhang X., Xu Q. and Song X. (2023). Understanding temporal patterns and determinants of ground-level ozone. Atmosphere, 14(3), 604, DOI: 10.3390/atmos14030604.

Watson L., Wang K.-Y., Hamer P. and Shallcross D. (2006). The potential impact of biogenic emissions of isoprene on urban chemistry in the United Kingdom. Atmospheric Science Letters, 7, 96-100, DOI: 10.1002/asl.140.

Xie Y., Cheng Ch., Wang Z., Wang K., Wang Yu. et al. (2021). Exploration of O3-precursor relationship and observation-oriented O3 control strategies in a non-provincial capital city, southwestern China. Science of the Total Environment, 800, 149422, DOI: 10.1016/j.scitotenv.2021.149422.

Zhang J., Wei Y. and Fang Z. (2019). Ozone pollution: a major health Hazard worldwide. Frontiers in Immunology, 10, 2518, DOI: 10.3389/fimmu.2019.02518.

Check for updates

CC BY

RESEARCH PAPER

EVALUATION OF NEW RELEASE GLOBAL GEOPOTENTIAL MODEL (GGMS) OVER EAST MALAYSIA

Noorhurul A. Othman[1], Muhammad F. Pa'suya[1*], Ami H. Md Din[2], Mohamad A. Che Aziz[1], Nurul S. Hazelin Noor Azmin[1], Mohd A. Abd Samad[1], Mohd A. Abdullah[3]

[1] Environment and Climate Change Research Group (ECC), Collage of Built Environment, Universiti Teknologi MARA, Perlis Branch, Arau Campus, 02600 Arau, Perlis, Malaysia

[2] Geospatial Imaging and Information Research Group (GI2RG), Faculty of Built Environment and Surveying, Universiti Teknologi Malaysia, 81310 Johor Bahru, Johor, Malaysia

[3] UO Geomatics Resources Sdn. Bhd, No. 306A, Jalan Sungai Korok, Alor Setar, 05400 Alor Setar, Kedah, Malaysia

***Corresponding author:** faiz524@uitm.edu.my

Received: March 24th 2024 / Accepted: November 27th 2024 / Published: December 31st 2024

https://doi.org/10.24057/2071-9388-2024-3304

ABSTRACT. Global Geopotential Model (GGM) is a mathematical representation of the Earth's gravity field and geoid, which is developed to provide accurate information about the variations in the Earth's gravitational potential across the entire globe. Recently numerous organizations and research centres have developed multi GGMs derived from several types of available gravity and height datasets to estimate orthometric heights from GNSS measurements. In this study, we present an accuracy evaluation and assessment of the nineteen recent and popular GGMS using actual GNSS/levelling points, and gravity anomaly points. The goal of this research is to find the optimum model for the study area which is located in the East Malaysia for further determination of geoid modelling in the regional scale. The selection of these areas basically is due to their renowned for uncontrolled topography and various datums. The results indicate that for geoid undulation, the XGM2019e_2159 with value of 0.195 model is the best fit GGM for the estimation model for East Malaysia. For gravity anomalies, the most reliable GGM for the study area is GO_CONS_GCF_2_DIR_R5 with RMSE of 32.456

KEYWORDS: sGlobal Geopotential Models (GGMs), GNSS Levelling, East Malaysia

CITATION: Othman N. A., Pa'suya M. F., Md Din A. H., Che Aziz M. A., Nurul S. Hazelin Noor Azmin, Mohd A. Abd Samad, Abdullah M. A. (2024). Evaluation of new release global geopotential model (ggms) over east malaysia. Geography, Environment, Sustainability, 4(17), 235-246

https://doi.org/10.24057/2071-9388-2024-3304

ACKNOWLEDGEMENTS: The authors are grateful to the Ministry of Higher Education (MOHE), Malaysia for their financial funding through FRGS 2022 (Reference code: FRGS/1/2022/WAB07/UITM/02/2 and to the Department of Survey and Mapping Malaysia (DSMM) for providing terrestrial and GNSS-levelling data over East Malaysia. Additionally, the author acknowledges the International Centre for Global Earth Models (ICGEM) for supplying the data used in this study.

Conflict of interests: The authors reported no potential conflict of interest.

INTRODUCTION

The geoid is a surface which the gravitational potential is uniform, and it is corresponds to a continuous sea level across the globe. It serves as the precise reference for height measurement and physically represents the Earth's shape (Perdana and Heliani, 2017). Nowadays, the ultimate goal of geodesist is to produce 1cm accuracy of local geoid model. However, it has yet been realised for most of the areas around the world. This is only possible with the optimal usage of all available data and methods. Various methods and approach in geoid determination have been introduced by different groups, such as Least Square Modification of Stokes' Formula (Sjöberg, 2003a, 2003b), Curtin University of Technology's (CUT) method (Goyal et al. 2019), Remove Compute-Restore (RCR) method (Schwarz et al. 1990), UNB Stokes-Helmert method (Ellmann and Vaníček. 2007), etc. Each method has different philosophy and steps in geoid computation but all those methods use similar input data which are Global Geopotential Model (GGMs). This data become the crucial input in the geoid computation as they provide essential long-wavelength information combined with Stokes' integration over local gravity data collected from terrestrial measurements. Notably, advancements in satellite gravity missions, such as Gravity Recovery and Climate Experiment 9GRACE) (Tapley et al. 2003; Tapley et al. 2005) and Gravity Field and Steady-State Ocean Circulation Explorer (GOCE) (Pail et al. 2011) have substantially improve our understanding of the global gravity field, particularly in the long-wavelength bands (Bruinsma et al. 2013; Brockman et al. 2014) are now available to the scientific community through public domain resources at (http://icgem.gfz-potsdam.de/ICGEM).

Global Geopotential Models (GGMs) are mathematical representation of Earth's gravitational potential achieved through a spherical harmonic expansion. These models employ fully normalised Stokes' coefficients (C_{nm} and S_{nm}) for each degree (n) and order (m) to characterise the gravitational potential. These coefficients enable the

derivation of various Earth-related parameters, including geoid undulation, normal gravity, gravity anomaly, vertical deflection, and gravity disturbance (Mainville et al. 1992). GGMs can be categorised into three main types: satellite-only models, combined models, and tailored models (Rapp et al. 1997; Chen et al. 2022). For satellite-only GGMs, the coefficients are derived by analysing the orbital deviations of satellites, such as those collected during missions like CHAMP, GRACE, and GOCE. However, the accuracy and resolution of these models are limited due to their low degree. Meanwhile the combined models are created by merging gravity data from various sources, including satellites, terrestrial gravity measurements, airborne gravity data, and satellite altimeter data in marine regions. As a result, these models achieve higher degrees and provide more accurate results compared to satellite-only models. Tailored GGMs are a product of enhanced GGMs harmonic coefficients using specialised mathematical techniques found within the first and second groups. These models are primarily designed to elevate the degree of accuracy within the models.

Prior to the geoid computation, the crucial step is to identify the optimal GGM that fit to the local geometrical vertical datum and gravity field data (Amos and Featherstone 2003; Benahmed 2010; Ellmann 2010; Strykowski and Forsberg 2010; Doganalp 2016; Saari and Bilker 2018). This selection process is imperative because the published error metrics associated with GGMs cannot be readily applied to assess their performance in a specific region, as they may be overly optimistic or represent global averages. Therefore, it is crucial for users to evaluate the GGMs to ensure their applicability for geoid computations in their target regions (Kiamehr and Sjöberg 2005)

Based on the literature records, there are numerous published studies investigated the accuracy of the GGMs in their interest regions using various methods and approaches, for example see Doganalp (2016), Al Shouny et al (2023), Alemu (2023), Al-Othman et al. (2016) and El-Ashquer et al (2016), etc. One of the most frequently employed methods to determine the best GGM for an area's gravity field is to compare GGMs through independent datasets of GNSS levelling (e.g., Yilmaz et al, 2016; Lee et al. 2020; Goyal et al. 2019)), terrestrial gravity anomalies (e.g., Hirt et al. 2011; Alemu 2021; Alemu 2023), and both (e.g., El-Ashquer et al. 2016; Benahmed, 2010, Guimarães et al.2012; Al Shouny et al. 2023). The main objective of this study is to identify the optimal GGMs that align with the characteristics of East Malaysia, a crucial step for subsequent geoid determination in this specific region. Consequently, we have selected a total of nineteen (19) GGMs released between 2014 and 2022 for evaluation. This evaluation is based on comparisons with a geometrical geoid derived from GNSS levelling, free air anomalies obtained from terrestrial gravity measurements, and a local precise gravimetric geoid model.

STUDY AREA

The study area is located in East Malaysia, encompasses of -3° N ≤ Latitude ≤ 9.75° N, 108° E ≤ Longitude ≤ 120.75° E, as illustrated in Fig. 1. The total land area within this study region spans approximately 198,447 square kilometers. It is further divided into two states namely Sabah in the northern region and Sarawak in the southern region.

SOURCES OF DATA

In this study, the performances of the nineteen (19) selected GGMs have been assessed using three datasets, which are GNSS levelling derived geoid height, terrestrial gravity anomalies, and official gravimetric geoid over East Malaysia obtained from the Department of Survey and Mapping Malaysia (DSMM). These datasets are crucial to evaluate the accuracy of the GGMs in East Malaysia. The details of the data are as follows:

GNSS Levelling

In total, 53 observation points have been generously provided by the DSMM. The spatial distribution of these observation points is illustrated in Fig. 2(a). However, since the levelling datum over the Sarawak region is referenced to the three different datums, 30 points over this state area have been excluded in the evaluation process to avoid any inconsistencies caused by the different datums. The GNSS levelling data was collected through a GNSS field campaign by DSMM from October to December 2016 with a minimum of 12 hours of observation period (Jamil et al. 2017) and processed using Bernese software.

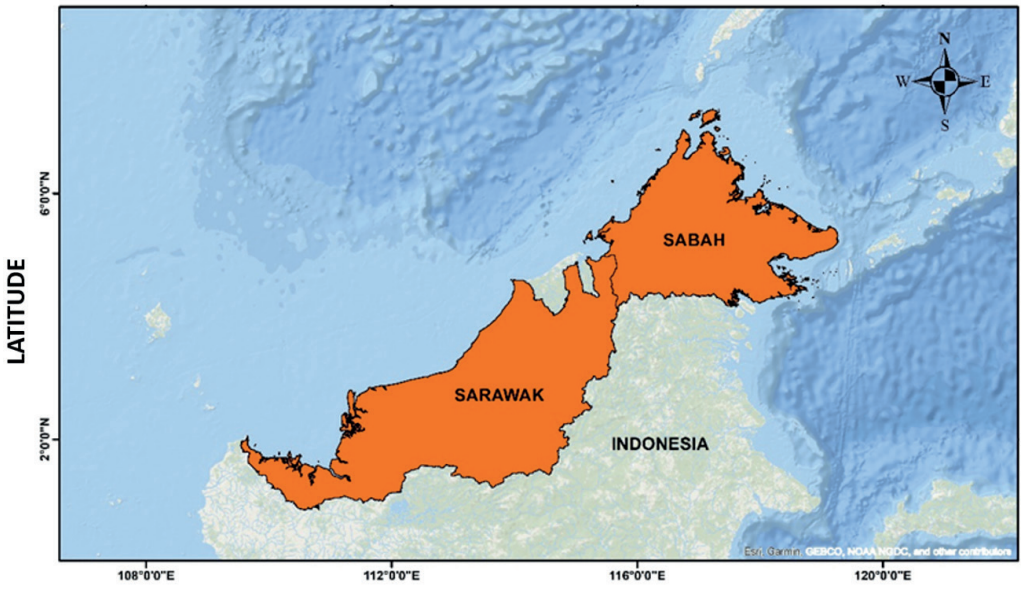

Fig. 1. Study area over East Malaysia

Terrestrial Gravity anomalies

In the second method of evaluation, a comparison has been conducted between all the selected GGMs and the terrestrial gravity anomalies, Δg_{FA} . These gravity anomalies have been computed using data collected from 690 terrestrial gravity measurement points across East Malaysia. The distribution of these terrestrial gravity data points is depicted in Fig. 2(b).

LOCAL GRAVIMETRIC GEOID MODEL

The performance assessment of all selected GGMs also includes a comparison with geoid height extracted from precise local gravimetric geoid. This gravimetric geoid was meticulously computed by the DSMM as part of the Marine Geodetic Infrastructure Project (MAGIC). The computation process involves the use of various data sources, including the mixed spherical harmonic model EGM08/GOCE, SRTM digital elevation model, DTU15 satellite altimeter-derived gravity anomalies at sea, and airborne gravity data. Notably, this gravimetric geoid achieves an accuracy level of approximately 3 to 5 cm across most of East Malaysia (Jamil et al. 2017). In this study, the geoid height obtained from each GGM has been compared with the corresponding local gravimetric geoid data at the same grid spacing. Fig. 3 provides a visual representation of the gravimetric geoid over East Malaysia, as provided by DSMM. This comparison is instrumental in assessing the accuracy and suitability of the GGMs' for geoid determination within the East Malaysian region.

GLOBAL GEOPOTENTIAL MODELS (GGMs)

In the fields of science and engineering, improving the understanding of the Earth's gravity field is crucial for precise orbit determination and height measurement systems (Rummel et al. 2002). Achieving a thorough understanding of the Earth's gravity field requires continuous advancements in both accuracy and spatial resolution. GGMs play a crucial role in representing the Earth's gravitational field, particularly in capturing the long-

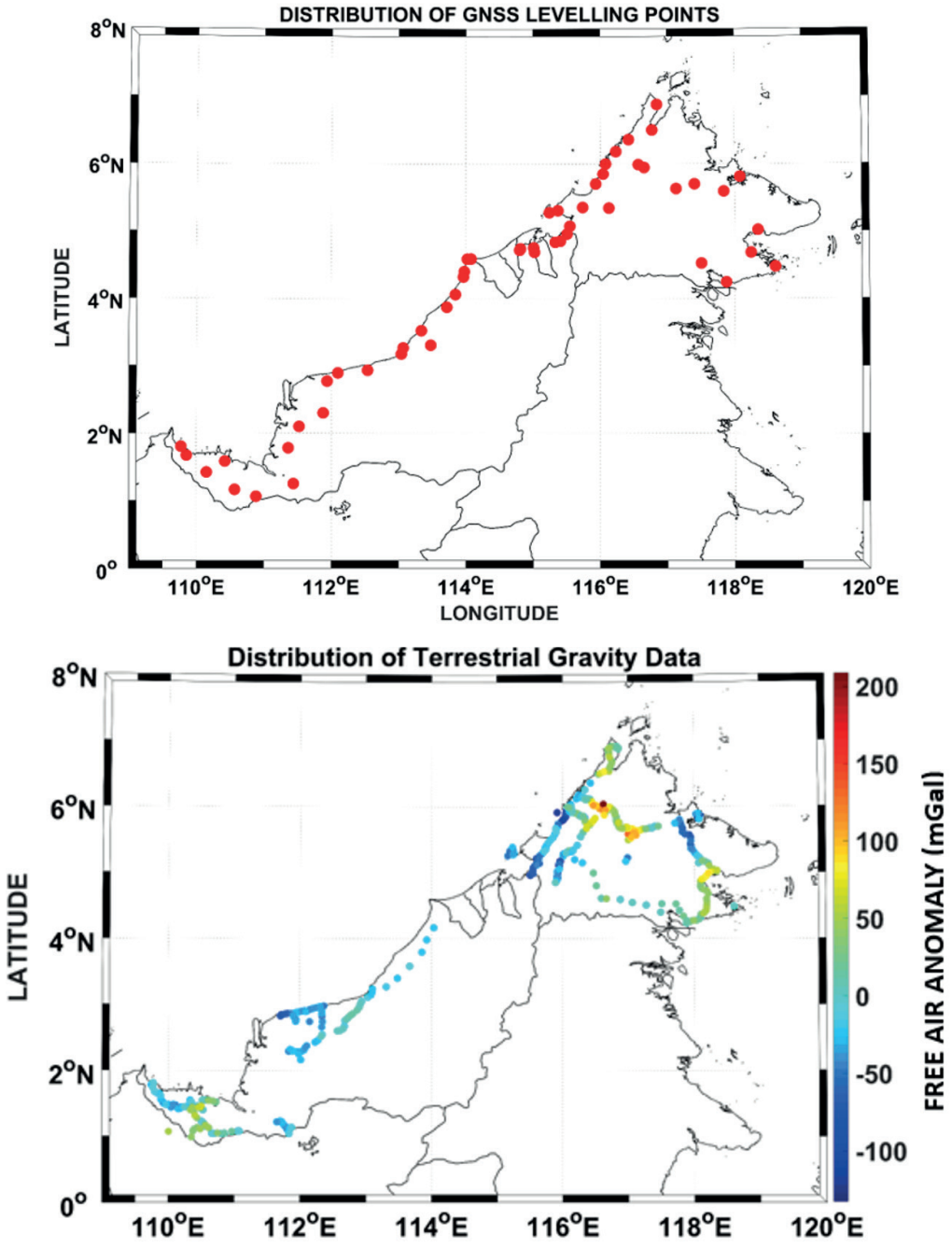

Fig. 2. Study area over East Malaysia

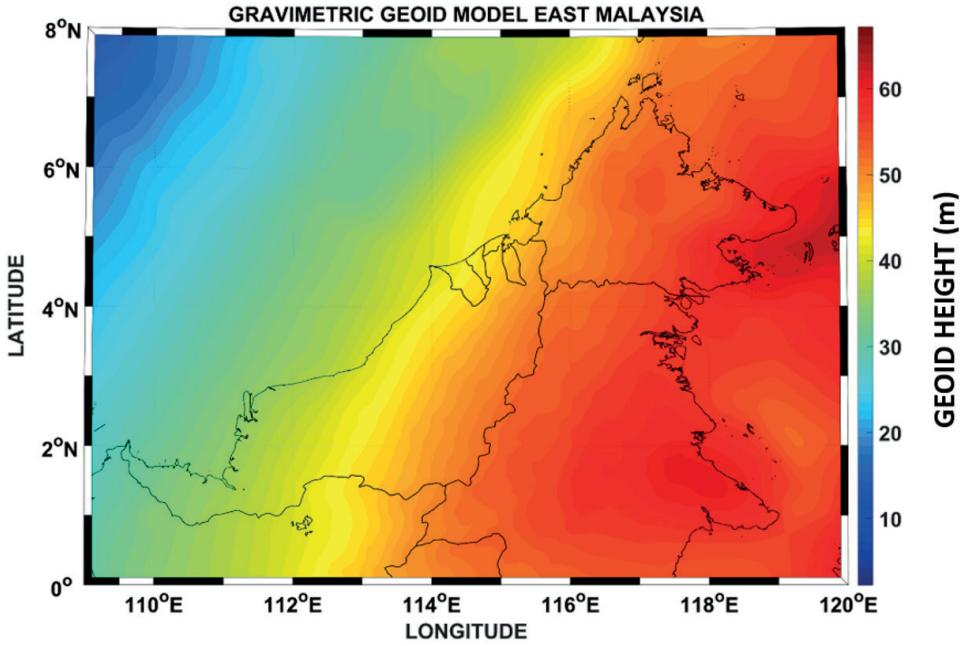

Fig. 3. Local gravimetric geoid model over East Malaysia

wavelength components (Amos and Featherstone, 2003; Kiamehr and Sjöberg, 2005). These models are built using a set of fully normalized spherical harmonic coefficients, which are derived from geopotential solutions (Mainville et al. 1992). The development of GGMs relies on integrating multiple data sources, including satellite observations, terrestrial gravity measurements, marine gravity anomalies from satellite altimetry, and airborne gravity data (Chen et al., 2022; Hirt et al., 2011; Rapp, 1997). Such comprehensive data integration ensures that the models provide an accurate representation of the Earth's gravity field across different spatial scales and environments. In the scope of this study, have conducted an evaluation of 19 GGMs, with four of them being categorized as combination GGMs and the remainder classified as satellite-only GGMs. To the best of our knowledge, no prior research has been conducted specifically addressing GGMs in the context of East Malaysia. Table 1 provides a comprehensive summary of the 19 GGMs evaluated in this study, and the spherical coefficients used were sourced from the ICGEM website (http://icgem.gfz-potsdam.de/tom_longtime) (Barthelmes, 2013). These GGMs, released between 2014 and 2022, encompass a wide range of models, including satellite-only ones (utilizing data from missions like GOCE and/or GRACE) and combined geopotential models. The geoid height (N) derived from these GGMs can be represented using a set of spherical harmonic coefficients, as described in equation (Rummel et al. 2002).

$$N_{GM} = \frac{GM}{\gamma r}\sum_{n=o}^{n_{max}}\left(\frac{R}{r}\right)\sum_{m=0}^{n} P_{nm}(\cos\theta)\left(C_{nm}\cos m\lambda + S_{nm}\sin m\lambda\right) \quad (1)$$

where θ, λ, and r are the point's co-latitude, longitude, and geocentric radius, respectively; R is the reference ellipsoid's major axis radius; GM is created by multiplying the Earth's mass by the gravitational constant; γ is the reference ellipsoid's mean gravity; C_{nm} and S_{nm} are the series development Stokes coefficients; $P_{nm}n$ -degree and m-order representation of the associated Legendre functions. Meanwhile, the gravity anomaly derived from GGMs up to spherical harmonic degree n_{max} can be calculated with the following equation (Heiskanen et al. 1967).

$$\Delta g_{GM} = \frac{GM}{r^2}\sum_{n=0}^{n_{max}}\left(\frac{R}{r}\right)(n-1)\times\sum_{m=0}^{n} P_{nm}(\cos\theta)\left(C_{nm}\cos m\lambda + S_{nm}\sin m\lambda\right) \quad (2)$$

DATA PROCESSING

The evaluation of the GGMS in this study was conducted using two distinct sets of data which is GNSS levelling and terrestrial gravity anomalies dataset. The GGM geoid heights and gravity anomalies were computed using the MATLAB based software EGMlab which developed by Kiamehr and Eshagh (2008), from the Division of Geodesy at the Royal Institute of Technology in Stockholm, Sweden. For the consistency of the comparison and minimize biases due to differences in reference ellipsoid, tide conventions and geoid reference, all the GGMs used are in the Tide-Free system and use GRS80 as the normal field. In the first evaluation, the GGMs gravity anomalies was compared with the 690 terrestrial gravity points. Prior to the comparison, the gravity data have been processed to compute free air anomalies, Δg_{FA} with the following equation:

$$\Delta g_{FA} = g + F - y_0 \quad (3)$$

where g is gravity value on the topographic surface, F is the free-air correction (approximately 0.3086H), H is the orthometric height and γ_0 is the normal gravity on the GRS80 ellipsoidal surface which can be computed using the Somigliana Formula as follows:

$$\gamma_o = \gamma_e \frac{1 + k\sin^2\varphi}{\sqrt{\left(1 - e^2\sin^2\varphi\right)}} \quad (4)$$

$$k = \frac{b\gamma_P - a\gamma_e}{a\gamma_e} \quad (5)$$

where γ_e is the gravity on the equator, γ_p is the gravity at the pole, b is the semi-major axis of the ellipsoid, e is the semi-minor axis of the ellipsoid, e is the first eccentricity and φ is the geodetic latitude. In order to analyse the performance of each GGMs, a basic statistical analysis was performed by calculating the Mean Error (ME) and Root-Mean Square Error (RMSE) by comparing the GGM gravity anomalies, Δg_{GCM} and terrestrial gravity anomalies, Δg_{FA} as follows:

$$\Delta g = \Delta g_{GCM} - \Delta g_{FA} \quad (6)$$

Table 1. Global Geopotential Models that are evaluated in this paper (S: Satellite, G: Gravity, A: Altimetry)

Model	Year	Max Degree	Data Source	Reference
SGG-UGM-2	2020	2190	A, EGM2008, S(Goce), S(Grace)	Liang et al. 2020
XGM2019	2019	2190	A,G, S(GOCO06s), T	Zingerle et al. 2019
SGG-UGM-1	2018	2159	EGM2008, S(Goce)	Xu et al. 2017
GECO	2015	2190	EGM2008, S(Goce)	Gilardoni et al. 2016
TONGJI-GMMG2021S	2022	300	S (Goce), S (Grace)	Chen et al. 2022
GO_CONS_GCF_2_TIM_R6e	2019	300	G(Polar), S(Goce)	Zingerle et al. 2019
GO_CONS_GCF_2_TIM_R6	2019	300	S(Goce)	Brockmann et al. 2021
GO_CONS_GCF_2_DIR_R6	2019	300	S	Bruinsma et al. 2014
TONGJI-GRACE02K	2018	180	S(Grace)	Chen et al, 2018
GOSG01S	2018	220	S(Goce)	Xu et al. 2017
IfE_GOCE05s	2017	250	S	Wu et al, 2017
GO_CONS_GCF_2_SPW_R5	2017	330	S(Goce)	Gatti et al, 2016
Tongji-Grace02s	2017	180	S(Grace)	Chen et al, 2016
ITU_GGC16	2016	280	S(Goce), S(Grace)	Akyilmaz, et al, 2016
GO_CONS_GCF_2_SPW_R4	2014	280	S(Goce)	Gatti et al, 2014
GO_CONS_GCF_2_TIM_R5	2014	280	S(Goce)	Brockmann et al, 2014
GO_CONS_GCF_2_DIR_R5	2014	300	S(Goce), S(Grace), S(Lageos)	Bruinsma et al, 2013
JYY_GOCE04S	2014	230	S(Goce)	Yi et al, 2013
GOGRA04S	2014	230	S(Goce), S(Grace)	Yi et al, 2013

The ME and RMSE are computed by using following equations:

$$ME = \frac{\sum_{i=1}^{n} N_{GCM} - h - H_{MSL}}{n} \quad (7)$$

$$RMSE = \sqrt{\frac{\left(\sum_{i=1}^{n}\left(N_{GCM} - h - H_{MSL}\right)\right)^2}{n}} \quad (8)$$

In the second comparison, the GGMs geoid height, N_{GCM} have been compared with the geometrical geoid from GNSS levelling, $N_{GNSS\ levelling}$ as follows:

$$N_{GNSS\ levelling} = h - H_{MSL} \quad (9)$$

$$\Delta N = N_{GCM} - N_{GNSS\ levelling} \quad (10)$$

where the h and H_{MSL} is the ellipsoidal height and mean sea level height at the benchmark. Subsequently, ME and RMSE of the difference were computed using Equation (6) and (7). The same procedure also be implemented to compare the GGMs geoid height and local gravimetric geoid. Notably, the comparison between GNSS levelling and GGMs derived geoid height may be influenced by several errors including the datum inconsistencies (Yilmaz et al. 2016; Goyal et al. 2019), the commission and omission errors of the GGMs as well as the biases /errors introduced by GNSS and levelling (Ssengendo 2015). Thus, to minimize the effect of all the systematic biases, the absolute differences have been fitted using a 4-parameter model based on:

$$\Delta N_i = a_i^T x + v_i \quad (11)$$

$$a_i = \left[1 \cos\varphi_i \cos\lambda_i \sin\lambda_i \sin\varphi_i\right]^T \quad (12)$$

$$x = \left[x_1 x_2 x_3 x_4\right]^T \quad (13)$$

where, a_i and x is a vector of unknown parameters and known coefficients, respectively. Details of the strategy of GGMs evaluation is illustrated in the Fig. 4.

RESULTS AND ANALYSIS

In this section, the results of the comparison are summarized in Tables 2 and 3 for the GNSS levelling and terrestrial gravity anomaly datasets, respectively. Each GGM listed was evaluated up to its maximum available degree and order. The computations were conducted point by point, with the GGM-derived gravity field values determined at the geocentric latitude and longitude corresponding to each observation point. Based on the statistical analysis of the comparison with geometrical geoid height, as presented in Table 2, the XGM2019e-2159 GGM model emerges as the best fit with GNSS levelling data among the combined GGMs, with a ME of 0.530 meters and a RMSE of 0.195 meters. This result aligns closely with an earlier study by Tocho et al. (2022), which reported an accuracy of approximately 0.219 meters for the XGM2019e-2159 model. However, the GECO GGM model can also be considered a strong contender, as the statistical analysis shows that its RMSE is only slightly different from that of XGM2019e-2159, with ME and RMSE values of

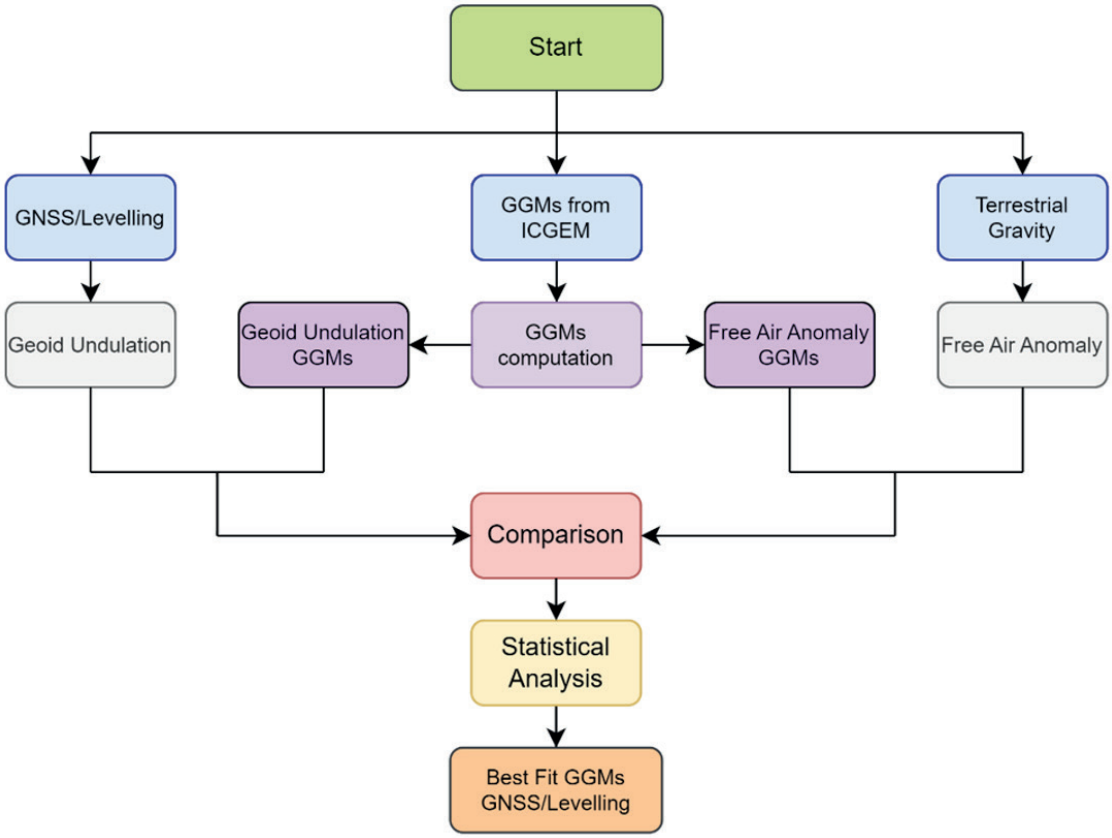

Fig. 4. Methodology of the study

0.525 meters and 0.198 meters, respectively. Additionally, the SGG-UGM-2 and SGG-UGM. -1 models exhibit RMSE values of 0.240 meters and 0.244 meters, respectively. The accuracy of GECO obtained in this study is consistent with the previous studies by Tocho et al. (2022) and Goyal et al. (2019).

Among the satellite-only GGMs, it is evident that the GO_CONS_GCF_2_SPW_R5 model (maximum degree 330) exhibits the best fit with the GNSS levelling data, characterized by a ME of 0.729 meters and a RMSE of 0.209 meters. However, the performance of several GGMs model such as GO_CONS_GCF_2_TIM_R6e, GO_CONS_GCF_2_DIR_R6, GO_CONS_GCF_2_TIM_R5, GO_CONS_GCF_2_TIM_R6, and ITU_GGC16 also show good performance. Statistical analysis shows the RMSE of those models only marginally different from GO_CONS_GCF_2_DIR_R6 which is below than 1cm (in the range of 0.214m–0.217 m). The RMSE of other satellite-only GGM fall in the range of 0.222m to 0.682 with Tongji-Grace02s having the poorest RMSE. The differences (after fitting) between the geoid height from the optimum GGM (XGM2019e-2159 and GO_CONS_GCF_2_SPW_R5) and geometrical geoid height over East Malaysia are illustrated in Figure 6. The range of the different (after fitting) between XGM2019e-2159 GGMs and GNSS levelling falls within the range of 29.112mGal-60.372mGal. Meanwhile, the range of the different (after fitting) for the GO_CONS_GCF_2_SPW_R5 GGM fall within the range of 28.959mGal - 60.644mGal.

The statistics regarding the differences between terrestrial gravity anomalies and GGMs gravity anomalies are presented in Table 3. From the statistical results, it is observed that the RMSE of the combined GGMs falls within the range of 32.780 mGal to 32.760 mGal. Among these, the GECO GGM model exhibits the best fit with terrestrial gravity anomalies, characterized by a ME of 46.669 mGal and an RMSE of 32.760 mGal. Interestingly, the statistical analysis in this table reveals that the XGM2019e-2159 model has the poorest RMSE (32.780 mGal), compared to the SGG-UGM-1 and SGG-UGM-2 models, which have RMSE values of 32.775 mGal each. However, it's worth noting that the accuracy of the combined GGMs does not exhibit significant differences, with variances of less than 0.01 mGal. Among the satellite-only GGMs, the GO_CONS_GCF_2_DIR_R5 model demonstrates the best agreement with terrestrial gravity anomalies, with an ME of 46.494 mGal and an RMSE of 32.456 mGal, as indicated in Table 3. In contrast, the accuracy of the GO_CONS_GCF_2_SPW_R5 GGM markedly differs from that of the other satellite-only GGMs. The RMSE values for the latter group fall within the range of 32.456mGal to 32.907mGal, with the Tongji-Grace02s model having the poorest RMSE. To visually depict the differences between the gravity anomalies derived from the optimal GGMs (GECO and GO_CONS_GCF_2_DIR_R5) and the geometrical geoid height over East Malaysia, Fig. 8 provides an illustration. Meanwhile Fig.7 display the geoid heights over East Malaysia derived from the GO_CONS_GCF_2_DIR_R5 and GECO GGMs. These illustrations provide insight into the variations in the geoid height across different regions of East Malaysia, indicating how each model represents the Earth's gravity field and the shape of the geoid in the study area. As shown in Fig. 8, the differences between GECO and terrestrial gravity anomalies fall within the range of 29.112 mGal to 60.372 mGal. Meanwhile, the differences between GO_CONS_GCF_2_DIR_R5 and terrestrial gravity anomalies are within the range of 28.959 mGal to -60.644 mGal. Relating to the GECO and GO_CONS_GCF_2_DIR_R5 spike, the sharp deviation a mismatch between the predicted gravity values from the model and the actual terrestrial gravity measurements.

CONCLUSIONS

This study evaluated the performance of GGMs in developing geoid models for East Malaysia by comparing their accuracy against terrestrial gravity anomalies and

Table 2. Statistical analysis of the difference between GGMs and GNSS levelling observations

GGM	Min	Max	Mean	RMSE
SGG-UGM-2	0.000	1.555	0.556	0.240
XGM2019e-2159	**0.175**	**1.583**	**0.530**	**0.195**
SGG-UGM-1	0.016	1.777	0.577	0.244
GECO	0.029	1.546	0.525	0.198
GO_CONS_GCF_2_TIM_R6E	0.184	1.586	0.641	0.217
GO_CONS_GCF_2_DIR_R5	0.187	1.692	0.713	0.230
GO_CONS_GCF_2_DIR_R6	0.208	1.664	0.693	0.213
GO_CONS_GCF_2_SPW_R4	0.024	1.567	0.468	0.260
GO_CONS_GCF_2_SPW_R5	**0.181**	**1.847**	**0.729**	**0.209**
GO_CONS_GCF_2_TIM_R5	0.212	1.625	0.699	0.214
GO_CONS_GCF_2_TIM_R6	0.187	1.579	0.642	0.217
GOGRA04S	0.000	1.843	0.728	0.331
GOSG01S	0.000	2.152	0.531	0.378
IfE_GOCE05s	0.068	2.104	0.742	0.307
ITU_GGC16	0.188	1.549	0.653	0.214
JYY_GOCE04S	0.001	1.980	0.780	0.330
Tongji-GMMG2021S	0.114	1.896	0.732	0.222
Tongji-Grace02k	0.000	4.212	0.891	0.656
Tongji-Grace02s	0.001	4.685	0.966	0.682

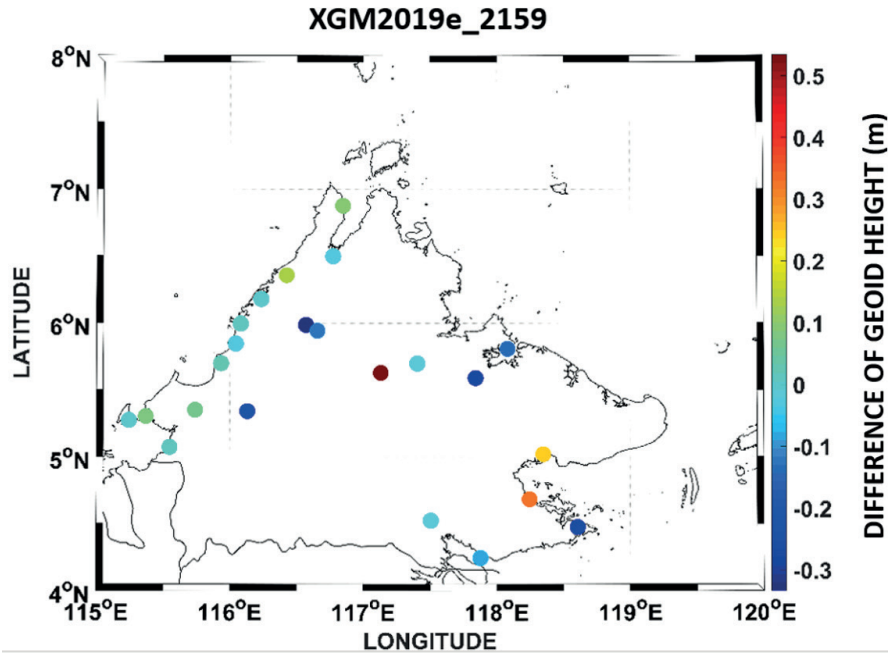

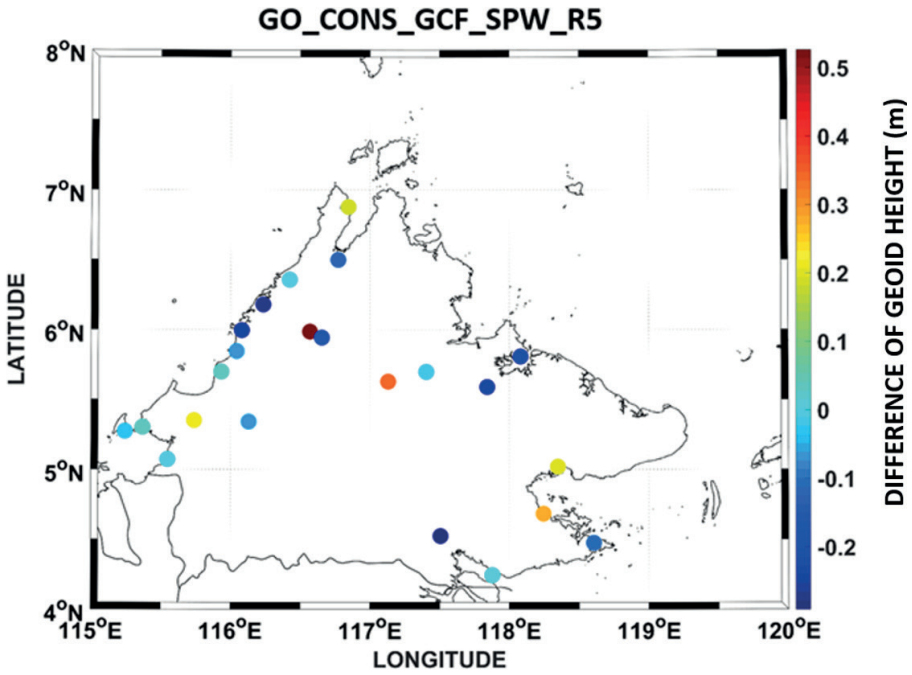

Fig. 5. Differences between (a) XGM2019e_2159 GGM and (b) GO_CONS_GCF_SPW_R5 GGM geoid height with GNSS levelling derived geoid height over Sabah region

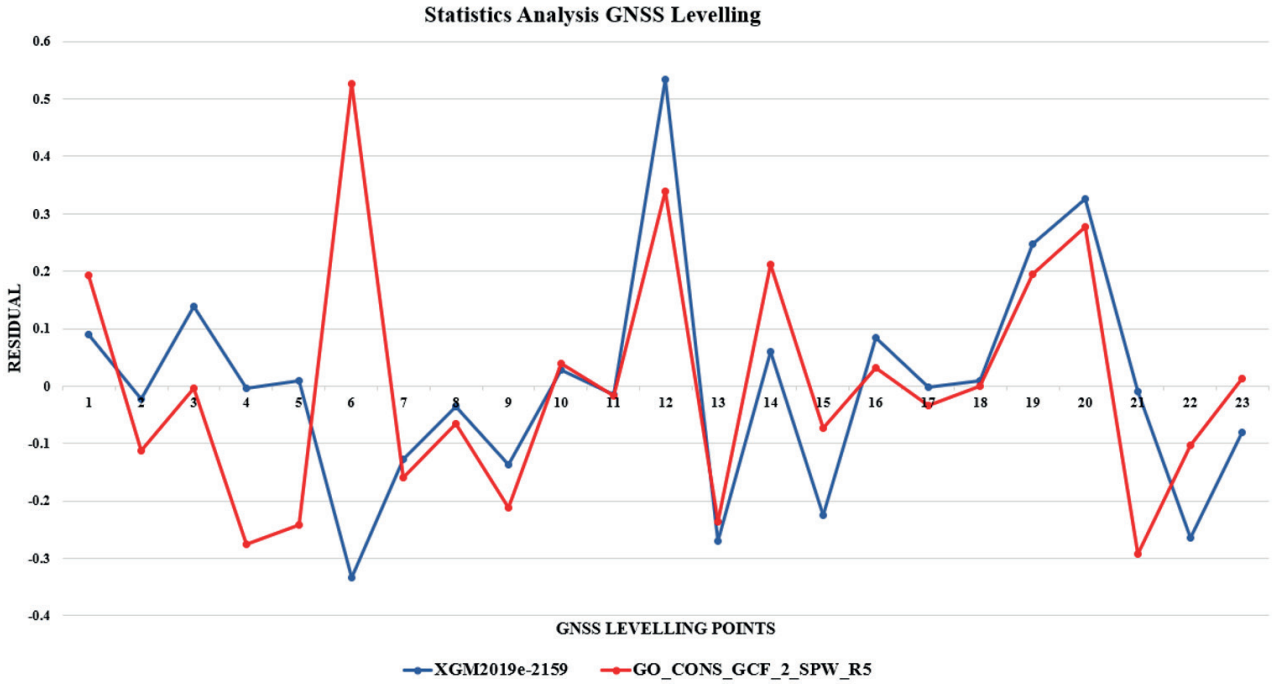

Fig. 6. Differences between GGMs and GNSS levelling over Sabah region

Table 3. Statistical analysis of the difference between GGMs and terrestrial gravity anomaly [unit:mGal]

GGM	Min	Max	Mean	RMSE
SGG-UGM-2	29.108	60.384	46.690	32.777
XGM2019e-2159	29.115	60.371	46.695	32.780
SGG-UGM-1	29.083	60.394	46.657	32.775
GECO	**29.112**	**60.372**	**46.669**	**32.760**
GO_CONS_GCF_2_TIM_R6E	29.065	60.597	46.530	32.760
GO_CONS_GCF_2_DIR_R5	**28.959**	**60.644**	**46.494**	**32.456**
GO_CONS_GCF_2_DIR_R6	28.993	60.577	46.496	35.754
GO_CONS_GCF_2_SPW_R4	29.106	60.779	46.661	32.800
GO_CONS_GCF_2_SPW_R5	28.786	60.469	46.505	32.761
GO_CONS_GCF_2_TIM_R5	28.964	60.613	46.492	32.759
GO_CONS_GCF_2_TIM_R6	29.064	60.600	46.530	32.760
GOGRA04S	28.678	60.896	46.493	32.779
GOSG01S	28.752	61.356	46.632	32.828
IfE_GOCE05s	28.958	60.811	46.478	32.779
ITU_GGC16	28.993	60.643	46.522	32.765
JYY_GOCE04S	28.675	60.899	46.488	32.779
Tongji-GMMG2021S	29.075	60.634	46.523	32.759
Tongji-Grace02k	29.132	60.698	46.510	32.903
Tongji-Grace02s	29.120	60.797	46.514	32.907

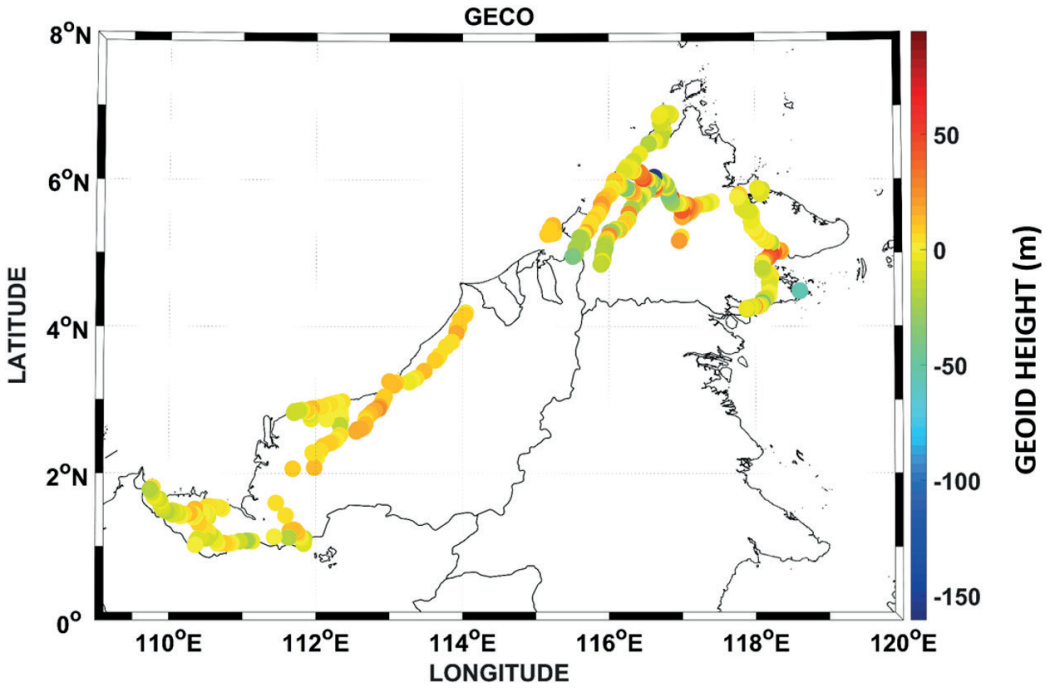

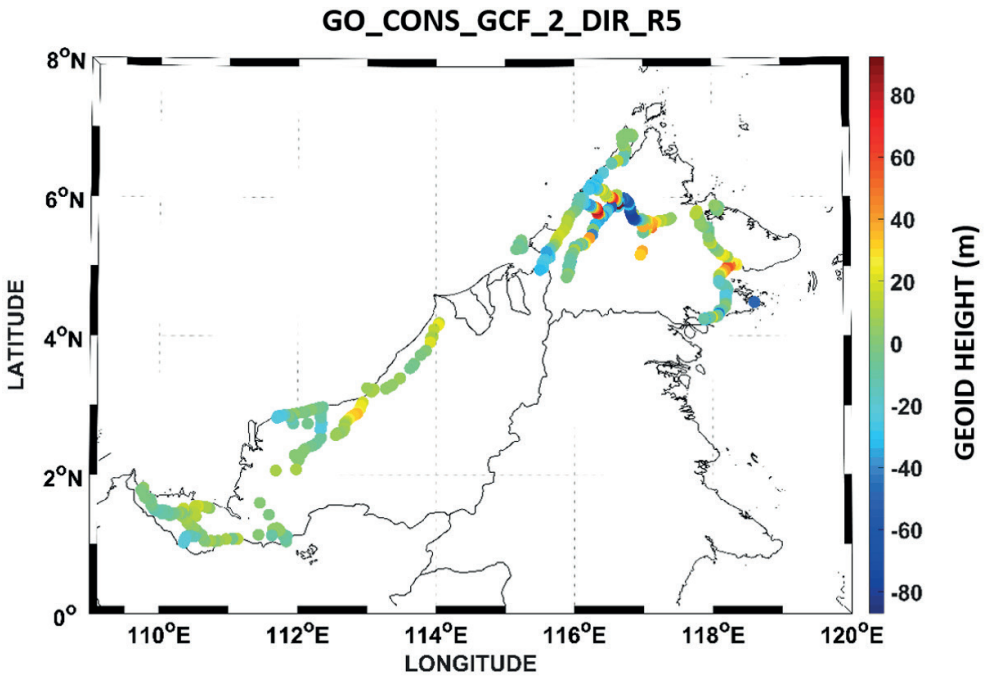

Fig. 7. Differences between (a) GECO GGM and (b) GO_CONS_GCF_2_DIR_R5 GGM with 680 terrestrial gravity anomalies

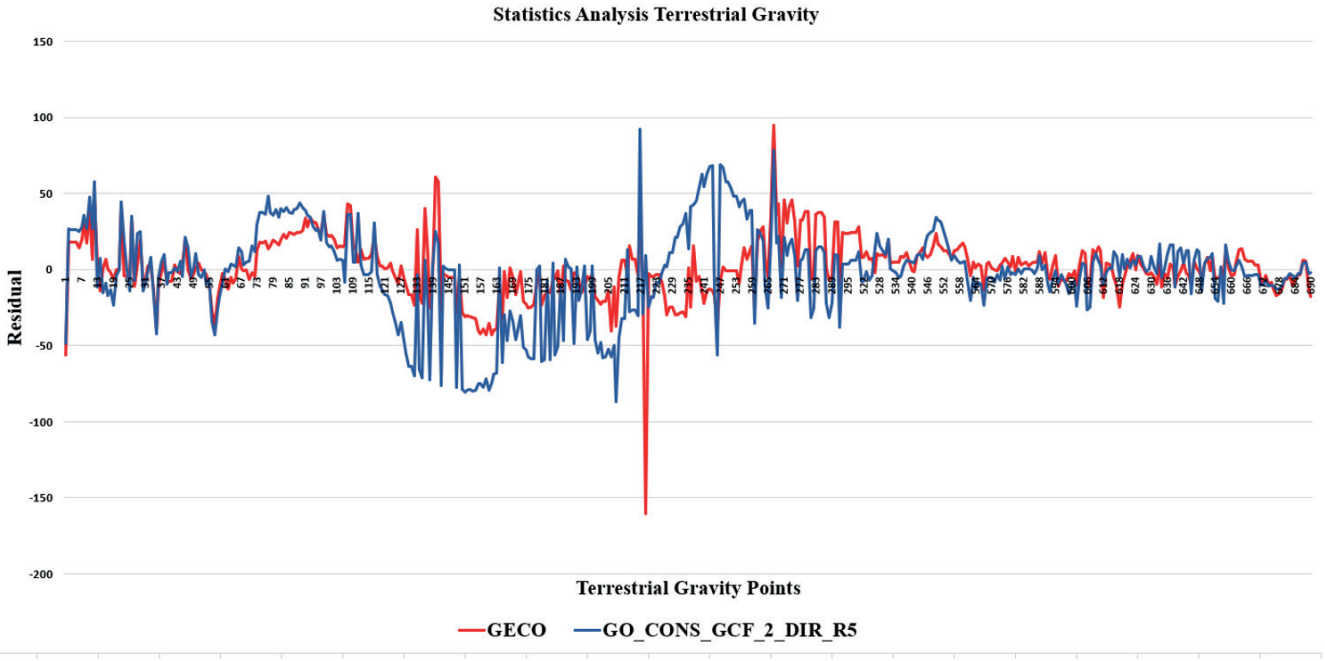

Fig. 8. Differences between two GGMs and terrestrial gravity anomalies over East Malaysia

GNSS leveling data. One of the key challenges identified is the uneven distribution of GNSS leveling points, which influences the reliability of models, particularly in inland mountainous areas. This uneven distribution directly affects the evaluation and validation of GGMs. Meanwhile, coastal and lowland regions, where infrastructure is more developed, provide better accessibility for setting up GNSS reference stations, ensuring more reliable and accurate measurements. This makes it easier to validate GGMs like GECO and GO_CONS_GCF_2_DIR_R5 in these areas. In contrast, the mountainous interior of East Malaysia, characterized by challenging terrain, sparse population, and limited infrastructure, has fewer GNSS points. This lack of data coverage limits the ability to properly assess the accuracy of the GGM models in these regions, contributing to the variability in performance among different GGMs. The results show that combined GGMs, which integrate data from multiple satellite missions, perform consistently across the region. Among the combined models, the GECO GGM showed the best fit with terrestrial gravity anomalies, achieving a mean error (ME) of 46.669 mGal and root mean square error (RMSE) of 32.760 mGal. However, the differences in RMSE values among the combined models were minimal, indicating stable performance across the set. For satellite-only GGMs, the GO_CONS_GCF_2_DIR_R5 model had the closest agreement with terrestrial gravity data, with an Mean of 46.494 mGal and RMSE of 32.456 mGal. Other satellite-only models, such as Tongji-Grace02s, displayed higher RMSE values, highlighting some variability in their accuracy. These findings suggest that satellite-only models can effectively capture large-scale gravity variations, but their precision may vary depending on the model used. Interestingly, the analysis reveals that combined GGMs perform better than satellite-only GGMs

when evaluated with GNSS leveling data, indicating that integrating data from multiple sources improves overall reliability. In contrast, satellite-only GGMs align more closely with terrestrial gravity anomalies, suggesting they are better suited for detecting broad-scale gravity variations. In conclusion, GECO GGM is identified as the most suitable combined model, while GO_CONS_GCF_2_DIR_R5 performs best among satellite-only models. As shown in fig 8, the differences between GECO and terrestrial gravity anomalies range from 29.112 mGal to 60.372 mGal, and for GO_CONS_GCF_2_DIR_R5, from 28.959 mGal to -60.644 mGal. These findings highlight the importance of selecting appropriate GGMs based on the type of analysis and data available. While combined GGMs provide robust solutions across datasets, satellite-only models may offer better alignment with specific gravity measurements, contributing to more precise geoid model development for the region.

REFERENCES

Akyilmaz, O., Ustun, A., Aydin, C., Arslan, N., Doganalp, S., Guney, C., Mercan, H., Uygur, S.O., Uz, M., Yagci, O.; GRACE time-variable gravity field recovery using an improved energy balance approach; Geophysical Journal International, Vol 203, No. 3, p. 1773-1786, doi: 10.1093/gji/ggv392.

Alemu, E. (2021). Evaluation of GGMs Based on the Terrestrial Gravity Data of Gravity Disturbance and Moho Depthin Afar, Ethiopia. Artificial Satellites, 56(3), 78–100. https://doi.org/10.2478/arsa-2021-0007

Alemu, E. (2023). Global geopotential models evaluation based on terrestrial gravity data over Ethiopia. Journal of Applied Geodesy, 17(3), 217–236. https://doi.org/10.1515/jag-2022-0051

Alothman, A., Godah, W., & Elsaka, B. (2016). Gravity field anomalies from recent GOCE satellite-based geopotential models and Terrestrial Gravity Data: A comparative study over Saudi Arabia. Arabian Journal of Geosciences, 9(5). https://doi.org/10.1007/s12517-016-2393-y

Al Shouny, A., Khalil, R., Kamel, A., & Miky, Y. (2023). Assessments of recent global geopotential models based on GPS/levelling and gravity data along Coastal Zones of Egypt. Open Geosciences, 15(1). https://doi.org/10.1515/geo-2022-0450

Amos, M., and Featherstone, W. (2003). Comparisons of recent global geopotential models with terrestrial gravity field observations over New Zealand and Australia. Geomatics Research Australasia, 79, 1–20.

Barthelmes, F. & K. (2013). International Centre for Global Earth Models (ICGEM). Journal of Geodesy, The Geodesists Handbook, 1–10. Retrieved from http://icgem.gfz-potsdam.de/ICGEM/

Benahmed Daho, S. A. (2010). Assessment of the EGM2008 Gravity Field in Algeria Using Gravity and GPS/Levelling Data. In International Association of Geodesy Symposia (Vol. 135, pp. 459–466). https://doi.org/10.1007/978-3-642-10634-7_61

Brockman, JM, Zehentner N, Höck E, Pail R, Loth I, Mayer-Gürr T, Schuh WD (2014) EGM_TIM_RL05: An independent geoid with centimeter accuracy purely based on the GOCE mission Geophys Res Lett 41:8089–8099, https://doi.org/10.1002/2014GL061904

Brockmann, J. M., Schubert, T., Schuh WD An Improved Model of the Earth's Static Gravity Field Solely Derived from Reprocessed GOCE Data Surveys in Geophysics, doi: 10.1007/s10712-020-09626-0, 2021

Bruinsma, S. L., Förste, C., Abrikosov, O., Marty, J. C., Rio, M. H., Mulet, S., & Bonvalot, S. (2013). The new ESA satellite-only gravity field model via the direct approach. Geophysical Research Letters, 40(14), 3607–3612. https://doi.org/10.1002/ grl.50716

Chen, Q., Luo, Z., Qian, C., Zhu, M., & Zhang, X. (2022). A comparison of satellite-only, combined, and local geoid models: A case study in Australia. Journal of Applied Geodesy, 16(2), 89–101. https://doi.org/10.1515/jag-2021-0032.

Chen, Q., Shen, Y., Chen, W., Zhang, X., Hsu, H., 2016: An improved GRACE monthly gravity field solution by modelling the non-conservative acceleration and attitude observation errors. Journal of Geodesy, 90(6), 503-523. http://doi.org/10.1007/s00190-016-0889-6.

Chen, Q., Shen, Y., Francis , O., Chen, W., Zhang, X., Hsu, H., 2018:Tongji-Grace02s and Tongji-Grace02k: high-precision static GRACE-only global Earth's gravity field models derived by refined data processing strategies. Journal of Geophysical Research: Solid Earth, doi: 10.1029/2018JB015641, 2018

Doganalp, S. (2016). An Evaluation of Recent Global Geopotential Models for Strip Area Project in Turkey. Earth Sciences Research Journal, 20(3), 1. https://doi.org/10.15446/esrj.v20n3.55440

El-Ashquer, M., Elsaka, B., & El-Fiky, G. (2016). On the Accuracy Assessment of the latest releases of Goce Satellite-based geopotential models with EGM2008 and terrestrial GPS/levelling and gravity data over Egypt. International Journal of Geosciences, 07(11), 1323–1344. https://doi.org/10.4236/ijg.2016.711097

Ellmann, A. (2010). Validation of the new earth gravitational model EGM08 over the Baltic countries. Gravity, Geoid and Earth Observation, 489–496. https://doi.org/10.1007/978-3-642-10634-7_65

Ellmann, A., & Vaníček, P. (2007). UNB application of stokes–Helmert's approach to geoid computation. Journal of Geodynamics, 43(2), 200–213. https://doi.org/10.1016/j.jog.2006.09.019

Gatti, A., Reguzzoni, M., Migliaccio, F., Sanso, F.; Space-wise grids of gravity gradients from GOCE data at nominal satellite altitude; Paris, 2014.

Gatti, A., Reguzzoni M., Migliaccio, F., Sansò F., (2016) Computation and assessment of the fifth release of the GOCE-only space-wise solution: Presented at the 1st Joint Commission 2 and IGFS Meeting, 19-23 September 2016, Thessaloníki, Greece.

Gilardoni, M., Reguzzoni, M., Sampietro, D.; GECO: a global gravity model by locally combining GOCE data and EGM2008; Studia Geophysica et Geodaetica, Vol 60, p. 228-247, doi: 10.1007/s11200-015-1114-4, 2016

Goyal, R., Dikshit, O., & Balasubramania, N. (2019). Evaluation of global geopotential models: A case study for India. Survey Review, 51(368), 402–412. https://doi.org/10.1080/00396265.2018.1468537

Guimarães, G., Matos, A., & Blitzkow, D. (2012). An evaluation of recent GOCE geopotential models in Brazil. Journal of Geodetic Science, 2(2), 144–155. https://doi.org/10.2478/v10156-011-0033-8

Hirt, C., Gruber, T., & Featherstone, W. E. (2011). Evaluation of the first GOCE static gravity field models using terrestrial gravity, vertical deflections and EGM2008 quasigeoid heights. Journal of Geodesy, 85(10), 723–740. https://doi.org/10.1007/s00190-011-0482-y

Heiskanen, W.A., Moritz, H. (1967). PhysicalGeodesy.W.H. Freeman, San Francisco

Jamil, H., Kadir, M., Forsberg, R., Olesen, A., Isa, M. N., Rasidi, S., Mohamed, A., Chihat, Z., Nielsen, E., Majid, F., Talib, K., & Aman, S. (2017). Airborne geoid mapping of land and sea areas of East Malaysia. Journal of Geodetic Science, 7(1), 84–93. https://doi.org/10.1515/jogs-2017-0010

Kiamehr, R., and Sjöberg, L. E. (2005). Effect of the SRTM global DEM on the determination of a high-resolution geoid model: A case study in Iran. Journal of Geodesy, 79(9), 540–551. https://doi.org/10.1007/s00190-005-0006-8

Kiamehr, R., & Eshagh, M. (2008). EGMlab, a scientific software for determining the gravity and gradient components from global geopotential models. Earth Science Informatics, 1(2), 93–103. https://doi.org/10.1007/s12145-008-0013-4

Lee, J., & Kwon, J. H. (2020). Precision evaluation of recent global geopotential models based on GNSS/leveling data on unified control points. Journal of the Korean Society of Surveying, Geodesy, Photogrammetry and Cartography, 38(2), 153–163. https://doi.org/10.7848/ksgpc.2020.38.2.153

Liang W.; Li J.; Xu, X; Zhang, S.; Zhao, Y. 2020: A High-Resolution Earth's Gravity Field Model SGG-UGM-2 from GOCE, GRACE, Satellite Altimetry, and EGM2008. Engineering, 860-878. doi: 10.1016/j.eng.2020.05.008.

Mainville, A., Forsberg, R., Sideris, M.G. (1992). Global positioning system testing of geoids computed from geopotential model and local gravity data: a case study.

Pail R, et al. (2011) First GOCE gravity field models derived by three different approaches. J Geod 85(11):819–843. https://doi.org/10.1007/s00190-011-0467-x

Perdana, A. D. P., & Heliani, L. S. (2017). Evaluation of global geopotential model and digital terrain model to the accuration of local geoid model: Case study in work field of PT Pertamina EP asset 4 field cepu. 2017 7th International Annual Engineering Seminar (InAES). https://doi.org/10.1109/inaes.2017.8068576

Rapp, R.H. (1997). Past and future developments in geopotential modelling, in : Forsberg, R, Feissl, M., Dietrich, R. (Eds.) Geodesy on the Move, Springer, Berlin, pp. 58-78

Rummel, R., Balmino, G., Johannessen, J., Visser, P., Woodworth, P. Dedicated gravity field missions-principles and aims, J Geodyn (2002) 33 3-20

Saari, T., & Bilker-Koivula, M. (2018). Applying the GOCE-based GGMs for the quasi-geoid modelling of Finland. Journal of Applied Geodesy, 12(1), 15–27. https://doi.org/10.1515/jag-2017-0020

Schwarz, K. P., Sideris, M. G., & Forsberg, R. (1990). The use of FFT techniques in physical geodesy. Geophysical Journal International, 100(3), 485–514. https://doi.org/10.1111/j.1365-246x.1990.tb00701.x

Sjöberg, L. E. (2003a). A computational scheme to model the geoid by the modified Stokes formula without gravity reductions. Journal of Geodesy, 77(7–8), 423–432. https://doi.org/10.1007/s00190-003-0338-1

Sjöberg, L. E. (2003b). A general model for modifying stokes? formula and its least-squares solution. Journal of Geodesy, 77(7–8), 459–464. https://doi.org/10.1007/s00190-003-0346-1

Ssengendo, R. (2015). A height datum for Uganda based on a gravimetric quasigeoid model and Gnss/levelling (thesis). Architecture and the Built Environment, KTH Royal Institute of Technology, Stockholm.

Strykowski, G., & Forsberg, R. (2010). Testing EGM2008 on Leveling Data from Scandinavia, Adjacent Baltic Areas, and Greenland. In International Association of Geodesy Symposia (Vol. 135, pp. 505–509). https://doi.org/10.1007/978-3-642-10634-7_67

Tapley B, Chambers D, Bettadpur S, Ries J (2003) Large scale ocean circulation from the GRACE GGM01 geoid. Geophys Res Lett 30(22):2163. https://doi.org/10.1029/2003GL018622

Tapley B, Ries J, Bettadpur S, Chambers D, Cheng M, Condi F, Gunter B, Kang Z, Nagel P, Pastor R, Pekker T, Poole S, Wang F (2005) GGM02 – An improved Earth gravity field model from GRACE. J Geod 79:467– 478. https://doi.org/10.1007/s00190-005-0480-z

Tocho, C. N., Antokoletz, E. D., Gómez, A. R., Guagni, H., & Piñon, D. A. (2022). Analysis of high-resolution global gravity field models for the estimation of International Height Reference System (IHRS) coordinates in Argentina. Journal of Geodetic Science, 12(1), 131–140. https://doi.org/10.1515/jogs-2022-0139

Wu, H., Müller, J., and Brieden, P. (2016) The IfE global gravity field model from GOCE-only observations: Presented at the International Symposium on Gravity, Geoid and Height Systems, 19-23 September 2016, Thessaloníki, Greece.

Xu X., Zhao Y., Reubelt T., Robert T. 2017 A GOCE only gravity model GOSG01S and the validation of GOCE related satellite gravity models Geodesy and Geodynamics, 8(4): 260-272, http://dx.doi.org/10.1016/j.geog.2017.03.013

Yi, Weiyong, Rummel, Reiner, Gruber, Thomas Gravity field contribution analysis of GOCE gravitational gradient components; Studia Geophysica et Geodaetica, Vol 57, No. 2, p. 174-202, doi: 10.1007/s11200-011-1178-8, 2013.

Yilmaz, M., Turgut, B., Gullu, M., & Yilmaz, I. (2016). Evaluation Of Recent Global Geopotential Models By Gnss/Levelling Data: Internal Aegean Region. International Journal of Engineering and Geosciences, 1(1), 15–19. https://doi.org/10.26833/ijeg.285221.

Zingerle P, Pail R, Gruber T, Oikonomidou X. The Experimental Gravity Field Model XGM2019e. GFZ Data Services; 2019. doi: 10.5880/ICGEM.2019.007.

Zingerle, P., Brockmann, J.M., Pail, R.; Gruber, T., Willberg, M. (2019): The polar extended gravity field model TIM_R6 doi: 10.5880/ICGEM.2019.005 2019.

ges.rgo.ru/jour/

ISSN 2542-1565 (Online)